UNIVERSITY OF CALIFORNIA, IRVINE

Costs and Operating Dynamics of Integrating Distributed Energy Resources in Commercial and Industrial Buildings with Electric Vehicle Charging

DISSERTATION

Submitted in partial satisfaction of the requirements

for the degree of

DOCTOR OF PHILOSOPHY

In Mechanical and Aerospace Engineering

By

Robert Joseph Flores

Dissertation Committee:

Professor Jack Brouwer, Chair

Professor G. Scott Samuelsen

Professor Faryar Jabbari

2016

For Louisa and Elijah

나의 상어와 아기 곰에게 바칩니다

Table of Contents

List of Figures

List of Tables

Nomenclature

AC – Absorption chiller

CAISO – California Independent System Operator

CARB – California Air Resource Board

CHP – Combined heat and power

CCHP – Combined cooling heat and power

DER – Distributed energy resources

DER-CAM – Distributed Energy Resource Customer Adoption Model

DG – Distributed generation

EES – Electrical energy storage

EVSE – Electric vehicle supply equipment

FC – Fuel cell

GT – Gas turbine

HRU – Heat recovery unit

LBNL – Lawrence Berkeley National Laboratory

MILP – Mixed integer linear programming

MIRR – Modified internal rate of return

MTG – Microturbine generator / Micro gas turbine

NHTS – National Household Travel Survey

non-TOU – non-Time of use

O&M – Operations and maintenance

PEV – Plug-in electric vehicle

PV – Photovoltaic

SCAQMD – South Coast Air Quality Management District

SCE – Southern California Edison

SCG – Southern California Gas Company

TES – Thermal energy storage

TOU – Time of use

UCI – University of California, Irvine

Acknowledgements

I would like to thank Professor Jack Brouwer for serving as my advisor and dissertation committee chair. His mentorship and support has allowed for me to grow my work from the simple analyses performed for my masters to the models and analyses tools presented in this current work.

I would also like to thank Professor Scott Samuelsen for serving on my dissertation committee and also for giving me the opportunity to come to University of California, Irvine and join the Advanced Power and Energy Program.

Thank you to Professor Faryar Jabbari for also serving on my dissertation committee and for providing a dose of common sense when needed. Thank you to Professor Moshen Jafari for providing advice on optimization and for being willing to meet with me all of those Saturday mornings.

Thank you to Brendan Shaffer for inspiring the Level 3 EVSE analysis and for providing a good source to bounce ideas off of. Thank you to Rich Hack and Roberto Fonseca for their help in capturing and curating the database of building energy demand profiles that were critical to my work. Thank you to Dr. Lori Schell for her assistance with understanding the financial impacts of alternative energy investment.

Thank you to Analy Munoz for her assistance with estimating the carbon emissions associated with renewable fuel and understanding the Anteater Express system. Thank you Aaron Cheng for his support in resolving the California grid carbon emissions. Thank you to

James Soukup and Amber Fong for their support in producing nodes to use in the fleet sizing and mix portion of my work.

Thank you to David White for finding other ways to expand the use of my models and work. Thank you to Josh Eichman, Anh-Tuan Vu Do, Josh Payne, Dimas Avila, and Derek McVay for the support they have provided during my Ph.D. studies.

Thank you to my family because your teaching and love have allowed me to get this far (especially Mom and Dad). Most of all, I would like to thank my beautiful wife, Louisa, who works hard so that I can pursue my dreams and encourages me to overachieve each and every day. She has also provided me with the most beautiful son, Elijah, who has inspired me to work ever harder and reach even higher. Louisa and Elijah: all of my work is possible because of you and for you.

Curriculum Vitae

Robert Flores

rjf@apep.uci.edu
221 Engineering Laboratory Facility
University of California, Irvine
Irvine, California 92697-3550
(408) 234 – 7415

Education

University of California, Irvine June 2016
Doctor of Philosophy in Mechanical Engineering

University of California, Irvine December 2013
Master of Science in Mechanical Engineering
GPA: 3.71

Santa Clara University June 2009
Bachelor of Science in Mechanical Engineering
GPA: 3.48

Research Interests

Economics of energy systems; optimal design of distributed energy resource systems; dynamic control of distributed energy systems comprising of fuel cells, gas turbines, and ancillary technologies; integration of sustainable transportation with energy systems.

Research and Professional Experience

Advanced Power and Energy Program, University of California, Irvine
Graduate Researcher June 2010 – Present

- Designed a real-time, dynamic dispatch strategy for minimizing the cost of energy using distributed generation
- Built optimization models to maximize the economic benefit of distributed energy resources
- Developed models of distributed energy resources for use industrial and commercial buildings
- Performed parametric studies on the economic feasibility of distributed generation technologies used to provide energy for industrial and commercial buildings
- Assisted in the design and building of utility rate structure models for key energy markets in the United States

- Resolved the ability of micro gas turbines to meet or surpass regional air quality standards.
- Implement building energy monitoring equipment for the Engineering Laboratory Facility
- Evaluated the feasibility of infrastructure used for electric vehicle fueling

MAE 115 – Applied Engineering Thermodynamics, University of California, Irvine
Teaching Assistant September 2015 – December 2015

- Planned and implemented discussion lessons that aided in understanding of thermodynamic concepts and solution methods
- Developed exam and homework questions that effectively tested students' knowledge and comprehension
- Collaborated with the professor and other teaching assistant to ensure cohesion between all lectures and discussion sections
- Held additional office hours to assist students in preparation for exams
- Performed all necessary grading duties

MAE 91 – Introduction to Thermodynamics, University of California, Irvine
Teaching Assistant March 2015 – June 2015

- Shared teaching duties for all discussion sections with the professor
- Actively engaged students in discussions during group work periods aimed at teaching and developing fundamental thermodynamic concepts
- Performed all necessary grading duties

MAE 115 – Applied Engineering Thermodynamics, University of California, Irvine
Teaching Assistant September 2014 – December 2014

- Planned and implemented discussion lessons that aided in understanding of thermodynamic concepts and solution methods
- Developed exam and homework questions that effectively tested students' knowledge and comprehension
- Collaborated with the professor and other teaching assistant to ensure cohesion between all lectures and discussion sections
- Held additional office hours to assist students in preparation for exams
- Performed all necessary grading duties

Solar Decathlon, Santa Clara, CA
Solar Thermal Engineer September 2008 – June 2009

- Collaborated with other engineers to design a solar powered house that won 3rd place in the U.S. Department of Energy Solar Decathlon competition
- Designed a solar thermal system with a team of six students that received best design award in Santa Clara University Interdisciplinary Engineering Project Competition
- Led the solar collection team in the development of a solar thermal collection system
- Created and developed a solar thermal model demonstrating energy collection and usage in the solar house thermal system

Applied Materials, Santa Clara, CA
Corporate Accounting Intern April 2007 – May 2010

- Generated on a daily basis journal entries to update the general ledger based on company bank statements
- Engaged in continuous process improvement in order to improve work efficiency and accuracy
- Coordinated with other accountants to reconcile general ledger accounts
- Coordinated with the Business Transformation group to ensure that cash recording practices are compatible with newly implemented software systems

Refereed Journal Articles:

1. Flores, R.J., Shaffer, B.P., and Brouwer, J., *Dynamic distributed generation dispatch strategy for lowering the cost of building energy*, Applied Energy 123 (2014): 196-208

2. Flores, R. J., Shaffer, B. P., & Brouwer, J. *Economic and sensitivity analyses of dynamic distributed generation dispatch to reduce building energy cos*t. Energy and Buildings, 85 (2014), 293-304.

3. Flores, R. J., Shaffer, B. P., & Brouwer, J. *Electricity costs for an electric vehicle fueling station with Level 3 charging*. Applied Energy, 169 (2016) , 813-830.

Conference and Other Publications:

4. Flores, R.J., "Evolution of an Economically and Environmentally Viable 25 MW Microgrid", International Colloquium on Environmentally Preferred Advanced Power Generation Conference – Microgrid Global Summit, Irvine, CA. March 2016

5. Flores, R.J., "Optimal Dispatch of Building Integrated Distributed Generation and Vehicle Charging", 15th International Colloquium on Environmentally Preferred Advanced Power Generation Conference, Irvine, CA. March 2015.

6. Flores, R.J., “The Cost to Fuel Electric Vehicles Using Level 3 Chargers”, 15th International Colloquium on Environmentally Preferred Advanced Power Generation Conference, Irvine, CA. March 2015.

7. Flores, R.J., “Economic Analyses of Fuel Cells to Meet Building Thermal Demand”, Fuel Cell Seminar and Energy Exposition, Los Angeles, CA. November 2014.

8. Flores, R.J., “Building Operation Optimization (III/III): Distributed Generation”, 14th International Colloquium on Environmentally Preferred Advanced Power Generation Conference, Newport Beach, CA. April 2014.

9. Zhao, L., Flores, R.J., and Brouwer, J., “Economical Dispatch of CCHP Systems with Emissions Constraints and Thermal Load Following Capability”, California Energy Commission Energy Research and Development Division Final Project Report, PIR-09-13, In Press.

10. Flores, R.J., “Dynamic Dispatch and Control of MTGs for Building CHP”, 13th International Colloquium on Environmentally Preferred Advanced Power Generation Conference, Newport Beach, CA. April 2014.

Conference Papers (only abstract required):

11. Flores, R.J., “Control Methodologies for Minimizing cost of Energy using Distributed Generation in the Built Environment”, 2012 SACNAS National Conference, Seattle, WA. October 2012.

Community Service

- Peer reviewer: Journal of Fuel Cell Science and Technology, ASME 2014 12th Fuel Cell Science, Engineering, and Technology Conference.
- SACNAS Mentorship Program Organizer: Established and operated a program that paired science, engineering, and mathematics undergraduate with graduate student mentors.
- Solar Decathlon 2015: Provided initial leadership to the Team Orange mechanical engineering team for the 2015 Solar Decathlon Competition.

Abstract of the Dissertation

Costs and Operating Dynamics of Integrating Distributed Energy Resources in Commercial and Industrial Buildings with Electric Vehicle Charging

By:

Robert Joseph Flores

Doctor of Philosophy in Mechanical and Aerospace Engineering

University of California, Irvine 2016

Professor Jack Brouwer, Chair

Growing concerns over greenhouse gas and pollutant emissions have increased the pressure to shift energy conversion paradigms from current forms to more sustainable methods, such as through the use of distributed energy resources (DER) at industrial and commercial buildings. This dissertation is concerned with the optimal design and dispatch of a DER system installed at an industrial or commercial building. An optimization model that accurately captures typical utility costs and the physical constraints of a combined cooling, heating, and power (CCHP) system is designed to size and operate a DER system at a building. The optimization model is then used with cooperative game theory to evaluate the financial performance of a CCHP investment. The CCHP model is then modified to include energy storage, solar powered generators, alternative fuel sources, carbon emission limits, and building interactions with public and fleet PEVs. Then, a separate plugin electric vehicle (PEV) refueling model is developed to determine the cost to operate a public Level 3 fast charging station.

The CCHP design and dispatch results show the size of the building load and consistency of the thermal loads are critical to positive financial performance. While using the CCHP system to produce cooling can provide savings, heat production drives positive financial performance.

When designing the DER system to reduce carbon emissions, the use of renewable fuels can allow for a gas turbine system with heat recovery to reduce carbon emissions for a large university by 67%. Further reductions require large photovoltaic installations coupled with energy storage or the ability to export electricity back to the grid if costs are to remain relatively low.

When considering Level 3 fast charging equipment, demand charges at low PEV travel levels are sufficiently high to discourage adoption. Integration of the equipment can reduce demand charge costs only if the building maximum demand does not coincide with PEV refueling. Electric vehicle refueling does not typically affect DER design at low PEV travel levels, but can as electric vehicle travel increases. However, as PEV travel increases, the stochastic nature of PEV refueling disappears, and the optimization problem may become deterministic.

1 Introduction

1.1 Overview

Concerns over increasing greenhouse gas and pollutant emissions associated with energy conversion has caused our society to evaluate how we convert energy. Because of these concerns many are attempting to find efficient and effective methods of reducing these emissions in the energy conversion sectors for which the greatest impact can be made.

During the year 2012, the U.S. commercial and industrial sectors consumed approximately 2323 terawatt-hours of delivered electricity and 3038 terawatt-hours of natural gas [1–3]. In the past, technical and economic limitations have restricted how commercial and industrial buildings can meet this electrical and natural gas. Building operators relied on energy provided by utilities, on lower efficiency onsite sources, or small amounts of photovoltaic (PV) sources for energy. Today, alternative developing and some mature technologies and methods are available to commercial and industrial buildings that allow for a reduction in emissions while possibly maintaining positive economic performance.

Concurrently, the light duty transportation sector consumes approximately 4396 terawatt-hours of fuel (primarily gasoline), and is considered as a primary source of poor urban air quality. Increased availability of alternative fuel vehicles has allowed for customers to reduce their contribution to pollution and greenhouse gas emissions. In particular, the plug-in electric vehicle (PEV), can potentially reduce or eliminate any associated emissions, depending upon the source of electricity. While PEVs are typically refueled at home, prior work has shown that some public PEV refueling infrastructure is required if drivers are to maintain typical travel patterns

[4]. If some of this infrastructure is located at commercial or industrial buildings, the amount of electricity passing through these buildings could rise as PEV use increases.

Taking into account the tremendous amount of energy consumed onsite, the potential of supplying electricity to the transportation sector, and the emergence of clean and renewable technologies, commercial and industrial buildings are a potential location where the greenhouse gas and pollutant emissions associated with society's activities can be reduced. This research is concerned with determining what technologies are best suited to realizing a reduction in emissions while maintaining positive economic performance.

Ideally, research in this area would consider technologies and methods that provide access to managing energy demand, reducing energy intensity of building operations, and producing energy onsite and elsewhere. Also, realistically, the first two options would traditionally be considered before the production of energy is addressed. However, if it assumed that a building operator has already evaluated and possibly installed some of these technologies, reducing both cost and emissions, then the next option is to determine if installing onsite generation can further improve building performance. Onsite generation, or as commonly referred to as distributed generation (DG), can be coupled with other ancillary technologies that convert waste produced by generators into useful products, such as heating or cooling for a building, and energy storage. The combination of all of these technologies is known as distributed energy resources (DER).

The following work contributes to the understanding of optimal design of DER systems installed at commercial and industrial buildings with environmental constraints and PEV refueling. This is accomplished by:

1. Building an optimization model capturing the decision to purchase and operate DER and PEVs when environmental constraints apply.
2. Evaluation of Level 3 or direct current fast charging technology for refueling PEVs.
3. Economic and environmental analysis of different ancillary devices coupled with DG to improve understanding of the benefits of different types of CCHP energy products.
4. Determining the effect on optimal DER design when emission reduction goals are established.
5. Evaluating the impact of including the option of adopting public refueling infrastructure at a building on the design of optimal DER design.
6. Evaluating the impact of adopting PEV fleet vehicles at a building on the design of optimal DER design.

1.2 Literature Review

1.2.1 Distributed Generation and Distributed Energy Resources

Distributed generation involves the use of small-scale electrical generators to provide power at the point of use. Shifting from centralized generation to distributed generation provides numerous benefits to individual customers, utilities, and society as a whole, including the potential for increased system efficiency, reliability, and power quality, as well as reduced grid demand, delivery losses, central generation investment, maintenance, expansion, and emissions [5]. Despite these benefits, it is estimated that distributed generation accounts for less than three percent of all installed generation capacity in the United States, with distributed generation smaller than 1 MW accounting for less than one percent [6].

It has been argued that this may be due to utility-imposed electrical standby charges associated with DG, which can effectively increase the cost of utility-supplied electricity whenever a customer installs DG [7] and potentially limit the long term benefits of DG [8]. However, any decrease in profitability caused by such rate structures has only been shown to be prohibitive for those serviced by utilities with moderate to low congestion grids [9]. It has also been argued that the small DG market may be due to mandatory regulatory and interconnection requirements that must be satisfied before DG may be utilized [10]. Regardless of the specific causes of the small current market size, the primary barrier for DG installation and use is cost; as a practical matter, customers will not consider DG in the first instance if it is not shown to be profitable [9,10], and the relative capital cost of smaller energy conversion systems has typically been much higher than similar (i.e., same technology) larger energy conversion systems.

DG is currently not a practical option for all commercial and industrial buildings, even if it appears to be profitable on average. The practicality of DG depends upon the magnitude and dynamic coincidence of electric and thermal demand as compared to the dispatch and control capabilities of available DG systems. DG is typically a more attractive option for commercial and industrial sectors that may be subject to relatively high electric rates and may have coincident heat and power demand. For example, despite the significant variation in rates between regions and providers[6], in California, commercial and industrial customers paid an average of $0.131 per kWh and $0.098 per kWh respectively in 2010 [11]. Under these circumstances, DG has the potential to reduce the amount spent on electric energy when properly matched to the needs of a customer.

Numerous forms of DG that use natural gas are available today. These technologies include small gas turbines (GT), microturbine generators (MTG), and fuel cells (FC) [12]. These technologies can also be operated using renewable biogas [13,14]. In addition to electricity, many of these technologies can provide a source of high grade heat for combined heat and power via heat recovery units (CHP) [15–17] and absorption chillers for combined cooling, heating, and power (CCHP) [18–20]. They are also capable of providing base load and load-following power [21,22]. They can also provide power quality support when used in conjunction with proper power electronics [23]. Renewable DG systems that use photovoltaic panels (PV), which absorb and convert solar energy to direct current electricity, are popular today[5]. Energy storage can be used with or without DG and ancillary devices to store electrical or thermal energy for later use in a building [24,25]. DG, all ancillary devices, and energy storage are all considered to be distributed energy resources (DER).

Investment risks associated with natural gas fired DG include the high volatility of natural gas prices. Predictably, studies concerning the impact of fuel price uncertainty show that the risk of investment increases as the volatility of fuel price increases [26]. It has also been shown that payback is more likely to increase than decrease when faced with electric rate, fuel price, or capital cost volatility, particularly when the price of electricity may decrease suddenly while fuel price increase [27].

Multiple business models have been developed and presented by Siler-Evans et al. and Verbruggen et al. take advantage of DER technology in an attempt to create business prospects, including demand shifting, demand response, providing reserve power capacity, and grid balancing [28,29]. The same work also suggested that the ability to sell and trade on a power

exchange market, feed in tariffs, and stable regulations may further improve the business prospects of DG [28,30].

Studies on the economics of DG and CHP establish that detailed information regarding the dynamics of the electrical load, thermal load, characteristics of the DG source, and applicable electric rate structures are necessary to estimate the profitability of a project [29]. Further studies demonstrate that both FCs and MTGs are best suited for situations with a large and consistent electrical and thermal load as they take full advantage of all the products of the FC or MTG, and that for situations without a consistent thermal load, it is better to employ a generator with higher electrical efficiency [31] or to abandon attempts to recover heat in the DG system design [32]. It was also shown that buildings with low electrical load factors and large heating demand were well suited for GT installation [31].

A variety of methods to design and operate CCHP systems have been presented in the literature. Broadly, the studies can be grouped into work that dispatched predesigned systems under desired operating strategies (or "simple dispatch" strategies) and work that used optimization methods to design and/or operate a system. "Simple dispatch" strategies for the purpose of this work are defined as any operating strategy that is predefined or uses a heuristics based approach.

Research of DER systems controlled using "simple" dispatch strategies have studied various topics regarding CCHP applications. Some studies by Nanaeda et al. and Becker et al., for example, have incorporated physics-based models in order to determine physical as was as economic feasibility [17,33]. Other studies (e.g., Wang et al., Ziher and Poredos, Naimaster and Sleiti, Medrano et al., Maidment et al., Lai and Hui, and Knizley et al.) have examined pre-sized

CCHP systems for which desired operation strategies are already defined [34–40], or where a criteria such as cost is used to decide between predefined dispatch strategies (e.g., Flores et al., and Flores et al.) [41,42]. Simple models have also been used to define when certain types of technology become economically attractive [43,44].

Numerous optimization tools have been presented in the literature. Typically, the goal of the optimization studies have been to adopt a CCHP system that minimizes cost, CO_2, emissions, primary energy consumption, or some combination of all three metrics. Cardona et al. and Aki et al. both presented a linear program that attempts to minimize cost and environmental impact showing that these goals are sometimes in conflict with one another [45,46]. Linear programs built by Fang et al, Lozano et al., and Wang et al. have also been used to determine the operation of a pre-sized CCHP system [47], to explore the marginal costs of changing different parameters associated with the constraints of the system [48], and size DER systems that included a CHP system with thermal energy storage [49]. Mixed integer linear programs (MILP) building by Collazos et al. and Bozchalui and Sharma have been presented with the goal of being used to control predesigned systems [50,51] while Keirstead et al. presented a MILP to determine the optimal design of a CCHP system in which planning restrictions [52], Liu et al. presented a MILP that includes environmental impacts [53], Lozano et al. presented a MILP that included legal constraints [54], and Liu et al. presented a MILP that accounted for economies of scale associated with purchasing multiple generators [55]. Other MILPs proposed by Wakui and Yokoyama, and Bracco et al. have included optimization of electrical energy storage [56] and renewables [57] in addition to CCHP systems. Other non-linear optimization problems have been proposed by Wang et al., Li et al., and Zeng et al. for a CCHP system powered by solar thermal

collectors [58], a CCHP system that includes thermal energy storage for both residential and commercial buildings [59], a CCHP system that incorporates a ground source heat pump for producing heat [60].

Probably the most famous of DER optimization tools is the Distributed Energy Resource Customer Adoption Model (DER-CAM) [61] developed and supported by researchers at Lawrence Berkeley National Laboratory (LBNL), which produces an optimal set of DER technologies and dispatch schedules for a given building energy demand. The DER-CAM model was used in research performed by Firestone et al., Siddiqui et al., Siddiqui et al., Marnay et al., Stadler et al., Marnay et al., and Stadler et al. [9,32,62–66]. However, research performed by Pruitt et al. using a nonlinear mixed integer program that considered part load efficiencies of DG and quality of recovered heat showed that a program similar to the DER-CAM model is limited in its ability to optimally size CCHP systems [61]. Further research using DER-CAM by Milan et al. has shown how improving optimization model accuracy can produce different results, depending on the level of detail included [67].

Many models have been built to determine an optimal configuration (system design) and financial performance of DER systems. However, important characteristics that affect the decision to invest in these technologies are not present in many of the state-of-the-art models. These missing characteristics include detailed and realistic electrical and natural gas utility cost structures, absorption chiller physics, and flexible design of heat recovery equipment.

In addition, the value of individual components of DER systems or the different energy products are not typically determined or assessed in the current literature. While the return on investment for the whole DER system is the driving factor for making an investment decision,

how individual technologies or types of energy conversion considered add to or subtract from the overall economic performance is hidden. This can result in a model finding that maximum value occurs when a set of technologies are adopted, ignoring that suggested components add little to no value while increasing investment risk.

1.2.2 Refueling Plug-in Electric Vehicles

Three major perceived disadvantages of plug-in electric vehicles (PEV) are limited range, slow recharging time [68], and availability of charging infrastructure [69,70] . Numerous research efforts have been made towards improving PEV range and charging infrastructure in an effort to overcome these perceived barriers to widespread PEV adoption [71]. Improvements to infrastructure have led to the installation of three types of electric vehicle supply equipment (EVSE) across the United States: the Level 1 (3.3 kW output), Level 2 (up to 14.4 kW output but typically 6.6 kW), and Level 3 EVSE (up to 240 kW output but typically 44 kW – 120 kW) [72]. Research focused on Level 1 and 2 type chargers has shown that while increasing battery size may assuage concerns regarding PEVs, some public EVSE capable of providing power beyond what is available from a typical electric socket (i.e., Level 3 charging) can increase the feasibility of widespread PEV adoption [4]. As a result, many aspects of Level 3 EVSE are currently being investigated.

Dharmakeerthi et al. showed that the integration of EVSE with the electrical grid introduces new challenges to operating and maintaining the electrical grid [73]. According to Sadeghi-Barzani et al., grid reliability must be considered when selecting locations for EVSE installation [74]. Once the EVSE is installed, Eising et al. and Salah et al. showed that electric grid reliability may be reduced for densely populated areas as PEV adoption increases [75,76],

while Dharmakeerthi et al. showed voltage stability may also be reduced in areas of high PEV use [77]. In distribution circuits, Dubey et al. showed that losses are greater for secondary voltages than primary voltages [78]. However, other work performed by Razeghi et al. has shown that charging plug-in hybrid vehicles within residential distribution circuits has little effect on residential transformer life unless drivers start charging as soon as they arrive at home with Level 2 EVSE [79]. Also, Harris and Webber [80] showed that unscheduled PEV charging will only increase peak demand by 1% for some regions in the United States if moderate grid growth and improvement occurs.

The optimization of PEV charging is another area that has received significant research attention. Research performed by Foley et al. that was based on the Ireland grid has shown that charging PEVs at night versus during the day can result in lower greenhouse gas emissions and cost [81]. When controlled properly, Zhang et al., Zakariazadeh et al., Clement-Nyns et al., and Soares et al. show that PEV charging can also be used to improve overall grid performance [82–85]. Electricity cost to charge PEVs can also be minimized according to Iversen et al., Su et al., Xu et al., and Tushar et al. [86–89], while also minimizing emissions (Zakariazadeh et al.) [90] or grid losses (Yang et al.) [91] with smart PEV charging. Other work performed by Momber et al. has looked at the possibility of utilizing PEVs connected to EVSE to help minimize building energy costs through peak shaving and load shifting [92].

The optimal siting of EVSE has also been explored in the current literature. This problem has been formulated as a mixed integer nonlinear program that minimizes initial investment cost and grid losses by Sadeghi- Barzani et al. [74], and both investment and operational cost by Jia et al. [93]. Several integer programs have been proposed by Su et al., Gimènez-Gaydou et al.,

Wagner et al., Xi et al., and Xu et al. that optimize EVSE placement such that total power losses in the grid are minimized [94], customer coverage is maximized [95,96], PEV refueling is maximized subject to an EVSE investment limit [97], and transportation distance to the EVSE is minimized [98]. Corresponding work has focused on evaluating the economics and feasibility of public EVSE. Research performed by Petersen et al. focused on plug-in hybrid vehicles found that making public EVSE ubiquitous increases the overall cost of PEV operation substantially [99]. However, Zhang et al. showed that some public EVSE is required to maintain high feasibility for PEVs [4]. Other work performed by Ghavami and Kar, Bayram et al., and Williams and DeShazo has focused on developing pricing methods for public EVSE to minimize cost of operation [100] while reducing congestion at individual charge points [101], or to recover investment cost while remaining cost-competitive with conventional gasoline vehicles [102].

As of 2015, approximately 70% of all public PEV charging outlets are Level 2, 21.5% are Level 1, and 8.5% are Level 3 [103]. Despite being the least adopted charger type, Level 3 EVSE are capable of charging a PEV battery up to 80% state of charge quickly [72]. Schroeder and Traber showed that the currently high investment cost and uncertainty associated with PEV adoption rates make investment in fast charging equipment risky [104]. If this risk can be reduced and the number of Level 3 EVSE increases, it is important to understand the costs associated with operating a Level 3 charger in addition to understanding optimal placement, charging strategy, grid impacts, and pricing methods.

Current research on electric vehicle charging has focused on the macroscopic impact of fueling PEVs, such as the overall cost to society or grid impacts. While some work has been performed on the charging behavior and economic performance of individual public EVSE,

operation costs and accompanying feasibility studies on Level 3 charging equipment have not been presented in the literature. Similarly, the cost of charging individual PEVs has not been delineated.

From the perspective of integration with the built environment, little research has been performed on examining how electric vehicle charging affects the decision to invest in DG or CCHP. While work has been performed on using electric vehicles as a form of energy storage for buildings, the simple question of how does PEV charging impact how building operators should meet their energy demands has not been answered.

1.2.3 Electric Vehicles and Distributed Energy Resources

Research on electric vehicle integration with the built environment has focused primarily on optimal refueling schedules and the possibility of using PEVs as a form of energy storage for the buildings at which they are parked or will travel to [105–107]. Other work has focused on integrating the refueling of vehicles within a microgrid powered using renewable technology [108].

So far, some of the only work that has addressed the possible effects that PEV refueling may have on the optimal design of DER was performed by Cardoso et al. [109]. In this work, the DER-CAM model was reformulated as a stochastic mixed integer linear program and coupled with an aggregated PEV travel model to simulate the arrival and departure of vehicles. This work considered the possibility of vehicle to grid power delivery in addition to PEV refueling. This work suggests that the inclusion of PEV refueling will have little to no impact on the decision to purchase and operate DER.

Keep in mind that Cardoso et al. [109] focused on a single energy demand load profile. Prior work performed on DER system optimization has always shown that while equipment capital costs and fuel versus electricity prices have always been critical to determining optimal technology adoption, the size and shape of the building profile also has an impact on optimization results. As a result, it is almost certain that the refueling of PEVs in some likely scenarios will affect optimal DER adoption. While the results of [109] suggest that the public refueling of PEVs will not affect DER adoption, further work in this area is required to ensure that this statement is true across all scenarios.

Almost all of the work in the current literature has been concerned with the refueling of PEVs used by individual drivers. Many other paths towards PEV adoption exist other than through purchase by individual drivers. For example, Green et al. [71] has suggested that the adoption of electric fleet vehicles by businesses, organizations, and agencies would increase PEV adoption and support improvements to public refueling infrastructure. Prior research by Erodĝan and Miller-Hools, Lin et al., Juan et al., and Hiermann et al. on the electric fleet vehicles has focused on the routing of green vehicles [110–113]. The vehicle routing problem is a well-known and well-studied problem that is typically formulated as a mixed integer linear program, as done by Desrosiers et al., Bektas, Miller et al., Laporte et al., and Christofides et al. [114–118]. Different variations on the vehicle routing problem have included determining optimal fleet mix and size (Golden et al. and Braysy et al.) [119,120], operation of a predetermined mixed fleet of vehicles (Yuan and Mehrez.) [121], and optimal routing when multiple starting and ending locations exist (Chan and Baker) [122]. Since many DER adoption models are also formulated as a MILP, there is potential for integration of the two problems. Such a combined

problem would allow for the interactions between the purchase and refueling of fleet PEVs and the purchase and operation of DER to be understood simultaneously.

1.2.4 Optimization

Optimization is a powerful mathematical tool that can provide solutions to complex problems providing that a sufficiently accurate mathematical model of the problem can be formulated. Numerous methods have been developed for tackling many different problems, both linear and nonlinear [123–129]. Many of these methods have been used in the work previously mentioned and each type has benefits to certain types of optimization problems. One type of problem typically used for both DER system sizing is mixed integer linear programming. This method is particularly attractive due to the types of decisions that must be made during DER optimization and the extensive number of commercially available solvers capable of reliably solving MILP problems, such as CPLEX [130], Gurobi [131], Xpress [132], FortMP [133], and through the MATLAB Optimization Toolbox [134].

1.2.4.1 Mixed Integer Linear Programming

The software listed above used proprietary algorithms to solve MILP problems. Almost all solvers, however, use some combination of the brand and bound algorithm and the cutting plane method, or, when combined, the brand and cut method [135]. In order to find a solution to a MILP problem, the branch and bound algorithm first relaxes all integrality constraints imposed on the problem and solves the MILP as if it were a linear program. Once the solution to the linear program has been found, additional constraints are added to restrict and integer variables that were assigned non-integer values during the integrality relaxation, and the additional linear

programs are solved. This process is repeated until a linear program with additional constraints is found where an optimal solution is found and all integer variables retain their integrality [135].

The cutting plane method is applied before any integer relaxation occurs. Through application of this method, any difference between the feasible solution space between the linear program and the MILP program is determined. If the integer feasible set is a smaller subspace of the linear feasible set, additional constraints are added to restrict the problem only to the integer feasible set. These additional constraints are known as cutting planes [135].

1.2.4.2 Stochastic Optimization

Stochastic optimization is a branch of optimization that deals with making decisions when the future is unknown. At their core, all optimization problems are stochastic in the sense that the future on which current decisions are being based off of is not known [136]. For example, if a DER system is optimized for a particular building using past building data, the system is only optimized for the past. If future building operations change or energy efficiency and management technology is adopted such that the building energy profiles change in either dynamics or amplitude, the DER system cannot be considered optimal for the future. A common assumption made during DER optimization is that prior building improvements have been made such that the energy demand profiles cannot be considerably reshaped or reduced to decrease cost and that building operations will remain similar to the past for the next five to ten years. By making this assumption, the stochastic DER optimization problem can be reduced to a deterministic problem. However, sometimes this simplifying assumption cannot be made and the stochastic nature of the problem must be addressed.

Stochastic optimization has been used numerous times with regards to DER and energy systems [137–143]. Each of these formulations relies upon the assumption that the stochastic processes that define the problem can be described by some sort of probability distribution [136]. These distributions can be used to develop likely or representative scenarios for future behavior [136]. Once the likely future scenarios have been determined along with their probability of occurring, the stochastic problem can be formulated as a two stage problem where first a decision is made that impacts the second stage of the problem [144,145]. An applicable example of this would be the decision to purchase EVSE to supply electricity to publicly refueled PEVs. The first stage would be to decide if EVSE should be purchased, and if so, what type and how many. Once purchased, the second stage would be to wait and see how many vehicles show up, refuel, and pay the EVSE investor for the provided service. If the PEV traffic to the EVSE can be probabilistically modeled, then an expected high, average, and low number of vehicles visiting the station can be estimated, along with the corresponding revenue and operating costs. This model provides the information needed to model the second stage of the problem.

Stochastic optimization is not specific to any particular linear or non-linear method. Formulations can be made for linear, mixed integer linear, and non-linear models. The stochastic method dictates how the model is constructed, stating that the initial decision to perform a certain action occurs while taking into account all possible stochastic scenarios. As a result, the number of variables used to model a specific problem increases in total by the number of possible scenarios. For example, if a DER optimization problem containing a single investment variable and ten operational variables, the size of the deterministic problem would be 1+10, or 11. If the problem was reformulated as a stochastic problem with X scenarios, the number of variables

would increase by 1+10X. This may not be a problem for smaller linear problems, but becomes untenable as problems increase in size and complexity (i.e., a linear problem becomes a MILP). Care and consideration must be taken when designing a problem to ensure that the size and accuracy are balanced such that the problem can actually be solved while providing useful results [136].

1.3 Goals

The two goals of this work are to:

1. Determine and evaluate the optimal mix and operation of distributed energy resources for a commercial or industrial building while also taking into account possible environmental constraints and the presence of plug-in electric vehicles, and
2. Determine the feasibility of public Level 3 refueling equipment.

Goal 2 is created to determine the feasibility of Level 3 refueling, but also to determine if it is reasonable to include Level 3 EVSE in the analysis of PEV refueling interaction with a building. For the purposes of this dissertation, the work will focus upon CO_2 emissions as the environmental metric associated with building and EVSE operation.

1.4 Objectives

In order to reach the goals of determining and evaluating the optimal mix and operation of DER at a commercial or industrial building while accounting for environmental constraints and the presence of PEVs, and determining the feasibility of public Level 3 refueling equipment the following objectives were established:

1. Develop models to capture the cost of energy as supplied by local electrical and natural gas utilities,
2. Develop models of energy demand for various commercial and industrial buildings,
3. Develop a model of public Level 3 charging equipment,
4. Exercise PEV refueling models to determine the cost to operate public Level 3 EVSE either as a standalone system or integrated with a building and evaluate the results,
5. Develop a model that optimally sizes distributed energy resource systems for a building,
6. Exercise models to assess the value of different types of energy produced by a DER system that is adopted to meet the energy demand of a building and evaluate the results,
7. Exercise models to evaluate the effects of environmental constraints of selected DER systems at a building,
8. Modify a DER optimization model to include uncontrolled refueling of PEVs using public EVSE, and the purchase and subsequent refueling of fleet PEVs when vehicle routes are either determined or to be optimized, and
9. Exercise models that explore how the integration of PEV refueling affects the decision to invest in DER systems for a building and evaluate the results.

2 Approach

The following tasks have been defined in order to accomplish the objectives listed in Section 1.4. One task is established for each of the objectives.

Task 1: Utility Cost Models

This task is established to develop models to capture the cost of energy as supplied by local utilities. The two types of utilities that have the largest effect on building energy costs and PEV charging are electrical and natural gas utilities. Utilities located in Southern California will be used due to a relatively high cost of electricity that together with state policies support DER use. In addition, the largest markets for fuel cells and PEVs are located in California [146,147]. The largest electrical utility in Southern California is Southern California Edison (SCE) and the largest natural gas utility is Southern California Gas (SCG). The models of this dissertation will be developed using applicable SCE and SCG rates used for commercial and industrial buildings, and public PEV charging.

Task 2: Building Energy Models

Prior work has shown the importance of using time resolved building data that captures electrical, heating, and cooling load dynamics. Building models based on measured and dynamically resolved data will be developed that showcase a variety of building loads.

Task 3: Level 3 Refueling Behavior Model

Since Level 3 charging data is not readily available, a model based on travel patterns to public spaces and public EVSE charging scenarios must be built. This objective will be accomplished by producing two models.

The first model will use travel data collected by the U.S. National Household Travel Survey [148] to produce a set of probability density functions that define typical travel parameters (day and time of travel, time spent at destination, distance traveled). This will be combined with sales data of Level 3 capable PEVs to produce a set of demand at public charging facilities.

The second model will capture typical operation of public charging facilities. Numerous different strategies are in operation today, ranging from time limits to text message alerts that notify a driver to move their PEV once charging is complete. While future charging strategies and charging technologies may not resemble how public charging is operated today, the model will attempt to span how public charging equipment is operated today.

Task 4: Level 3 Refueling Model Simulation

Travel patterns for the most common types of trips will be used to analyze the cost to operate and refuel using Level 3 charging equipment. A range of commercial and industrial building models will also be used to explore the result of integrating the equipment with a building. The results of the models will then be used to accomplish Goal 2.

Task 5: DER Optimization Model

Many optimization methods for sizing DER systems (system design) are present in the literature. One of the most prevalent is mixed integer linear programing. This type of programming allows for many of the various parameters that define the cost of building energy and physical characteristics of DER to be included. A combination of both integer, binary, and continuous variables can be used to define a problem, increasing the accuracy and power of the

model at the expense of increased computational time. Despite this drawback, an optimal or near optimal solution can be found for many complex mixed integer linear programs.

A mixed integer linear program will be built that includes all relevant constraints presented in the current literature, with the addition of new constraints that improve the modeling of the cost of utility energy and the operation of heat recovery devices, such as an absorption chiller.

Task 6: DER System Evaluation

Applicable technologies will be selected to span possible distributed generators, absorption chillers, heat recovery units, and forms of energy storage. Possible operating costs and characteristics will be selected in order to project the performance of these systems assuming current performance capabilities and projected capabilities. Once the models have been run, the data will be analyzed to partially accomplish Goal 1.

Task 7: Environmental Constraint Effect on DER System Performance

The optimization model built for Task 5 will be executed with an additional constraint that limits the amount of carbon emitted during operation. The constraint will initially allow for unlimited carbon emissions, and will then be decreased until the minimum feasible level of carbon emissions are found. This approach will show how adopted technologies and fuel source change as carbon emission constraints become more stringent.

Task 8: Addition of PEV Refueling to DER System Optimization

The integration of PEV refueling into the DER optimization can occur under many different scenarios. The three scenarios that will be examined in this work are uncontrolled

refueling of PEVs, the design and operation of a fleet of vehicles when the routes to be travelled are predetermined, and the design and operation of a fleet of vehicles when only the destinations along the routes are known.

The first scenario will require a stochastic formulation of the DER optimization model built in Task 5. Using the PEV travel model built in Task 3, representative refueling patterns will be generated and integrated with the stochastic formulation of the DER optimization model, allowing for the optimal DER design to be determined while taking into account the public refueling of PEVs.

The second scenario applies to businesses where specific routes are required. An example of this would be a transportation business or agency with predetermined bus routes. Assuming that the routes are defined not only by specific locations that must be visited but also a schedule, the problem of determining the optimal fleet composition consisting of PEVs and conventional vehicles while also designing the optimal DER system can be viewed as deterministic. The extension of the optimal DER system design problem to a pre-routed fleet design problem will maintain the mixed integer linear programing structure, requiring only accounting for additional constraints regarding the fleet design and operation.

The third scenario applies to businesses where specific locations must be visited, but the routes between the locations are to be determined through optimization. This problem would combine an optimal fleet sizing and mix while considering route design with the optimal DER system problem. This problem is also deterministic, with the typical optimal fleet sizing and mix problem having mixed integer linear characteristics. As a result, this problem can be integrated

with the optimal DER system design by including a formulation of the fleet sizing and mix problem.

Task 9: Evaluate DER Optimization with PEV Refueling

Using the model created in Task 8, the impact of PEV refueling on CCHP adoption and operation decisions will be examined.

3 Model Development

The following sections describe the various models created to satisfy the objective discussed in Section 1.4.

3.1 Utility Models

3.1.1 Electrical Rate Model

Electric rate structures are typically broken down into fixed, energy (aka volumetric), and demand charges. The methods by which these charges are calculated vary amongst utilities and rate structures (e.g., time of use, declining block, and fixed rate). As a result, the calculation of utility costs can vary significantly between utilities and depend strongly upon the specific tariffs that are applied. It is therefore important to capture the general characteristics of an electric rate structure and how it functions as a whole, in addition to the specific individual charges associated with a particular rate structure.

The electrical rate structures used in this work were based upon the rate structures that are currently used by Southern California Edison (SCE). SCE rate structures for commercial and industrial buildings are broken down by maximum yearly customer demand. These rates use the same types of charges with variations in the exact cost of each charge. There are three charges that can be summarized by examining TOU-8, the rate structure applicable for customers with a maximum demand of 500 kW or greater [149]. Under TOU-8 rates, demand and energy charges vary between summer and winter season. In addition, charges have both a time of use (TOU) component that depends upon the time during which the energy or demand is purchased, and non-time of use components (non-TOU) that do not vary with time.

SCE defines "summer" as June 1st through October 1st, and "winter" as all other times. During the summer, the on-peak hours are 12:00 p.m. to 6:00 p.m., the mid-peak hours from 8:00 a.m. to 12:00 p.m. and 6:00 p.m. to 11:00 p.m., and off-peak hours are all other hours. During the winter, on-peak hours do not exist, mid-peak hours are from 8:00 a.m. to 9:00 p.m., and off-peak hours are all other hours. Energy charges versus time of day for summer and winter season are shown in Figure 3-1. Figure 3-2 shows the percentage of a year for which each peak period is applicable. A non-TOU demand charge of $14.88 per KW is applicable for all months and is determined by the highest 15 minute average demand in a month. During the summer, TOU demand charges exist for both on-peak and mid-peak, and are $23.74 per KW and $6.55 per KW respectively. These are determined by the highest 15 minute average demand during the peak period in a month.

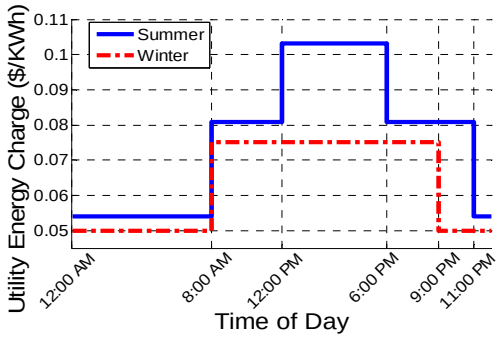

Figure 3-1: Southern California Edison Energy Charges versus Time of Day for Summer and Winter Seasons

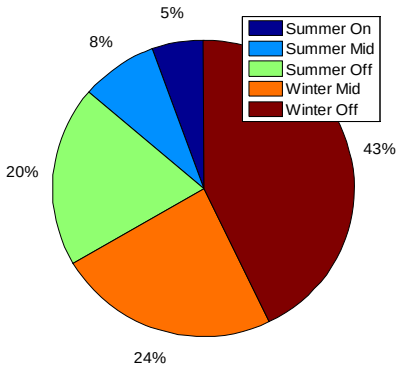

Figure 3-2: Percentage of year for Southern California Edison Peak Periods

For public PEV charging, two separate rates apply if maximum load is not greater than 500 kW. TOU-EV-3 applies if maximum demand is under 20 kW [150] and TOU-EV-4 if maximum demand is between 20 kW and 500 kW [151]. Otherwise, the TOU-8 rate is applicable. These two rates include an on-peak time for winter from 12:00 p.m. to 6:00 p.m., shifting mid-peak to either 8:00 a.m. to 12:00 p.m. or 6:00 p.m. to 11:00 p.m.

Table 3-1 shows Southern California Edison energy and demand charges for electric vehicle refueling and both commercial and industrial buildings.

Table 3-1: Electrical energy and demand charges for TOU-EV-3, TOU-EV-4, and TOU-8 rate structures for Southern California Edison for 2015

	Rate	TOU-EV-3	TOU-EV-4	TOU-8-A	TOU-8-B
Energy Charges ($/kW h)	Summer On-Peak	0.36386	0.29033	0.40067	0.13711
	Summer Mid-Peak	0.17469	0.12248	0.13597	0.08308
	Summer Off-Peak	0.09485	0.05356	0.05938	0.05938
	Winter On-Peak	0.16221	0.10763	N/A	N/A
	Winter Mid-Peak	0.14291	0.09402	0.08487	0.08487
	Winter Off-Peak	0.10374	0.06244	0.06473	0.06473
Demand Charges ($/kW)	Summer On-Peak	N/A	N/A	N/A	23.74
	Summer Mid-Peak	N/A	N/A	N/A	6.55
	Summer non-TOU	N/A	13.2	14.88	14.88
	Winter non-TOU	N/A	13.2	14.88	14.88

3.1.2 Natural Gas Rate Model

Natural gas utilities usually sell their gas in a block structure. These block structures can have a single price for all gas used in each block or comprise up to a three-tiered declining block structure, with gas typically becoming progressively cheaper as the customer reaches each new tier. The standard charge is in dollars per therm (unit of heat equivalent to 100,000 BTUs or 1.055×10^8 joules). Southern California Gas Company (SCG) is a major provider of natural gas to most customers in southern California, providing a declining block structure for commercial and industrial users. Like many natural gas utilities, SCG's rates take into account the distribution and fuel costs. While distribution costs have been observed to be relatively stable for SCG, fuel costs regularly change depending upon the market price of natural gas. As a result, while natural gas rate structures are relatively simple, changes in fuel cost cause regular variations and introduce uncertainty in customer prices. Prior work has shown that fuel price has a large impact on distributed generation economics. However, due to increased reserves and high production of natural gas recently, prices have been "depressed… to the lowest levels in a decade"[152], leading to price projections that remain low in the near future[153]. While energy price projections have been shown to be inaccurate [154], a distributed generation investment that pays back in a reasonable time period should reduce the risk of exposure to natural gas price volatility. As a result, the natural gas rate model used in the current work will follow SCG prices effective March 1st, 2015. This rate structure is as follows: \$0.8787/therm for the first 250 therms, \$0.62284/therm for the next 3,917 therms, and \$0.45129/therm for all subsequent therms.

3.2 Building Energy Model

Building models were developed using measured electrical load data showing energy consumption in 15 minute increments acquired from 39 buildings throughout southern California; 12 of which had corresponding heating and cooling loads [155]. All 12 buildings had a minimum of 12 months of data collected.

The building data cannot be directly used in the planned mixed integer linear program proposed to study CCHP systems due to computational constraints; there is simply too much data to be included in a full scale optimization model. As a result, a filtering method was adopted to reduce the collected data set for each building down to a representative set that captures the dynamics and level of consumption present in the captured data. The k-medoids method presented in [156] was adopted. This method is desirable because the representative data set is formed by parts of the original data set. The operation of the method is as follows: Each day consists of 96 time resolved data points for electricity, heating, and cooling. The days are arranged in the row of a matrix with electricity occupying columns 1 through 97, heat occupying columns 97 through 192, and cooling occupying columns 193 through 288. All subsequent days occupy the remaining rows in the same manner. This is shown in Equation 1

$$L = \begin{bmatrix} l_{1,1} & \cdots & l_{1,96} & l_{1,97} & \cdots & l_{1,192} & l_{1,193} & \cdots & l_{1,288} \\ \vdots & & \vdots & \vdots & & \vdots & \vdots & & \vdots \\ l_{i,1} & \cdots & l_{i,96} & l_{i,97} & \cdots & l_{i,192} & l_{i,193} & \cdots & l_{i,288} \\ \vdots & & \vdots & \vdots & & \vdots & \vdots & & \vdots \\ l_{365,1} & \cdots & l_{365,96} & l_{365,97} & \cdots & l_{365,192} & l_{365,193} & \cdots & l_{365,288} \end{bmatrix} \quad \text{(Eq. 1)}$$

The dissimilarity between the days is calculated using Equation 2, where *i* and *j* correspond to two different days in the year. Equation 2 is calculated for every combination of

two days in the data set, with the results being arranged in a dissimilarity matrix shown in Equation 3.

$$d(i,j) = \left(\sum_{k=1}^{288}\left(l_{i,k} - l_{j,k}\right)^2\right)^{1/2} \quad \text{(Eq. 2)}$$

$$D = \begin{bmatrix} 0 & d(1,2) & & d(1,365) \\ & 0 & & \\ & & \ddots & d(364,365) \\ sim & & & 0 \end{bmatrix} \quad \text{(Eq. 3)}$$

The dissimilarity matrix is then used in a binary program to determine the representative days. The binary program is analogous to the optimal plant location problem, where *n* stores need to be supplied by *k* plants, and the goal is to minimize the total distance between every store and the closest plant. The n stores can be considered the days in the full data set and the k plants are the number of representative days that for the reduced building demand data set. The binary program uses Equation 2 as the "distance" between days to determine representative days. The decision variables y and z are binary (limited to either 0 or 1). The binary program is as follows:

$$minimize \sum_{i=1}^{n}\sum_{j=1}^{n} d(i,j)\, z_{i,j} \quad \text{(Eq. 4)}$$

such that

$$\sum_{i=1}^{n} z_{i,j} = 1 \quad \text{(Eq. 5)}$$

$$z_{i,j} \leq y_i \quad \text{(Eq. 6)}$$

$$\sum_{i=1}^{n} y_i = k \quad \text{(Eq. 7)}$$

$$y_i, z_{i,j} \in \{0,1\}, \quad i,j = 1,2,\ldots,n \quad \text{(Eq. 8)}$$

Equation 5 ensures that each day is assigned to a representative day while Equation 6 ensures that a day can only be assigned to a single representative day. Equation 7 limits the number of representative days selected to *k*. Equation 8 establishes the decision variables as binary. Using the binary program presented above, the total annual building data set is reduced to a representative set that can be used in mixed integer programing with reasonable computational time. Two examples of the filtered data are shown in Figure 3-3.

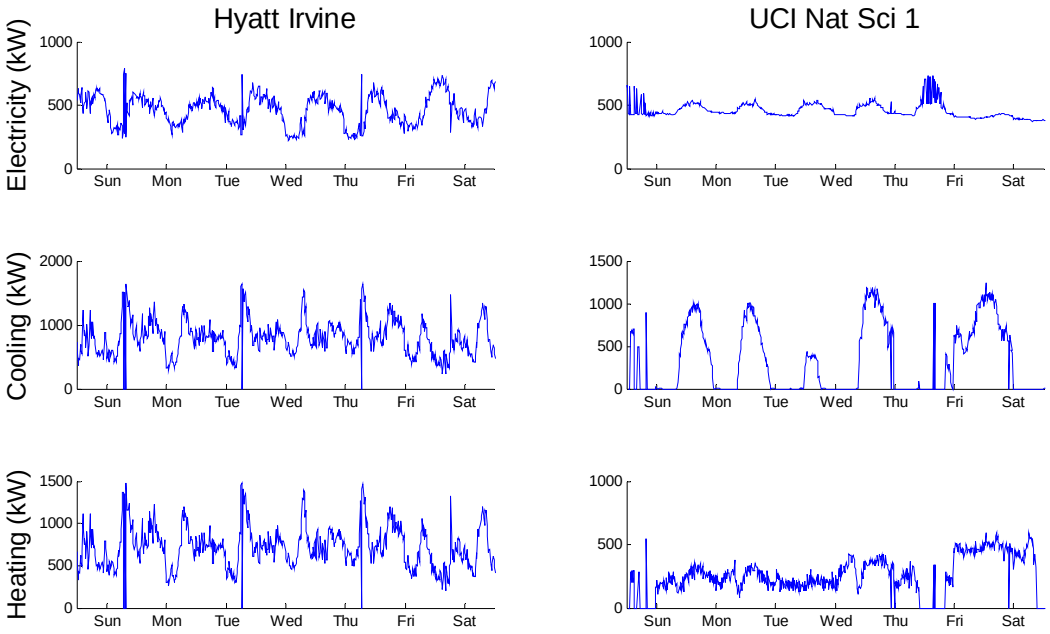

Figure 3-3: Representative week of electrical, cooling, and heating demand for the Hyatt Hotel in Irvine and UCI Natural Science 1 (Nat Sci 1) buildings

This method is also used to determine a representative month of building data to be used for Goal 2. Instead of building a model to integrate Level 3 charging equipment for an entire year, the building data can be broken down to a representative summer and winter month. Using

the reduced data set, the general behavior of charging for a single month can be examined, reducing the amount of time that must be explored to a single month or two.

3.3 PEV Refueling Model

Models were developed to determine the monthly electrical demand and cost of electricity for a Level 3 fast charging station. These models consisted of a travel model, an electric utility cost model, and a Level 3 charging station model. Using these models, the cost of the total load supplied to all PEVs and the cost incurred by each individual PEV can be calculated. Figure 3-4 shows a flowchart describing the simulation approach used in this study. Obround shapes represent model inputs using real data, squares represent built models or data selection processes, and diamonds represent model outputs.

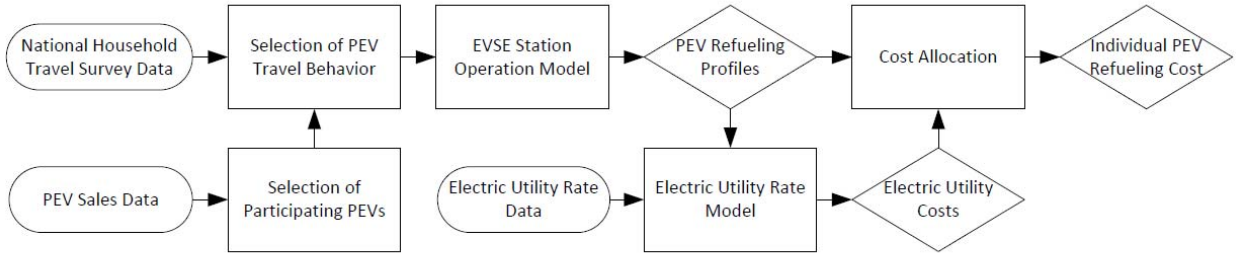

Figure 3-4: Flowchart of Level 3 EVSE electrical utility cost and cost allocation model

3.3.1 Travel Model

The purpose of the travel model is to determine the amount of electricity used by each PEV during travel. Since data on Level 3 charging stations was not readily available, the travel model was produced by generating vehicle travel profiles using probability density functions based upon PEV sales information and travel survey data. The PEV sales information was used to determine the model of PEV used for travel. The travel survey data was also used to determine

day of travel, time of arrival, time spent at destination (or dwell time), and vehicle miles traveled. This information was then used to determine the battery state of charge.

3.3.1.1 Type of PEV

Four PEV models capable of fast charging that are available today are the Nissan Leaf, the Tesla Model S, the Chevy Spark, and the Mitsubishi i-MiEV. The battery size [157], vehicle range [158], and cumulative sales in the United States since 2010 [159] for these four vehicles are shown in Table 3-2.

Table 3-2: Battery size [157]*, vehicle range* [158]*, and cumulative sales since 2010* [159] *for PEVs compatible with Level 3 charging*

PEV Model	Vehicles Sold Since 2010	Battery Size (kW h)	Range (Miles)
Nissan Leaf	47306	24	84
Tesla Model S	25141	60	208
Mitsubishi i-MiEV	1721	16	62
Chevrolet Spark	832	20	82

It was assumed that any car utilizing a Level 3 charger would be one of these four cars, and that the chance of any of these cars using the station could be determined using the probability distribution created by the number of each model sold in the United States. Using PEV sales, a probability density function was created to determine what type of PEV arrived at a Level 3 charging station to be charged.

For a given number of total PEVs visiting the Level 3 charging state, the probability density function was then used to determine the model of each vehicle to be charged. Using the battery size and range information associated with each PEV, the trip parameters (as are

described in Section 3.3.1.2) were used to determine how much electricity was used during travel.

For many of the PEVs listed in Table 3-2, Level 3 EVSE compatibility is optional and typically increases purchase cost. The cumulative sales data presented in Table 3-2 undoubtedly include PEVs purchased without the Level 3 option. However, since sales data cannot be conveniently differentiated between PEVs capable and incapable of Level 3 charging, this work assumes that the sales data is representative of all purchased PEVs that are Level 3 compatible.

3.3.1.2 Travel information

The 2009 U.S. National Household Travel Survey (NHTS) was used to determine the travel information [148]. The NHTS data was filtered so that only trips occurring in California were considered. Level 3 charging is not typically associated with PEV charging at home and approximately 92% of all Level 3 chargers are located at public locations [103], so all travel data that listed "home" as the destination were excluded. Finally, the travel data were separated by destination. Of the remaining travel data, the four most common trips in order of most to least common were for shopping (30.1%), work (15.7%), getting or eating a meal (12%), and pick up or drop off someone (11.7%). For these four data sets, the following parameters were extracted: day of travel, time of arrival at destination, time spent at destination (or dwell time), and vehicle miles traveled from the beginning of the day on all trips leading to the destination. These four parameters are shown, separated by season (winter and summer), for shopping travel in Figure 3-5 and for work travel in Figure 3-6. The individual parameters have little-to-no correlation with all other parameters and were considered to be independent of each other for all types of travel.

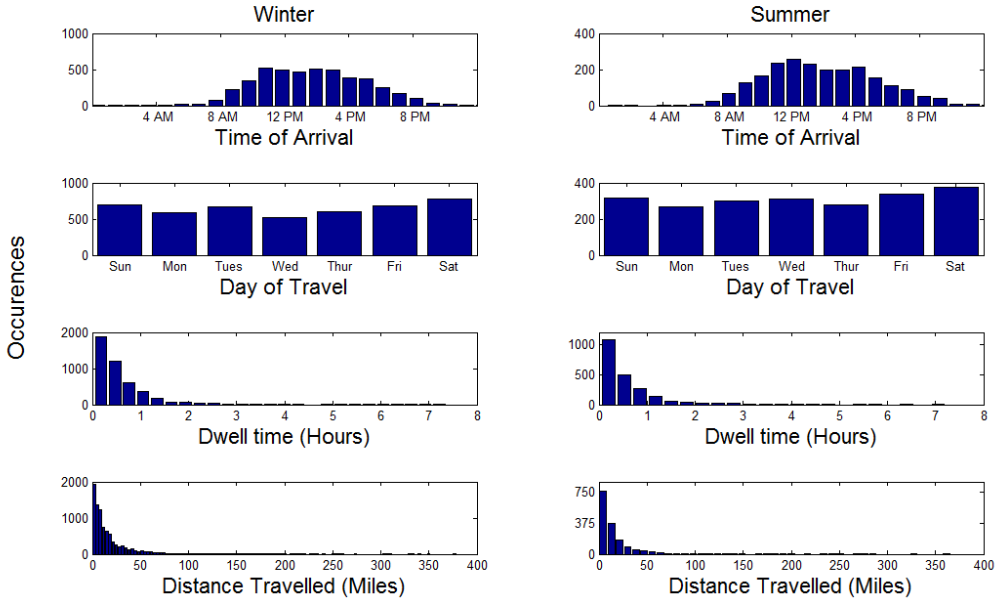

Figure 3-5: NHTS arrival time, day of travel, dwell time, and distance travelled data for shopping trips in Southern California

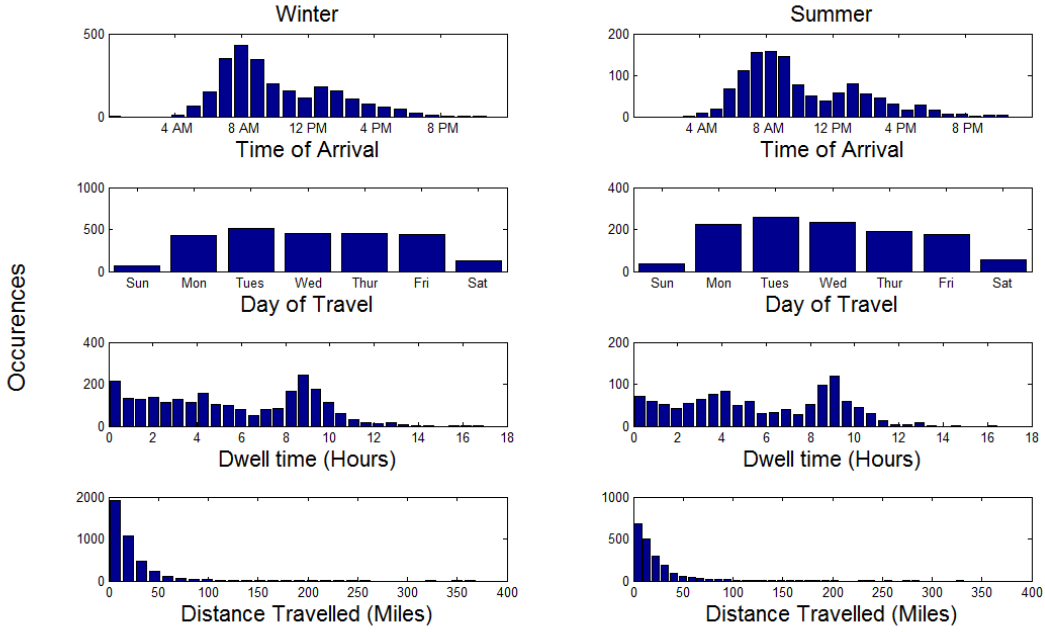

Figure 3-6: NHTS arrival time, day of travel, dwell time, and distance travelled data for work trips in Southern California

As shown in Figure 3-5, travel for shopping primarily occurs between 8 A.M. and 6 P.M., occurs frequently throughout the week, results in short dwell times, and involves travel close to the drivers origin. As seen in Figure 3-6, travel for work occurs primarily in the morning, occurs during the work week with few weekend trips, results in long dwell times, and involves travel that is further from a driver's origin than shopping travel.

Qualitatively, the distance travelled and dwell time properties of the travel data to pick or drop off someone are similar to shopping travel data, while the day of travel property is similar to work travel with an increase in weekend day of travel. Data for getting or eating a meal travel are also similar to shopping data except for increasing travel during the weekend and an increased number of trips resulting in a dwell time between 30 and 60 minutes. In this case, day of arrival for travel to get or eat a meal occurs most frequently during the weekend. However, since all travel to pick up or drop off someone and three of the four getting or eating a meal parameters are similar to either shopping or work travel and to simplify the analysis, only shopping and work travel were used in the travel model.

The NHTS data for shopping and work travel were used to create probability density functions for the four independent parameters. These probability density functions were then used to create travel information for each PEV model that arrives at the Level 3 EVSE. Coupling the vehicle miles traveled with the type of PEV, the amount of electricity used during travel was determined. If the vehicle miles traveled produced by the probability density function was ever greater than the range of the vehicle model, the vehicle miles travelled were reduced to the range of the PEV (i.e., assuming some refueling must have previously taken place).

3.3.2 Level 3 Charging Station Operation Model

While much research is focused on developing optimal charging strategies for public EVSE, PEV charging is typically determined by availability of charging equipment and systems or rules used to increase the number of PEVs charged. These systems and rules include, but are not limited to, valet operations, charging time limits, and text messaging services that notify customers when PEV charging is finished.

Instead of attempting to capture any single type of system or EVSE operation strategy, two forms of EVSE operations are used to span the potential impacts of all systems or sets of rules that typically govern PEV charging. The "conventional parking" and "valet parking" forms of operation are selected and described below. The "valet parking" form could be accomplished by one or more of the strategies outlined above (e.g., text messaging) to make sure that fully charged PEVs are removed from the charger in a timely fashion increasing EVSE availability.

A typical gasoline fuel dispenser works with most conventional vehicles, regardless of brand or model, Level 3 EVSE is not necessarily compatible with all Level 3 capable PEVs. Numerous types of Level 3 EVSE exist, each with a unique power rating, PEV connector, and set of PEV models that are compatible. Even though adaptors that allow connection between previously incompatible PEVs and Level 3 EVSE are being introduced, a typical PEV can only be charged with a single type of Level 3 EVSE. As a result, any specific Level 3 EVSE can only provide charging to a fraction of Level 3 compatible PEVs.

Despite this compatibility issue, the following operation strategies assume that either a standard PEV connection has been adopted or EVSE adapters are available, allowing for all Level 3 compatible PEVs to charge using the Level 3 EVSE examined. This assumption allows

for the full fleet of Level 3 EVSE compatible PEVs to have access to the tested refueling station configurations. Two different EVSE power ratings are explored (44 kW and 120 kW) corresponding to the range of Level 3 charging rates for vehicles currently available in the market. This work considers EVSE powered by a dedicated utility meter (electrical demand is determined only by PEV refueling).

3.3.2.1 Conventional Parking Operation

Conventional parking assumes that no rules or systems are implemented regarding EVSE operation. If a PEV arrives at an available EVSE equipped parking spot, the PEV will be parked and the battery charged to the desired level. If the driver returns to leave before the PEV is finished charging, the PEV is partially charged and the EVSE parking spot is vacated. Otherwise, the PEV is fully charged and the EVSE equipped parking spot is occupied until the drivers dwell time is finished. All other PEVs that arrive while the EVSE parking spot is occupied leave to find another spot and are not charged using the EVSE at that particular charging station.

3.3.2.2 Valet Parking Operation

Valet parking assumes that some system or technology is used to remove a PEV once charging is complete. According to this form of operation, if a PEV arrives at an available EVSE equipped parking spot, the PEV will be parked and the battery charged until either the battery is charged to the desired level or the driver returns to leave. If another PEV arrives while the EVSE equipped parking spot is occupied, the new PEV is queued and connected to the EVSE as soon as the currently charging PEV finishes charging or leaves. However, if the dwell time of the queued PEV is shorter than the time to charge the current PEV, the queued PEV leaves without being charged. Partial charges are also allowed under the valet parking scenario. Note that the

assumptions of this valet parking scenario maximize the potential use of the EVSE installed, thus spanning the other potential methods of EVSE and PEV charging operations.

3.4 DER Optimization Model

Mixed integer linear programming is selected as the method for modeling and determining the optimal DER system for a building. Due to the mixture of integer and continuous variables, a mixed integer linear programing formulation captures the decisions created while deciding if investment in DER is wise. For example, a building operator is capable of purchasing a generator only in discrete quantities. However, the decision to purchase the generator is informed by how the generator will be operated. If the generator is capable of part load operation, then each individual decision of how much energy to produce using the generator can change through time. As a result, the integer decision of purchasing a generator is mixed with the continuous decision of how much energy to produce at each time step.

The mixed integer linear program is designed to find the least expensive combination of utility energy purchases, CCHP investment, and CCHP system operation while meeting the electrical, heating, and cooling demand of a building. Operational and physical limitations of the CCHP technology is taken into account along with electrical and utility rate models. A schematic of the system being sized is shown in Figure 3-7. The schematic presents a building with a legacy vapor compression and boiler system installed to meet cooling and heating demands. The decision to be made is whether or not a generator (either a fuel cell or gas turbine) and photovoltaic panels should be adopted with a heat recovery unit, absorption chiller, electrical energy storage (EES), and thermal energy storage (TES), to meet part or all of the building energy demand. Additional decisions on the layout of the heat recovery unit and absorption

chiller must be made by deciding if duct work connecting the heat recovery unit to the generator and/or to the absorption chiller is to be installed. The labeling of this duct work is made relative to the absorption chiller, with a connection directly from the generator being a device in parallel with the absorption chiller (duct-parallel or duct-p) and a connection from the absorption chiller being in series with the chiller (duct-series or duct-s). In addition to DER adoption, the option of purchasing renewable natural gas to power fossil fuel fired DG and the option of exporting/selling electricity back to the grid are also included in the formulation. The parameters and decision variables that define this problem are shown in Table *3-3* and Table 3-4.

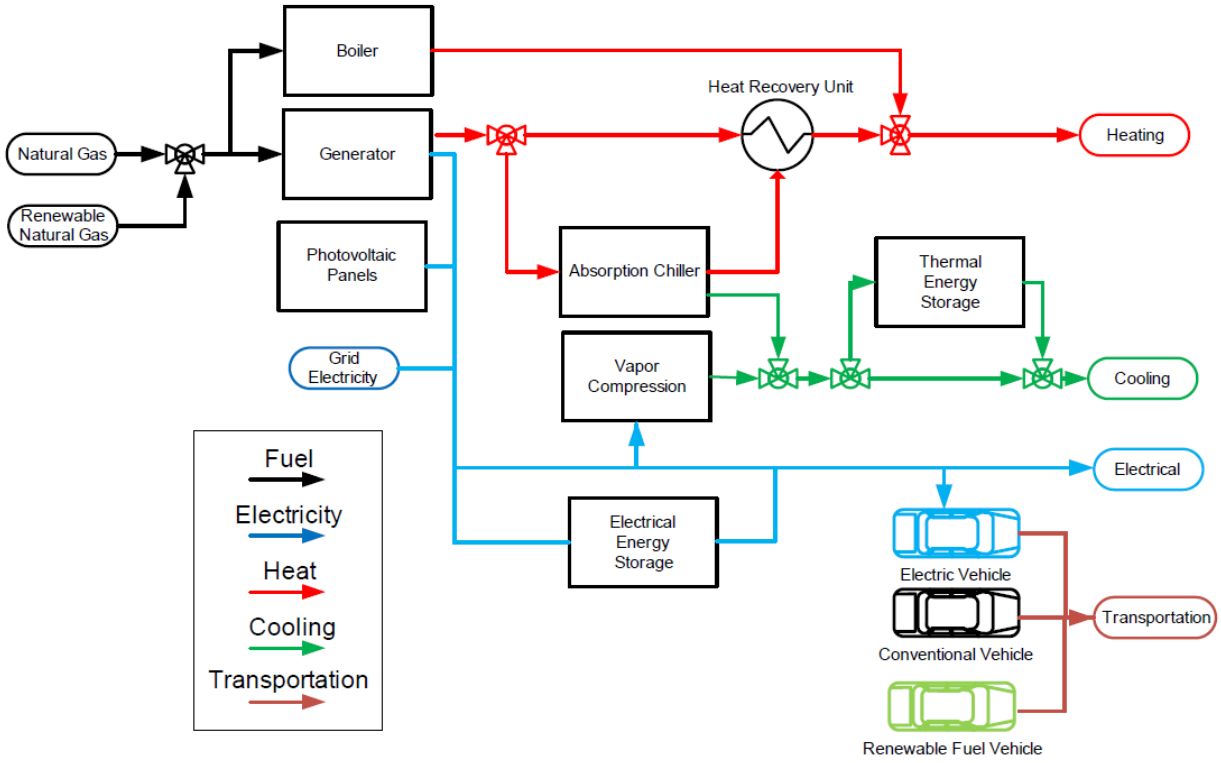

Figure 3-7: Schematic of the modeled system

Table 3-3: Parameters that define the DER system optimization

Sets	**Description**
$n \in N$	Set of all months
$m \in M$	Set of all summer months ($M \subset N$)
$h \in H_n$	Set of all 60 min increments in month n
$t \in T_n$	Set of all 15 min increments in month n
$o \in O_m$	Set of all 15 min increments during on-peak in summer month m ($O \subset T$)
$p \in P_m$	Set of all 15 min increments during mid-peak in summer month m ($P \subset T$)
$k \in K$	Set of all generator types
Building Parameters	
$E_{Bldg\ Elec,t}$	Building electrical demand at time t (kWh)
$E_{Bldg\ Heat,t}$	Building heating demand at time t (kWh)
$E_{Bldg\ Cool,t}$	Building cooling demand at time t (kWh)
Bldg Area	Area available for a photovoltaic installation (m^2)
$e_{solar,t}$	Available insolation at the building at time t (kW/m^2)
$\Delta T_{bldg.-1}$	Difference in temperature between the heat exchanger providing cooling to the building and the temperature of the used storage working fluid (^oC)
ΔT_{2-bldg}	Difference in temperature between the charged thermal energy storage working fluid and the heat exchanged providing cooling to the building (^oC)
Utility Cost Parameters	
$C_{grid,t}$	Electrical utility energy charge at time t ($/kW h)
$C_{DC,n}$	Non-TOU demand charge in month n ($/kW)
$C_{onDC,m}$	On-peak demand charge in summer month m ($/kW)
$C_{midDC,m}$	Mid-peak demand charge in summer month m ($/kW)
$C_{NG,n,i}$	i component of piece-wise function of natural gas cost for month n ($)
$C_{rng,n}$	Cost of renewable natural gas during month n ($/therm)
$C_{ex,t}$	Price at which electrical utility purchases energy from the building at time t ($/kWh)
$C_{CO2\ Grid,t}$	Carbon emissions associated with utility electricity at time t (lbs CO_2/kWh)
DG Parameters	
$C_{om\ DG,k}$	O&M cost for DG of type k ($/kWh)
$C_{cap\ DG,k}$	Capital cost for DG of type k ($)
$C_{start\ DG,k}$	Startup cost for DG of type k ($/start)
$\eta_{DG,k}$	Electrical efficiency for DG of type k (%)
$\bar{\eta}_{DG,k}$	Maximum efficiency for DG of type k (%)
$S_{DG,k}$	Rated power for DG of type k (kW)
$\delta_{DG,k}$	Minimum turndown for DG of type k (%)

$\bar{\mu}_{DG,k}$	Maximum ramp up rate for DG of type k (%/15 minutes)
$\underline{\mu}_{DG,k}$	Maximum ramp down rate for DG of type k (%/15 minutes)
Absorption Chiller Parameters	
$C_{cap\ AC}$	Capital cost for absorption chiller ($/kW)
$C_{om\ AC}$	O&M cost for absorption chiller output ($/kWh)
$C_{om\ AC\ Charge}$	O&M cost to charge absorption chiller output ($/kWh)
COP_{AC}	Coefficient of performance for absorption chiller
Δ_{AC}	Heat input for absorption chiller for 1 kW h of cooling out (kWh heat in / kWh cool out)
Υ	Thermal storage required for 1 kWh of cooling out (kWh stored / kWh cool out)
β	Stored energy retained from prior time step (%)
δ_{AC}	Minimum turndown for absorption chiller (%)
$E_{COOL\ MAX}$	Maximum cooling load for building (kWh)
Heat Recovery Unit / Duct Parameters	
$C_{cap\ HRU}$	Capital cost for heat recovery unit ($/kW)
$C_{cap\ duct\text{-}p}$	Capital cost for duct in parallel with absorption chiller ($/kW)
$C_{cap\ duct\text{-}s}$	Capital cost for duct in series with absorption chiller ($/kW)
$C_{om\ HRU}$	O&M cost for heat recovery unit ($/kWh)
$C_{om\ duct\text{-}p}$	O&M cost for duct in parallel with absorption chiller ($/kWh)
$C_{om\ duct\text{-}s}$	O&M cost for duct in series with absorption chiller ($/kWh)
ε_{HRU}	Effectiveness of heat recovery unit (%)
$\varepsilon_{duct\text{-}p}$	Effectiveness of duct in parallel with absorption chiller recovery unit (%)
$\varepsilon_{duct\text{-}s}$	Effectiveness of duct in series with absorption chiller recovery unit (%)
Photovoltaic Parameters	
$C_{cap\ PV}$	Capital cost for photovoltaic system ($/kW)
$C_{om\ PV}$	O&M Cost for photovoltaic system ($/kWh)
η_{PV}	Photovoltaic efficiency at nominal conditions
Electrical Energy Storage Parameters	
$C_{cap\ EES}$	Capital cost for EES ($/kWh)
$C_{om\ EES\ chrg}$	O&M cost to charge EES ($/kWh)
$C_{om\ EES\ dchrg}$	O&M cost to discharge EES ($/kWh)
α_{EES}	Retained EES storage between 15 minute time periods (%)
$\eta_{EES\ chrg}$	EES charging efficiency (%)
$\eta_{EES\ dchrg}$	EES discharging efficiency (%)
$\bar{\delta}_{EES}$	Maximum EES state of charge (%)
$\underline{\delta}_{EES}$	Minimum EES state of charge (%)
$\bar{\mu}_{EES}$	Maximum EES charging rate (%)

$\underline{\mu}_{EES}$	Maximum EES discharging rate (%)
Thermal Energy Storage Parameters	
$C_{cap\ TES}$	Capital cost for TES ($/kWh)
$C_{om\ TES\ chrg}$	O&M cost to charge TES ($/kWh)
$C_{om\ TES\ dchrg}$	O&M cost to discharge TES ($/kWh)
α_{TES}	Retained TES storage between 15 minute time periods (%)
$\eta_{TES\ chrg}$	TES charging efficiency (%)
$\eta_{TES\ dchrg}$	TES discharging efficiency (%)
$\bar{\delta}_{TES}$	Maximum TES state of charge (%)
$\underline{\delta}_{TES}$	Minimum TES state of charge (%)
$\bar{\mu}_{TES}$	Maximum TES charging rate (%)
$\underline{\mu}_{TES}$	Maximum TES discharging rate (%)
Legacy System Parameters	
$C_{om\ VC}$	O&M cost for vapor compression chiller output ($/kWh)
COP_{VC}	Coefficient of performance for vapor compression chiller
$C_{om\ Boil}$	O&M cost for boiler ($/kWh)
η_{Boil}	Boiler efficiency (%)

Table 3-4: Decision variables that define the DER system optimization

Utility Decision Variables	**Description**	**Variable Type**
$e_{grid,t}$	Electricity purchased from grid at time t (kWh)	Continuous
$P_{max,n}$	Maximum demand during month n (kW)	Continuous
$P_{on\ max,m}$	Maximum on-peak demand during summer month m (kW)	Continuous
$P_{mid\ max,m}$	Maximum mid-peak demand during summer month m (kW)	Continuous
$C_{ng,n}$	Cost of natural gas purchased during month n ($)	Continuous
$\lambda_{i,n}$	i component of piece-wise function of natural gas cost for month n	Continuous
$\delta_{j,n}$	j component to impose special order set type 2 constraint of natural gas piece-wise function for month n (n/a)	Binary
e_{rng}	Renewable natural gas purchased (kWh)	Continuous

$e_{ex,t}$	Electricity sold back to the grid at time t (kWh)	Continuous
Generator Decision Variables	**Description**	**Variable Type**
$N_{DG,k}$	Number of DG of type k purchased	Integer
$n_{DG\ on,k,h}$	Number of DG of type k active during hour h	Integer
$n_{DG\ Start,k,h}$	Number of DG of type k starting during hour h	Integer
$e_{DG,k,t}$	Aggregated power output from DG of type k during time t (kWh)	Continuous
$g_{DG,k,t}$	Aggregated fuel consumption of DG of type k during time t (kWh)	Continuous
$g_{rDG,k,t}$	Aggregated renewable fuel consumption of DG of type k during time t (kWh)	Continuous
Absorption Chiller Decision Variables		
$P_{max\ AC}$	Absorption chiller capacity purchased (kW)	Continuous
$e_{AC,t}$	Absorption chiller output at time t (kWh)	Continuous
$e_{AC\ Store,t}$	Absorption chiller thermal storage at time t (kWh)	Continuous
$e_{AC\ Charge,t}$	Absorption chiller charging at time t (kWh)	Continuous
$e_{AC\ Cool,t}$	Absorption chiller output due to a charge system at time t (kWh)	Continuous
$e_{AC\ Dcharge,t}$	Absorption chiller discharging at time t (kWh)	Continuous
$N_{AC,t}$	Absorption chiller operational state at time t	Binary
Heat Recovery Unit / Duct Decision Variables		
$P_{max\ HRU}$	Heat recovery unit size purchased (kW)	Continuous
$P_{max\ duct\text{-}p}$	Parallel duct size purchased (kW)	Continuous
$P_{max\ duct\text{-}s}$	Series duct size purchased (kW)	Continuous
$e_{HRU,t}$	Heat recovery unit output during time t(kWh)	Continuous
$e_{duct\text{-}p,t}$	Parallel duct output during time t (kWh)	Continuous

$e_{duct\text{-}s,t}$	Series duct output during time t (kWh)	Continuous
Photovoltaic Decision Variables		
P_{PV}	Photovoltaic system size purchased (kW)	Continuous
$e_{pv,t}$	Photovoltaic system output during time t (kWh)	Continuous
Electrical Energy Storage Variables		
$e_{EES\ size}$	EES purchased (kWh)	Continuous
$e_{EES\ chrg,t}$	Electricity stored during time t (kWh)	Continuous
$e_{EES\ dchrg,t}$	Electricity discharged from storage during time t (kWh)	Continuous
Thermal Energy Storage Variables		
$e_{TES\ size}$	TES purchased (kWh)	Continuous
$e_{TES\ chrg,t}$	Thermal energy stored during time t (kWh)	Continuous
$e_{TES\ dchrg,t}$	Thermal energy discharged from storage during time t (kWh)	Continuous
Legacy System Decision Variables		
$e_{VC,t}$	Vapor compression chiller output at time t (kWh)	Continuous
$e_{boil,t}$	Boiler output at time t (kWh)	Continuous
$e_{boil\ rng,t}$	Boiler output using renewable natural gas at time t (kWh)	Continuous

3.4.1 DER MILP Formulation

The proposed cost function for the MILP formulation is shown in Equation 9.

$$
\begin{aligned}
minimize \sum_t C_{grid,t} e_{grid,t} + \sum_n C_{DC,n} P_{max,n} + \sum_m C_{on\ DC,m} P_{on\ max,m} + \sum_m C_{mid\ DC,m} P_{mid\ max,m} \\
+ \sum_n C_{ng,n} + C_{rng,n} e_{rng} \\
+ \sum_k C_{cap\ DG,k} S_{DG,k} N_{DG,k} + \sum_k \sum_t C_{om\ DG,k} e_{DG,k,t} + \sum_k \sum_h C_{start\ DG,k} n_{DG\ start,k,h} \\
+ C_{cap\ AC} P_{\max AC} + \sum_t C_{om\ AC} e_{AC,t} + \sum_t C_{om\ AC\ \ Charge} e_{AC\ Charge,t} \\
+ C_{cap\ HRU} P_{\max HRU} + \sum_t C_{om\ HRU} e_{HRU,t} \\
+ C_{cap\ duct-p} P_{\max duct-p} \sum_t C_{om\ duct-p} e_{duct-p,t} \\
+ C_{cap\ duct-s} P_{\max duct-s} + \sum_t C_{om\ duct-s} e_{duct-s,t} + C_{cap\ PV} P_{\max PV} \\
+ \sum_t C_{om\ PV} e_{PV} + C_{cap\ EES} E_{EES} + \sum_t C_{om\ EES\ dchrg} e_{EES\ chrg} \qquad (Eq.\ 9) \\
+ \sum_t C_{om\ EES\ chrg} e_{EES\ hrg} + C_{cap\ TES} E_{TES} + \sum_t C_{om\ TES\ dchrg} e_{TES\ chrg,t} \\
+ \sum_t C_{om\ TES\ chrg} e_{TES\ dchrg,t} + \sum_t C_{om\ VC} e_{VC,t} + \sum_t C_{om\ Boil} e_{boil,t} \\
+ \sum_t C_{om\ Boil\ r} e_{boil\ rng,t} - \sum_t C_{ex,t} e_{ex,t}
\end{aligned}
$$

All decision variables must be equal to or greater than zero. Equation 10 through Equation 42 present the constraints that must be satisfied by the optimal solution. Equations 10

through 12 ensure that the electrical, heating, and cooling demand of the building is always met. Equation 10 also ensures that the vapor compression system is powered by either electrical utility energy or energy produced onsite, and that the changes in the electrical energy storage state of charge are accounted for in addition to electrical energy production and consumption.

$$E_{grid,t} + \sum_{k} e_{DG,k,t} + e_{pv,t} + e_{EES\ dchrg,t} = E_{Bldg\ Elec,t} + \frac{e_{VC,t}}{COP_{VC}} + e_{EES\ chrg,t} + e_{ex,t} \quad \text{(Eq. 10)}$$

$$e_{HRU,t} + e_{boil,,t} + e_{boil\ rng,t} = E_{Bldg\ Heat,t} \quad \text{(Eq. 11)}$$

$$e_{AC,t} + e_{VC,t} + e_{TES2\ dchrg,t} = E_{Bldg\ Cool,t} + e_{TES2\ chrg,t}\left(1 + \frac{\Delta T_{bldg-1}}{\Delta T_{2-bldg}}\right) \quad \text{(Eq. 12)}$$

As seen in Equation 9, the only natural gas cost is already associated with the total cost of natural gas per month. This is because the natural gas cost is modeled as a piece-wise continuous function. Figure 3-8 shows the piece-wise function for total cost versus total consumption for a single month. The start and stop of each line segment occurs at the different natural gas cost tiers as outlined in Section 3.1.2. Equation 13 shows the monthly consumption of natural gas due to boiler and generator operation equal to sum of the tier limits (natural gas cost starts at 0 therms and changes when 250 and 4167 therms have been consumed) and total consumption limit (set to 150,000 therms) times $\lambda_{i,n}$, or the piece-wise function variables. Equation 14 shows the same variables multiplied by the cumulative costs associated with the tier limits. Equation 15 through 20 ensure that only two adjacent $\lambda_{i,n}$ can be non-zero and that the $\lambda_{i,n}$ must sum to zero.

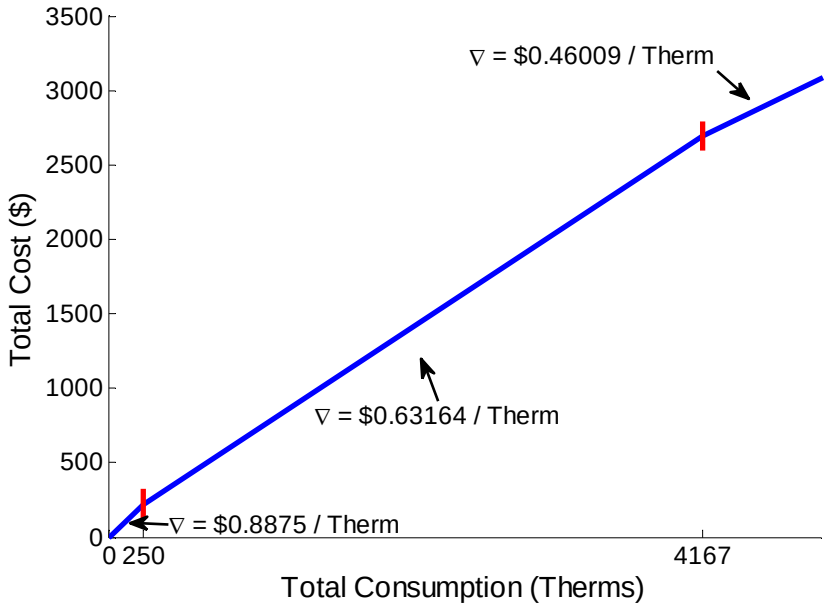

Figure 3-8: Piece-wise function that captures the total monthly cost of natural gas versus total consumption

$$0\lambda_{1,n} + 250\lambda_{2,n} + 4167\lambda_{3,n} + 150{,}000\lambda_{4,n} = \sum_t \frac{C_1 e_{boil,t}}{\eta_{boil}} + \sum_k \sum_t C_1 g_{DG,k,t} \quad \text{(Eq. 13)}$$

$$C_{ng,n} = 0\lambda_{1,n} + C_{ng,n,1}\lambda_{2,n} + C_{ng,n,2}\lambda_{3,n} + C_{ng,n,1}\lambda_{4,n} \quad \text{(Eq. 14)}$$

$$\lambda_{1,n} + \lambda_{2,n} + \lambda_{3,n} + \lambda_{4,n} = 1 \quad \text{(Eq. 15)}$$

$$\lambda_{1,n} - \delta_{1,n} \leq 0 \quad \text{(Eq. 16)}$$

$$\lambda_{2,n} - \delta_{1,n} - \delta_{2,n} \leq 0 \quad \text{(Eq. 17)}$$

$$\lambda_{3,n} - \delta_{2,n} - \delta_{3,n} \leq 0 \quad \text{(Eq. 18)}$$

$$\lambda_{4,n} - \delta_{3,n} \leq 0 \quad \text{(Eq. 19)}$$

$$\delta_{1,n} + \delta_{2,n} + \delta_{3,n} = 1 \quad \text{(Eq. 20)}$$

Equations 21 through 27 govern the operation of any set of adopted generators. Equation 21 limits active generators to generators purchased. Equation 22 sets fuel consumption to be proportional to the aggregated electricity produced. Equation 23 establishes when a generator is started. Equation 24 sets the maximum power that can be produced with the active generators while Equation 25 sets the minimum power that must be produced with the active generators. Equations 26 and 27 limit the ability of the generators to change power settings to the maximum ramp up and down capabilities of the active generator.

$$n_{DG\ on,k,h} \leq N_{DG,k} \quad \text{(Eq. 21)}$$

$$\eta_{DG,k} g_{DG,k,t} + \eta_{DG,k} g_{rDG,k,t} = e_{DG,k,t} \quad \text{(Eq. 22)}$$

$$n_{DG\ on,k,h} - n_{DG\ on,k,h-1} \leq n_{DG\ start,k,h} \quad \text{(Eq. 23)}$$

$$e_{DG,k,t} \leq S_{DG} n_{DG\ on,h} \quad \text{(Eq. 24)}$$

$$\delta_{DG,k} S_{DG,k} n_{DG\ on,k,h} \leq e_{DG,k,t} \quad \text{(Eq. 25)}$$

$$e_{DG,k,t} - e_{DG,k,t-1} \leq \bar{\mu}_{DG,k} S_{DG,k}\, n_{DG\ on,k,h} \quad \text{(Eq. 26)}$$

$$e_{DG,k,t-1} - e_{DG,k,t} \leq \underline{\mu}_{DG,k} S_{DG,k}\, n_{DG\ on,k,h} \quad \text{(Eq. 27)}$$

Equations 21 through 27 do not explicitly require that a generator to be operated for a certain period of time when started or remain turned off for an extended period before being reactivated. However, the aggregated power variable is on a 15 minute time scale while the active generator variable is on an hourly time scale. As a result, behavior that resulted in rapid on-off operation can be partially eliminated. Mandatory on- or off-time constraints have been presented in the literature for determining optimal operation after a CCHP system has been sized, but require triple the number of integer variables associated with the state of each generator at each time step [51]. By keeping active generator and aggregated power variables on different time scales, an increase in integer decision variables can be avoided while implementing a partial constraint on minimum generator up and down time. In addition, by setting the active generator variable to an hourly time scale, the number of integer variables can be reduced, decreasing computational time. While some optimality is sacrificed due to this approach, the program benefits from partially incorporating desired operating characteristics while reducing integer variables.

Equations 28 through 33 govern the absorption chiller operation. Since the vapor generation process in an absorption chiller is thermally activated, the solution must be heated and maintained at a high temperature in order to operate. This can be modeled by considering the energy storage that occurs within the absorption chiller during start up and operation. Equation 28 is an energy balance for the absorption chiller system. Equation 29 states that the maximum amount of energy stored at any time is limited by the size of the absorption chiller, or by the amount of solution in the chiller. Likewise, Equation 30 limits the cooling output of the chiller by the extent to which the chiller has been thermally activated. Equation 31 sets the total output

of the absorption chiller to energy input into a thermally activated absorption chiller and any energy extracted from storage. Equations 32 and 33 are used to establish a minimum cooling output during operation, allowing for operation to be restricted where performance of the chiller can be approximated by a linear system.

$$e_{AC\ Store,t} + e_{AC\ Dcharge,t} - \beta e_{AC\ Store,t-1} - e_{AC\ Charge,t} = 0 \quad \text{(Eq. 28)}$$

$$e_{AC\ Store,t} \leq \Upsilon P_{\max AC} \quad \text{(Eq. 29)}$$

$$e_{AC,t} \leq \frac{e_{AC\ Store,t}}{\Upsilon} \quad \text{(Eq. 30)}$$

$$e_{AC,t} = \frac{\Delta_{AC}}{COP_{AC}} e_{AC\ Dcharge,t} + e_{AC\ Cool,t} \quad \text{(Eq. 31)}$$

$$e_{AC,t} \leq E_{COOL\ MAX} N_{AC,t} \quad \text{(Eq. 32)}$$

$$\delta_{AC} P_{\max AC} \leq e_{AC,t} + \alpha\left(1 - N_{AC,t}\right) \quad \text{(Eq. 33)}$$

Equations 34 and 35 limit the output of the heat recovery unit to the installed size and to the energy transferred through the different ducts. Equations 36 and 37 limit the output of the ducts to the installed size.

$$e_{HRU,t} \leq P_{\max HRU} \quad \text{(Eq. 34)}$$

$$\frac{e_{HRU,t}}{\epsilon_{HRU}} = e_{duct-p,t} + e_{duct-s,t} \quad \text{(Eq. 35)}$$

$$e_{duct-p,t} \leq P_{\max duct-p} \quad \text{(Eq. 36)}$$

$$e_{duct-s,t} \leq P_{\max duct-s} \quad \text{(Eq. 37)}$$

Equation 38 limits the amount of heat that can be recovered to heat available from the generators. Equation 39 limits the amount of heat that can be passed to the heat recovery unit through the duct in series with the absorption chiller to heat rejection from the chiller.

$$\frac{e_{duct-p,t}}{\epsilon_{duct-p}} + \Delta\frac{e_{AC\,Cool,t}}{COP_{AC}} + e_{AC\,Charge,t} \leq \sum_k \frac{\overline{\eta}_{DG,k} - \eta_{DG,k}}{\eta_{DG,k}} e_{DG,k,t} \quad \text{(Eq. 38)}$$

$$\frac{e_{duct-s,t}}{\epsilon_{duct-s}} \leq \frac{\Delta - 1}{COP_{AC}} e_{AC,t} \quad \text{(Eq. 39)}$$

Equations 40 through 42 govern the adoption and operation of a photovoltaic system. Equation 40 limits the output of the PV system to the available insolation that falls on the PV panels. Since Equation 40 is formulated as an inequality, the PV output can be lower than the available insolation. This considers the PV as curtailable, or that the building operator can choose to leave or take the renewable power produced by the PV depending upon the state of other DER systems. If Equation 40 were changed to an equality constraint, then all power produced by the PV system would be considered "must-take" power. Equation 41 limits the output of the PV system by the installed capacity. Equation 42 limits the size of the installed PV system to the available space for such a system at the building.

$$e_{pv,t} \leq e_{solar,t}\frac{P_{pv}}{\eta_{pv}} \quad \text{(Eq. 40)}$$

$$4e_{pv,t} \leq P_{pv} \quad \text{(Eq. 41)}$$

$$\frac{P_{pv}}{\eta_{pv}} \leq Bldg\ Area \quad \text{(Eq. 42)}$$

Equations 43 through 47 govern the operation of any adopted EES. Equation 43 is the EES energy balance, ensuring that any charging or discharging are linked to the prior and current EES states of charge. Equations 44 and 45 limit the EES state of charge to reside between the limits required to maintain the EES. Equations 46 and 47 limit the rate at which the EES can be charged or discharged.

$$e_{EES\ store,t} = \alpha_{EES} e_{EES\ store,t-1} + \eta_{EES\ chrg} e_{EES\ chrg,t} - \frac{e_{EES\ dchrg,t}}{\eta_{EES\ dchrg,t}} \quad \text{(Eq. 43)}$$

$$e_{EES\ store,t} \leq \bar{\delta}_{EES} e_{EES\ size} \quad \text{(Eq. 44)}$$

$$e_{EES\ store,t} \geq \underline{\delta}_{EES} e_{EES\ size} \quad \text{(Eq. 45)}$$

$$e_{EES\ dchrg,t} \leq \bar{\mu}_{EES} e_{EES\ size} \quad \text{(Eq. 46)}$$

$$e_{EES\ chrg,t} \leq \underline{\mu}_{EES} e_{EES\ size} \quad \text{(Eq. 47)}$$

Equations 48 through 52 govern the operation of any adopted TES. Equation 48 is the TES energy balance, ensuring that any charging or discharging are linked to the prior and current TES state of charge. Equation 49 and 50 limit the TES state of charge to reside between the limits required to maintain the TES. Equations 51 and 52 limit the rate at which the TES can be charged or discharged.

$$e_{TES\ store,t} = \alpha_{TES} e_{TES\ store,t-1} + \eta_{TES\ chrg} e_{TES\ chrg,t} - \frac{e_{TES\ dchrg,t}}{\eta_{TES\ dchrg,t}} \quad \text{(Eq. 48)}$$

$$e_{TES\ store,t} \leq \bar{\delta}_{TES} e_{TES\ size} \quad \text{(Eq. 49)}$$

$$e_{TES\ store,t} \geq \underline{\delta}_{TES} e_{TES\ size} \quad \text{(Eq. 50)}$$

$$e_{TES\,dchrg,t} \leq \bar{\mu}_{TES} e_{TES\,size} \quad \text{(Eq. 51)}$$

$$e_{TES\,chrg,t} \leq \underline{\mu}_{TES} e_{TES\,size} \quad \text{(Eq. 52)}$$

Equations 53 through 55 set all demand charges equal to the maximum demand drawn from the electrical utility during all months, and on-peak and mid-peak during summer months. Since the energy purchased from the grid variable is on a 15 minute increment, multiplying the variable by four-per-hour (four 15 minute periods per hour) converts the variable to power, allowing the demand charges to be calculated.

$$4e_{Grid,t} \leq P_{max,n} \quad \text{(Eq. 53)}$$

$$4e_{Grid,o} \leq P_{on\,max,m} \quad \text{(Eq. 54)}$$

$$4e_{Grid,p} \leq P_{mid\,max,m} \quad \text{(Eq. 55)}$$

3.4.2 Environmental Constraints

The general DER adoption problem described in Section 0 describes the components of the model required to design and operate a DER system based solely on cost. As described in Section 1, the development of recent DER technologies has allowed for a building operator to control the greenhouse gas or pollutant emissions associated with a building. The desire to control building emissions can be factored into the optimization model. One method of including the building environmental impact is to include emissions in the cost function, resulting in the optimization routine attempting to minimize emissions. Another approach is to constrain the emissions. Under an environmental constraint, the goal of the optimization is still to minimize

cost, but with the additional requirement that a certain reduction of emissions occurs. The later approach is selected for this work.

Legislation in California limiting carbon emissions place future goals in terms of a reduction from prior year's levels [160]. As a result, the most likely application of the optimization presented in this paper is to determine the optimal DER mix such that cost is minimized while also reducing total carbon emissions. Carbon emissions associated with a building are tied to the utility electricity imported and utility fuel that is purchased and used onsite. One option that is consistently used as a way to reduce the carbon associated with fuel combustion is to switch from a non-renewable fuel to a renewable fuel. This option is considered in the optimization. However, most renewable fuels have a carbon signature associated with the cleanup of a dirtier version of the gas in order to eliminate potential pollutants. As a result, the use of renewable fuel still is associated with a small carbon signature. In addition, it export is allowed during the optimization, then the other grid production is offset by the electricity sold back to the grid. Therefore, carbon emissions associated with the grid are avoided. Keep in mind that if the exported electricity was produced by inefficient generation onsite, then the total carbon emissions will increase due to increased fuel consumption.

Equation 56 shows the carbon constraint as formulated in the DER optimization problem. C_1 and $C_{1,rng}$ are constants that account for the amount of carbon released per unit of fuel consumed for both non-renewable and renewable fuels respectively used at the building.

$$\sum_t C_{CO_2\ grid,t} e_{grid,t} + \sum_n C_1\left(0\lambda_{1,n} + 250\lambda_{2,n} + 4167\lambda_{3,n} + 150{,}000\lambda_{4,n}\right)_n + C_{1,rng} e_{rng} - \sum_t C_{CO_2\ grid,t} e_{ex,t} \leq CO_2\ Limit \quad \text{(Eq. 56)}$$

As mentioned prior, the carbon emission constraint is typically coupled with an option of purchasing renewable fuel. The total renewable natural gas consumed per month is accounted for in the constraint shown in Equation 57. Equation 57 is typically omitted from the optimization and the renewable fuel variables associated with DG and boiler operation are not included because renewable fuel cost is typically higher than purchased natural gas. In this case, the additional scenarios add unneeded complexity since it is known that no renewable fuel will be purchased during the optimization.

$$\sum_k \sum_t g_{rDG,k,t} + \sum_t e_{boil\,rng,t} = e_{rng} \quad \text{(Eq. 57)}$$

3.4.3 PEV Integration

PEV integration with the DER problem will change depending upon the specific problem. The two general problems addressed in this work are the uncontrolled refueling of PEVs at a building and the purchase and refueling of fleet PEVs.

The first problem is concerned with whether or not the building operator should purchase and install EVSE at the building. The second problem is concerned with whether or not the building operator should purchase PEVs or conventional vehicles to meet a given set of business transportation requirements. These requirements can come in many different forms. The two forms examined in this work are for when vehicles are being purchased to operate along pre-selected routes and along routes that are to be determined to specific nodes or customers.

3.4.3.1 Uncontrolled PEV Refueling

PEV traffic to and from the building is an approximately deterministic process from the perspective of the individual driver. The driver knows the final destination, is assumed to be fairly familiar with the travel time to the final destination, the vehicle miles travelled, and the

approximate dwell time at the final destination. None of this information is known by the building operator about any individual driver.

Despite this lack of information, the travel of vehicles to a building typically can be described by using probability density functions based off of information such as the National Household Travel Survey. Using this information in conjunction with a PEV refueling station model similar to what is described in Section 3.3 coupled with a rate at which PEV refueling customers will be charged, the expected revenues associated with installing different EVSE types and configurations can be estimated.

For this work, the DER optimization model presented in Section 0 is reformulated as a stochastic problem. The stochastic process is assumed to only be the PEV traffic to the building. Using the PEV refueling model described in Section 3.3, likely travel scenarios can be generated along with the probability of each scenario occurring. Using these scenarios, the electrical demand profile associated with different types and number of installed EVSE can be generated, along with the projected revenue created by charging PEV drivers to refuel. These projected refueling profiles and associated revenues are implemented into the stochastic formulation of the DER optimization model.

The stochastic formulation of the MILP presented in 0 is limited to only non-renewable CCHP systems (no form of energy storage is currently modeled). The constraints regarding DG, HRU, and AC operation are all the same. The only difference is that each set of constraints exist for each possible PEV refueling scenario. For example, if three likely scenarios exist, three sets of each technology constraints exist for the individual scenarios. As such, the individual

constraints will not be relisted unless a modification occurs as a result of the stochastic formulation.

Table 3-5 list the additional sets and parameters required for the stochastic formulation. The two additional decision variables are $n_{ev\ chargers,j}$, which defines the option of purchasing the EVSE configuration *j,* and $n_{ev\ option,\omega}$, which ensures that the purchased EVSE configuration j is operated in each of the possible scenarios. Both variables are binary.

Table 3-5: Additional parameters that define the stochastic DER and EVSE system optimization

Sets	**Description**
$\omega \in \Omega$	Set of possible PEV refueling scenarios that are likely to occur
$j \in J$	Set of possible EVSE types and configurations
Parameters	
p_{ω}	Probability that PEV refueling scenario ω will occur (%)
$C_{ev,j}$	Capital cost of purchasing EVSE type and configuration j ($)
$D_{j,\omega,t}$	Electrical demand associated with EVSE type and configuration j under PEV refueling scenario ω at time t

Equation 58 is the modified cost function for the stochastic formulation. The first set of variables represents possible investment that will occur. The second set of variables defines the operation occurring in each of the possible scenarios.

$$
\begin{aligned}
minimize \sum_j C_{ev,j}\, n_{ev\ chargers,j} + \sum_k C_{cap\ DG,k} S_{DG,k} N_{DG,k} + C_{cap\ AC} P_{\max AC} + C_{cap\ HRU} P_{\max HRU} \\
+ C_{cap\ duct-p} P_{\max duct-p} + C_{cap\ duct-s} P_{\max duct-s} \\
+ \sum_\omega p_\omega \left(\sum_j R_{ev,j} n_{ev\ option,\omega} \sum_t C_{grid,t} e_{grid,t,\omega} + \sum_n C_{DC,n} P_{max,n,\omega} \right. \\
+ \sum_m C_{on\ DC,m} P_{on\ max,m,\omega} + \sum_m C_{mid\ DC,m} P_{mid\ max,m,\omega} + \sum_n C_{ng,n,\omega} \\
+ \sum_k \sum_t C_{om\ DG,k} e_{DG,k,t,\omega} + \sum_k \sum_h C_{start\ DG,k} n_{DG\ start,k,h,\omega} + \sum_t C_{om\ AC} e_{AC,t,\omega} \\
+ \sum_t C_{om\ AC\ \ Charge} e_{AC\ Charge,t,\omega} \\
+ \sum_t C_{om\ HRU} e_{HRU,t,\omega} + \sum_t C_{om\ duct-p} e_{duct-p,t,\omega} + \sum_t C_{om\ duct-s} e_{duct-s,t,\omega} \\
\left. + \sum_t C_{om\ VC} e_{VC,t,\omega} + \sum_t C_{om\ Boil} e_{boil,t,\omega} \right)
\end{aligned}
\qquad \text{(Eq. 58)}
$$

Equation 59 ensures that any selected EVSE configuration *j* is operated during all scenarios. Equation 60 ensures that, at most, only a single EVSE configuration is purchased. Equation 60 shows the modified energy balance equation (originally shown in Equation 10) that states that the additional PEV refueling load must be met at all times for all scenarios.

$$n_{ev\ chargers,j} = n_{ev\ option,\omega} \qquad \text{(Eq. 59)}$$

$$\sum_j n_{ev\ chargers,j} \leq 1 \qquad \text{(Eq. 60)}$$

$$E_{grid,t,\omega} + \sum_k e_{DG,k,t,\omega} + e_{pv,t,\omega} + e_{batt\ dchrg,t,\omega} = E_{Bldg\ Elec,t,\omega} + \frac{e_{VC,t,\omega}}{COP_{VC}} + e_{batt\ chrg,t,\omega} + \sum_j D_{j,\omega,t} n_{ev\ option,\omega} \qquad \text{(Eq. 61)}$$

3.4.3.2 Fleet PEV Purchase and Refueling

Under some scenarios, the decision to purchase and refuel fleet PEVs can remain a stochastic problem. However, many other scenarios exist where the problem is reduced to a deterministic problem. The extension of the DER optimization problem to fleet PEV purchasing

and refueling falls under the latter category. If the vehicles being purchased are to travel along pre-specified routes, depart from, and arrive back at the building being optimized, the problem can be viewed as deterministic. Similarly, if the vehicles are leaving the building at a specific time to travel to specific nodes and are guaranteed to arrive no later than a given time, the problem remains deterministic despite not knowing the particular routes to be traveled. Both of these problems are modeled for the full DER optimization problem.

Unlike the uncontrolled PEV refueling problem, the fleet PEV problems require the purchase of vehicles. As such, the competing potential purchase of conventional vehicles must be included, resulting in the possibility of PEVs never being adopted.

3.4.3.2.1 Optimal Purchase of Pre-routed PEV and Conventional Vehicles

If the building operator is to purchase a new set of vehicles to meet some transportation requirement when the vehicle routes are already determined, the additional constraints described in this section are applicable. One possible application of this problem is determining bus fleet mix for public transportation. This formulation assumes that there are r routes. Each route r requires $n_{req,r}$ vehicles to be purchased. The additional sets and parameters included in this formulation are shown in Table 3-6, and additional decision variables in Table 3-7.

Table 3-6: Parameters that define the pre-routed fleet mix optimization

Sets	**Description**
r ∈ R	Set of routes
l ∈ L	Set electric vehicles that can be purchased
m ∈ M	Set of conventional vehicles that can be purchased
n ∈ N	Set of EVSE that can be purchased
Route Parameters	
$n_{req,r}$	Number of vehicles required to be purchased for route r
$\bar{r}_{ev,l}$	Miles travelled on route r by a vehicle (miles)
PEV Parameters	

$C_{ev,l}$	Capital and operations cost of PEV l ($)
$C_{evse,n}$	Capital cost of EVSE n ($)
$\eta_{ev\ mpkWh,l}$	Electricity used during PEV travel (Miles/kWh)
$S_{ev,l}$	Number of refueling ports for PEV l (number of refueling ports)
$S_{evse,n}$	Power rating of EVSE n (kW)
Conventional Vehicle Parameters	
$C_{con,m}$	Capital and operations cost of conventional vehicle m ($)

Table 3-7: Decision variables that define the pre-routed fleet mix optimization

PEV Decision Variables	**Description**	**Variable Type**
$n_{ev,l,r}$	Number of purchased PEVs of type l for route r	Integer
$n_{evse,n}$	Number of purchased EVSE of type n	Integer
PEV Decision Variables	**Description**	**Variable Type**
$n_{con,m,r}$	Number of conventional vehicles of type m for route r	Integer

The cost function is modified to include the additional cost of purchasing vehicles and EVSE, as presented in Equation 62 to include the additional cost associated with the purchase of convention vehicles, PEVs, and EVSE. The cost for the vehicles includes both the capital cost and the operation cost of each vehicle over the length of the simulation. Equation 63 is the modified energy balance, showing that the refueling of PEVs must be accounted for when electricity is procured or generated. Equation 64 ensures that the proper number of vehicles for each route is purchased. Equation 65 states that the amount of electricity delivered to any purchased PEVs must equal the amount required to complete the route the following day. Equation 66 aggregated the refueling of all PEVs for all routes into a single variable that is input into Equation 62. Equation 67 ensures that the aggregated refueling of PEVs is limited by the number and size of EVSE purchased. Equation 68 limits the number of purchased EVSE by the number of refueling ports on the purchased PEVs.

$$cost\ func + \sum_r \left(\sum_l C_{ev,l} n_{ev,l,r} + \sum_m C_{con,m} n_{con,m,r} \right) + \sum_n C_{evse,n} n_{evse,n} \qquad \text{(Eq. 62)}$$

$$E_{grid,t,\omega} + \sum_k e_{DG,k,t,\omega} + e_{pv,t,\omega} + e_{EES\ dchrg,t,\omega} = E_{Bldg\ Elec,t,\omega} + \frac{e_{VC,t,\omega}}{COP_{VC}} + e_{EES\ chrg,t,\omega} +$$

$$ev_{r,agg,,t} \quad \text{(Eq. 63)}$$

$$\sum_l n_{ev,l,r} + \sum_m n_{con,m,r} = n_{req,r} \quad \text{(Eq. 64)}$$

$$\sum_{t\epsilon day} ev_{r,t} = \sum_l \frac{\bar{r}_{ev,l}}{\eta_{ev\ mpkWh,l}} n_{ev,l} \quad \text{(Eq. 65)}$$

$$ev_{r,agg,,t} = \sum_r ev_{r,t} \quad \text{(Eq. 66)}$$

$$ev_{r,agg,,t} \leq \sum_n S_{evse,n} n_{evse,n} \quad \text{(Eq. 67)}$$

$$\sum_n n_{evse,n} \leq \sum_l \sum_r S_{ev,l} n_{ev,l,r} \quad \text{(Eq. 68)}$$

3.4.3.2.2 Optimal Fleet Size and Mix Vehicle Routing Problem

If the building operation includes some delivery component that requires vehicles to travel to specific locations or nodes, then the business owner may elect to purchase PEVs, conventional vehicles, or a mix of both, and design the routes of the vehicles such that cost is minimized. This problem, as discussed before, is known as the fleet size and mix vehicle routing problem. This problem has been studied extensively [114], and the extensions of the vehicle routing to electric vehicle travel have been formulated [110]. As a result, instead of a new formulation, the formulations from these two cited works will be adopted directly as the fleet size and mix vehicle routing problem that takes into account PEVs and integrated into the DER optimization formulation.

In the problem formulation, *n* number of customers or nodes must be visited. The distance between each customer and all other customers and the building are known. Each

customer must be visited within a certain time limit. The assigned routes to any vehicle, including travel back to the building, must be within the range of that specific vehicle.

Table 3-8: Parameters that define the pre-routed fleet mix optimization

Sets	**Description**
$n \in N$	Set of nodes to be visited
$i \in I$	Set of trips that result in arrive from node i
$j \in J$	Set of trips that depart from node j
$v \in V$	Set of all conventional and electric vehicles
$r \in R$	Set of PEVs that can be purchased
Route Parameters	
A_i	Time at which delivery at node i can start to occur (Time)
B_i	Time at which delivery at node i has to occur (Time)
$T_{i,j}$	Time required to travel from node i to node j (Time)
$d_{i,j}$	Distance between node i and node j (Miles)
Vehicle Parameters	
Q_v	Range of vehicle v (Miles)
C_v	Capital cost of vehicle v ($)
$c_{i,j,v}$	Operational cost of vehicle v to travel from node i to node j ($)
PEV Parameters	
$C_{evse,m}$	Capital cost of EVSE m ($)
$\eta_{ev\ mpkWh,r}$	Electricity used during PEV travel (Miles/kWh)
$S_{ev,l}$	Number of refueling ports for PEV l (number of refueling ports)
$S_{evse,m}$	Power rating of EVSE m (kW)

Table 3-9: Decision variables that define the pre-routed fleet mix optimization

Vehicle/Travel Decision Variables	**Description**	**Variable Type**
$x_{i,j,v}$	Selection of route between node i and j using vehicle v	Binary
t_i	Time of arrival at node i	Continuous
$y_{i,v}$	Remaining range of vehicle v after arriving at node i	Continuous
PEV Decision Variables	**Description**	**Variable Type**
$e_{agg,t}$	Aggregated energy delivered to purchased PEVs (kWh)	Continuous

The problem formulation uses the constraints developed in [110,114] to describe the fleet mix and size vehicle routing problem with PEVs. Equation 69 through Equation 80 define the fleet mix and size vehicle routing problem. Equation 69 shows the modified Equation 9 cost function to include the cost of purchasing the different vehicles and EVSE and the cost to travel between the different nodes. The cost to travel between the different nodes for conventional vehicles includes maintenance and fuel cost. For PEVs, the cost to travel between nodes only considers maintenance cost since the cost to fuel the PEVs will be determined by the cost of purchasing electricity for the building.

$$cost\ func + \ \sum_v \left(\sum_{j=1}^{n} C_v x_{0,j,v} + \sum_{i=0}^{n}\sum_{j=0}^{n} c_{i,j,v} x_{i,j,v}\right) + \sum_m C_{evse,m} n_{evse,m} \qquad \text{(Eq. 69)}$$

Equation 70 ensures that all nodes are visited while Equation 71 forces a vehicle arriving at a node to depart from the same node. Equation 72 ensures that all nodes are visited within a specific time window. Equation 73 ensures that travel from node to node occurs in sequential order. This constraint also suppresses any subtour formation where an optimal solution suggests that a vehicle travels between the nodes and never returns to the building. A subtour is a routing solution between nodes that does not start or end with travel back to the base. Equation 74 reduces the vehicle range as a result of traveling between nodes while Equation 75 states that each vehicle leaves the building after being completely refueled. Equation 76 ensures that all vehicles traveling always have enough range to return to the building.

$$\sum_v \sum_{j=0}^{n} x_{i,h,v} = 1 \qquad i = 1, \ldots., n \qquad \text{(Eq. 70)}$$

$$\sum_{i=0}^{n} x_{i,l,v} = \sum_{j=0}^{n} x_{l,j,v} \quad l = 1, \ldots, n \qquad \text{(Eq. 71)}$$

$$A_i \leq t_i \leq B_i \; i = 1, \ldots, n \qquad \text{(Eq. 72)}$$

$$t_i + T_{i,j} - t_j \leq \sum_v max\big(B_i + T_{i,j} - A_j, 0\big)\big(1 - x_{i,j,v}\big)\ \ i,j = 1, \dots, n \quad \text{(Eq. 73)}$$

$$y_{j,v} \leq y_{i,v} - d_{i,j}x_{i,j,v} + Q_v\big(1 - x_{i,j,v}\big)\ i = 1, \dots, n \quad \text{(Eq. 74)}$$

$$y_{1,v} = Q_v \quad \text{(Eq. 75)}$$

$$y_{j,v} \geq d_{j,0} \quad \text{(Eq. 76)}$$

Equation 77 through 80 only relate to any purchased PEVs. Equation 77 is Equation 10 with the addition of the refueling requirements. Equation 78 ensures that all purchased PEVs are refueled after arriving back at the building based on the route performed during the day. Equation 79 limits the refueling rate to the number and size of the EVSE purchased and Equation 80 limits the number of purchased EVSE to by the PEVs purchased times the number of refueling sockets per PEV.

$$E_{grid,t,\omega} + \sum_k e_{DG,k,t,\omega} + e_{pv,t,\omega} + e_{batt\ dchrg,t,\omega} = E_{Bldg\ Elec,t,\omega} + \frac{e_{VC,t,\omega}}{COP_{VC}} + e_{batt\ chrg,t,\omega} + ev_{agg,,t} \quad \text{(Eq. 77)}$$

$$\sum_{t \epsilon day} e_{agg,t} = \sum_r \sum_{i=0}^{n} \sum_{j=0}^{n} \frac{d_{i,j}}{\eta_{mpkWh,r}} x_{i,j,r} \quad \text{(Eq. 78)}$$

$$e_{agg,t} \leq \sum_n S_{evse,n} n_{evse,n} \quad \text{(Eq. 79)}$$

$$\sum_n n_{evse,n} \leq \sum_l \sum_r S_{ev,l} n_{ev,l,r} \quad \text{(Eq. 80)}$$

3.5 Cost and Emission Allocation

3.5.1 Cost to Fuel PEVs

The total electrical utility cost can easily be calculated by using the applicable rate structure model as described in Section 3.1. The cost produced by this model is the aggregated

cost to charge a set of PEVs during a winter or summer month with Level 3 EVSE. This total cost model, however, does not resolve the marginal cost to charge each of the individual PEVs in each scenario.

Determining the cost of charging individual PEVs using pubic Level 3 EVSE can be viewed as a cooperative game with all utility costs being allocated to the charging of the individual vehicles. While individual drivers may not work together to minimize total electricity cost for the refueling station, they may cooperate so that they each pay a fair price to refuel. No customer wishes to subsidize the charging of another customer's PEV, so a method that efficiently and fairly allocates electric utility cost must be used. One possible solution to this problem is the Shapley value [161]. The Shapley value is not applied in real time. Rather, it is applied a posteriori to determine the fair share of total electricity charges for each customer. This method can be used to assist with the design and evaluation of PEV customer refueling rates used to charge drivers to use public Level 3 EVSE by determining if a rate fairly allocates electric utility charges.

The Shapley value is a method to determine the "fair" allocation to a coalition of players. In the case of PEVs charged using public EVSE, the coalition of players, as defined by set N of n players, are all of the PEVs that are charged. S is any coalition of PEVs that form a subset of N. The function v(S) is the characteristic function, which determines the cost incurred by the subset S. The characteristic function for this work is either the utility demand or energy charge. With these definitions, the Shapley value can be found using the following equation to find the allocation φ_i of player (or PEV) i:

$$\varphi_i(i) = \sum_{S \subseteq N \setminus \{i\}} \frac{|S|!(n-|S|-1)!}{n!} \big(v(S \cup \{i\}) - v(S)\big) \quad \text{(Eq. 81)}$$

3.5.1.1 Allocation for Standalone Level 3 EVSE

The Shapley value is deemed a fair allocation due to all costs being allocated, any two participants with the same contribution (same total electric energy used to recharge their PEV) receive the same allocation, participants who contribute nothing receive no allocation, and scaling the cooperative game up by any real number *a* results in the Shapley value of each member being scaled by *a*. Note that the allocation of demand charges is analogous to the runway problem explored by Littlechild and Owen [162], resulting in a simplified calculation of the Shapley value that is determined by the following solution:

1. Divide the cost of providing the minimum power for which a demand charge is incurred (20 kW) by all PEVs that incur a demand of 20 kW or greater.
2. Divide the incremental cost of providing power to the next smallest power demand incurred by all PEVs that draw at the next smallest power demand or greater.

Step two is repeated until the incremental cost created by the PEVs that create the largest power demand is divided equally among all PEVs that create this level of demand. Note that while the Level 3 charging creates a demand of over 20 kW, any PEV or group of PEVs that are fueled by Level 3 EVSE but do not create an aggregated demand that averages 20 kW or greater for a 15 minute period receives no allocation for the given 15 minute period because this level of charging would fall under TOU-EV-3, which has no demand charge.

3.5.1.2 Allocation for Level 3 EVSE Integrated with a Building

The Shapley value for the building and aggregated PEV load can be found directly by using Equation 81. This type of analysis is useful in determining the fair cost incurred by PEVs refueling at a building. While the rate that is applicable to the aggregated PEV and building load

is determined by the utility, the Shapley value will show any value created by EVSE integration and assign the cost fairly. For example, if PEVs experience a lower cost of energy due to integration, the building should experience a benefit due to providing access to the lower cost utility rate. Also, if the aggregation of building and PEV loads does not significantly increase overall demand charges, both parties should experience a cost reduction as a result of being able to split a demand charge that did not increase as a result of integration.

3.5.2 Cost to Purchase and Operate DER

A DER system is considered a single resource that is used to make multiple products. All utility and equipment purchases and subsequent operation are made to produce multiple types of energy. The interactions between these different types of building energy can be separated through cost allocation. Similar to PEV charging, the allocation of building energy costs can be viewed as a cooperative game. This allows for the Shapley value to be used.

If the set of players is considered to be the different types of energy demand (electricity, heating, cooling, and transportation), the Shapley value can be determined for all costs by determining the optimal DER and PEV configuration of all possible coalitions formed by players, or combinations of energy types. This is accomplished by using the DER optimization model to size a system for meeting each individual and all possible combinations of energy demand types and transportation requirements. This answers the question of if only one or two types of energy were to be produced using a CCHP system in conjunction with the legacy technology, what would the optimal system configuration be? With this known, the marginal costs associated with meeting the other types of energy can be determined.

Once the investment and operational costs have been allocated, the value of each type of energy can be determined. This will allow for the performance of the investment made into meeting different types of building energy to be made. The metric used to determine energy value will be levelized cost of energy. The metric used to determine investment performance will be marginal internal rate of return. Marginal internal rate of return is similar to the internal rate of return with the primary difference being that any positive cash flow is reinvested using a separate interest rate. Both metrics are discussed in further detail in Section 3.7.

This method can also be used to determine the sources of any emissions. By determining the emissions produced by each combination of energy conversion technology use, the contribution to the overall emissions can be determined. Particularly when a reduction in emissions are desired, the energy type for which reductions are easiest or least expensive can be determined.

3.6 Utility Emission Model

Operation of a building using non-renewable forms of energy produce CO_2 emissions. For any fuel used onsite, the emissions are simply traced to the carbon content of the fuel. The same is for carbon emissions associated with an electrical utility. However, from the perspective of the building, it is unknown the types of generators producing the electricity and the types and quantities of fuels being burned. In addition, generator dispatch varies throughout the day, resulting in a changing CO_2 emission factor throughout the day.

Instead of tracking down the dispatch of each individual generating plant that produces power for California, the California Independent System Operator (CAISO) website [163] was used to determine the percent of total power delivered to California customers produced by

carbon free generating sources (renewable, geothermal, nuclear, hydro, etc.) for each one hour period for the year 2015. By making the assumption that the rest of the electricity was produced using natural gas fired combined cycle power plants, a time resolved emissions factor was produced for California. This time resolved emissions factor was then normalized to the average emission factor for the State of California reported in the Department of Energy eGrid report [164]. The emissions factor was then reduced to a representative set of winter and summer emissions using the clustering method described in Section 0 for filtering building data. The resulting emission factor profile for electricity purchased from a utility in California is shown in Figure 3-9.

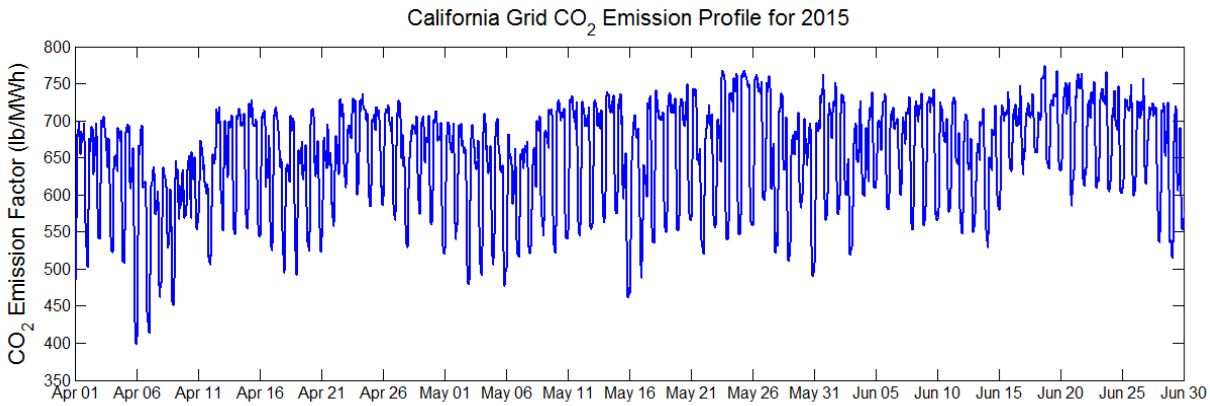

Figure 3-9: Time resolved CO_2 emissions factor for the State of California in 2015 during two winter and one summer months

Figure 3-10 shows two typical winter and summer weeks as presented in Figure 3-9. By focusing on a smaller time period than three months, the dynamics of the time resolved grid emissions factor can be better understood. The X axis tick marks in Figure 3-10 correspond to noon each day. It is clear from Figure 3-10 that grid electrical energy during the early to middle

part of each day is the least carbon intensive, with carbon emissions per unit of energy increasing at night.

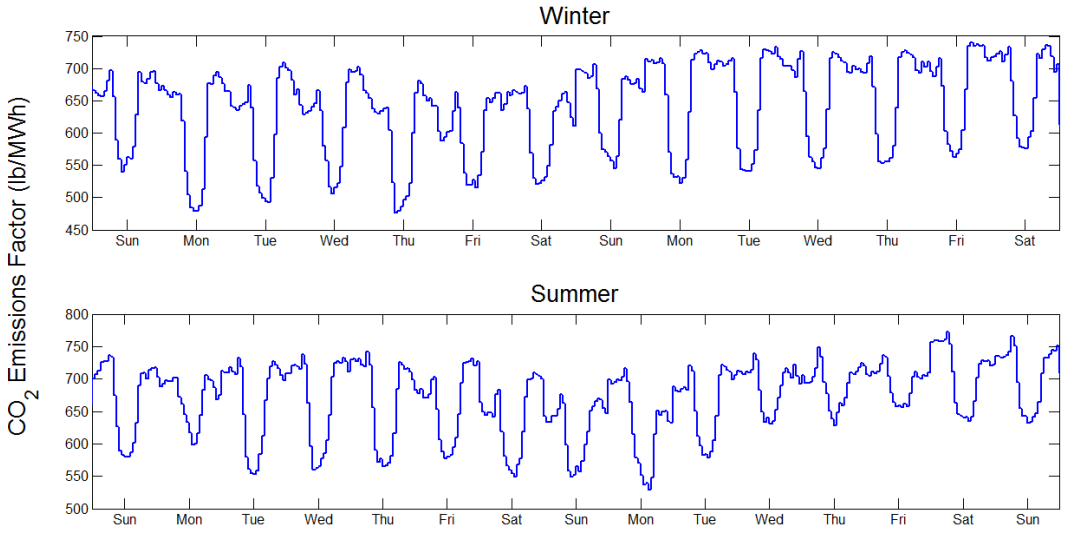

Figure 3-10: Time resolved CO_2 emissions factor for the State of California in 2015 during two winter weeks and two summer weeks

3.7 DER Financial Metrics

Many of the cost components associated with the installation and operation of a DER system can be easily determined based on manufacturer provided information, information in the current literature, or from projections on costs into the future. This information is critical to determining the total cost of operation for a DER system. Some costs, such as operations and maintenance (O&M), can be either presented in terms of or converted to cost per unit of energy produced or stored. With the O&M cost simplified to a single variable O&M cost, the total cost of operating and maintaining a DER technology can be easily found by multiplying the variable O&M cost by the total amount of energy produced or stored.

Capital cost for a purchased piece of equipment must be converted from the initial total cost of purchase and installation into the equity supplied by the investor and the loan supplied by a borrower to assist with the financing of the equipment. This work assumes that the investor will always pay for 20% of all equipment purchased, with the remaining 80% supplied in the form of a loan. The loan details are assumed to be as follows: yearly interest rate is 8%, the life of the loan is 10 years, and monthly debt payments occur. The monthly debt payment required for the loan can be determined using Eq. 82, where i is the interest rate, n is the life of the loan in months, and *Principal* is the borrowed 80% of the DER system cost.

$$\textbf{\textit{Monthly Debt Payment}} = \frac{\textit{Principal} \times i}{1-(1+i)^{-n}} \qquad \text{Eq. 82}$$

Once the amount invested, debt payments, O&M costs, and utility purchase costs have been determined, a valuation of the investment can be made versus if the energy load met by a new DER system had been met using traditional energy sources, such as an electrical utility. The metrics selected for comparison in this work are the modified internal rate of return (MIRR) and the levelized cost of energy (LCOE).

The MIRR for any particular investment weights the savings produced by any specific investment versus the cost of investment. Specifically, any savings that are produced are discounted forward to their future value (FV) in time using a reinvestment rate j associated with the business or organization investing in the DER technology. Any losses are discounted backward to their present value (PV) at the borrowing rate i, or loan rate, as if the loss were to be originally borrowed from a lender. The MIRR is determined for n number of periods. The equation used to determine the MIRR is shown in Eq. 83.

$$MIRR = \sqrt[n]{\frac{FV(Savings,j)}{PV(Losses,i)}} - 1 \qquad \text{Eq. 83}$$

The LCOE relates the cost to invest in a particular DER technology or to meet a type of energy demand over an extended period of time. Typically, the LCOE is determined over the entire lifetime of a specific piece of technology or system. By determining the LCOE, multiple types of generators and energy sources can be compared on an economic basis using the same scale. The equation for the LCOE is shown in Eq. 84. In Eq. 84, I_t is the investment cost at time period t, M_t is the O&M cost at time t, F_t is the fuel cost at time t, E_t is the energy produced or consumed during time t , r is the discount rate over the time period, and n is the number of time periods.

$$LCOE = \frac{\sum_{t=1}^{n} \frac{I_t + M_t + F_t}{(1+r)^t}}{\sum_{t=1}^{n} \frac{E_t}{(1+r)^t}} \qquad \text{Eq. 84}$$

4 Operational Data Sets

4.1 Building Data

Two separate sets of building data are used in this work. The first set is the prior mentioned building data set collected in [155]. The second set is for the campus energy demand for the University of California at Irvine (UCI). UCI currently uses a combination of a CCHP plant local PV systems and utility electricity to meet all campus energy demand. The CCHP system consists of a 13.5 MW gas turbine, a heat recovery steam generator used to convert gas turbine waste heat to steam, and a 4.5 MW steam turbine. Approximately 4 MW of photovoltaic systems, seven electric chillers, one steam chiller, and a 4.5 million gallon cold thermal energy storage tank that provides 60,000 ton-hours of cooling storage [165] are also installed. In order to operate the CCHP central plant, extensive monitoring is used to determine the operational state of all installed technologies, providing a dataset from which the time resolved campus energy demand can be determined. Prior work by McLarty resolved this set of data to three years of 15-minute resolved electrical, cooling, and heating demand associated with the campus [166].

Direct use of the building data is either difficult or unnecessary for this current work. For DER optimization, including a years' worth of building energy demand produced an intractable MILP problem that cannot be solved quickly enough using a typical computer. For EVSE integration evaluation, by focusing upon the cost of electricity associated with Level 3 operation, the maximum data length required is set by the length of a utility billing period, or typically one month. As a result, the building energy data sets either must or should be filtered to create a representative building energy data set. This is accomplished by filtering the building energy data using the clustering method described in Section 3.2.

4.1.1 Commercial and Industrial Buildings

4.1.1.1 CCHP System Design

The 12 buildings that have a complete set of electrical, cooling, and heating demand are used for the CCHP system design. The results of processing the building data are shown in Figure 4-1 through Figure 4-12.

Table 4-1 through Table 4-3 contain general information about the building electrical, heating, and cooling demand, respectively. The buildings are arranged from smallest average electrical demand to largest. A wife variety of behavior is experienced across the buildings. For example, the Long Beach and Loma Linda VA Hospital building, shown in Figure 4-12 and Figure 4-11 respectively, both have relatively flat electrical demand and thermal loads that coincide with the middle of the day and are similar in size to the electrical demand. The Patton Hospital Building, St. Regis Hotel, and Hyatt Irvine Hotel , shown in Figure 4-10, Figure 4-9, and Figure 4-7 respectively, have a diurnal electrical and cooling load matched with a consistent thermal load. The SCAQMD and UCI Croul buildings, as seen in Figure 4-8 and Figure 4-2 respectively, has an electrical demand that is highly dynamic during the early morning, a cooling load that is large but only occurs during the day, and a heating load that occasionally appears to be consistent, but experiences periods where it only coincides with the cooling demand. Both the UCI Natural Sciences 1 and 2 buildings, shown in Figure 4-5 and Figure 4-6 respectively, have a combination of relatively flat electrical demand with transient electrical behavior. This is mixed with transient thermal loads. The UCI Cal IT2 has a relatively flat electrical demand that is paired with a diurnal cooling load and a consistently inconsistent heating demand, as seen in Figure 4-4. The US Navy Palmer Hall building has a diurnal electrical and cooling load, as seen

in Figure 4-3. The thermal loads, however, are relatively small compared to the electrical load. Finally, the smallest building included is the UCI Bren building, which has a diurnal electrical and cooling load with an inconsistent heating load, as seen in Figure 4-1.

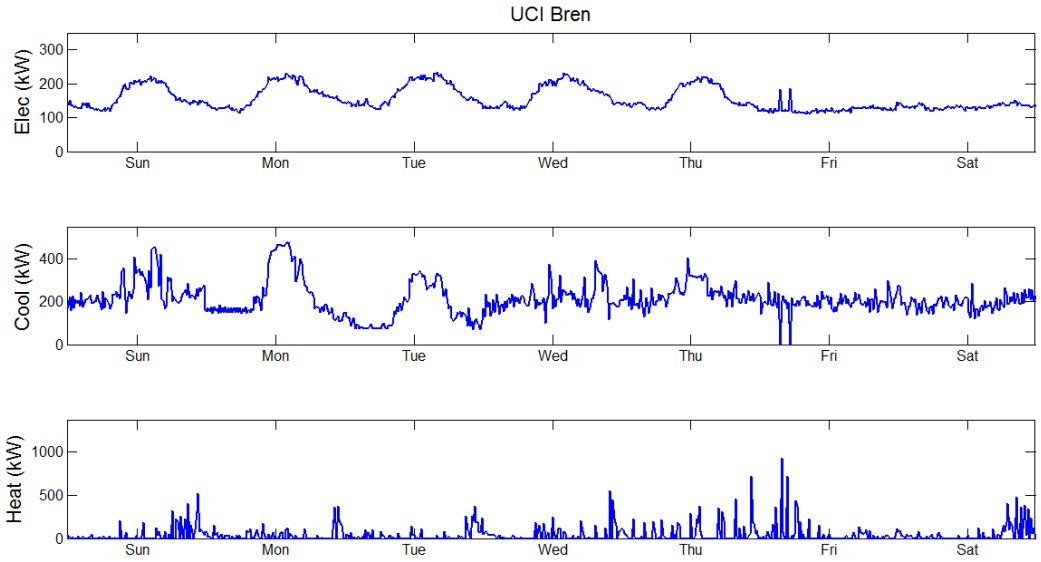

Figure 4-1: Filtered UCI Bren building (university) energy demand data

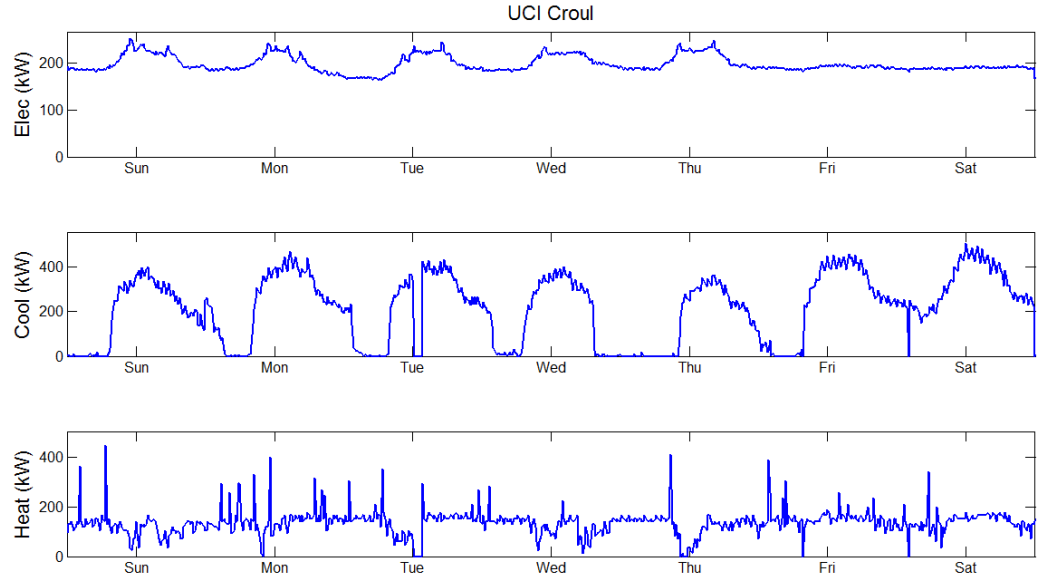

Figure 4-2: Filtered UCI Croul building (university) energy demand data

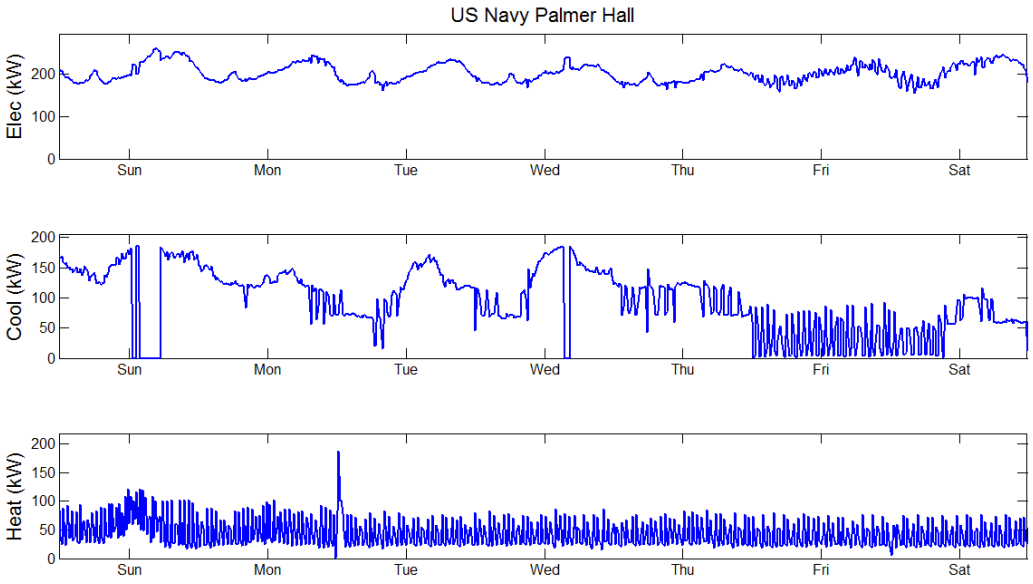

Figure 4-3: Filtered US Navy Palmer Hall building (hotel) energy demand data

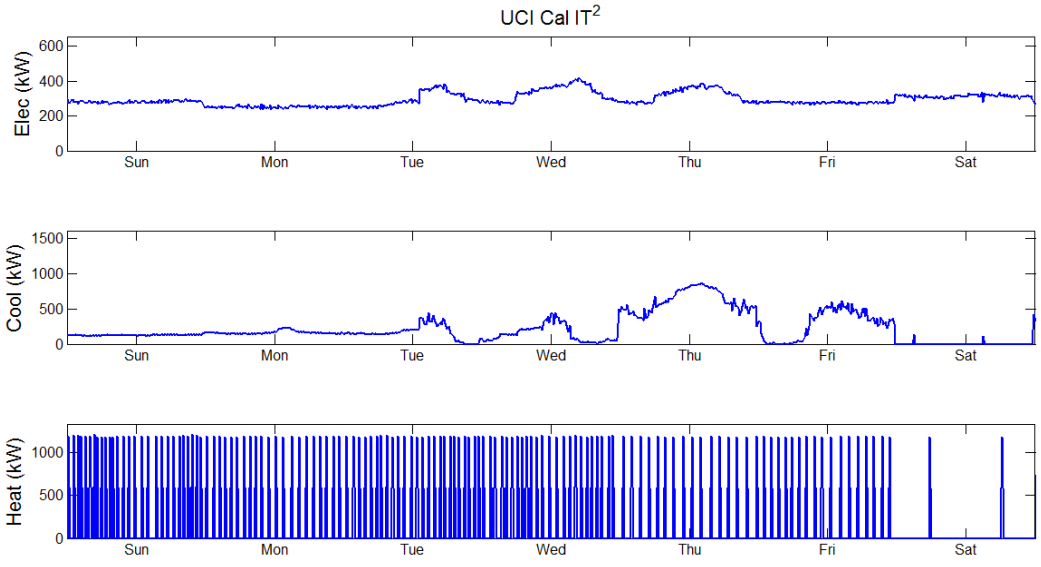

Figure 4-4: Filtered UCI Cal IT^2 building (university) energy demand data

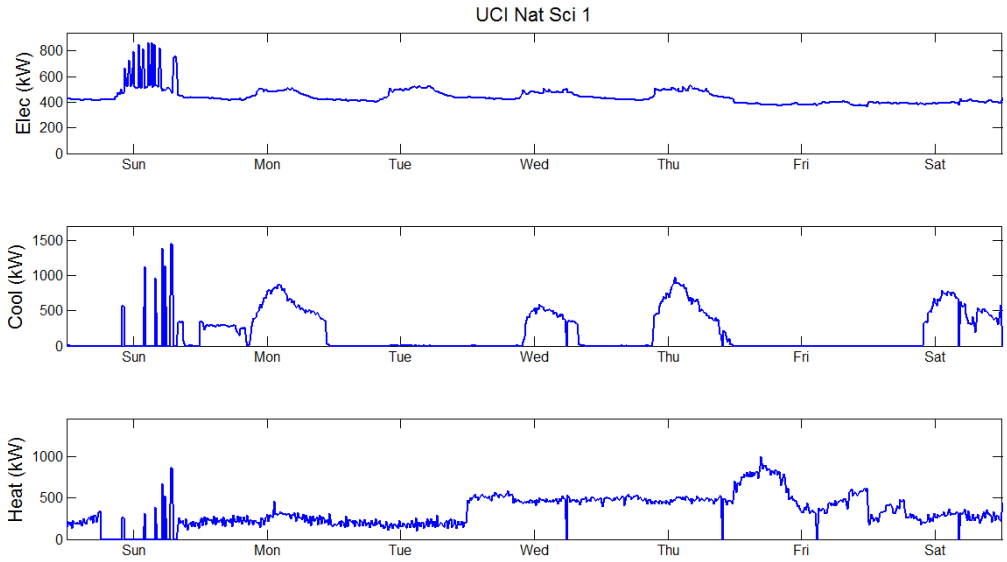

Figure 4-5: Filtered UCI Natural Sciences 1 building (university) energy demand data

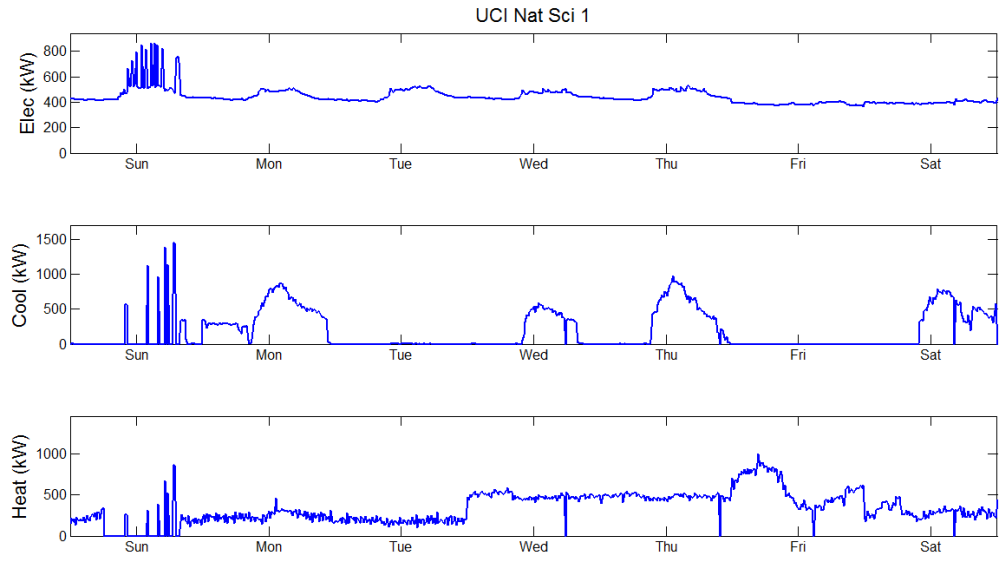

Figure 4-6: Filtered UCI Natural Sciences 2 building (university) energy demand data

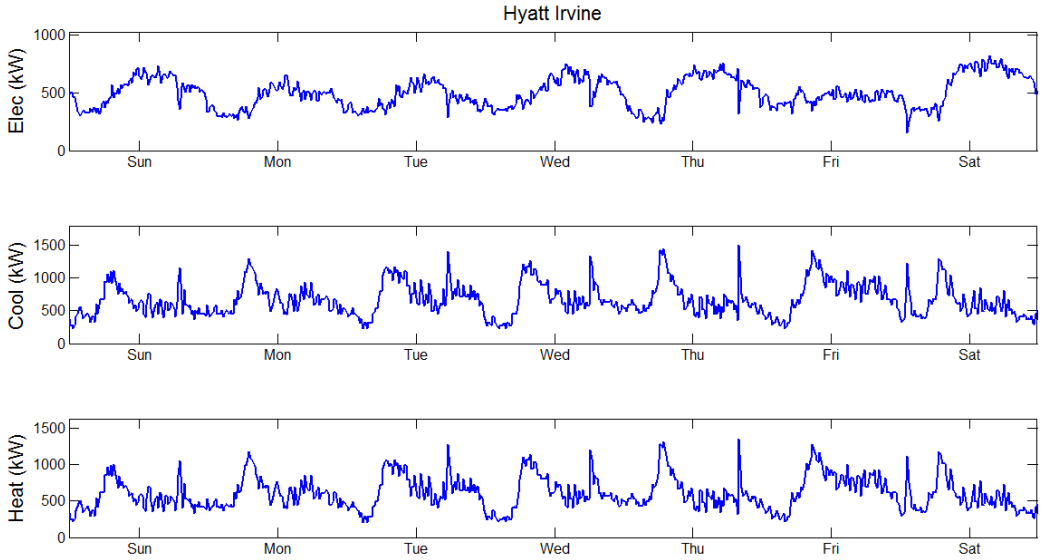

Figure 4-7: Filtered Hyatt Irvine building (hotel) energy demand data

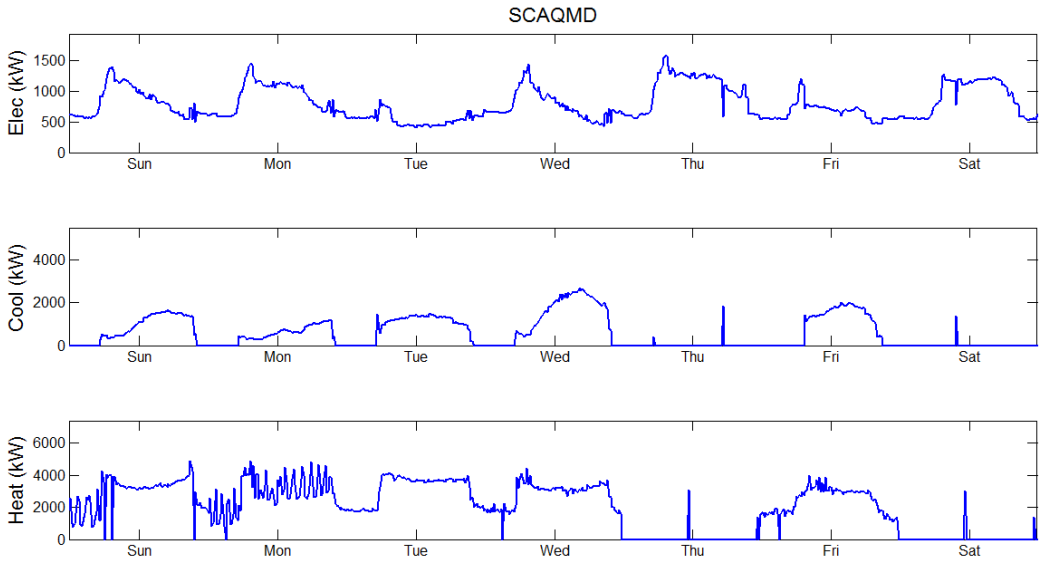

Figure 4-8: Filtered SCAQMD building (regulatory agency, office/laboratory) energy demand data

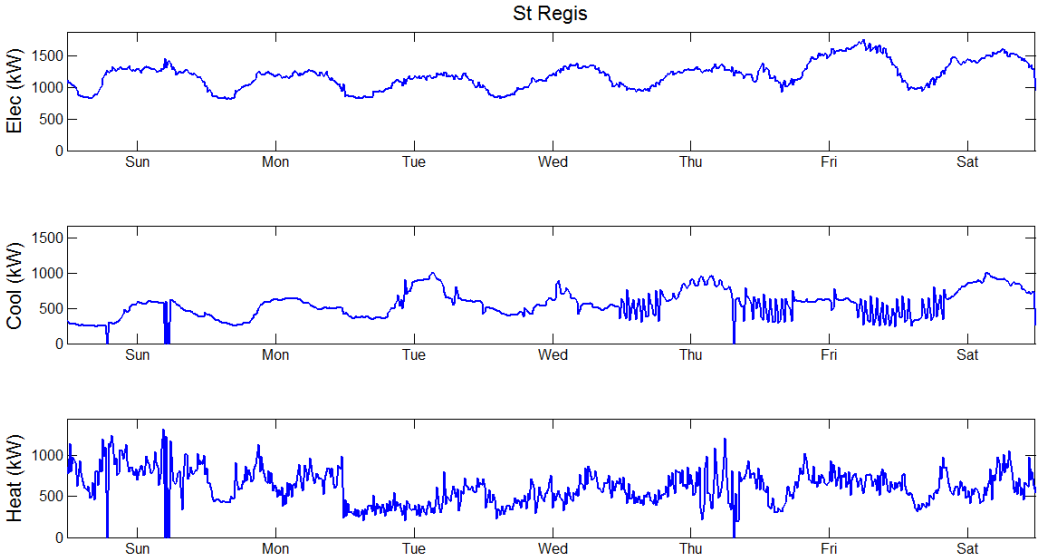

Figure 4-9: Filtered St. Regis building (hotel) energy demand data

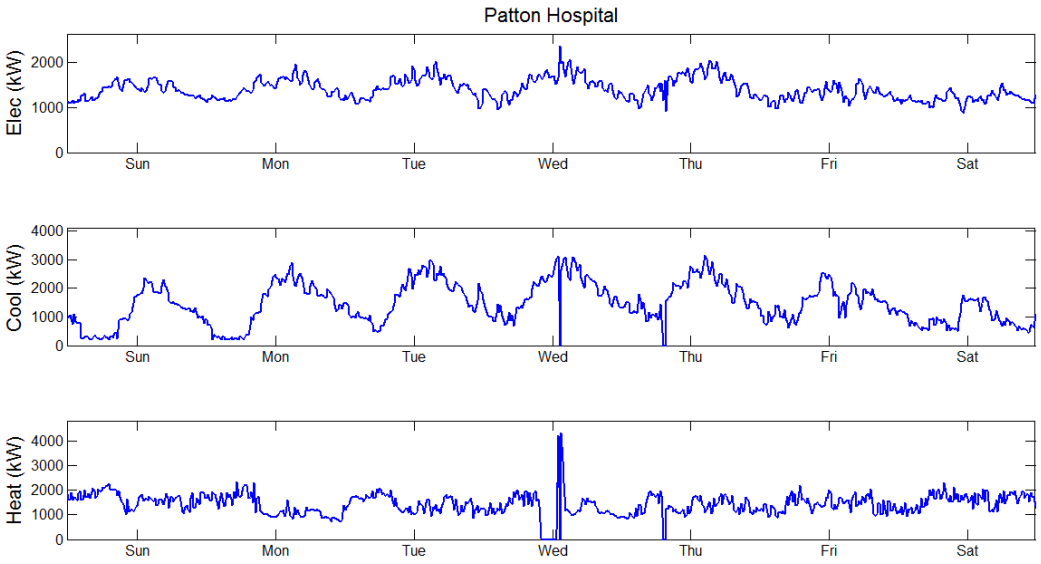

Figure 4-10: Filtered Patton Hospital building energy demand data

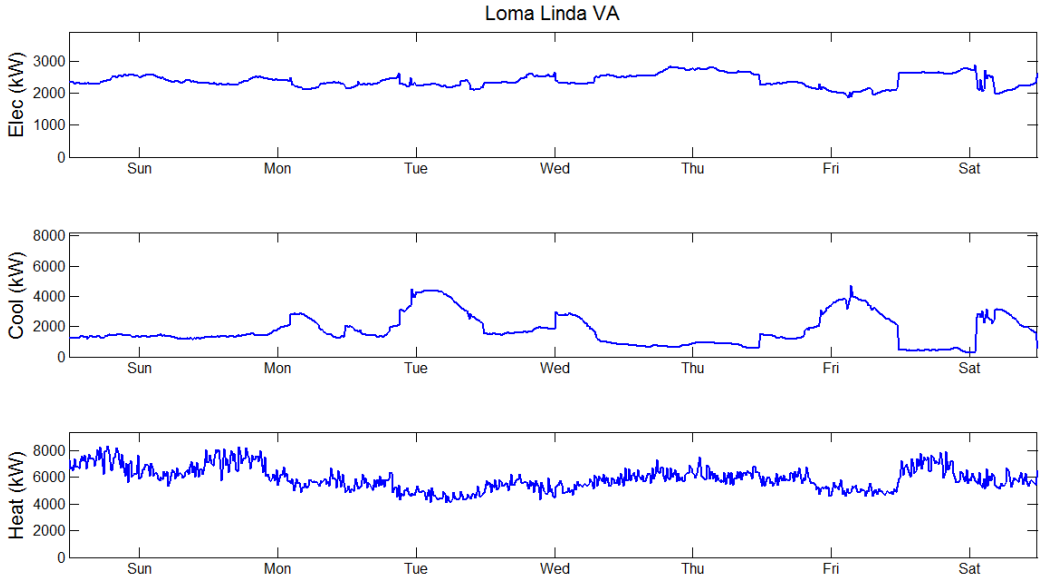

Figure 4-11: Filtered Loma Linda VA building energy demand data

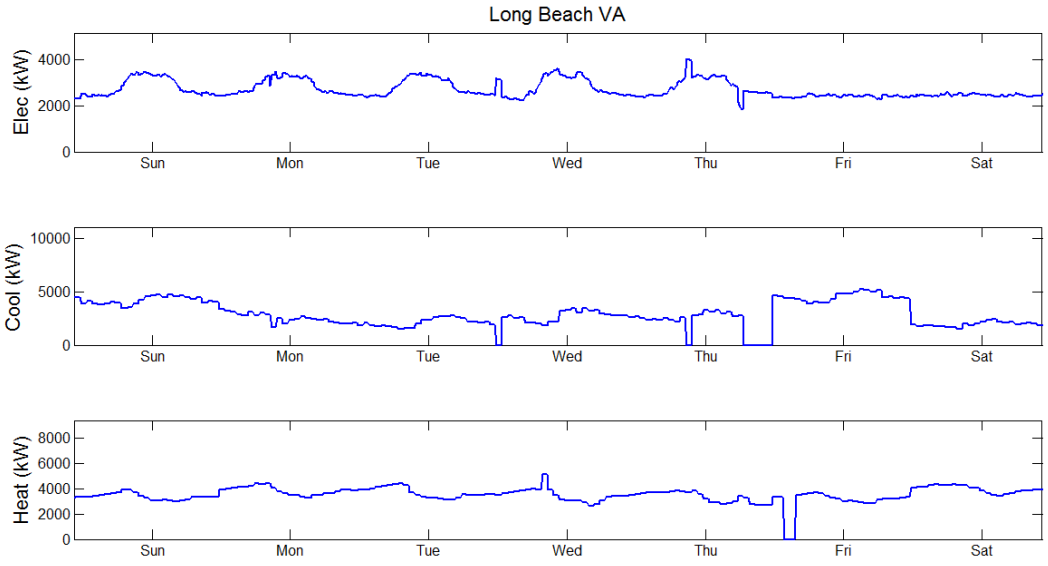

Figure 4-12: Filtered Long Beach VA building energy demand data

Table 4-1: Summary of electrical demand for the 12 filtered building energy demand data sets

Building Name	Avg. Elec Demand (kW)	Max Elec Demand (kW)

UCI Bren	157	349
UCI Croul	188	253
US Navy Palmer Hall	195	281
UCI Cal IT2	323	688
UCI Nat Sci 2	397	888
UCI Nat Sci 1	431	865
Hyatt Irvine	552	996
SCAQMD	781	1920
St Regis	1212	1790
Patton Hospital	1400	2374
Loma Linda VA	2570	3871
Long Beach VA	2893	4832

Table 4-2: Summary of heating demand for the 12 filtered building energy demand data sets

Building Name	**Avg. Heat Demand (kW)**	**Max Heat Demand (kW)**	**Heating Coincidence w/ Elec**	**Heat/Elec Ratio**
UCI Bren	74	1252	0.40	0.47
UCI Croul	84	457	0.68	0.45
US Navy Palmer Hall	56	199	0.89	0.29
UCI Cal IT2	189	1208	0.17	0.58
UCI Nat Sci 2	477	2579	0.39	1.20
UCI Nat Sci 1	253	1325	0.93	0.59
Hyatt Irvine	531	1477	1.00	0.96
SCAQMD	1280	6721	0.62	1.64
St Regis	594	1313	1.00	0.49
Patton Hospital	1488	4409	0.87	1.06
Loma Linda VA	3253	8512	0.93	1.27
Long Beach VA	2251	8508	0.63	0.78

Table 4-3: Summary of cooling demand for the 12 filtered building energy demand data sets

Building Name	Avg Cool Demand (kW)	Max Cool Demand (kW)	Cooling Coincidence w/ Elec	Cool/Elec Ratio
UCI Bren	175	499	0.86	1.11
UCI Croul	88	507	0.46	0.47
US Navy Palmer Hall	29	187	0.76	0.15
UCI Cal IT2	344	1465	0.81	1.06
UCI Nat Sci 2	212	1380	0.38	0.53
UCI Nat Sci 1	336	1545	0.61	0.78
Hyatt Irvine	591	1641	1.00	1.07
SCAQMD	742	5012	0.49	0.95
St Regis	554	1524	0.91	0.46
Patton Hospital	1204	3738	0.98	0.86
Loma Linda VA	1806	7490	0.61	0.70
Long Beach VA	2251	10093	0.65	0.78

4.1.1.2 Level 3 EVSE Integration

The primary interest of this part of the study is the cost of refueling PEVs using Level 3 EVSE charging at these types of buildings. However, the impact of EVSE integration into a preexisting building will alter the load profile serviced by a utility, and possibly the resulting cost of electricity for both the refueled PEVs and the building. No two buildings are identical in either load dynamics of quantity of electricity consumed. A robust building model is required to capture the majority of behavior that can be commonly found in the built environment.

Since the only applicable building energy demand required for this analysis is the electrical demand created by the combined electrical and cooling load, different buildings can be selected from the set of 39 buildings for which building data exists. Not all 39 buildings are

required to perform this study, so ten buildings from the set of 39 that span high and low load factor were selected to be used in this work. Since the study is interested in the cost of electricity, and the typical billing period for a utility is a calendar month, only a summer and winter month of building data was required. Instead of using averaged building data, the k-medoids clustering method described by Domínguez-Muño in [156] was used to filter the building data to one representative summer and winter month. The filtered summer and winter month are shown in Figure 4-13 and Figure 4-14 respectively. Note that the demand profiles for summer and winter were built using data from the respective seasons only, with the season being defined by the utility as described in Section 3.1.1. As a result, all representative months are different for each of the buildings in each season.

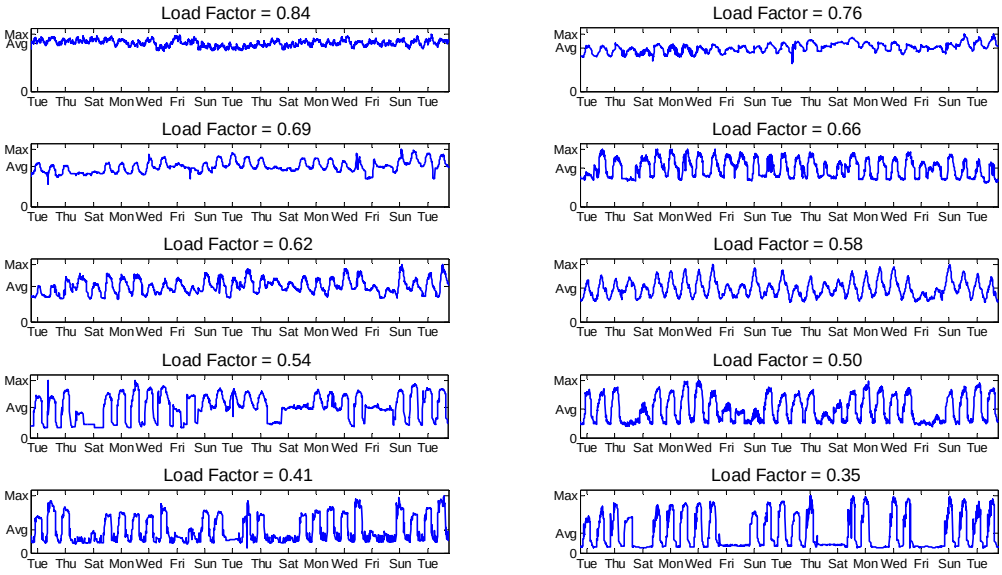

Figure 4-13 Representative electrical demand during the summer for the 10 buildings

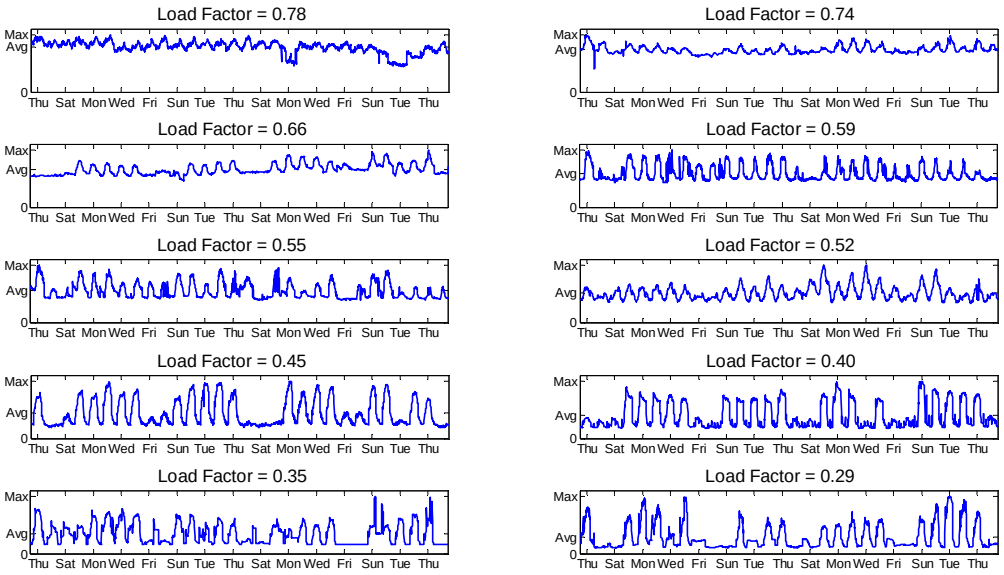

Figure 4-14: Representative electrical demand during the winter for the 10 buildings

After the data has been filtered, each building electrical data set is normalized by an average electrical demand to remove any effects created by differences in total energy consumed. Each data set was normalized to 100 kW, 500 kW, 1000 kW, and 2000 kW. The normalized representative data sets were used to test the effects of integrating Level 3 EVSE with building electrical demand. Building specific results in Section 0 will be identified by the corresponding load factor of the building load profiles presented in this section. The winter and summer building data sets were kept separate during any simulation with the cost, with winter building loads being associated with winter energy cost and summer building loads with summer energy costs.

4.1.2 UCI Energy Demand

The UCI energy demand data for 2012 was filtered, producing the energy demand profile shown in Figure 4-15. Table 4-4 contains summary values of the UCI campus electrical, cooling, and heating demand for the filtered data set.

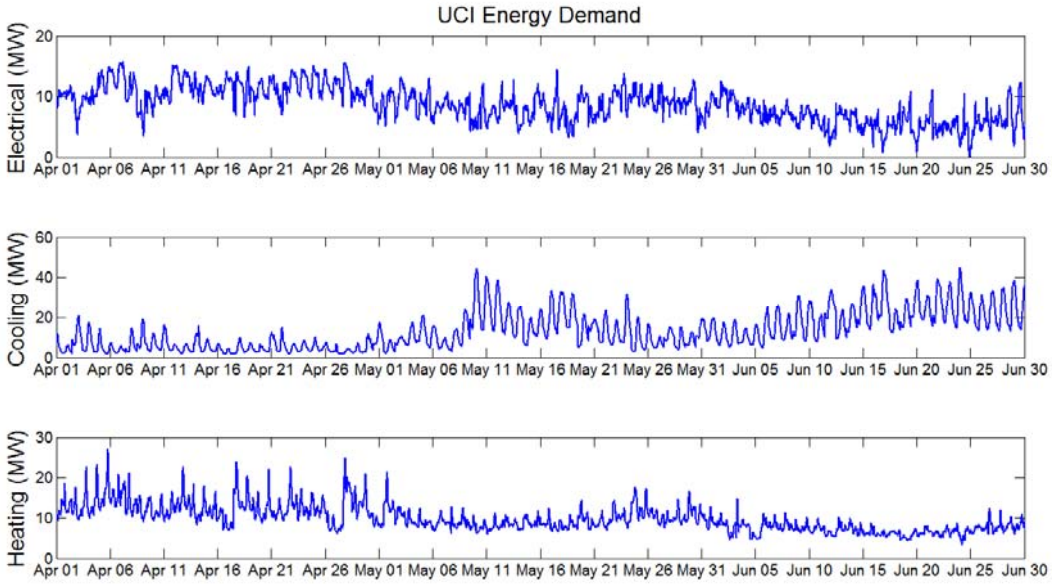

Figure 4-15: Filtered UCI campus energy demand data

Table 4-4: Summary of electrical, heating, and cooling demand for the filtered UCI Campus energy demand data set

Season	All	Summer	Winter
Average Electrical Demand (MW)	8.69	6.33	9.84
Max Electrical Demand (MW)	15.74	12.50	15.74
Electrical Load Factor	0.55	0.51	0.63
Average Heating Demand (MW)	9.84	7.18	11.14
Max Heating Demand (MW)	27.03	14.74	27.03
Heating Load Factor	0.36	0.49	0.41

Ratio of Heating to Electrical Load	1.13	1.14	1.13
Average Cooling Demand (MW)	13.17	20.16	9.75
Max Cooling Demand (MW)	45.08	45.08	44.70
Cooling Load Factor	0.29	0.45	0.22
Ratio of Cooling to Electrical Load	1.52	3.19	0.99

4.2 Fleet Vehicle Travel Behavior and Electric Vehicles

The building energy profiles described above include the relevant information to study the interactions between a DER system and a building. This information, however, is not sufficient to make informed decisions on whether electric vehicles should be adopted for use by the business operator to perform certain required tasks. Addition information governing either the vehicle routes or locations that must be visited is required.

Fleet vehicle behavior for some applications (e.g., a taxi fleet) is similar to the uncontrolled vehicle behavior described in the travel model discussed in Section 3.3.1. Other applications, however, have more regular travel patterns and can be described as nearly deterministic. Two examples of this are the operation of public buses traveling along specific routes on a schedule and the use of delivery vehicles that leave an origin at a specified time and travel to a set number of customers or locations. The information describing these two types of travel is unique to each application. This work uses data sets that are defined for each type of travel and specific to the buildings examined.

4.2.1 UCI Operations Fleet and Anteater Express Bus System

The University of California, Irvine maintains a fleet of vehicles to support university operations. The travel of much of the UCI fleet is specific to the individual daily tasks required

of the employees, and can be viewed as stochastic from the perspective of the work. One portion of the fleet (the Anteater Express bus system) provides public transportation around the UCI campus and surrounding neighborhoods to UCI students. A map of the system provided by UCI is shown in Figure 4-16. The Anteater Express route travel information for each bus is shown in Table 4-5. Any pre-routed fleet optimization will use the information displayed in Table 4-5 as the basis for the transportation system to be optimized.

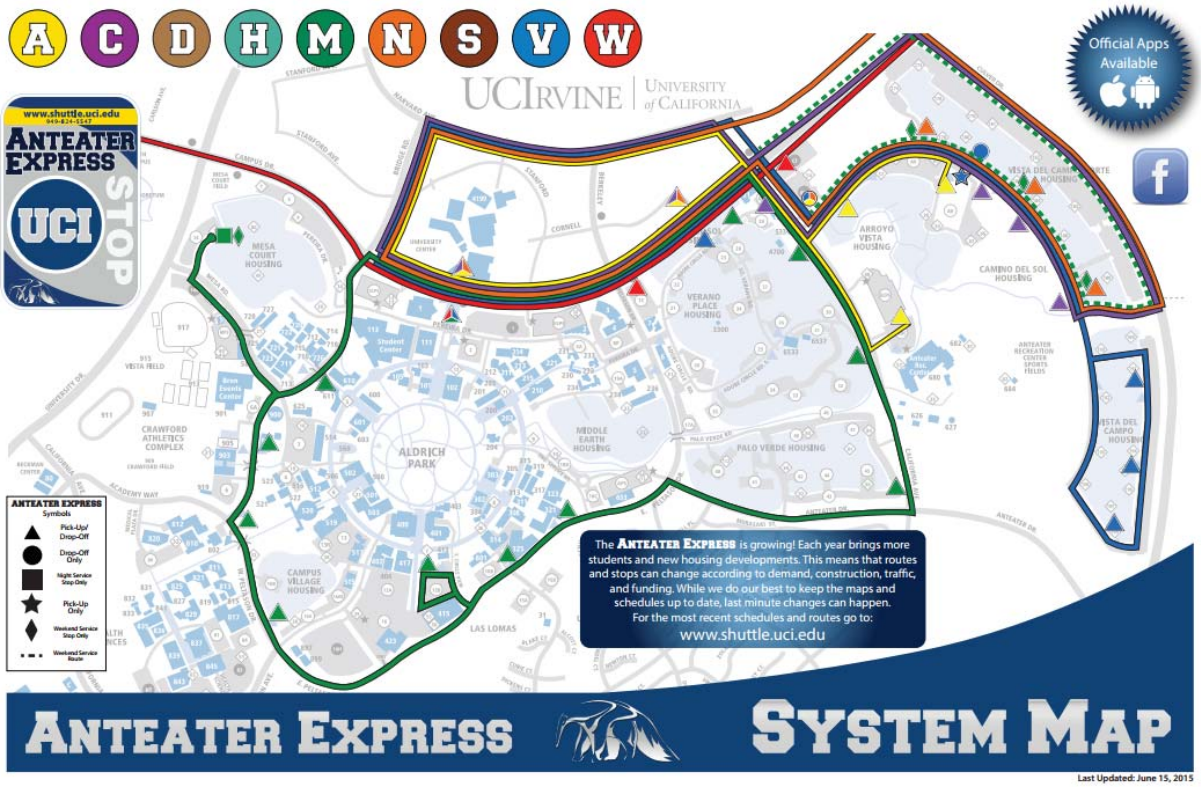

Figure 4-16: System map of Anteater Express public transportation system at UCI for 2015 through 2016 [167]

Table 4-5: Travel behavior for busses used by the Anteater Express System

Route	Miles per Day (M-Th)	Miles per Day (F)	Quarters in Service (F, W, Sp, Su)	Service Schedule (M-Th)	Service Schedule (F)

AV Bus 1	156.8	118.4	Fall, Winter, Spring	7:17am - 11:21pm	7:17am - 7:21pm
AV Bus 2	115.2	115.2	Fall, Winter, Spring	7:27am - 7:00pm	7:27am - 7:11pm
Main Bus 1	178	135	Fall, Winter, Spring	7:25am - 11:31pm	7:25am - 7:17pm
Main Bus 2	131.25	131.25	Fall, Winter, Spring	7:35am - 6:52pm	7:35am - 7:07pm
Newport	271.2	220.35	Fall, Winter, Spring	7:20am - 11:15pm	7:20am - 8:00pm
Park West - Carlson	195.2	152.5	Fall, Winter, Spring	6:58am - 10:48pm	6:58am - 7:18pm
Vista del Campo Bus 1	112	60	Fall, Winter, Spring	7:21am - 6:53pm	7:21am - 1:45pm
Vista del Campo Bus 2	112	60	Fall, Winter, Spring	7:30am - 7:02pm	7:30am - 1:37pm
Vista del Campo Bus 3	112	56	Fall, Winter, Spring	7:38am - 7:10pm	7:38am - 1:20pm
Vista del Campo Norte Bus 1	119	61.2	Fall, Winter, Spring	7:27am - 7:00pm	7:27am - 1:20pm
Vista del Campo Norte Bus 2	119	61.2	Fall, Winter, Spring	7:34am - 7:06pm	7:34am - 1:30pm
Vista del Campo Norte Bus 3	119	61.2	Fall, Winter, Spring	7:41am - 7:15pm	7:41am - 1:40pm
Camino del Sol Bus 1	122.4	64.6	Fall, Winter, Spring	7:22am - 7:15pm	7:22am - 1:35pm
Camino del Sol Bus 2	119	61.2	Fall, Winter, Spring	7:32am - 7:05pm	7:32am - 1:25pm
Morning Overflow	20	20	Fall, Winter, Spring	7:15am - 11:15am	7:15am - 11:15am
Evening Overflow	24	24	Fall, Winter, Spring	4:30pm - 9:00pm	NA
ACC Combined Bus 1	36.9	49.2	Fall, Winter, Spring	7:00pm - 11:16pm	1:20pm - 7:06pm
ACC Combined Bus 2	36.9	36.9	Fall, Winter, Spring	7:15pm - 11:31pm	1:25pm - 5:41pm

ACC Combined Bus 3	0	49.2	Fall, Winter, Spring	NA	1:30pm - 7:16pm
ACC Combined Bus 4	0	36.9	Fall, Winter, Spring	NA	1:35pm - 5:51pm
ACC Combined Bus 5	0	49.2	Fall, Winter, Spring	NA	1:40pm - 7:26pm
ACC Combined Bus 6	0	32.8	Fall, Winter, Spring	NA	1:45pm - 5:31pm
Summer Combined Bus 1	121.5	121.5	Summer	7:10am - 8:24pm	7:10am - 8:24pm
Summer Combined Bus 2	139.5	108	Summer	7:18am - 10:09pm	7:18am - 7:04pm
Summer Combined Bus 3	103.5	103.5	Summer	7:25am - 6:44pm	7:25am - 6:44pm
Summer Combined Bus 4	36	36	Summer	7:33am - 11:17am	7:33am - 11:17am
Summer Overflow	18	18	Summer	8:15am - 12:15pm	8:15am - 12:15pm

4.2.2 Node Set for Fleet Vehicle Travel

The optimization formulation presented in Section 3.4.3.2.2 allows for a building or business operator that also manages a fleet of vehicles used to travel to a set of nodes or locations to determine the optimal fleet size and composition while taking into account the delivery or travel requirements created by the fleet. The interaction with the building is created if electric vehicles are adopted and are refueled at the building. If this occurs, then the cost of electricity at the building can impact the decision to route a specific electric vehicle such that overall energy and transportation costs are minimized. If the building or business operator is also deciding to

adopt and operate a DER system, the interaction between the electric vehicles and DER system may affect the adoption and operation of the other.

The set of nodes a building or business operator is concerned with is specific to the individual application. For example, a small business may provide a mobile service that requires for the adoption of a vehicle to travel relatively close to the business building. On the other hand, large delivery depot may service thousands of nodes near and far from the business, requiring for the adoption of a large fleet of vehicles.

For this current work, a random set of nodes is generated using geographic information system software to produce a set of locations to be visited that are relatively close to a specified origin such that an electric vehicle theoretically can be used to travel from the origin to each node and back to the origin. Including nodes with a resulting round trip distance greater than any available electric vehicle range is not included in the current work, although such a scenario does occur in actual application.

The origin in this case is assumed to the University of California at Irvine. Fourteen locations were randomly selected from retail locations and shopping centers surrounding UCI, with the only constraint being that no location could be farther than 60 miles from the university. In addition to the distance between the 14 nodes and the UCI, the distance between all node combinations was also determined. The corresponding travel time between all nodes was also determined using geographic information system software. The information associated with the distance and time to travel between all nodes can be arranged in matrix form, and is called the origin-destination distance matrix and origin-destination time matrix respectively.

Table 4-6: Origin-destination distance matrix for travel between the UCI origin and all 14 nodes with all distances in miles

Nodes	**1**	**2**	**3**	**4**	**5**	**6**	**7**	**8**	**9**	**10**	**11**	**12**	**13**	**14**	**15**
1	0	32	37	40	9	21	58	63	25	52	10	7	57	47	24
2	32	0	43	50	26	22	45	48	13	31	35	26	45	56	26
3	36	43	0	7	34	39	37	41	39	31	33	32	36	16	45
4	40	50	8	0	40	46	43	47	46	37	35	39	35	10	51
5	9	26	34	41	0	9	56	60	10	50	17	5	55	46	15
6	21	23	40	46	9	0	61	66	10	48	26	14	60	54	6
7	58	45	37	43	56	61	0	6	53	19	58	54	6	43	67
8	63	48	41	47	60	65	7	0	55	21	63	58	12	48	70
9	25	14	40	47	10	10	52	56	0	38	28	14	52	54	14
10	52	31	31	37	50	47	19	22	38	0	52	48	19	43	53
11	11	35	34	34	17	28	61	66	29	55	0	16	60	40	34
12	7	26	32	39	4	14	54	58	14	48	16	0	53	44	20
13	58	44	36	34	55	60	6	12	52	18	58	53	0	37	66
14	45	57	17	10	46	53	44	48	54	44	39	44	38	0	59
15	24	26	45	52	15	6	67	71	14	53	31	20	66	59	0

Table 4-7: Origin-destination time matrix for travel between the UCI origin and all 14 nodes with all time to travel in minutes

Nodes	**1**	**2**	**3**	**4**	**5**	**6**	**7**	**8**	**9**	**10**	**11**	**12**	**13**	**14**	**15**
1	0	38	45	49	16	29	66	71	33	60	18	12	68	54	36
2	38	0	54	60	35	30	55	57	19	40	41	31	57	68	35
3	43	52	0	11	42	44	44	48	48	38	38	38	46	21	51
4	50	59	13	0	50	52	50	54	56	44	42	45	44	15	58
5	16	35	44	50	0	14	65	70	17	59	25	8	67	54	20
6	29	31	46	52	14	0	69	74	15	57	34	20	71	60	9
7	66	54	46	51	66	70	0	9	61	24	71	61	11	58	76
8	70	56	49	54	69	73	9	0	62	25	75	65	17	63	79
9	33	20	51	57	17	14	61	63	0	46	35	24	63	63	19
10	59	39	39	44	58	56	25	26	46	0	64	54	27	53	62
11	18	41	40	41	25	34	71	75	36	65	0	21	73	47	41
12	12	32	39	45	8	20	61	65	24	55	21	0	63	49	27
13	68	56	48	43	68	71	11	18	62	26	73	63	0	50	78
14	55	68	23	15	54	60	58	62	63	54	48	50	50	0	66
15	35	36	52	58	20	9	76	80	19	63	41	27	78	66	0

5 Optimal Design and Operation of CCHP Systems with Heat Recovery

The primary barrier to the widespread adoption of DER technologies is a high investment cost of many of the associated technologies. As these technologies begin to mature, and the cost to purchase and install DER systems begins to decrease, careful matching of technology to energy demand must be made to ensure that the goals of an investor are met in an economically efficient manner. Much of the work presented in Section 1.2.1 has been focused on developing optimization models to design DER systems such that some goal is met. The most common goal is to minimize energy cost.

From the perspective of the investor hoping to minimize energy costs, one of the most important metrics associated with the design of a DER system is the rate of return on the investment made. Achieving a high rate of return on an investment indicates an efficient and desirable investment of limited resources, and can propel an investor to purchase a DER system. If the DER system produces multiple types of energy, such as heating and cooling in addition to electricity, a single rate of return fails to determine the benefit or hindrance created by creating these different types of energies.

Determining the value created by producing multiple types of energy can be useful prior to and after investment. From the investors perspective, this knowledge can determine what type of energy production is driving the system economic performance, risk associated with any specific technology of projected energy demand, and the critical components of the system. From the perspective of an equipment manufacturer, this knowledge can establish what types of technologies pair together well and the exact value provided by the manufacturer's products.

From a subsidizers perspective, such as a government entity providing incentives for the purchase of DER technology, this knowledge can show which technologies perform well and which need some additional economic assistance to improve financial performance. Many of these concerns can be reduced to the following question: how much does it cost to supply cooling or heating using a DER system?

This current work is concerned with determining the cost to produce electricity, cooling, and heating using a CCHP system operated using utility supplied natural gas, acting in parallel with an electrical utility. Numerous DER technologies could be included in this work. However, initially, this study will focus on a reduced system consisting of a fuel cell or gas turbine producing electricity for a building and waste heat that can be captured using an absorption chiller or heat recovery unit. A CCHP system consisting of the above listed technologies will be designed for a building already equipped with a vapor compression and boiler system properly sized to meet the associated cooling and heating load. The particular buildings are selected from the set of buildings described in Section 4.1.1.1. Using the DER optimization model described in Section 3.4 and cost allocation method described in Section 3.5, the investment made in, cost to produce, and financial performance associated with electricity, cooling and heating for each building can be determined.

The process of DER system optimization will occur for three separate CCHP systems. The first system will consist of a fuel cell and microturbine supplying heat to a heat recovery unit. The second will consist of the same system as the first configuration, plus an absorption chiller with investment and operating costs comparable to currently available absorption chillers. The final CCHP system includes the same technology as the second configuration, with the only

difference being that the absorption chiller operations and maintenance cost is the same as a vapor compression system.

A typical DER system is based on DG providing a heat to a heat recovery unit, the first system captures what a baseline DER system will look like for each building. Adding an absorption chiller to the technology mix in the second system introduces the question of what is the best use of heat produced by DG. Since a heat recovery unit is in the most basic terms just a heat exchanger, the cost to purchase and operate a HRU is low relative to the price of other components in a DER system. It is unlikely that future developments to heat recovery technology (or heat exchangers) will reduce either capital or operation cost substantially. Likewise, the capital cost of an absorption chiller is relatively small compared to the DG producing heat. However, the operations and maintenance cost for an absorption chiller can be nearly twice the cost as a vapor compression chiller [168,169]. As a result, the third system is the same as the second, only with a reduced absorption chiller O&M cost.

5.1 Optimization Parameters and Assumptions

The three separate technology scenarios are denoted using the following titles:

- HRUo (Heat recovery unit only): Consists of fuel cells, microturbines, and a heat recovery unit
- AC-h (Absorption chiller with high O&M cost): HRUo with an absorption chiller at current capital and O&M costs
- AC-l (Absorption chiller with low O&M cost): HRUo with an absorption chiller at current capital costs. O&M costs are reduced to the same O&M cost as a vapor compression system

The capital and O&M cost parameters for the heat recovery unit, absorption chiller, vapor compression chiller, and boiler were taken from Hosford, and DiMola [168,169]. The fuel cell O&M costs were also taken from [168,169]. All other fuel cell and microturbines cost parameters were taken from [12]. Current capital costs for both fuel cells and microturbines proved to be prohibitive to DG adoption. As a result, future projected values for these technologies were adopted for this work. By using these projected cost values, it is assumed that future events will occur that reduce the cost of DG for the end user or investor. The technical parameters for the fuel cells, microturbine, and heat recovery unit were taken from [170–172] and the absorption chiller technical parameters were derived from the work performed on a double effect absorption chiller studied in [173]. Table 5-1 shows the parameters and values used in the optimization work for all included technology.

Table 5-1: Parameters of CCHP system optimization for determining the value of heat recovery in an absorption chiller and heat recovery unit

DG Parameters	**Description**	**Value (Microturbine/Fuel Cell)**
$C_{om\ DG,k}$	O&M cost for DG of type k ($/kWh)	0.02 / 0.023
$C_{cap\ DG,k}$	Capital cost for DG of type k ($/kW)	1600 / 2200
$C_{start\ DG,k}$	Startup cost for DG of type k ($/start)	10 / 10
$\eta_{DG,k}$	Electrical efficiency for DG of type k (%)	25 / 47
$\bar{\eta}_{DG,k}$	Maximum efficiency for DG of type k (%)	90% / 90%
$S_{DG,k}$	Rated power for DG of type k (kW)	65 / 100
$\delta_{DG,k}$	Minimum turndown for DG of type k (%)	80% / 50%
$\bar{\mu}_{DG,k}$	Maximum ramp up rate for DG of type k (%/15 minutes)	50% / 10%
$\underline{\mu}_{DG,k}$	Maximum ramp down rate for DG of type k (%/15 minutes)	50% / 10%
Heat Recovery Unit / Duct Parameters	**Description**	**Value**

$C_{cap\ HRU}$	Capital cost for heat recovery unit ($/kW)	100
$C_{cap\ duct\text{-}p}$	Capital cost for duct in parallel with absorption chiller ($/kW)	10
$C_{om\ HRU}$	O&M cost for heat recovery unit ($/kWh)	0.001
$C_{om\ duct\text{-}p}$	O&M cost for duct in parallel with absorption chiller ($/kWh)	0
ε_{HRU}	Effectiveness of heat recovery unit (%)	90%
$\varepsilon_{duct\text{-}p}$	Effectiveness of duct in parallel with absorption chiller recovery unit (%)	90%
Absorption Chiller Parameters	**Description**	**Value (AC-h / AC-l)**
$C_{cap\ AC}$	Capital cost for absorption chiller ($/kW)	170 / 170
$C_{om\ AC}$	O&M cost for absorption chiller output ($/kWh)	0.0266 / 0.014
$C_{om\ AC\ Charge}$	O&M cost to charge absorption chiller output ($/kWh)	0.001 / 0.001
COP_{AC}	Coefficient of performance for absorption chiller	1 / 1
Δ_{AC}	Heat input for absorption chiller for 1 kW h of cooling out (kWh heat in / kWh cool out)	1.4 / 1.4
Υ	Thermal storage required for 1 kWh of cooling out (kWh stored / kWh cool out)	1.5 / 1.5
β	Stored energy retained from prior time step (%)	95% / 95%
δ_{AC}	Minimum turndown for absorption chiller (%)	50% / 50%
$E_{COOL\ MAX}$	Maximum cooling load for building (kWh)	(Max Building Cooling Load)x(1.15)
Legacy System Parameters	**Description**	**Value**
$C_{om\ VC}$	O&M cost for vapor compression chiller output ($/kWh)	0.014
COP_{VC}	Coefficient of performance for vapor compression chiller	3.4
$C_{om\ Boil}$	O&M cost for boiler ($/kWh)	0.001
η_{Boil}	Boiler efficiency (%)	90%

The two primary assumptions made during this work are that a) the building electrical, heating, and cooling demand have already been reduced and managed through energy efficiency measures, and b) future building demand will be similar to the building data used to perform the current optimization. One of the least expensive ways to decrease the cost of building energy is to implement energy efficiency technologies or techniques. These types of building improvements are typically carried out prior to the installation of a DER system, and can significantly reduce energy cost. This work assumes that any financially desirable energy efficiency measures have already been implemented, meaning that no additional improvements can be made that reduce building energy demand and the next set of technologies to be evaluated are DER technologies.

The first assumption of minimum building energy demand is coupled with the second assumption that building energy use in the future will be similar to that of the past. In order for the optimal DER system to remain optimal, building energy consumption in the future must exhibit approximately the same dynamics and magnitude in the future. While a DER system in the future may continue to be optimal even if building energy profiles change, this cannot be guaranteed. If the building energy profile does not change, then the DER system will remain optimal and can perform as indicated by the optimization results.

5.2 Building Results

Five buildings were selected for close examination in this study. A total of twelve buildings are available for study, as described in Section 4.1.1.1. However, a full discussion of each building is not necessary as the trends shown in the four selected buildings are indicative of all available buildings. The four selected buildings are US Navy Palmer Hall, UCI Cal IT^2,

SCAQMD, St. Regis Hotel, and Patton Hospital. The buildings are presented from the lowest to highest average electrical demand. Results for the seven other buildings fall within the range of the buildings included in this study, and are not included.

For the sake of clarity, the term "combined electrical demand" will be defined as the electrical demand created when the electrical load and the electrical demand created by vapor compression chiller operation occurring to meet the cooling demand at any given moment are added together. Also, fuel utilization for a CCHP system will be defined as the sum of all useful energy produced either directly from the generator, or from thermally activated devices downstream of the generator, divided by the energy content of the fuel used. When a DG system is combined with an absorption chiller and heat recovery unit, the electricity, heating, and cooling are all considered useful and are included in determining CCHP fuel utilization. Finally, the environmental impact considered only deals with CO_2 emissions. The terms CO_2 and carbon are used interchangeably throughout this work and are intended to represent the total CO_2 emissions released in order to produce all types of energy required bythe building. This work does not take into account CO_2 equivalent emissions, such as the equivalent carbon emissions associated with a natural gas leak in a connection between an adopted type of DG and the utility gas pipe. All results are presented in terms of "tonnes" or metric tons.

All presented results are produced using the CCHP optimization model. For each technology combination, the adopted system and resulting operation is optimal from the perspective of minimizing total energy cost for a building. While specific to each building, the results show how a DER system is designed and operated in order to achieve minimum energy

cost with the available options. No non-optimal DER system designs or resulting dispatch is presented for any building or technology scenario.

5.2.1 US Navy Palmer Hall

The US Navy Palmer Hall (USN) building has an average electrical demand of 195 kW and an electrical load factor of 0.69. The ratio of the total heating load to the total electrical load of 0.29 and the heating load coincides with the electrical load 89% of the time. When the cooling demand is met through the use of electricity, the combined electrical and cooling demand produce a combined average electrical demand of 203 kW, with a load factor of 0.65.The ratio of the total cooling load to the electric load is 0.15, and the cooling load is coincidence with the electric load 76% of the time. From the perspective of integrating a CHP or CCHP system with the building, the high level of coincidence between the two thermal loads and the electrical load allow for the use of waste head produced by any onsite DG. However, both the heating and cooling loads are small relative to the electrical load, possibly reducing the amount of waste heat that is utilized during heat recovery.

Prior to DER system integration, the cost of electricity, cooling, and heating can each be individually determined. Assuming that the electrical and cooling load are both powered through the purchase of electrical imports from the local utility, the combined cost of both loads can be determined using the electrical utility rate structure modeled in Section 3.1.1. Then, using the cost allocation method described in Section 3.5, the cost of the individual electrical and cooling load can be determined. The cost of the heating load is determined by assuming that a boiler fired with natural gas purchased from the local utility that charges customers under the rate structure described in Section 3.1.2. The resulting cost to provide electricity, cooling and heating

are as follows: $0.0891 per kWh for electricity, $0.0541 per kWh for cooling, and $0.0265 per kWh for heating. Note that the cooling cost includes the cost of purchasing electricity to power a vapor compression chilling system. Also, the heating cost is relatively high due to the limited natural gas consumption associated with the USN building. When a declining block natural gas utility rate structure is in effect, as in this case, buildings will relatively small heating loads pay more per therm of natural gas purchased than buildings with higher heating loads.

The USN building was optimized for the three DER technology scenarios, and the technology adopted during optimization is shown in Table 5-2. Two 100 kW fuel cells are adopted under every technology scenario. When allowed, a 60 kW absorption chiller is adopted, and a 132 kW heat recovery unit is adopted during every technology scenario.

Table 5-2: Optimal CCHP system design for all technology scenarios operating at the USN building

Technology Scenario	Fuel Cell (100 kW)	Microturbine (65 kW)	AC (kW)	HRU (kW)	Duct - Parallel (kW)	Duct - Series (kW)
HRUo	2	0	n/a	133	148	n/a
AC-h	2	0	61	132	147	13
AC-l	2	0	60	132	147	23

5.2.1.1 CCHP System Operation

The average electrical demand of the combined electrical and cooling demand is 203 kW, and the capacity of the installed fuel cell system is 200 kW. Figure 5-1 shows the source of electrical energy for the three technology scenarios. As expected, the fuel cell system provides the majority of electricity consumed onsite. Not shown in Figure 5-1 is the decrease in total electrical consumption onsite as a result of adopting an absorption chiller. Since it is assumed

that a legacy vapor compression system is used to meet the building cooling load, shifting a portion of the cooling load to the newly adopted absorption chiller system results in a reduction in total electricity consumed onsite. Total electrical consumption decreases by 2.5% under the AC-h technology scenario and 2.6% under the AC-l scenario. The reduction in electrical consumption is primarily due to absorption chiller operation, which meets the cooling load through the utilization of waste heat instead of through the use of electricity in a vapor compression chiller. The decrease in total electrical energy is accomplished by decreasing electrical imports by 19% when moving from the HRUo scenario to the AC-h scenario, and 22% when moving from the HRUo scenario to the AC-l scenario.

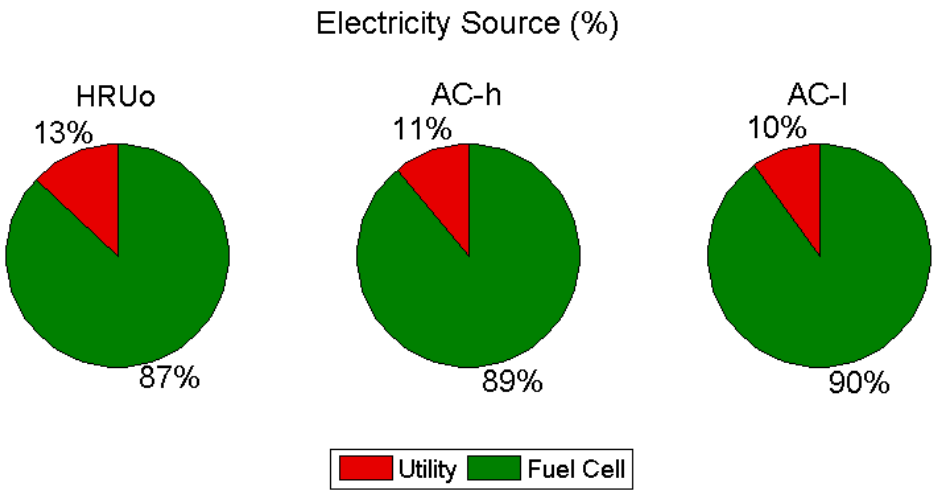

Figure 5-1: Source of electricity for the three optimal CCHP systems adopted at the USN building

Figure 5-2 shows the source of cooling. The HRUo scenario is not shown since the entire load is met by the vapor compression chiller system. Once installed, the absorption chiller provides the majority of the cooling load. When the AC O&M is reduced to the same cost as VC

O&M, the portion of the cooling load that is optimally met by the absorption chiller increases slightly.

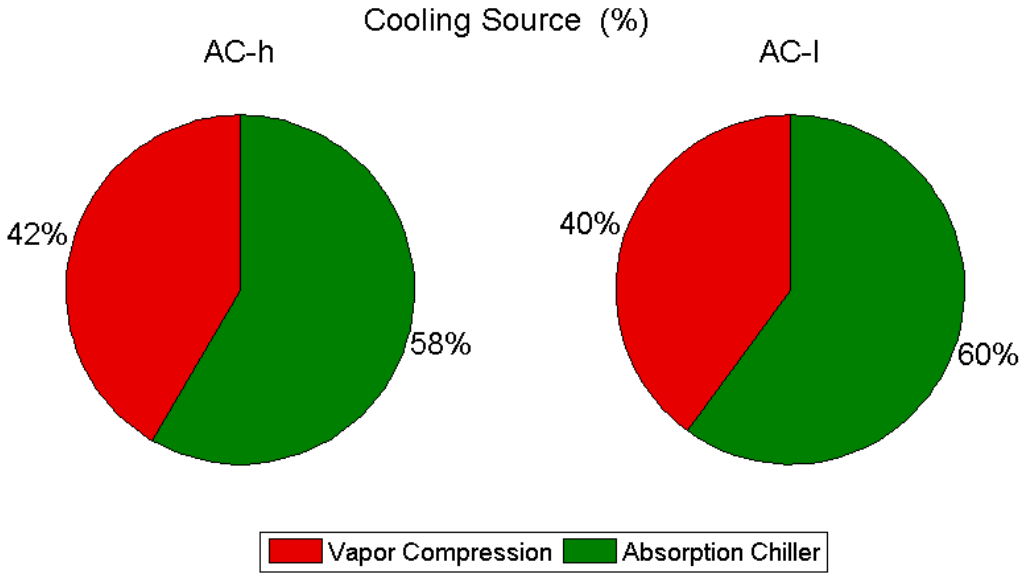

Figure 5-2: Source of cooling to meet the USN building cooling demand for all technology scenarios

Figure 5-3 shows the source of heating. Since the total heating load is a fraction of the electrical load, and the heating load is highly coincident with the electrical demand, the vast majority of all heating is provided by the heat recovery unit powered by captured waste heat produced by the two fuel cells.

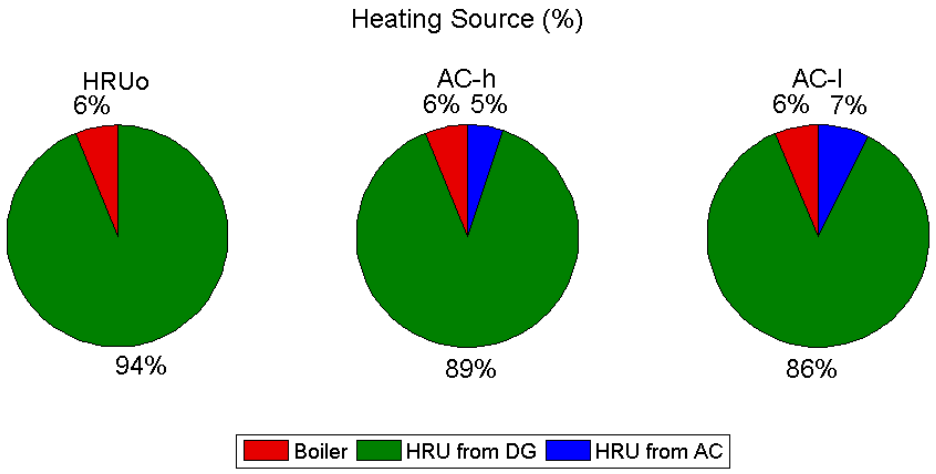

Figure 5-3: Source of heating to meet the USN building heating demand for all technology scenarios

Due to the high coincidence of both the heating and cooling load with the electrical load, the majority of both thermal loads can both be met using captured waste heat provided by the fuel cells. However, utilization of the fuel energy released during fuel cell operation is 61% for the HRUo scenario, and 65% for both AC-h and AC-l scenarios.

Figure 5-4 shows electrical operation over the course of a week for the three technology scenarios. When the building electrical demand exceeds 200 kW, the fuel cells are operated at full power, and electricity is imported from the utility to provide the remaining load. When the electrical demand dips below 200 kW, the fuel cells perform load following, and grid imports are eliminated. In Figure 5-4, the thin black line represents the electrical demand, including cooling, met by the grid prior to CCHP system integration. Adoption of an absorption chiller reduces the overall electrical demand slightly, but the difference in operation between the overall electrical operation under the AC-h and AC-l technology scenarios is marginal.

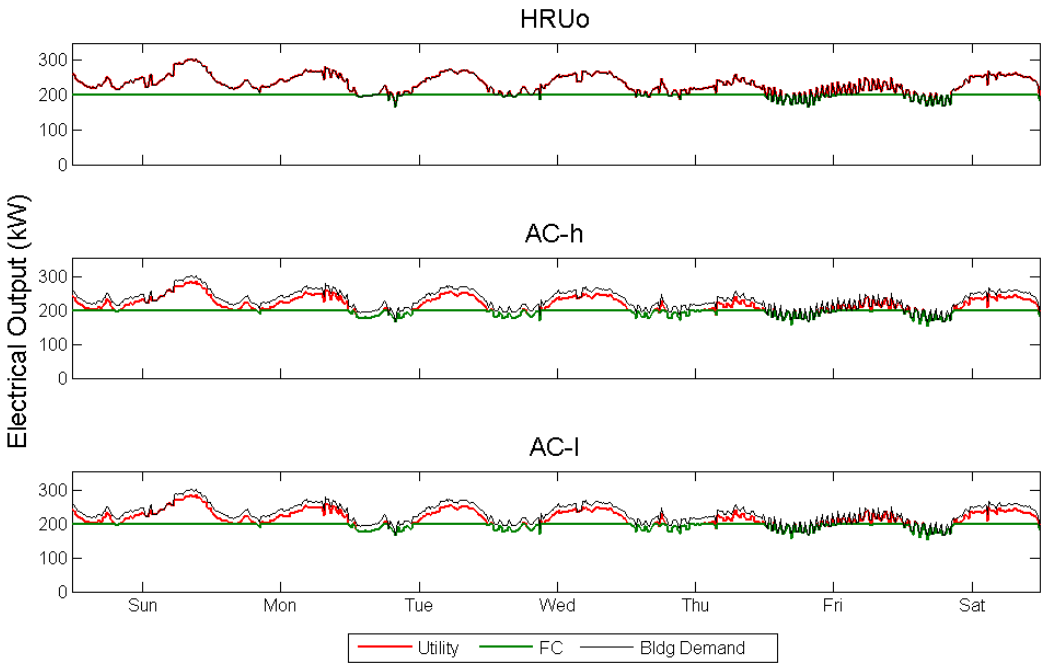

Figure 5-4: Winter electrical operation for all technology scenarios adopted at the USN building

Figure 5-5 and Figure 5-6 show the heating and cooling operation respectively over the same winter week as Figure 5-4. The HRU supplies the majority of the heating demand during the entire week except for one instance occurring early in the morning of Tuesday. Figure 5-5 also shows when the HRU is powered using waste heat directly from the fuel cells or from the absorption chiller. As suggested by Figure 5-3, the base and much of the dynamic heating load is met using heat directly supplied from the fuel cells. Simultaneously, the absorption chiller is also used to provide a base cooling load, with the vapor compression system being used to meet the cooling load dynamics. Waste heat from the fuel cells is always provided first to the absorption chiller, with the heat recovery unit being powered by a mix of heat from between the fuel cells and absorption chiller.

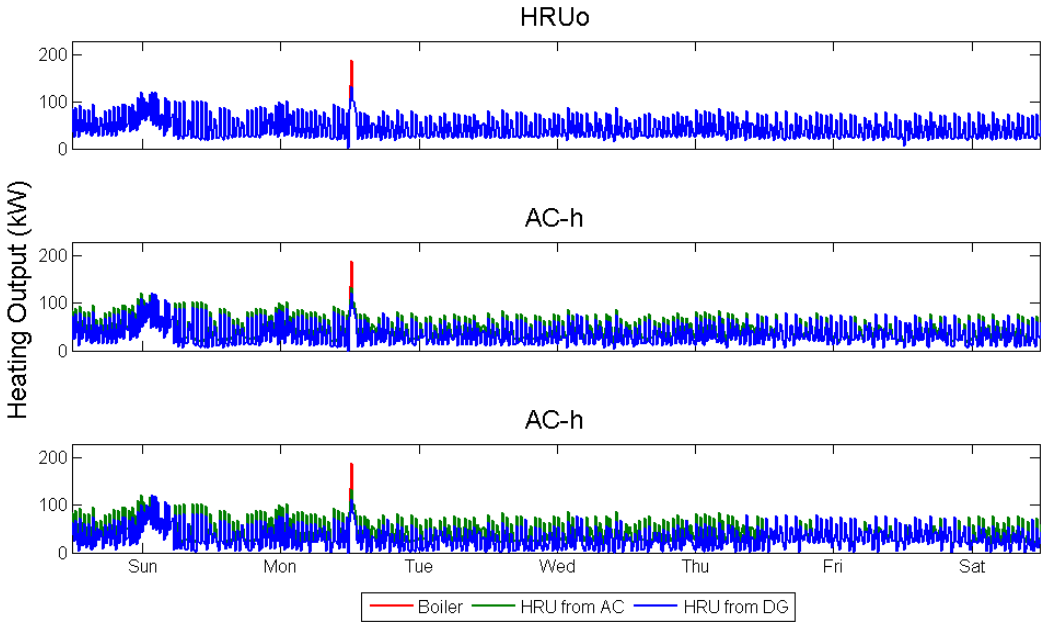

Figure 5-5: Winter heating operation for all technology scenarios adopted at the USN building

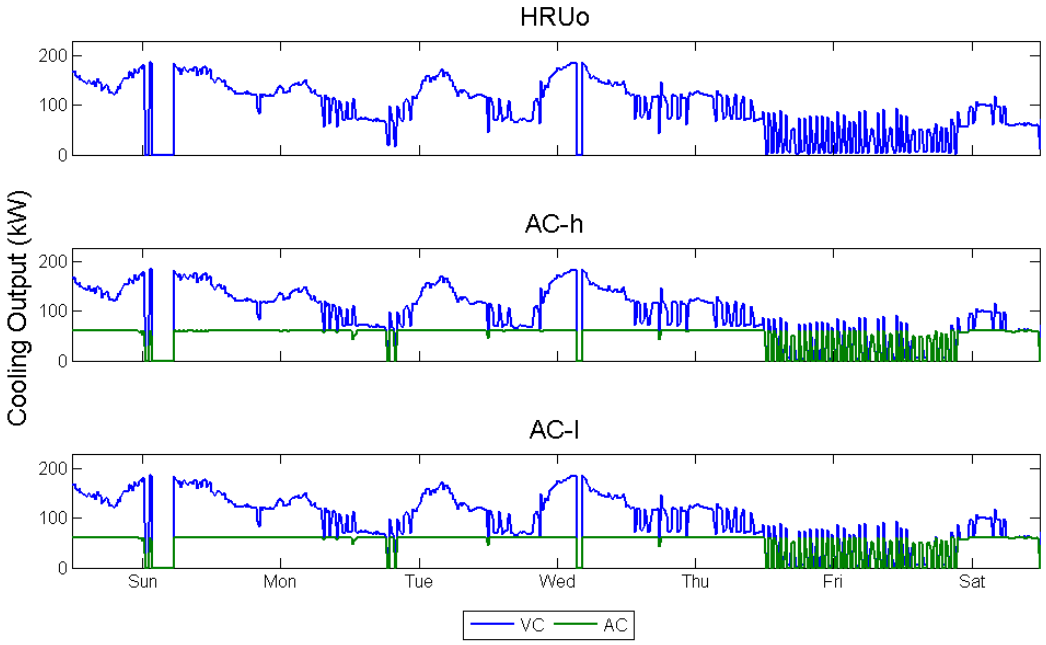

Figure 5-6: Winter cooling operation for all technology scenarios adopted at the USN building

Figure 5-7 shows the absorption chiller operation during the same week as shown during the cooling operation in Figure 5-6. In order to provide the base cooling load, the absorption

chiller is nearly always maintained in an operational state, with reduced operation only occurring when the building cooling load is low.

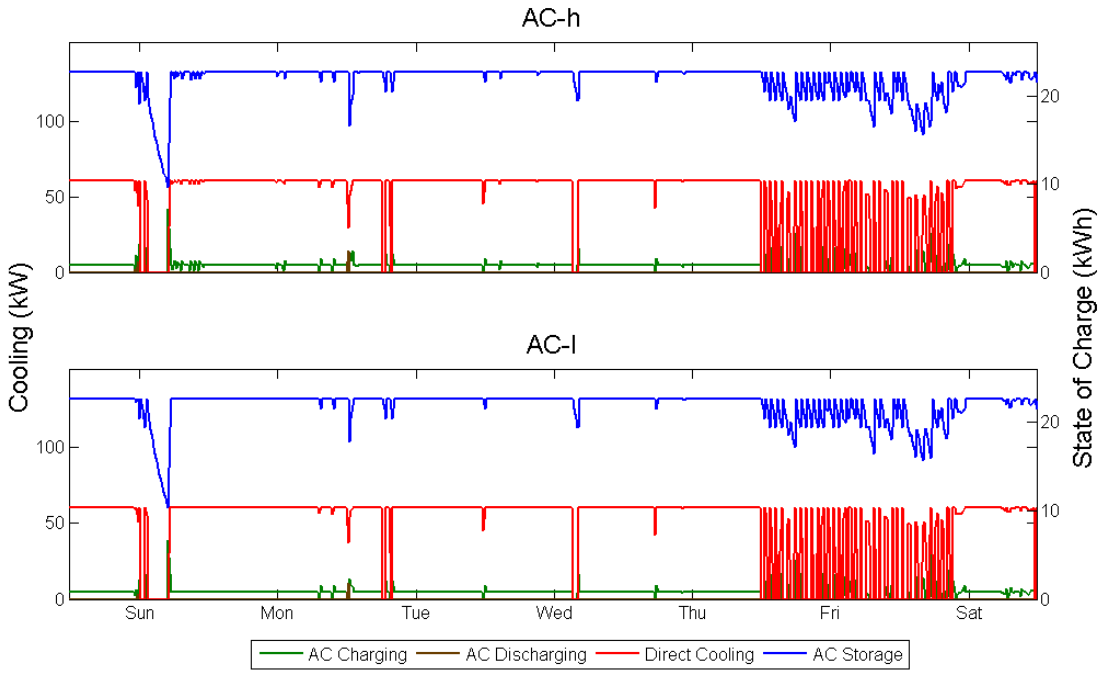

Figure 5-7: Winter absorption chiller operation for all technology scenarios adopted at the USN building

Figure 5-8, Figure 5-9, Figure 5-10, and Figure 5-11 show the electrical, heating, cooling, and absorption chiller operation respectively during a summer week. The primary difference between summer and winter operation is how the fuel cells are operated during the summer off-peak period During the winter off-peak period, the fuel cells are continuously operated at the maximum possible load, with the fuel cell only being turned down to a lower than maximum power setting when the building electrical demand is lower than 200 kW, or the capacity of the two fuel cells. During winter, the fuel cells are turned down and grid imports increase. The fuel cells provide a form of electrical load following, but continuously import electricity. Fuel cell operation also increases when the building heating load increases, as seen during late Saturday

evening. The corresponding cooling load is relatively small, allowing for the absorption chiller to meet nearly the entire cooling load. However, with the output of the absorption chiller limited by the small cooling load, little heat is provided to the heat recovery unit through the absorption chiller. Throughout most of this week, the absorption chiller is maintained in a barely operational state, with enough heat being directed to the system to maintain the cooling fluid generation process.

Since the operation of an absorption chiller offsets vapor compression chiller operation, an absorption chiller can be used to reduce the maximum combined electrical demand created by supplying both the electrical and cooling load with electricity. For the USN building, the maximum combined demand is reduced by approximately 18 kW for both the AC-h and AC-l technology scenarios.

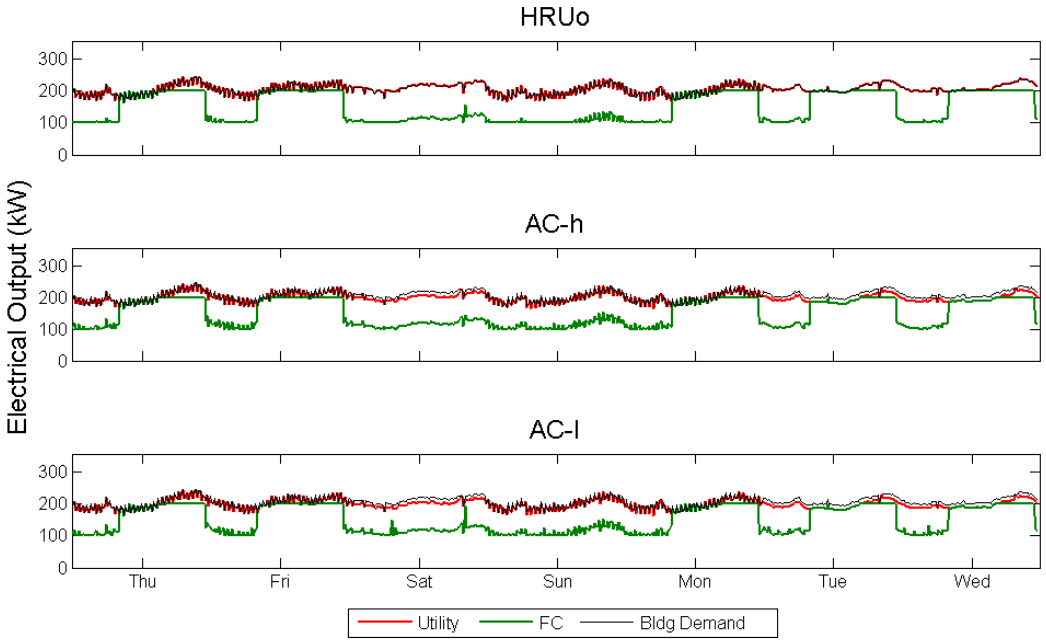

Figure 5-8: Summer electrical operation for all technology scenarios adopted at the USN building

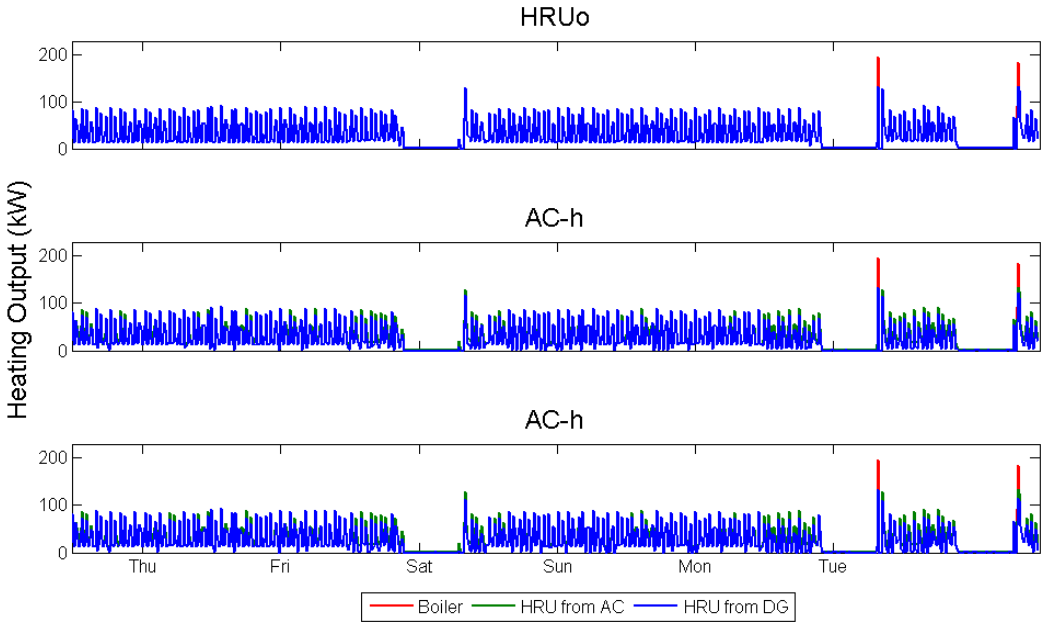

Figure 5-9: Summer heating operation for all technology scenarios adopted at the USN building

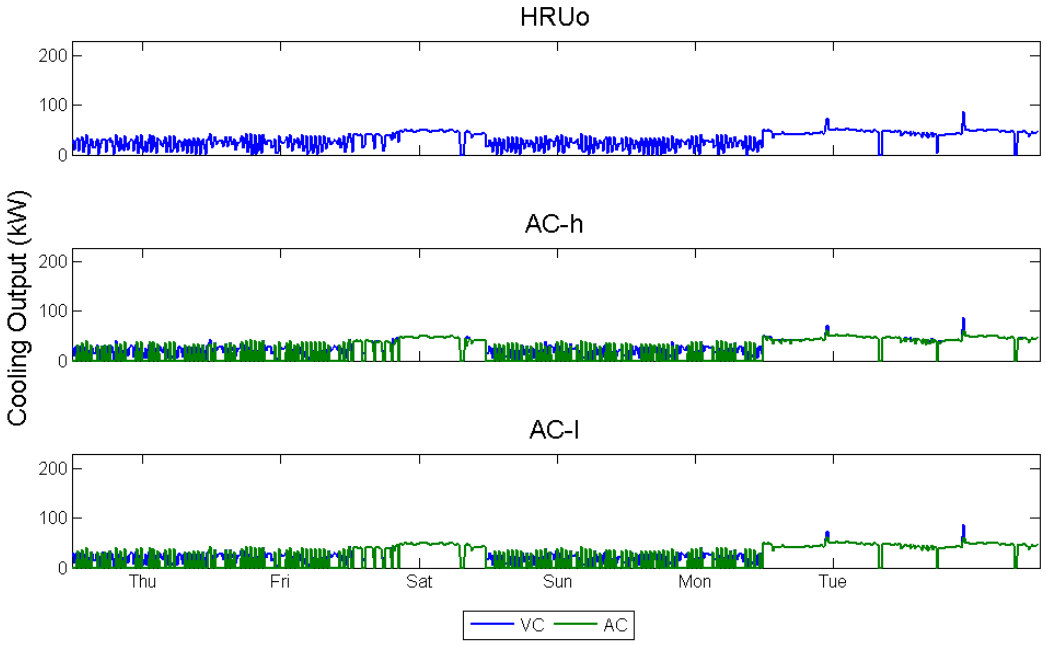

Figure 5-10: Summer cooling operation for all technology scenarios adopted at the USN building

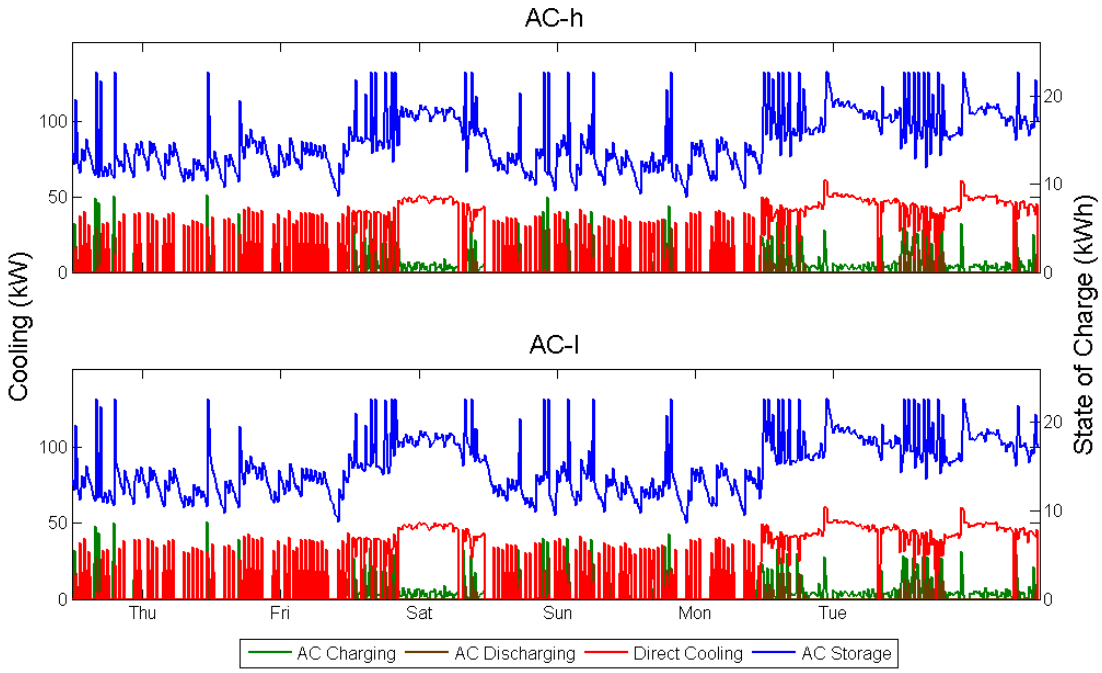

Figure 5-11: Summer absorption chiller operation for all technology scenarios adopted at the USN building

5.2.1.2 Financial Performance

The overall financial performance of the three technology scenarios is presented in Figure 5-12, which shows the modified internal rate of return over the course of 20 years, assuming that the CCHP system is able to maintain both operation and the savings predicted during the optimization process over the length of time at which the rate of return is calculated. The rate of return is determined by weighing the savings produced by adopting and operating a CCHP system versus how the building energy demand would traditionally be met (through the use of utility electricity and natural gas exclusively). As discussed in Section 3.7, the reinvestment rate is 8%. None of the technology scenarios produce a return above 8% until after ten years have passed, or the loan has been paid off in full. Allowing for an absorption chiller to be adopted improves the financial performance of the overall system, and reducing absorption chiller O&M

increases the rate of return further. However, since none of the investments result in a rate of return higher than 8%, an investment in another area would provide more financial benefit.

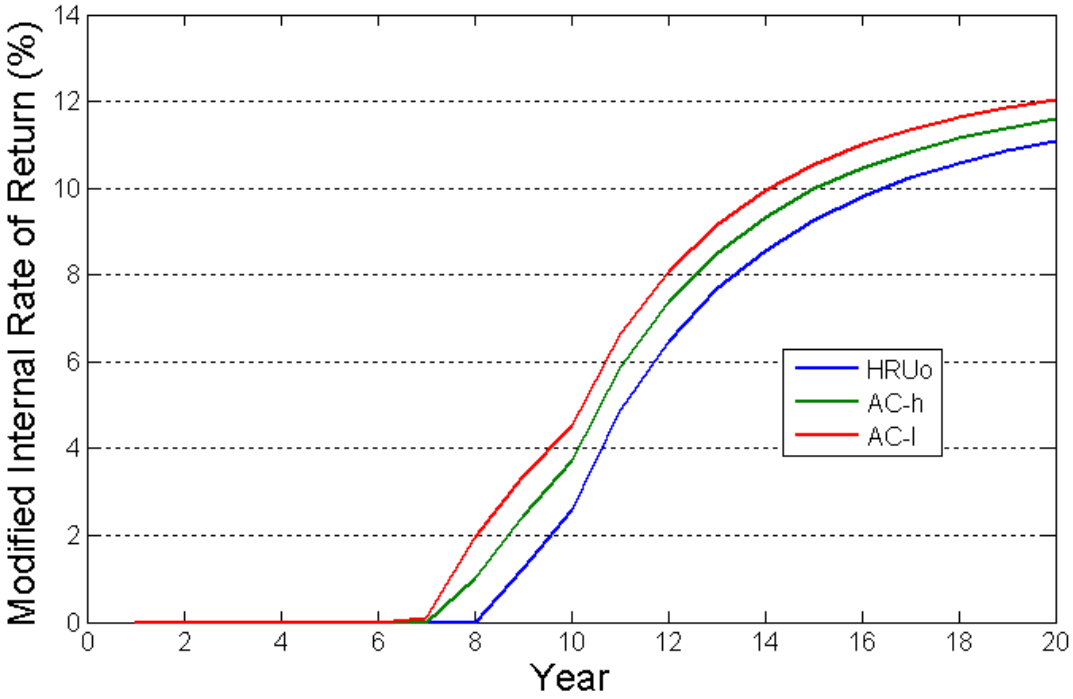

Figure 5-12: Modified internal rate of return for all three technology scenarios when adopted and operated at the USN building

Figure 5-12 provides enough information for an investor to decide if an investment in the optimal CCHP system should be made. However, since the financial performance may not be desirable, investment in this type of system is unlikely. Qualitatively, it is easy to state that the initial investment cost created by high equipment capital cost or operations cost is too high due to high fuel cost, but no additional quantitative information is provided in Figure 5-12. If investment in such a system as what has been suggested for the USN building is desirable, it is of great interest to quantitatively determine what components of the investment are holding the financial performance of the system back.

One path to quantitative understanding of the investment components is through the application of the Shapley value, as described in Section 3.5.2. By viewing the CCHP system as a shared system that is cooperating to provide multiple products or energies at the lowest cost possible, the Shapley value can be determined for each type of energy. This method of cost allocation can be used to determine which types of energy are driving CCHP investment, and how the individual cost components (i.e., utility energy and demand charge cost, natural gas cost, CCHP system O&M, and CCHP system investment costs, etc.) are incurred while meeting the building energy demand. By determining the Shapley value, the invidious cost components can be broken down into the portion of the total cost created by meeting an individual building energy demand. If the cost allocation is positive, the result suggests that the individual energy demand has incurred a cost. If the cost allocation is negative, the result suggests that a particular type of energy has helped avoid the incursion of a specific cost during CCHP system integration. By allowing for this individual energy type to be met during CCHP system integration, a service is provided to the entire building in the form of a cost reduction, for which the individual type of energy driving the cost reduction is compensated. The actual cost incurred for each cost component is the sum of the cost allocated individually to electricity, cooling, and heating.

Figure 5-13 shows the utility costs allocated to electricity, cooling, and heating for the three technology scenarios. A positive utility energy cost is allocated to both electrical and cooling loads, while a negative allocation is assigned to the heating load. This result shows that the electrical and cooling allocation are responsible for the import of electrical energy. However, the heating load results in the operation of the two fuel cells, offsetting imported electrical energy. This service provided by shifting the electrical demand from imported utility electricity

to the fuel cells is compensated by providing the heating load a negative utility energy cost allocation. While the cooling load always experiences a positive utility energy allocation, the allocation shrinks when an absorption chiller is adopted, showing that the reduced electrical demand required to meet the cooling load has been reduced.

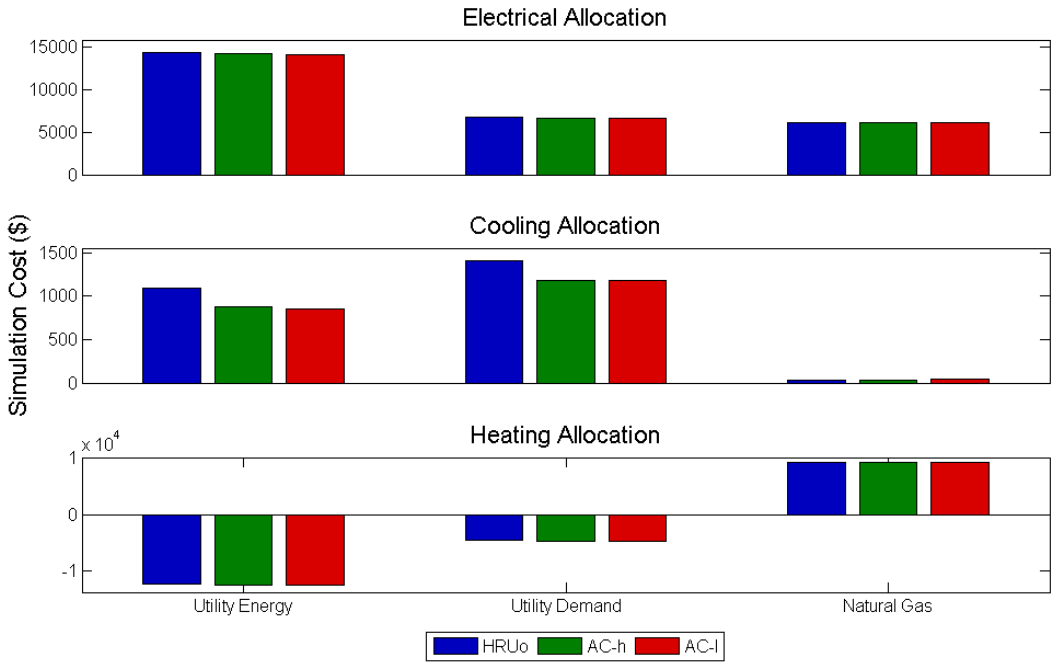

Figure 5-13: Utility costs allocated to the production of electricity, cooling, and heating for the three technology scenarios at USN building

Utility demand charges are also positively allocated to the electrical and cooling load and negatively allocated to the heating load. The negative amount allocated to the cooling load is a fraction of the negative utility energy allocation. While the heating demand is in part responsible for the shift in electrical energy from the utility to the two fuel cells, the heating load does not assist with demand charge reduction to the same degree. Referring to Figure 5-8 and Figure 5-9, fuel cell operation is reduced during summer off-peak, with the fuel cell ramping up when

heating demand is high. However, even though the heating demand is met entirely through the capture of waste heat from the two fuel cells, the heating demand is not sufficiently high enough to continually increase fuel cell operation, and the utility demand charge increases during this peak. As a result, the heating demand can be found responsible only for a small decrease to utility demand charge.

Utility natural gas is allocated to both electrical and heating demand. Since the cooling demand is relatively small, a small natural gas allocation is assigned to this energy type. This result also suggests that, even though the absorption chiller is used to meet over 50% of the cooling demand in the AC-h and AC-l technology scenarios, the primary driver for fuel cell operation (and the corresponding consumption of natural gas) is not driven by cooling, but by the electrical and heating load.

Figure 5-14 shows the O&M cost allocation for fuel cells and microturbines. The fuel cell O&M cost is evenly distributed between the electrical and heating load, with the cooling load receiving a marginal cost allocation. The small O&M allocation received by cooling further supports the result found in Figure 5-13 that the cooling load does not drive fuel cell operation. Concurrently, the O&M allocation result suggests that fuel cell operation would not occur if either only the electrical or heating load were present. In order for fuel cell operation to occur, the coincidence of the electrical and heating load is required and the waste heat produced by the fuel cell must be used to meet the building heating load.

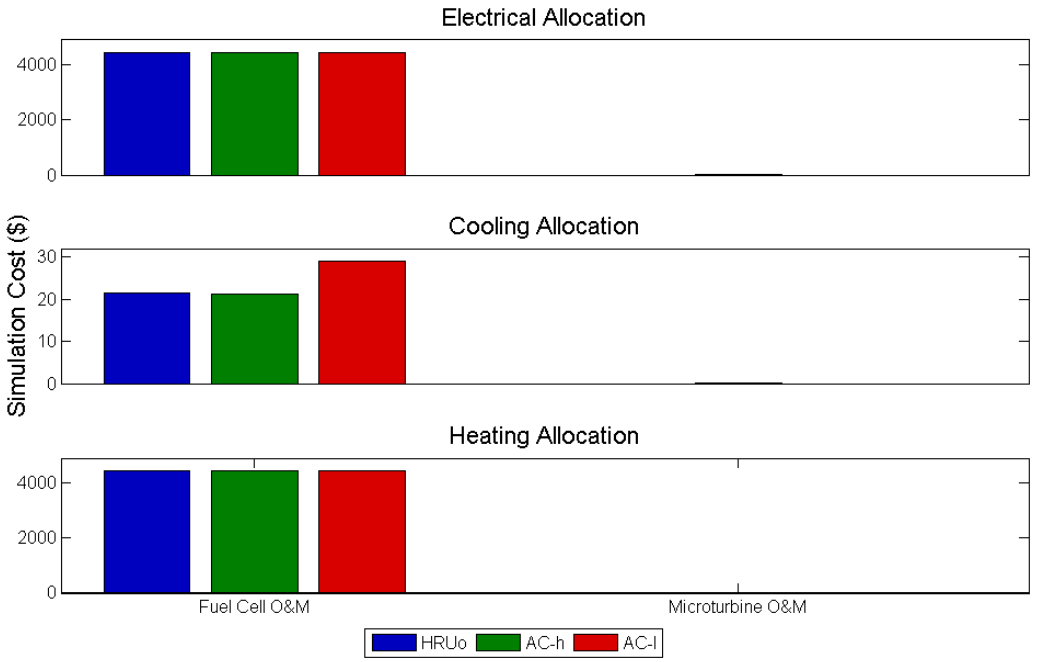

Figure 5-14: Fuel cell and microturbine O&M costs allocated to the production of electricity, cooling, and heating for the three technology scenarios at USN building

Figure 5-15 shows the O&M associated with the vapor compression and absorption chiller systems operating at the USN building under the three technology scenarios. Under the HRUo scenario, only the cooling load received a vapor compression O&M allocation since this type of energy is solely responsible for VC operation. However, when an absorption chiller is adopted, and vapor compression operation is curtailed, both the electrical and heating load receive a negative allocation. While the electrical and heating load simultaneously drive fuel cell operation, excess heat is available for use in the absorption chiller. Vapor compression operation is reduced as a result, and the financial benefit is attributed to the electrical and heating load.

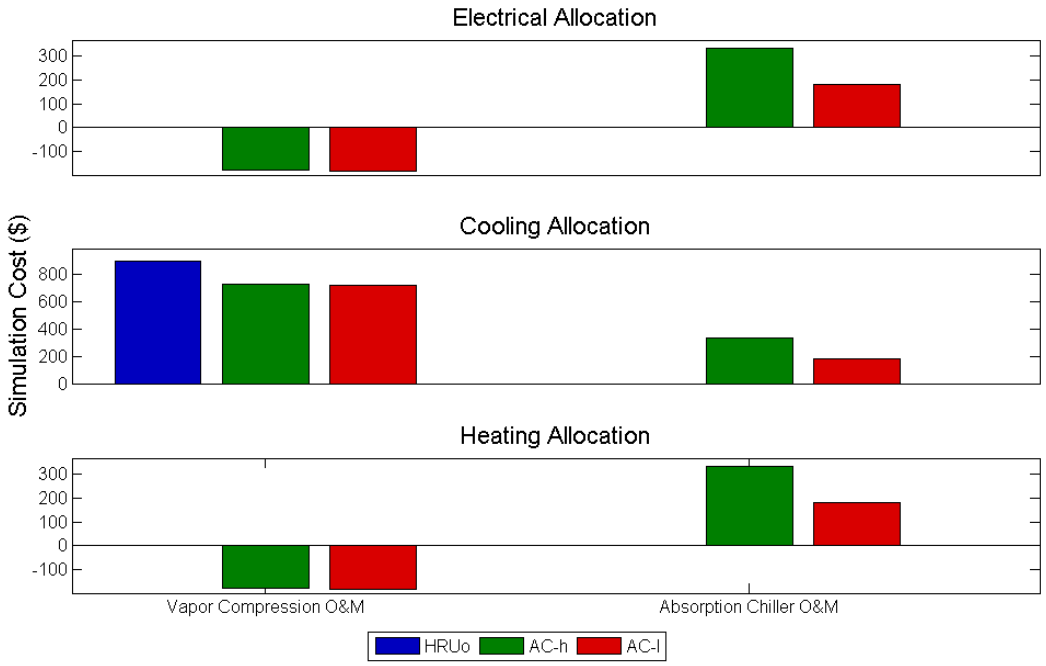

Figure 5-15: Vapor compression and absorption chiller O&M costs allocated to the production of electricity, cooling, and heating for the three technology scenarios at USN building

Figure 5-16 shows the allocated boiler and heat recovery unit O&M cost for the three technology scenarios. The cooling demand receives a maximum allocation on the order of $0.05, also suggesting that cooling load does not impact the overall fuel cell system operation. The electrical load receives a negative boiler and positive HRU O&M allocation, showing that fuel cell operation occurring to meet the electrical demand reduces boiler operation while increasing HRU operation. The heating load receives a positive allocation for both technologies.

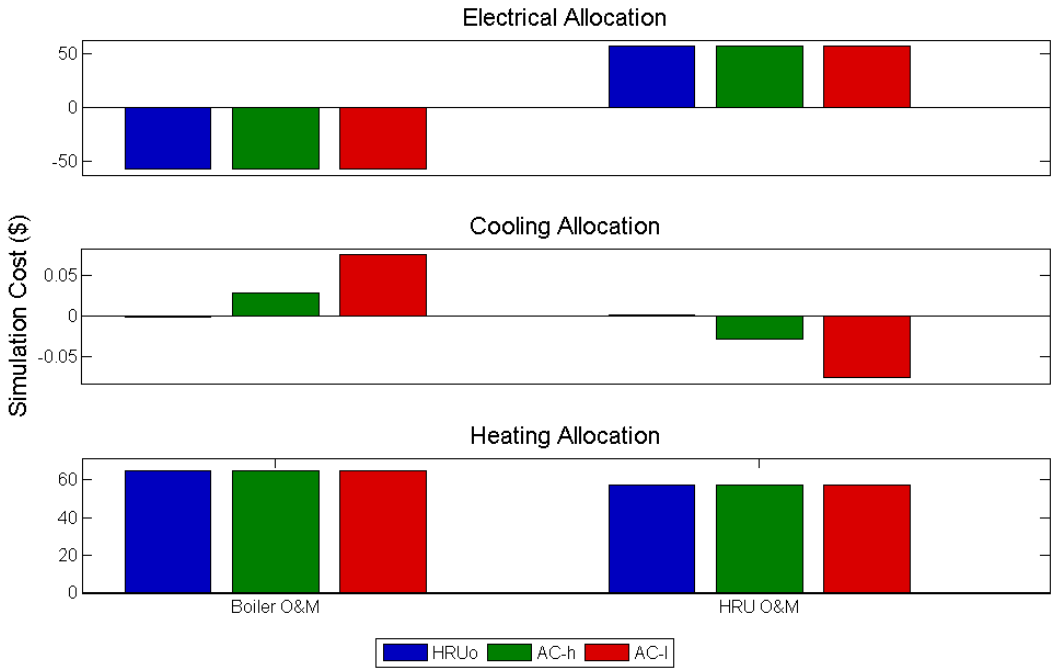

Figure 5-16: Boiler and heat recovery unit O&M costs allocated to the production of electricity, cooling, and heating for the three technology scenarios at USN building

Since fuel cell operation is attributed to both the electrical and heating load, allowing for excess waste heat to be captured by the absorption chiller, the electrical and heating loads are equally responsible for absorption chiller operation, and receive an equal AC O&M cost allocation as cooling for both the AC-h and AC-l technology scenarios. Note that the allocated absorption chiller O&M cost is not completely offset by the negative vapor compression O&M cost received by the electrical and heating load.

Figure 5-17 and Figure 5-18 show the allocated loan costs for the different adopted CCHP technologies. Figure 5-17 shows the loan payments associated with the adopted DG while Figure 5-18 shows the loan payments for the adopted heat recovery devices. Using the information provided in both figures allows for the investment made in each energy stream to be

determined. When the loan payment cost is allocated, the loan portion has an associated capital investment component, which is the amount invested in the individual energies.

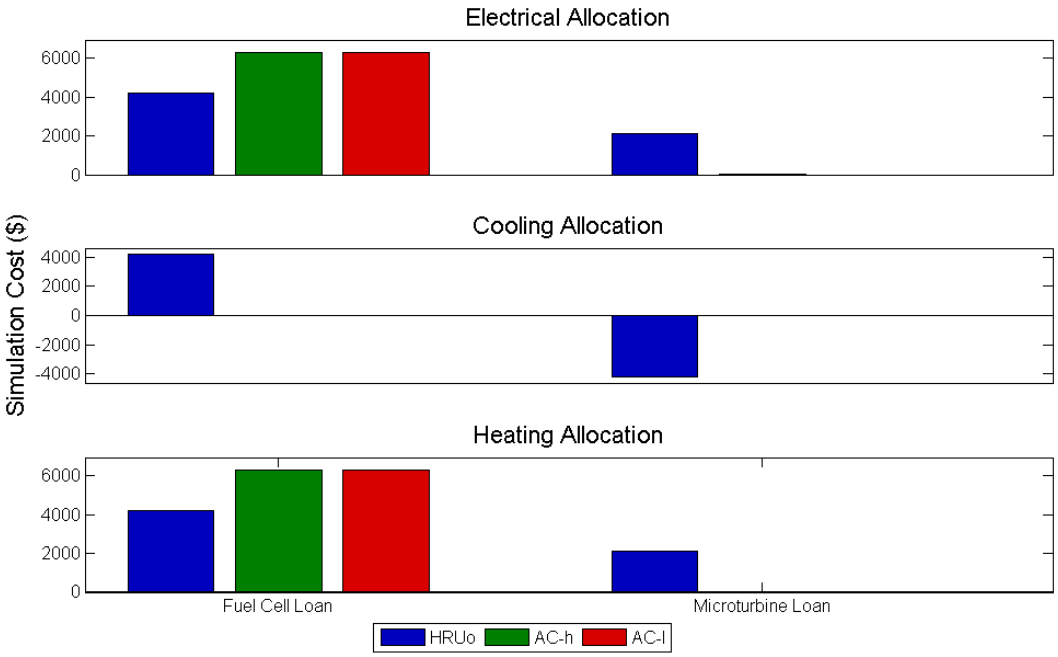

Figure 5-17: Fuel cell and microturbine loan costs allocated to the production of electricity, cooling, and heating for the three technology scenarios at USN building

Figure 5-17 shows that the fuel cell capital loan payments should be equally allocated across the three different energy types under HRUo technology scenario. This suggests that all three types of energy are necessary for fuel cell adoption to occur. Under the same technology scenario, the electrical and heating allocation receive a positive microturbine loan payment allocation, while the cooling load receives a negative and offsetting loan allocation. If the electrical and heating loads were to exist without the cooling load, investment in a microturbine system would have occurred. However, the inclusion of cooling blocks microturbine adoption, and cooling receives a negative allocation under this cost component. Including the option of

adopting an absorption chiller results in the fuel cells only being adopted as a result of the electrical and heating load, with the cooling load receiving no allocation.

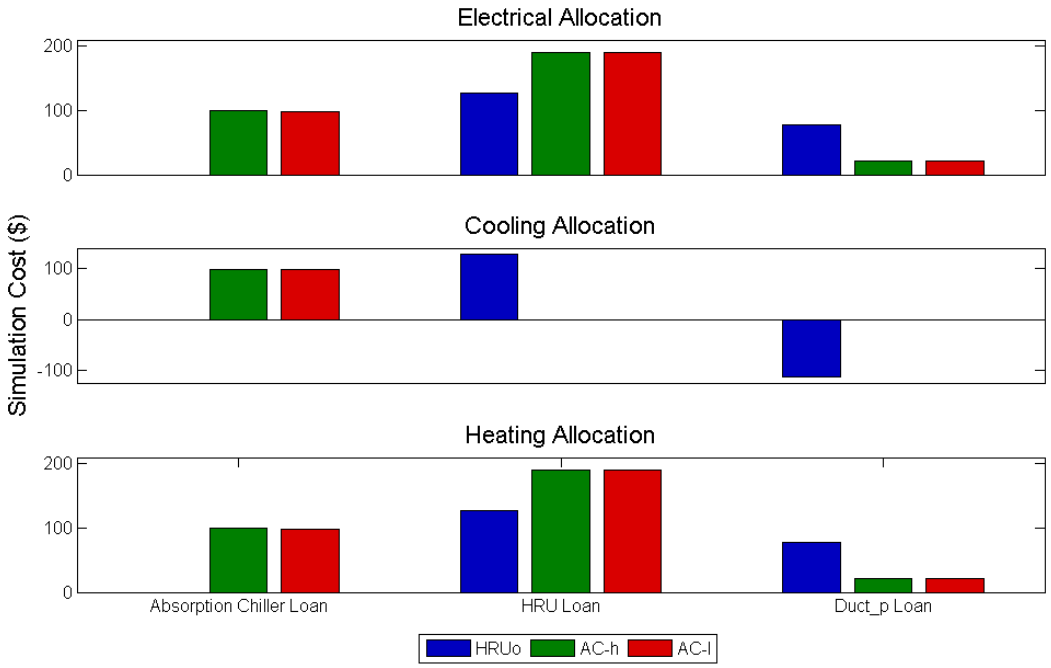

Figure 5-18: Absorption chiller, heat recovery unit, and duct-parallel loan costs allocated to the production of electricity, cooling, and heating for the three technology scenarios at USN building

Figure 5-18 shows that the adoption of an absorption chiller only occurs when all three energy types are present, resulting in the equal allocation of AC loan payments between electrical, cooling, and heating load. Under the HRUo scenario, the same behavior is experienced for the heat recovery unit. Once the absorption chiller is made available, the cooling load stops supporting the adoption of the HRU, and receives no cost allocation. Under the AC-h and AC-l scenarios, the HRU cost is shared equally between the electrical and heating load. The same is true for the duct connecting the HRU to the two fuel cells. Cooling, however, receives a negative allocation in this category. Since some heat is still available in the exhaust stream exiting the

absorption chiller, the cooling load supports the adoption of a duct in between the absorption chiller and heat recovery unit, reducing the size of the duct in parallel with the absorption chiller (or directly from the fuel cells to the HRU).

The allocated costs form a basis from which a more detailed analysis can be made for each type of energy. As discussed before, the allocated loan payments can be used to determine the investment associated with each type of energy. Then, savings for each type of energy can be determined by comparing the allocated costs to the cost if the building energy demand had been met using traditional methods. Using the combined investment and subsequent savings, a rate of return for each type of energy can be determined. In addition, the levelized cost of energy can also be determined, showing if the adoption of a CCHP system increased or decreased energy costs. The CCHP system is compared to the baseline scenario, where building demand is met through the use of utility electricity and natural gas. Under this scenario, the cost to provide electricity, cooling and heating are as follows: $0.0891 per kWh for electricity, $0.0541 per kWh for cooling, and $0.0265 per kWh for heating.

Figure 5-19 shows the difference in levelized cost of energy between the cases when a CCHP system is adopted and when the baseline scenario applies at year five, seven, and nine for the three technology scenarios. Figure 5-19 also shows to associated rate of return for the three technology scenarios across electricity, cooling, and heating.

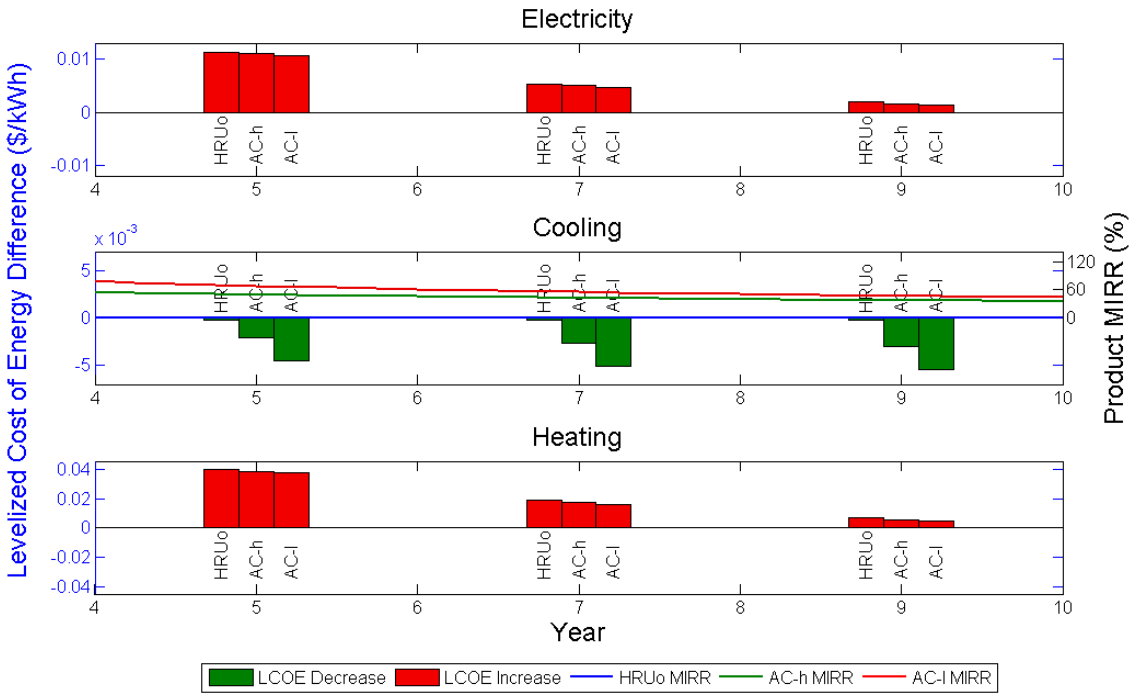

Figure 5-19: Levelized cost of energy difference at years five, seven, and nine and corresponding modified internal rate of return for electricity, cooling, and heating when CCHP systems are adopted according to the three technology scenarios at the USN building

For a single technology scenario, the levelized cost of energy decreases with time due to the reduced effect of capital costs. The levelized cost at year five and nine take into account the same capital payments. However, energy production after year nine is 40% greater than year five. Even after taking into account the discounting factor associated with the additional energy, the effects of capital cost towards increasing levelized energy cost decrease as time moves along. Since Figure 5-19 only shows the difference in LCOE between a CCHP and baseline scenario, the decrease in LCOE is manifested by a difference decreasing. For example, for the HRUo scenario, the cost of electricity is increased by approximately $0.01 per kWh at year five, but is only increased by approximately $0.001 per kWh at year nine.

According to Figure 5-19 the adoption of the optimally designed CCHP system always increases the cost of electricity and heating. At year five, electricity is increased by approximately $0.01 for all technology scenarios, while heating is increased by nearly $0.04 per kWh for the HRUo scenario. Adopting an absorption chiller always decreases the CCHP system levelized cost of electricity or heating, especially when the AC can operate at the same cost as the competing vapor compression system. If the system can be maintained for nine years, then the cost of electricity and heating nearly approaches the baseline scenario.

The large increase to heating is due to a relatively high capital cost allocation and high fuel costs. Despite being small relative to the electrical load, the heating load is required for adoption of the two fuel cells. As a result, the high capital cost is partially allocated to the heating. For this particular building, the total heating load is 70% smaller than the electrical load. Even though the fuel cell capital cost component in the numerator of the levelized cost of electricity and heating equations are the same, the denominator for the heating is 70% smaller for the heating calculation.

Despite the high capital cost, fuel costs are also high due to the small size of the building. Operational costs remain high as a result, allowing for the electrical and heating levelized cost to approach parity with the baseline scenario at best. Since no reduction to either electricity or heating is achieved, no positive rate of return is observed for either type of energy (electricity or heating).

Cooling, on the other hand, is reduced for every technology scenario. Under the HRUo scenario, no capital investment is made in the cooling production since the fuel cell investment is balanced by the avoidance of microturbine investment. No rate of return exists under this

scenario since an investment of $0 that yields positive savings has an infinite rate of return. Slight savings are realized by producing electricity onsite to power the vapor compression system, and the levelized cost of cooling is the same in all years.

Investment is preferred under the AC-h and AC-l scenarios, primarily due to the purchase of an absorption chiller. Again, no capital investment in either fuel cells or gas turbines occurs, reducing the initial investment substantially. As a result, a reduction to levelized cost of cooling can be realized by year 5. These savings increases, with the cost of cooling under the AC-l scenario being reduced by nearly $0.005 per kWh in year nine. Note that the drop in levelized cost for cooling is not nearly as large as for electricity and heating since the capital cost invested for the sake of cooling is small. With a small investment occurring, the effects of stretching the capital cost over more years is muted for cooling.

5.2.1.3 Building Carbon Emissions

Using the same method to allocate the different cost components, CO_2 emissions associated with the import of electrical energy and the use of natural gas in a CCHP system or boiler can be allocated to electricity, cooling and heating. A baseline carbon emissions scenario can be built using information about the electrical utility and the fuel combusted in the legacy boiler for heating. Assuming that the electrical utility produces carbon emissions at a time resolved rate as described in Section 3.6, and heating is met through the combustion of natural gas, the baseline carbon emissions can be determined. The resulting baseline carbon emissions associated with the building is shown in Figure 5-20 for an entire year. In total, the USN building energy use results in the emission of 633 tonnes of CO_2 per year.

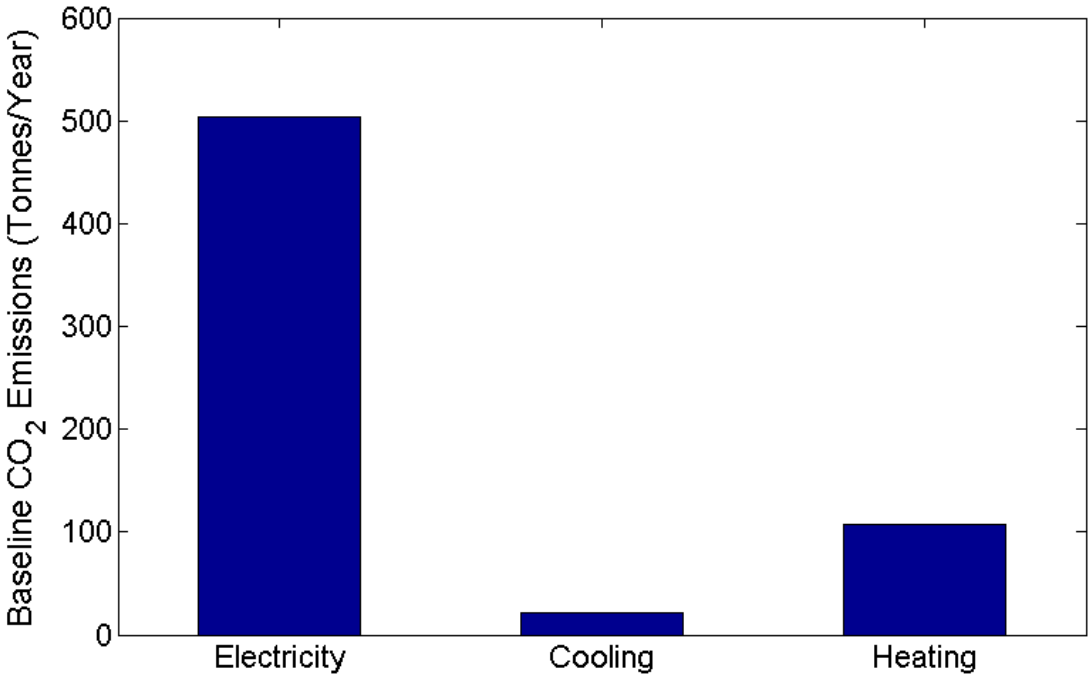

Figure 5-20: Yearly baseline carbon emissions for the USN building

At the USN building, integration of a CCHP system designed to minimize total cost always results in an increase to carbon emissions, as seen in Figure 5-21. The HRUo system experiences the largest increase to carbon emissions, while the other two scenarios experience roughly the same increase.

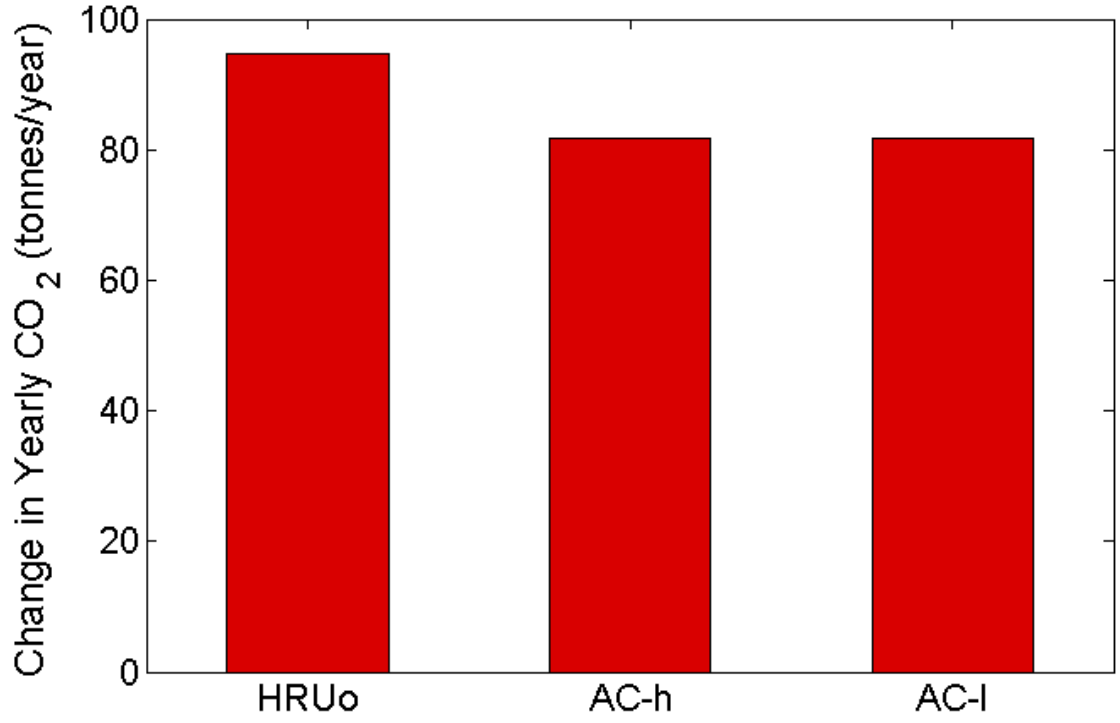

Figure 5-21: Change in yearly carbon emissions for the USN building as a result of CCHP system adoption

The energy type that causes the carbon emissions increase can be determine by calculating the Shapley value for carbon emissions. Figure 5-22 shows the increase in emissions allocated to the three types of energy supplied to the building for the three technology scenario. Figure 5-22 shows that the electricity and heating loads are equally responsible for increasing carbon emissions. These two energy loads are responsible for the adoption and operation of the two fuel cells, and are also responsible for the additional emissions generated during CCHP adoption. The cooling load, however, reduces carbon emissions. Under the HRUo technology scenario, the inclusion of the cooling load blocked the adoption of a microturbine. Under the AC-h and AC-l scenarios, the absorption chiller was used to capture waste heat that would not

have been used, increasing fuel utilization in the CCHP system while reducing the amount of vapor compression operation required.

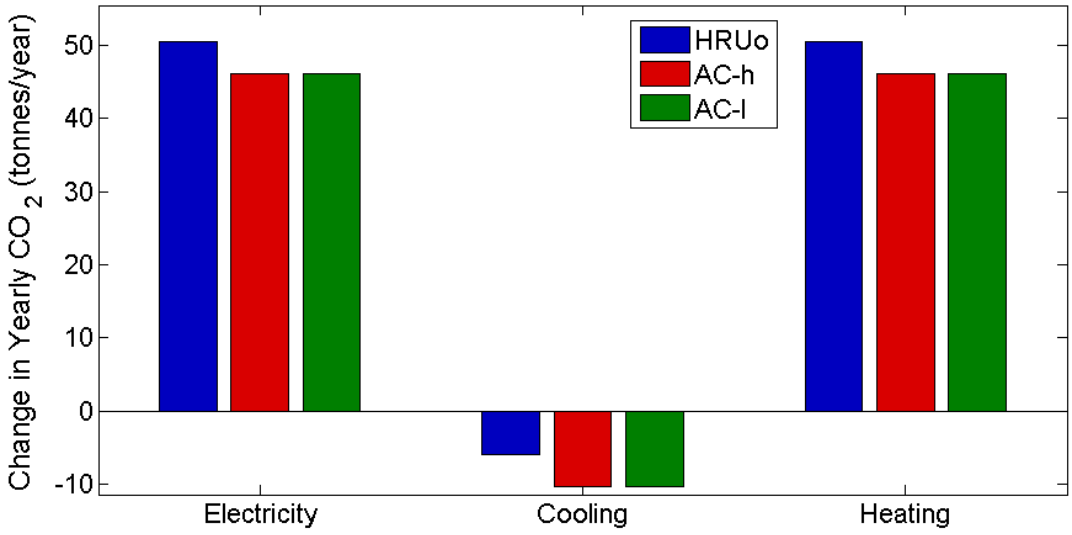

Figure 5-22: Change in yearly carbon emissions for individual types of energy for the USN building as a result of CCHP system adoption

5.2.2 UCI Cal IT^2

The UCI Cal IT^2 building has an average electrical demand of 323 kW and an electrical load factor of 0.47. The ratio of the total heating load to total electrical load is 0.58, and the heating load is coincident with the electrical load 17% of the time. The ratio of the total cooling load to electric load is 1.06, and the cooling load is coincident with the electrical load 81% of the time. Prior to CCHP system integration, the cost to meet the building energy demand is $0.095 per kWh for electricity, $0.0477 per kWh for cooling, and $0.0239 per kWh for heating.

Table 5-3 shows the optimal CCHP system for all technology scenarios when designed for the UCI Cal IT^2 building. Four fuel cells are always adopted, with a single under scenario C. As absorption chiller O&M cost decreases, the size of the adopted chiller increases slightly. The

HRU decreases in size as an AC is adopted and AC O&M decreases. The duct directly from the DG to the HRU (duct-parallel or duct-p) decreases in size along with the HRU. As the AC increases in size, the duct connecting the HRU to the AC also increases in size.

Table 5-3: Optimal CCHP system design for all technology scenarios operating at the UCI Cal IT^2 building

Technology Scenario	Fuel Cell (100 kW)	Microturbine (65 kW)	AC (kW)	HRU (kW)	Duct - Parallel (kW)	Duct - Series (kW)
HRUo	4	0	n/a	326	362	n/a
AC-h	4	0	261	295	306	99
AC-l	4	1	275	238	264	110

5.2.2.1 DER System Operation

Figure 5-23, Figure 5-24, and Figure 5-25 show the source of energy for the electrical, cooling, and heating demand respectively. Figure 5-23 shows that the fuel cell is the primary source of electrical energy for all system types. Note that the electrical consumption is the combined demand created by all electrical usage plus electricity used to operate the building vapor compression systems to produce cooling. Since an absorption chiller is not included in HRUo, the cooling demand under this technology scenario is met entire through the use of an electrically powered vapor compression system. By adopting and operating an absorption chiller, the total amount of electricity required to power the cooling demand decreases as a result of shifting part of the cooling load from an electrically operated vapor compression system to a thermally activated absorption chiller. The difference in electrical consumption as a result of absorption chiller adoption for AC-h versus HRUo and AC-l versus HRUo is 8.5% and 10.2%,

respectively. These reductions are solely due to a decrease in the purchase of utility supplied electricity. This type of electricity is reduced from the HRUo level by 31% for the AC-h scenario and 72% for the AC-l scenario. Total electrical energy produced by the fuel cell decreases by 3% for AC-h and increases by 2.7% under AC-l. A single microturbine is adopted.

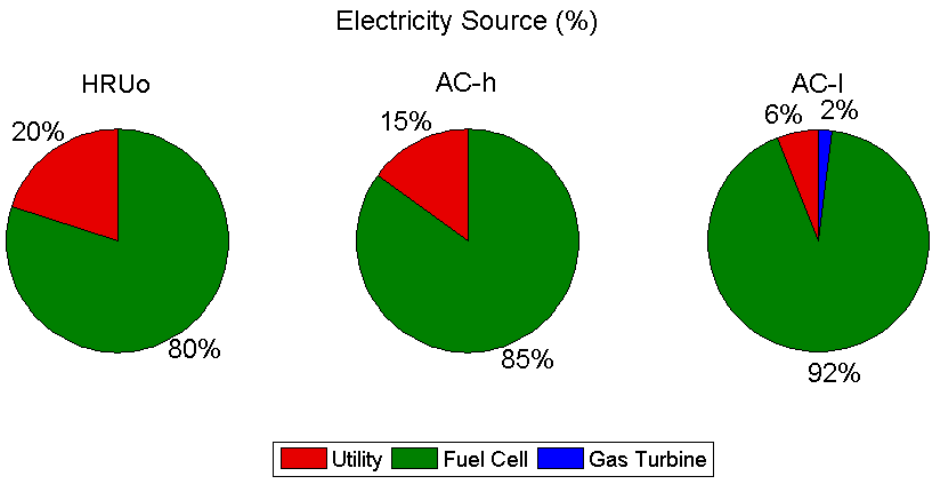

Figure 5-23: Source of electricity to meet the UCI Cal IT² electrical demand for all technology scenarios

This reduction in electrical consumption is matched with an increase in absorption chiller cooling production, as seen in Figure 5-24. While electrical imports decrease by 31% and 72 percent for AC-h and AC-l respectively, vapor compression operation does not decrease at the same rate. Instead, additional fuel cell operation and production from the single microturbine supplant additional grid imports, allowing for the vapor compression system to continue operation while imports decrease.

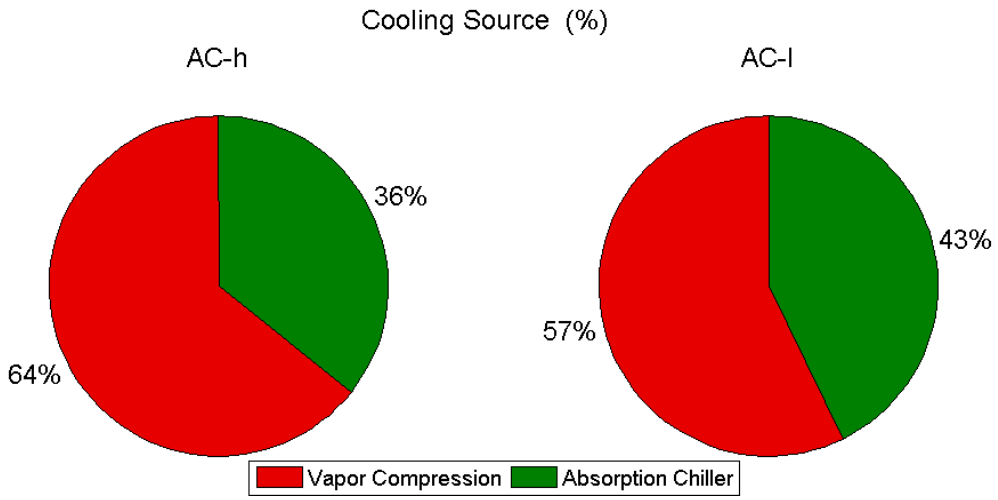

Figure 5-24: Source of cooling to meet the UCI Cal IT² cooling demand for all technology scenarios

The amount of heat supplied from the adopted DG into the heat recovery unit initially supplies 26% of the building heating demand, but decreases as an absorption chiller is adopted and operated more frequently.

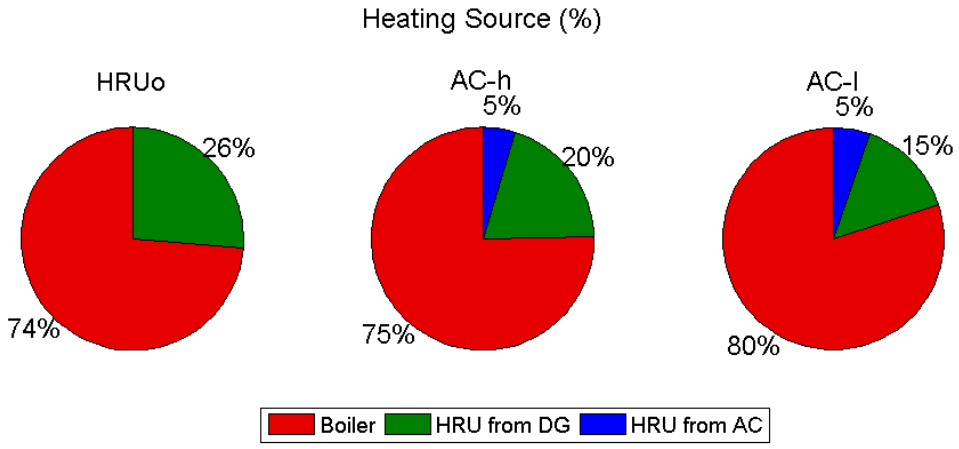

Figure 5-25: Source of heating to meet the UCI Cal IT² heating demand for all technology scenarios

Electrical operation over the course of a week is shown for the three technology scenarios in Figure 5-26. In Figure 5-26, the combined electrical demand created when meeting the full cooling load using only a vapor compression system is shown by the black line in all three subplots. The four fuel cells provide baseload power for the building for all three technology scenarios. In both AC-h and AC-l, the adoption of an absorption chillers allows for the electrical demand to be decreased in both instances. When a microturbine is adopted under the AC-l technology scenario, the turbine is operated to provide peak power only, with operation occurring only during the middle of the day.

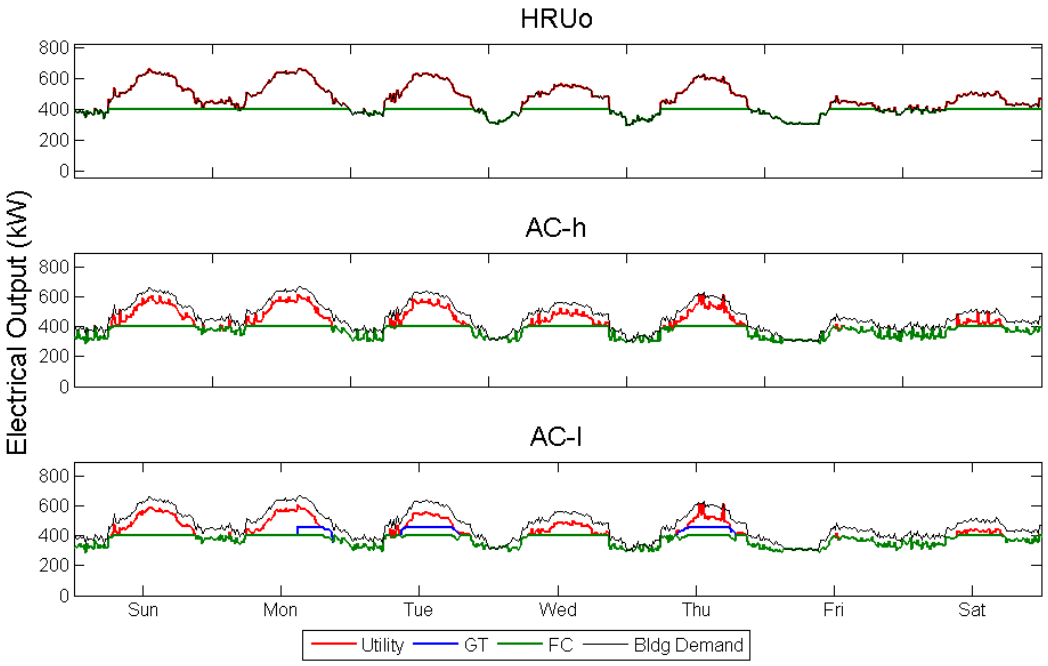

Figure 5-26: Winter electrical operation for all technology scenarios adopted at the UCI Cal IT² building

The heating operation is shown in Figure 5-27. Due to the transient nature of the heating demand, the actual energy demanded at any given moment is nearly twice the corresponding electrical demand. Even though the four fuel cells (and single microturbine under AC-l), are

capable of producing the total heating energy demanded by the building, the adopted CCHP systems for the three technology scenarios are incapable of providing the heating power required, leading to continual boiler operation throughout the week. This mismatch of the heating to the electrical demand results in an overall fuel utilization under HRUo of 54%. Note that the adopted fuel cells each have an electrical efficiency of 47%, suggesting that only a fraction of the available waste heat is captured from the fuel cells for actual operation.

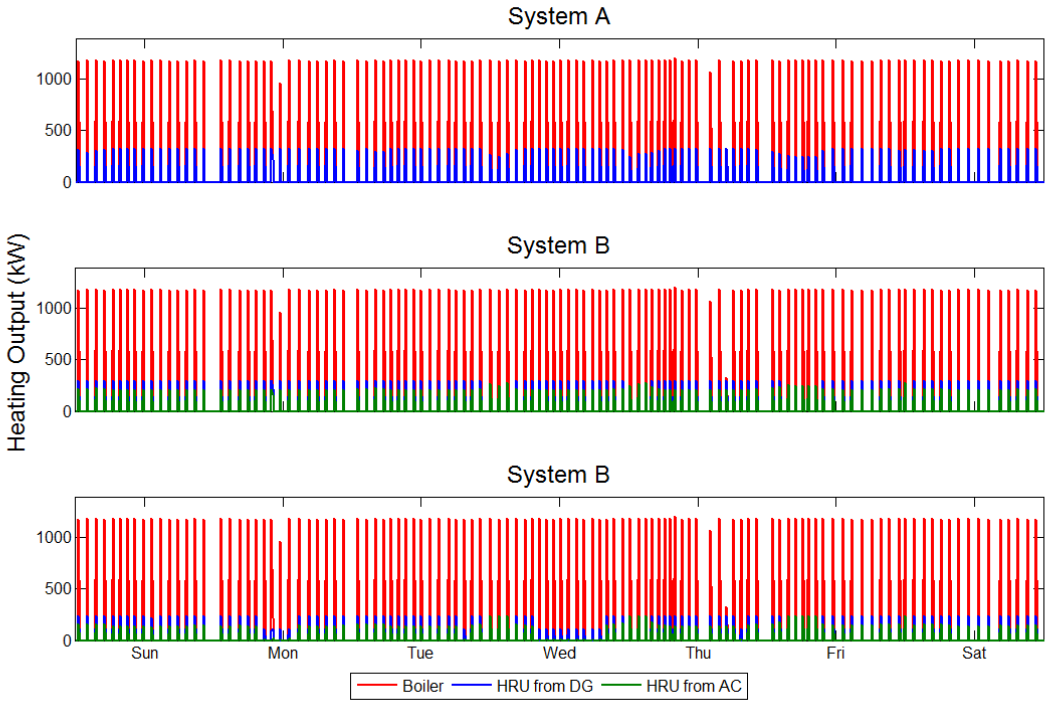

Figure 5-27: Winter heating operation for all technology scenarios adopted at the UCI Cal IT^2 building

Allowing for an absorption chiller to be adopted helps to increase fuel utilization. As discussed earlier and seen in in Figure 5-26, fuel cell operation between the all technology scenarios experiences minimal changes. Due to continuous fuel cell operation, a nearly constant stream of waste heat is available for use in an absorption chiller, leading to the adoption of

similar sized systems for both the AC-h and AC-l scenarios. The operation of these systems in conjunction with the legacy vapor compression system for the same winter week can be seen in Figure 5-28.

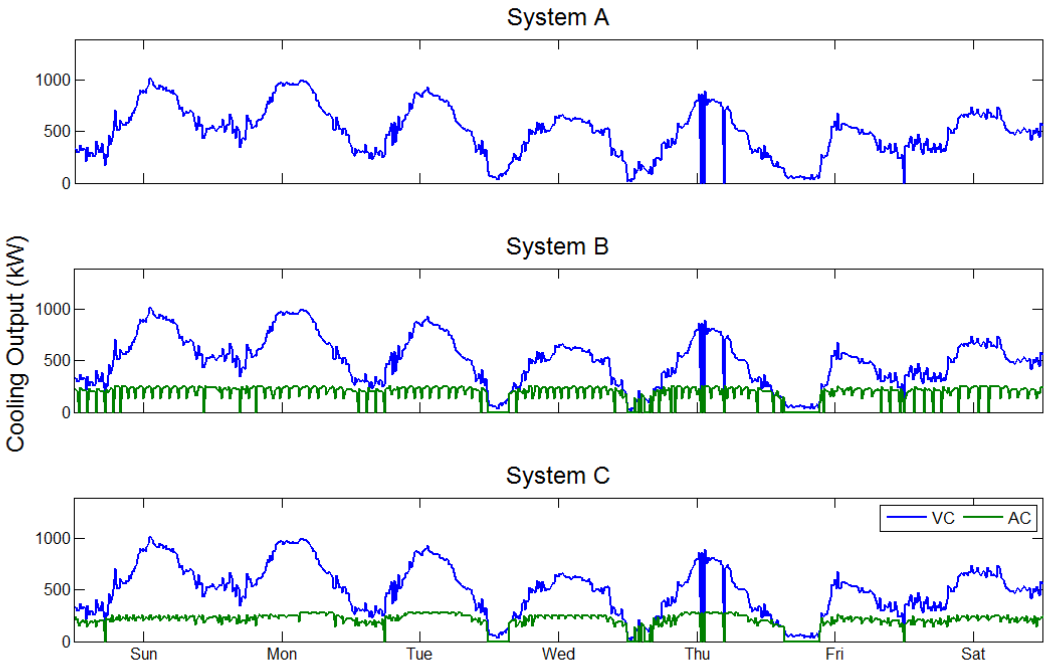

Figure 5-28: Winter cooling operation for all technology scenarios adopted at the UCI Cal IT² building

The steady stream of unused waste heat allows for the base cooling load to be shifted from the vapor compression system to the newly adopted absorption chiller. Under the AC-h scenario, when heating demand does occur, heat is directed to the HRU in order to meet as much of the heating demand as possible, resulting in a dip in absorption chiller cooling output. Under the AC-l scenario, this behavior still occurs, but with a smaller impact to the overall amount of cooling produced. Both scenarios increase fuel utilization from 54% under the HRUo scenario to 71% and 70% under the AC-h and AC-l scenario respectively.

Note that the extremely transient behavior of the heating demand forces the absorption chiller to also operate in an extremely transient manner Figure 5-29. Figure 5-29 shows the charging of the absorption chiller (AC Charging), the discharging of any stored thermal energy in the form of cooling (AC Discharging), the heat passed to a thermally activated chiller and directly turned into cooling (Direct Cooling), and the resulting absorption chiller state of charge (AC Storage). The combined Direct Cooling and AC Discharging form the absorption chiller cooling output seen in Figure 5-28. While the total cooling output is relatively constant, Figure 5-29 shows constant charging and discharging of the absorption chiller. When heating demand does occur, waste heat supply to the absorption chiller is reduced and the stored heat in the chiller is converted to cooling. This results in the absorption chiller state of charge to decrease. In subsequent time steps, when heating demand is nonexistent, the waste heat from the fuel cells is diverted back to the absorption chiller, recharging the system so that cooling can continually produce. This behavior is not as extreme under the AC-l scenario, indicating that as cooling can be produced using an absorption chiller at lower cost, it becomes more valuable to continually provide waste heat to the absorption chiller in lieu of providing heat to the HRU.

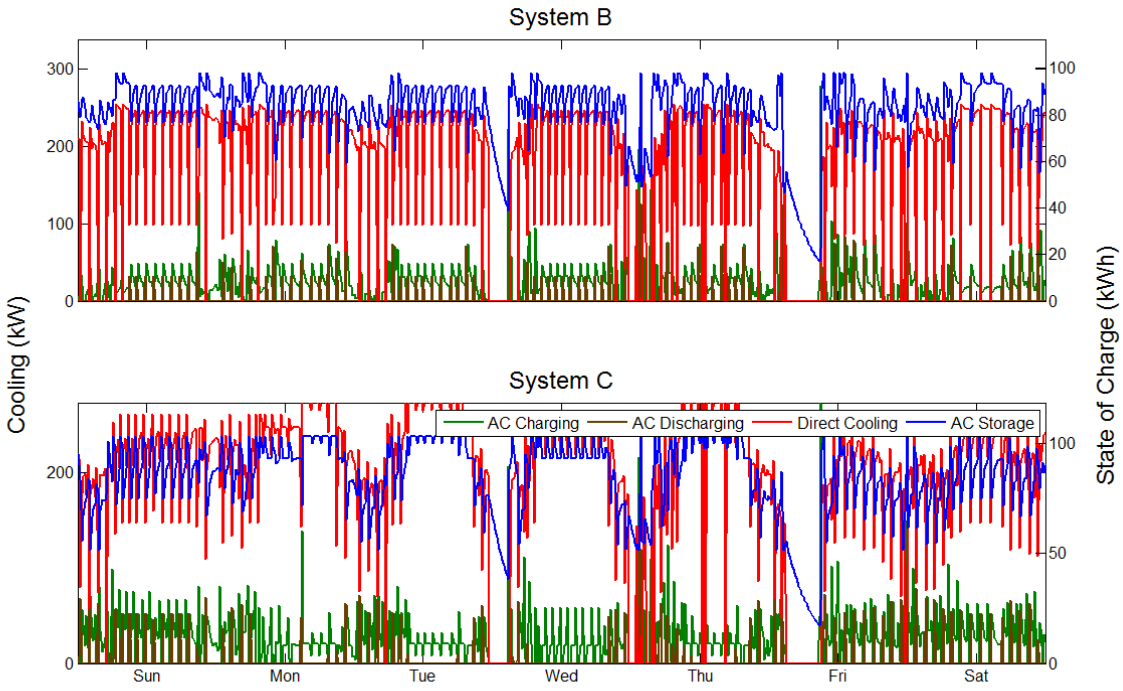

Figure 5-29: Winter absorption chiller operation for all technology scenarios adopted at the UCI Cal IT^2 building

As more waste heat is passed through the absorption chiller, less heat is available for use by the HRU. However, the fuel cell exhaust stream still has some useful heat content after passing through the absorption chiller, which can be used by the HRU. The leftover thermal energy can be directed through a duct in series with the absorption chiller into the HRU. Under the AC-h scenario, approximately 19% of the total heating production from the HRU is produced using energy captured from the exhaust stream exiting the absorption chiller. This percentage increases to 26% in the AC-l scenario.

Figure 5-30, Figure 5-31, Figure 5-32, and Figure 5-33 show the electrical, heating, cooling, and absorption chiller operation during the summer for the UCI Cal IT ^{2} building. Comparing these figures to the winter counterparts shows that in general, winter and summer

operation are similar, except that the fuel cell system experiences greater turndown during off-peak period.

Absorption chiller operation reduced the maximum combined electrical demand created by the combination of the electrical and cooling load by 75 kW for the AC-h scenario and 81 kW for the AC-l scenario.

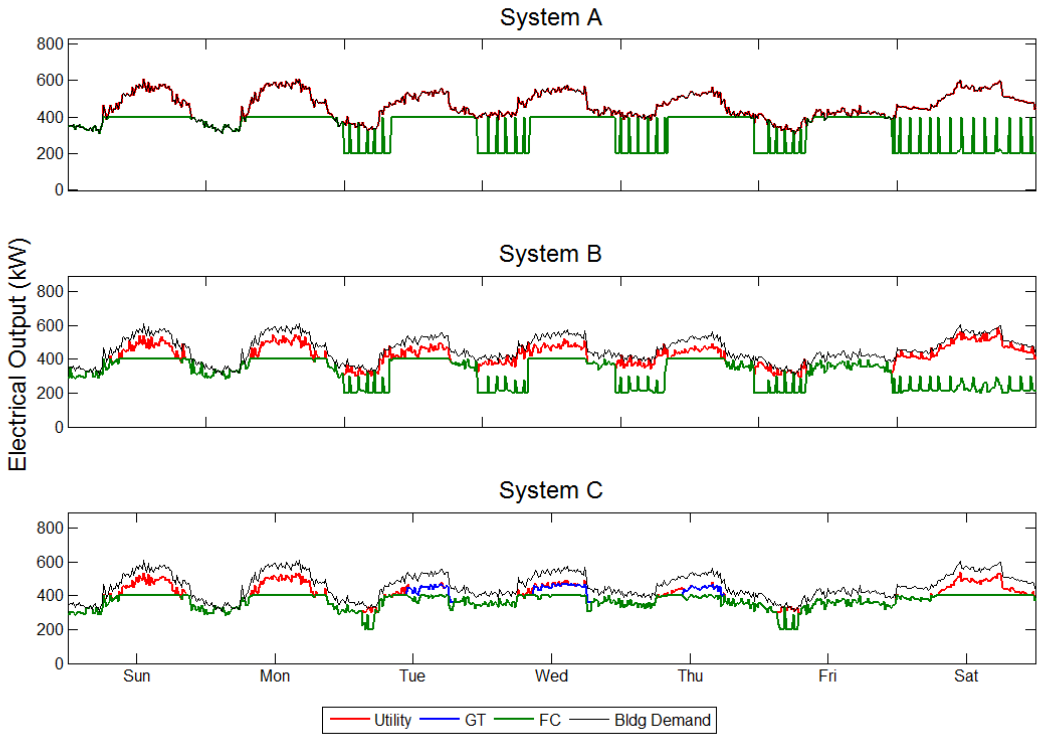

Figure 5-30: Summer electrical operation for all technology scenarios adopted at the UCI Cal IT^2 building

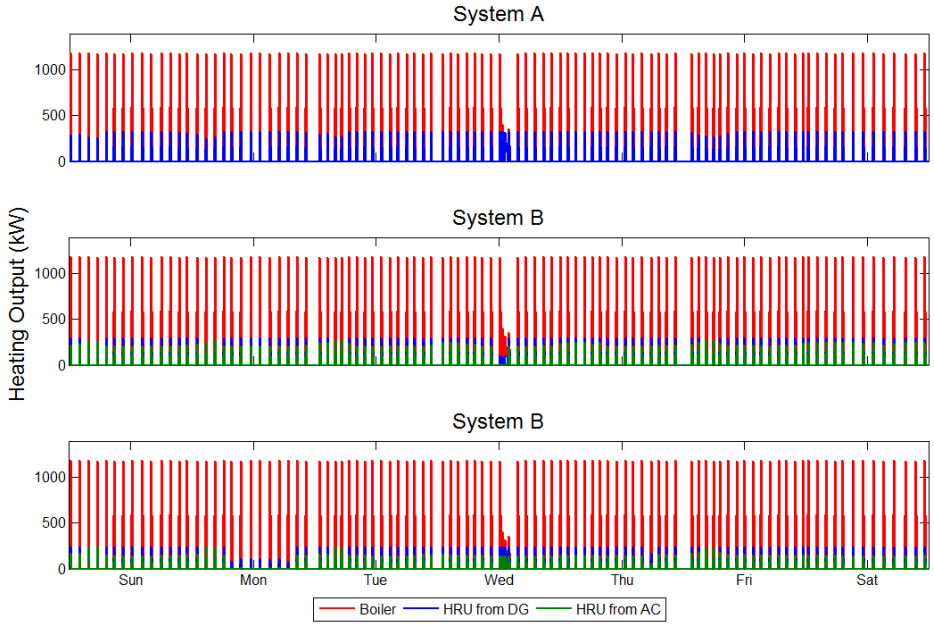

Figure 5-31: Summer heating operation for all technology scenarios adopted at the UCI Cal IT² building

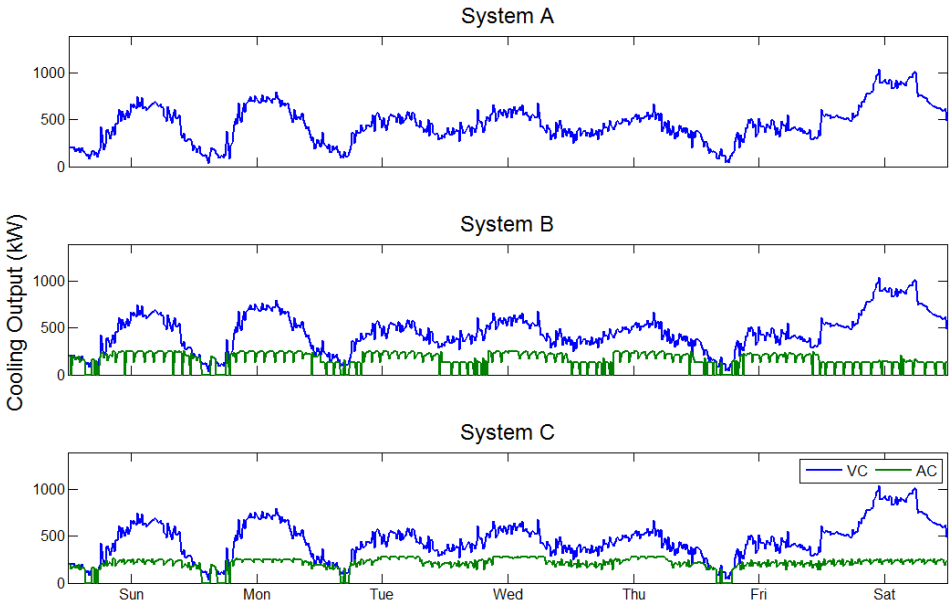

Figure 5-32: Summer cooling operation for all technology scenarios adopted at the UCI Cal IT² building

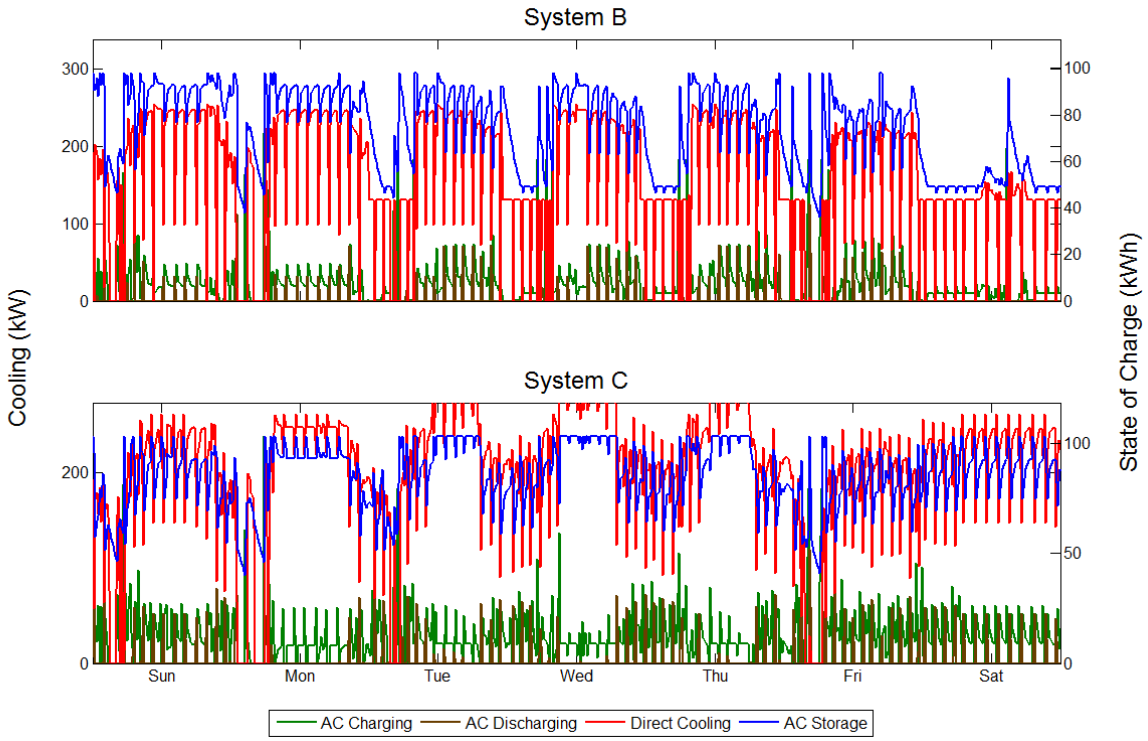

Figure 5-33: Summer absorption chiller operation for all technology scenarios adopted at the UCI Cal IT^2 building

5.2.2.2 A Note on UCI Cal IT^2 Suggested Operation

One of the primary assumptions made prior to optimization is that the building energy demand has already been modified such that energy consumption has been minimized in an economically efficient manner. While this may be true of a building like UCI Cal IT^2, the transient behavior exhibited by the heating load suggests that this is not the case. Also, the optimization results produced for the UCI Cal IT^2 building present obvious operational issues, particularly for the fuel cells and absorption chillers. Some portions of the suggested fuel cell operation require a sharp increase in electrical power output, followed by a sharp decline. While a fuel cell may be capable of following such transients, it is most likely not desirable from the perspective of maintaining the durability (lifetime) of the fuel cell systems. This behavior would

not even be acceptable for a more mechanically robust device, such as a microturbine. Combined with the thermal cycling of the absorption chiller, the suggested operation may lead to premature degradation of the adopted technologies.

It would be desirable to implement additional constraints into the CCHP system optimization model limiting the behavior of the adopted technologies. From an optimization perspective, such a modification is most likely undesirable unless it reduces the number of active constraints or decision variables included in the optimization. If the opposite is true, it is unlikely that an optimal or near optimal solution to what technologies should be adopted in a reasonable amount of time. It is obvious that the suggested fuel cell and absorption chiller operation are most likely undesirable and would not be implemented in real life. Instead of abandoning the overall optimization results and optimization model, the optimal system suggestion should be tested with a more realistic dispatch to determine if the resulting cost of realistic operation continues to reduce the cost of energy. For example, the fuel cell cycling appears to primarily occur during summer off-peak periods when the transient heating demand occurs. If the fuel cell cycling is performed for the sake of providing heat to the HRU, and the increased operation results in a marginal savings, then this behavior may be ignored while maintaining the financial integrity of an investment in the CCHP system. Similar analysis can be carried out for the other adopted technology, such as the absorption chiller.

Considering all of this, it important to note that this particular building will most likely need some additional improvements, especially to modify the heating dynamics, prior to CCHP system integration. From the perspective of this work, the UCI Cal IT^2 provides a relatively small building with inconsistent thermal loads, providing insight into how the utilization of waste

heat to produce heat and cooling can improve overall fuel utilization, which is one of the largest primary benefits associated with CHP and CCHP systems.

5.2.2.3 Financial Performance

The overall financial performance of the three technology scenarios can be seen in Figure 5-34, which shows the modified internal rate of return over the course of 20 years, assuming that the CCHP system is able to maintain operation over the length of time at which the rate of return is calculated. The rate of return is determined by weighing the savings produced by adopting and operating a CCHP system versus how the building energy demand would traditionally be met (through the use of utility electricity and natural gas exclusively). As discussed in Section 3.7, the reinvestment rate is 8%. Neither of the HRUo and the AC-h technology scenarios produce above an 8% return until after ten years, or after the loan associated with the CCHP purchase, has been paid off. From the perspective of a business, the funds invested in a CCHP system with the characteristics the same as either the HRUo or AC-h scenarios would result in an undesirable investment since the same funds could be invested elsewhere with an 8% return.

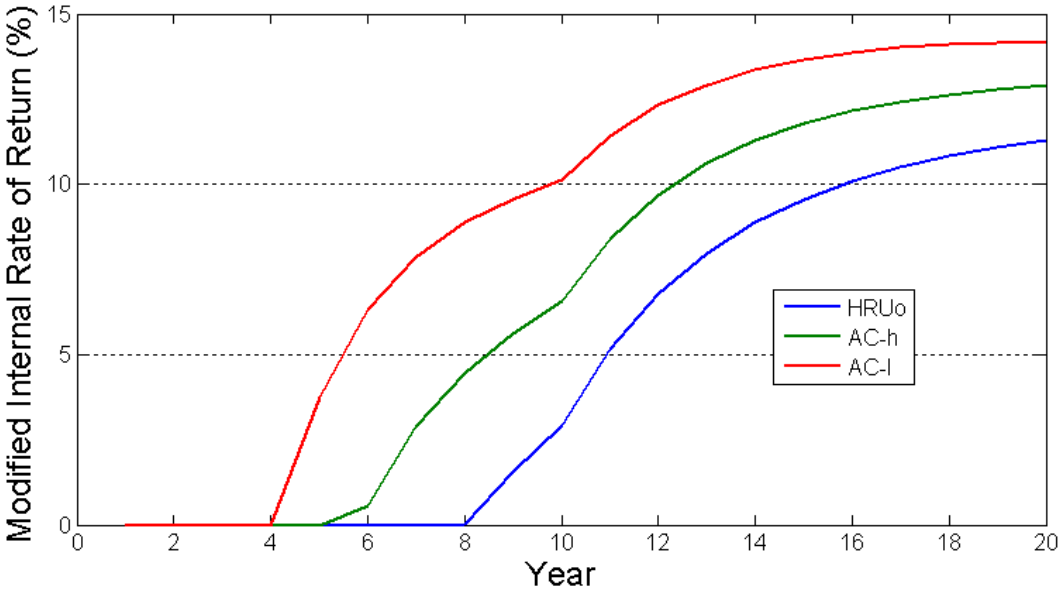

Figure 5-34: Modified internal rate of return for all three technology scenarios when adopted and operated at the UCI Cal IT^2 building

The AC-l scenario does achieve over an 8% return at year ten, with the system producing a 10% return. If the system in question were capable of consistent operation over the course of ten years, then investment in this CCHP system could be deemed desirable by a business or organization operating within the UCI Cal IT^2 building.

Most importantly, however, is the improvement in the rate of return, first, by providing another type of technology that can be adopted, and second, by reducing the operating cost of the new technology to parity with the other competing option. Particularly for the UCI Cal IT^2 building, the ability to meet part of the building load using an absorption chiller allows for the utilization of an unused stream of energy; the waste head produced by the fuel cells. In total, the absorption chiller is able to meet only 43% of the total cooling demand. This level of absorption chiller operation is leveraged to decrease utility imports, adopt a microturbine, and power the legacy vapor compression system primarily using electricity generated onsite. For the bottom

line, the addition of a low O&M cost absorption chiller appears to singlehandedly make an undesirable investment desirable.

The cost to purchase and operate the different adopted CCHP systems can be broken down to determine the cost contribution of each type of energy to the individual cost categories by using the method described in Section 3.5 and Section 3.5.2. Figure 5-35 shows the utility costs allocated to electricity, cooling, and heating production for the three technology scenarios. The actual cost incurred by operation using the system would compose of the sum of the individual electrical, cooling, and heating allocation. For example, for the HRUo scenario, the electrical energy cost incurred would be the sum of the blue bar from each of the subplots that belong to the utility energy portion of each subplot. This plot, and all other cost allocation plots similar to Figure 5-35 should be interpreted as each individual energy stream either results in the purchase or avoidance of a particular cost. For example, the electrical utility energy cost is increased naturally by the electrical load since the electrical utility energy can be used directly to meet the building demand. The heating load, however, encourages the use of other sources for supplying energy to the building (such as the adoption of four fuel cells). Since the heating demand supports the purchase of electricity from other sources other than the electrical utility, the heating portion of the utility energy cost is negative. By shifting the electrical energy use away from the electrical utility, the heating load has performed a "service" by reducing the utility energy demand and is compensated as a result.

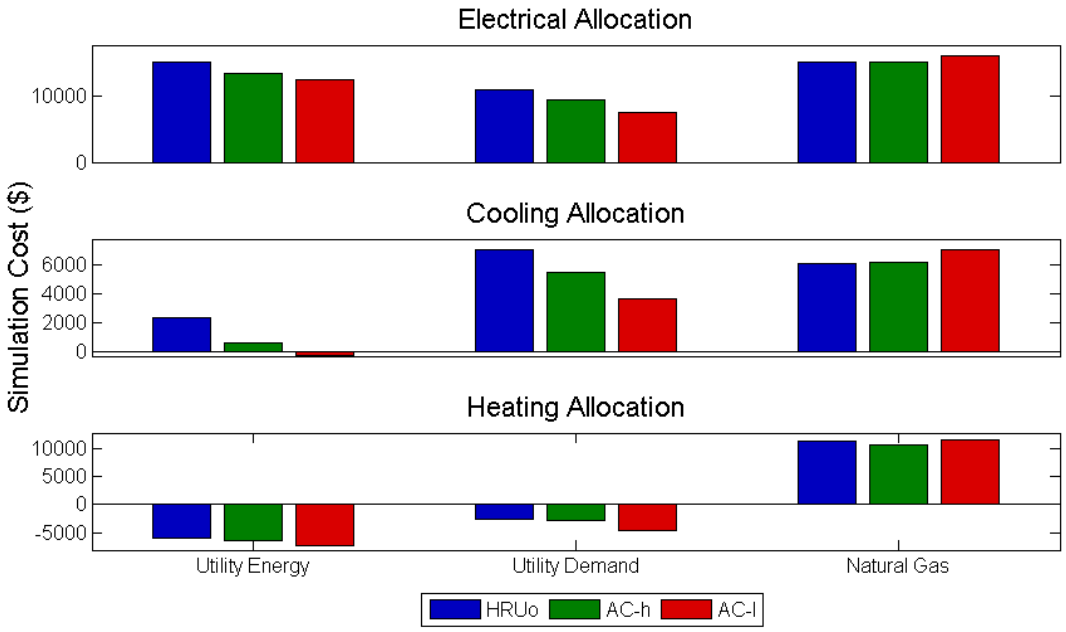

Figure 5-35: Utility costs allocated to the production of electricity, cooling, and heating for the three technology scenarios at UCI Cal IT²

For both utility energy and demand charges, total cost for all three types of energy decrease as the technology scenarios change from HRUo, to AC-h, to AC-l. Simultaneously, natural gas cost increases as electrical production is shifted from imported electricity to generation onsite using fuel cells. Note that the negative allocation to heating for utility energy balances out a large portion of the utility energy allocation to electricity and cooling, but not for utility demand charge, suggesting that the heating load is responsible for shifting a large portion of the overall energy procurement to onsite sources, but is unable to significantly reduce overall demand charges. Coupled with the knowledge of the transient nature of the UCI Cal IT^2 heating load, the heating load cannot continually drive fuel cell operation in a way that significantly reduces demand charges, resulting in a small negative allocation.

The cooling utility energy allocation only turns negative under the AC-l technology scenario. This suggests that absorption chiller operation does not drive fuel cell operation until absorption chiller O&M costs reach parity with vapor compression O&M. Prior to this occurrence, electrical energy is still imported in order to produce cooling onsite.

Figure 5-36 shows the allocated fuel cell and microturbine operations and maintenance costs. Since a microturbine is used to supply only a fraction of the overall building energy demand, the microturbine O&M cost is marginal compared to fuel cell O&M cost. The allocation to the three types of energy show that fuel cell operation does not change significantly across the technology scenarios, a fact already shown by the small different in overall fuel cell output. The primary driver for fuel cell operation is shown to be the electrical load due to the large size of the fuel cell O&M cost allocated to electricity relative to both cooling and heating.

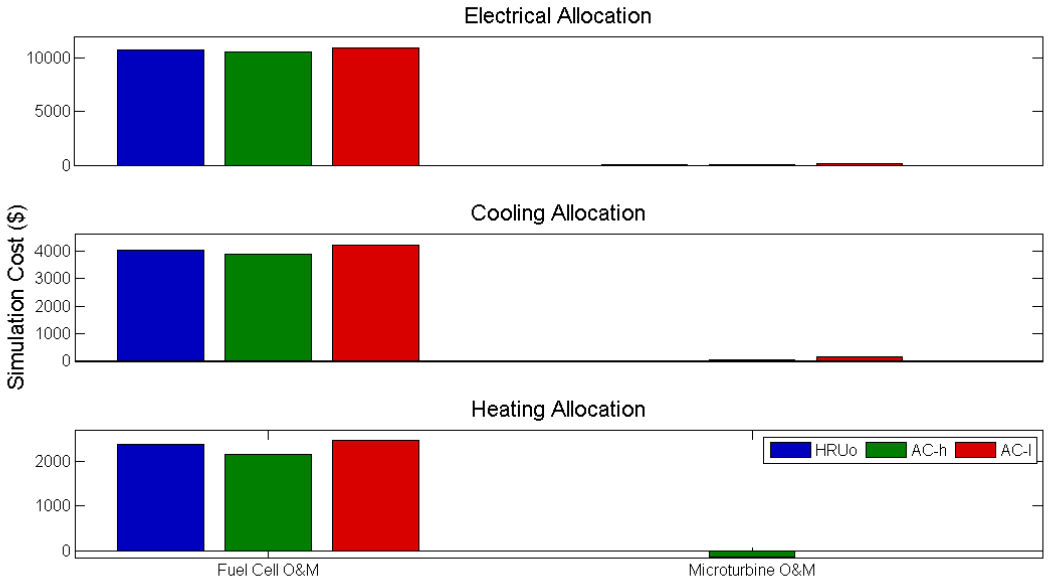

Figure 5-36: Fuel cell and microturbine O&M costs allocated to the production of electricity, cooling, and heating for the three technology scenarios at UCI Cal IT²

Figure 5-37 shows the vapor compression and absorption chiller costs allocated for the three technology scenarios to the electrical, cooling and heating load. As expected, vapor compression and absorption chiller O&M costs are allocated to the cooling load. Both the electrical and heating load receive a negative vapor compression O&M allocation. This suggest that both loads drive a shift away from vapor compression operation. Since the electrical load is the primary driver for fuel cell operation, the electrical load can be viewed as responsible for the production of the waste heat used to power the absorption chiller, which offsets vapor compression operation. Likewise, the heating load is also responsible for the adoption and operation of the fuel cells, also assisting in shifting the cooling load away from the vapor compression system to the absorption chiller. Due to the role played in increasing absorption chiller use, both the electrical and heating loads are allocated a portion of the total absorption chiller O&M cost.

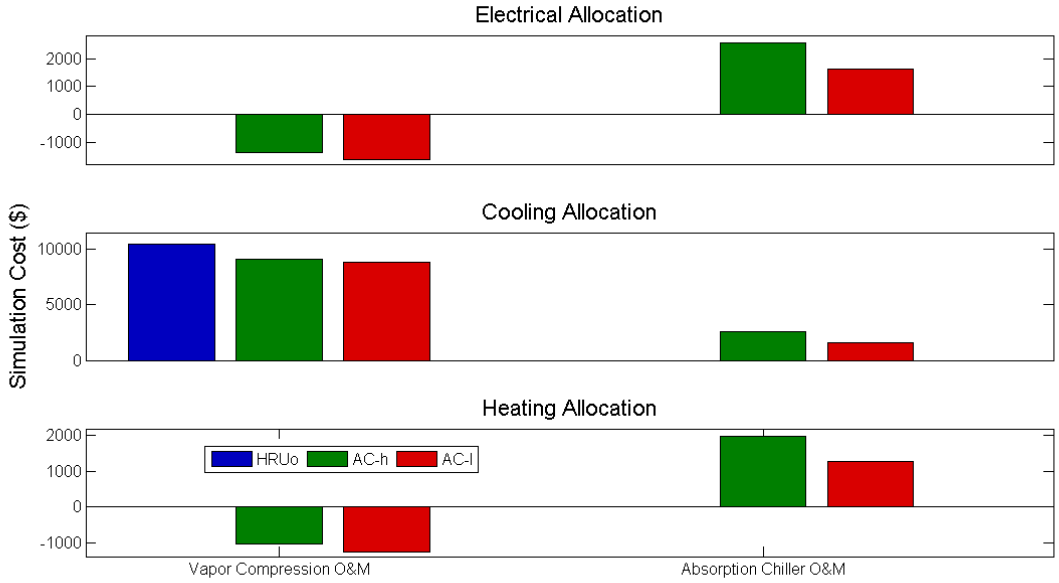

Figure 5-37: Vapor compression and absorption chiller O&M costs allocated to the production of electricity, cooling, and heating for the three technology scenarios at UCI Cal IT²

Figure 5-38 shows the cost allocation for boiler and heat recovery unity O&M cost. Similar to cooling, the legacy system O&M costs are primarily allocated to the applicable type of energy, or boiler costs are primarily allocated to heating. Notice, however, that cooling receives a small boiler O&M allocation under the AC-l technology scenario. Due to the increased absorption chiller operation under this scenario, heat that normal is provided to the heat recovery unit under the other two technology scenarios is diverted to the absorption chiller, resulting in increased boiler operation and a slight boiler O&M cost allocation to cooling (although the actual allocation is on the order of less than one dollar). Heat recovery unit O&M cost is almost equally shared by all three energy types, suggesting that any HRU operation is driven not primarily by heat, but simultaneously by all types of energy. Similar to the absorption chiller, HRU operation occurs due to the presence of an electrical and cooling load in addition to a heating load.

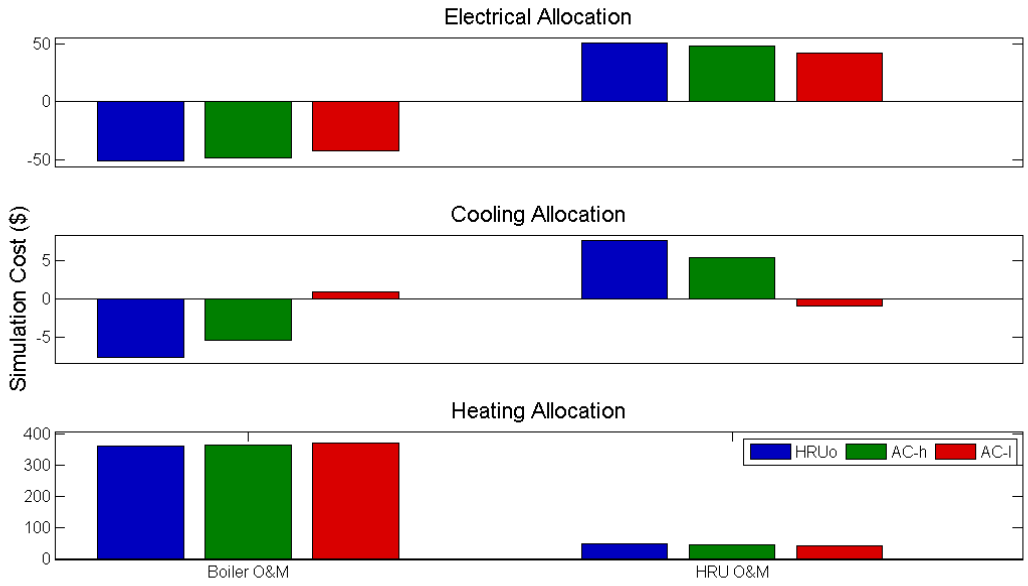

Figure 5-38: Boiler and heat recovery unit O&M costs allocated to the production of electricity, cooling, and heating for the three technology scenarios at UCI Cal IT²

Figure 5-39 shows the fuel cell and microturbine loan allocation for the electrical, cooling, and heating load for the three technology scenarios. Another way to view Figure 5-39 is as which type of energy drives the adoption of the different available technology. For the HRUo scenario, only the electrical and cooling loads are responsible for the adoption of the four fuel cell systems. Under this scenario, the electrical and heating load combined would adopt a microturbine. However, the cooling load blocks this investment in favor of more fuel efficient fuel cell systems.

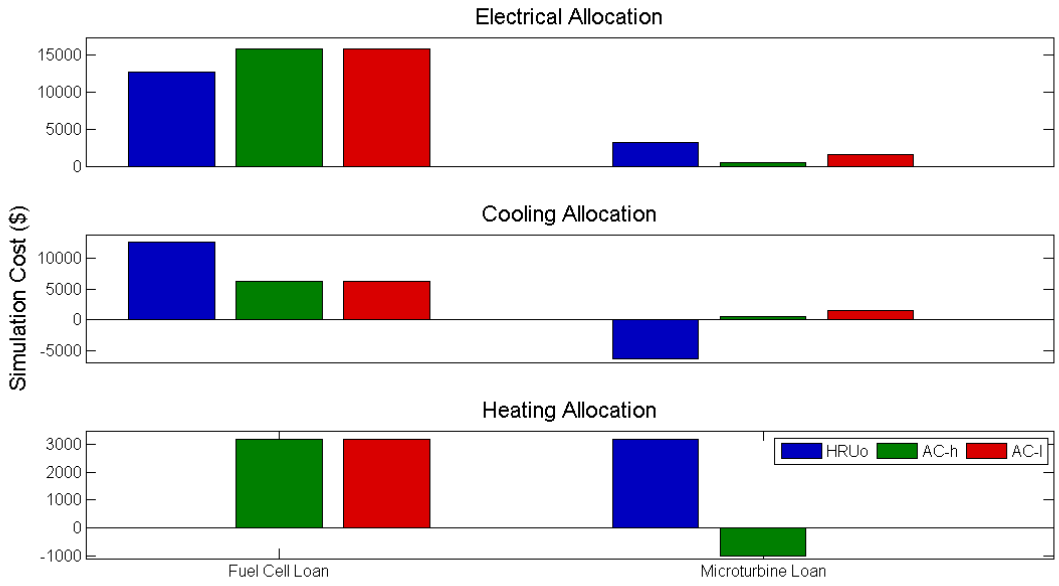

Figure 5-39: Fuel cell and microturbine loan costs allocated to the production of electricity, cooling, and heating for the three technology scenarios at UCI Cal IT²

Under the AC-h scenario, where an absorption chiller can be purchased, all types of energy support the purchase and operation of four fuel cell systems. The decision to purchase a fuel cell, however, is driven primarily by the electrical load. The cooling load actually supports the purchase of a smaller set of fuel cells. Since the absorption chiller can offset the use of

electricity provided to the vapor compression system, the absorption chiller system reduces the overall electrical load created by the building, reducing the number of fuel cells that need to be purchased. In fact, the absorption chiller option drives the decision to invest in a microturbine, with the heating load blocking this decision in the AC-h scenario.

Figure 5-40 shows the absorption chiller, heat recovery unit, and duct-parallel loan payment allocations to the three types of energy for the three technology scenarios. When available for adoption, the absorption chiller loan payment cost is shared equally by all three energy types. The heat recovery loan payment cost is shared equally across all three types of energy under the HRUo technology scenario, but only across electrical and heating load under any scenario that includes an absorption chiller. The duct-parallel loan payment is supported by the electrical and heating load but receives a negative allocation towards the cooling load. Since some heat is still available in the exhaust stream exiting the absorption chiller, the cooling load supports the adoption of a large duct-series instead of duct-parallel. The duct-series allocations are not shown because they are small compared to the allocations associated with all other technologies shown in Figure 5-40.

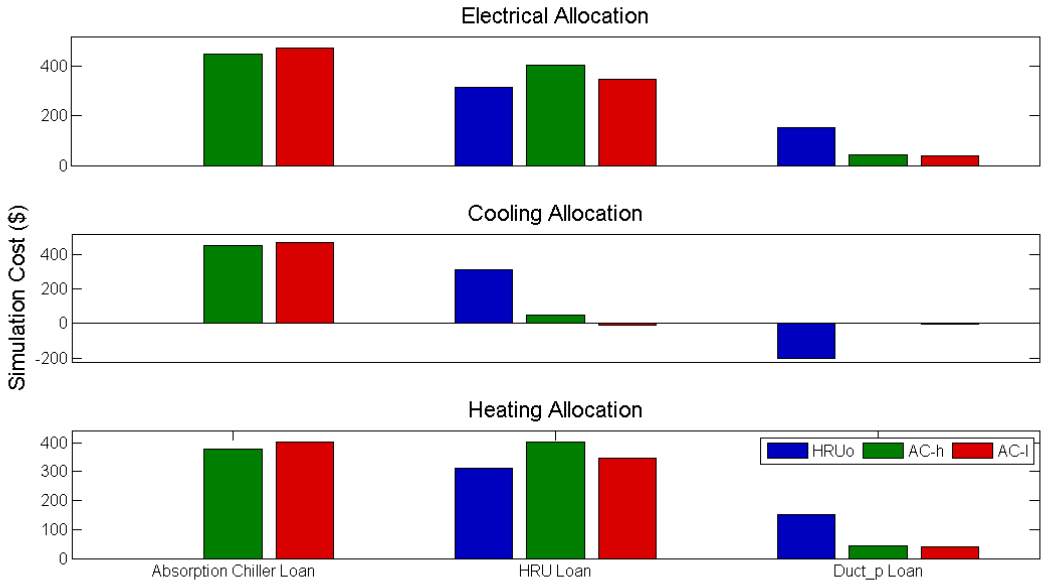

Figure 5-40: Absorption chiller, heat recovery unit, and duct-parallel loan costs allocated to the production of electricity, cooling, and heating for the three technology scenarios at UCI Cal IT²

The results presented in Figure 5-35 through Figure 5-40 represent the cost of meeting the UCI Cal IT² building energy demand. Figure 5-35 through Figure 5-38 show the operational cost and Figure 5-39 and Figure 5-40 show the financing cost for a CCHP system. The same method used to allocate the CCHP system operation costs can be used to determine the cost of meeting all building energy demand through the purchase of utility electricity and natural gas exclusively. With the cost to meet building energy using local utilities only established, the difference in cost for each type of energy as a result of CCHP adoption can be assessed. Finally, the results presented in Figure 5-40 and Figure 5-41 also indicate the energy type responsible for the adoption, or investment, in any particular CCHP technology, allowing for the initial investment made to be allocated across the three types of energy. With a defined investment and resulting savings associated with each type of energy, the financial performance of the investment in each type of energy can be evaluated.

The case against which the CCHP investment is compared is the scenario where the building electrical and cooling loads are met through the purchase of utility electricity and the heating load is met through the use of a boiler fired using natural gas. This baseline scenario produces a baseline levelized cost for the three types of energy as follows: $0.095 per kWh for electricity, $0.0477 per kWh for cooling, and $0.0239 per kWh for heating.

Using the allocated costs and associated investment made in each type of energy, the financial performance versus the baseline scenario can be determined. The resulting difference to the levelized cost of energy and modified internal rate of return is shown in Figure 5-41 for the three types of energy and the three technology scenarios analyzed. For all scenarios, the investment in electricity results almost always in an increased cost of electricity, with the levelized cost of electricity at five years increasing by over $0.01 per kWh. If the CCHP system remains operational, the levelized cost of electricity shrinks, reducing the loss associated with producing electricity onsite. If the CCHP system remains operational for nine years, near parity with the baseline system is achieved. While the adoption of a CCHP system almost always increases the cost of electricity, allowing for other technologies, such as an absorption chiller reduces the cost of electricity. If that absorption chiller can be maintained at a cost comparable to the baseline scenario (or a vapor compression system), then the cost of electricity can be reduced to the point of actually reducing the cost of electricity, as seen in year nine for the AC-l system. With nearly all systems increasing the cost of electricity, no rate of return occurs, signifying that the investment results in an increased cost of electricity.

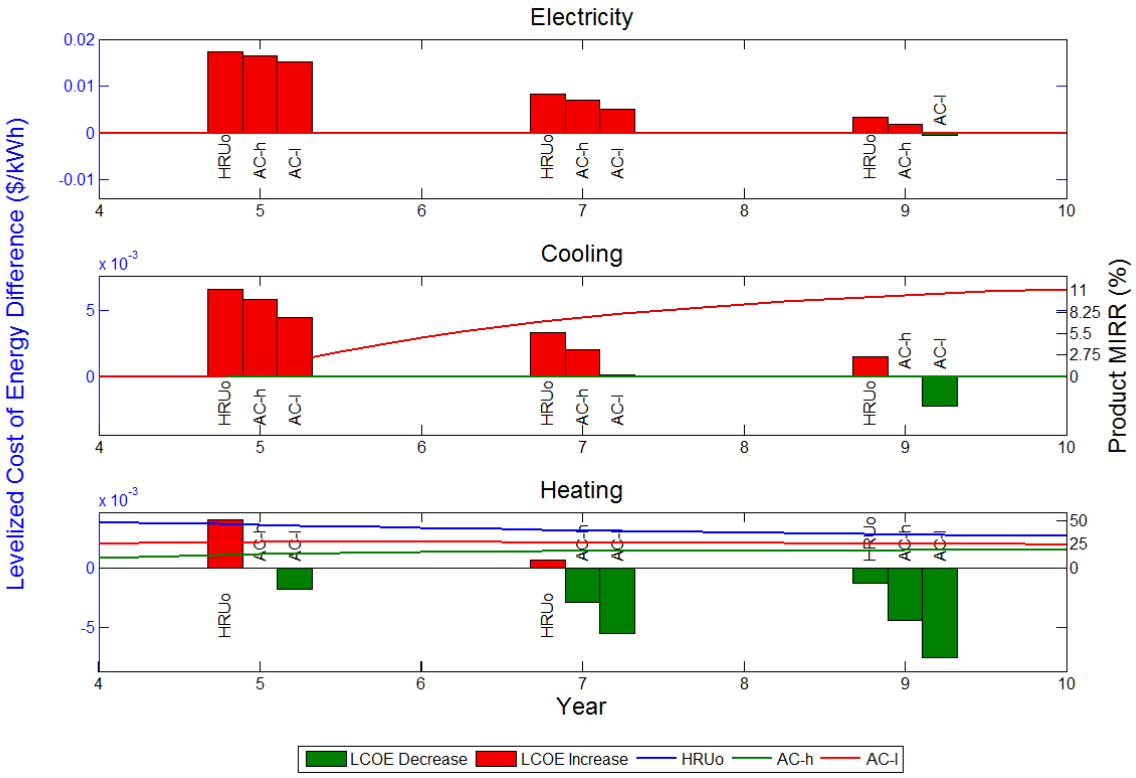

Figure 5-41: Levelized cost of energy difference at years five, seven, and nine and corresponding modified internal rate of return for electricity, cooling, and heating when CCHP systems are adopted according to the three technology scenarios

The levelized cost of cooling and heating both experience similar behavior to electricity. Increasing the years over which the system is operational results in a decreased levelized cost. Also, allowing for the adoption of an absorption chiller (especially if the chiller can be maintained at a cost comparable to a vapor compression system) reduces the cost of each type of energy at each year. Similar to electricity, cooling is also initially produced at a loss for all technology scenarios. The cost of cooling never reaches parity with the baseline scenario, while the AC-h reaches parity at year nine. The AC-l scenario, however, reaches near parity with baseline cooling costs in year seven followed by a decrease in cost of cooling in year nine. As a

result, the only cooling investment that produces a positive return is the AC-l scenario, with a return of over 8% being realized in year nine.

Unlike electricity and cooling, the investment associated with heating always produces a lower cost of heating by year nine. While a loss is still realized in year five under the HRUo technology scenario, the AC-h scenario reaches parity with the baseline scenario, and the AC-l scenario produces a savings. Increasing the time over which the CCHP system remains operational only improves the financial performance associated with heating. As a result of the reduction to heating costs, the corresponding rates of return are incredibly high. The highest rate of return experienced is for the HRUo system, which achieves a modified internal rate of return over 51% by year three. Under this scenario, the heating load is allocated no fuel cell investment cost, and the heat recovery unit cost is split between electricity, heating and cooling. With a low initial investment cost associated with heating, relatively large savings are produced, resulting in a large rate of return. Note that since any savings are reinvested at 8% while calculating the modified internal rate of return, the rate of return associated with heating decreases as the effect of large savings are muted by a more reasonable return from reinvestment.

Allowing for the adoption of an absorption chiller results in the allocation of a portion of the fuel cell investment cost to heating. With a larger initial investment, the rate of return decreases from the HRUo technology scenario to the AC-h scenario. Despite the larger investment, heating reaches parity with the baseline scenario faster under the AC-h scenario. While saddled with a larger investment cost, excess heating can be provided from the absorption chiller to the heat recovery unit for capture. This waste heat only has a portion of the original heat content remaining. In addition, much of the cost associated with the production of the waste

heat is absorbed by the cooling load, allowing the HRU access to an even lower cost source of heat than a fuel cell or absorption chiller. Heating enjoys even better performance under the AC-l technology scenario, where the absorption chiller utilizes waste heat from the four fuel cells and microturbine first more consistently, increasing the amount of low cost waste heat available to the HRU.

5.2.2.4 Building Carbon Emissions

Using the same method to allocate the different cost components, CO_2 emissions associated with the import of electrical energy and the use of natural gas in a DER system or boiler can be allocated to electricity, cooling and heating. Assuming that the baseline scenario is where all electrical energy required by the building to meet any electrical or cooling load is met using a utility with a CO_2 emissions profile as described in Section 3.6, and all heating is met using a natural gas fired boiler, the carbon emissions associated with the baseline energy supply to the building is shown in Figure 5-42 for an entire year. In total, UCI Cal IT^2 energy use results in the emission of 1,445 tonnes of CO_2 per year.

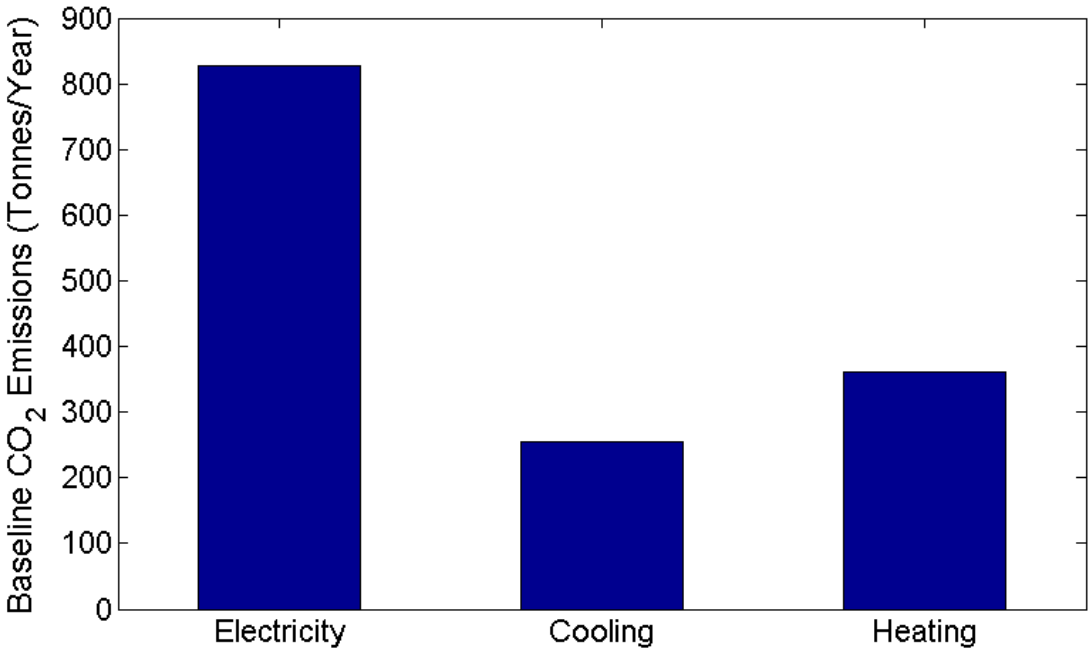

Figure 5-42: Yearly baseline carbon emissions for the UCI Cal IT² building

The adoption of DER systems affects total CO_2 emissions. In the case of UCI Cal IT², the adoption of a DER system increases carbon emissions for all technology scenarios, as seen in Figure 5-43. Note that CO_2 emissions were not constrained during optimization. Also, the utility grid from which electricity is imported operates with one of the lowest carbon emissions factors in the United States [174]. The result that carbon emissions increase as a result of DER system adoption is due primarily to the reduced carbon emissions emitted while producing utility electricity, not low efficiency associated with onsite generation.

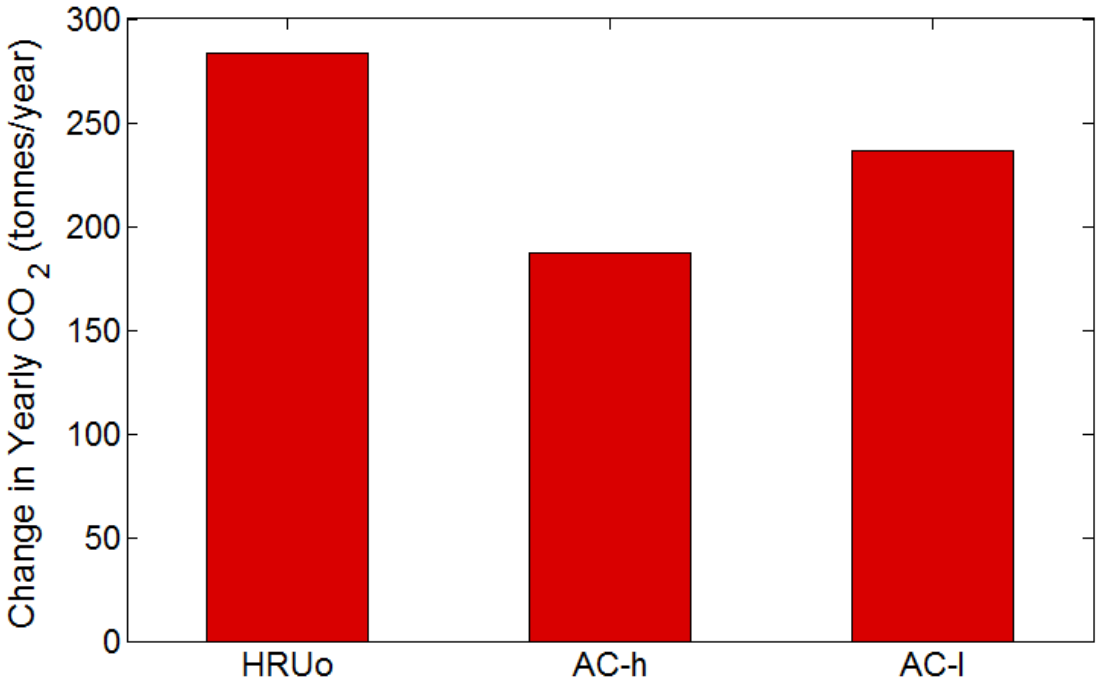

Figure 5-43: Change in yearly carbon emissions for the UCI Cal IT² building as a result of DER system adoption

The source of carbon emissions increase can be traced back to the individual type of energy producing an increase in emissions. Figure 5-44 shows the increase in emissions allocated to the three types of energy supplied to the building for the three technology scenario. Figure 5-44 clearly shows that carbon emissions increase greatest for electrical energy. Heating also always produces an increase in carbon emissions, while cooling produces an increase when an absorption chiller is not available under the HRUo technology scenario, but decreases carbon emissions when the absorption chiller is available.

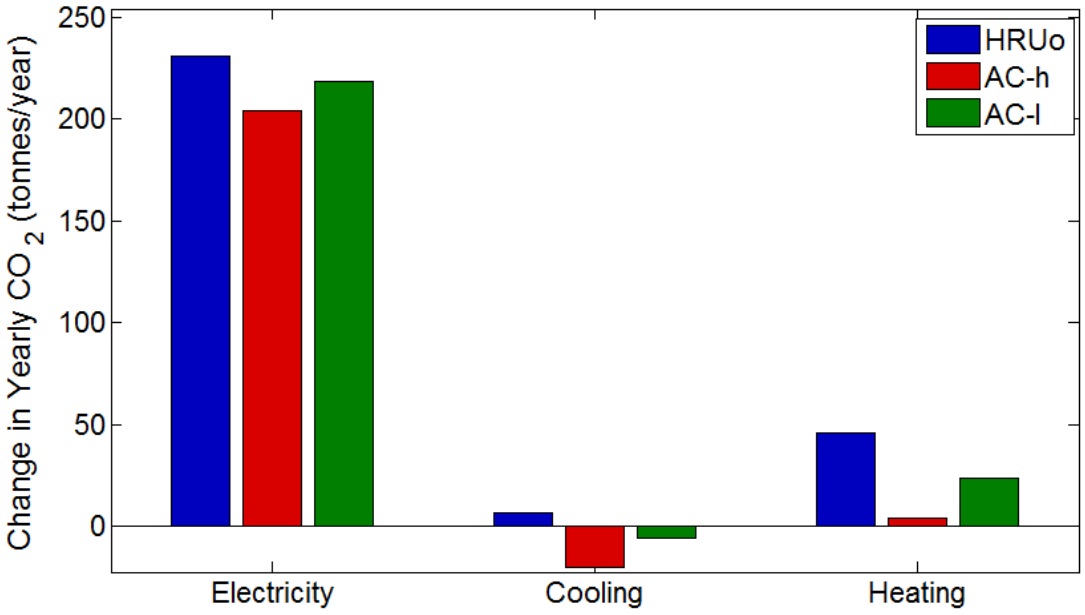

Figure 5-44: Change in yearly carbon emissions for individual types of energy for the UCI Cal IT² building as a result of DER system adoption

Under the HRUo technology scenario, only 54% of fuel energy used in the DER system is utilized in the form of electricity and heat supplied to the building. Combined with the low carbon emission factor associated with grid electricity, this scenario experiences the greatest increase to carbon emissions. Allowing for absorption chiller adoption tempers the increase to carbon emissions due to electricity and heating, while producing a decrease in cooling emissions from baseline carbon emissions. Under the AC-h technology scenario, total fuel cell electrical energy output is reduced by 3.1% from output under the HRUo scenario while grid imports also decrease by 30.1%. While an overall increase to carbon emissions are experienced under the AC-h scenario, the combined attributes of reducing both onsite generation output and grid imports allows for this scenario to achieve the lowest total carbon emissions for any of the DER technology scenarios. Shifting to the AC-l scenario reduces grid imports by 72% from the HRUo

scenario, but fuel cell operation increases by 2.7%. As a result, carbon emissions increase over AC-h scenario levels.

5.2.3 SCAQMD Building

The South Coast Air Quality Management District (SCAQMD) building has an average electrical demand of 781 kW and an electrical load factor of 0.41. The heating load is coincident with the electrical load 62% of the time and the ratio of the total heating load to the electrical load is 1.64. The cooling load is coincident with the electrical load 49% of the time, and the ratio of the total cooling load to the electrical load is 0.95. When the electrical, cooling, and heating loads are met by traditional utility sources, the cost of energy is $0.0986 per kWh for electricity, $0.0486 per kWh for cooling, and $0.0193 per kWh for heating.

Table 5-4 shows the optimal DER system design for SCAQMD under the three technology scenarios. A combination of fuel cells and microturbines are always adopted. Absorption chiller adoption also always occurs when allowed, and increases significantly when absorption chiller O&M is reduced during the AC-l technology scenario. When moving from the HRUo to AC-h scenario, heat recovery unit adoption increases, then decreases when moving to the AC-l scenario.

Table 5-4: Optimal CCHP system design for all technology scenarios operating at the SCAQMD building

Technology Scenario	Fuel Cell (100 kW)	Microturbine (65 kW)	AC (kW)	HRU (kW)	Duct - Parallel (kW)	Duct - Series (kW)
HRUo	7	3	n/a	1033	1147	n/a
AC-h	6	4	150	1102	1225	60
AC-l	6	5	531	741	823	213

5.2.3.1 DER System Operation

Figure 5-45 shows the source of electrical energy for the three technology scenarios. The total amount of electricity consumed onsite under the HRUo scenario is the same as the baseline scenario. Total electricity consumption falls by 0.5% under the AC-h scenario and by 6.5% under the AC-l scenario. Across these three scenarios, the installed fuel cells provide the majority of the power. While producing 59% of the total electricity consumed at the SCAQMD building, fuel cell output falls by 12% when moving from the HRUo to AC-h scenario, and 9.2% when moving from the HRUo to AC-l scenario. These reductions are primarily due to the number of fuel cells installed changing from seven to six once an absorption chiller is made available for adoption. Electrical imports increase by 11% when moving from the HRUo to AC-h scenario, and then decrease by 20% when moving from the HRUo to the AC-l scenario. Moving across the same scenarios, microturbine output increases by 34% and 41% respectively, increasing as more microturbines are adopted.

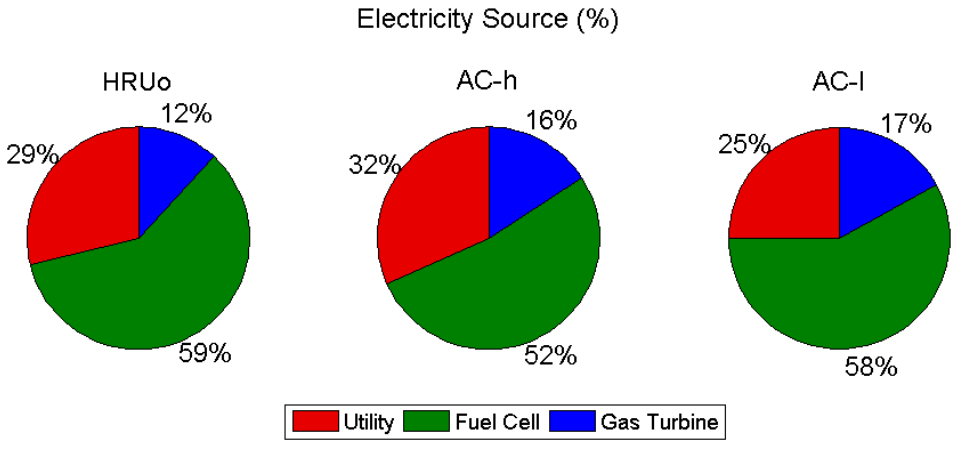

Figure 5-45: Source of electricity to meet the SCAQMD electrical demand for all technology scenarios

Figure 5-46 shows the source of cooling for the AC-h and AC-l technology scenario. When first adopted under the AC-h technology scenario, the absorption chiller is used to meet a fraction of the total cooling load. As the absorption chiller O&M is reduced to parity with vapor compression O&M, the size of the absorption chiller increases 354%, and the total amount of cooling produced by the absorption chiller increases by 1,342%. Despite the increase, the majority of the cooling load is met by the legacy vapor compression chiller.

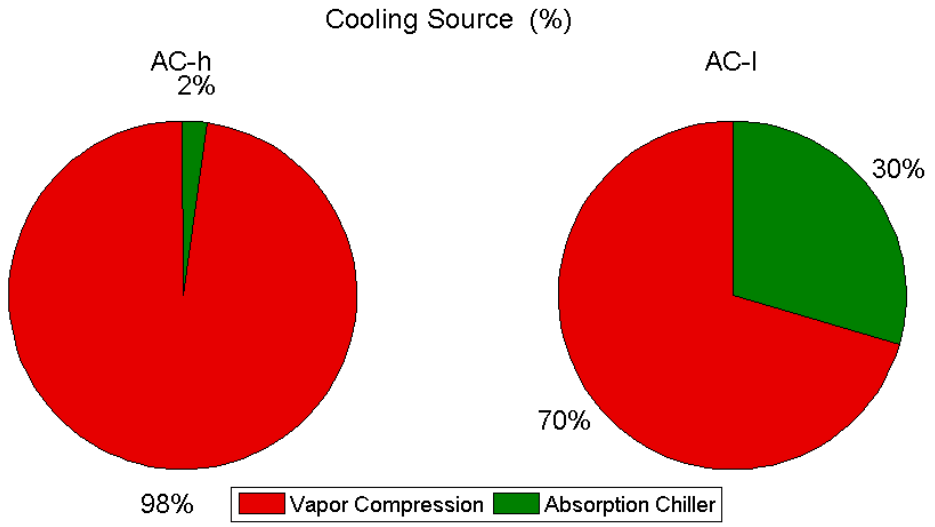

Figure 5-46: Source of cooling to meet the SCAQMD cooling demand for all technology scenarios

Figure 5-47 shows the source of heating for the three technology scenarios installed at SCAQMD. For all three technology scenarios, the legacy boiler is sued to meet the majority of the building heating load. The heat recovery unit meets a large portion of the heating demand, but this portion decreases as absorption chiller operation increases. Overall, the DER system

achieves a relatively high DER system fuel utilization, with, the HRUo, AC-h, and AC-l systems achieving fuel utilizations of 73%, 75%, and 75% respectively.

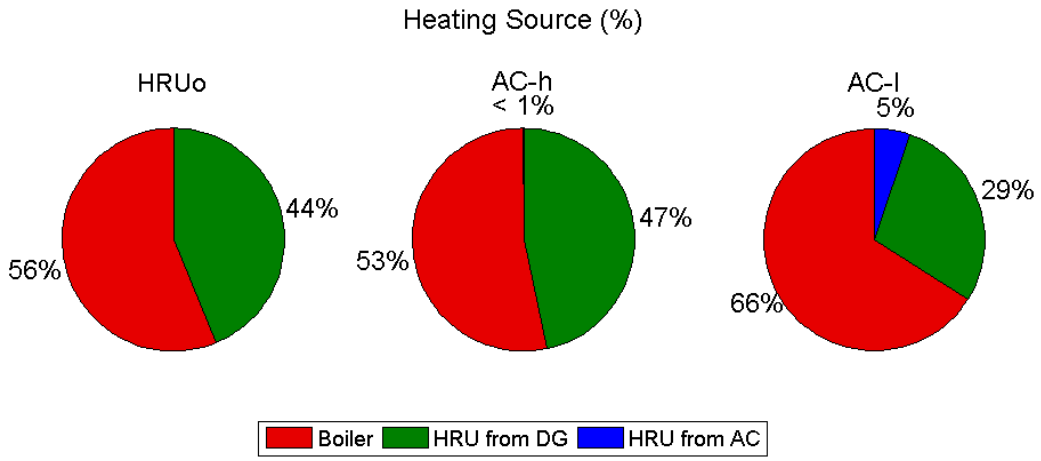

Figure 5-47: Source of heating to meet the SCAQMD heating demand for all technology scenarios

Figure 5-48 shows a week of electrical operation during the winter for all three technology scenarios at the SCAQMD building. Similar to the prior buildings studied, the installed fuel cells perform load following, producing the maximum amount of electricity possible across the three scenarios. The microturbines are only operated during the middle of the day. A single instance where all fuel cells shut down while the microturbines continue to provide power occurs during the Wednesday morning under the HRUo scenario.

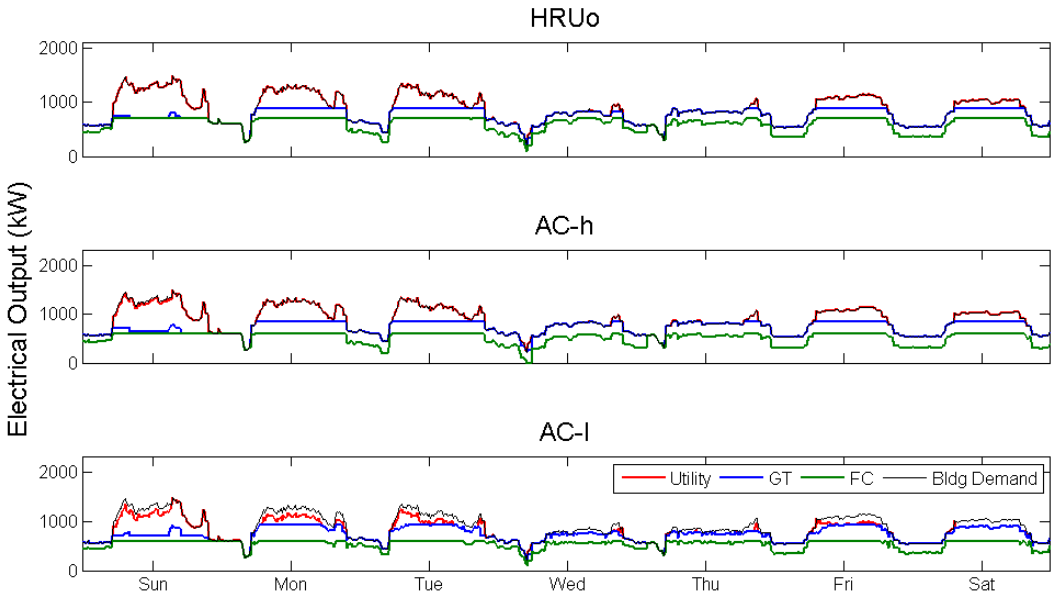

Figure 5-48: Winter electrical operation for all technology scenarios adopted at the SCAQMD building

Figure 5-49 shows the heating operation for the same week as the electrical operation. The particular instance where the fuel cells shut down correspond to a period where heating demand is high. The fuel cells are shut off so that the microturbines can meet the electrical demand while supplying a large stream of waste heat to be captured using the heat recovery unit. Under the HRUo and AC-h scenario, the HRU is used to provide a base heating load. The majority of the heating load continues to be met using the legacy boiler. HRU operation decreases under the AC-h scenario, and HRU output decreases occasionally throughout the day. This reduction in HRU output is due to fuel cell operation occurring during the Wednesday morning when the electrical demand decreases. Under this scenario, the microturbines are not operated, resulting in a reduced waste heat stream for use in the HRU.

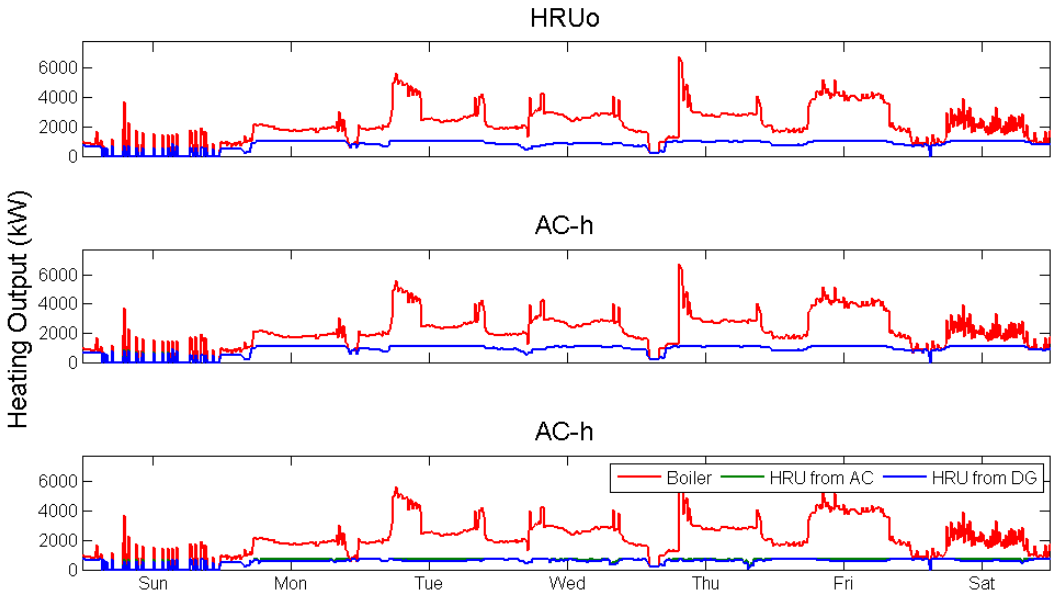

Figure 5-49: Winter heating operation for all technology scenarios adopted at the SCAQMD building

Figure 5-50 shows the cooling operation that corresponds to the electrical and heating operation during the winter week shown in Figure 5-48 and Figure 5-49. Figure 5-51 shows the corresponding absorption chiller operation during the winter week for the AC-h and AC-l technology scenarios. Cooling demand only occurs during the middle of the day. When an absorption chiller is first adopted under the AC-h scenario, the chiller is only operated during Sunday. Comparing Figure 5-50 to Figure 5-48 shows that microturbine operation does not occur during the first Sunday. During this instance, the absorption chiller is used to reduce the total electrical demand, reducing demand charges incurred during building operation.

Under the AC-l scenario, the absorption chiller is operated whenever a cooling demand exists. The cooling produced, however, depends on the combined electrical and cooling demand. During the days where the combined demand is high, the absorption chiller is used to produce

the maximum possible amount of cooling, shifting the cooling load from the electrically operated vapor compression system to the thermally activated absorption chiller. However, on Wednesday, when the combined electrical and cooling demand is relatively low, the absorption chiller is operated at a lower setting, producing cooling. The waste heat is instead used in the heat recovery unit.

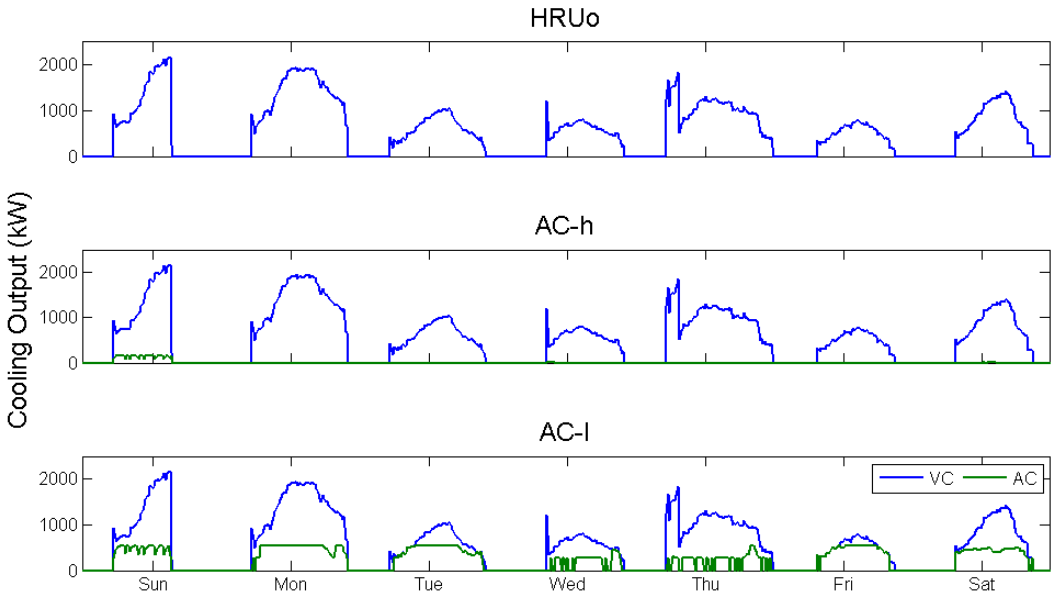

Figure 5-50: Winter cooling operation for all technology scenarios adopted at the SCAQMD building

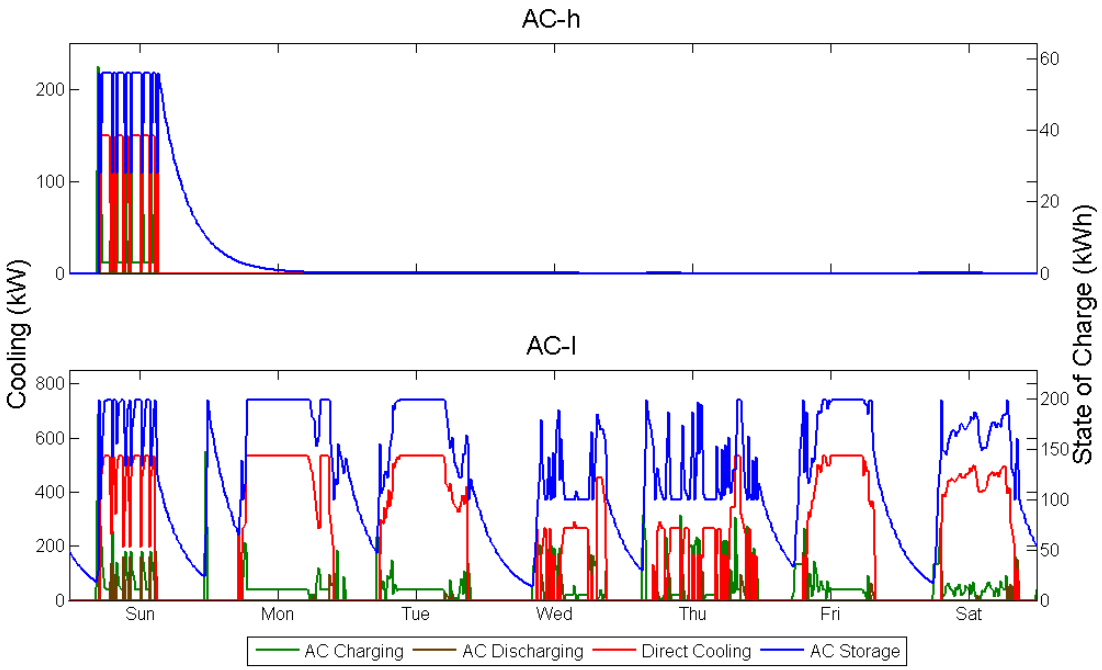

Figure 5-51: Winter absorption chiller operation for all technology scenarios adopted at the SCAQMD building

Electrical, cooling, and absorption chiller operation during a summer week is shown in Figure 5-52, Figure 5-53, and Figure 5-54 respectively. Summer electrical operations differs in the same way from winter operation as the USN and UCI Cal IT^2 buildings, with the adopted fuel cells and microturbines producing the maximum amount of electricity during on-peak and mid-peak, and turning down to the minimum power output during off-peak. Heating operation during the summer is similar to operation during the winter, and is not shown. The largest difference between the SCAQMD building operation during the summer and winter is the absorption chiller operation under the AC-h technology scenario. During the winter, the AC-h absorption chiller is periodically operated to assist with reducing the demand charge associated with electrical utility imports. In addition to reducing the peak utility demand, the absorption chiller is also operated when utility imports occur during mid-peak and on-peak periods. During

these periods, the import of grid electricity may not increase demand charges, but the absorption chiller is operated so that the purchase of expensive grid electricity is avoided. An example of this is seen during Tuesday morning, where absorption chiller operation occurs while grid imports are low. During the winter, the absorption chiller would not have been operated in the same situation, but the summer cost of grid electricity is more expensive during the middle of the day, and the absorption chiller is dispatched to reduce the amount of imported grid electrical energy.

While the absorption chiller has the potential to reduce the maximum combined electrical demand created by the combined electrical and cooling load, no reduction is experienced under the AC-h scenario. The maximum demand is reduced by 64 kW for the AC-l technology scenario.

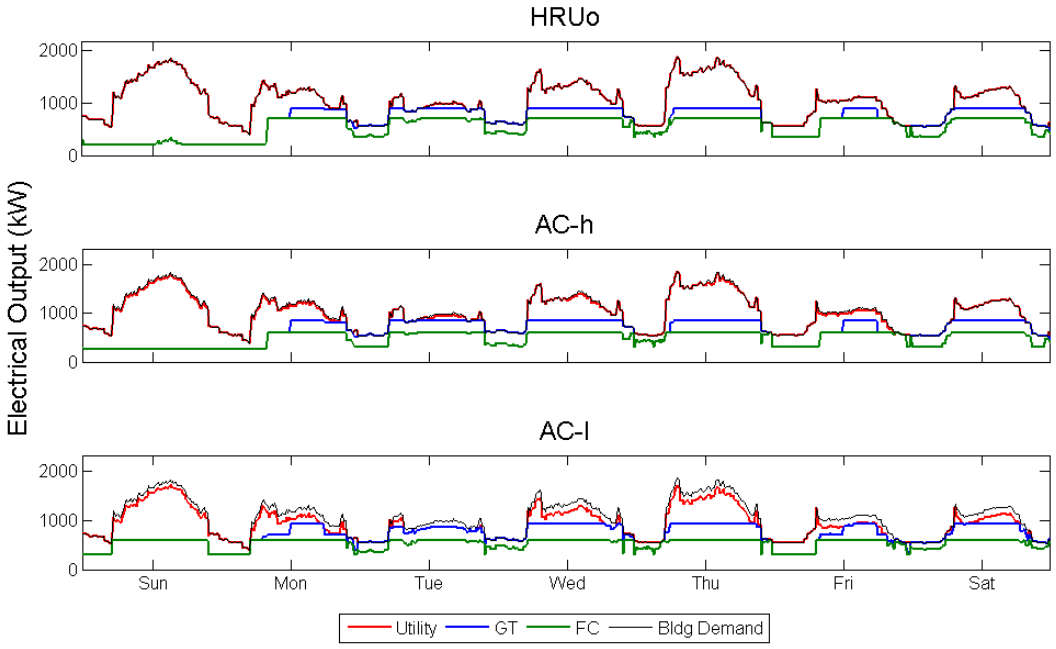

Figure 5-52: Summer electrical operation for all technology scenarios adopted at the SCAQMD building

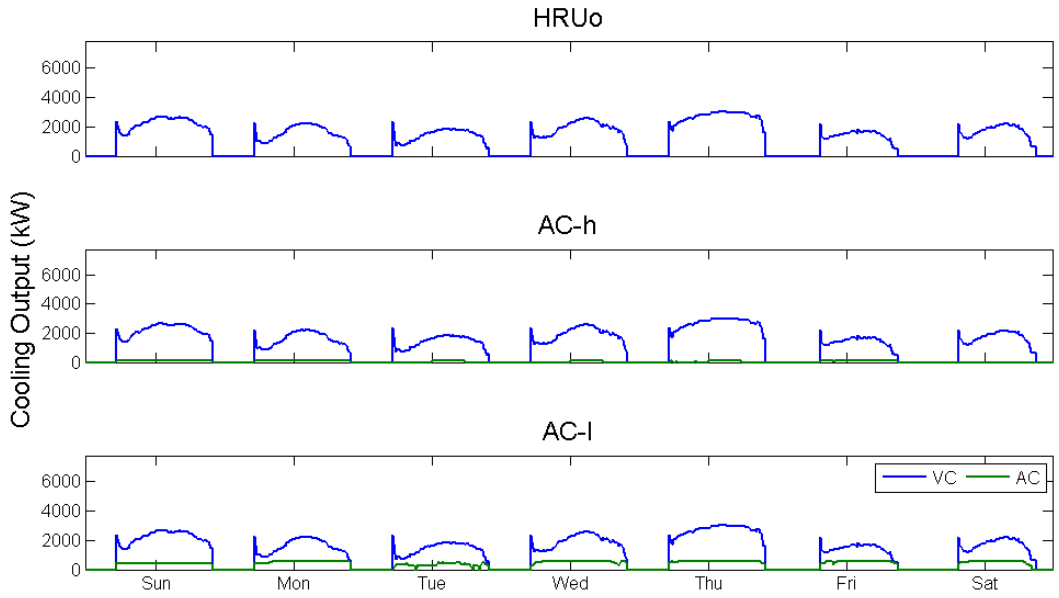

Figure 5-53: Summer cooling operation for all technology scenarios adopted at the SCAQMD building

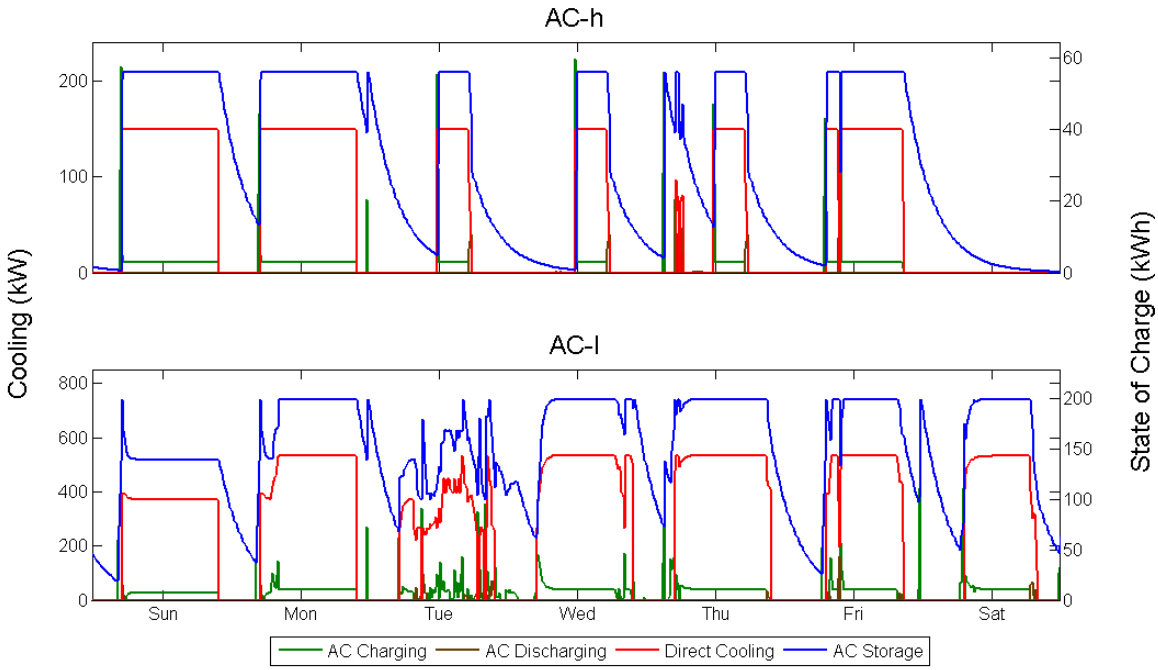

Figure 5-54: Summer absorption chiller operation for all technology scenarios adopted at the SCAQMD building

5.2.3.2 Financial Performance

Figure 5-55 shows the overall financial performance of the three adopted DER systems at the SCAQMD building. While the adoption of an absorption chiller continues to improve the overall investment performance, the improvements experienced at the SCAQMD building are smaller than as experienced in either the USN or UCI Cal IT^2 building.

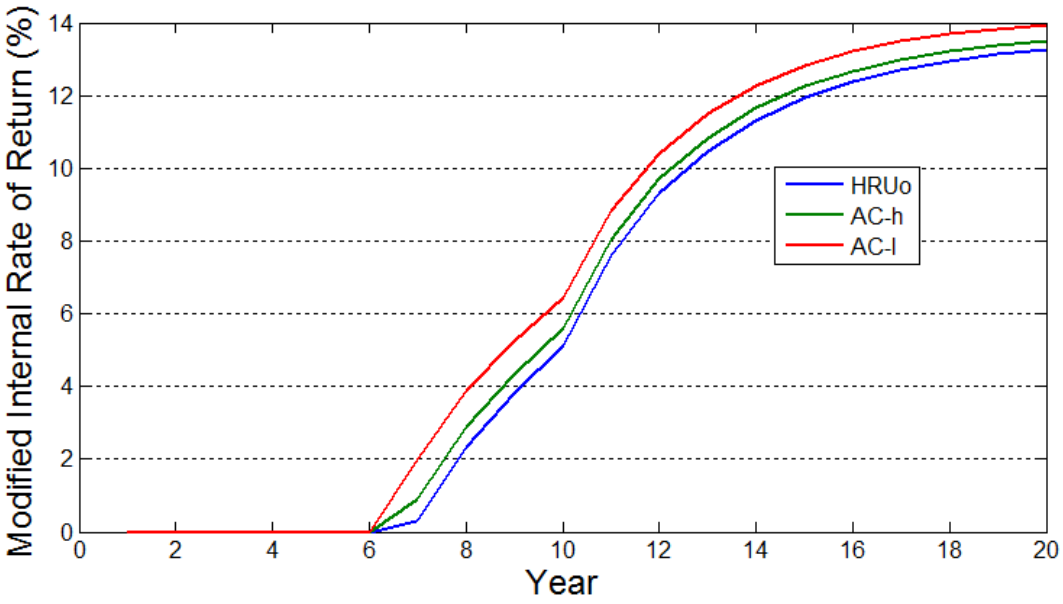

Figure 5-55: Modified internal rate of return for all three technology scenarios when adopted and operated at the SCAQMD

Figure 5-56 shows the allocated utility costs associated with DER systems operation at the SCAQMD building. The overall results presented in Figure 5-56 are similar to the corresponding USN results. However, the USN building uses utility imports to meet between 11% and 13% of the total building electrical demand, whereas the SCAQMD building imports between 25% and 32% of the total electrical demand. Also, Figure 5-48 and Figure 5-52 both show that the majority of grid imports occur during the middle of the day, when the cost of electricity is highest. As a result, the heating load receives a relatively small negative allocation

for both utility energy and demand charges. DER system adoption reduces the amount of exported electricity, by the portion of the building demand met onsite is the electrical and cooling base load. The more expensive dynamic load is still met primarily through the import of grid electricity, reducing the savings generated by DER system adoption.

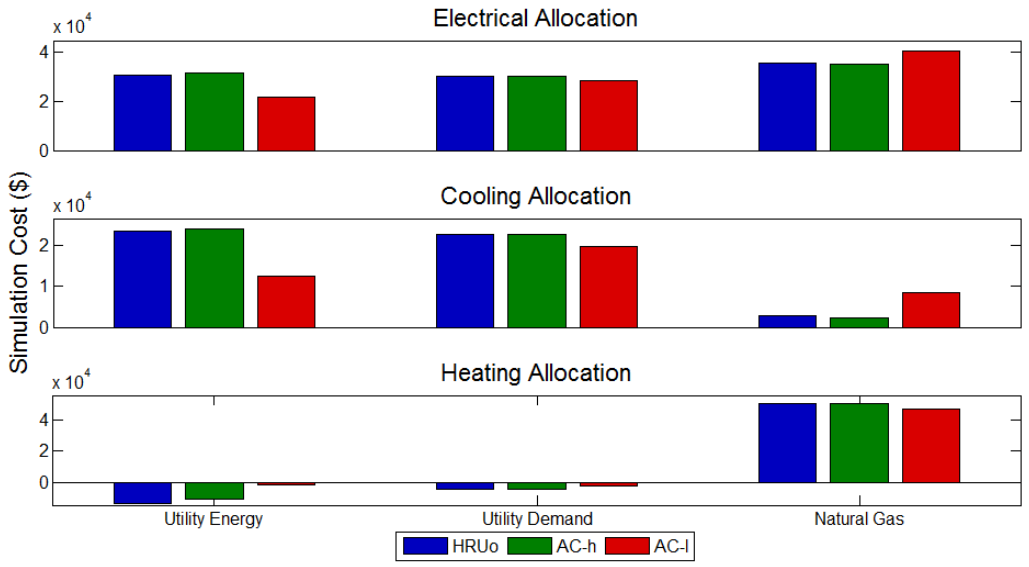

Figure 5-56: Utility costs allocated to the production of electricity, cooling, and heating for the three technology scenarios at the SCAQMD building

Figure 5-57 shows the allocated fuel cell and microturbine cost allocation. The electrical load receives the largest fuel cell O&M cost allocation. Although the cooling load also receives a fuel cell O&M cost allocation, the size of the allocation combined with the relatively large utility and demand charge allocations show that the cooling load is primarily met through the import of grid electricity even after DER system adoption. Similarly, the heating load receives a small fuel cell O&M allocation, even receiving a negative allocation under the AC-l technology scenario. At the same time, the heating load receives approximately half of the microturbine O&M cost. The other half is shared by the electrical load, showing that the combined electrical and heating

load is required for the adoption and operation of microturbines to occur. The cooling load receives either a negative or small microturbine O&M allocation, suggesting the cooling load either suppresses or is indifferent to microturbine operation.

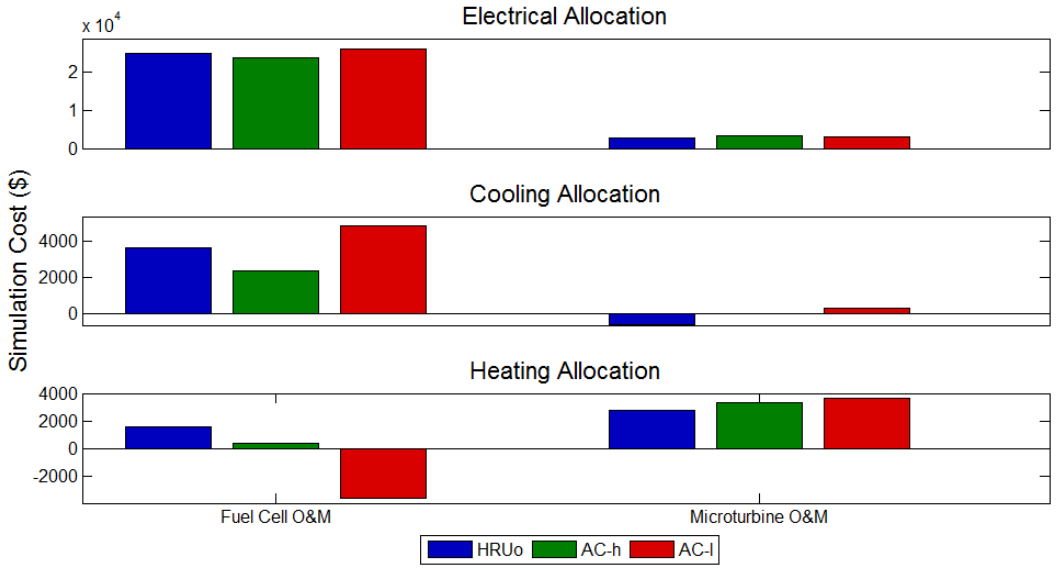

Figure 5-57: Fuel cell and microturbine O&M costs allocated to the production of electricity, cooling, and heating for the three technology scenarios at SCAQMD building

From the perspective of system design, the results shown in Figure 5-57 indicate that the microturbines are used to meet the electrical and heating loads only. The fuel cells are used to meet a small part of the heating load except under the AC-l scenario, where the heating load actively reduces fuel cell operation. Instead of designing an actual system where ducting between all generators and heat recovery technologies needs to be installed, the systems can be separated such that the microturbines and heat recovery unit are connected, and the fuel cells and absorption chiller are connected, but the systems are viewed as separate DER systems. This result is reflected in Figure 5-47, which shows that only a fraction of the building heating load is

met through the capture of waste heat provided to the heat recovery unit from the absorption chiller.

Figure 5-58 shows the vapor compression and absorption chiller O&M cost allocations for the three technology scenarios. The allocation of these two types of cost are dissimilar to the previously studied buildings. Like the other two buildings, the vapor compression cost is allocated primarily to the cooling load. DER system operation due to the electrical load reduces vapor compression operation due to the generation of heat that can be used to power the absorption chiller. The heating load, however, receives a positive vapor compression allocation cost under the AC-h and AC-l scenario. In the prior two buildings, a negative vapor compression O&M cost was allocated to the heating load. Those two buildings also had heating and cooling loads that were small relative to the electrical load. In addition, the DG operation for both buildings resulted in excess production of waste heat that could not be fully utilized by the adopted DER systems. The SCAQMD has the opposite problem, where each individual thermal load is sufficiently large during the middle of the day where either load could fully utilize the waste heat produced by the fuel cells and microturbines. As a result, the heating load encourages the use of the legacy vapor compression chiller to meet the cooling load, while suppressing absorption chiller operation.

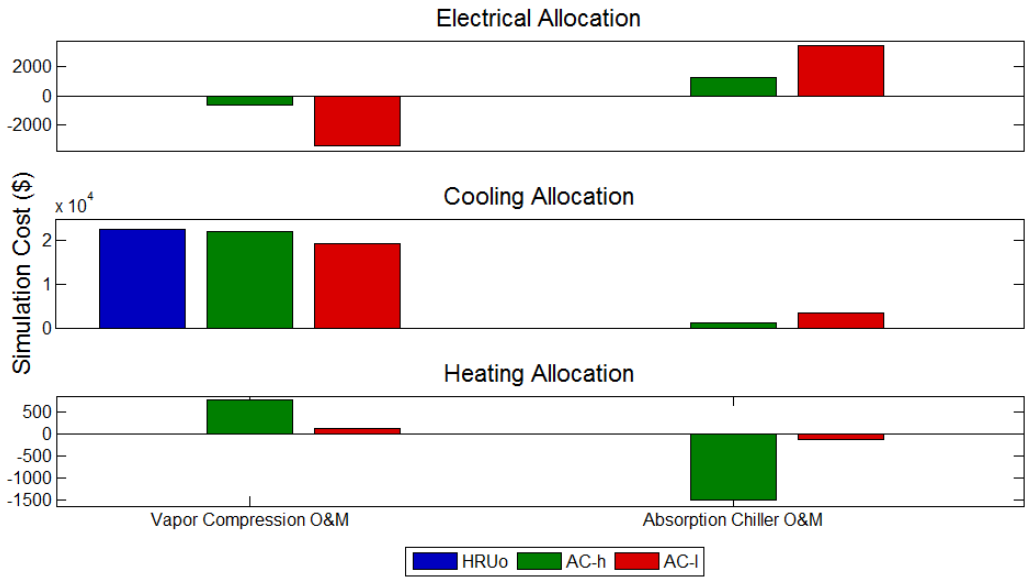

Figure 5-58: Vapor compression and absorption chiller O&M costs allocated to the production of electricity, cooling, and heating for the three technology scenarios at SCAQMD building

This behavior is not completely reciprocated by the cooling load with respect to heat recovery unit operation. Figure 5-59 shows the boiler and heat recovery unit cost allocation for the three technology scenarios. The boiler and HRU O&M cost allocation is similar to the allocation experienced for the UCI Cal IT^2 building for the same technologies. While the cooling load does suppress HRU operation under the AC-l technology scenario, the cooling load actually encourages HRU operation under the AC-h scenario. While the heating load desires to utilize all of the available heat produced by the adopted DG, the cooling load derives some benefit from passing waste heat stream used by the absorption chiller to the heat recovery unit in order to fully capture the available heat.

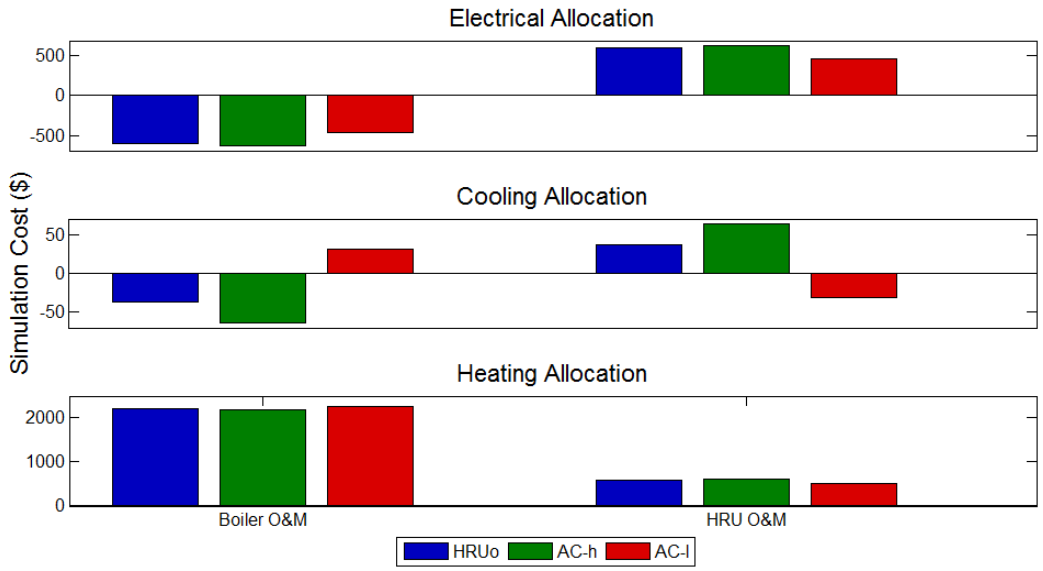

Figure 5-59: Boiler and heat recovery unit O&M costs allocated to the production of electricity, cooling, and heating for the three technology scenarios at SCAQMD building

Figure 5-60 shows the fuel cell and microturbine loan allocation for the three technology scenarios. The primary difference between Figure 5-60 and the results for the USN building and UCI Cal IT^2 building is the negative or nonexistent fuel cell loan allocation received by the heating load. Contrary to all prior results, the SCAQMD heating load discourages the adoption of fuel cells in favor of microturbines. Microturbines can be purchased at a lower capital cost and produce more heat per kWh of electricity generated. From the perspective of the electrical and heating load only, microturbine technology appears well suited to assist with meeting the building electrical base load while also supplying all of the heating load simultaneously. The overall DER system optimization elects to adopt fuel cells in addition to microturbines, but the resistance shown by the heating load to fuel cells is manifested in a negative fuel cell loan allocation, reducing the investment associated with the heating load.

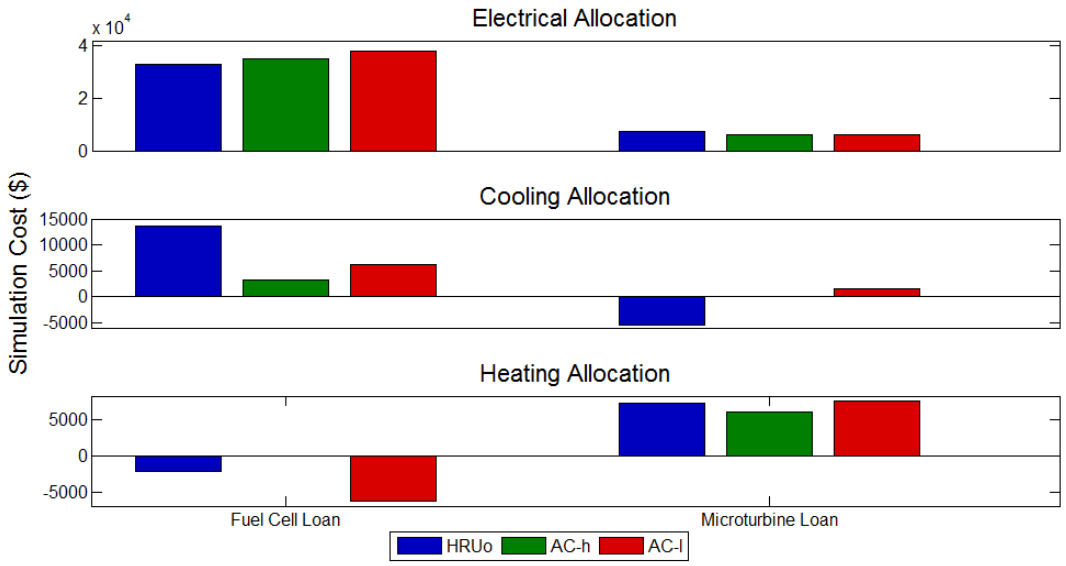

Figure 5-60: Fuel cell and microturbine loan costs allocated to the production of electricity, cooling, and heating for the three technology scenarios at SCAQMD

Figure 5-61 shows the allocated absorption chiller, heat recovery unit, and duct-parallel loan payments for the three technology scenarios. Nearly all allocations are similar to what is seen for the previous two buildings. Due to the competitive nature for the use of available waste heat between the cooling and heating load at SCAQMD, the heating load receives either a negative or nearly zero absorption chiller loan payment allocation.

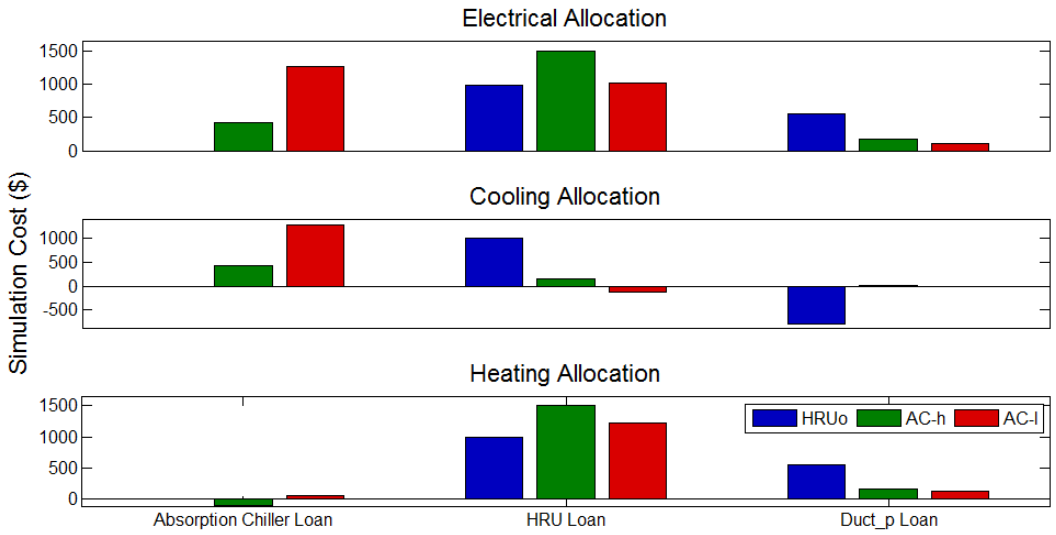

Figure 5-61: Absorption chiller, heat recovery unit, and duct-parallel loan costs allocated to the production of electricity, cooling, and heating for the three technology scenarios at SCAQMD

The levelized cost of energy and rate of return for the three technology scenarios are shown for the electrical, cooling, and heating loads in Figure 5-62. The financial performance of the different products is similar to the same energy types at the UCI Cal IT^2 building, with the levelized cost being consistently reduced for heating only. The best financial performance is seen by the AC-l technology scenario, which experiences the highest return. However, the reduction to the levelized cost of heating is similar between the HRUo and AC-l scenario. The difference in financial performance is created by the cooling operation under the AC-l scenario. Despite requiring a higher initial investment due to the adoption of the largest absorption chiller, savings can be generated for the cooling load by year nine, resulting in the realization of a small rate of return of approximately 0.2% at year ten.

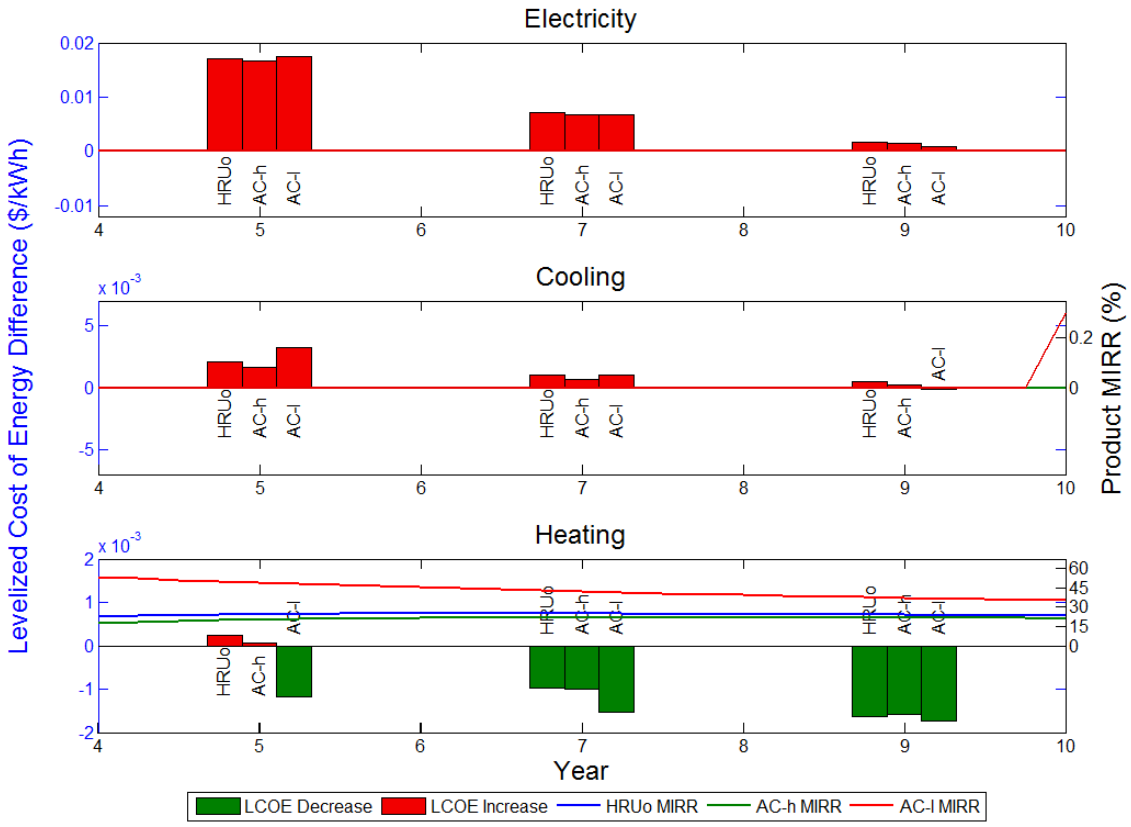

Figure 5-62: Levelized cost of energy difference at years five, seven, and nine and corresponding modified internal rate of return for electricity, cooling, and heating when DER systems are adopted according to the three technology scenarios at the SCAQMD building

5.2.3.3 Building Carbon Emissions

Approximately 4,986 tonnes of CO_2 per year are emitted due to SCAQMD building energy use. The allocation between electricity, heating, and cooling is similar to what has been presented for the USN and UCI Cal IT^2 building. Adopting a DER system with the goal of minimizing cost of energy results in an increase to emissions, as seen in Figure 5-63.

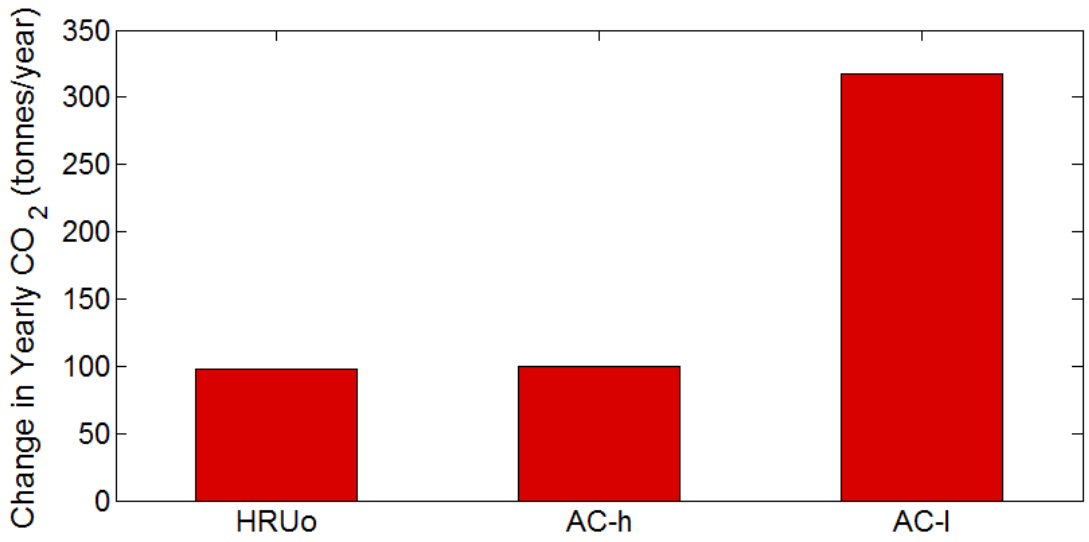

Figure 5-63: Change in yearly carbon emissions for the SCAQMD building as a result of DER system adoption

Figure 5-64 shows the increase in carbon emissions shown in Figure 5-63 allocated between electricity, heating, and cooling. The energy type responsible for an increase to carbon emissions for every technology scenario is electricity. The high utilization of waste heat to meet both the heating and cooling reduces carbon emissions for both loads. The AC-h technology scenario experiences the smallest increase to carbon emissions. Under this scenario, the HRU is sued to meet the largest portion of the building heating load. Under this scenario, the cooling load receives the largest carbon emissions reduction, suggesting that the adoption and infrequent operation of the absorption chiller allows for the utilization of additional waste heat, even if the largest increase in overall DER system operation is experienced through the increased capture of waste heat in the heat recovery unit.

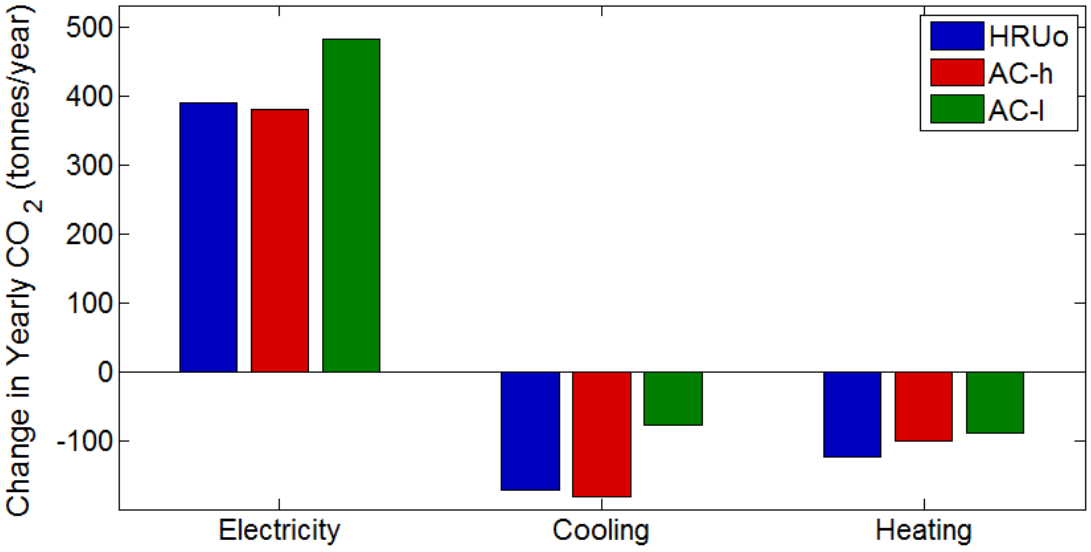

Figure 5-64: Change in yearly carbon emissions for individual types of energy for the SCAQMD building as a result of DER system adoption

5.2.4 St. Regis Hotel

The St. Regis hotel has an average electrical demand of 1212 kW and an electrical load factor of 0.677. The heating load is coincident with the electrical demand 100% of the time and the ratio of the heating to electrical load is 0.49. The cooling load is coincident with the electrical load 91% of the time and the ratio between the cooling and electrical load is 0.46. The baseline cost of energy is $0.0906 per kWh for electricity, $0.0455 per kWh for cooling, and $0.0202 per kWh for heating.

Table 5-5 shows the optimal DER system design for the St. Regis building for the three DER system technology scenarios. Fuel cells and a heat recovery unit is always adopted. An absorption chiller is adopted whenever allowed along with one or two microturbines.

Table 5-5: Optimal CCHP system design for all technology scenarios operating at the St. Regis building

Technology Scenario	Fuel Cell (100 kW)	Microturbine (65 kW)	AC (kW)	HRU (kW)	Duct - Parallel (kW)	Duct - Series (kW)
HRUo	14	0	0	844	938	0
AC-h	13	1	375	809	899	150
AC-l	13	2	610	750	834	244

5.2.4.1 DER System Operation

Figure 5-65, Figure 5-66, and Figure 5-67 show the source of electricity, cooling, and heating respectively for the three DER systems adopted by the St. Regis Hotel. Total electrical usage decreases by 5.5% and 7.8% under the AC-h and AC-l technology scenarios respectively. Shifting from the HRUo scenario to the AC-h results in electrical imports dropping by 6.4% and total fuel cell electrical output by 5.7%. Shifting from the HRUo to AC-l scenario results in electrical imports dropping by 66% and fuel cell output by 1.6%.Microturbine operation contributes a marginal amount of electricity to the overall electrical production.

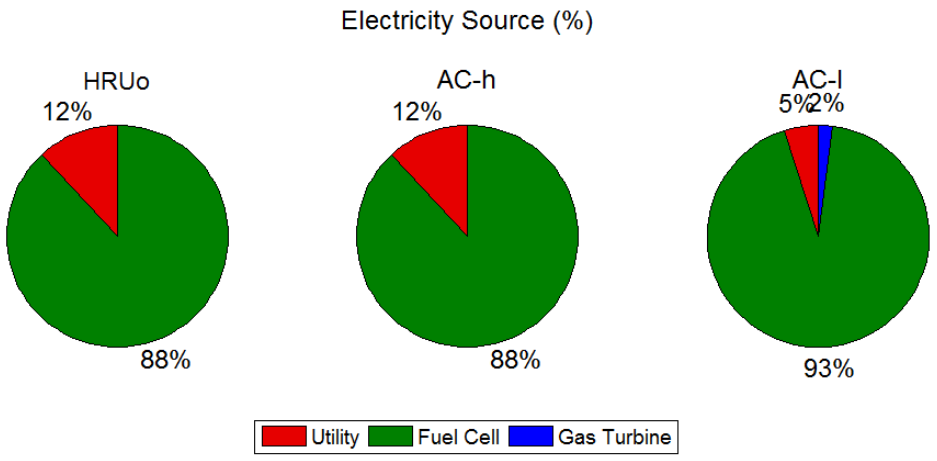

Figure 5-65: Source of electricity to meet the St. Regis electrical demand for all technology scenarios

Similar to the USN building, when adopted, the absorption chiller is used to provide a large portion of the total cooling demand. The heat recovery unit is used to provide nearly the entire heating demand for the building. As absorption chiller operation increases, the boiler is used more frequently, but the combination of waste heat from the fuel cells, microturbines, and absorption chiller allow for the heat recovery unit to provide 95% of the building heating demand. Overall utilization of the fuel energy used in the DER system is 70% for the HRUo scenario, 81% for the AC-h scenario, and 82% for the AC-l scenario.

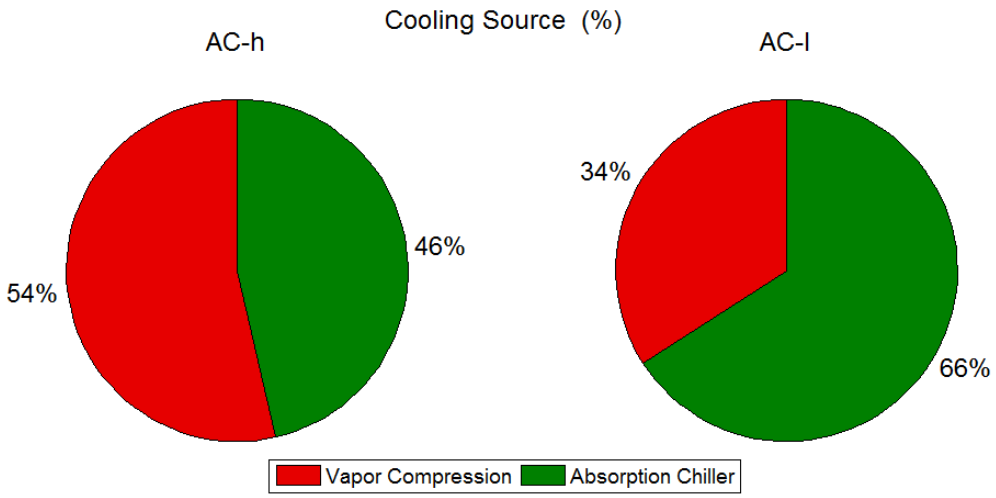

Figure 5-66: Source of cooling to meet the St. Regis electrical demand for all technology scenarios

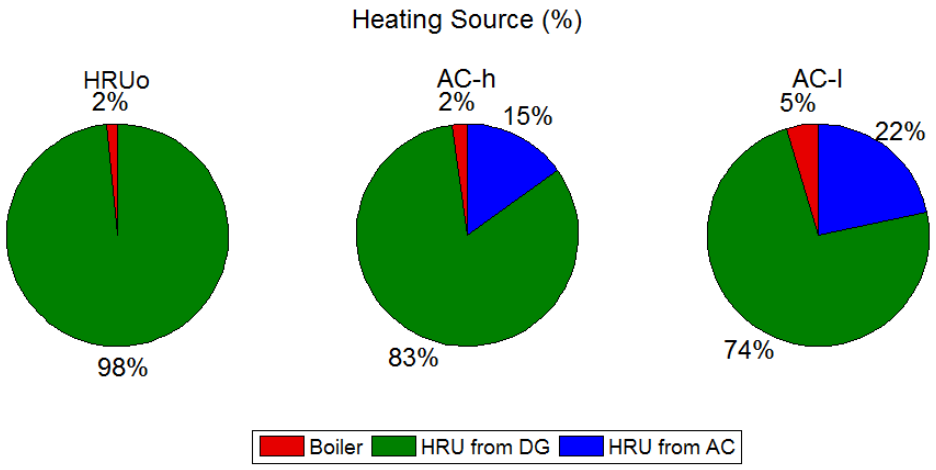

Figure 5-67: Source of heating to meet the St. Regis electrical demand for all technology scenarios

Winter operation of the different systems is similar to DER system operation occurring at the previous buildings studied, as seen for St. Regis in Figure 5-68. Figure 5-69 and Figure 5-70 show the heating and cooling operation respectively. When adopted, the absorption chiller is operated to reduce electrical imports as much as possible. During Monday, the combined electrical and cooling load is sufficiently large that electrical imports are unavoidable. During this day, the fuel cells and absorption chiller are operated at maximum capacity. During the following Tuesday, the combined electrical and cooling load produces a combined load that can be met entirely onsite. During this day, the absorption chiller is used to produce enough cooling such that the combined electrical load is low enough to be met entirely using the adopted DG. The heating demand throughout these two days is nearly completely met using the heat recovery unit. As absorption chiller operation increases, so does the amount of heat captured from the waste heat exiting the absorption chiller. When both the heating and cooling loads are high (for example, mid-day Saturday), the cooling load is given priority and the absorption chiller is operated before the heat recovery unit.

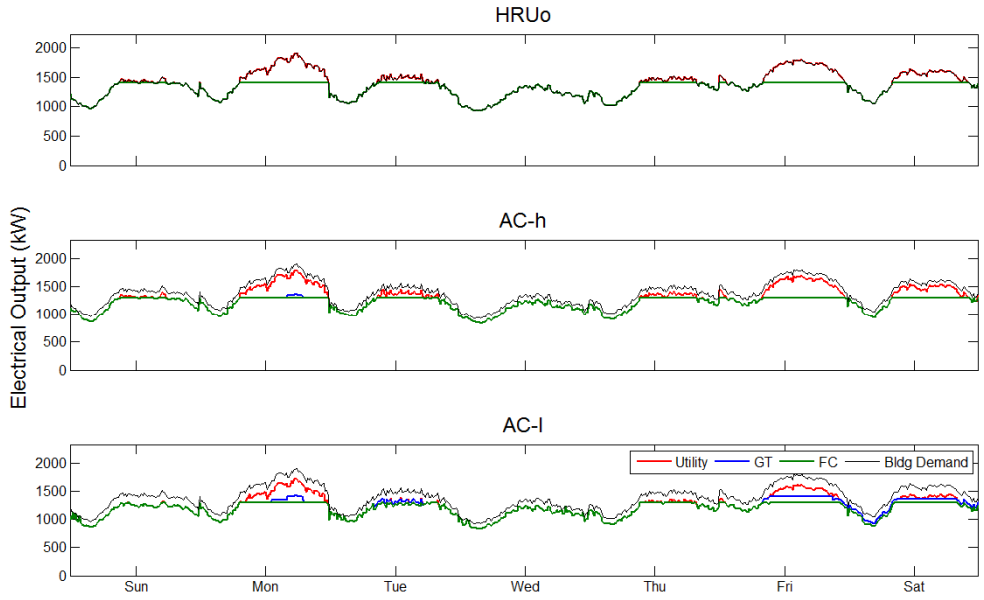

Figure 5-68: Winter electrical operation for all technology scenarios adopted at the St. Regis building

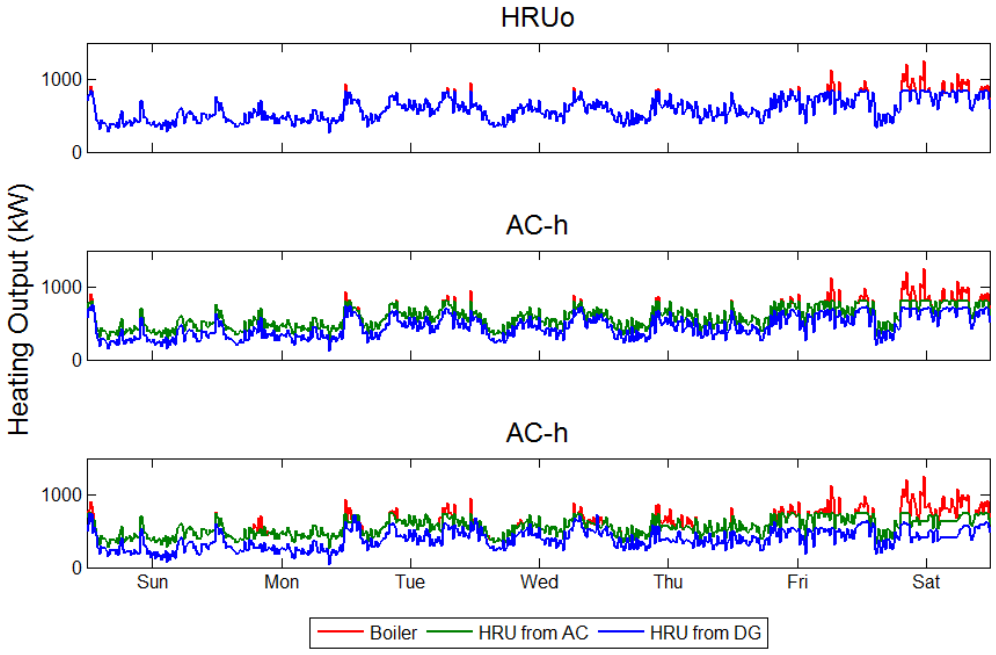

Figure 5-69: Winter heating operation for all technology scenarios adopted at the St. Regis building

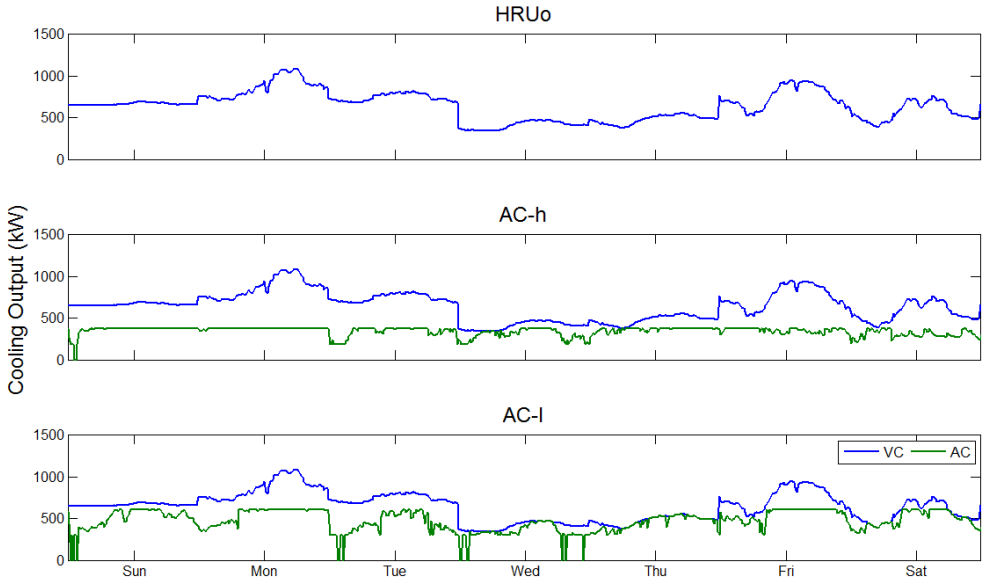

Figure 5-70: Winter cooling operation for all technology scenarios adopted at the St. Regis building

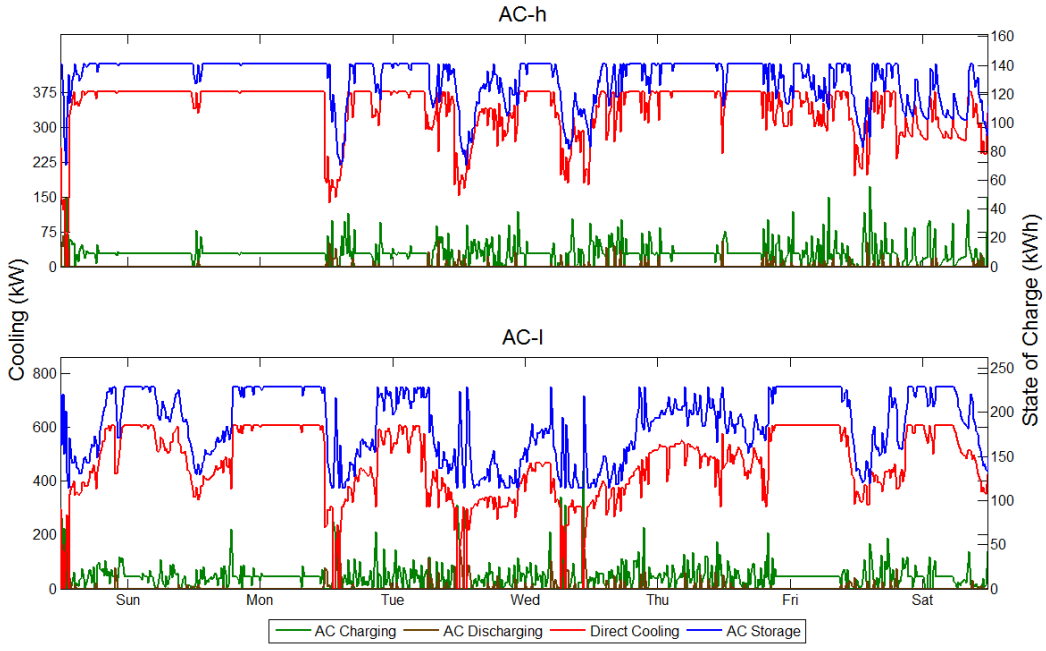

Figure 5-71: Winter absorption chiller operation for all technology scenarios adopted at the St. Regis building

Operation during the summer changes from the winter in the same ways as the DER operation changes at the other studied buildings, as seen in Figure 5-72. The adopted fuel cells are turned down to part load during off-peak. Load following occurs, but instead of supplying the entire building demand, a constant supply of electricity is imported, with the fuel cells operated to maintain the demand charge at a certain level. Cooling and heating operation during the summer mirror operation during the winter, and are not shown.

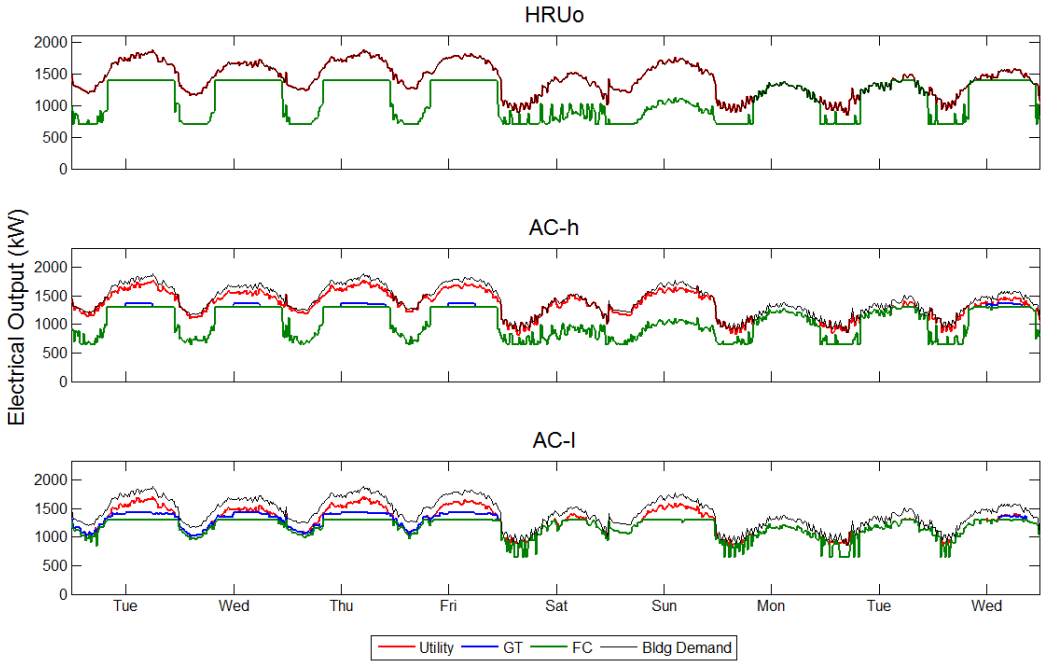

Figure 5-72: Summer electrical operation for all technology scenarios adopted at the St. Regis building

As a result of absorption chiller adoption, the maximum combined electrical demand for the St. Regis building is reduced by 110 kW under the AC-h scenario and 179 kW under the AC-l scenario. Compared to the generator sizes included in this study, the level of demand reduction

created by absorption chiller operation is the equivalent to having an additional fuel cell operating under the AC-h scenario and two fuel cells operating under the AC-l scenario.

5.2.4.2 Financial Performance

The DER systems adopted at the St. Regis building produce savings sufficiently large to produce a desirable return on DER investment, as seen in Figure 5-73. The HRUo system nearly achieves a rate of return of 8% by year ten. When an absorption chiller is adopted, a return of 8% is achieved by year eight under the AC-h scenario, and between four and six years under the AC-l scenario.

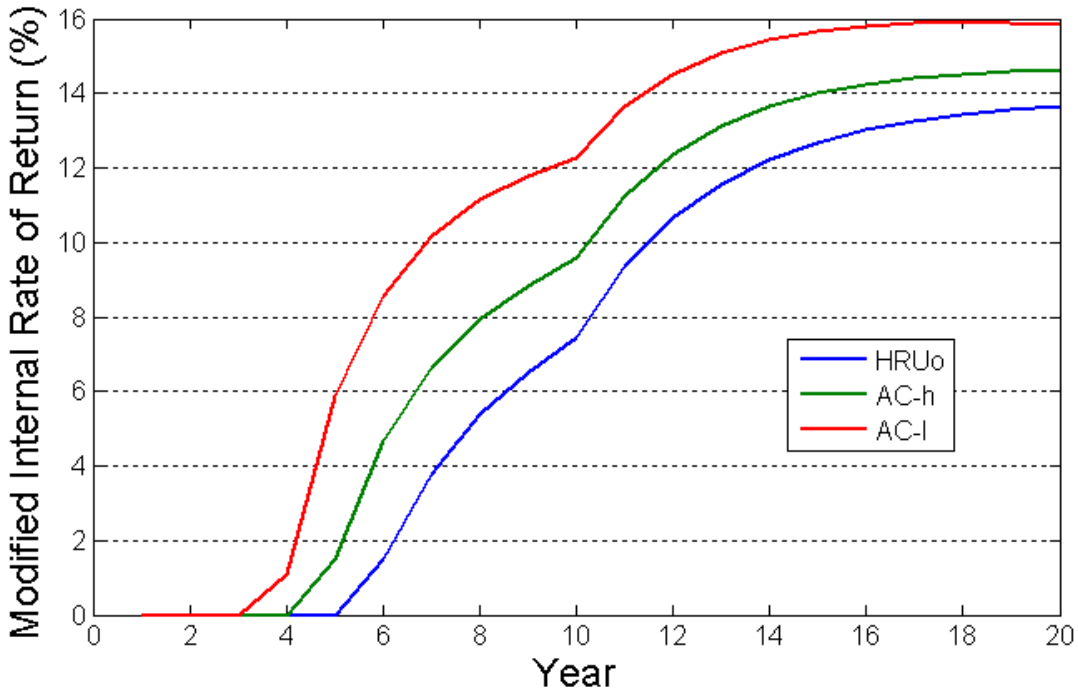

Figure 5-73: Modified internal rate of return for all three technology scenarios when adopted and operated at the St. Regis building

Even with objectively desirable financial performance for the two systems that include an absorption chiller, allocating the different cost components will allow for an investor to

understand how a better return can be obtained or which loads are critical to positive financial performance.

Figure 5-74 shows the allocated utility costs for the three technology scenarios. The general results are similar to prior buildings analyzed, with electricity and cooling receiving a positive allocation for all utility costs, and heating receiving a negative allocation for electrical utility costs and a positive allocation for natural gas cost. The main difference presented in these results is seen for the electrical load allocations, particularly in the relative size of the three types of costs. The St. Regis and USN buildings are similar in the sense that after DER adoption, only a fraction of the combined electrical demand is met using grid imports. However, the USN building electrical load utility energy and demand charges cost allocations are twice the size of the natural gas cost allocation. Note that the cost allocation for the USN building revealed that both the electrical and heating load were both required for fuel cell adoption and operation to occur. This requirement appears to disappear for the St. Regis building, where the electrical load produces DER system operation that incurs a large natural gas fuel cost.

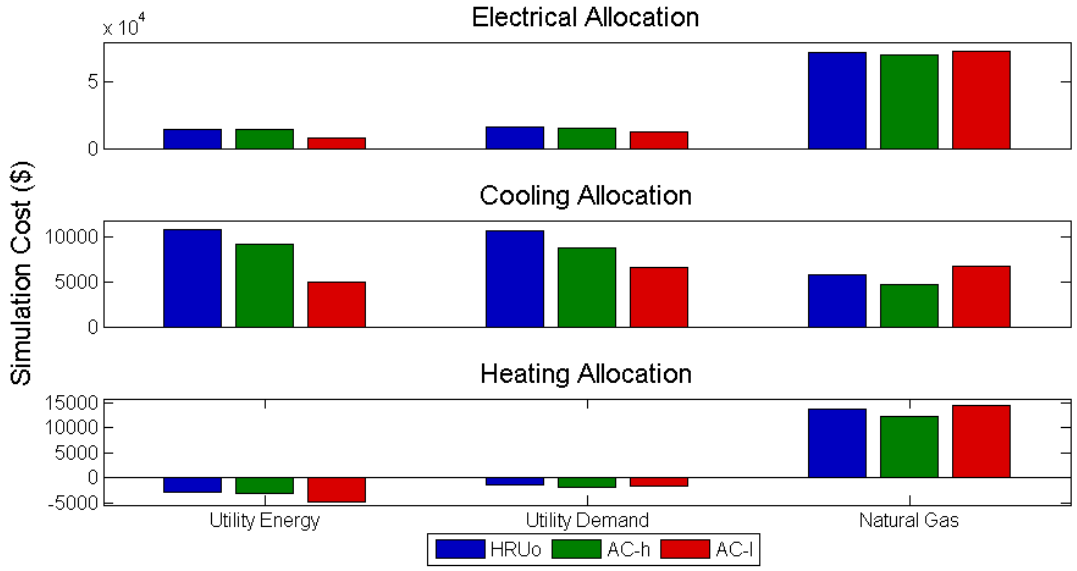

Figure 5-74: Utility costs allocated to the production of electricity, cooling, and heating for the three technology scenarios at the St. Regis building

Figure 5-75, which shows the allocated fuel cell and microturbine O&M cost, confirms the result that the electrical load singlehandedly drives fuel cell operation. The majority of fuel cell O&M cost across the three technology scenarios is allocated to the electrical load. Cooling allocation also receives a positive fuel cell O&M cost allocation. However, the heating load receives a small allocation under the HRUo technology scenario, a negative allocation under the AC-h scenario, and no allocation under the AC-l scenario. Instead, the heating load receives the largest microturbine O&M cost allocation. The cooling load receives a slightly smaller microturbine allocation, but the electrical load receives a negative microturbine O&M cost allocation for all three technology scenarios.

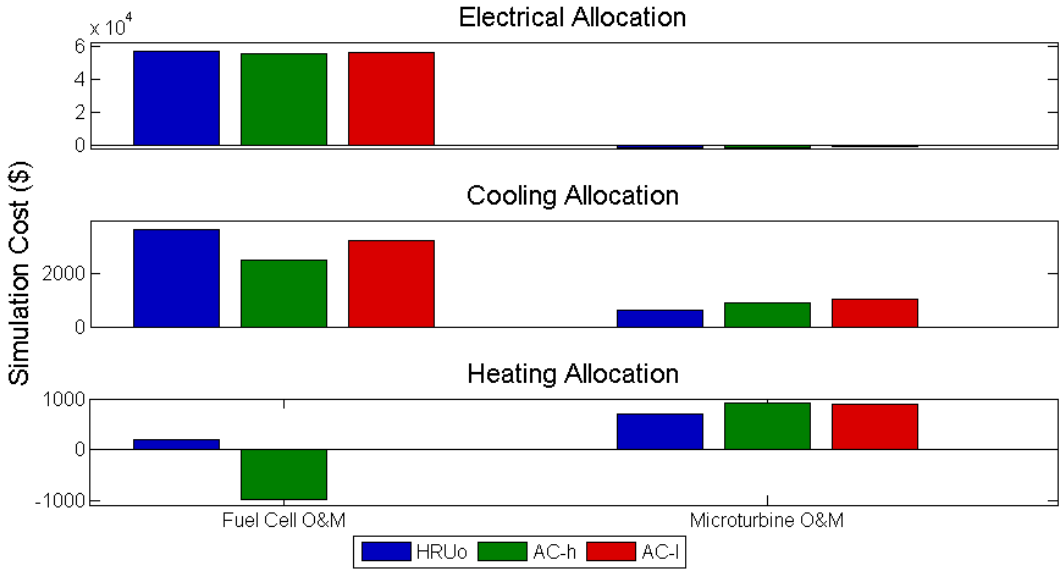

Figure 5-75: Fuel cell and microturbine O&M costs allocated to the production of electricity, cooling, and heating for the three technology scenarios at the St. Regis building

Allocating the different cost components associated with O&M for technologies that produce heating and cooling are similar in shape to the allocation for the same technologies when adopted at the UCI Cal IT^2 building. In general, the allocation of the thermal energy producing technologies operating at the UCI Cal IT^2 building (and the St. Regis building) show that the electrical load drives a shift in thermal energy from production from the legacy systems to production from the technologies that operate off of the waste heat generated by the adopted DG.

Figure 5-76 shows the allocated loan payments for the three technology scenario. Since the prior results showed that the electrical load is primarily responsible for fuel cell operation, it is a natural result that the electrical load is also responsible for fuel cell adoption.

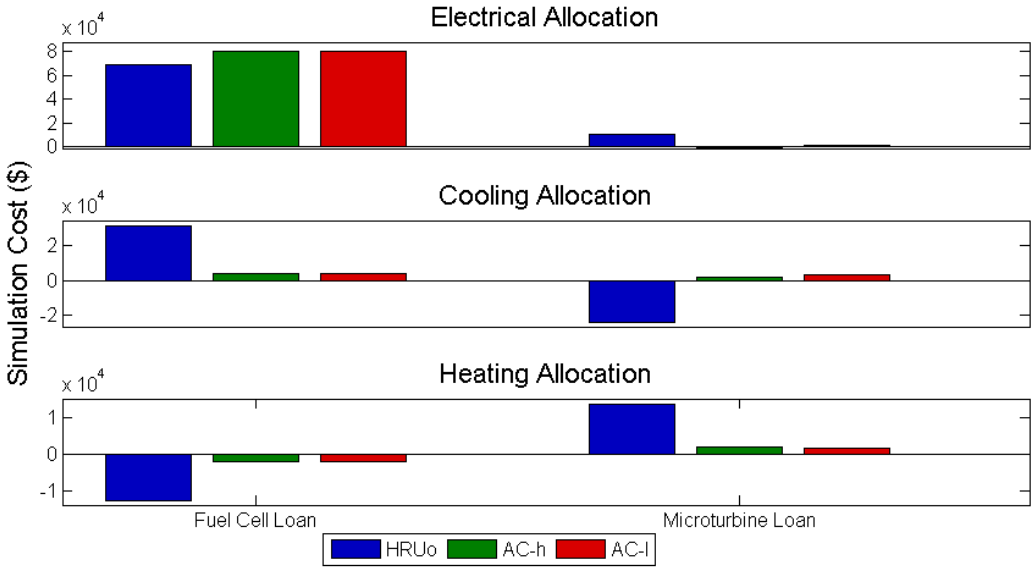

Figure 5-76: Fuel cell and microturbine loan costs allocated to the production of electricity, cooling, and heating for the three technology scenarios at the St. Regis building

The allocation of absorption chiller, heat recovery unit, and duct-parallel loan payments are similar to the allocation for the same technologies for the UCI Cal IT^2 building. The results for the UCI Cal IT^2 building, as seen in Figure 5-40, showed that the adoption of an absorption chiller was due to the combination of all three energy loads, and the corresponding loan payment was split across the three energy types. Under the HRUo technology scenario, the heat recovery unit cost allocation was due to presence of all three energy loads, and the loan payment associated with the HRU was split evenly across the three energy loads. When an absorption chiller is available for adoption, the HRU was adopted due to the electrical and heating load only, and the HRU loan payment was split among the two loads.

Using the allocated costs, the levelized cost of energy and corresponding rate of return for the three types of energy was calculated and is shown in Figure 5-77. The levelized cost of electricity increases due to the high investment cost associated with driving the purchase of the

fuel cells. However, the impact of the investment is reduced over time, with parity with the baseline scenario being achieved in year nine. Under the AC-l scenario, a small decrease in the levelized cost of electricity is produced, resulting in a rate of return of 1% being achieved in year ten.

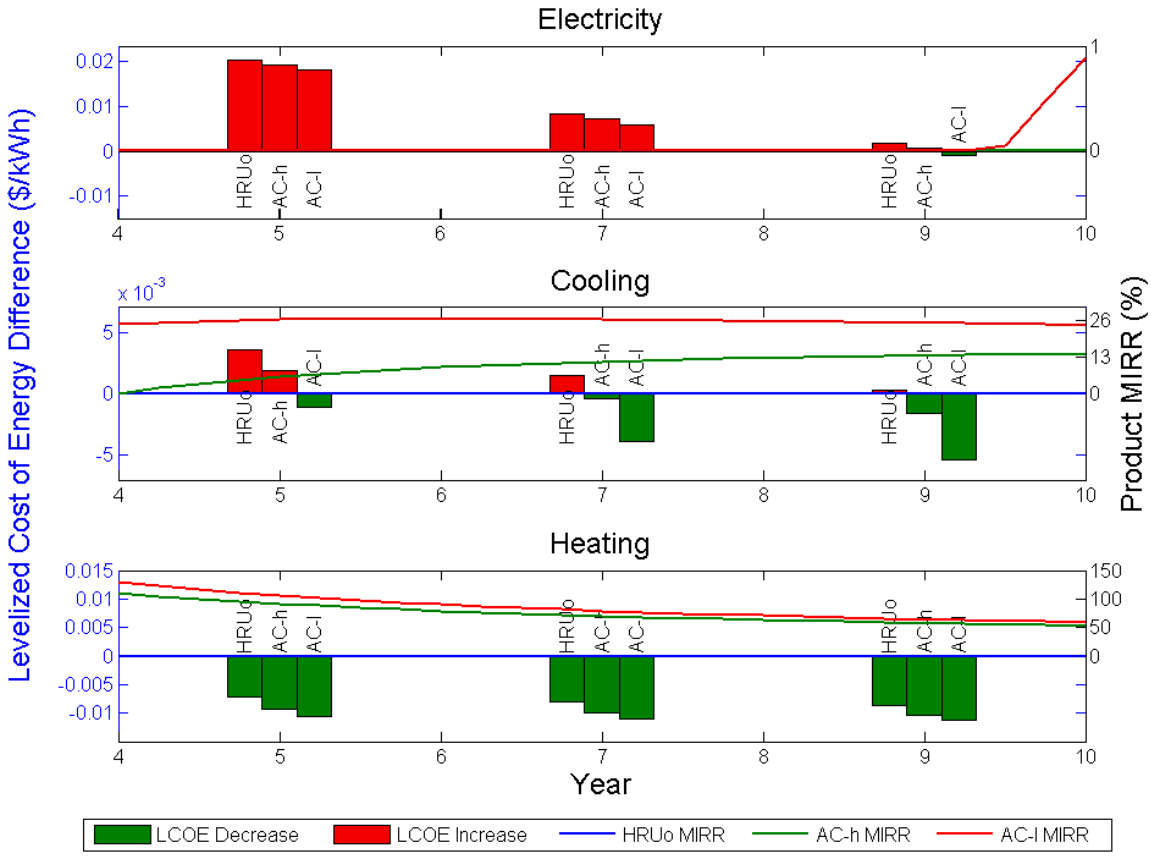

Figure 5-77: Levelized cost of energy difference at years five, seven, and nine and corresponding modified internal rate of return for electricity, cooling, and heating when DER systems are adopted according to the three technology scenarios at the St. Regis building

The cooling load also initially experiences an increase in cost of cooling for the HRUo and AC-h scenario. While the HRUo scenario only reaches parity with the baseline cost of cooling (resulting in no positive rate of return), the AC-h scenario produces cooling at a lower

cost than the baseline scenario by year seven, producing a rate of return approaching 13% by year ten. Cooling under the AC-l scenario immediately produces lower cost cooling in year five. As the investment cost effects are reduced by time, the savings produced under the AC-l scenario increase to a reduction of $0.005 per kWh cooling in year ten, and the corresponding rate of return exceeds 26%.

Unlike the electrical and cooling loads, the heating load immediately achieves lower cost after DER system adoption. Since minimal investment occurred due to the heating load, it is not hard for heating operation to produce savings. With savings produced almost immediately, the rate of return on heating investment is higher for the St. Regis building than any other tested building. The HRUo building has no rate of return due to a lack of initial investment associated with the heating load, resulting in an infinite rate of return.

Both the UCI Cal IT^2 and SCAQMD experience good performance on any heating load investments. These buildings, however, do not have an electrical load which can absorb the cost of DG adoption. The primary investment cost allocated to both the heating and cooling loads are associated with the corresponding technology. During daily operation, fuel cell operation is driven by the electrical load, which receives the bulk of the fuel cell O&M cost. From the perspective of the thermal loads, the waste heat provided to the absorption chiller and heat recovery is supplied free of charge, with the only cost incurred being associated with converting the waste heat into a usable product. As a result, both cooling and heating loads experience reduced cost when an absorption chiller is available for adoption, driving the positive financial performance of the entire DER system.

5.2.4.3 Building Carbon Emissions

Meeting the St. Regis energy loads produces 4,661 metric tons of CO_2 per year. While all other DER systems have increased carbon emissions up until this point, the St. Regis building provides one technology scenario where the adoption of a DER system that was selected to minimize overall cost of energy reduces total carbon emissions, as seen in Figure 5-78. Carbon emissions under the AC-h scenario experience a reduction as a result of DER system adoption.

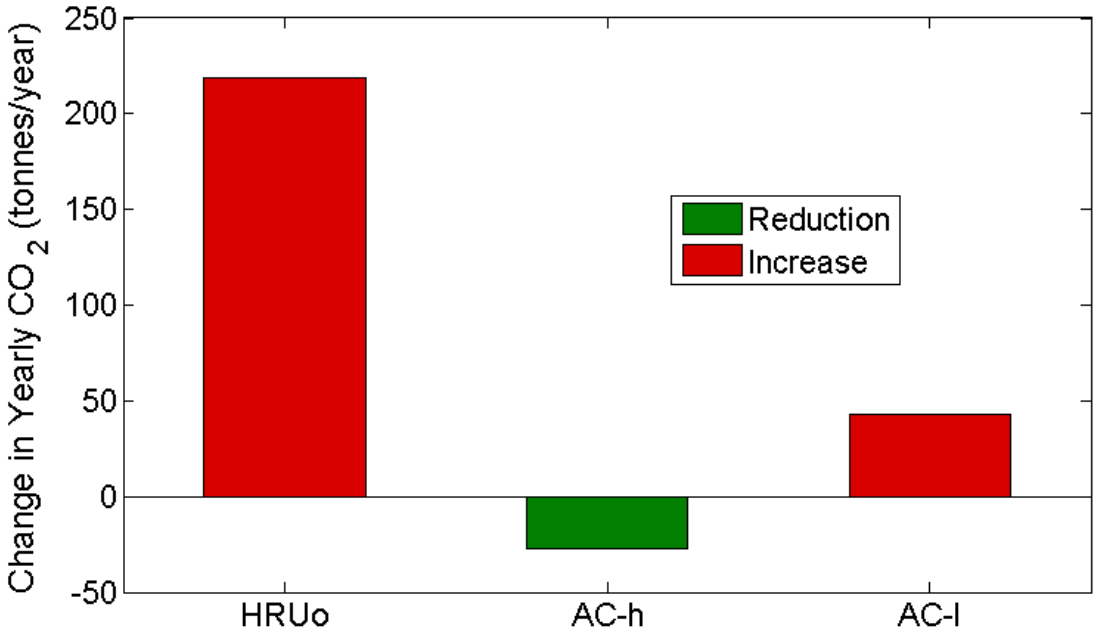

Figure 5-78: Change in yearly carbon emissions for the St. Regis building as a result of DER system adoption

Figure 5-79 shows the impact of the different energy loads on changing overall carbon emissions per year for the three different technology scenarios. As seen in all other scenarios, DER system operation due to the electrical load decrease carbon emissions. The carbon emission associated with both cooling and heating are reduced due to DER system operation. The reduction in carbon emissions associated with the AC-h technology scenario associated with the

largest reduction in carbon emissions for both the cooling and heating load. Note that the reduction in carbon emissions for heating decreases as a result of reducing absorption chiller O&M. Reducing AC O&M resulted in a slight reduction to heat recovery unit operation and a large increase in absorption chiller operation.

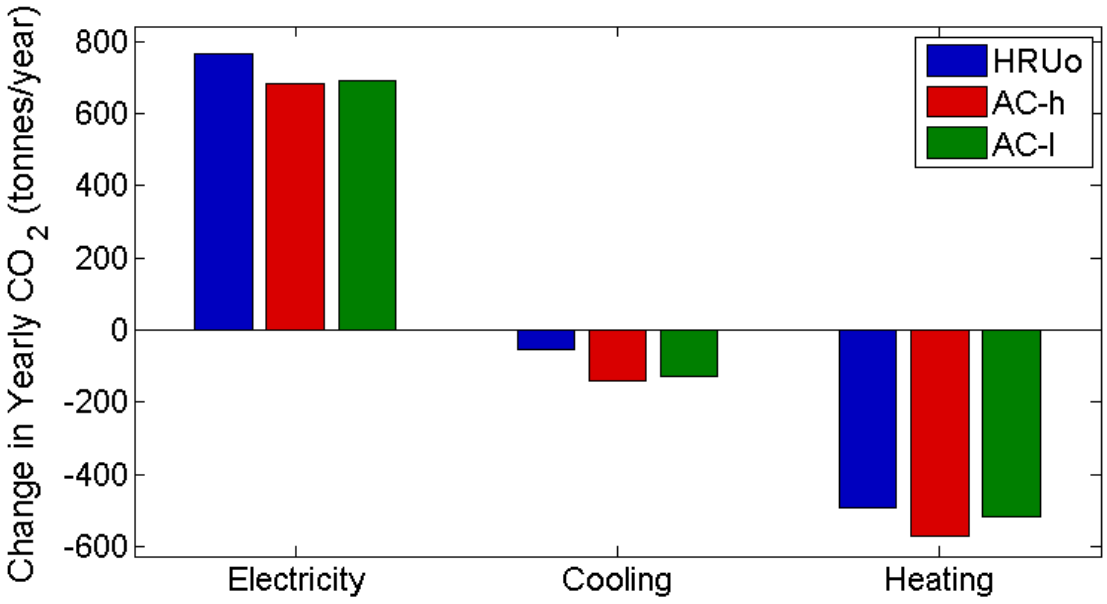

Figure 5-79: Change in yearly carbon emissions for individual types of energy for the St. Regis building as a result of DER system adoption

5.2.5 Patton State Hospital

The Patton State Hospital (Patton) building has an average electrical demand of 1400 kW and an electrical load factor of 0.59. The cooling load is coincident with the electrical load 95% of the time and the ratio of cooling to electrical load is 0.86. The heating load is coincident with the electrical load 100% of the time, and the ratio of heating to electrical load is 1.06. The baseline cost of energy for the Patton building is $0.094 per kWh for electricity, $0.0492 per kWh for cooling, and $0.0192 per kWh for heating.

Table 5-6 shows the adopted DER systems under the three different technology scenarios. The Patton building is the first building studied where a shift in adopted generation capacity away from fuel cells towards microturbines. Also, unlike all other studied buildings, the size of the adopted HRU increases along with the absorption chiller when shifting from the AC-h to the AC-l technology scenario.

Table 5-6: Optimal CCHP system design for all technology scenarios operating at the Patton building

Technology Scenario	Fuel Cell (100 kW)	Microturbine (65 kW)	AC (kW)	HRU (kW)	Duct - Parallel (kW)	Duct - Series (kW)
HRUo	17	4	0	1400	1555	0
AC-h	17	5	1262	1400	1555	505
AC-l	11	13	1850	1732	1925	740

5.2.5.1 DER System Operation

Figure 5-80 shows the source of electricity for the three technology scenarios at the Patton building. Overall, total electricity consumption decreases by 4.2% under the AC-h scenario and 10% under the AC-l scenario. Grid imports are reduced by 53% when moving from the HRUo to AC-h scenario, and 63% when moving from the HRU to AC-l scenario. Fuel cells provide the bulk of the consumed electricity, with microturbine operation increasing significantly under the AC-l scenario. The reduction in total electricity consumed onsite is due to absorption chiller operation, which is used to meet 24% of the cooling load under the AC-h scenario, and 50% of the cooling load under the AC-l scenario.

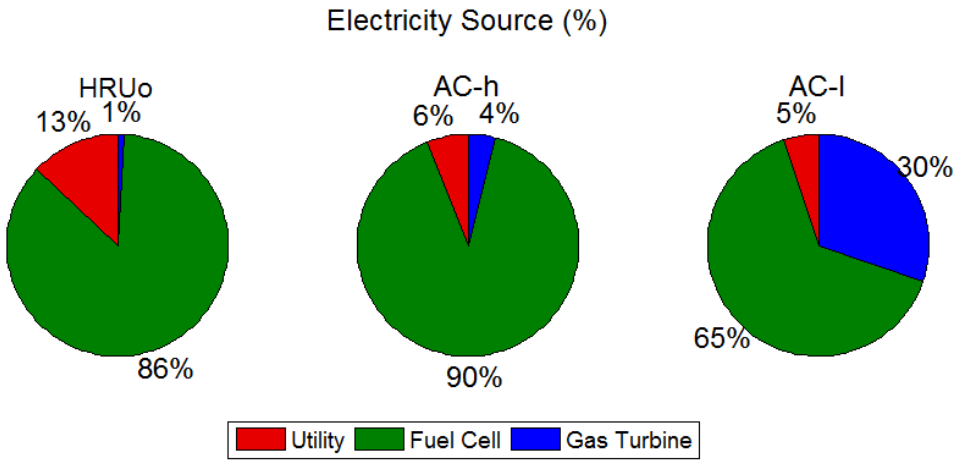

Figure 5-80: Source of electricity to meet the Patton building electrical demand for all technology scenarios

Waste heat is used to meet the majority of the heating load through the use of a heat recovery unit. Figure 5-81 shows that the amount of heat supplied from the HRU under the HRUo and AC-h scenario is roughly the same, but increases under the AC-l scenario. The high level of coincidence between the two thermal loads and the electrical load coupled with the size of the loads allows for the technology scenarios to achieve the following fuel utilizations: 78% for HRUo, 82% for AC-h, and 81% for AC-l.

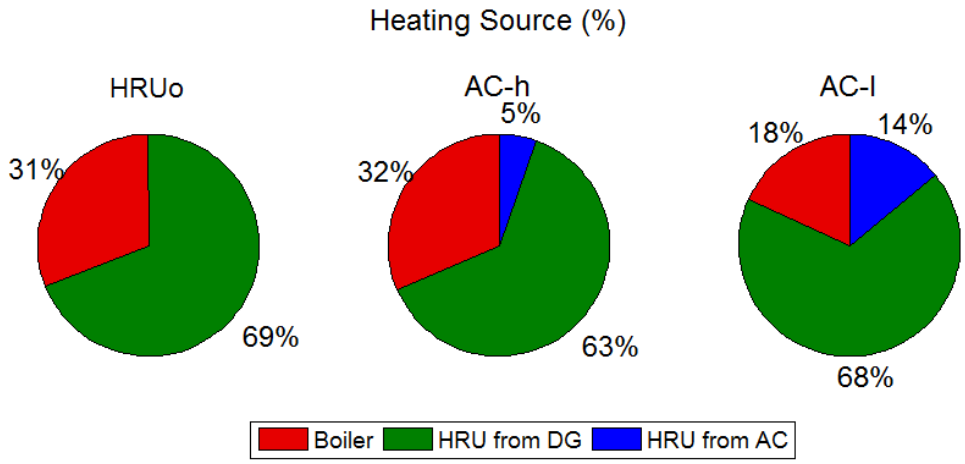

Figure 5-81: Source of heating to meet the Patton building electrical demand for all technology scenarios

Figure 5-82, Figure 5-83, and Figure 5-84 show electrical, heating, and cooling operation respectively for the same winter week for the Patton building. Electrical operation for the HRUo and AC-h scenario is similar to all other buildings previously studied, with the fuel cell providing baseload or load following power while the microturbine is used to perform peak shaving, particularly during the winter mid-peak period. Heat recovery unit operation mirrors fuel cell operation, with the HRU being used to meet the entire heating load when possible. Under the AC-h scenario, the absorption chiller is dispatched to manage electrical imports, with operation only occurring during the day. The maximum electrical load produced by the combined electrical and cooling demand is reduced by 322 kW under the AC-h technology scenario.

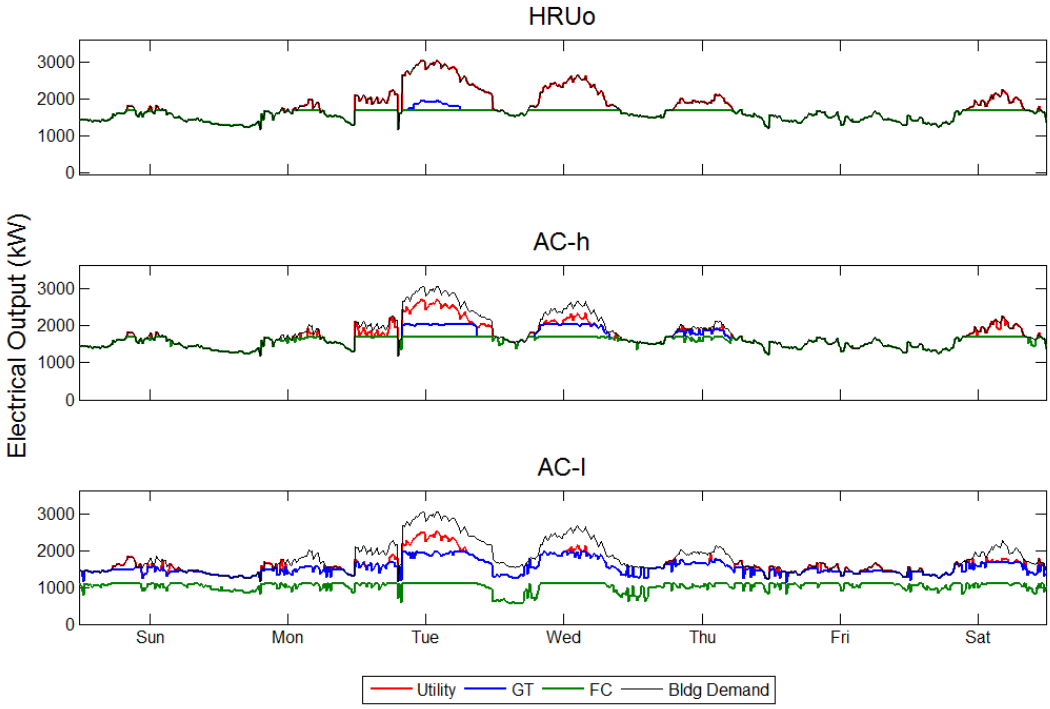

Figure 5-82: Winter electrical operation for all technology scenarios adopted at the Patton building

Electrical operation under the AC-l scenario differs from winter operation seen in previously studied buildings. Since approximately 43% of the installed capacity is due to microturbine adoption, microturbine operation expands from dispatch during the middle of the day to continuous operation. The coordination of fuel cell and microturbine operation depends on more than the building electrical load at any given moment, but relies on the thermal loads as well. For example, the relatively low electrical load occurring Sunday night decreases through time. Instead of reducing microturbine operation while maintaining fuel cell operation, the fuel cells are turned down since the extra waste heat produced by the microturbines can be utilized by the heating load. Later, during early Wednesday morning, the electrical demand drops, and

microturbine operation is again maintained, favoring the additional production of waste heat for use to meet thermal loads.

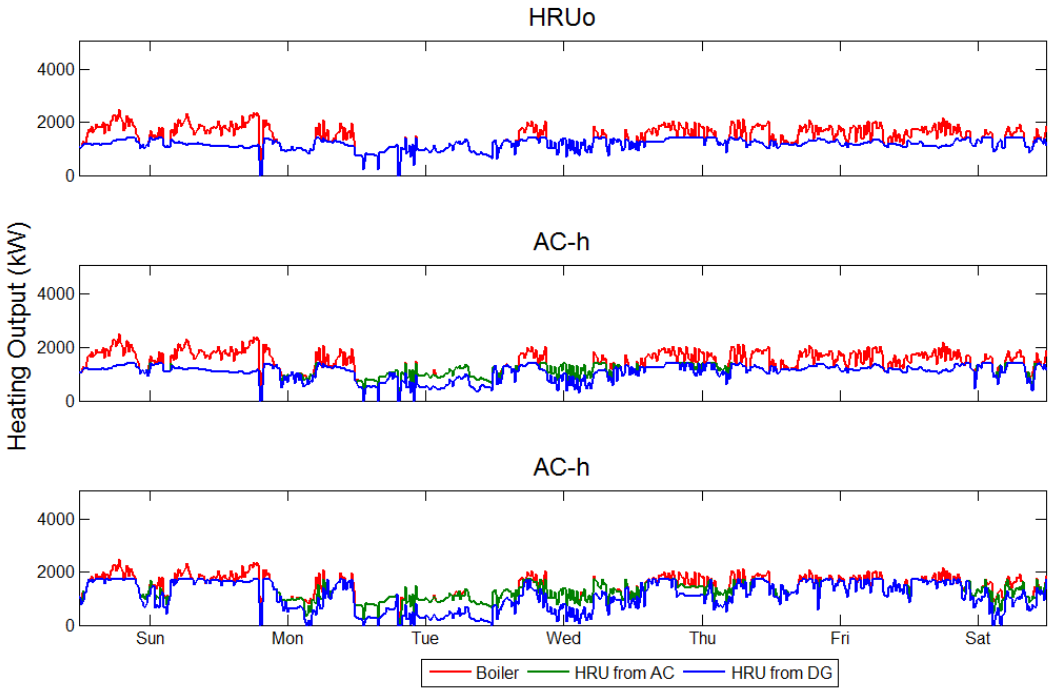

Figure 5-83: Winter heating operation for all technology scenarios adopted at the Patton building

During the two instances occurring mid-day Tuesday and Wednesday where electrical and cooling loads are high while the heating load is low, both fuel cells and microturbines are operated at near power, with the waste heat being first diverted to the absorption chiller in order to reduce the overall electrical demand. During this period, the heat recovery unit is still used to meet the majority of the heating demand, but the capture of waste heat from the absorption chiller is greatest during these two time periods.

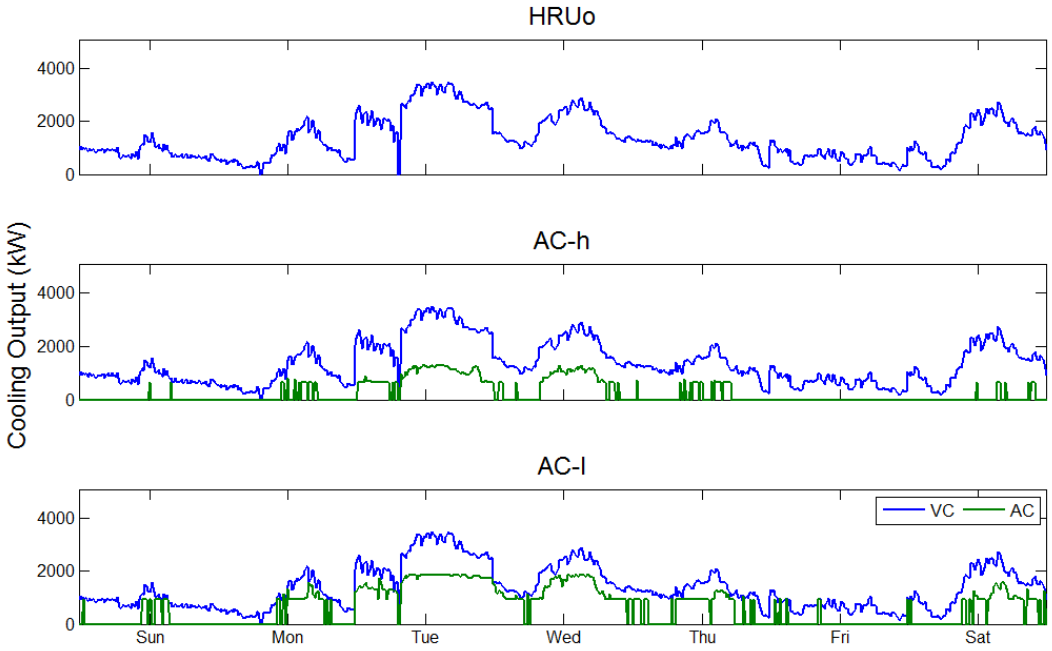

Figure 5-84: Winter cooling operation for all technology scenarios adopted at the Patton building

Summer electrical, heating, cooling, and absorption chiller operation are shown in Figure 5-85, Figure 5-88, Figure 5-86, and Figure 5-87 respectively. Similar to winter operation, summer electrical operation is similar to how similar systems are operated at the other studied buildings. Operation under the AC-l scenario is similar to operation of the same system during the winter, with the operation of all systems being managed to reduce utility imports while meeting the waste heat requirements of the adopted HRU and absorption chiller.

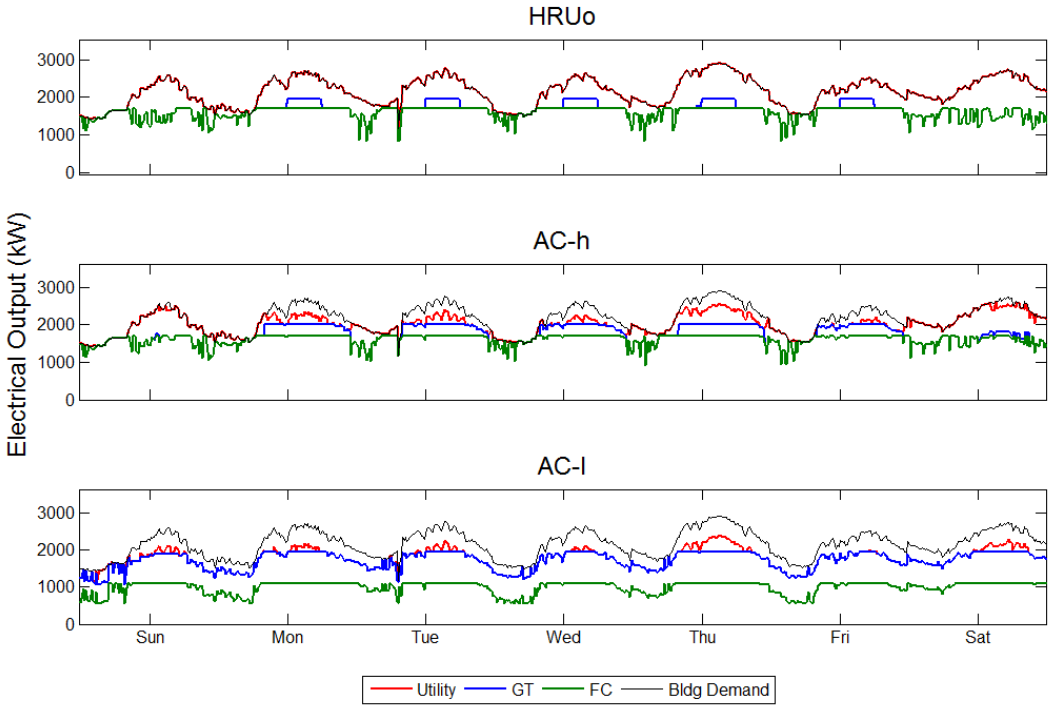

Figure 5-85: Summer electrical operation for all technology scenarios adopted at the Patton building

Absorption chiller at other buildings are operated continuously during the summer for both the AC-h and AC-l technology scenarios. AC operation at the Patton building differs in that dispatch only occurs during the middle of the day, with the load occurring during off peak being met using the vapor compression system. Shifting to the AC-l scenario, absorption chiller operation increases, with a large portion of off-peak cooling being met through AC operation. Under this scenario, the maximum combined electrical demand is reduced by 544 kW due to absorption chiller operation.

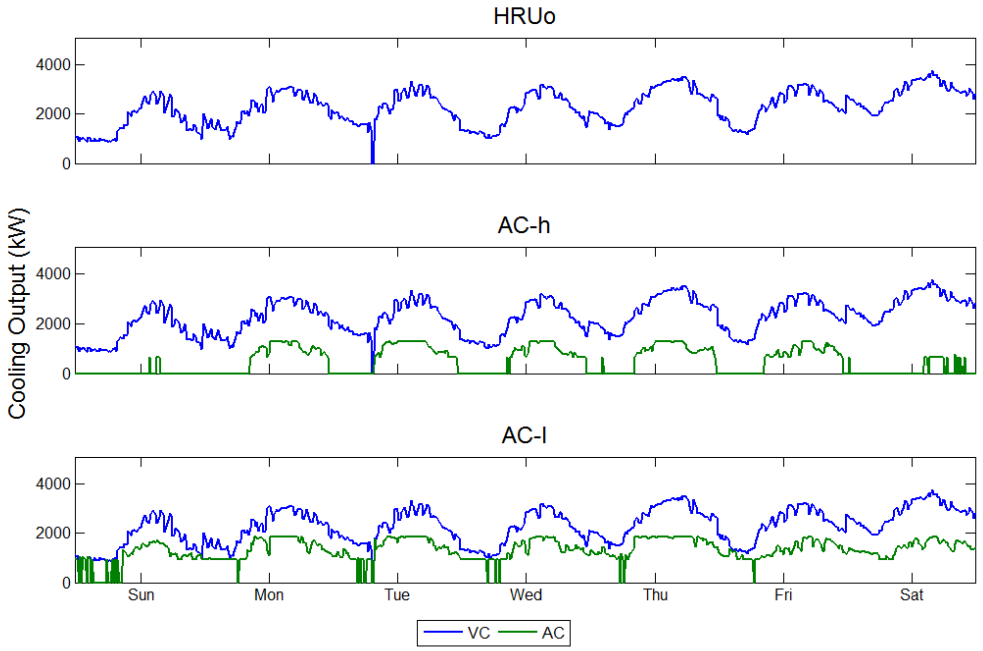

Figure 5-86: Summer cooling operation for all technology scenarios adopted at the Patton building

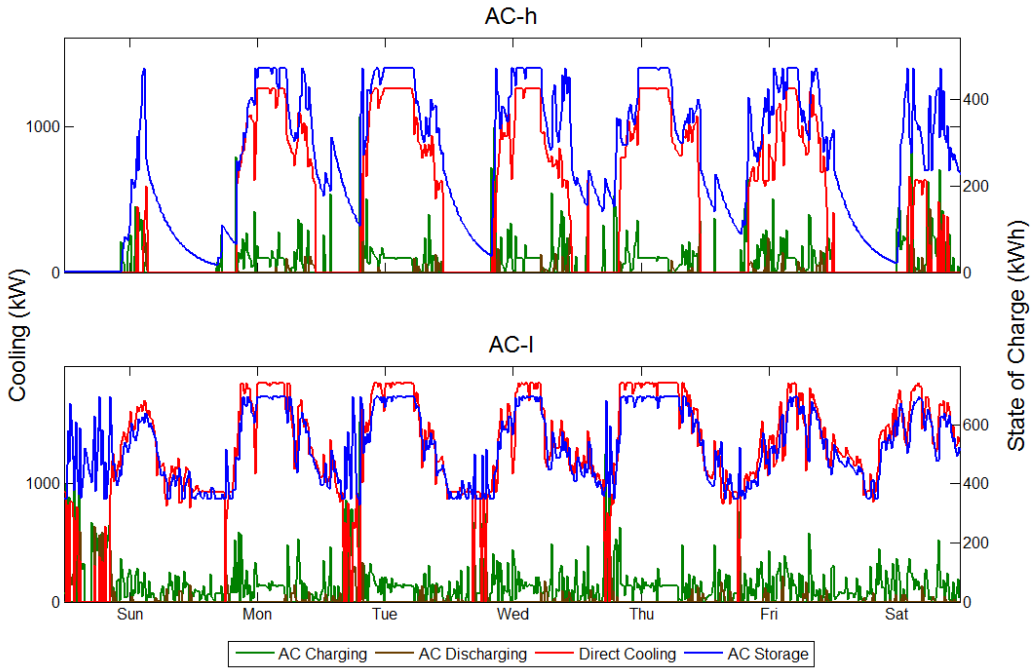

Figure 5-87: Summer absorption chiller operation for all technology scenarios adopted at the Patton building

Instead of being dispatched to continuously provide cooling, the absorption chiller output is managed to reduce the electrical demand associated with the cooling load while also providing enough waste heat to the heat recovery unit, as seen in Figure 5-88. Note that heating operation between the AC-h and AC-l scenario does not change significantly, with the HRU providing more of the heating load under the AC-l scenario.

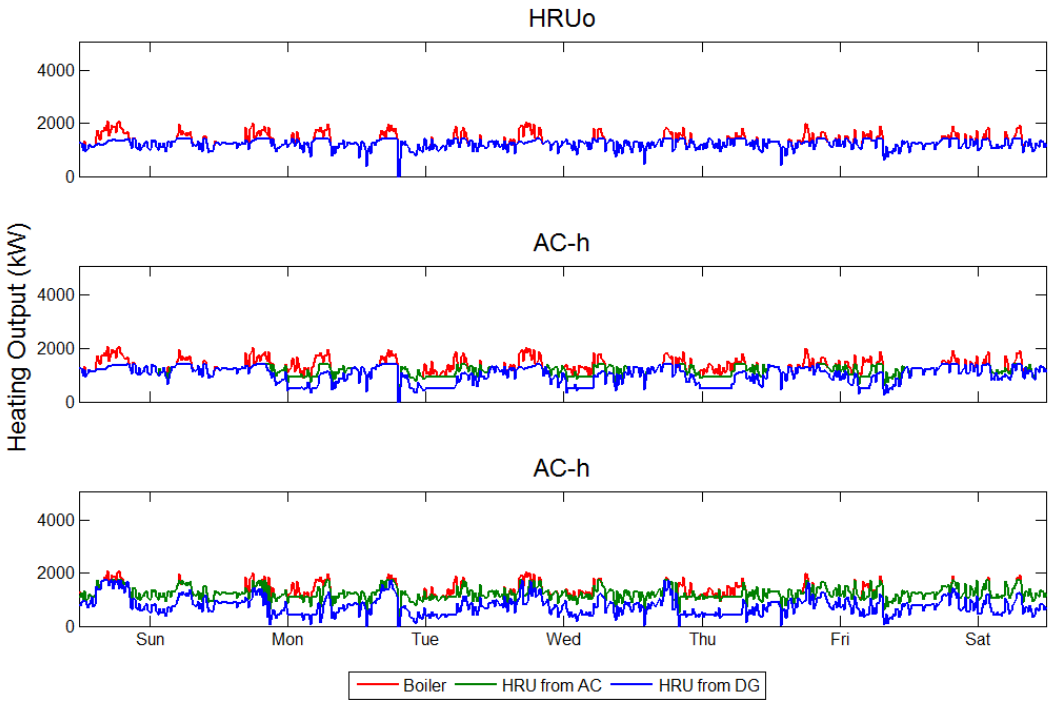

Figure 5-88: Summer heating operation for all technology scenarios adopted at the Patton building

Overall, the additional operation of the absorption chiller allows for more of the heating load to be met by the heat recovery, and also reduced the maximum combined electrical demand by 544 kW.

5.2.5.2 Financial Performance

All three DER systems adopted at the Patton State Hospital experience good financial performance, as seen in Figure 5-89. In particular, the adoption of a low O&M cost absorption chiller improves the rate of return from approximately 9% under the HRUo scenario to above 14% under the AC-l scenario at year ten. Adoption and operation of an absorption chiller is not responsible for the increase alone. HRU operations increase under the AC-l scenario, but more importantly, a shift from fuel cells to a mix between fuel cells and microturbines occur, reducing the initial investment cost associated with the purchase of the DER system. As seen in the figures showing DER system operation, the management of fuel cells and microturbines to continuously meet or reduce the electrical demand while supplying nearly all of the heating load and managing the cooling load during mid-peak and on-peak periods, the flexibility of changing the available waste heat to meet the current thermal demand added flexibility in operation that has not been seen in any of the smaller buildings examined.

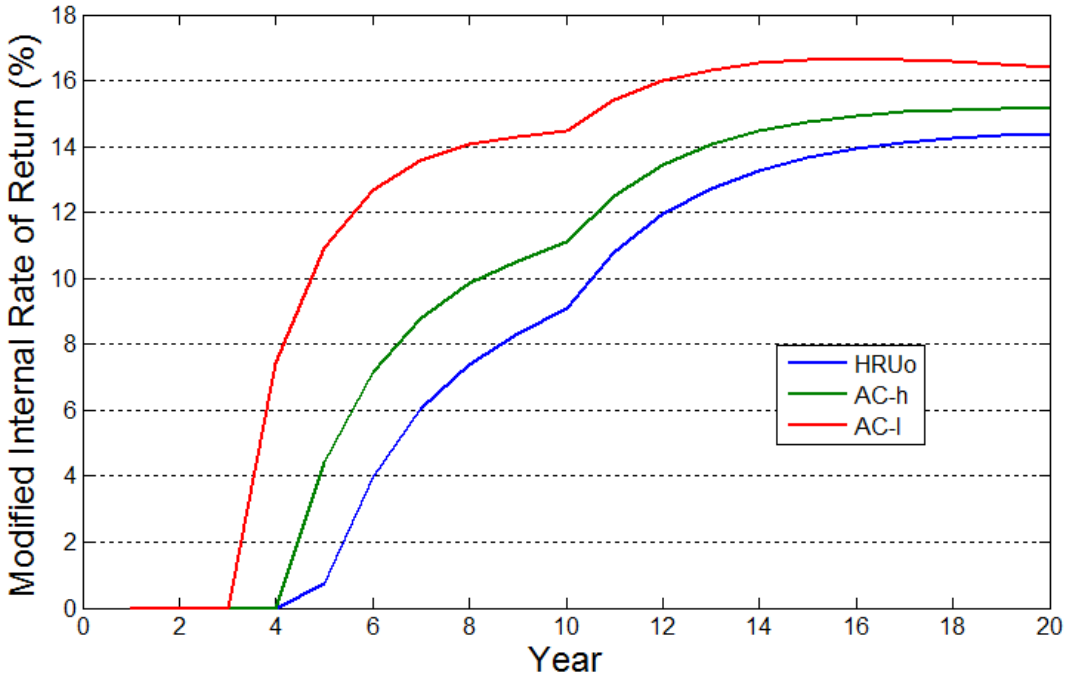

Figure 5-89: Modified internal rate of return for all three technology scenarios when adopted and operated at the Patton building

Allocating the cost components reveals more information on the financial performance of the DER systems. Figure 5-90 shows the allocated utility costs. The allocated costs for the AC-h and AC-l scenario are similar to results for prior buildings, and do not require further discussion. All past results have shown that the heating load typically receives a large negative utility energy and demand cost allocation. This does not occur under the Patton building. A negative allocation for these costs suggest that DG operation occurs in part due to the ability to recover waste heat through the use of a HRU to meet the building heating load. For this particular building, this is not the case, and the heating load does not drive the shift from supplying electricity using imported electricity to onsite generation. Similar financial behavior is experienced under all technology scenarios for the St. Regis hotel building, suggesting that under the HRUo scenario, the electrical load is the primary driver for the adoption and operation of multiple fuel cells.

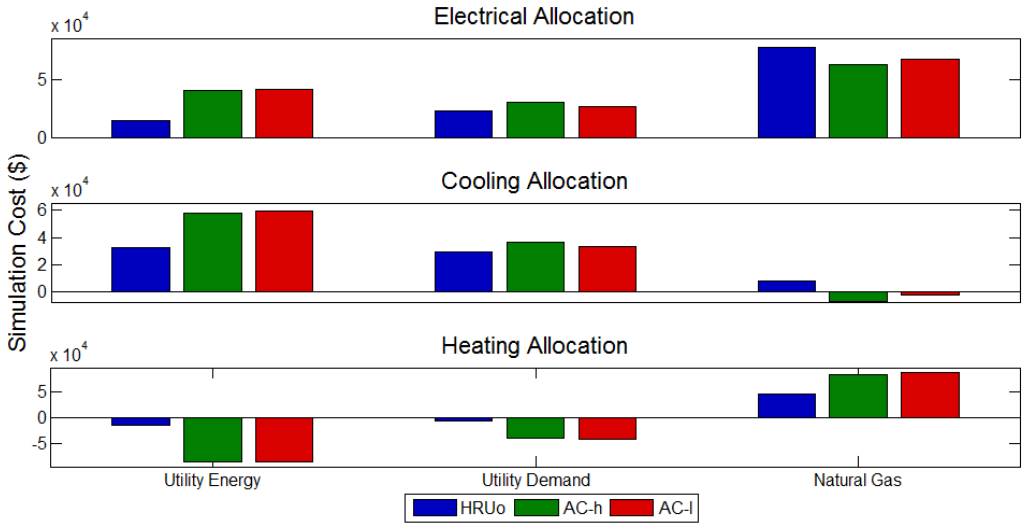

Figure 5-90: Utility costs allocated to the production of electricity, cooling, and heating for the three technology scenarios at the Patton building

This result is further confirmed by the allocation of fuel cell and microturbine O&M costs, as seen in Figure 5-91. Under the HRUo scenario, the majority of fuel cell O&M cost is allocated primarily to the electrical load. However, under any scenario where an absorption chiller may be adopted, fuel cell O&M is shared by both the electrical and heating load. Meanwhile, the cooling load suppresses fuel cell operation in favor of increased microturbine operation. Similar behavior can be seen at the SCAQMD building, where the different thermal loads prefer the operation of different generators. Under the AC-h and AC-l scenarios, both the cooling and heating load receive large portions of DG O&M cost.

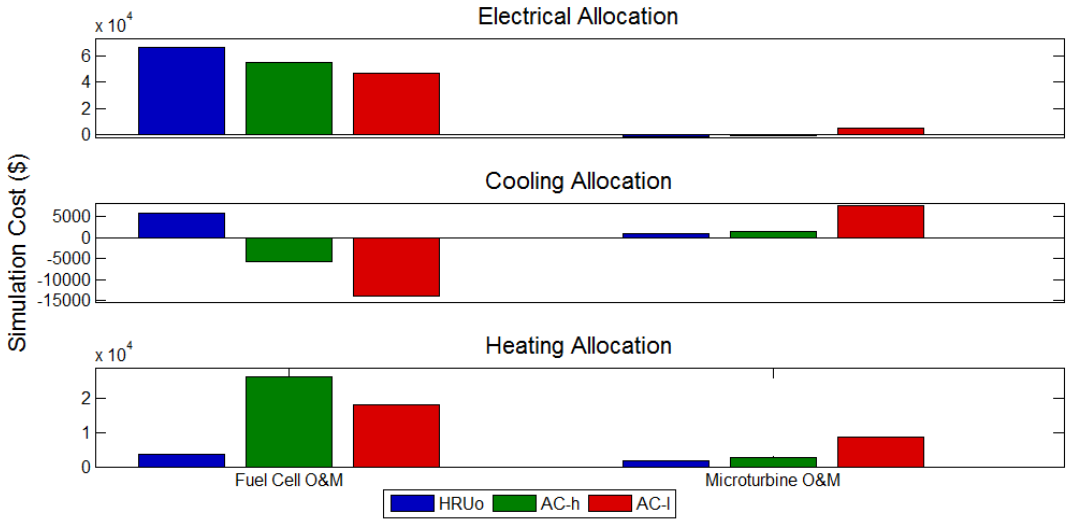

Figure 5-91: Fuel cell and microturbine O&M costs allocated to the production of electricity, cooling, and heating for the three technology scenarios at the Patton building

Despite supporting different types of power generation, the cooling and heating loads both support a mutual switch from the traditional methods of thermal energy generation towards the methods powered by the use of waste heat. Figure 5-92 and Figure 5-93 show O&M associated with technology used to produce cooling and heating respectively. The heating load receives a negative vapor compression allocation when an absorption chiller is available as an option, while the cooling load receives a negative boiler O&M allocation. The scenario in which the absorption chiller produces 50% of the building cooling load is also the scenario in which the cooling load is allocated the largest reduction in boiler O&M.

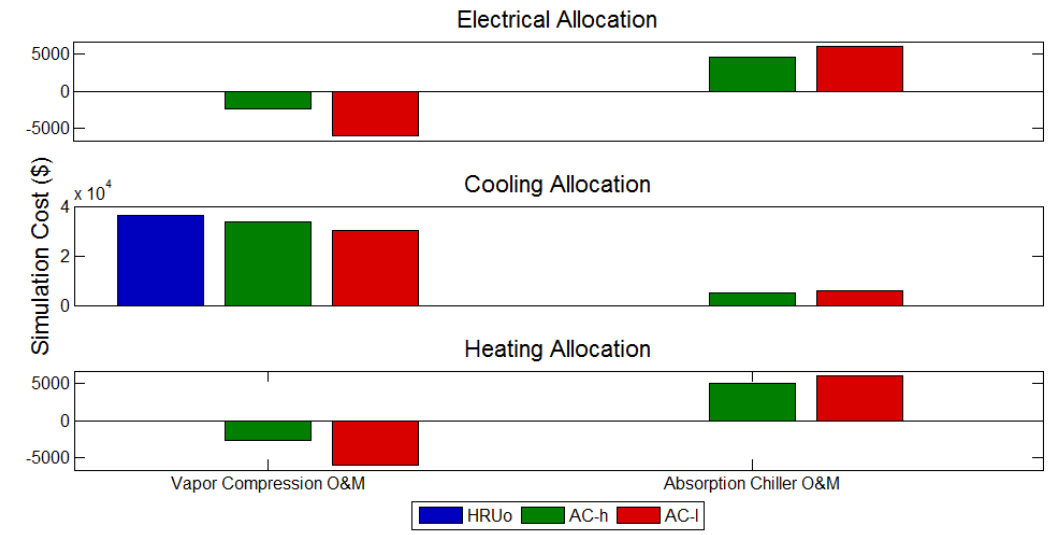

Figure 5-92: Vapor compression and absorption chiller O&M costs allocated to the production of electricity, cooling, and heating for the three technology scenarios at the Patton building

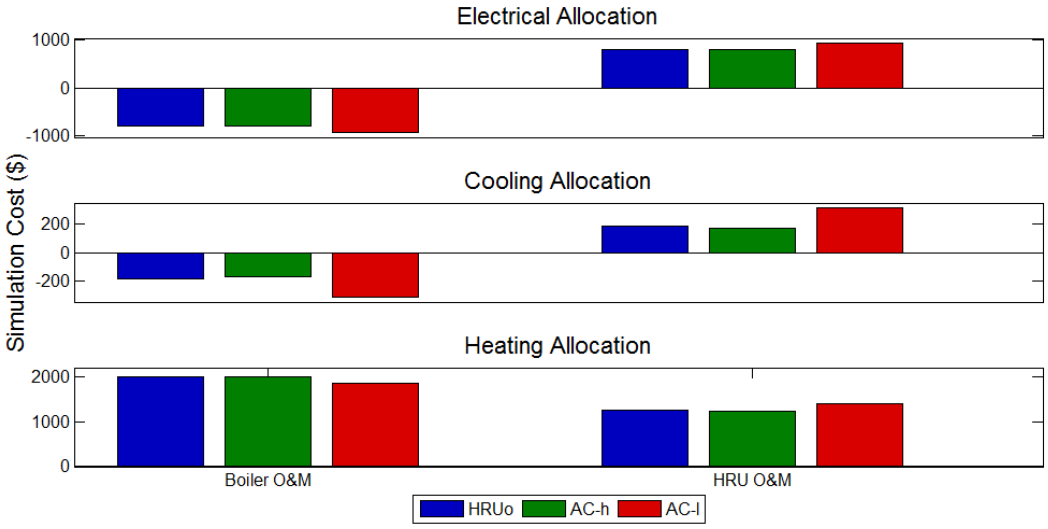

Figure 5-93: Boiler and heat recovery unit O&M costs allocated to the production of electricity, cooling, and heating for the three technology scenarios at the Patton building

Using the allocated costs, the corresponding levelized cost of energy and modified internal rate of return were calculated for electricity, cooling and heating, and are shown in Figure 5-94. The same levelized cost of electricity increase is seen for the three technology

scenarios during year five. However, both scenarios that include an absorption chiller are able to produce savings and generate a positive rate of return by year eight for the AC-h scenario and year 6 for the AC-l scenario. Parity with the baseline scenario is achieved in year nine for the cost of cooling under the HRUo scenario. If an absorption chiller is available for adoption, then the cooling load suppressed the addition of additional fuel cells in favor of microturbines. The resulting change in investment results in a reduced initial investment cost and a negative allocation investment cost for cooling. In other words, the cooling load deserves to be compensated by electricity and heating loads as an investment, the cooling load is still allowed to adopt an absorption chiller and take advantage of produced waste heat from the adopted fuel cells, and savings are realized. This results in an infinite rate of return for both the AC-h and AC-l scenarios, and an instant reduction to the levelized cost of cooling. The heating load is allocated a portion of the fuel cell investment cost, resulting in a positive investment associated with cooling. However, savings are significant enough that a reduction in levelized cost of heating is realized for all scenarios by year seven. By year nine, the levelized cost of heating has been reduced by at least $0.005 per kWh for all three technology scenarios.

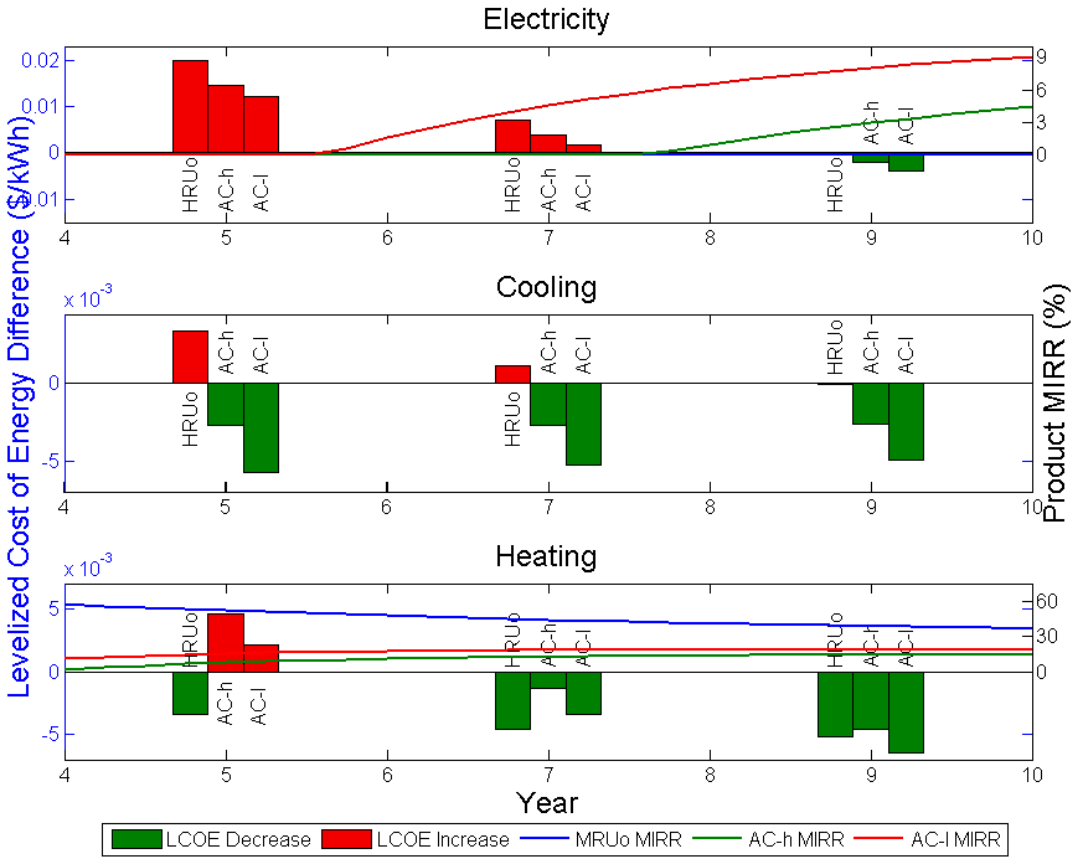

Figure 5-94: Levelized cost of energy difference at years five, seven, and nine and corresponding modified internal rate of return for electricity, cooling, and heating when DER systems are adopted according to the three technology scenarios at the Patton building

5.2.5.3 Building Carbon Emissions

Under baseline operations, 7,350 tonnes of CO_2 per year is emitted in order to meet the energy loads of the Patton building. Adopting a DER system results in an overall reduction in the HRUo and AC-h technology scenarios and an increase in the AC-l scenario, as seen in Figure 5-95. Figure 5-96 shows the difference broken down by the change in carbon emissions due to the electrical, cooling, and heating loads.

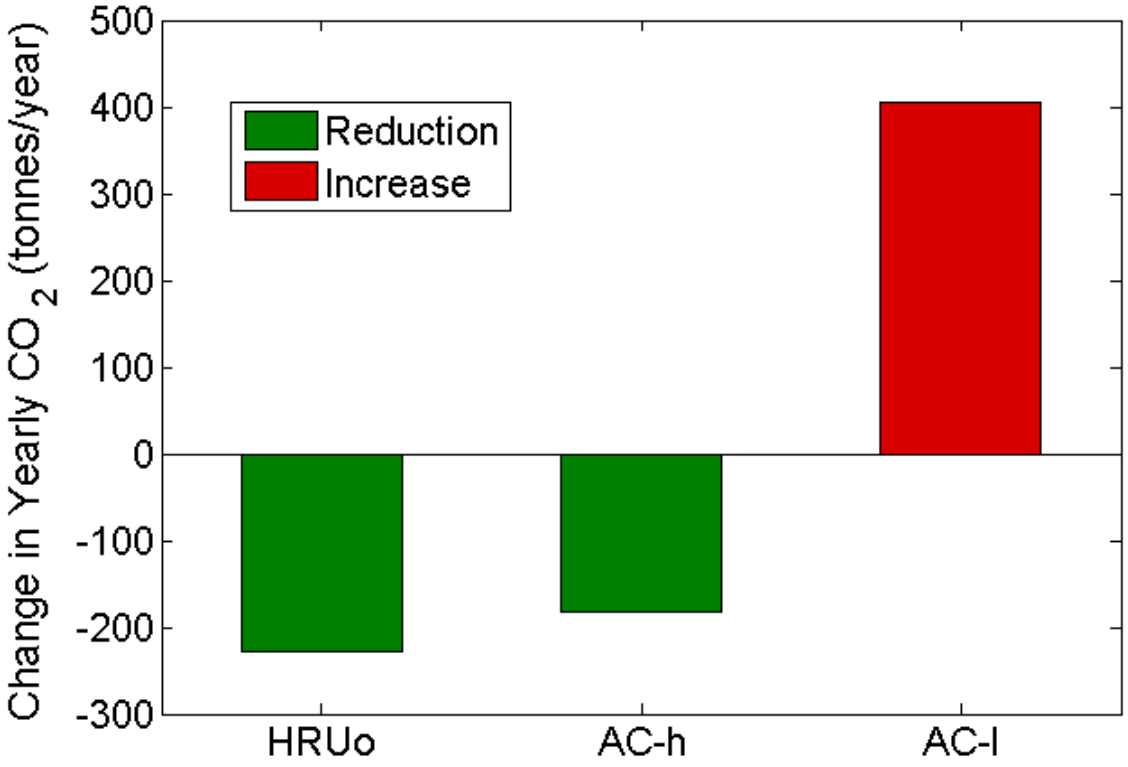

Figure 5-95: Change in yearly carbon emissions for the Patton building as a result of DER system adoption

When total carbon emissions are reduced, both the heating and cooling load contributed to the overall reduction. One reason why the cooling load is capable of achieving an associated reduction is that the operation of the adopted DG occurs due to a combination of the electrical and heating load. As a result, the carbon emissions are attributed to these two loads (primarily to the electrical load), allowing for the absorption chiller to have access to waste heat for which the associated carbon has already been assigned to another load. In essence, the same mechanisms that result in extremely good financial performance for both cooling and heating (or the fact that the electrical load drives DG operation) also benefit both thermal loads in being assigned less carbon.

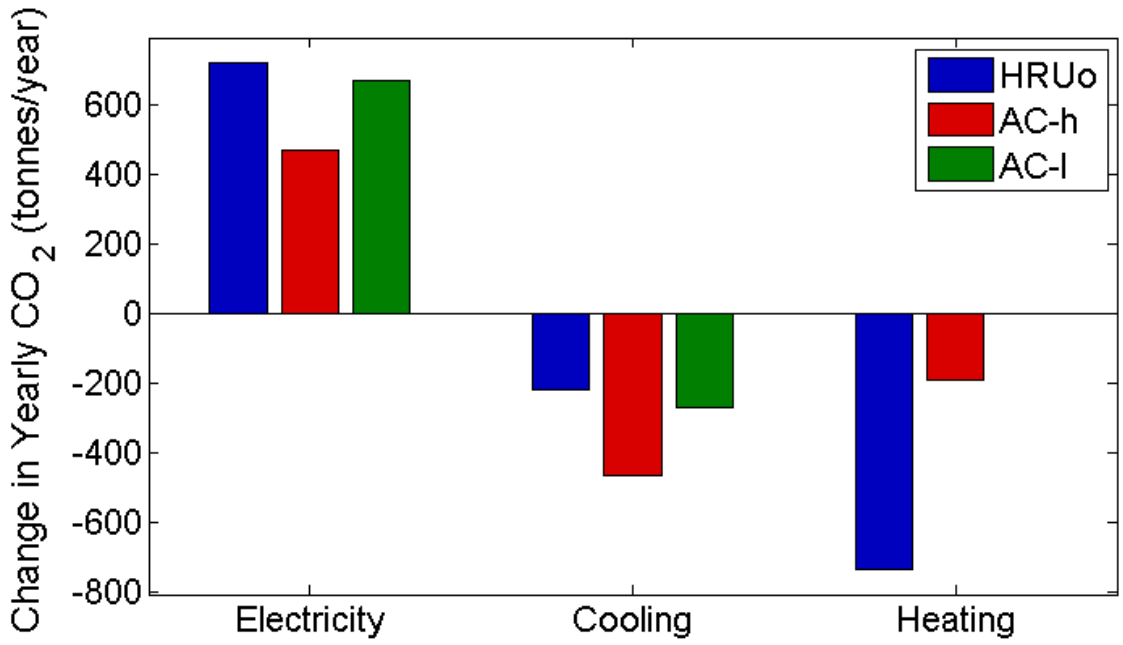

Figure 5-96: Change in yearly carbon emissions for individual types of energy for the Patton building as a result of DER system adoption

5.3 Discussion

The buildings included in this study range in average electrical demand from 195 kW to 1400 kW. The size and dynamics of the thermal loads includes small but consistent (USN building), average size but inconsistent (UCI Cal IT^2), large and coinciding with maximum electrical demand (SCAQMD), average and consistent (St. Regis), and large and consistent (Patton). By no means are all types of building operation captured in this study. For example, the most dynamic electrical load tested has an electrical load factor of 0.41 (SCAQMD) much more dynamic load profiles exist, particularly for industrial operations. However, many buildings have operation within the range of the buildings evaluated, or should have similar results to the buildings evaluated.

One of the most commonly determined results in the literature is also found through this work. Reducing fuel cell capital cost to approximately around $2,000 per kW results in large scale adoption at many building types. Despite having higher capital and O&M cost than the other competing option (a microturbine), the high electrical efficiency propels the fuel cell into being selected by the optimization routine as the primary provider of electrical energy for all buildings investigated.

Another common finding in the literature is that fuel costs are important to the financial success of an investment in a CCHP system. This work agrees with this finding, but extends it to how real world natural gas utility rates impact the adoption and performance of a CCHP or DER system. From a practical perspective, the amount of fuel consumed by any installed system is limited by the amount of electrical energy demanded by the building. Due to the structure of the declining block rate structure, any DG operating at a building with a relatively small electrical load will never convert enough natural gas into electricity to reach the lower cost natural gas blocks, as seen for the USN building. On the other hand, a building like Patton State Hospital easily consumed enough natural gas through DG operation to quickly reach the least expensive natural gas block, and the cost to purchase a therm of natural gas was reduced by 13% from the rate paid by the USN building. Even if the electrical load dynamics and ratios between total thermal loads and the electrical load were similar, a smaller building will always have higher fuel costs. This inherent advantage provides a boost to financial performance for large buildings.

From the perspective of comparing the financial usefulness of using heat to power a heat recovery unit or absorption chiller, there is no clear winner. In the situation in which the best financial performance was achieved (Patton State Hospital), the supply of waste heat was

managed in a way that improved operation of all systems. Under the scenario with the best financial performance (the AC-l scenario), the absorption chiller operation was leveraged to increase heat recovery unit capacity and operation, and vice versa. In addition, the composition of the installed DG system changed, with numerous fuel cells being replaced with microturbines. The overall installed DG capacity barely changed versus the installed capacity under the AC-h scenario. However, the mix of DER technologies allowed for the overall system to respond differently depended upon the particular load requirements at any given time. When thermal loads were high but the electrical load was low, fuel cells were turned down in favor of microturbine operation that produced sufficient heat to maintain operation of all thermally activated technologies. When the thermal loads were low, microturbine operation was reduced in favor of the more efficient fuel cell systems. The best attributed of the different technologies could be realized, improving overall system performance. Note that this level of operation was not achieved until the absorption chiller O&M cost was reduced to parity with vapor compression O&M. Prior to this scenario, fuel cells dominated the adopted DG capacity, the absorption chiller was primarily used to reduce the electrical load in order to manage the utility demand charge, and cooperation between the absorption chiller and heat recovery unit was rare. While waste heat from the absorption chiller was still captured downstream in the heat recovery unit, the systems operated independently of each other.

The scenario presented by the Patton State Hospital is obviously CCHP friendly since the thermal loads are consistent and large, providing great opportunity for the capture of waste heat produced by adopted DG. Notice that the key to unlocking the synergistic CCHP operation was not low fuel cell capital cost or low natural gas cost, but low absorption chiller O&M cost. Prior

to reaching party with vapor compression chiller systems, the absorption chiller at Patton State Hospital was dispatched to manage the electrical demand such that demand charges did not increase or the electrical demand of the building could be met using the installed DG system. Whenever the cooling demand either was low or did not coincide with a large electrical load demand, absorption chiller operations ceased. The value created by the absorption chiller was limited to reducing demand charges since every kWh of cooling produced increased O&M costs above what it would cost to simply use the legacy vapor compression system. Under this scenario, the economic potential of the absorption chiller is limited. Lowering absorption chiller O&M cost not only expands the chiller economic value, but provides new avenues through which a CCHP system can collectively operate to increase energy savings. Allowing for absorption chiller adoption to occur expands the flexibility of the CCHP system and creates new ways in which the building energy loads can be managed to increase savings. Achieving a low absorption chiller O&M only increases this flexibility, improving the financial performance in every scenario tested.

The flexibility of a DER system is heavily dependent on the building energy loads. For example, the St. Regis building is also able to provide low cost natural gas, but the economic performance of any adopted system is not as attractive as the optimal systems adopted by Patton State Hospital. Even though the thermal loads are consistent and are not small (the ratio of heating to electrical and cooling to electrical load is 0.49 and 0.46 respectively), the loads are small enough to discourage the adoption of a large set of microturbines. The installed fuel cells are capable of meeting the majority of the electrical load while also supplying waste heat to meet both thermal loads.

The SCAQMD building presents a case where a mixed CCHP system is adopted, but the opportunistic behavior exhibited during AC-l operation at the Patton State Hospital does not occur. Since the cooling load primarily only occurs during the day, and is large, the value of an absorption chiller is limited. Microturbine operation also only occurs during the middle of the day, as if the sole purpose of the turbines were to power the vapor compression and absorption chiller system. In this respect, the microturbine and absorption chiller system operate in a nearly independent state away from the fuel cell and heat recovery unit system. Of course some transfer of waste heat from the fuel cell to absorption chiller and microturbine to heat recovery unit does occur, but the limited time over which the cooling load occurs limits the economic usefulness of any connection between the absorption chiller and heat recovery unit.

Both the UCI Cal IT^2 and USN buildings have associated energy loads that appear to integrate well with a CCHP system. The UCI Cal IT^2 building, however, has an inconsistent heating load that is unable to capture large amounts of waste heat in an economically efficient manner. The USN building is simply too small for the adoptable generators. While the thermal loads are consistent, the available generators cannot operate at a part load low enough to tailor CCHP operation to follow either the heating or cooling load. AS a result, the USN building experiences the lowest fuel utilization of any building except for under the HRUo technology scenario.

Note that the primary benefit provided by an absorption chiller is not the supply of cooling, but the augmentation of the electrical demand created by the combined electrical and cooling load. By shifting the cooling load from a vapor compression chiller system to an absorption chiller, the original electric demand can be reduced. If this reduction occurs when the

electrical load is high, then the size of the combined electrical demand can be reduced in a manner that resembles the adoption of additional DG. The buildings that experience the greatest reduction in combined electrical demand also experience the greatest savings and best economic results. For example, the adoption and operation of an absorption chiller at the Patton building reduces the maximum combined electrical demand being reduced by 10% (or 322 kW) under the AC-h scenario, and 17% (or 544 kW) under the AC-l scenario. This electrical demand is equivalent to the purchase and operation of 322 kW or 544 kW of photovoltaic panels at that given moment, only at a fraction of the initial investment cost. The combined electrical demand reduction occurring at the other four buildings are as follows: St. Regis: 5% under AC-h and 9%under AC-l, SCAQMD: 0% under AC-h, and 3% under AC-l, UCI Cal IT^2: 10% under AC-h, and 11% under AC-l, and USN: 5.7% under both. The inability of a DER system to reduce the combined electrical demand through the dispatch of an absorption chiller contributed to the poor economic performance of CCHP systems at both the SCAQMD and USN building. The savings created by an absorption chiller at these buildings is muted, since the large benefit of reducing combined electrical demand does not exist to counteract and increased cost, such as O&M costs, incurred as a result of absorption chiller operation.

In addition, the building with the highest electricity cost (SCAQMD at $0.0986 per kWh), was not able to achieve the best financial performance as a result of DER system integration. On the contrary, this building experienced the poorest financial buildings other than the small USN building. Despite having access to relatively low cost fuel, having a consistent heating load, and a cooling load that coincided nicely with desired microturbine operation, the financial performance of the adopted DER systems suffered from not being able to sue the

absorption chiller to reduce the combined electrical demand. Instead, two buildings with a lower baseline cost of electricity and smaller overall thermal loads (which would suggest less room to produce savings), were able to achieve better financial performance. Particularly, the attributes of the Patton building energy loads allowed for the adopted DER systems to excel financially.

Breaking down the financial performance into an investment and savings associated with each type of energy product provided additional insight into the overall financial performance. Of all the buildings studied, desirable financial performance did not occur unless the cost of the building heating load was reduced. The savings generated through the use of waste heat in a heat recovery unit form a basis from which additional savings derived from the cooling and electricity load can increase financial performance. For the scenarios where good financial performance occurs, the heating load was never the primary driver for DG adoption. Instead, the electrical or cooling load supported DG adoption, allowing waste heat to be provided to a heat recovery unit with little or no DG investment or O&M cost to the heating load. In order for this to happen, DG adoption must be desirable at the building even without the capture of waste heat. When this scenario occurs, and the thermal loads are not required for DG operation, the operation of the waste heat recovery technologies is allowed to produce savings without needing to offset any increased cost to the electrical load as a result of DG adoption.

Naturally, the buildings for which electricity producing DG would be most desirable would be at large buildings due to the combined factors of possibly achieving economies of scale as a result of adopting a large DG system, while also providing access to low cost fuel. Reducing the size of the building, even if the building has relatively large and consistent thermal loads, will reduce the economic performance of any installed CCHP system. In other words, buildings that

have traditionally been accepted as desirable locations for CCHP system integration, such as supermarkets or schools, may not be the best candidates for CCHP adoption. Likewise, large buildings with relatively small thermal loads may prove to be very desirable locations for CCHP system integration.

The optimization of CCHP system at the five buildings almost always resulted in an increase to CO_2 emissions. This result, however, is not an indictment of CCHP technology in general, but is more a product of the carbon emissions associated with the baseline scenario. The California electric grid produced electricity with one of the lowest carbon signatures in the country. In addition, current boiler technology is able to combust a low carbon content fuel like natural gas, and capture upwards of 90% of the released thermal energy. Likewise, currently available vapor compression chillers are capable of operation with a coefficient of performance much greater than the 3.4 value using in this current work.

In fact, the ability of any CCHP system to reduce carbon emissions overall without explicitly including either a cost or constraint limiting carbon emissions are impressive. These scenarios only occurred when high fuel utilization occurred, although high fuel utilization did not always correspond to reduced carbon emissions. In fact, the systems for which a carbon emissions reduction occurred had a combination of high fuel utilization, extensive HRU system operation, and an absorption chiller O&M cost higher than vapor compression O&M cost. For all buildings, carbon emissions increased with absorption chiller operation.

Two separate reasons create this result. The first reason is that an absorption chiller is not able to fully utilize the entire energy content provided in a waste heat stream. Due to the elevated

operating temperature of the refrigerant generator in an absorption chiller, heat transfer from the waste heat stream to the absorption chiller will not occur after a certain point.

The second, and more important, reason is that the competing option of a vapor compression system powered by grid electricity operates with a very small carbon signature. For example, if a vapor compression system with a COP of 3.4 operates in the middle of the day when the electrical grid carbon emissions factor is relatively low (600 lbs. CO_2 per MWh of electricity), carbon emissions per unit of cooling are extremely low (176 lbs. CO_2 per MWh of cooling). Taking this into account, the chances of reducing carbon emissions are slim-to-none when an absorption chiller is used to provide a large portion of a building cooling load because the baseline option already has a low carbon signature to begin with.

As stated before, these results are indicative of the relatively low carbon signature associated with baseline operation. If this analysis were to take place in almost any other state, where the carbon content of the primary electrical utility fuel source is higher (e.g., coal), then a carbon reduction would certainly occur as a result of installing a fuel cell and absorption chiller system.

6 Optimal DER System Design with a CO_2 Emission Constraint

The purpose of Section 5 is to explore the decision to install a CCHP system and use the DG waste heat to produce either heating, cooling, or both. The optimal CCHP adoption model did not include any environmental constraints. From a practical perspective, the environmental impact of a CCHP system located in California can be ignored if two conditions are met. First, if carbon dioxide emissions associated with building activity are less than 25,000 metric tons, then the building does not need any carbon emission permits [175]. Second, if the generators selected during optimization produce oxides of nitrogen, carbon monoxide, and volatile organic compounds at rates lower than the levels required by the California Air Resource Board (CARB) for generators of their size [176], the generators may be installed and operation. By limiting the optimization to buildings that have associated carbon emissions lower than 25,000 metric tons and optimizing only for generators that meet the CARB pollutant emission requirements, the applicable environmental constraints are implicitly satisfied. Any decrease to the carbon or pollutant emissions are voluntary and would only occur if the building operator places a priority on reducing carbon or pollutant emissions.

If the focus is shifted from smaller to larger buildings, total carbon emissions will most likely increase and must be accounted for during optimization. Under the current carbon cap and trade market used in California, a carbon emitter (such as a building operator) must purchase a permit to emit a certain amount of carbon if total yearly carbon emissions are estimated to be more than 25,00 metric tons [175]. This additional cost of purchasing the permit can be included in the optimization by increasing fuel cost to include the cost associated with the carbon content

of the fuel. Unless the total permitted amount of carbon emissions for all of California is reduced, a carbon constraint is not required during DER optimization.

For some institutions and businesses, objectives other than cost may motivate the desire to reduce carbon. One institution, the University of California, has committed "…to emitting net zero greenhouse gases from its buildings and vehicle fleet by 2025…" in order to remain a world leader in sustainability [177]. This commitment requires that the ten campuses, five medical centers, and three national laboratories that make up the university system collectively reduce carbon emissions. Such a reduction can be accomplished in part by purchasing utility electricity from renewable electricity providers or purchasing carbon offsets, but will also include the adoption of on-site and off-site renewable energy technology at/for individual campuses [178].

Ideally, the path towards carbon neutrality would simultaneously consider all University of California campuses, medical centers, and national laboratories. However, the resolution required by some of these decisions, such as how much solar energy capacity should be installed at each campus, can require that a more granular approach be used to evaluate each individual institution. From the perspective of what renewable or sustainable DER systems can be used to help achieve the carbon neutral goal, the DER optimization model presented in Section 3.4, including the carbon emission constraint presented in Section 3.4.2, can be used to find the path required to achieve carbon neutrality at the lowest cost possible.

It is unlikely that the final set of decisions that will lead to carbon neutrality will be implemented overnight. In addition, prior carbon reduction goals have been placed in terms of specific emission reduction goals throughout time [178]. In addition, from a broader perspective, other institutions other than the University of California may adopt similar goals that do not

include full carbon neutrality. With these considerations, it is important to understand how the optimal design of a DER system and subsequent operation will change as carbon emission constraints become tighter. While this work is particular to the University of California, Irvine energy demand profile developed in Section 4.1.2, the process of reducing carbon emissions through adopting progressively more sustainable DER systems is illustrated.

6.1 Optimization Parameters and Assumptions

The analyses on DER adoption with a carbon constraint focuses on the UCI campus demand shown in Section 4.1.2. While UCI is a campus with numerous buildings at which a DER system could potentially be installed, the optimization will assume that a central DER plant will be optimized to meet the energy demand of the whole campus. This work also assumes that the campus demand profile used during the optimization is representative of future energy demand during the summer and winter.

The DER technologies included in the optimization are a 13.5 MW gas turbine, one MW fuel cell, a heat recovery unit, photovoltaic system, thermal energy storage, and electrical energy storage. The optimization assumes that a legacy vapor compression and boiler system exists that is large and flexible enough to meet the UCI campus cooling and heating demand. All applicable parameters are shown in Table 6-1.

Another option included in the optimization is the ability to export electricity from UCI back to the utility operated grid. This work assumes that the campus will be compensated to export electrical energy at a rate comparable to the rate at which electrical energy is imported. According to SCE, the cost to transmit and distribute electrical energy is approximately two cents [149]. Since the campus is only providing production of electrical energy, not transmission

or distribution services, this work assumes that the campus is compensated at a rate of the energy charges for TOU-8 Option B energy charges shown in Table 3-1 less two cents.

The optimization will occur with multiple sets of technology options in order to show the effect of allowing for certain combinations to be adopted. The baseline optimization scenario will include gas turbine, fuel cell, photovoltaic, and heat recovery units. An EES scenario will include all baseline technologies with the additional option of purchasing EES. A TES scenario will include all baseline technologies with the additional option of purchasing TES. An EES and TES scenario will include all baseline technologies with the additional option of purchasing EES and TES. Finally, an export scenario will include only baseline technologies (no energy storage options) but will be allowed to export electricity. All scenarios are labeled based on the additional technology that can be adopted beyond the baseline scenario (GT, FC, PV, and HRU). For example, the TES scenario includes all baseline technologies and a TES option. In total, five technology scenarios are included in this work.

The prior Section 5 assumed that the capital cost of certain technologies, such as fuel cells, would be reduced according to future system cost projections [12]. The current analyses on DER system adoption for UCI shifts the focus from future systems with projected costs to current systems. As a result, the parameters used for optimization change, particularly for the capital cost associated with fuel cells.

The optimization also assumes that the electric and natural gas utility rate models developed in Section 3.1 are applicable. In the current work on the UCI campus, it is assumed that the campus has an unlimited supply of renewable natural gas at a price of $1 per therm. It is also assumed that some non-renewable carbon emissions were produced during the production of

the renewable natural gas, resulting in the renewable natural gas emitting two pounds of CO_2 per therm converted. Note that if the procurement process of the renewable natural gas were to be powered using renewable energy also, then the carbon associated with renewable fuel production would disappear.

Since the current formulation of the DER system optimization allows for the heating demand to be met only from thermal energy produced from firing a boiler or from recovering gas turbine or fuel cell waste heat using a heat recovery unit, and it is assumed that some carbon emissions are associated with renewable natural gas production, it is infeasible to design a DER system that is carbon neutral without including other technologies or carbon reduction options that are available to the actual campus. As a result, the carbon constraint will be continually applied until a further reduction results in an infeasible formulation of the problem.

In particular, a required carbon reduction will be based on the amount of carbon emitted if the UCI campus energy demand shown in Figure 4-15 was met only using utility electricity with a time resolved carbon emission rate described by Figure 3-9 and non-renewable natural gas. Under this scenario, approximately 12,932 metric tons of CO_2 are emitted over the year. While the first optimization will not include a carbon emissions constraint, subsequent DER system optimizations that include a carbon constraint will base the amount of allowable carbon compared to 12,932 metric tons. The first optimization to include a carbon constraint will ensure that the adoption of a DER system does not result in the emissions of no more than the baseline emissions. Subsequent optimizations will state that carbon emissions must be reduced by some percentage (33%, 66%, 80%, etc.). The carbon emission constraint will be reduced for the baseline technology scenario until further reductions are infeasible.

An arbitrarily large amount of area is allowed for a PV installation. In actual practice, this area would be limited to space on top of buildings, parking structures, and other developed or open areas. The actual area allowable may be much smaller in reality, but the current work assumes a large area is available in order to establish the unconstrained land use level of PV installation required at each level of CO_2 reduction.

Table 6-1: Parameters of DER system optimization for the UCI campus when a carbon constraint applies

Building Parameters	**Description**	**Value**
Bldg Area	Area available for a photovoltaic installation (m^2)	10,000,000,000
$\Delta T_{bldg.-1}$	Difference in temperature between the heat exchanger providing cooling to the building and the temperature of the used storage working fluid (^oC)	3
$\Delta T_{2\text{-}bldg}$	Difference in temperature between the charged thermal energy storage working fluid and the heat exchanged providing cooling to the building (^oC)	5
DG Parameters	**Description**	**Value (Gas Turbine/Fuel Cell)**
$C_{om\ DG,k}$	O&M cost for DG of type k ($/kWh)	0.01 / 0.023
$C_{cap\ DG,k}$	Capital cost for DG of type k ($)	1400 / 4000
$C_{start\ DG,k}$	Startup cost for DG of type k ($/start)	100 / 100
$\eta_{DG,k}$	Electrical efficiency for DG of type k (%)	32 / 47
$\bar{\eta}_{DG,k}$	Maximum efficiency for DG of type k (%)	90% / 90%
$S_{DG,k}$	Rated power for DG of type k (MW)	13.5 / 1
$\delta_{DG,k}$	Minimum turndown for DG of type k (%)	60% / 50%
$\bar{\mu}_{DG,k}$	Maximum ramp up rate for DG of type k (%/15 minutes)	50% / 10%
$\underline{\mu}_{DG,k}$	Maximum ramp down rate for DG of type k (%/15 minutes)	50% / 10%

Heat Recovery Unit / Duct Parameters	**Description**	**Value**
$C_{cap\ HRU}$	Capital cost for heat recovery unit ($/kW)	100
$C_{cap\ duct\text{-}p}$	Capital cost for duct in parallel with absorption chiller ($/kW)	10
$C_{om\ HRU}$	O&M cost for heat recovery unit ($/kWh)	0.001
$C_{om\ duct\text{-}p}$	O&M cost for duct in parallel with absorption chiller ($/kWh)	0
ε_{HRU}	Effectiveness of heat recovery unit (%)	90%
$\varepsilon_{duct\text{-}p}$	Effectiveness of duct in parallel with absorption chiller recovery unit (%)	90%
Photovoltaic Parameters	**Description**	**Value**
$C_{cap\ PV}$	Capital cost for photovoltaic system ($/kW)	2000
$C_{om\ PV}$	O&M Cost for photovoltaic system ($/kWh)	0.001
η_{PV}	Photovoltaic efficiency at nominal conditions	20%
Electrical Energy Storage Parameters	**Description**	**Value**
$C_{cap\ EES}$	Capital cost for EES ($/kWh)	200
$C_{om\ EES\ chrg}$	O&M cost to charge EES ($/kWh)	0.001
$C_{om\ EES\ dchrg}$	O&M cost to discharge EES ($/kWh)	0.001
α_{EES}	Retained EES storage between 15 minute time periods (%)	99.5%
$\eta_{EES\ chrg}$	EES charging efficiency (%)	95%
$\eta_{EES\ dchrg}$	EES discharging efficiency (%)	95%
$\bar{\delta}_{EES}$	Maximum EES state of charge (%)	95%
$\underline{\delta}_{EES}$	Minimum EES state of charge (%)	30%
$\bar{\mu}_{EES}$	Maximum EES charging rate (%)	25%
$\underline{\mu}_{EES}$	Maximum EES discharging rate (%)	25%
Thermal Energy Storage Parameters	**Description**	**Value**
$C_{cap\ TES}$	Capital cost for TES ($/kWh)	50
$C_{om\ TES\ chrg}$	O&M cost to charge TES ($/kWh)	0.0001
$C_{om\ TES\ dchrg}$	O&M cost to discharge TES ($/kWh)	0.0001

α_{TES}	Retained TES storage between 15 minute time periods (%)	99.9%
$\eta_{TES\ chrg}$	TES charging efficiency (%)	95%
$\eta_{TES\ dchrg}$	TES discharging efficiency (%)	95%
$\bar{\delta}_{TES}$	Maximum TES state of charge (%)	99%
$\underline{\delta}_{TES}$	Minimum TES state of charge (%)	5%
$\bar{\mu}_{TES}$	Maximum TES charging rate (%)	25%
$\underline{\mu}_{TES}$	Maximum TES discharging rate (%)	25%
Legacy System Parameters	**Description**	**Value**
$C_{om\ VC}$	O&M cost for vapor compression chiller output ($/kWh)	0.0139734
COP_{VC}	Coefficient of performance for vapor compression chiller	3.4
$C_{om\ Boil}$	O&M cost for boiler ($/kWh)	0.001
η_{Boil}	Boiler efficiency (%)	90%

UCI also operates a public bus system as described in Section 4.2.1. Since a component of the carbon neutrality commitment includes a reduction to carbon emissions associated with transportation, the current work will also include the optimization of the Anteater Express bus system in the optimization. The bus route data described in Section 4.2.1 are used to build a set of routes for which fleet vehicles will be adopted for. The set of routes input into the model are shown in Table 6-2. All summer routes and ACC Combined Bus 3 through 5 were omitted from the aggregated bus data. It is assumed that the routes listed in Table 6-2 occur daily throughout the entire year.

Table 6-2: Aggregated Anteater Express bus route data for input into DER optimization model

Route	Range (Miles)	Required Vehicles	Time of Arrival at Base (Time)	Time at Base (Hours)
AV	136	2	21:00	10
Main	153	2	21:00	10
Newport/Park West	150	2	23:00	8
VDC	101	3	19:00	12

VDC Norte	107	3	19:00	12
CdS	108	2	19:00	12
ACC Combined	38	2	23:00	8

While a full fleet of vehicles are currently in operation, this work assumes that a new fleet is to be adopted. Three separate vehicles can potentially be adopted: a conventional vehicle, a conventional vehicle operated using a renewable fuel source, and an electric vehicle. The parameters for all three vehicle types are shown in Table 6-3. The electric vehicle parameters are based on a commercially available bus produced by BYD Company [179]. The seven routes listed in Table 6-3 are included in the optimization of the five technology scenarios.

Table 6-3: Parameters for fleet vehicles for DER system optimization at the UCI campus when a carbon constraint applies

PEV Parameters	**Description**	**Value**
$C_{ev,l}$	Capital and operations cost of PEV l ($)	1,200,000
$C_{evse,n}$	Capital cost of EVSE n ($)	10,000
$\eta_{ev\ mpkWh,l}$	Electricity used during PEV travel (Miles/kWh)	2.1
$S_{ev,l}$	Number of refueling ports for PEV l (number of refueling ports)	2
$S_{evse,n}$	Power rating of EVSE n (kW)	30
Conventional Vehicle Parameters	**Description**	**Value (Conventional/Renewable Conventional)**
$C_{con,m}$	Capital and operations cost of conventional vehicle m ($)	500,000 / 750,000

6.2 DER System Optimization Results for UCI

The DER systems optimization model was executed with no carbon emission constraint. Following optimization simulations included a carbon constraint limiting total carbon emissions produced while meeting campus energy demand by the following percentages of 12,932 metric tons of CO_2 associated with campus operation if the only sources of energy are from an electrical and non-renewable natural gas utility: 0%, 33%, 66%, 80%, and 85%. Further carbon emission reductions beyond 85% are difficult to achieve under the baseline technology scenario, and further tightening to the emissions constraint resulted in an infeasible optimization problem.

DER systems optimization for all other technology scenarios occurred using the same emissions reduction constraints used for the baseline technology scenario. For all technology scenarios, carbon emissions increased by approximately 28% when the carbon constraint was not implemented. When the carbon constraint was implemented, the minimum cost was always achieved when carbon emissions were reduced by the required amount only.

The optimization results suggested what type and how much of tech technology should be adopted in order to minimize total cost while meeting a carbon emissions target. The technologies adopted during the optimizations are shown below.

Table 6-4 shows the number of gas turbines and fuel cells and size of PV and HRU systems adopted for all technology scenarios and carbon emission reductions.

Table 6-5 shows the amount of electrical and thermal energy storage adopted for the scenarios that included either EES and/or TES technologies. Table 6-6 show the vehicles adopted for the Anteater Express fleet.

Table 6-4: DER optimization results for adopted energy producing technologies for the UCI campus

Technology	**Gas Turbine (13.5 MW)**						**Fuel Cell (1 MW)**					
CO2 Reduction	UC	0%	33%	67%	80%	85%	UC	0%	33%	67%	80%	85%
Baseline	1	1	1	1	1	1	0	0	0	0	0	11
EES	1	1	1	1	1	1	0	0	0	0	0	0
TES	1	1	1	1	1	1	0	0	0	0	0	1
EES + TES	1	1	1	1	1	1	0	0	0	0	0	0
Export	1	1	1	1	1	1	0	0	0	0	0	0
Technology	**PV (MW)**						**HRU (MW)**					
CO2 reduction	UC	0%	33%	67%	80%	85%	UC	0%	33%	67%	80%	85%
Baseline	0.0	2.8	2.8	2.8	8.0	31.6	14.5	14.8	14.8	15.6	17.1	17.2
EES	0.2	2.5	2.5	2.5	8.5	20.4	14.6	15.4	15.4	15.4	16.7	17.1
TES	0.0	3.0	3.0	3.0	7.4	19.8	14.5	15.3	15.3	15.3	16.7	16.8
EES + TES	0.0	3.0	3.0	3.0	8.4	20.8	14.6	15.4	15.4	15.4	16.7	16.1
Export	0.4	2.8	2.8	2.8	11.9	17.2	14.6	15.4	15.4	15.4	16.7	16.6

Table 6-5: DER Optimization results for adopted energy storage technologies for the UCI campus

Technology	EES (MWh)						TES (MWh)					
CO2 Reduction	UC	0%	33%	67%	80%	85%	UC	0%	33%	67%	80%	85%
EES	3.9	3.6	3.6	3.6	7.8	20.5	n/a	n/a	n/a	n/a	n/a	n/a
TES	n/a	n/a	n/a	n/a	n/a	n/a	18.8	7.5	7.5	7.5	21.8	44.3
EES + TES	0.9	0.8	0.8	0.8	4.4	16.8	18.0	4.8	5.0	5.0	7.9	31.8

Table 6-6: DER Optimization results for adopted vehicles for Anteater Express bus system

Vehicle Type	Electric					Renewable - Conventional					Conventional				
CO2 Reduction	UC	0%	33%	67%	85%	UC	0%	33%	67%	85%	UC	0%	33%	67%	85%
Baseline	0	0	0	0	0	14	14	14	14	3	0	0	0	0	11
EES	0	0	0	0	0	14	14	14	14	0	0	0	0	0	14
TES	0	0	0	0	0	14	14	14	14	0	0	0	0	0	14
EES + TES	0	0	0	0	0	14	14	14	14	5	0	0	0	0	9
Export	0	0	0	0	0	14	14	14	14	14	0	0	0	0	0

Table 6-4 shows that a 13.5 MW gas turbine was adopted for every technology scenario optimization across all carbon constraints tested. Fuel cells were not purchased except under the baseline and TES technology scenario and a required 85% reduction in carbon emissions with the current capital cost assumption ($4,000/kW). When carbon emissions are unconstrained, little to no PV was adopted. As a carbon constrain limit was implemented and tightened up to a 66% reduction, approximately three MW's of PV was adopted under every scenario. The PV system size increased for every technology scenario as the carbon constraint was tightened beyond a 66% reduction. A HRU sized to the heat output of the selected generators was always purchased

for every technology scenario and carbon constraint tested. The size of the HRU increased slightly as the carbon constraint was tightened for every scenario.

Under the applicable technology scenarios, EES was always adopted. Between 3.6 and 3.9 MWh for the EES scenario and 0.8 and 0.9 MWH for the EES and TES scenario of EES was adopted when carbon emissions were unconstrained or constrained by up to a 66% reduction. Increasing the carbon reduction resulted in an adoption of a larger EES system that mirrors the increase seen for the PV system size.

Under the applicable technology scenarios, TES was also always adopted. When no carbon constraint was enforced, 18 and 19 MWh of TES was adopted for the TES and EES and TES technology scenarios respectively. Once a carbon constraint was implemented, the TES size was reduced to 7.5 MWh for the TES scenario and 4.8 for the EES and TES scenario for a carbon reduction between 0% and 66%. Once the carbon reduction increased beyond 66%, TES size increased with the corresponding PV system.

All scenarios in which energy storage is an option, once a carbon constraint has been implemented, storage size increases with the size of the PV system. For both EES and TES, the increase in storage size corresponds to an increase in renewable energy production. However, since the PV output is dictated only by the available insolation, not the present UCI campus energy demand, both forms of storage are used to manage any mismatch between the PV production and the campus demand. Otherwise, any excess renewable energy production would be curtailed. The EES is used directly to store electrical energy for later use, while the TES is sued to store chilled water produced by any vapor compression chillers operated using excess renewable electricity. By storing excess renewable energy in the form of electricity or chilled

water produced using electrically fired vapor compression chillers, future energy demand can be met using renewable energy even when the adopted PV system produces little or no electricity.

Table 6-6 shows that conventional vehicles were always adopted over renewable fuel or electric vehicles except when carbon emissions were reduced by 80% for the baseline technology scenario or 85% for all technology scenarios except the Export scenario.

6.3 Optimal DER System Operation

In addition to selecting a set of technologies, each optimization simulation provides the dispatch schedule of all adopted technologies and import schedule for electrical and natural gas utilities such that the optimal DER system is operated to minimize cost while meeting the carbon emission constraint. While the operation of each technology scenario under each carbon emission constraint case differs from other scenarios, some overall characteristics can be elucidated from the dispatch results of the optimization simulations.

The first optimization that occurred for each technology scenario occurred without a carbon constraint. As a result, the installed DER system was free to increase carbon emissions if the resulting system was able to reduce overall costs. Coupled with the higher cost associated with the purchase of renewable fuel, only non-renewable natural gas is purchased for any natural gas fired DG purchased. Renewable gas was only purchased when a carbon constraint was applied.

The adoption and subsequent operation of a gas turbine for every scenario resulted in an increase to total carbon emissions by approximately 28% for all technology scenarios, despite the use of a heat recovery unit to provide heating to the campus. Note that this result is more indicative of the carbon emissions associated with the California grid and not the operation of a

combined heat and power system. According to the United States Department of Energy, the average carbon emission factor associated with the California electricity grid is 43% lower than the national average emission factor [174]. In other words, electricity produced in California is generated through methods that produce, on average, less carbon than the typical methods used elsewhere in the United States. In order to ensure that the adoption of a DER system results in reduced, or at least does not increase carbon emissions, the carbon emission constraint must be activated.

Once activated, the carbon emission constraint results in different behavior for the procurement of natural gas. Figure 6-1 shows the portion of total fuel purchases that are from renewable natural gas. As stated earlier, no renewable natural gas is purchased when the carbon emission constraint is inactive. Activating the carbon constraint results in the purchase of renewable natural gas, starting with purchasing a small quantity when a 0% reduction is required and increasing until nearly all purchased fuel is renewable at a 67% CO_2 reduction constraint. Only renewable natural gas is purchased past a 67% reduction in carbon emissions.

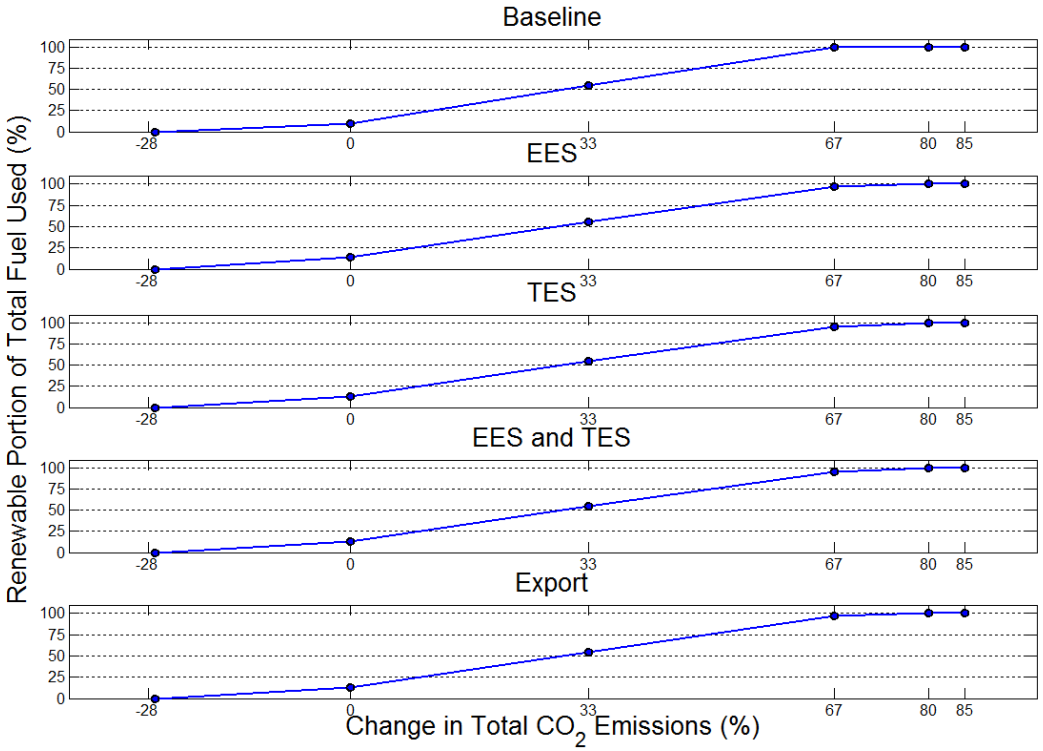

Figure 6-1: Percent of total fuel use that is renewable for all technology scenarios and carbon emission limits

The subsequent DER system operation also changes depending on the carbon emission constraint, as seen in Figure 6-2 and Figure 6-4. Figure 6-3 shows the capacity factor for gas turbines and fuel cells versus the carbon reduction and Figure 6-4 shows the percent of total produced electricity by all generation technologies and purchased from the electrical utility. The highest gas turbine capacity factor is experienced when carbon emissions are not constrained. Virtually all of the UCI electrical and cooling load is met by the gas turbine, with any additional load being supplied using utility electricity. As a carbon constraint is instituted, gas turbine operation is reduced for a 0%, 33%, and 67% carbon reduction while utility electricity purchases increase. PV systems are consistently installed when the carbon constraint is active, with the percent of the total load being met using solar power increasing as the carbon constraint requires

larger emission reductions. However, the amount of total energy produced by an adopted PV system remains a fraction of the total electrical energy produced unless carbon emissions are to be reduced by 85%. At this level of carbon reduction, solar energy is responsible for approximately one quarter of all electrical energy generation and procurement for the UCI campus.

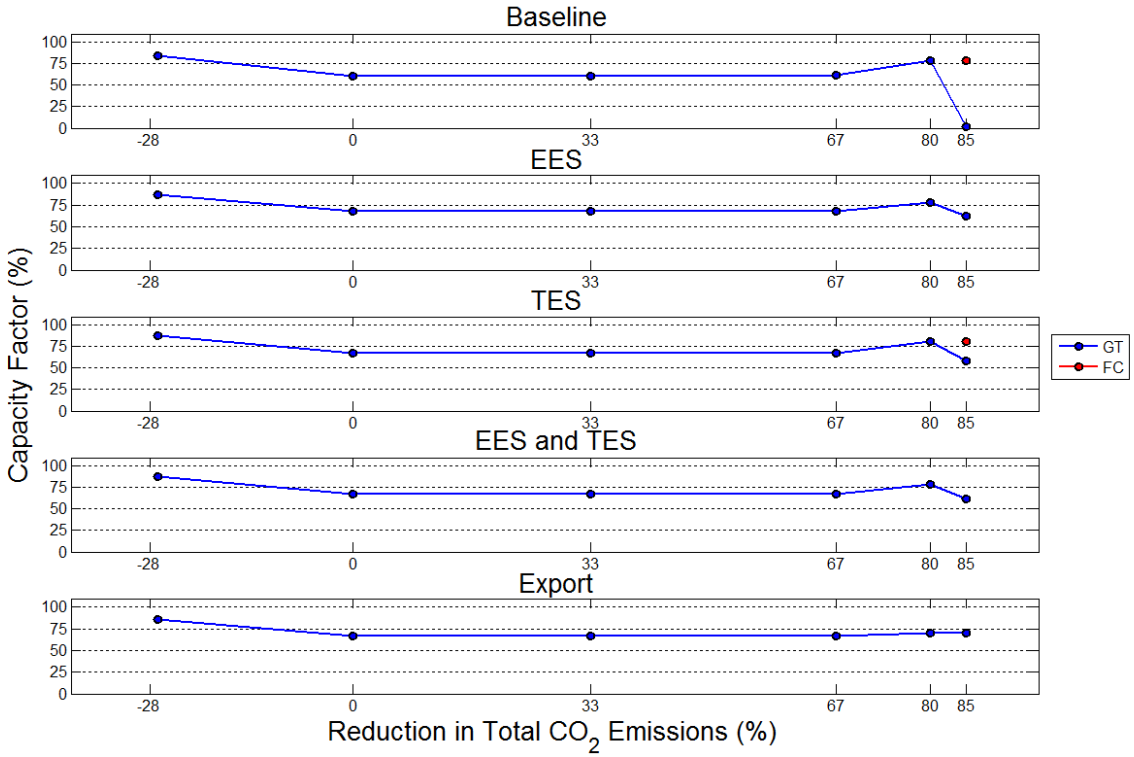

Figure 6-2: Gas turbine and fuel cell capacity factors for all technology scenarios and carbon emission limits

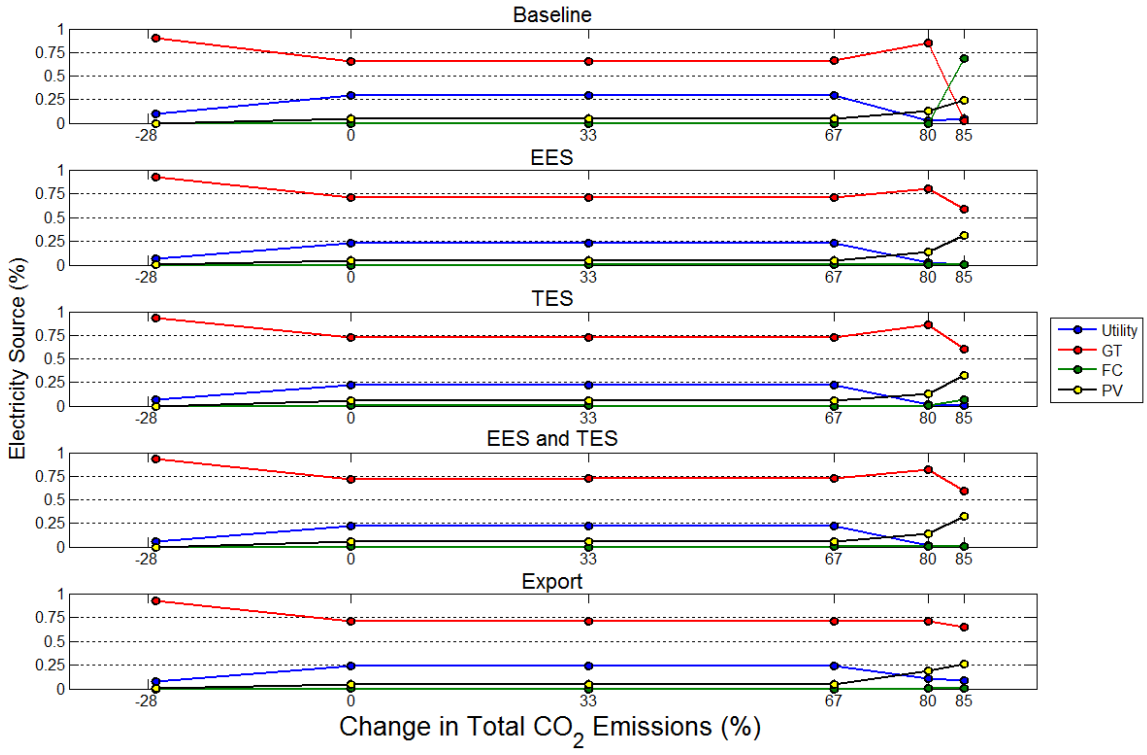

Figure 6-3: Source of electrical production for all technology scenarios and carbon emission limits

Utility electricity is virtually eliminated when carbon emissions are unconstrained, but increases when carbon emissions are reduced by 0% (or not increased by DER adoption), 33%, and 67%. At an 80% to 85% carbon emissions reduction, PV power increases, supplanting imported utility electricity.

When fuel cells are adopted for the baseline and TES technology scenario, the installed systems are operated at a high capacity factor, as seen in Figure 6-2. However, the contribution to total generation depends on the size of the installed system, with the TES technology scenario system providing approximately 6% of the overall amount of generation.

Under the export scenario, gas turbine capacity factor and contribution to total energy generated stays relatively constant across the different levels of carbon emissions reduction. The remaining energy is met using a combination of solar energy and the utility, with solar generation increasing as the carbon emission reduction increases.

With the majority of the electrical demand being supplied by the gas turbine or fuel cells for nearly all technology scenarios and carbon emission reduction levels, sufficient waste heat is produced to supply nearly all of the campus heating demand. Figure 6-4 shows the percent of the total heating load that was met using either the heat recovery unity used to capture waste heat produced by the adopted gas turbine or fuel cells, and the natural gas fired boiler. Boiler operation is virtually eliminated until the carbon emissions reduction reaches 85%. Gas fired generator operation is reduced at this level of carbon reduction in favor of electricity produced using the large PV system. At this point, the boiler is fired much more frequently, using only renewable natural gas as the fuel. The export technology scenario is the exception to this behavior, with gas turbine operation remaining high even when an 85% carbon emissions reduction is required. Since gas turbine operation remains high, sufficient waste heat is available to satisfy the campus heating demand.

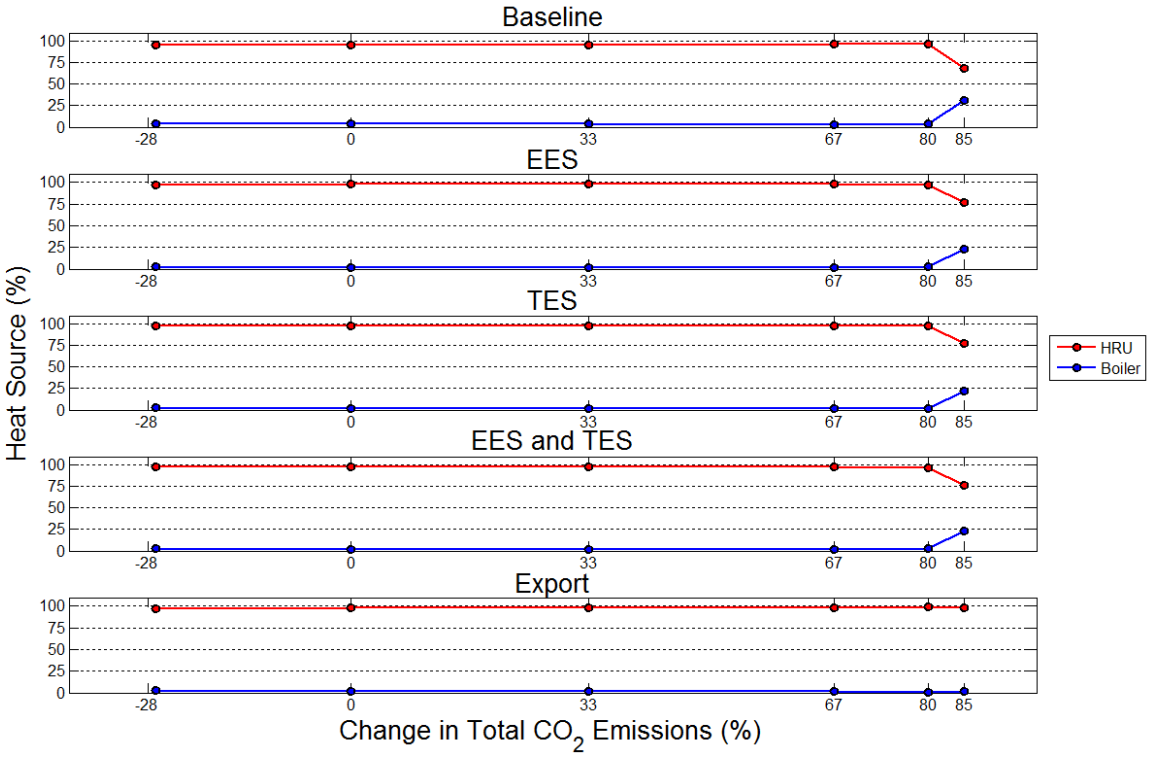

Figure 6-4: Source of heat production for all technology scenarios and carbon emission limits

and Figure 6-3 both show that PV system size and solar generation increase as carbon emissions are reduced. The optimization model that determines the PV system size is to allow curtailment whenever economically desirable considering the level of required carbon emissions. Figure 6-5 shows for all technology scenarios when PV is adopted the percent of available solar energy that is actually used by the campus. As expected, the technology scenarios that allow for some form of storage or electrical energy export utilize nearly all available solar energy, resulting virtually no curtailment to PV system output. The baseline system also experiences full PV system utilization when carbon emissions are reduced by up to 67%. However, reducing carbon further results in the progressively lower PV system utilization. Curtailment for the 80% carbon reduction case occurs rarely, but further reduction results in significant curtailment, with less than 50% of the available solar power being captured and used.

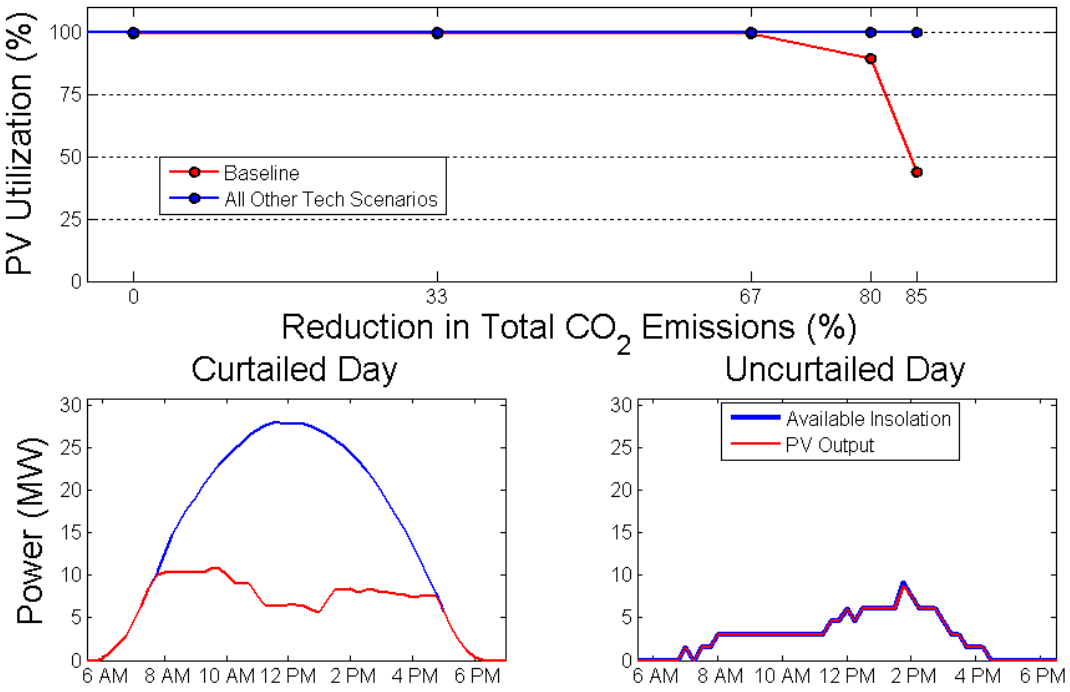

Figure 6-5: PV utilization for baseline and all other technology scenarios for the various carbon emission limits with the corresponding PV utilization for two days for the baseline scenario with maximum carbon reduction tested

The time resolved curtailment for the baseline technology scenario when carbon emissions are reduced by 85% is also shown in Figure 6-5. Another day when the all energy produced by the same PV system is also shown in the bottom right. Clearly, the bottom right subfigure presents the day for which the PV system is sized in order to ensure that carbon emissions for the entire simulation are reduced by 85%. On this day, the available insolation is reduced from a typical sunny day, resulting in the requirement for an oversized system in order to meet the carbon reduction goal. Since no form of storage exists, excess solar from prior days where available insolation is more similar to what is presented in the bottom left subfigure cannot be captured and stored for days when insolation is reduced. As a result, the PV system

size required to meet the 85% carbon reduction goal must be sized to continually reduce carbon every day, even when other factors result in a reduced yield in useable solar energy. The optimal system design in this case is generally oversized, resulting in significant curtailment.

6.3.1 Baseline operation

Figure 6-6 shows the electrical dispatch during a winter month for the technology scenario when carbon emissions are unconstrained, reduced by 33%, and reduced by 85%. The dispatch profiles for when carbon emissions are reduced by 0%, 67%, and 80% are similar to when emissions are reduced by 33%. The main difference between the 33% reduction operation and other levels of carbon reduction is the amount of renewable fuel purchased to operate the gas turbine and boiler, as seen in Figure 6-1. The campus electrical demand in this figure and all proceeding electrical operations figures consists of the electrical demand and resulting electrical consumption produced by using vapor compression chillers to meet the cooling demand. The total electrical load assumes that all electrical and cooling demand is met instantaneously. Obviously, the resulting electrical load may be altered if technologies such as TES are adopted.

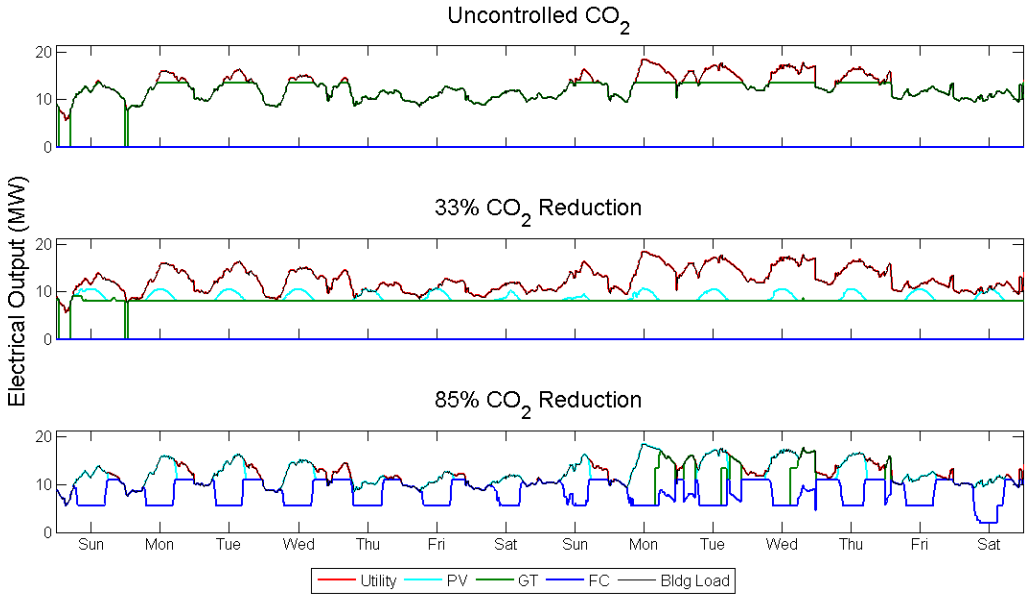

Figure 6-6: Electrical operation during the winter for the baseline technology scenario when CO_2 is uncontrolled, reduced by 33%, and reduced by 85%

Figure 6-6 shows that the gas turbine follows the UCI electrical demand when carbon emissions are unconstrained. Whenever the campus load is greater than the capacity of the gas turbine, electrical energy is imported from the local utility. Also, two short periods can be seen during the first Sunday and Figure 6-6 where the campus electrical demand is too low for the gas turbine to remain operational, resulting in a shutdown of the turbine. As a result of incurring a large demand charge during this forced shutdown, it becomes economical to shut down for a brief period of time during the following Monday.

When carbon emissions are reduced by 33%, the gas turbine is continuously operated. However, instead of load following, the turbine is operated at the lowest possible power setting. The PV system is able to produce power during the day, but electrical imports increase, particularly during the middle of the day. According to Figure 3-9, grid carbon emissions are

lowest in the middle of the day, providing UCI energy with lower carbon intensity than at night despite the higher cost of electricity during the day.

Reducing carbon emissions virtually eliminates gas turbine operation in Figure 6-6 except during the second Monday, Tuesday, and Wednesday, when the gas turbine is operated to provide peak power. The 11 adopted fuel cells provide the majority of the demanded electricity. During the night, the fuel cells perform electrical load following, but are turned down to the minimum power setting during the day when solar power is available from the PV system. Utility imports are commonplace in the late afternoon as the sun sets and PV output is reduced.

Heating operation for the same time period as Figure 6-6 is shown in Figure 6-7. For both the uncontrolled carbon emissions and 33% reduction case, waste heat from the gas turbine is captured using the heat recovery unit and used to supply the entire campus heating demand except for the two instances occurring on the first Sunday and Monday when the gas turbine must shut down due to insufficient electrical demand. At 85% reduction, the heating demand is nearly completely satisfied during the evenings when fuel cell operation is highest. However, during the day, when the fuel cells are turned down in favor of solar energy, the boiler must be fired using renewable natural gas in order to meet the campus heating demand.

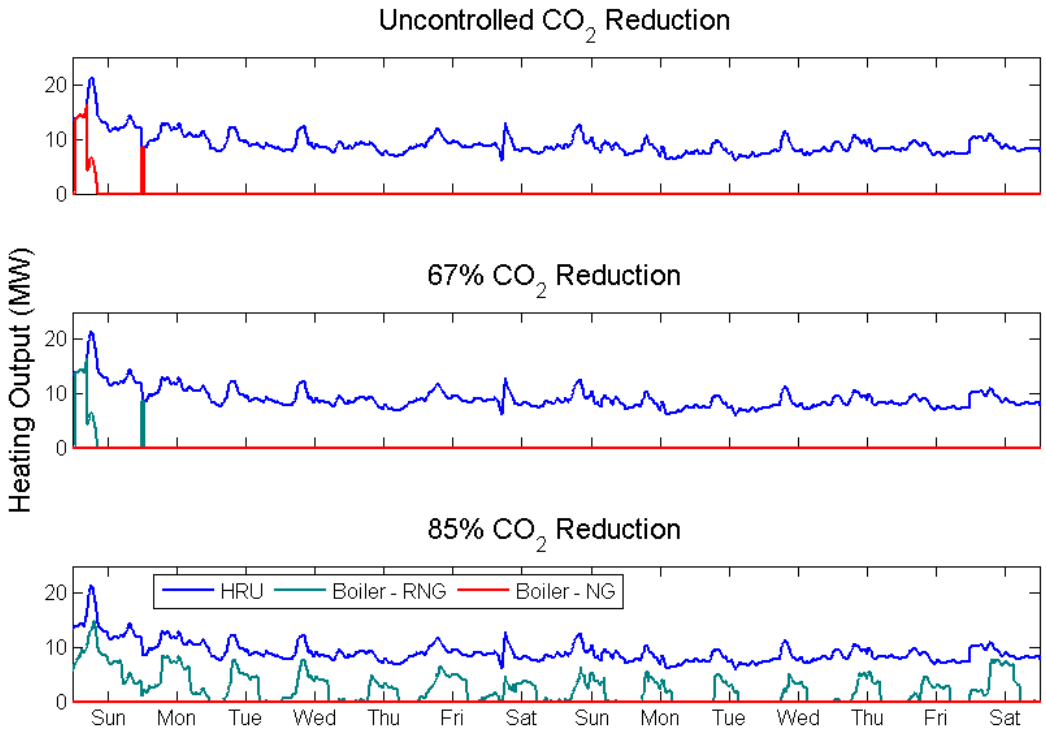

Figure 6-7: Heating operation during the winter for the baseline technology scenario when CO_2 is uncontrolled, reduced by 33%, and reduced by 85%

Figure 6-8 shows the electrical operation of the adopted DER systems and electrical utility imports for two weeks during the summer when carbon emissions are uncontrolled, reduced by 33%, and reduced by 85%. Operation for the 0%, 67%, and 80% reduction case are similar to the 33% reduction case with the difference being the amount of renewable natural gas purchased. During the summer, gas turbine during off-peak periods is reduced to the minimum power output due to the low cost of utility electricity. During on-peak and mid-peak periods, the turbine performs load following operations, importing electricity whenever the campus electrical demand is greater than the maximum output of the gas turbine.

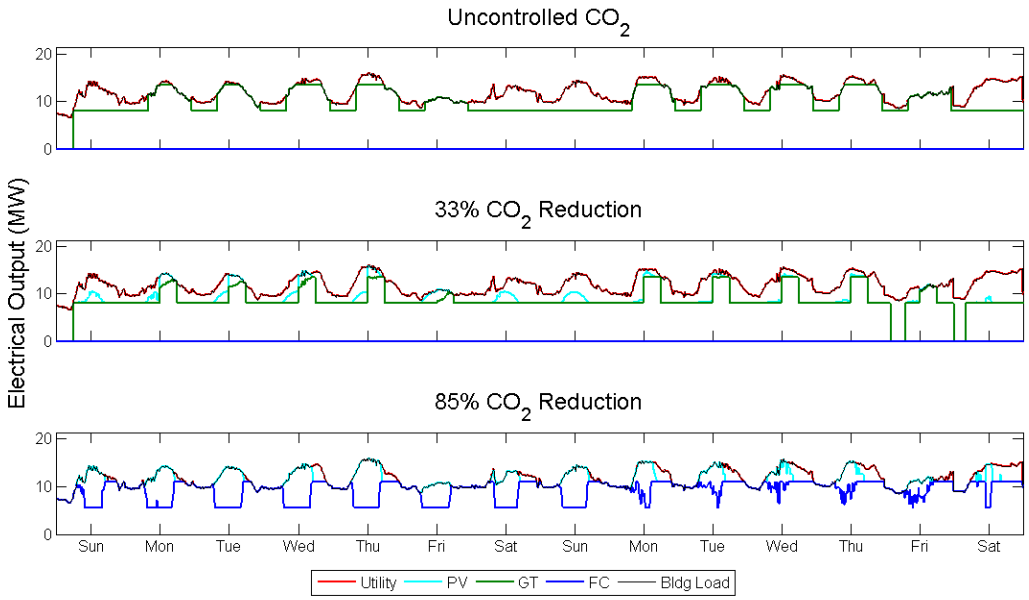

Figure 6-8: Electrical operation during the summer for the baseline technology scenario when CO_2 is uncontrolled, reduced by 33%, and reduced by 85%

When carbon emissions are reduced by 33%, the gas turbine is operated at the lowest possible power setting during mid-peak and off-peak. However, during on-peak, the turbine is turned up to full power, with part load operation only occurring when the campus electrical demand is low or when solar energy is available, as seen during the first Friday. Electrical operations when emissions are reduced by 85% are similar to winter operations for the same level of carbon reduction.

Similar to the winter, any available waste heat is captured from the gas turbine or fuel cells. When the gas turbine is operated, the recovered heat is sufficient to meet the entire campus heating load, with the boiler needing to be fired whenever a gas turbine shutdown occurs. When carbon emissions are reduced by 85%, the fuel cells perform load following during off-peak, producing sufficient heat to meet the entire campus demand. During the day, the fuel cells are

turned down in favor of solar energy, resulting in the firing of the boiler using renewable natural gas.

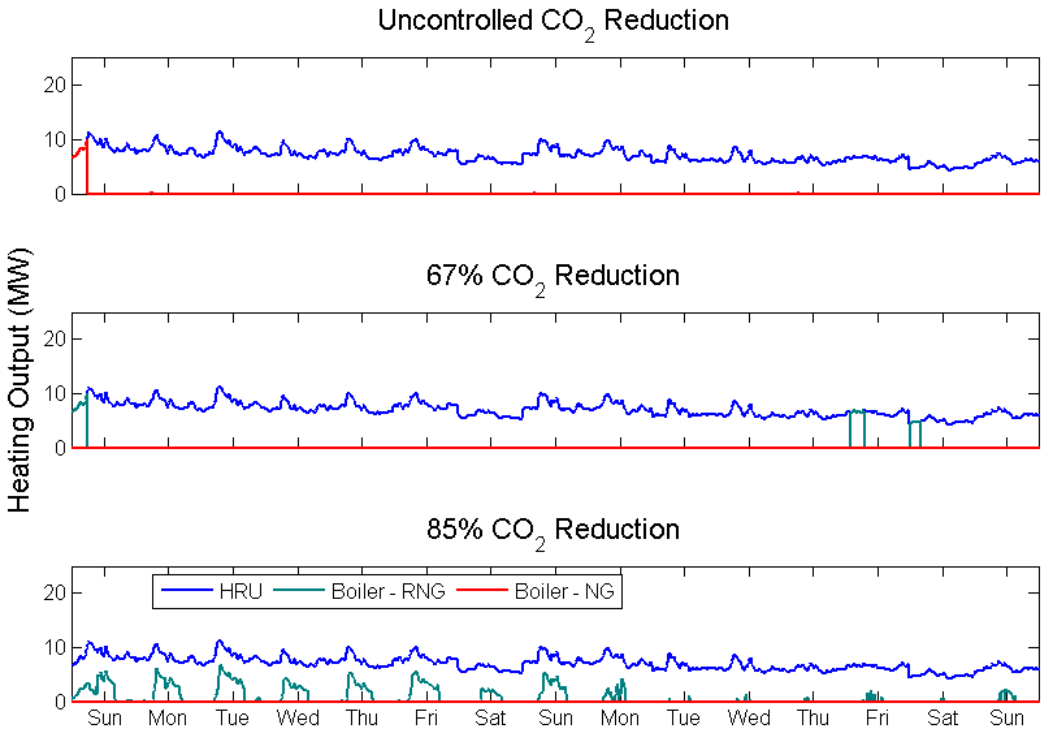

Figure 6-9: Heating operation during the summer for the baseline technology scenario when CO_2 is uncontrolled, reduced by 33%, and reduced by 85%

The only technology scenario for which PV curtailment is an issue is the baseline technology scenario when carbon emissions are reduced by 85% as seen in Figure 6-5. This occurs primarily because no EES or export can be adopted in the baseline scenario. A brief example of curtailment under this scenario is shown in Figure 6-5. Figure 6-10 shows how the curtailment fits in with the electrical operation of other purchased resources and imported electrical energy. Figure 6-10 presents the same dispatch profiles for the baseline technology scenario with an 85% carbon emissions reduction as seen in Figure 6-6 during the winter and

Figure 6-8 during the summer. Figure 6-10 includes the possible solar energy that could be captured with the installed PV system, but is curtailed due to an inability to store or sell the excess renewable energy. As discussed earlier, the sizing of the PV system was based to produce carbon free energy even on days when relatively little insolation is available, such as during the second summer week where no curtailment occurs. Note that the presented scenario is the only scenario for which a large fuel cell system is adopted. With no ability to consistently provide carbon free energy, fuel cells were selected in order to produce a more efficient form of energy conversion for meeting the UCI campus electrical demand.

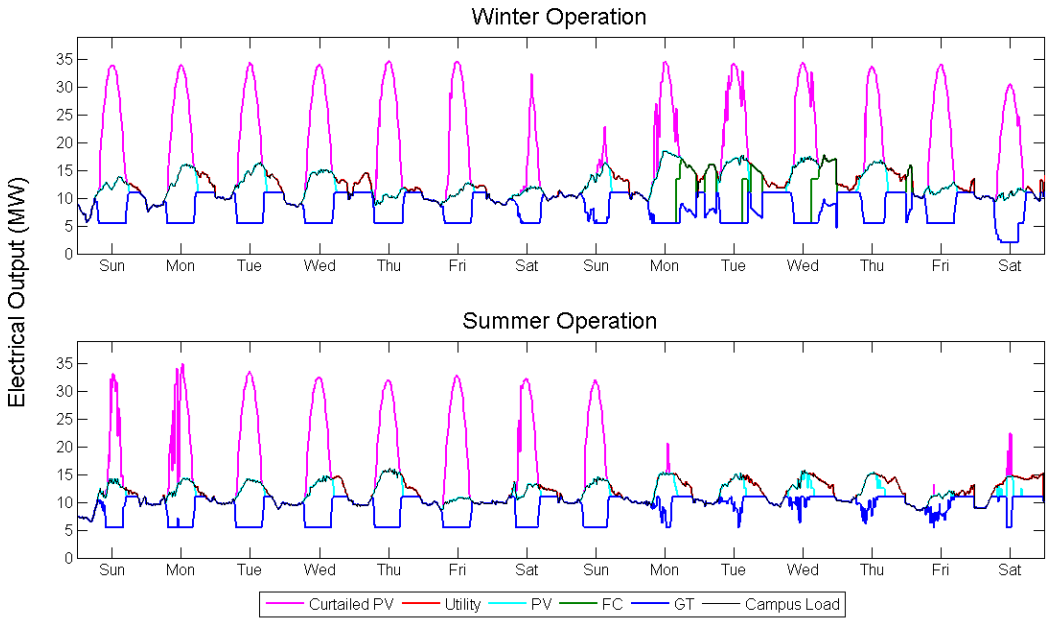

Figure 6-10: Electrical operation including curtailed PV power for summer and winter operation for the baseline scenario when CO_2 emissions are reduced by 85%

The heating operation for all other technology scenarios is nearly identical to the baseline scenario for the heat recovery unit and boiler fired using both renewable and non-renewable natural gas.

6.3.2 Energy Storage Technology

An obvious technology that will help reduce the curtailment of solar energy is energy storage. Figure 6-5 shows that curtailment can be avoided while reducing carbon emissions by up to 67% for all technology scenarios. However, curtailment for the baseline technology scenario appears to exponentially increase as carbon emissions are reduced further. This issue is unique only to the baseline technology scenario. For the scenarios where energy storage is an option, the PV system and energy storage can be sized to simultaneously meet part of the campus demand while the sun is shining while storing excess solar energy for later use after the sun has set.

If any adopted form of storage is to be used in this manner, then it is safe to assume that a larger portion of the total campus electrical or cooling load will pass through storage. Figure 6-11 shows the amount of energy generated onsite or procured using utility electricity that is stored for the EES, the TES, and the EES and TES technology scenarios and every level of carbon reduction. Figure 6-12 shows the percent of the campus electrical or cooling demand that is pulled from energy storage for the same technology scenarios and level of carbon reduction. As expected, Figure 6-11 and Figure 6-12 appear to be nearly identical in shape and magnitude. Simply put, whatever amount of energy that is stored is eventually used, so the two figures should be nearly identical.

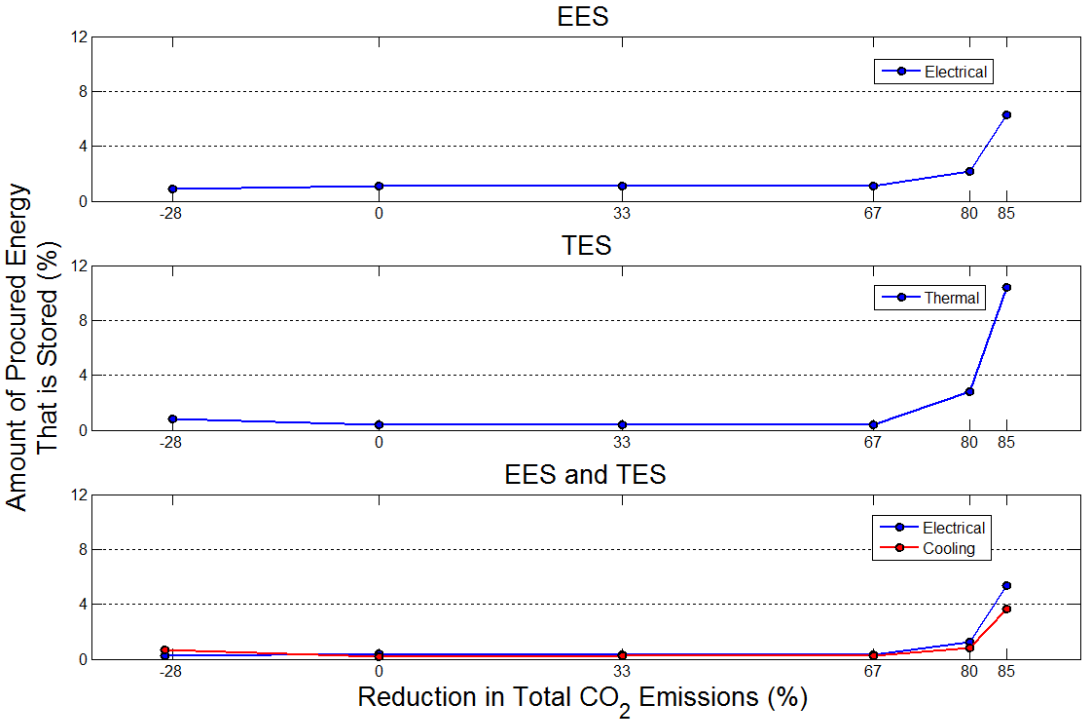

Figure 6-11: Amount of energy purchased from a utility or produced on-site that is stored for the technology scenarios that include some form of energy storage for all carbon emission limits

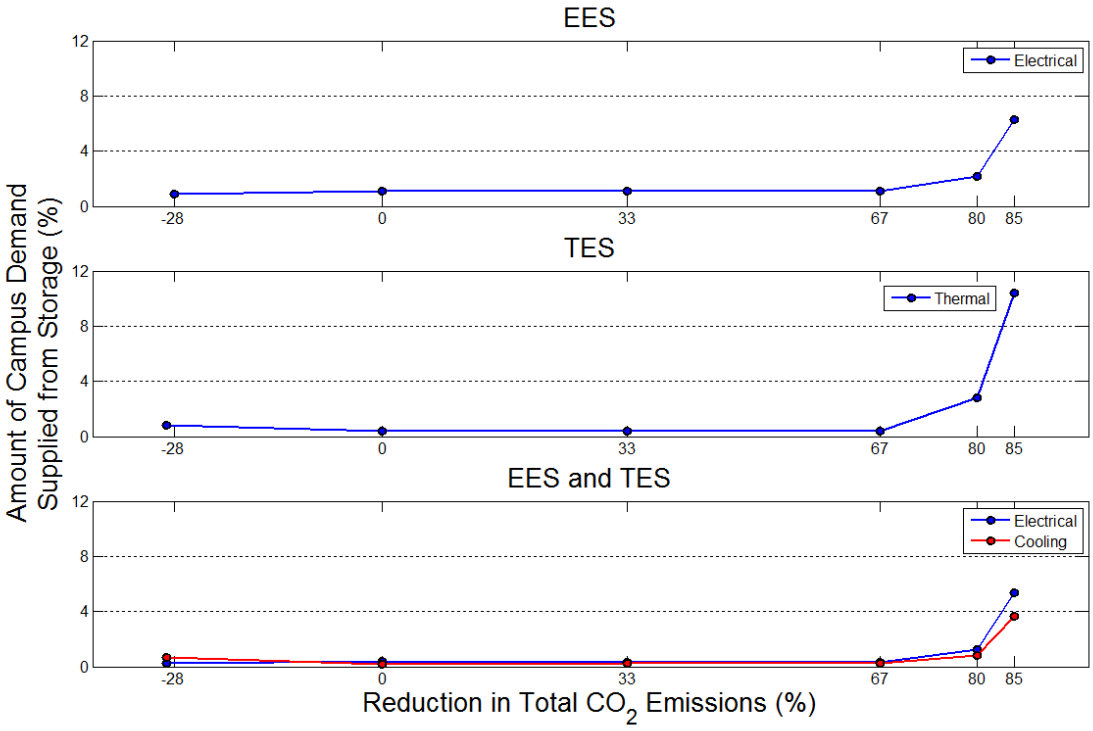

Figure 6-12: Percent of total electrical or Amount of energy purchased from a utility or produced on-site that is stored for the technology scenarios that include some form of energy storage for all carbon emission limits

For both Figure 6-11 and Figure 6-12, any energy passing through storage is fraction of the total energy consumed by the campus. It is not until carbon emissions are reduced by up to 80% and 85% that storage begins to play a larger role for the campus. However, even at an 85% reduction, less than 12% of either the campus electrical or cooling load passes through storage. While this is still a relatively small percentage of the total campus demand, the increase in storage use coincides with an increase in solar energy production relative to cases with greater carbon emissions with smaller PV systems relative to the baseline technology scenario at an 85% carbon reduction. By allowing for energy storage to be adopted, the same carbon reduction goals can be met with a smaller PV system that experiences better utilization.

6.3.2.1 EES Operation

Figure 6-13 shows the electrical operation during a two week period in the winter for the EES technology scenario when carbon emissions are unconstrained, reduced by 33%, and reduced by 85%. Figure 6-14 shows the corresponding EES operation, including state of charge, for the same time period and carbon emission reduction levels as seen in Figure 6-13. Note that EES modeled in the optimization can have a maximum and minimum state of charge of 95% and 5% respectively. Figure 6-14 only includes the usable portion of the EES, ignoring the EES capacity that is unusable due to a desire to maintain safe EES operation and EES integrity. Also, charging of the EES is represented as negative power, meaning that generation technologies produce electricity beyond what is currently demanded by the campus, with the excess being subtracted from the overall generation by being stored in EES for later use.

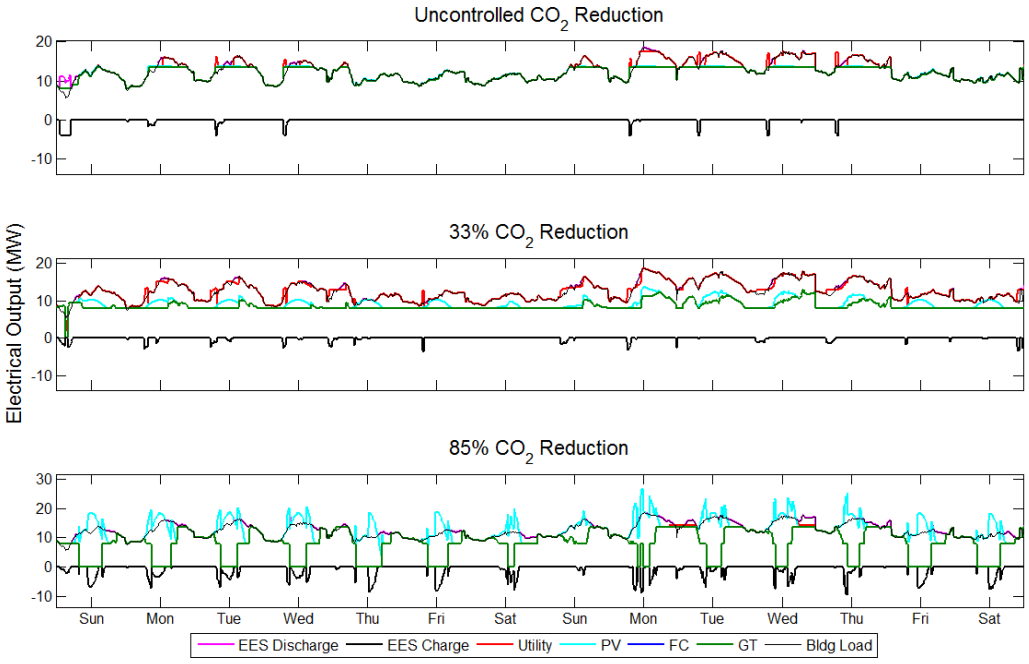

Figure 6-13: Electrical operation during the winter for the EES technology scenario when CO_2 emissions are uncontrolled, reduced by 33%, and reduced by 85%

When carbon emissions are unconstrained, overall system operation is similar to the corresponding baseline technology scenario operation. A slight difference can be seen as a result of EES adoption. First, the addition of EES technology allows for the gas turbine to remain operational during the first Sunday when the campus load is low. Instead of shutting down, the turbine is operated at the minimum power setting, with the excess power being used to charge the EES up to full state of charge. Shortly after the campus electrical demand begins to increase, the EES is discharged to meet the campus demand. Second, the EES performs peak shaving, as seen on the second Monday of Figure 6-13. Off peak electricity is imported from the local utility, charging the EES up to full state of charge. The EES is then slowly discharged when campus demand is highest, shaving the maximum utility demand and reducing the demand charge. Third, the EES is used to perform cost arbitrage, as seen during the second Tuesday, Wednesday, and Thursday. During the morning of these days, excess off-peak utility energy is purchased, stored in the EES, and immediately discharged when the mid-peak arrives. The discharge of the energy does not occur when the campus demand is highest, suggesting that the point of EES dispatch at that time was not to reduce demand charges, but to procure a portion of the daily electrical demand earlier when electrical energy costs are lower.

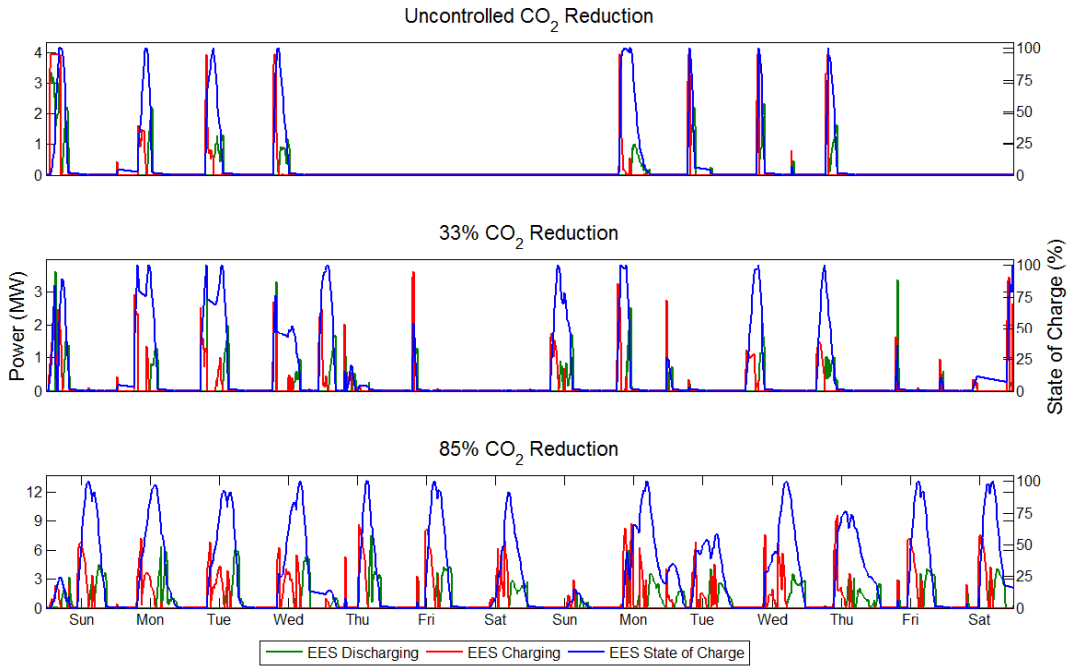

Figure 6-14: EES discharging, charging, and state of charge during the winter for the EES technology scenario when CO_2 emissions are uncontrolled, reduced by 33%, and reduced by 87.5%

Operation for the EES scenario with a 33% carbon emissions reduction is similar to the baseline scenario. Gas turbine operation is reduced, the PV system is used to provide a portion of the energy during the day, and utility imports increase. The EES performs a similar function as for the unconstrained carbon emissions case, and EES operation does not appear to correspond to PV system operation. Charging of the EES during the off-peak period still occurs in order to perform arbitrage and peak shaving. While total carbon emissions must be reduced by 33% in this simulation, the purchase of off-peak electricity for the purposes of peak shaving and cost arbitrage actually increase total CO_2 emissions associated with the UCI campus load due to an increase carbon emissions factor during off-peak (night) associated with electricity purchased from a California utility, as seen in Figure 3-10. However, this must be offset by either running

the gas turbine using renewable natural gas or importing utility electricity when the grid carbon emission factor is low.

The gas turbine is still used to provide the majority of the campus power when carbon emissions are reduced by 85%. However, during the middle of the day, when solar generation is greatest, the gas turbine is routinely shut down and the entire campus electrical load is met using the PV system.

EES operation also changes. Instead of primarily being used for peak shaving, arbitrage, and to provide an energy dump for the gas turbine when campus demand is low, the EES is charged using excess solar energy produced by the PV system. This allows for the full utilization of the PV system, allowing for excess PV generation during the middle of the day to be stored and used during the evening and night. Utility imports at this level of carbon reduction are virtually eliminated.

Figure 6-17 and Figure 6-18 show electrical system and EES operation over a two week period in the summer. Electrical operation is similar to the baseline technology scenario for the uncontrolled carbon emissions and 33% emission reduction case, with the gas turbine operating at near or full power during on-peak and the minimum power during off-peak. However, under the baseline technology scenario with a 33% reduction to carbon emissions, gas turbine operation during the mid-peak period is reduced to the minimum power outlet for the baseline technology scenario. Under the EES technology scenario, gas turbine power output is increased during mid-peak period, but continues to produce less than the allowable maximum power (either the campus electrical demand or the maximum output of the turbine, whichever is lower). Instead grid imports continue consistently. Similar to winter EES operation, EES during the summer is

used to provide peak shaving, arbitrage, and a dump for excess electricity produced by the gas turbine when campus electrical demand is low. Operation at the 85% carbon emission reduction level is similar to operation during the winter.

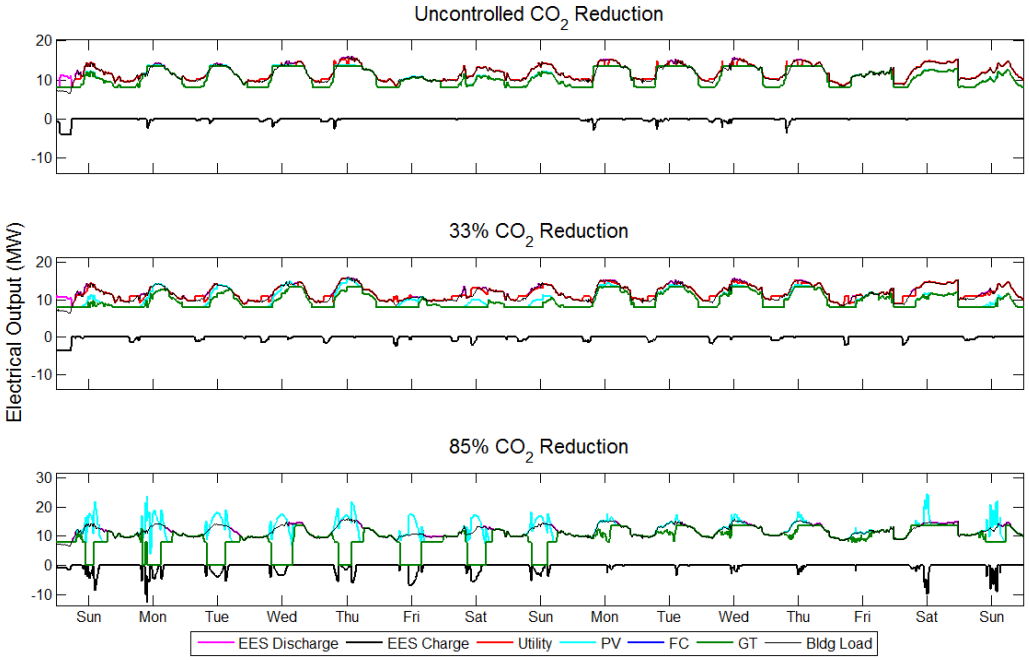

Figure 6-15: Electrical operation during the summer for the EES technology scenario when CO_2 emissions are uncontrolled, reduced by 33%, and reduced by 87.5%

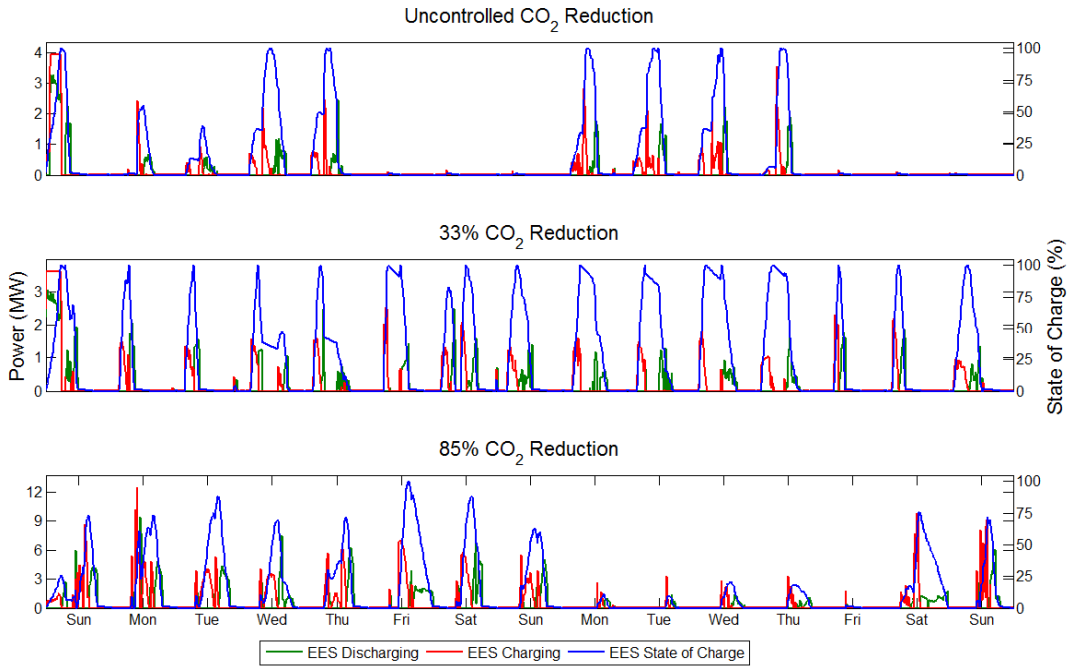

Figure 6-16: EES discharging, charging, and state of charge during the summer for the EES technology scenario when CO_2 emissions are uncontrolled, reduced by 33%, and reduced by 87.5%

6.3.2.2 TES Operation

Figure 6-17 shows electrical operation for the TES scenario system and electrical imports for two winter months. Figure 6-18 and Figure 6-19 show the cooling system and TES operation, respectively, for the same two weeks as Figure 6-17. The gas turbine, PV system, and electrical import operation shown in Figure 6-17 is similar to the same technologies and resources under the EES scenario, as seen in Figure 6-13. The single fuel cell adopted to help reduce carbon emissions by 85% operates in a similar fashion to the gas turbine, where operation occurs primarily when the PV system is not producing electricity. However, instead of operating at a reduced capacity during night hours, like the turbine, the single fuel cell produces at the maximum power setting.

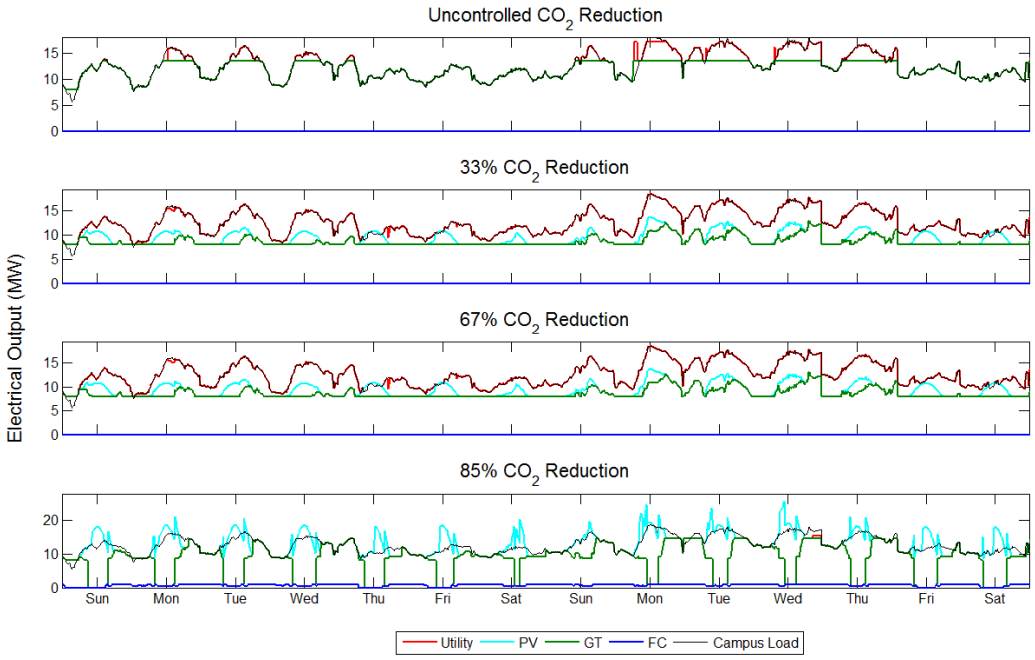

Figure 6-17: Electrical operation during the winter for the TES technology scenario when CO_2 emissions are uncontrolled, reduced by 33%, reduced by 66%, and reduced by 85%

The primary difference with the EES technology scenario, besides the form of energy storage included in this scenario, is that by having TES as an adoptable option, the actual campus load can be changed while still meeting the full cooling and electrical demand. Since the electrical campus load shown in Figure 6-17 is a combination of the electrical demand and the cooling demand assuming that all cooling is met at time of demand, the expected combined electrical demand may be altered through use of TES. For example, in the unconstrained carbon emissions case, the expected electrical demand during the second Monday is decreased. This is accomplished by charging the TES storage prior to the peak electrical and cooling demand, allowing for the cooling peak demand to be reduced, resulting in a reduction to overall electrical demand. This type of peak shaving is also seen for the same peak in the EES technology scenario shown in Figure 6-13.

The optimization results show that the TES system adopted when carbon emissions are unconstrained is larger than systems adopted when carbon emissions are required to be reduced by 0%, 33%, and 67%. As a result, the impact TES has on changing the combined electrical demand is marginal, as seen in Figure 6-17. Since the output of the adopted PV system for the case where carbon emissions are constrained is small enough that there is never any risk of curtailment, thermal storage is not required to ensure full utilization of available solar power. Considering that thermal energy is lost when cooling is passed through the TES from a vapor compression system, into a storage tank, and then to the campus to meet demand, storage will increase the carbon emissions if the cooling is produced using an energy source other that solar power. As a result, TES size shrinks when instituting a carbon constraint reducing total emissions up to 67% versus if carbon emissions are not constrained.

TES size does start to increase when carbon emissions are to be reduced by 80% or 85%. This increase is coupled with an increase in size for the PV system. With an increased PV system size, excess renewable energy is available, resulting in the adoption of a large TES. The excess solar energy is used to operate vapor compression systems to charge the TES, as seen when comparing Figure 6-17, Figure 6-18, and Figure 6-19 for the 85% carbon emission reduction case. When the desired carbon reduction results in an increase in PV system size, TES is operated in a manner that has the greatest impact of the resulting combined electrical demand. In particular, the combined electrical and cooling load is augmented in the early evening as the sun is setting, PV system production drops, and the controllable DG are being turned back on. While combined electrical and cooling demand is dropping, the TES is dispatched to reduce the combined load so that the fuel cell and gas turbine can continue to operate at part load. This style

of operation is not always possible, especially when available insolation is low, resulting in reduced PV system output. When insolation is low, the TES system is not utilized since sources of energy that produce carbon emissions are required to charge the TES. Instead of producing additional carbon to produce cooling that will lose energy content as it is stored in the TES, the cooling demand is continuously met using electricity produced by the gas turbine.

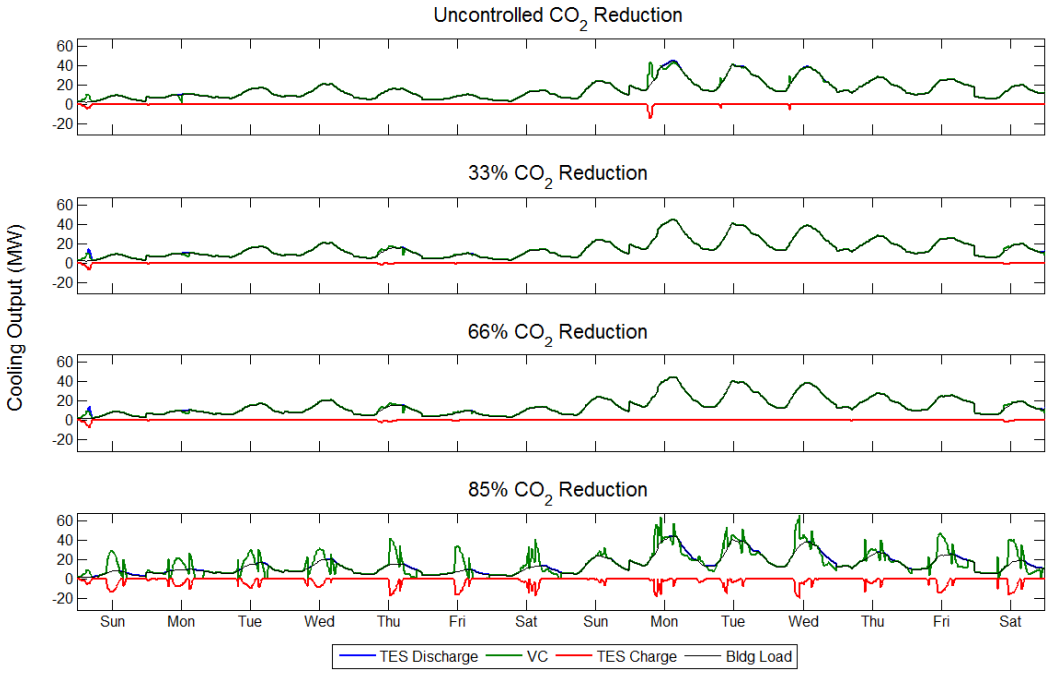

Figure 6-18: Cooling operation during the winter for the TES technology scenario when CO_2 is uncontrolled, reduced by 33%, reduced by 66%, and reduced by 85%

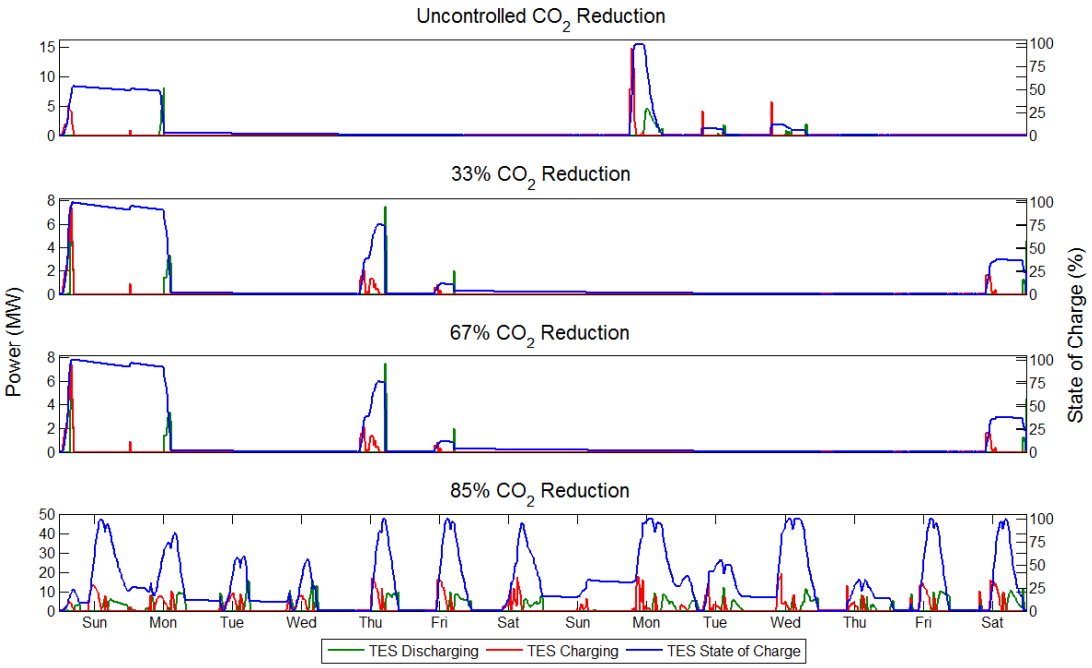

Figure 6-19: TES operation during the winter for the TES technology scenario when CO_2 is uncontrolled, reduced by 33%, reduced by 66%, and reduced by 85%

Figure 6-20, Figure 6-21, and Figure 6-22 show the electrical, cooling, and TES system operation respectively for the TES scenario during two weeks in the summer. The operation of all electricity producing systems is similar to operation experienced for the EES technology

scenario. Also, cooling and TES operation over the two summer weeks is similar to operation during the winter.

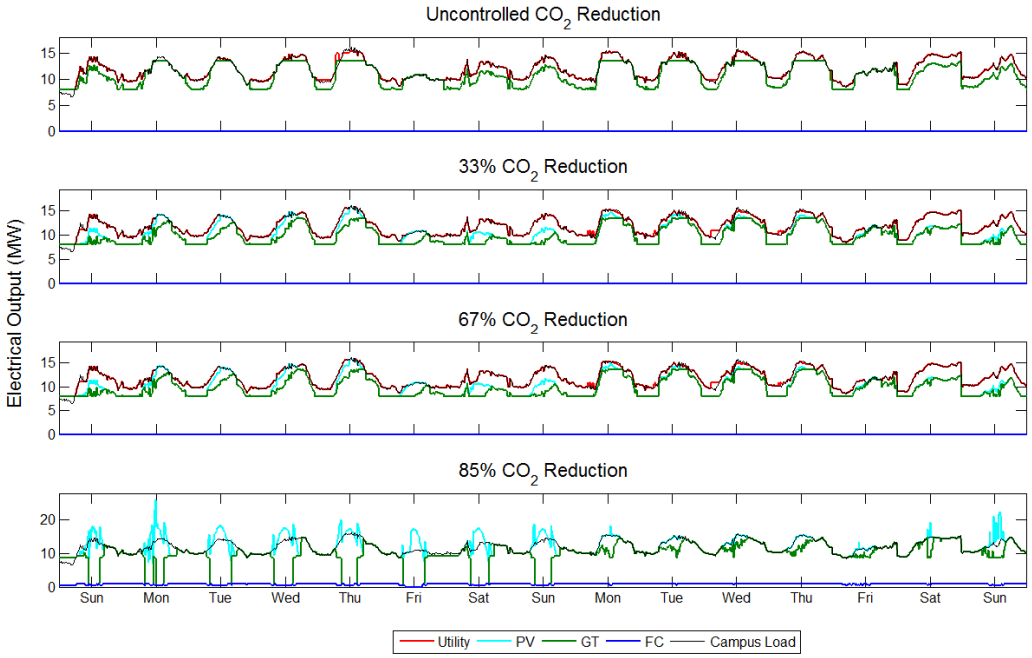

Figure 6-20: Electrical operation during the summer for the TES technology scenario when CO_2 is uncontrolled, reduced by 33%, reduced by 66%, and reduced by 85%

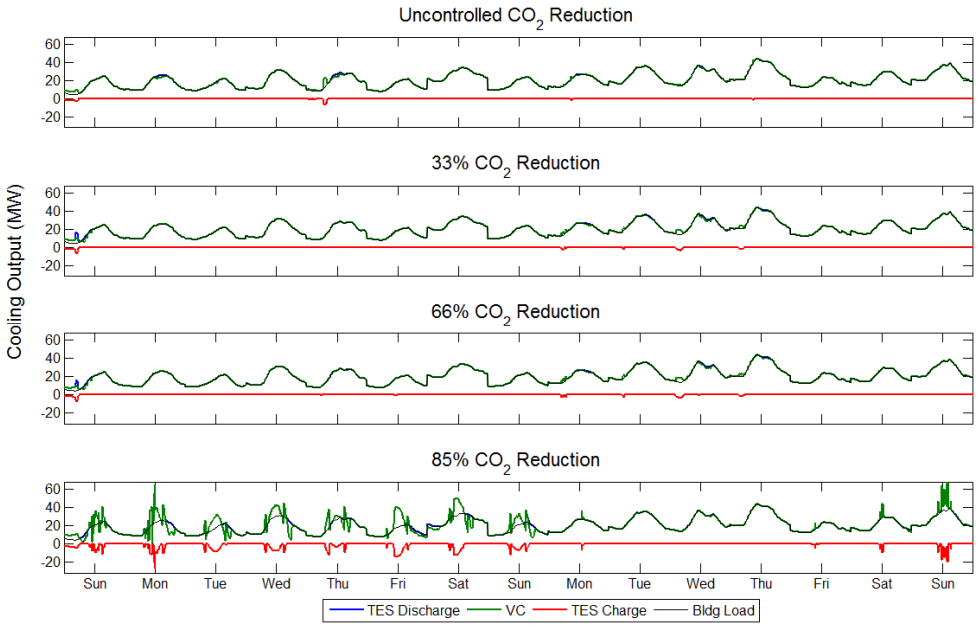

Figure 6-21: Cooling operation during the summer for the TES technology scenario when CO_2 is uncontrolled, reduced by 33%, reduced by 66%, and reduced by 85%

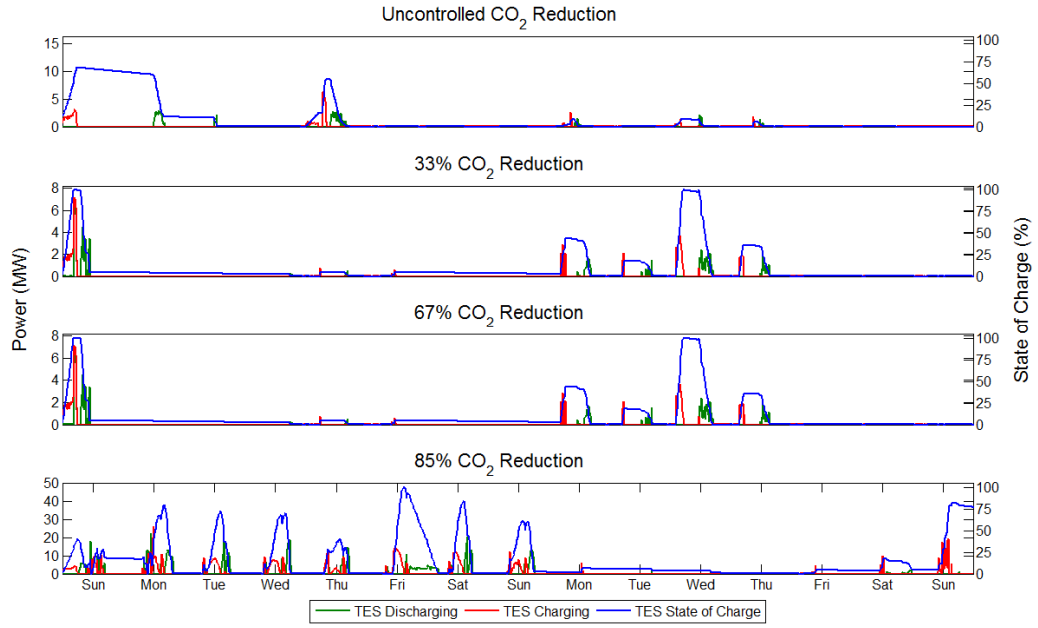

Figure 6-22: TES operation during the summer for the TES technology scenario when CO_2 is uncontrolled, reduced by 33%, reduced by 66%, and reduced by 85%

6.3.2.3 EES and TES

When both EES and TES are allowed to be adopted, both forms of energy storage are adopted for every level of carbon reduction. EES system size when carbon emissions are unconstrained or reduced by 0%, 33%, or 67% shrinks by approximately 76%. TES system size also shrinks, but only by 4% when carbon emissions are unconstrained and 33% to 36% when carbon emissions are reduced by 0%, 33%, and 67%. While the quantity of each individual storage is reduced, the potential for supplying the cooling demand using stored energy is increased for all carbon reduction cases while adding some additional flexibility of keeping some of the stored energy in the form of electricity.

Since the source of cooling production during the optimization is assumed to be only electrically powered vapor compression systems, the electricity stored in EES can be discharged to produce cooling. The assumed coefficient of performance for the installed vapor compression system is 3.4, meaning that every kWh of electrical energy input into the vapor compression system produces 3.4 kWh of cooling out. This conversion effectively allows a single MWh of electrical energy storage to be equivalent to approximately 3.4 MWh of cooling. So by allowing for the selection of both EES and TES, overall cooling storage is increased for all carbon reduction scenarios while also providing the flexibility of storing some energy in the form of electricity, which can be used for purposes other than cooling.

Figure 6-23 shows electrical operation for the EES and TES technology scenario during two winter weeks when carbon emissions are uncontrolled and reduced by 33% and 85%. Figure 6-24, Figure 6-25, and Figure 6-26 show the EES operation, cooling dispatch, and TES operation respectively for the same two winter weeks. Electrical operation for the uncontrolled and 33%

reduction case are similar to the TES technology scenario operation for the same two weeks, as shown in Figure 6-17. When carbon emissions are unconstrained, the TES is used to increase the load during the morning of the first Monday to allow for gas turbine operation to occur. Later, the TES tank is again used to shave the peak demand. Throughout the two weeks, the EES is used to perform arbitrage. However, the size of the EES is small relative to the total load, reducing the ability of the EES to impact overall operations.

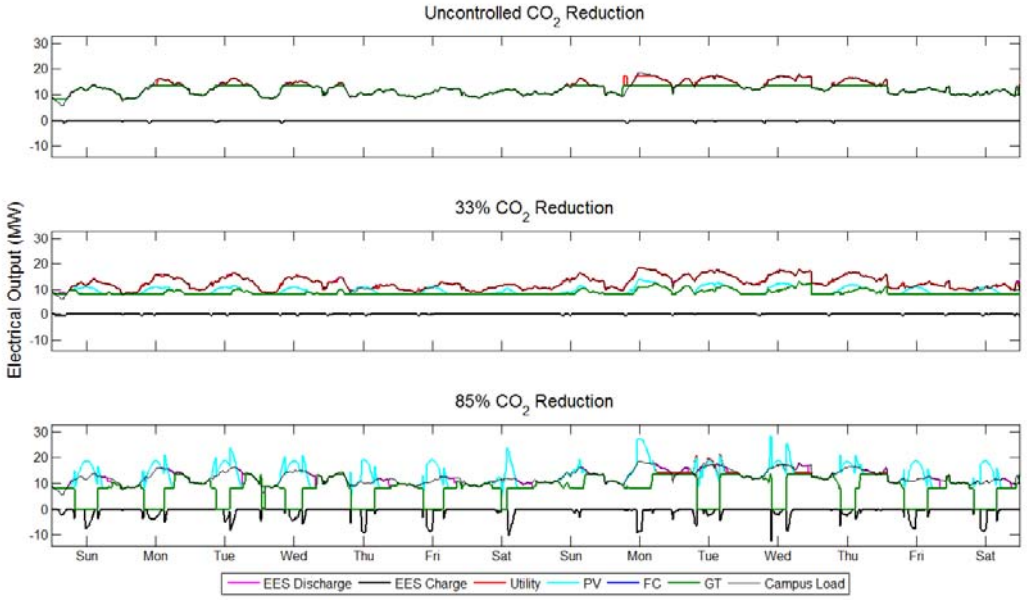

Figure 6-23: Electrical operation during the winter for the EES and TES technology scenario when CO_2 is uncontrolled, reduced by 33%, and reduced by 80%

DER system operation when carbon emissions are reduced by 33% is also similar to the TES technology scenario operation with the same level of carbon reduction. Despite a difference in system size, TES operation for the EES and TES technology scenario is nearly identical in shape during these two weeks as with the TES only technology scenario. While EES operation is

similar also to the EES only scenario, the size of the EES system in the current technology scenario is much smaller, resulting in a reduced impact on the campus demand.

Operation with an 85% carbon emissions reduction under the EES and TES scenario is similar to the individual energy storage technology scenarios. The gas turbine performs load following when PV production is zero, turns down as solar energy becomes available, and shuts off when the PV system is able to meet the full UCI campus electrical and cooling demand. Excess solar energy is then stored in either the EES or TES. As seen in Figure 6-23 and Figure 6-24, the EES is regularly charged during the day with excess solar energy, and later discharged as PV system production ramps down as the sun sets. While the TES is regularly charged to full capacity, TES charging tends to occur after EES charging. Intuitively, the EES should be charged first since the stored electricity is more flexible in its end use than stored cooling. While a vapor compression chiller can easily convert electricity into cooling, no technology that converts cooling back to electricity can be adopted during the optimization. Regardless, both the EES and TES appear to be discharged to either meet or reduce the combined electrical demand as solar power production decreases at the end of each day.

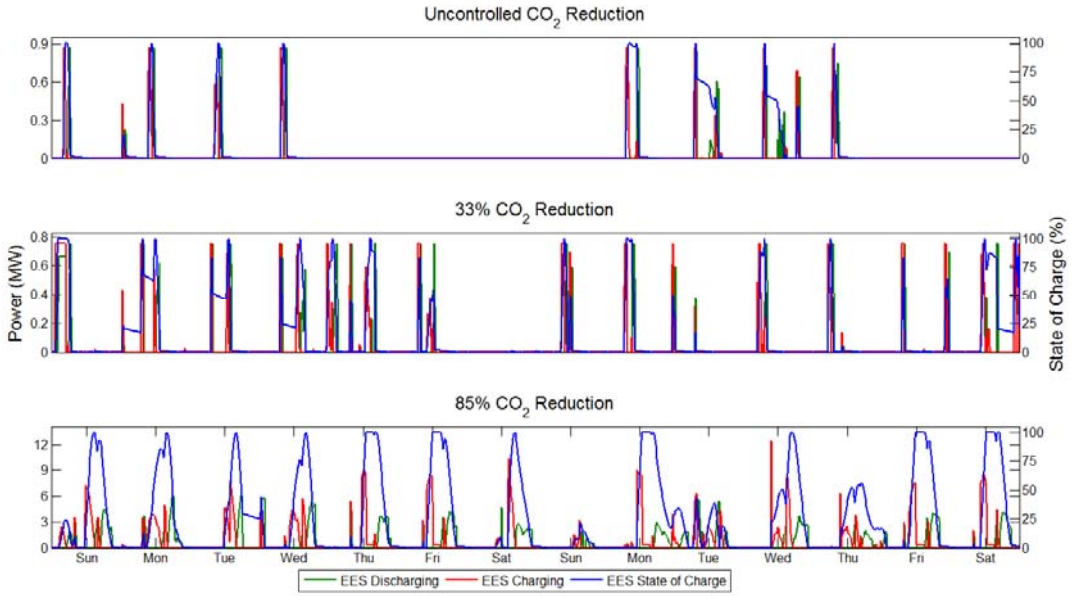

Figure 6-24: EES operation during the winter for the EES and TES technology scenario when CO_2 is uncontrolled, reduced by 33%, and reduced by 80%

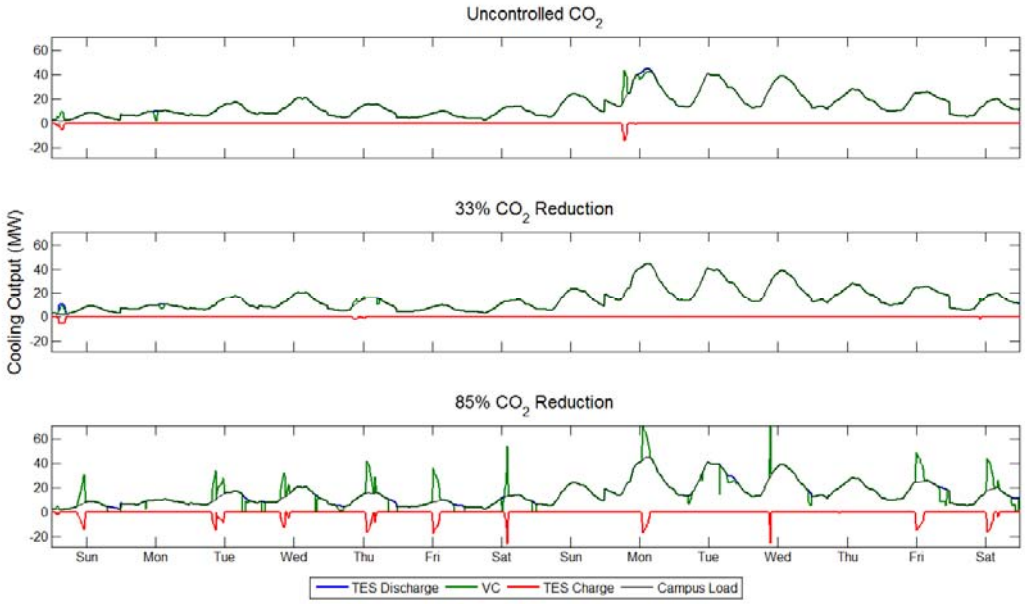

Figure 6-25: Cooling operation during the winter for the EES and TES technology scenario when CO_2 is uncontrolled, reduced by 33%, and reduced by 80%

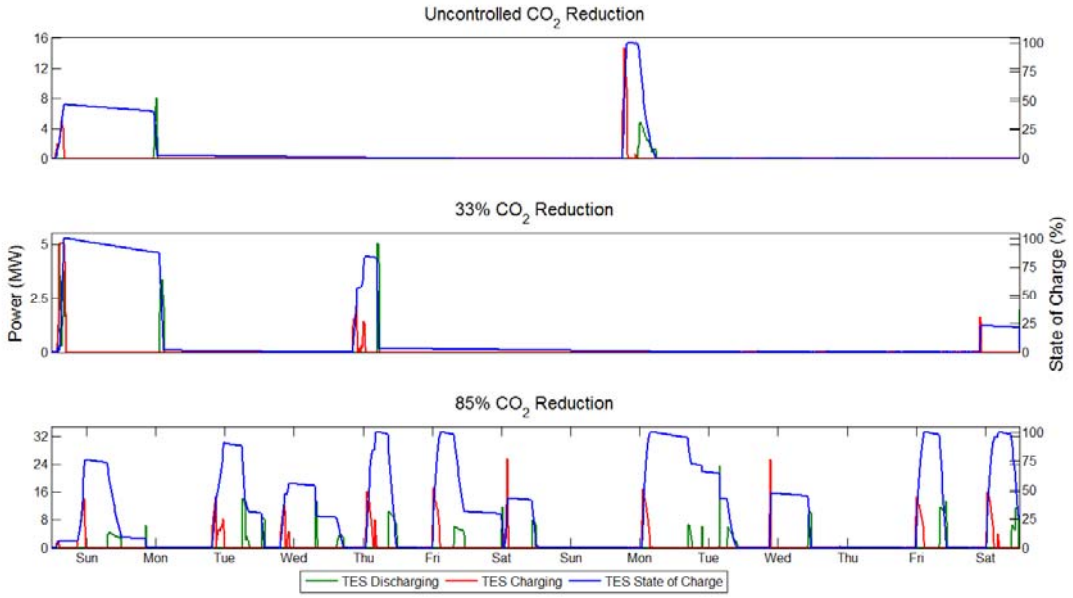

Figure 6-26: TES operation during the winter for the EES and TES technology scenario when CO_2 is uncontrolled, reduced by 33%, and reduced by 80%

Figure 6-27, Figure 6-28, Figure 6-29, and Figure 6-30 show the electrical, EES, cooling, and TES operation respectively during two summer weeks when CO_2 emissions are uncontrolled, reduced by 33%, and reduced by 85%. Electrical operation is similar to the EES technology scenario. As seen in Figure 6-30, TES use is sparse during the two week period. During the first week, the solar energy production is sufficiently large enough to meet the campus combined electrical and cooling demand while charging the EES. During the next week, PV production is limited, and the EES experiences some charging when excess solar energy exists, but no useful energy is sent to the TES for storage.

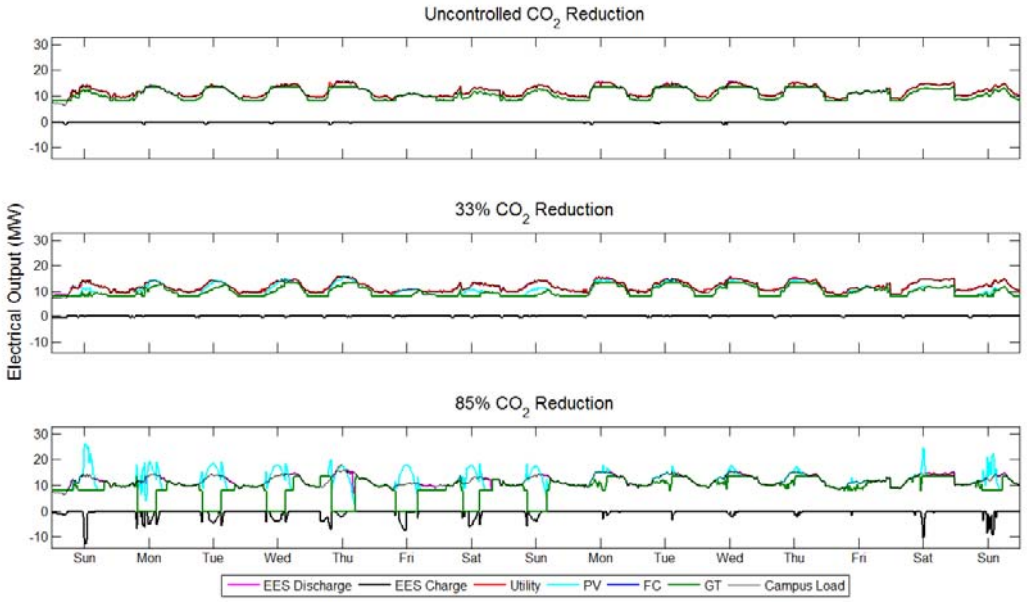

Figure 6-27: Electrical operation during the summer for the EES and TES technology scenario when CO_2 is uncontrolled, reduced by 33%, and reduced by 80%

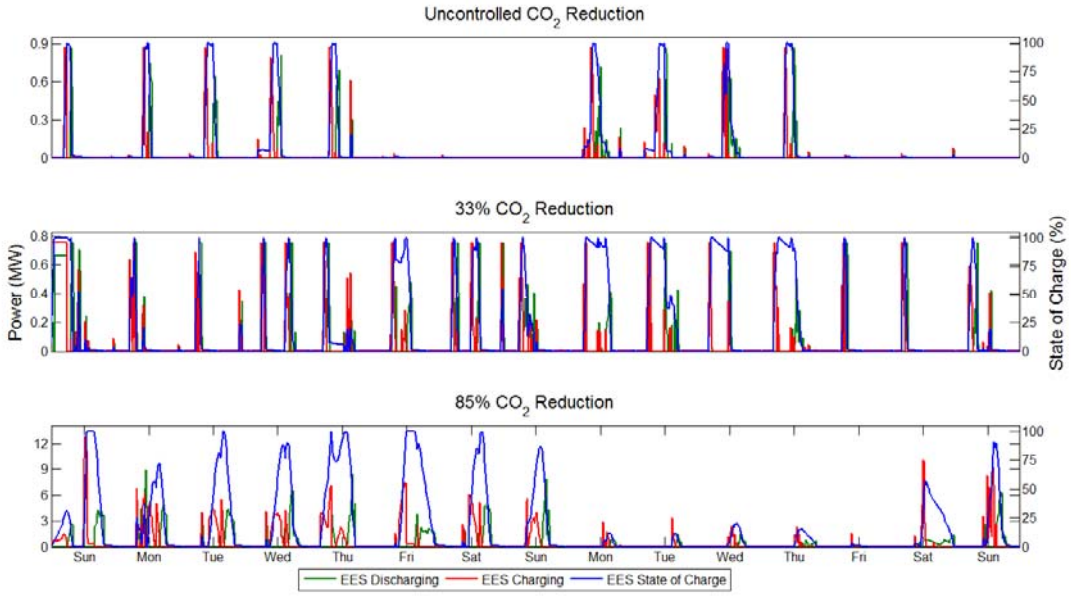

Figure 6-28: EES operation during the summer for the EES and TES technology scenario when CO_2 is uncontrolled, reduced by 33%, and reduced by 80%

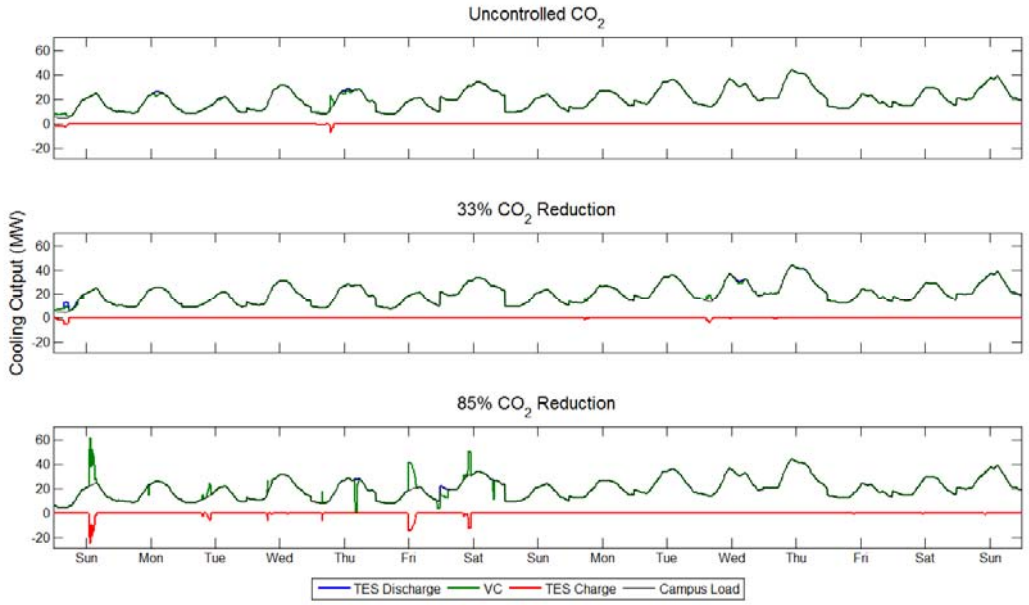

Figure 6-29: Cooling operation during the summer for the EES and TES technology scenario when CO_2 is uncontrolled, reduced by 33%, and reduced by 80%

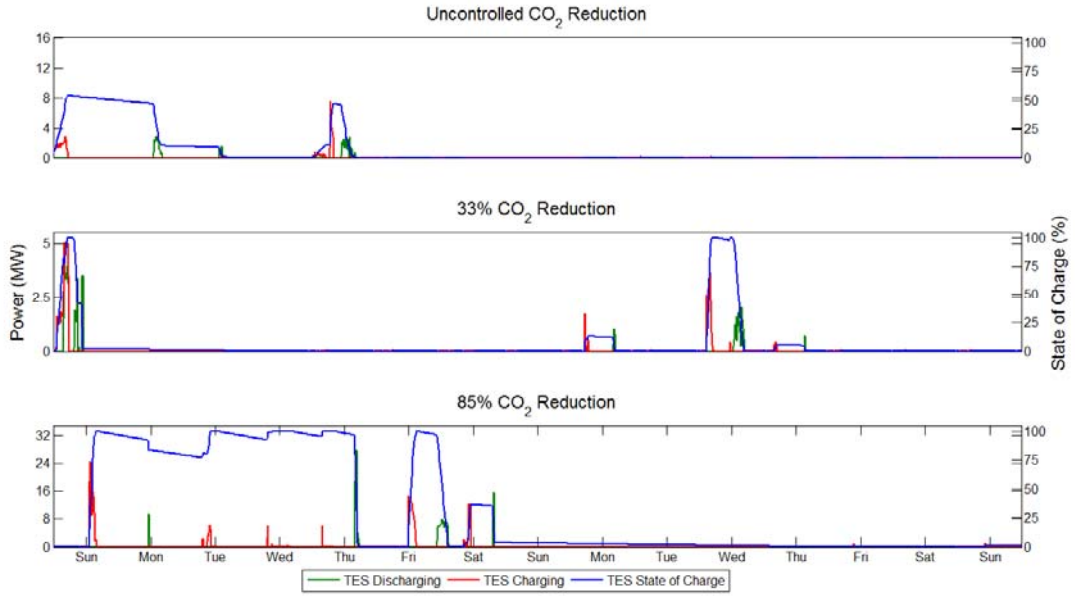

Figure 6-30: TES operation during the summer for the EES and TES technology scenario when CO_2 is uncontrolled, reduced by 33%, and reduced by 80%

6.3.3 Export Scenario

The export technology scenario optimizes the same set of technology available under the baseline technology, but with the ability of selling any excess energy generated onsite back to the utility. All of the electricity exported back to the utility is assumed to be exported under a net metering agreement similar to what is currently available to solar PV systems today. That is, power is exported to the utility at the retail price it would be charged to the customer at that same time of day and year. This work, however, assumes that the rate the DER system operator in this case receives is only the utility energy rate associated with generation, and does not include transmission and distribution charges. The applicable utility rates can be seen in Table 3-1. Note that transmission and distribution charges for the applicable SCE rate structure are approximately $0.02 per kWh, resulting in the revenue generated by exporting electrical energy at any time is the cost to purchase utility electrical energy minus the approximate $0.02 per kWh charge associated with transmission and distribution.

In addition to providing an additional revenue stream, the export of electricity generated onsite theoretically offsets utility generation, reducing carbon emissions produced by the grid. Figure 6-31 shows the percent of electricity generated onsite that is sold back to the grid. When carbon emissions are uncontrolled or reduced by 0%, 33%, and 67%, only a fraction of onsite generation is exported. As the carbon emission reduction increases from 67% to 80% and 85%, the size of the PV system increases. Under the baseline scenario, the renewable energy produced by the larger PV size exceeds the campus demand, and curtailment occurs. Under the export scenario, the excess energy is sold to the grid, reducing total costs while also decreasing the net carbon emissions associated with the UCI campus. Reducing carbon emissions past 67% results

in the installation of increasingly larger PV systems. As the PV system size increases, so does the amount of electricity sold back to the grid.

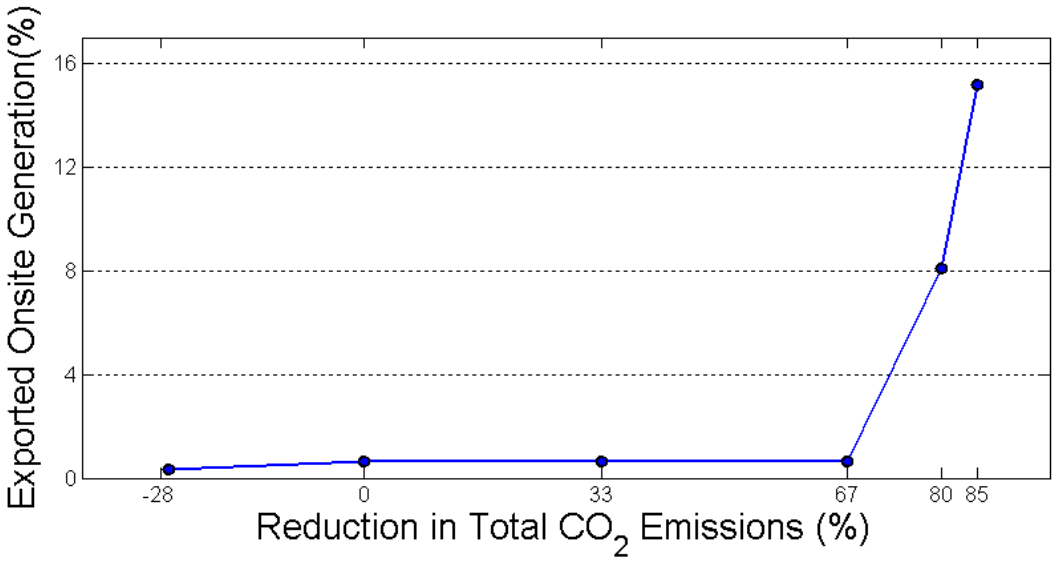

Figure 6-31: Percent of onsite generated electricity that is exported for all carbon reduction cases

Figure 6-32 shows electrical operation for the DER system optimized for the export technology scenario when carbon emissions are uncontrolled, reduced by 33%, and reduced by 85%. Electrical operation when carbon emissions are unconstrained is nearly identical to the baseline technology scenario. The only primary difference is when the campus electrical demand is low during the first Sunday, the gas turbine continues operation, with the excess electricity being sold back to the grid. No additional export occurs during the next two weeks, suggesting that the little to no value exists for selling electricity back to the grid during the winter using a gas turbine. The one instance where export does occur allows for demand charges to be avoided, which would be substantially larger if incurred versus any losses created by selling electricity back to the grid.

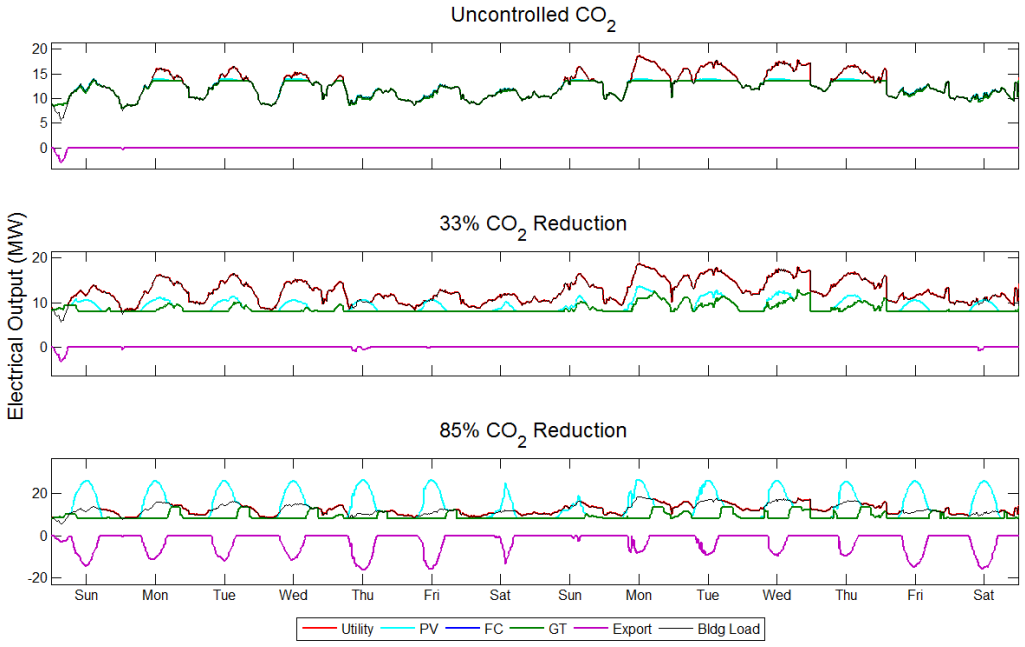

Figure 6-32: Electrical operation during the winter for the export technology scenario when CO_2 is uncontrolled, reduced by 33%, and reduced by 87.5%

System operation when carbon emissions are reduced by 33% are also similar to the baseline scenario. However, since the gas turbine is allowed to remain operational during the first Sunday under the export scenario, and demand charges are avoided, the gas turbine is operated dynamically in the late noon and evening each day in order to ensure that demand charges do not increase. Under the baseline scenario, the utility imports required while the gas turbine is shut down during the first Sunday create demand charges large enough such that the gas turbine does not need to be operated dynamically to keep maximum utility demand low.

When carbon emissions are reduced by 85%, gas turbine operations are maintained throughout the day. This is the only example of a controllable form of DG (either a fuel cell or gas turbine) where sustained operations occur throughout the day. Like all other technology scenarios, the largest PV system installed occurs for the 85% carbon reduction case. However,

whereas the baseline scenario required a large PV system to produce renewable energy on low insolation days and all energy storage scenarios stored solar energy for later use in the day, the export technology scenario leverages the renewable energy generated onsite using the sun to offset gas turbine operation. As long as the carbon reduction goal is in terms of net carbon reduction, the ability to produce and export solar energy creates leverage that the campus can use to maintain gas turbine operation while meeting the overall carbon emission reduction goal.

Figure 6-33 shows electrical operation for the export technology scenario during the summer. For both the uncontrolled and 33% carbon reduction cases, the ability to export once again allows the gas turbine to operate during the first Sunday and not shut down due to low campus demand. Later, whenever campus demand is low during the middle of the day (on-peak), the gas turbine can be operated at full capacity, with any excess electricity being exported back to the grid. While dynamic operation still occurs during the mid-peak period, operation during all of on-peak and for much of off-peak have been simplified, with the gas turbine operating at full capacity during on-peak and near or at the minimum power setting during off-peak.

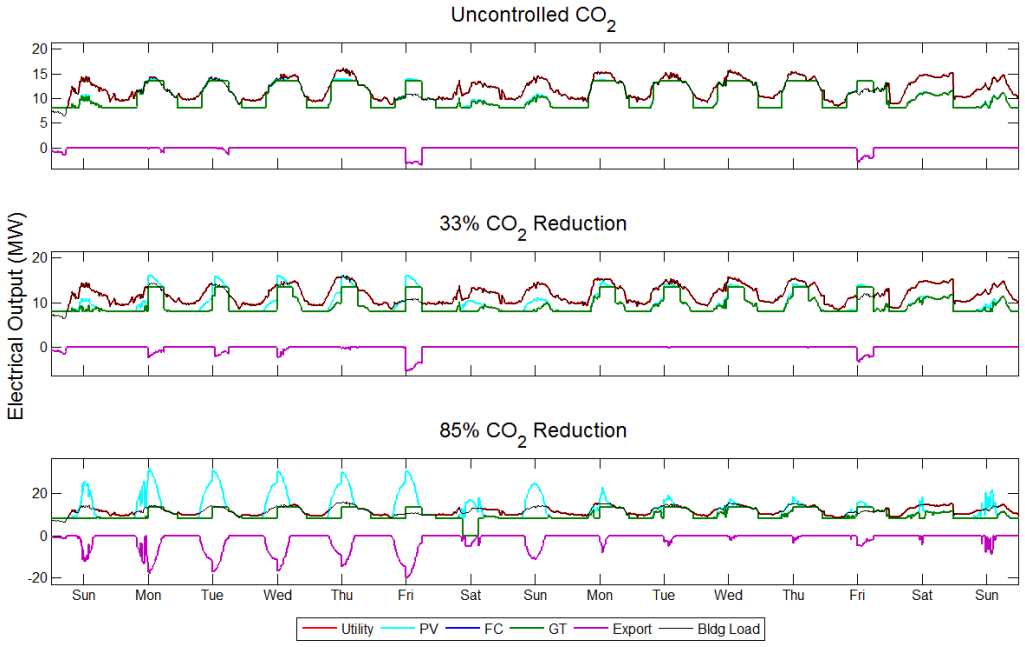

Figure 6-33: Electrical operation during the summer for the export technology scenario when CO_2 is uncontrolled, reduced by 33%, and reduced by 87.5%

Similar to operation during the winter, gas turbine operation is maintained throughout all days during the summer except for the first Saturday. Unlike the winter time period, the gas turbine is operated at full capacity during all on-peak days, even though sufficient solar power exists to meet the portion of the UCI campus demand that is now met by the increase gas turbine power. On-peak electricity is the most valuable electricity, and the campus experiences the greatest compensation per unit energy for exporting electricity during this period. As a result, the ability to export creates an opportunity to produce additional revenue while meeting the 85% carbon emissions reduction.

6.4 DER System Cost and Carbon Reduction

Figure 6-34 shows the yearly operating cost for all technology scenarios and carbon reduction cases without the monthly debt payment associated with the purchase of the DER

system on top and with the monthly debt payment on bottom. While the cost to operate the DER system increases carbon emissions decrease, the cost increase is primarily due to the purchase of more expensive renewable natural gas, and the cost increases are small relative to the increase in yearly cost due to the additional loan payments. In other words, the cost to operate a DER system increases as carbon emissions are reduced, but the additional operations and maintenance costs are relatively small compared to financing cost. Also, as a result of an increased use of solar energy, operating costs actually decrease when moving from an 80% reduction to 85%. However, the loan payment associated with the increase in PV system size results in an overall large increase to the size of the loan payment required, erasing any potential benefit created by using energy sources with low operating costs.

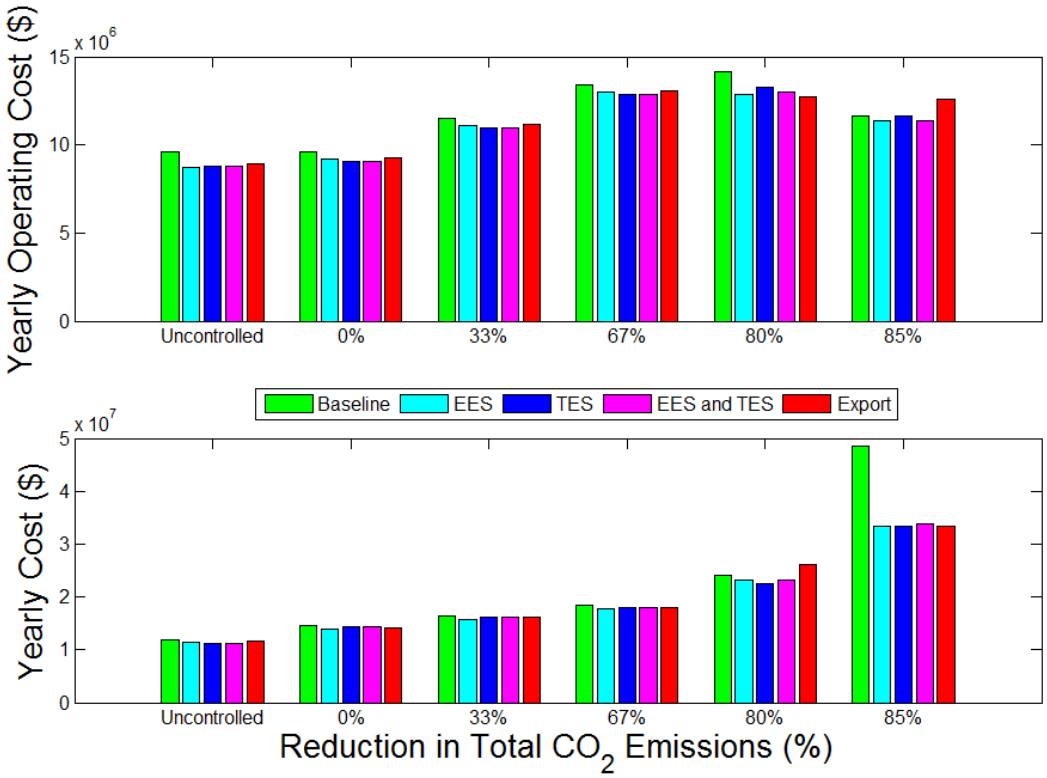

Figure 6-34: Yearly operating cost without and with debt payment required for optimal DER system for all technology scenarios and carbon emission limits

Figure 6-35 shows the initial investment required when 20% of the total install cost is covered by the investor for all technology scenarios for all carbon reduction cases. In general, the initial investment cost tends to increase as carbon emissions are reduced. However, since the set of adopted technology between the 0% reduction and 67% reduction case are nearly identical, the investment costs are the same. If another source of renewable natural gas with a lower carbon signature associated with gas clean up were to be made available to the UCI campus, further carbon emission reduction would be possible beyond 67% without installing any additional technology or increasing the initial investment.

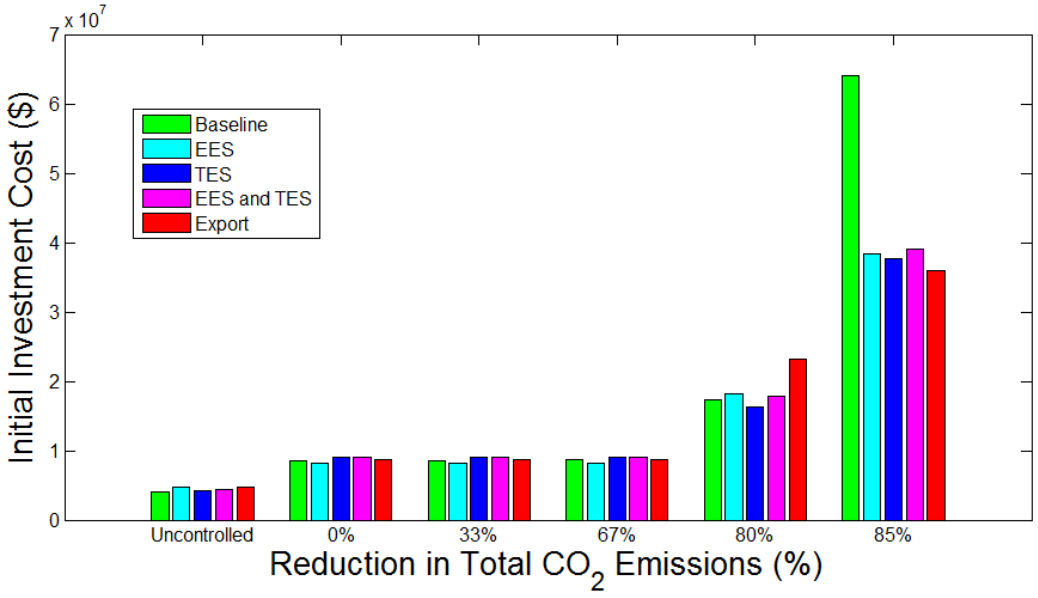

Figure 6-35: Initial investment cost required by an investor for all technology scenarios and carbon emission limits

Further emission reductions beyond 67% occur due to the installation of larger PV systems. This results in an increase to the initial capital investment cost. Initial investment cost at an 80% carbon emission reduction is similar across all technology scenarios. The export technology scenario experiences the adoption of the largest PV system, resulting in the largest

initial investment. However, as the carbon emission reduction increases from 80% to 85%, the baseline technology scenario is forced to adopt the largest PV system in order to provide solar energy every day, even on days when sunlight is diminished. The resulting initial investment for the optimal DER system is 50% larger under the baseline technology scenario than the next largest scenario (the EES and TES technology scenario). Note that if export to the grid is allowed, the resulting initial investment is the lowest of all technology scenarios even though the physical technology options are the same as the baseline technology scenarios.

Figure 6-36 shows the modified internal rate of return for all technology scenarios and carbon reduction cases. As discussed in Section 3.7, the MIRR assumes that any savings produced by DER operation are reinvested by the business or organization. The reinvestment rate is the rate at which a business or organization produced returns at during normal operations, and is assumed to be 8% for this work. A return of 0% is equivalent to the statement that DER investment and operation results in a financial loss. The extent of this loss is not quantified by the MIRR since an overall loss would result in the root of a negative number being determined, resulting in a non-real rate of return in the number of periods is an even number.

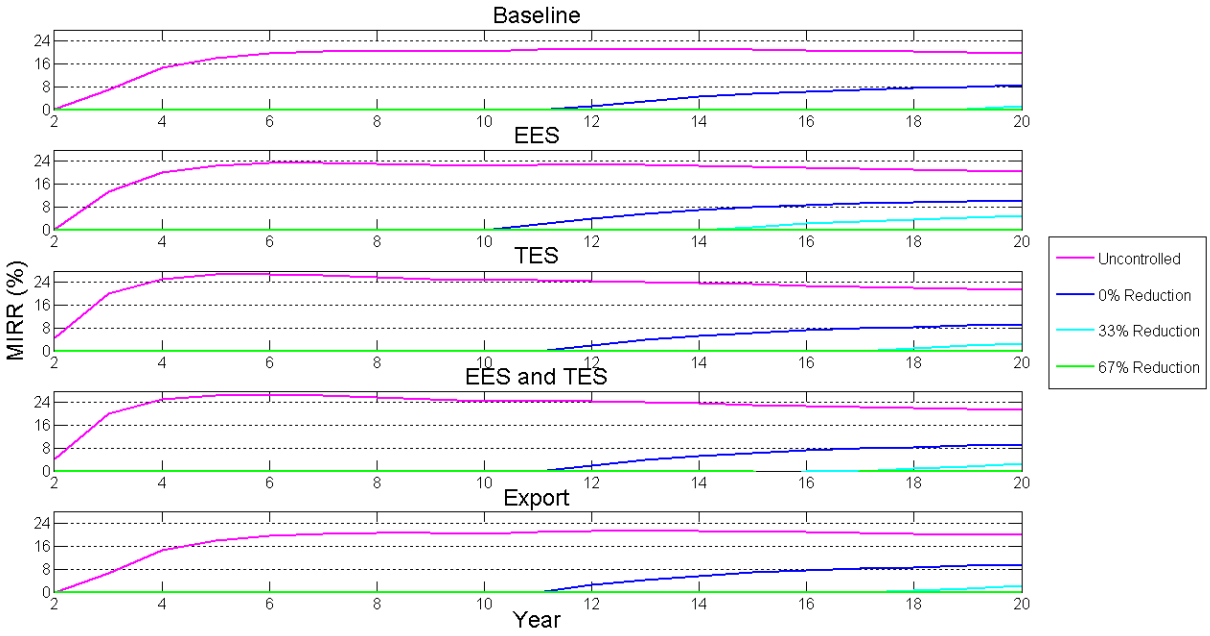

Figure 6-36: Marginal internal rate of return for all technology scenarios when carbon emissions are uncontrolled and reduced by 0%, 33%, and 67%

From an investment perspective, the best return on money invested is obtained when carbon emissions are uncontrolled. Under this case, all technology scenarios produce extremely positive returns on the initial investment, with the TES technology scenario providing the greatest return on investment. If carbon emissions are constrained to not increase when a DER system is adopted, the economic performance deteriorates for all scenarios, and a positive return is not seen until ten years, of the loan has been paid off. Reducing carbon emissions results in an even smaller on no positive return associated with the DER system.

Other considerations must be made when attempting to reduce carbon emissions. Earlier, it was argued that other motivations may exist that create the desire to reduce carbon emissions. If this is the case, other metrics must be used to evaluate the performance of a DER system. The simplest metric is to determine the additional cost incurred above the baseline cost divided by the

amount of carbon emissions that were eliminated by DER system purchase and operation, or the cost per unit mass of carbon reduction. Figure 6-37 shows the cost to reduce carbon for all technology scenarios when emissions are reduced by 33%, 67%, 80%, and 85%. The initial investment cost is included in Figure 6-37 by determining the payment required to be made to the initial investor such that the initial investment is paid back in ten years at an interest rate of 8%.

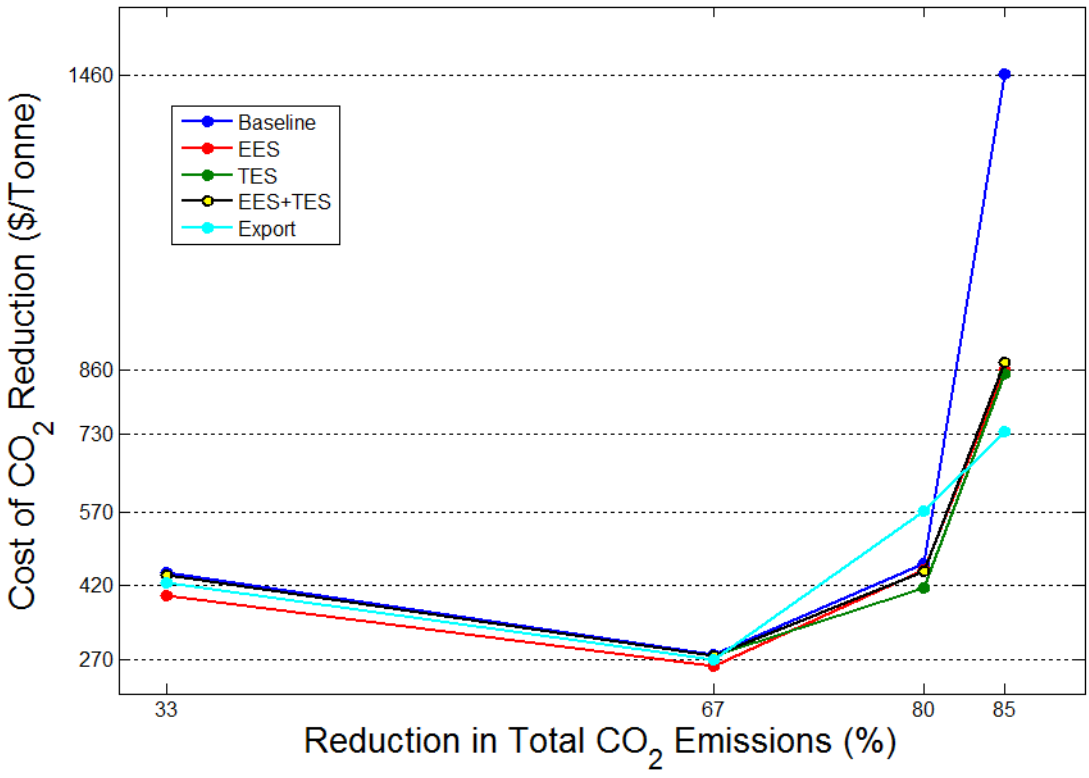

Figure 6-37: Cost of CO_2 reduction for all technology scenario and carbon emission limit

Figure 6-37 shows that the cost to reduce carbon decreases from 33% to 67% reduction. Since the technology purchased at these levels of reduction are identical for all technology scenarios, and the additional carbon reduction from 33% to 67% is achieved by switching from a non-renewable to renewable fuel, the initial investment and loan payments do not increase as a

result of reducing carbon emissions further. Reducing carbon emissions beyond 67% requires for the set of purchased technology to change, with a shift to higher efficiency or solar technology driving the increase in total cost. As a result, the cost to carbon begins to increase in an exponential fashion as it becomes more difficult to reduce carbon emissions.

When carbon emissions are reduced by 85%, the technology scenario with the highest cost versus reduced carbon emissions are the baseline technology scenario. Allowing for the adoption of energy storage decreases the cost to reduce carbon by 41%. Allowing for export of electrical energy and by determining total carbon reduction on a net carbon emissions basis, the cost to reduce carbon can be reduced from the baseline technology scenario by approximately 50%.

6.5 Discussion

With the set of technologies and energy source options included in the current work, attempting to reduce carbon emissions always results in a cost increase. How the cost is increased depends on the desired level of carbon reduction. The particular parameters of the renewable natural gas explored in this current work showed that a system designed to minimize cost of energy regardless of carbon emissions can be slightly modified with some additional PV and achieve a carbon emissions reduction of up to 67%. When the reduction to carbon emissions are at or below 67%, the DER system adopted and style of operation under every technology scenario is nearly identical. Obviously, energy storage and export ability increase the flexibility of the overall system, but the economic performance and cost to reduce carbon are similar across all technology scenarios. It is not until carbon emissions have been reduced to 67% that the economic performance and cost to reduce carbon start to diverge.

If the carbon emissions associated with the production of renewable fuel can be reduced, then the same system that was adopted across all technology scenarios for a carbon reduction of 0%, 33%, and 67% could achieve even greater emissions reduction. From an economic perspective, this would allow the campus to put off investment in other expensive technologies until later while reducing the amount of ancillary technology required to support the future operation of uncontrollable but carbon free PV.

Reducing carbon emissions beyond what can be achieved by switching to renewable fuel increases cost significantly. Predictably, the cost increase is greatest when excess energy production cannot be accommodated through the use of storage or export back to the grid. Of these two options, the option that achieved an 85% reduction to carbon emissions at the lowest cost was the export technology scenario. Realistically, the rate at which an individual can sell electricity back to the grid would most likely be lower than the rates used in this current work, and the economic benefit created by exporting electricity presented in the current results may be overstated. At the same time, electricity exported back to the grid is likely to supplant energy generated from fossil fuel fired power plants, resulting in a greater reduction in carbon emissions compared to that assumed in this work. Further model refinement would likely result in an optimal DER system adopting a smaller PV system with worse financial performance but improved environmental impact.

Note that renewable fuel was modeled as an infinite resource in the sense that there was no limit to how much could be purchased. If this source does not exist, and there is a limit to the amount of renewable fuel that can be purchased, then PV system size will start to increase in order to actually achieve any carbon emissions reduction. With this taken into consideration, the

cost to reduce carbon presented in Figure 6-37 are likely lower than what can be actually achieved. Coupled with the currently low price to purchase a permit to emit carbon (according to [180], a permit to emit carbon has never been sold at a price higher than $23 per tonne and is currently being sold at approximately $12 per tonne), a carbon constraint will always need to be included in any DER optimization that desires carbon emissions reductions. Or else, outside carbon market factors must increase the cost of carbon to accurately reflect the true cost of reducing emissions. These carbon emission costs could be readily included in the optimization. Other factors may reduce the cost to reduce carbon, such as by installing utility size PV systems in a central location instead of many small PV systems at the point of use or by using renewable fuel in a more efficient central power plant. However, unless the price to emit carbon increases or the cost of renewable generation sources and energy storage plummets, no DER optimization model that minimizes cost will suggest the adoption of a system that significantly reduces carbon emissions without enforcing a constraint that requires such an action.

7 Cost of Electricity for Public Level 3 EVSE Operation

When a Level 3 EVSE charger is purchased for public use, the equipment can be connected to the utility in two different ways: a dedicated utility meter can be installed and used to supply electricity to the EVSE exclusively, or the EVSE can be integrated with a building by connecting the equipment to the building electrical system. Under this second scenario, the EVSE and building receive electric utility service under a single utility meter, and the utility bill is determined by the combined building and EVSE refueling load. PEV refueling cost depends upon whether the EVSE is serviced by a dedicated utility meter (or the "Standalone" scenario) or has been integrated with a building (or the "Integrated" scenario).

7.1 Standalone Level 3 EVSE Analysis

The travel model described in Section 3.3.1 was used to produce a set of trips made by Level 3 compatible PEVs. The number of trips considered per simulation ranged from 50 PEV trips per month to 10,000 PEV trips per month. Using the assumption that the PEVs started each day with a fully charged battery, the end state of charge was determined. The trips were then separated between PEVs with a battery state of charge greater than and less than 80%. All PEVs with less than an 80% state of charge were charged according to the Level 3 EVSE operation model as described in Section 3.3.2. The resulting electricity demand profile was used with the utility rate model described in Section 3.1.1 and cost allocation model described in Section 3.5.1.1 to determine the total utility cost and demand charge cost incurred by each individual PEV.

These simulations and calculations, described above, were performed for Level 3 EVSE with two power ratings; 44 kW and 120 kW. For both the 44 kW and 120 kW chargers, one, two,

four, and eight EVSE supplied by a single utility meter were evaluated. Under these scenarios, the applicable utility rate structure is either TOU-EV-3 or TOU-EV-4, depending upon the maximum power demand.

The results of this work are the averaged results of numerous simulations. At each given number of PEV trips per month, the probability density functions described in section 3.3.1 are used to generate a randomly selected set of trips performed by PEVs. Using the randomly generated set of PEV trips, a charging profile is then determined using the Level 3 charging station operation model described in section 3.3.2. The resulting electrical load profile is then combined with the utility rate model as described in Section 3.1.1 to find the cost of electricity. This process is repeated until the average cost of electricity of all simulations performed at the given number of PEV trips per month experiences negligible changes due to an additional simulation. At this point, no additional simulations are performed for a given number of PEV trips per month. Variation in energy and demand charge cost results across the different simulations is presented in Section 7.1.3.

The results presented in this section have been published in a paper by Flores et al. [181].

7.1.1 Single 44 kW EVSE Results

A single Level 3 44 kW charger servicing either shopping or work trip types is examined in Section 7.1.1.1 and 7.1.1.2, respectively. Increasing both charger power and number of chargers per electricity meter is explored in 7.1.2.

7.1.1.1 Shopping Travel

Assuming that all PEVs start each day with a full battery, approximately 28% of all winter and summer shopping trips result in arriving with less than an 80% state of charge. Figure

7-1 shows example load profiles for a Level 3 charging station using both conventional and valet parking. The same set of PEV trips were used to simulate demand profiles for conventional and valet operations. The load profiles range from 27 to 2787 PEV shopping trips serviced per month by the charging station. These values correspond to a total number of PEV trips of 100 to 10,000 per month. The allocated cost for each time step is also included in Figure 7-1. The total cost includes the demand charge allocation as well as the energy charge cost using the cost of energy at the time of purchase. At low levels of PEV use, the demand profiles are similar between conventional and valet operations. However, as the number of PEV cars increases, the electrical demand for valet operations increases due to the queuing and subsequent refueling PEVs that arrive while the EVSE is occupied. This is apparent in the demand profiles at 696 PEV trips serviced per month. The total cost of operation also decreases as the number of PEV trips serviced increases.

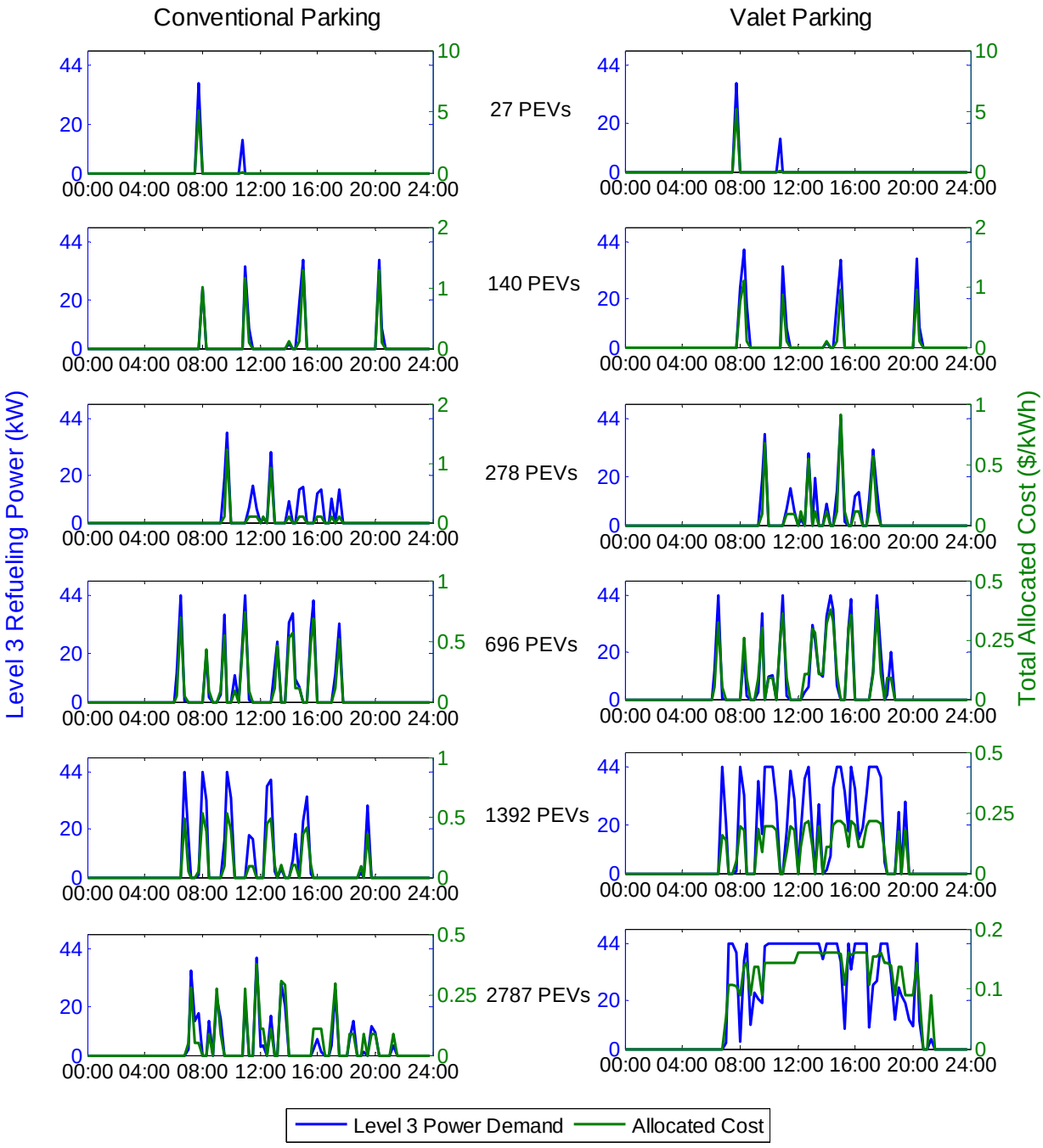

Figure 7-1: Example load profiles and resulting cost allocations for 27, 140, 278, 696, 1,392, and 2,787 shopping trips per month using PEVs

Figure 7-2 shows the percent of PEVs with a state of charge below 80% that are fully refueled, partially refueled, or unfueled for both conventional and valet parking scenarios. Predictably, valet parking provides greater access to the EVSE. The valet results show that approximately 20 % of all shopping travel has a corresponding dwell time that is shorter than what is required to completely refuel. While valet parking significantly increases the percent of PEVs refueled at moderate to high levels of traffic, additional EVSE is required if all Level 3 eligible PEVs are to be refueled.

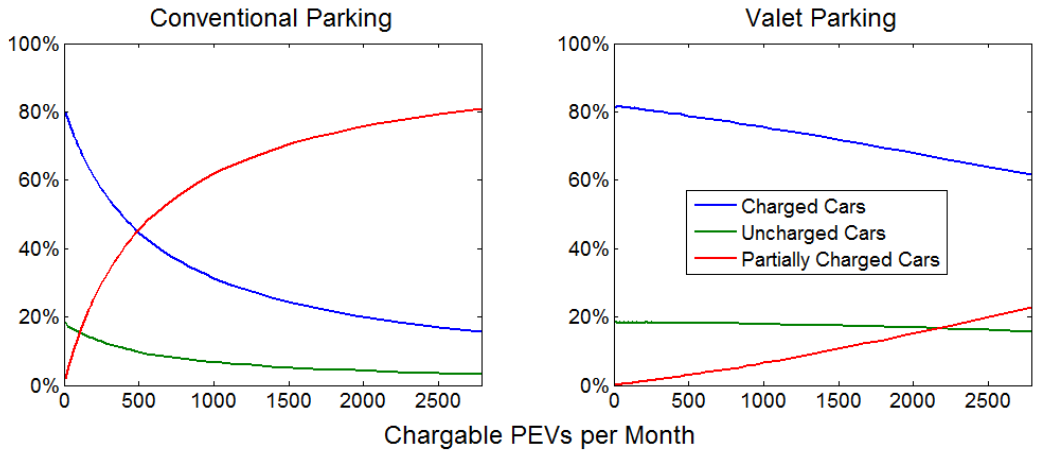

Figure 7-2: Percent of cars that are fully charged, partially charged, or uncharged by the 44 kW Level 3 charger after a shopping trip type for conventional and valet parking scenarios

The average energy charge costs for both the summer and winter seasons versus the number of chargeable PEVs per month are shown in Figure 7-3. The average energy cost for valet parking remains stable regardless of the number of PEVs refueled per month. While an increase in PEV traffic increases the number of PEVs refueling during on-peak times, PEV use during the weekend also increases. As a result, the increased EVSE utilization during summer and winter on-peak times due to increased PEV use is counter-balanced by increased usage during mid-peak and during the weekend (off-peak) leading to relatively stable energy costs.

With conventional parking, the average energy cost decreases as PEV traffic increases due to arrival of PEVs during off- and mid-peak, decreasing the access that PEVs have to the EVSE when arriving during on-peak.

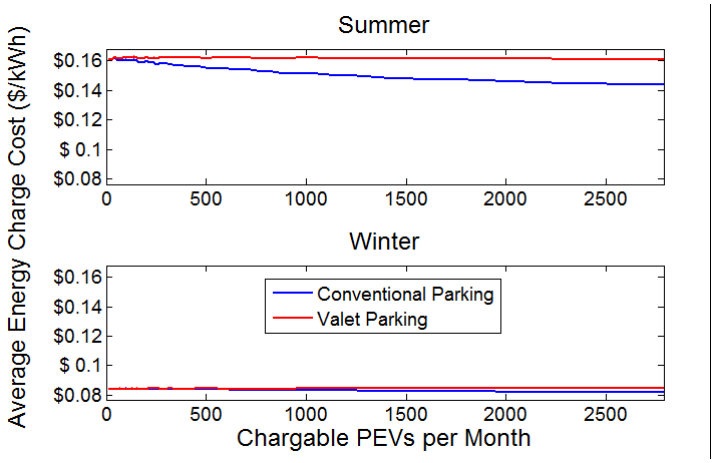

Figure 7-3: Average energy charge cost versus number of chargeable PEVs per month for shopping trips occurring during the summer and winter

On the other hand, Figure 7-4 shows the average demand charge cost for the winter season versus number of chargeable PEVs per month. Since summer and winter demand charges are the same and the difference between summer and winter shopping travel is small, the average demand charge cost versus chargeable PEVs for summer is nearly identical in amplitude and dynamics as that shown in Figure 7-4 for the winter demand charge costs. While it is clear from Figure 7-4 that the demand charge cost is the dominant electrical energy cost, increasing the number of PEVs charging per month can quickly reduce cost.

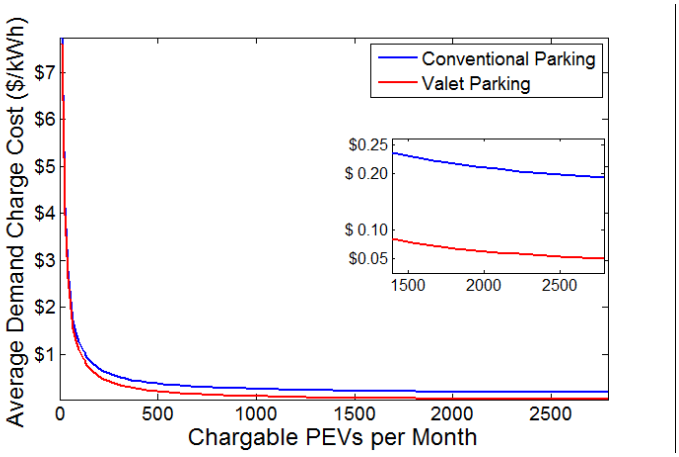

Figure 7-4: Average demand charge cost versus number of chargeable PEVs per month for shopping trips occurring during the winter

The demand charge cost shown in Figure 7-4 is the average demand charge cost that a Level 3 EVSE operator must pay the utility. This curve is the product of an aggregated refueling load produced by supplying electricity to numerous PEVs. The actual cost incurred by each individual PEV can be allocated using the method described in Section 3.5.1.1. The results of this analysis can be separated into the two categories of PEVs that do and those that do not receive demand charge allocations. PEVs that receive no demand charge allocation are PEVs that, when aggregated with all other refueled PEVs, do not produce an EVSE demand greater than 20 kW for any 15 minute period, or the electrical demand required to shift the EVSE from the utility rate TOU-EV-3 to TOU-EV-4. Figure 7-5 shows the percent of all refueled PEVs that received no demand charge allocation. PEVs that receive a demand charge allocation either directly produced or were aggregated with other vehicles to produce a maximum 15 minute average demand greater than 20 kW. Figure 7-6 shows the distribution of allocated demand charge costs for all simulations performed across various amounts of PEVs charged per month. This figure displays the percent of PEVs that receive an allocation that results in a specific

$/kWh cost for all simulations. The distribution shows the percent of vehicles that incur a specific demand charge cost for all simulations performed at each level of PEV trips per month.

Figure 7-5 shows that, under conventional parking, the majority of PEVs do not contribute to an EVSE demand greater than 20 kW and are not allocated any demand charge cost. If valet parking is implemented, the percent of vehicles contributing to a demand greater than 20 kW increases with PEV use, reducing the number of vehicles receiving no allocation. Figure 7-6 shows that the demand charge allocation can vary greatly depending upon the number of PEVs charged per month. At a low number of PEVs charged per month, allocations can vary drastically. As the number of PEVs refueled per month increases, this variability in allocation starts to disappear as the demand charge is allocated across a greater number of PEVs. This variability can be reduced even further if valet operations occur since more vehicles can be refueled through this method than through conventional parking. Although costs are lowest and cost allocation spread is the tightest at high PEV use, the EVSE is unable to meet the full demand as some PEVs remain uncharged regardless of operation type. As seen in Figure 7-2, at the highest levels of PEV use examined, 20% of PEVs receive no charging. Figure 7-6 also shows that, at low PEV use, some PEVs may deserve to pay a price of up to $20 per kWh for the demand charge incurred during recharging, and, on average, a PEV receiving a cost allocation averages approximately $4 per kWh. At the highest levels of PEV use tested, the cost allocation range shrinks to between no allocation and $0.50 per kWh for conventional parking and no allocation to $0.10 per kWh for valet parking.

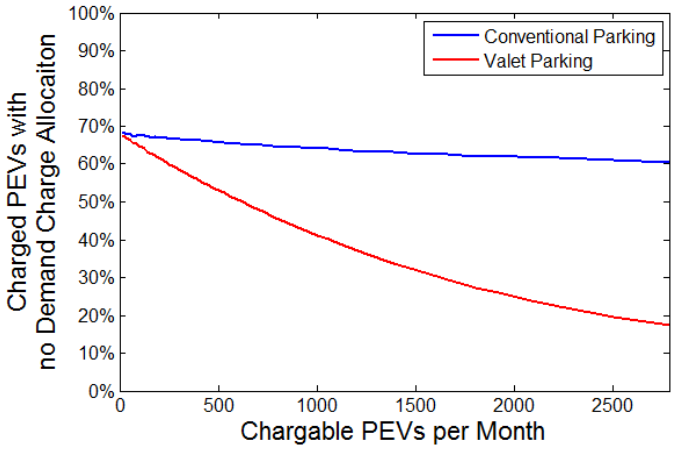

Figure 7-5: Percent of PEVs that are refueled but do not receive a demand charge allocation for shopping type travel during the winter

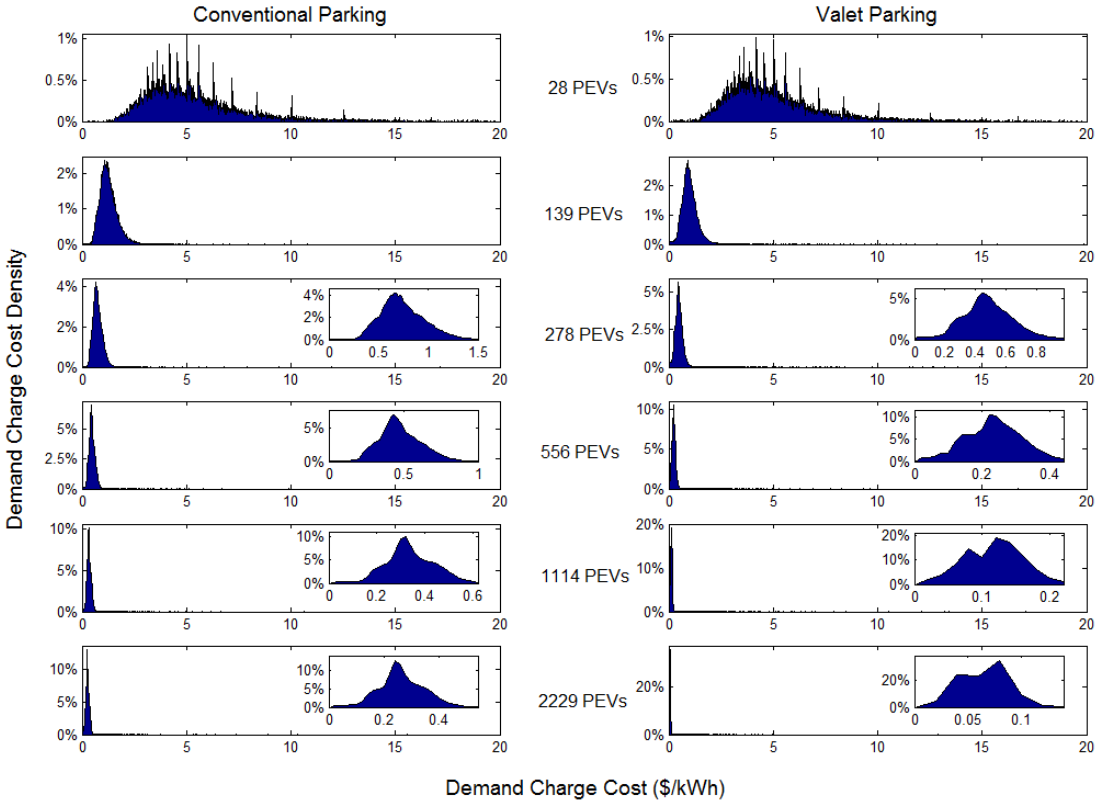

Figure 7-6: Distributions of demand charge cost allocations to individual PEVs used for shopping type travel during the winter

7.1.1.2 Work Travel

Assuming that PEVs start the day with a fully charged battery, approximately 37% of all work related travel results in a PEV with less than 80% state of charge. In addition to an increase in the number of PEVs that are eligible for Level 3 refueling, the long dwell time associated with work travel can have a significant impact on the resulting demand supplied to the EVSE. Figure 7-7 shows example load profiles for Level 3 EVSE under conventional and valet operations for various levels of PEV use and the corresponding refueling cost. The 37 and 3,711 PEVs per month correspond to approximately 100 and 10,000 total work trips per month made by Level 3 compatible PEVs. Figure 7-8 shows the percent of Level 3 eligible vehicles that are completely refueled or not fueled at all. Simulations using work type travel resulted in PEVs being either completely refueled or not fueled with virtually no PEVs receiving partial refueling.

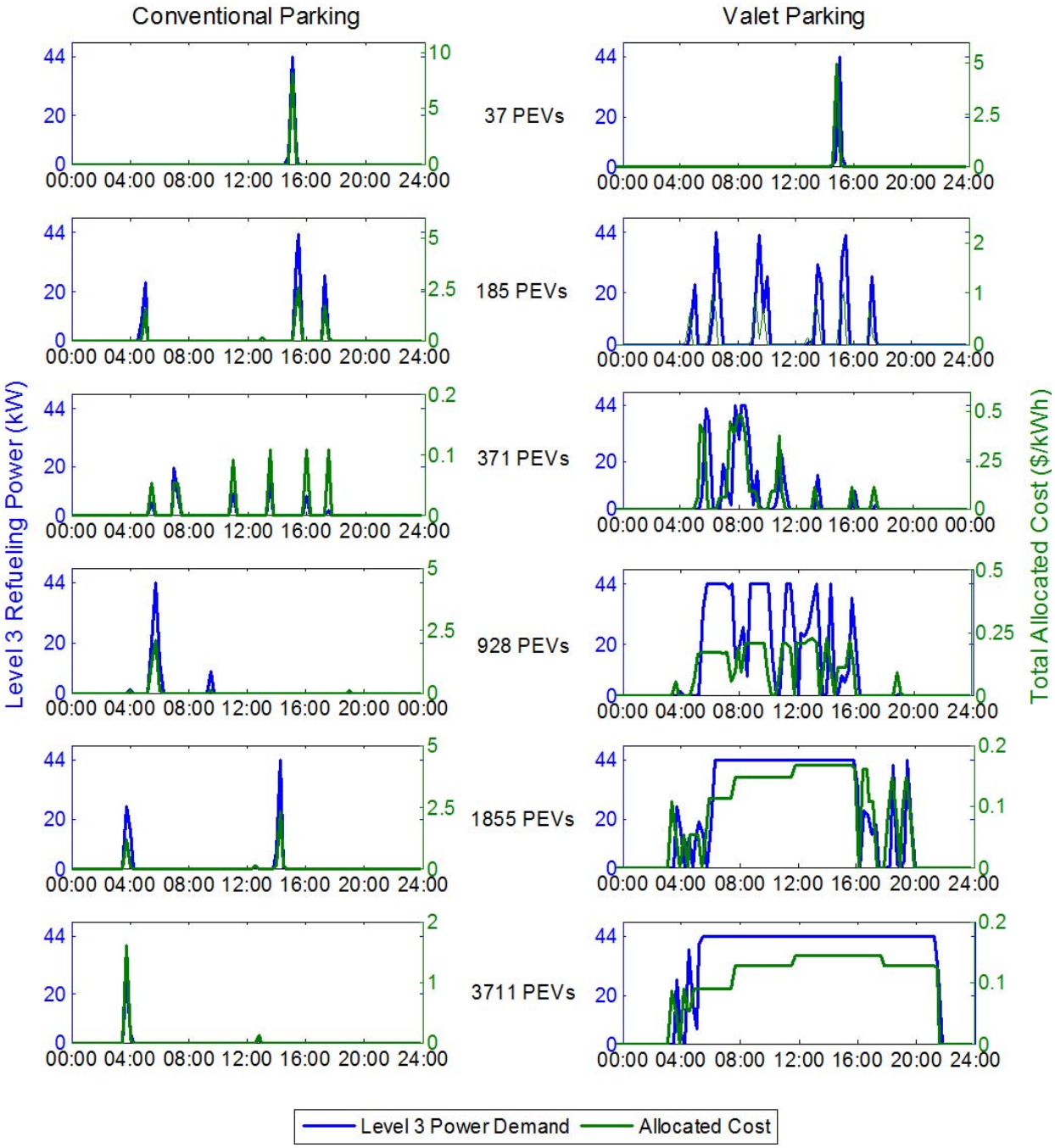

Figure 7-7: Example load profiles and resulting cost allocations for 37, 185, 371, 928, 1,855, and 3,711 work trips per month using PEVs

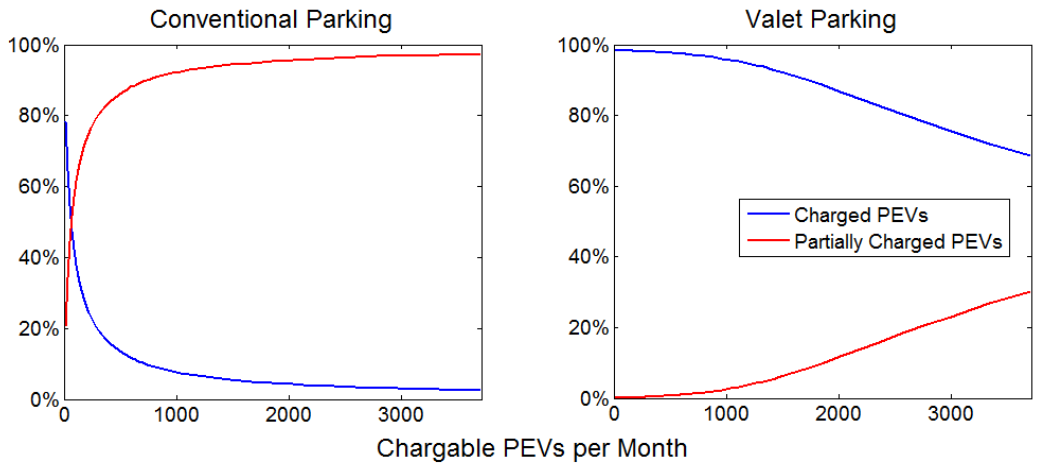

Figure 7-8: Percent of cars that are fully charged, or uncharged by the 44 kW Level 3 charger after a work trip type for conventional and valet parking scenarios

It is clear from Figure 7-7 that there is little difference between the demand produced by a small number of PEVs versus a large number for conventional operations. This is due to a long dwell time associated with work travel, resulting in PEVs occupying the EVSE long after refueling is complete. This also results in only a small fraction of Level 3 eligible PEVs having access to the EVSE. Compared with shopping type travel, a much smaller percent of PEVs used for work travel that are refueled even at a low number of total PEVs visiting the station, which results in and refueling costs that are high regardless of the number of eligible PEVs.

In contrast to conventional operations, valet operations benefit from the long dwell time. Even though the number of eligible PEVs is increased for work type travel, the extended dwell time ensures that a single 44 kW EVSE can refuel the majority of PEVs. As a result, total cost is reduced from approximately $10 per kWh at low number of PEVs to below $0.15 per kWh at a high number of PEVs if valet operations are implemented. However, as PEV use increases, so does the percent of unfueled PEVs.

Figure 7-9 shows the average energy charge cost versus number of chargeable PEVs per month. During summer and winter, a drop in average energy cost can be seen for conventional parking and low levels of PEV use. This is due to a switch in electric rate structure from TOU-EV-3 to TOU-EV-4. Referring to Table 3-1, energy charges are higher for TOU-EV-3 than TOU-EV-4. At low levels of PEV use, it is possible that the few eligible PEVs do not create an electrical demand of greater than 20 kW. In addition, the long dwell time associated with work travel coupled with low PEV use can result in a maximum monthly demand lower than 20 kW and the selection of TOU-EV-3 as the utility rate. If valet parking is implemented or PEV use increases beyond 100 total PEVs per month, EVSE demand surpasses 20 kW and TOU-EV-4 is selected as the utility rate.

With conventional parking, the early arrival and long dwell time associated with work type travel results in early arriving PEVs being refueled using off-peak electricity, but occupying the station through mid-peak and on-peak, resulting in the EVSE only using low cost utility energy. Conversely, the long dwell time results in a higher cost of energy for valet parking due to an increased use in mid-peak and on-peak electricity. While PEVs may arrive early in the morning, increasing the number of vehicles that are queued increases the amount of electricity purchased during mid-peak and on-peak, resulting in a higher overall cost of electrical energy. Between 2,500 and 3,000 PEVs refueled per month, the EVSE is constantly utilized during on-peak. If additional PEVs arrive, refueling occurs during the later mid-peak, reducing the average energy cost at high levels of PEV use. This behavior can also be seen in Figure 7-7 at 3,711 PEV trips per month, where the additional PEV traffic results in increased PEV refueling after the on-peak period.

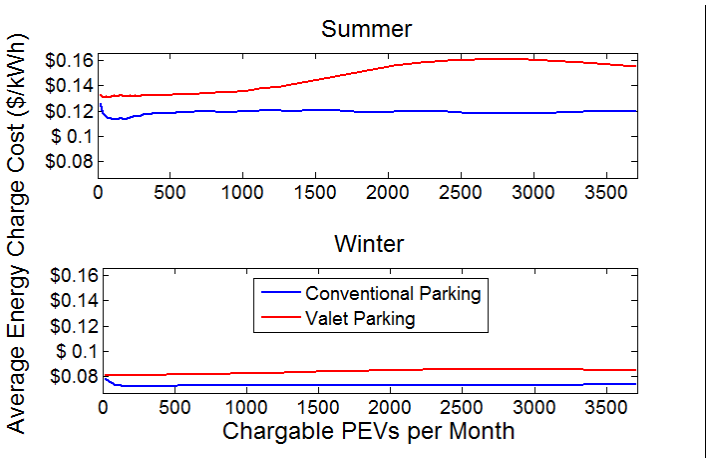

Figure 7-9: Average energy charge cost versus number of chargeable PEVs per month for work trips in the summer and winter

Similar to shopping type trips, there is negligible difference between summer and winter demand charge costs as a result of similar seasonal travel patterns and no difference in demand charge rates from summer to winter (for the rate structures considered). Figure 7-10 shows the average demand charge costs incurred for using Level 3 EVSE to refuel PEVs. Similar to shopping type travel, a low number of PEV trips per month results in a large demand charge cost. For conventional parking, demand charge cost remains high regardless of the number of PEVs available to be charged due to the long dwell time associated with work type travel. However, for valet parking, demand charge costs are reduced to being on the same order of magnitude as energy charge costs once a moderate number of PEV trips to the Level 3 EVSE occur (around 650 Level 3 eligible PEVs per month).

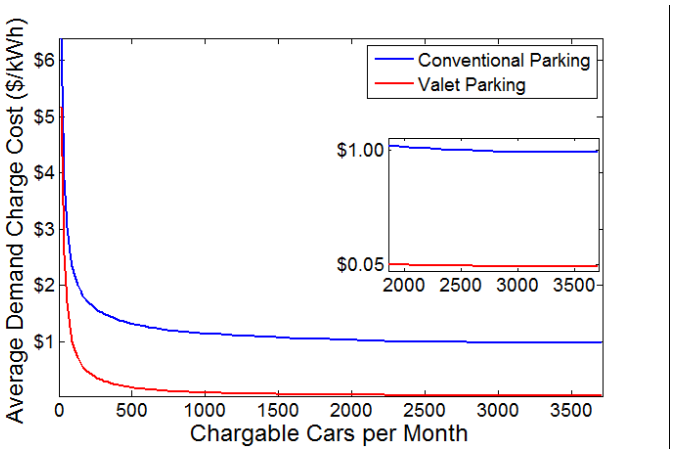

Figure 7-10: Average demand charge cost versus number of chargeable PEVs per month for work trips occurring during the winter

Using the method described in Section 3.5.1.1, the cost to fuel individual PEVs can be determined. Figure 7-11 shows the percent of PEVs that would receive no demand charge cost allocation. Figure 7-12 shows the resulting demand charge cost for PEVs that do receive an allocation. The density plot in Figure 7-12 represents the total percentage of cars that receive a demand charge allocation that results in the specified $/kWh cost. Similar to shopping type travel, the electrical demand incurred by most PEVs is not large enough to produce a demand charge allocation, as seen from the conventional parking results in Figure 7-11. With conventional parking, increasing the number of PEVs that can be charged using Level 3 EVSE has almost no impact on reducing demand charge cost once a small number of PEVs are available to be charged each month. As a result, only a small number of PEVs are responsible for incurring a demand charge, resulting in both a high cost to refuel those particular PEVs, but a large distribution of incurred costs. Under valet parking, the increase in eligible PEVs can be accommodated using the single EVSE, increasing the aggregated load while also increasing the number of vehicles that receive a demand charge allocation. More PEVs share the demand

charge, thus reducing the average cost of operation and the cost allocated to each PEV. Similar to the cost allocation for shopping travel, incurred demand charges are expensive at low PEV use, sometimes reaching up to $20 per kWh delivered to the PEV. As PEV use increases, the range of demand charge allocation shrinks for valet operations to between no allocation and $0.07 per kWh. Costs also decrease under conventional operations, but typically range between no allocation and $2 per kWh, with some vehicles incurring ng upwards of $5 per kWh to recharge.

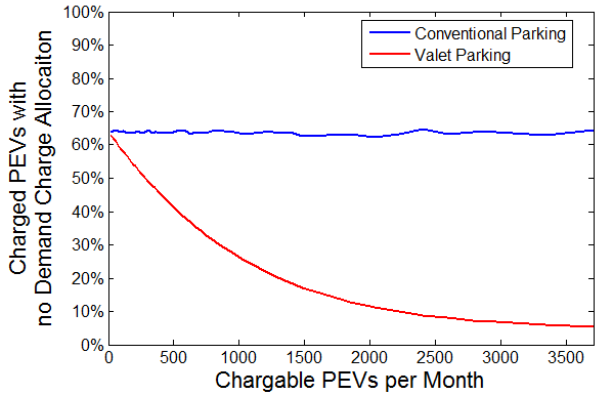

Figure 7-11: Percent of PEVs that are refueled but do not receive a demand charge allocation for work type travel during the winter

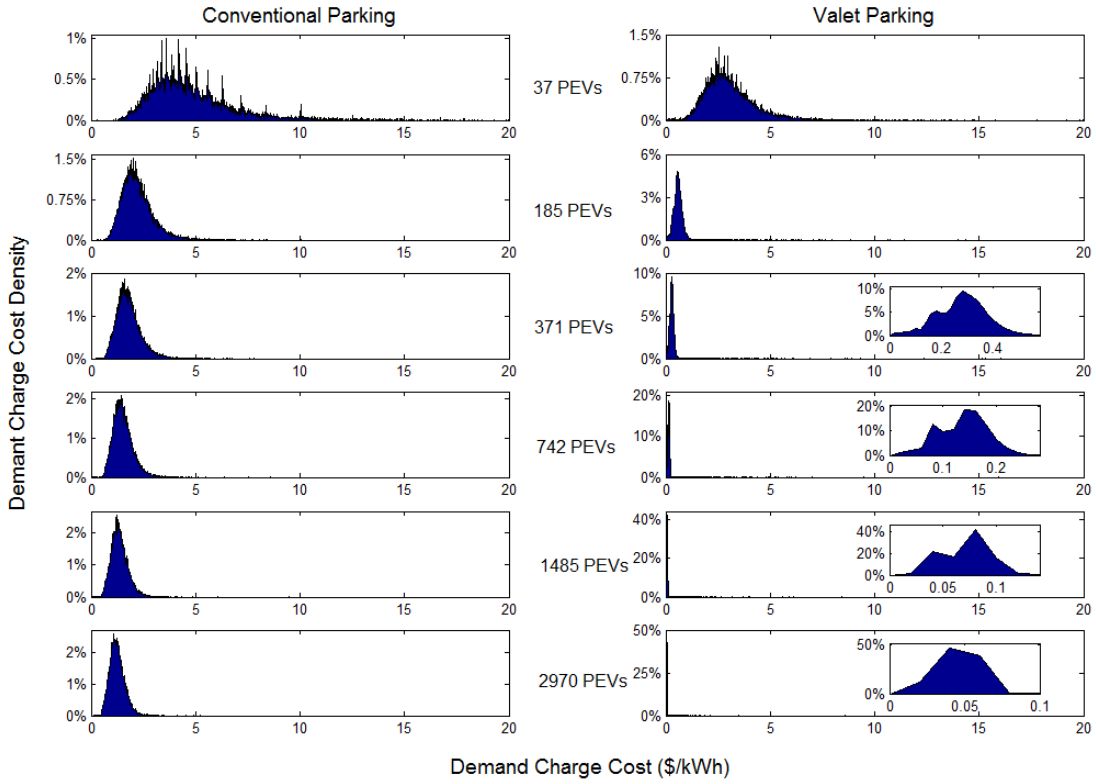

Figure 7-12: Distribution of demand charge cost allocations to individual PEVs used for work type travel during the winter

7.1.2 Increased Charger Power and EVSE Number

The 44 kW Level 3 charger considered in Sections 7.1.1.1 and 7.1.1.2 is the baseline for all other Level 3 charging analyses in this work. All scenarios presented can be expanded by increasing the number of EVSE supplied by a single utility meter and/or by selected Level 3 EVSE with higher power output. Both options are explored in this section. EVSE with a power output of 120 kW will be considered, and the number of EVSE per utility meter is increased from one to two, four, and eight for both 44 kW and 120 kW Level 3 EVSE.

Under valet operations, the increase in number of chargers and the increase of charger power output increases the number of PEVs that can be charged for both shopping and work trip

types. Figure 7-2 and Figure 7-8 show that, for the range of PEV use tested, a single 44 kW Level 3 charger is capable of refueling the majority of PEVs that are eligible for Level 3 refueling. However, at high levels of PEV use, either additional Level 3 EVSE must be installed or refueling power must be increased to satisfy the demand of all vehicles. Figure 7-13 and Figure 7-14 show the amount of PEVs that are fully refueled, partially refueled, or not refueled for shopping and work respectively when increasing refueling power and number of available EVSE. Both figures show that increasing the refueling power increases the number of vehicles that have access to the EVSE, nearly reducing the percent of unfueled PEVs to zero for all levels of PEV use tested. Increasing the number of EVSE has the same effect for 44 kW EVSE. At high levels of PEV use, either multiple 44 kW EVSE or higher power EVSE must be adopted if all eligible PEVs are to have access to being refuel.

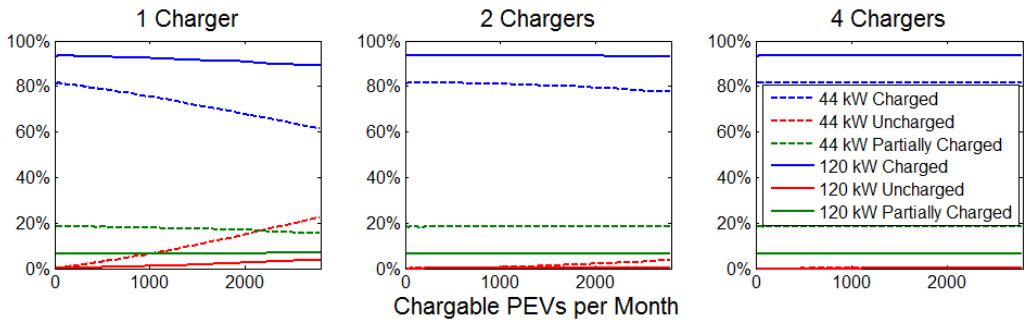

Figure 7-13: Percent of vehicles that are fully charged, partially charged, or uncharged during shopping trips to locations with one, two, and four Level 3 chargers with a power output of 44 kW or 120 kW under valet operations.

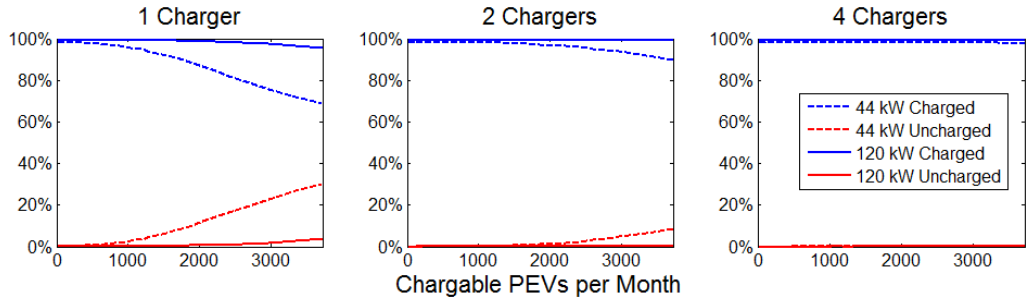

Figure 7-14: Percent of vehicles that are fully charged, partially charged, or uncharged during work trips to locations with one, two, and four Level 3 chargers with a power output of 44 kW or 120 kW under valet operations.

Figure 7-2 and Figure 7-8 also show that more than a single 44 kW EVSE is required to refuel the majority of PEVs if conventional parking occurs and PEV use is moderate. The impacts of increased EVSE power and number of available EVSE on the percent of PEVs refueled, partially refueled, or unfueled for conventionally operated EVSE servicing PEVs used for shopping travel are presented in Figure 7-15. This figure shows that increasing the number of EVSE reduces the percentage of Level 3 eligible PEVs that are unfueled. At the highest level of PEV use tested, installing two chargers reduces the percentage of unfueled PEVs from 80% to 65%, while installing four chargers reduces unfueled vehicles to 40%, and installing eight chargers reduces unfueled vehicles to 11%. At moderate levels of PEV use, additional EVSE must be installed if all eligible PEVs are to have access to being refueled. Increasing EVSE power only increases the rate at which PEVs are refueled, ensuring that more PEVs are fully refueled, not partially refueled. The number of PEVs unfueled does not decrease when EVSE power is increased.

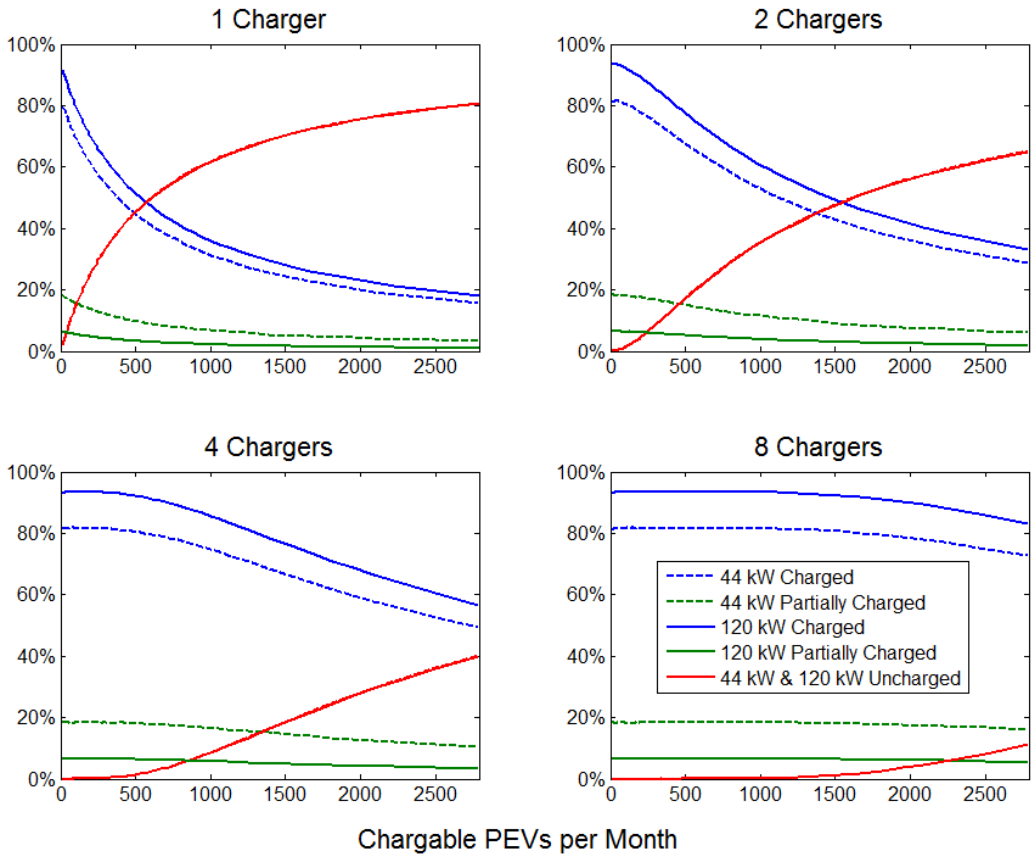

Figure 7-15: Percent of vehicles that are fully charged, partially charged, or uncharged during shopping trips to locations with one, two, four, and eight Level 3 chargers with a power output of 44 kW or 120 kW under conventional operations.

Likewise, increased EVSE power does not reduce the number of uncharged PEVs used for work travel. In addition, as a result of the extended dwell time associated with work travel, the number of PEVs refueled when using 44 kW and 120 kW EVSE is nearly identical across all ranges of PEV use, with any difference due to random variations in travel patterns (results fall on top of each other in Figure 7-16). Figure 7-16 shows the number of PEVs that are either charged or uncharged for the various numbers of EVSE station size tested for 44 kW EVSE. The results presented in Figure 7-16 are nearly identical to results produced using 120 kW EVSE and have

therefore have been omitted for the sake of brevity. Increasing the number of EVSE improves the number of PEVs serviced. However, due to the extended dwell time associated with work travel, the majority of PEVs do not have access to EVSE once a moderate amount of PEV traffic is present, and even eight EVSE is insufficient to refuel the majority of PEVs. These results suggest that increasing refueling rate is not necessary or useful for work travel.

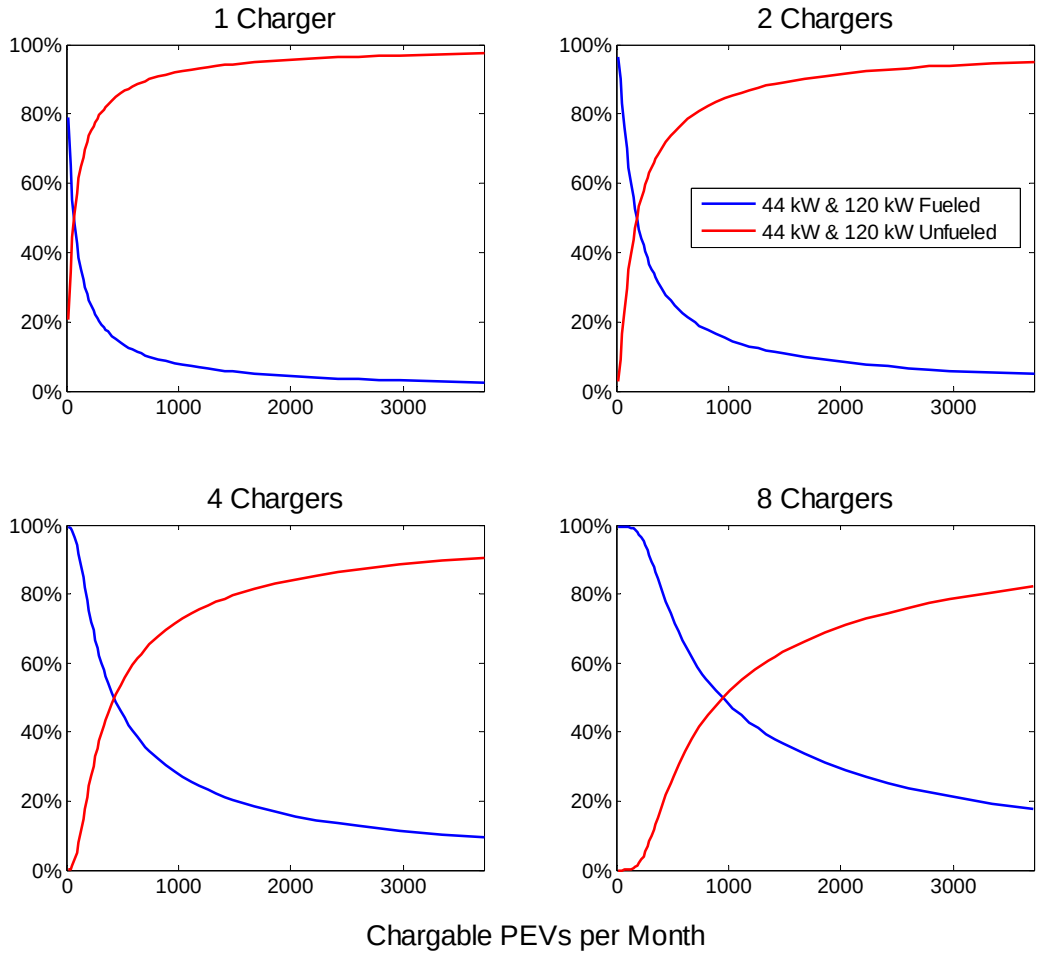

Figure 7-16: Percent of vehicles that are fully charged, partially charged, or uncharged during work trips to locations with one, two, four, and eight Level 3 chargers with a power output of 44 kW or 120 kW under conventional operations.

While increasing EVSE power has little to no effect on increasing the number of PEVs refueled over the range of PEV use tested, the demand charge cost increases. Figure 7-17 shows the change in demand charge due to increasing EVSE power output for both shopping and work travel. For all scenarios considered, increasing the refueling rate from 44 kW to 120 kW increases cost without providing either additional fast charging access or extent of recharge gains.

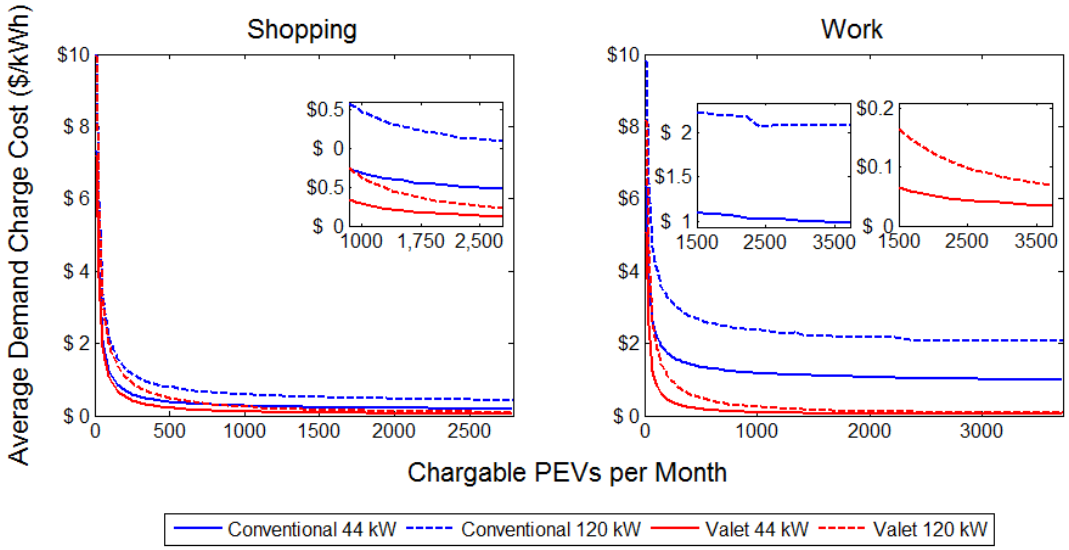

Figure 7-17: Average demand charge cost for 44 kW and 120 kW Level 3 EVSE used to service shopping and work type trips.

The impacts of increasing the number of EVSE supplied through a single electrical utility meter is not as clear as simply increasing EVSE power. Figure 7-18 and Figure 7-19 show the demand charge cost incurred by use of multiple EVSE behind a single utility meter to refuel PEVs for both shopping and work travel. As seen in both figures, if a charging station uses conventional parking, the impact ranges between a slight decrease in cost to negligible cost impact. Increasing the number of EVSE serviced by a single meter may potentially result in the

simultaneous refueling of multiple PEVs, leading to an increased demand charge. However, conventional operation results in EVSE being occupied by PEVs that are fully charged. As a result, the maximum power demand achieved by a single charger is typically not surpassed despite the presence of multiple EVSE. The demand charge is maintained at a low level relative to the maximum possible demand created by all EVSE refueling a group of PEVs. The number of PEVs refueled increases while not substantially increasing the maximum demand, and no change to the average demand charge cost.

Conversely, demand charge costs increase as the number of EVSE is increased under valet operations. Due to the instant availability of EVSE after refueling any individual PEV, the demand supplied through the electric meter can be maintained if another PEV either arrives or has been queued for refueling. As PEV use increases, arrival and dwell times of the individual PEVs start to coincide with the arrival and dwell time of other PEVs, resulting in sustained refueling. Without any additional management of when PEVs are refueled, the maximum utility demand is easily increased along with the average demand charge cost. Both shopping and work travel results shows that as more Level 3 eligible PEV vehicles arrive at a refueling station with multiple EVSE and valet operations, demand charge cost increases for the EVSE operator, and ultimately, for the individual PEV drivers.

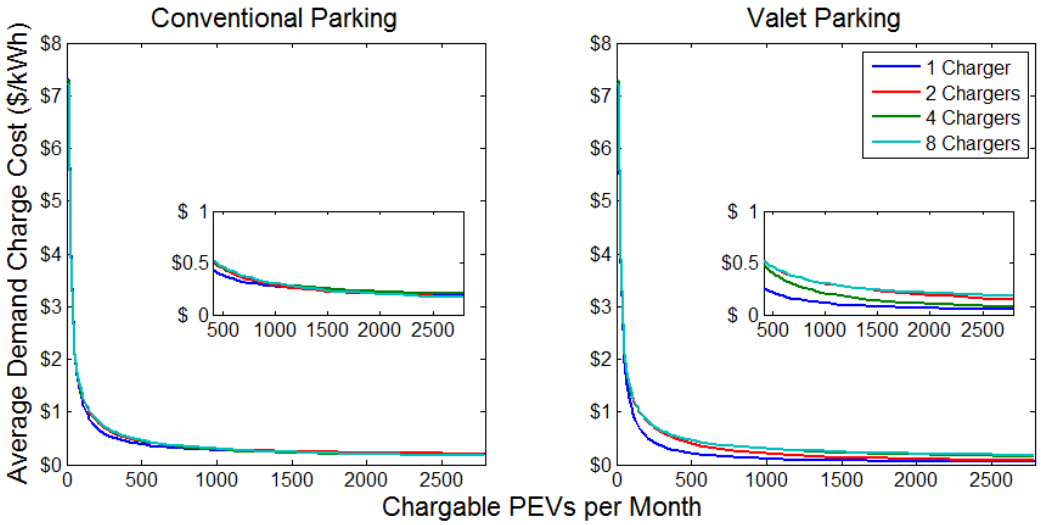

Figure 7-18: Average demand charge cost for multiple 44 kW EVSE to refuel PEVs used for shopping travel

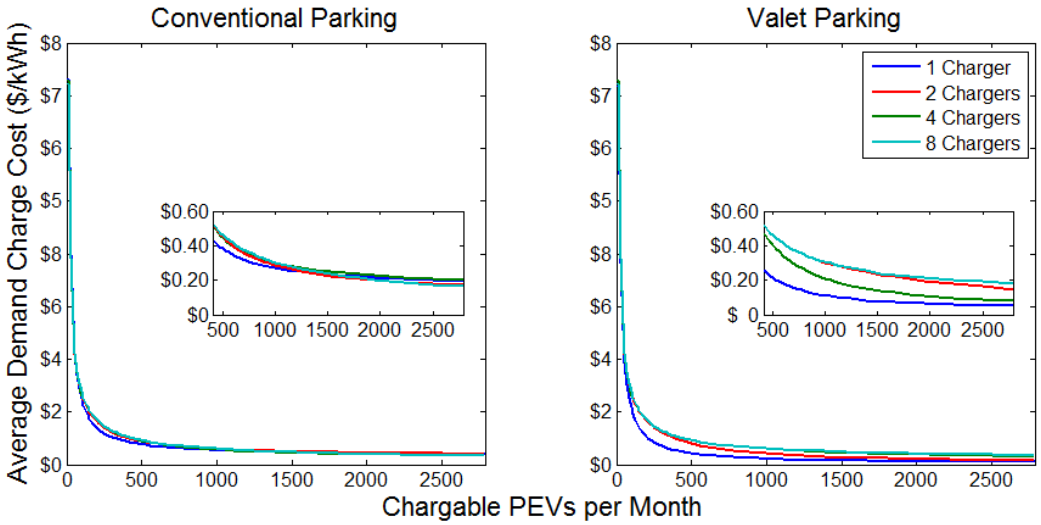

Figure 7-19: Average demand charge cost for multiple 44 kW EVSE to refuel PEVs used for work travel

Installing multiple 120 kW EVSE results in similar trends as seen in Figure 7-18 and Figure 7-19 for 44 kW EVSE and have therefore have been omitted for the sake of brevity. However, due to the increased power, the results are shifted up on the average demand charge

cost versus PEVs plot for all scenarios due to the higher demand charge incurred by using the higher power 120 kW EVSE.

Energy costs experience little to no change as a result of increasing either EVSE power or multiple EVSE because energy cost is determined by PEV time of refueling, not the maximum demand supplied during the refueling process.

7.1.3 Sensitivity of Utility Costs

The results presented in Section 7.1.1 and 7.1.2 are the averaged results of numerous simulations using the applicable model described in Section 0. Each individual simulation stochastically produces different energy and demand charge costs that are averaged to produce the results presented in Section 7.1.1 and 7.1.2. This section presents the variation of individual simulations versus the average results.

Figure 7-20 and

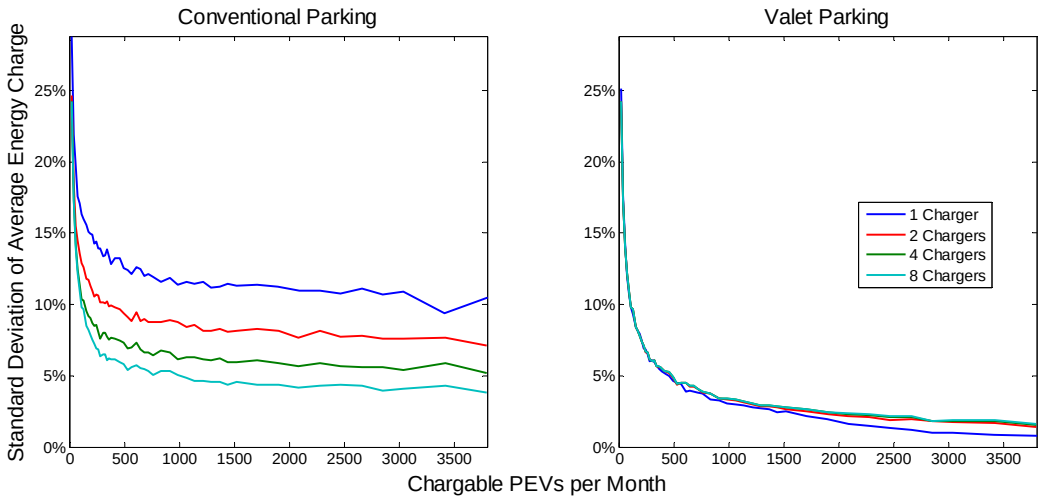

Figure 7-21 show the standard deviation of average energy charge during the summer versus number of chargeable PEVs per month for shopping and work travel respectively for one,

two, four, and eight 44 kW EVSE. For both shopping and work travel, the standard deviation decreases as PEV traffic increases. A high deviation is due to the arrival of PEVs at different utility peak periods during the day. With little PEV traffic, arrivals at unexpected times produce results that vary significantly from the average. As PEV traffic increases, and arrival time at expected hours becomes more common and then begins to dominate travel behavior, the effect of a PEV arriving at an unexpected hour is reduced and variation across simulations decreases except for work with conventional parking. Under this scenario, a PEV that arrives at an unexpected time may have a long dwell time. When this occurs during a peak period when PEV refueling does not typically occur, the simulation cost differs from the average energy cost. However, as more EVSE are installed, expected arrival behavior begins to dominate all of the simulations, reducing variation between simulations.

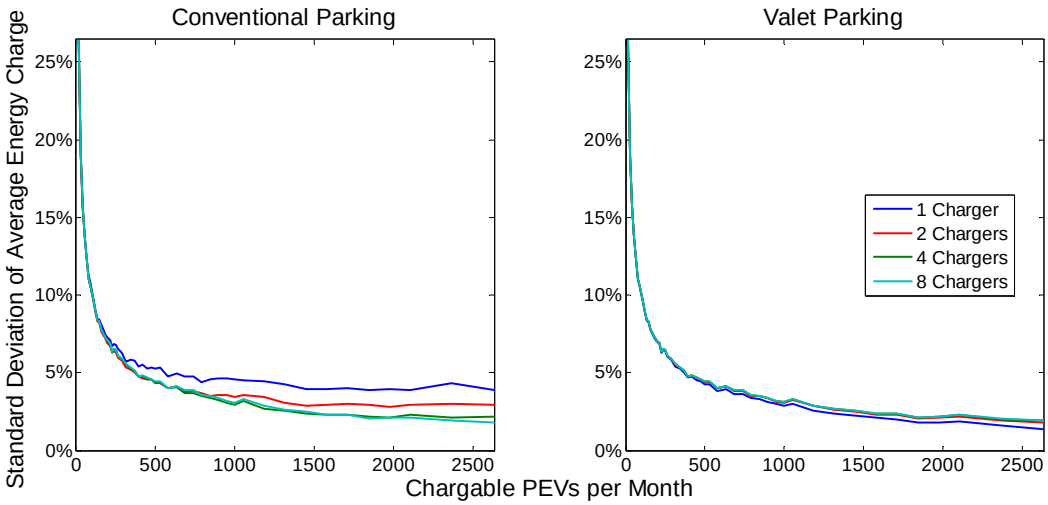

Figure 7-20: Standard deviation of average energy charge cost for shopping travel during the summer for one, two, four, and eight 44 kW EVSE

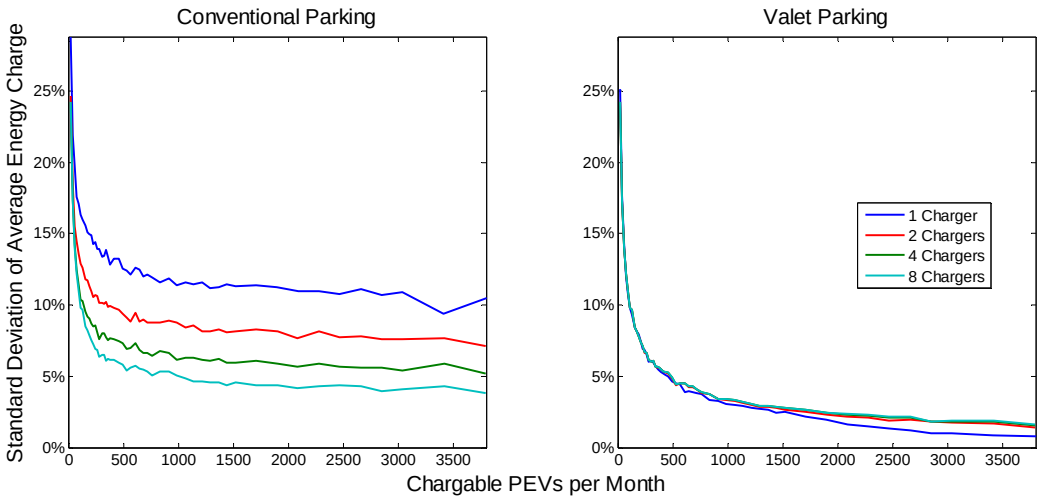

Figure 7-21: Standard deviation of average energy charge cost for work travel during the summer for one, two, four, and eight 44 kW EVSE

Winter results are similar to summer results, only shifted down due the elimination of the on-peak period, reducing the number of peak periods to two (summer has three). As a result, the cost difference between a PEV arriving during an expected peak period versus an unexpected peak period is reduced. Increasing EVSE power does not affect variations in the simulation results.

Figure 7-22 and Figure 7-23 show the standard deviation of average demand charge during the summer versus number of chargeable PEVs per month for shopping and work travel respectively for one, two, four, and eight 44 kW EVSE. Similar to the energy charge statistics, the standard deviation decreases as PEV traffic increases.

When considering a single EVSE and low levels of PEV traffic, the 20 kW threshold may not be exceeded during some simulations. This creates a large variation when compared to simulations that do surpass the 20 kW threshold. As PEV traffic increases and a demand charge occurs consistently, the standard deviation decreases, and any variation in demand charge is due

to differences in the total number of kWh delivered to the PEVs (which changes depending upon the randomly selected PEV trips).

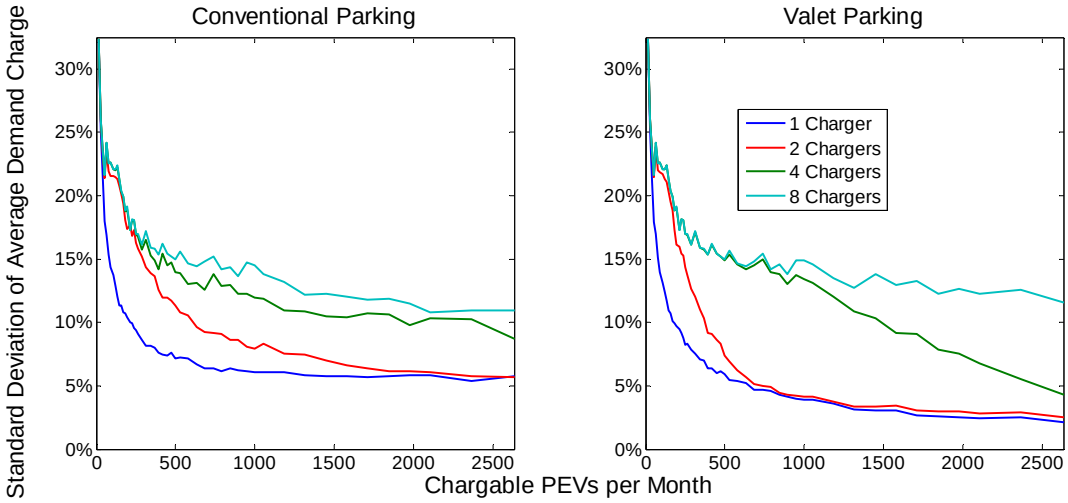

Figure 7-22: Standard deviation of average demand charge cost for shopping travel during the summer for one, two, four, and eight 44 kW EVSE

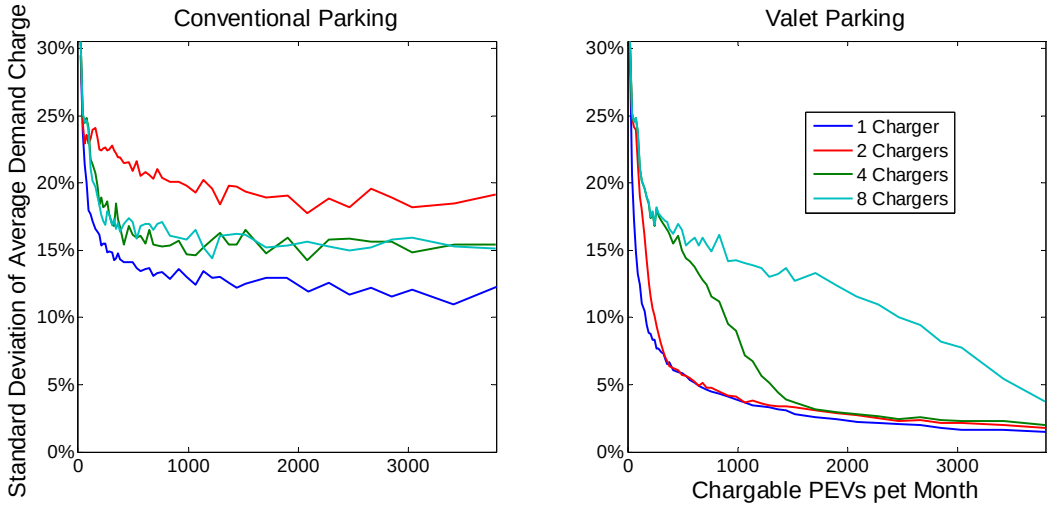

Figure 7-23: Standard deviation of average demand charge cost for work travel during the summer for one, two, four, and eight 44 kW EVSE

For all scenarios except work with conventional parking, increasing EVSE increases the number of PEVs required to consistently reach the new maximum demand charge, increasing

variation in demand charge cost between simulations. Once the demand charge is increased consistently across the simulations, variations are caused by differences in the total energy delivered to the PEVs.

Due to the typically long dwell time associated with work travel, a single EVSE operated under conventional parking can be occupied indefinitely by a PEV that does not incur a demand charge. With low PEV traffic levels, it is possible to have an entire simulation with no demand charge, increasing variation in the average demand charge across all simulations.

Increasing EVSE in this situation to two further increases variation in the simulation results, as shown in Figure 7-23, because multiple EVSE must arrive at approximately the same time to use available EVSE and refuel at the maximum power during the entire time window over which the demand charge is determined. When this occurs for some simulations, but not others, the standard deviation increases. However, increasing EVSE beyond two allows for a higher demand charge to be produced more consistently across the different simulations, reducing variation in simulation results. This increased demand charge can still vary between simulations, resulting in a permanently high standard deviation across all levels of PEV traffic.

7.1.4 Discussion

It is clear from the results that Level 3 EVSE can be prohibitively expensive with little PEV use. Average utility rates for these scenarios range from $0.08 to $7.90/kWh. For all scenarios tested, between 100 and 150 trips per month must be made by PEVs that are compatible with Level 3 EVSE and have a battery state of charge below 80% to reduce average demand charge costs below $1.00 per kWh. In some instances, such as for conventionally operated EVSE refueling PEVs used for work travel, average demand charge cost cannot be

reduced below $1.00 per kWh. If the EVSE is operated using valet parking, approximately 550 refueling events during the winter (or 1500 total PEV trips), and 800 charging events during the summer (or 2000 total PEV trips) must take place in order to reduce the average total utility cost below $0.25 per kWh. For shopping travel and valet operations, 670 refueling events per month during the winter (or 2400 total PEV trips), and 1400 refueling events per month during the summer (or 5000 total PEV trips) are required in order to reduce total average utility cost below $0.25 per kWh. Under conventional operations at shopping centers, costs never fall below $0.27 per kWh during the winter and $0.33 per kWh during the summer. If a goal of installing the Level 3 EVSE is to provide an economically competitive transportation fueling option, Level 3 compatible PEV use must significantly increase, and in some instances, parking management is required. Only in scenarios when both of these facts were considered (valet parking and high PEV use) did utility rates drop below $0.25 per kWh.

If PEV use does increase, certain types of travel are more conducive to improving EVSE availability and operational costs. The relatively small difference in average demand charge cost between conventional and valet operations for shopping travel suggest that trips resulting in a short dwell time do not need as much parking management as trips that result in a long dwell time, such as work travel. As dwell time increases (e.g., work travel), parking management must be implemented to maintain a driver satisfaction and keep utility costs low. The benefit of a long dwell time is the potential to fully refuel all PEVs that arrive at any particular charging station, regardless of the amount of PEV use. As such, the most attractive scenario is the situation where numerous PEVs arrive with below an 80% state of charge, stay near the EVSE for an extended period of time (e.g., work travel), and a system is enacted that follows the valet parking strategy.

This combination has the potential to reduce total average cost, including demand charge cost, to $0.13 per kWh during the winter and $0.21 per kWh for summer with shopping travel and $0.12 per kWh during the winter and $0.19 per kWh during the summer for work travel.

The results also clearly show that while increasing the number of available EVSE can improve access to refueling, using a "valet" system can significantly increase PEV refueling throughput and reduce cost of electricity while limiting the number of required EVSE. Increasing EVSE power, however, does not improve access while increasing cost of electricity.

When multiple Level 3 EVSE on a single utility meter, additional management beyond the simple "valet" system must be implemented in order to ensure that demand charges are not unnecessarily increased. Much work has been done on the optimal refueling of PEVs [86–89]. Including demand charge costs in PEV refueling optimization would ensure that PEVs are refueled while maintaining as low of a demand charge as possible.

The cost allocation analysis illustrates the challenge of rate design for PEV refueling. At low to moderate levels of PEV use, it is impossible to design a simple rate (fixed fee, time of use, $ per kWh) that fairly chargers drivers to refuel; the demand charge cost incurred by a few is borne by all. This task becomes easier as the number of PEV trips resulting in a battery state of charge below 80% increases. However, if the average trip length to the charger remains short, as with shopping travel, and only a fraction of the refueled PEVs will have incurred a demand charge, fair rate design will remain difficult. A shift towards rates that allocate costs fairly would help to eliminate this problem, which could be assisted by sharing information with incoming PEV drivers allowing them to opt out of charging if such would incur increased demand charges.

But such a system may create another barrier to increasing PEV adoption due to increased public confusion as to how much it costs to charge a PEV using public charging infrastructure.

The results presented in this paper are specific to utilities that have rate structures for PEV charging similar to Southern California Edison. If the EVSE were located within the territory of a different utility that did not apply demand charges to public PEV refueling in favor of increased energy charges, the high costs faced by charging stations when PEV use is low and/or conventional parking is in effect may be eliminated. For example, if the EVSE were located within the service territory of Pacific Gas and Electric, the second largest utility in California, the applicable rate structure would be either the A-1, A-1 TOU, or A-6 TOU rate structure if the maximum demand stayed below 200 kW. None of these three rates include demand charges, and with the exception of summer on-peak under A-6 TOU, feature energy charges that are between $0.14 per kWh and $0.28 per kWh. While the high capital cost associated with Level 3 EVSE may still block an investment decision, the issue of electricity being too expensive may be significantly reduced in this case.

7.2 Integrated Level 3 EVSE Analysis

Since the shopping and work trips are randomly produced using the NHTS data, the applicable models described in Section 0 are run multiple times for a given number of PEV trips per month to produce the averaged results presented in the current section. The total simulation is repeated until the averaged results experience marginal changes due to additional simulations. The number of trips considered in this work range from 50 to 10,000 trips per month. Scenarios with one, two, four, and eight EVSE integrated with a building are considered. The EVSE power levels considered are 44 kW and 120 kW.

The results are separated in this section by trip type and by season. EVSE integration under the winter utility rate will show the effects of PEV fueling at a building with time of use energy and demand charges. Summer results will also show the impact of time of use rates, but will also show the effect of when PEV refueling changes the utility rate that the building receives electrical service under.

The results presented in this work are concerned only with the cost implications to both the PEV drivers and building. The EVSE operation effect on driver accessibility to the EVSE for both conventional and valet operation was studied in [181]. The results in [181]predictably showed that conventional parking refuels a fraction of the vehicles that can be refueled when valet operation occurs. For a full discussion of the differences in EVSE accessibility between conventional and valet operations, as well as analyses of EVSE serviced by a dedicated utility meter (or not integrated with a building), please refer to [181].

Many of the results are in terms of a difference in cost.

- For EVSE operation, the difference in cost is between EVSE integrated with a building and EVSE serviced by a dedicated utility meter.
- For the building, the difference in cost is between the cost of electricity before and after EVSE integration occurs.

7.2.1 Shopping Travel

7.2.1.1 Winter Season and 44 kW EVSE

Results from [181] showed that approximately 28% of all Level 3 compatible PEVs used for shopping trips will arrive with less than an 80% state of charge. The minimum and maximum

number of trips tested per month (50 to 10,000 PEV trips per month) correspond to 14 and 2787 trips that can be serviced using Level 3 EVSE respectively.

EVSE integration into a building potentially provides access to lower cost of electricity, potentially leading to reduced cost of electricity. Figure 7-24 shows the average energy charge allocated to the individual PEVs (based on Shapley values) using one, two, four, and eight 44 kW EVSE during the winter. Since the price of electrical energy only depends on time of purchase, the results for Figure 7-24 are independent of building type or size and the presented results are consistent across all buildings included in this study. For valet parking, the cost of energy is the same regardless of number of vehicles serviced and number of EVSE since a single EVSE is capable of meeting almost any demand under valet parking, and the majority of PEV refueling occurs during the middle of the day, or mid-peak during the winter,. Under conventional parking, the cost of energy increases as more EVSE are installed. Since a single PEV can occupy an EVSE indefinitely and vehicles are more likely to arrive early as PEV traffic increases, a PEV that arrives during off-peak time can refuel before mid-peak prices become applicable and block other PEVs from refueling later, effectively lowering the cost of energy. Increasing the number of EVSE reduces the impact of first to arrive PEVs, allowing for later arriving PEVs to refuel using mid-peak electricity. Also, while the cost of energy is reduced for all PEV traffic levels and operating scenarios, the energy charge reduction is only on the order of $0.001 per kWh.

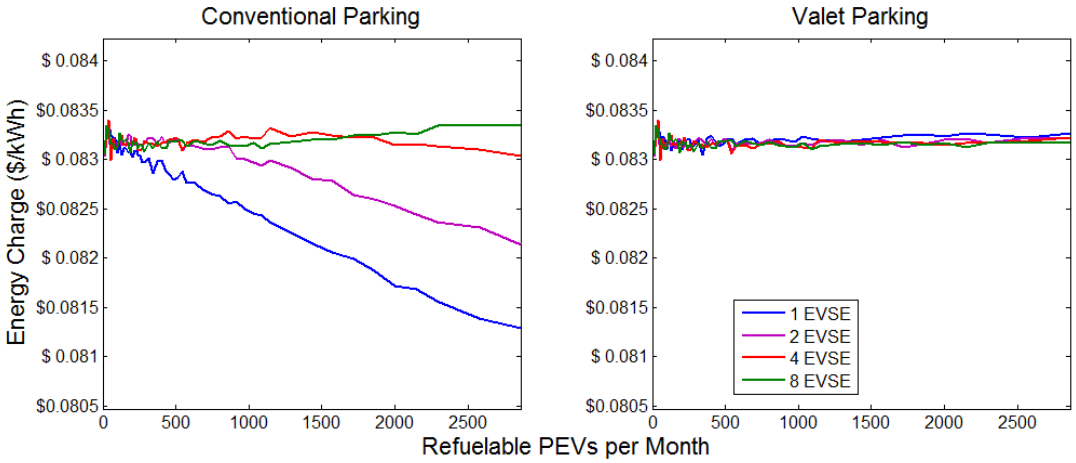

Figure 7-24: Energy charges for refueling PEVs performing shopping travel using one, two, four, and eight 44 kW EVSE for both conventional and valet parking during the winter

EVSE integration with a building provides PEV drivers access to lower energy charges during the winter. This implies that the building is providing a service in the form of creating access to lower cost electricity. Therefore, according to the Shapley value, the building receives some compensation for the benefit provided to PEV drivers in the form of slightly reduced energy costs. Figure 7-25 shows the difference in energy cost for the buildings as a result of integrating one, two, four, and eight 44 kW EVSE during the winter for a 100 kW average demand. The savings provided to the building appears as the inverted amount of energy purchased for EVSE operation, as shown in Figure 7-26. The benefit provided by the building to the PEVs depends only on the amount of energy consumed by the vehicles. An increase in energy delivered produced by either increased PEV traffic or additional EVSE increases the amount of energy that can be sold for refueling PEVs, which increases savings. However, since the savings are tied to the amount of energy sold to PEV drivers, not the building size, the total savings produced by EVSE integration is fixed across all building size. On a savings per energy sold basis, as Figure 7-25 is presented, savings are reduced as building size increase since

savings do not increase while building size does. Keep in mind that while a cost reduction does occur, the maximum benefit shown using multiple EVSE and valet operations results in an energy charge savings of $14.40 total for all building profiles and sizes.

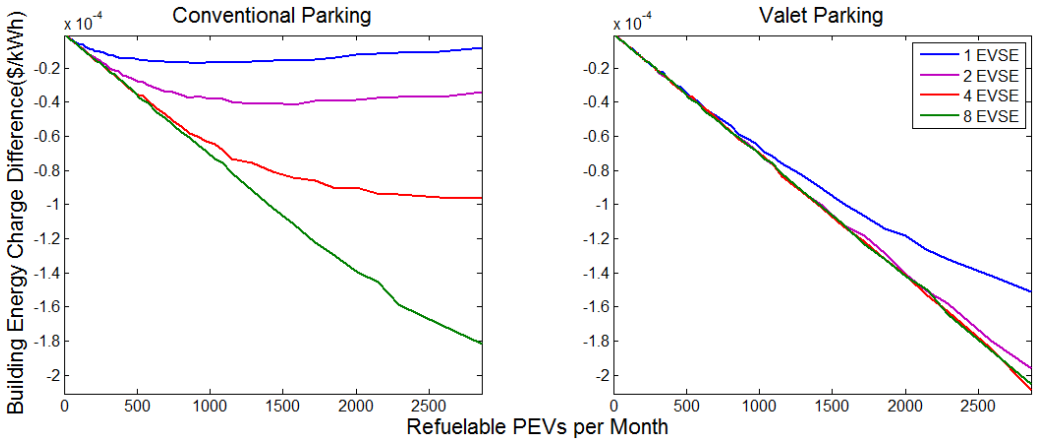

Figure 7-25: Building energy charge difference for a 100 kW average demand as a result of integration one, two, four, and eight 44 kW EVSE using conventional and valet parking operation during the winter

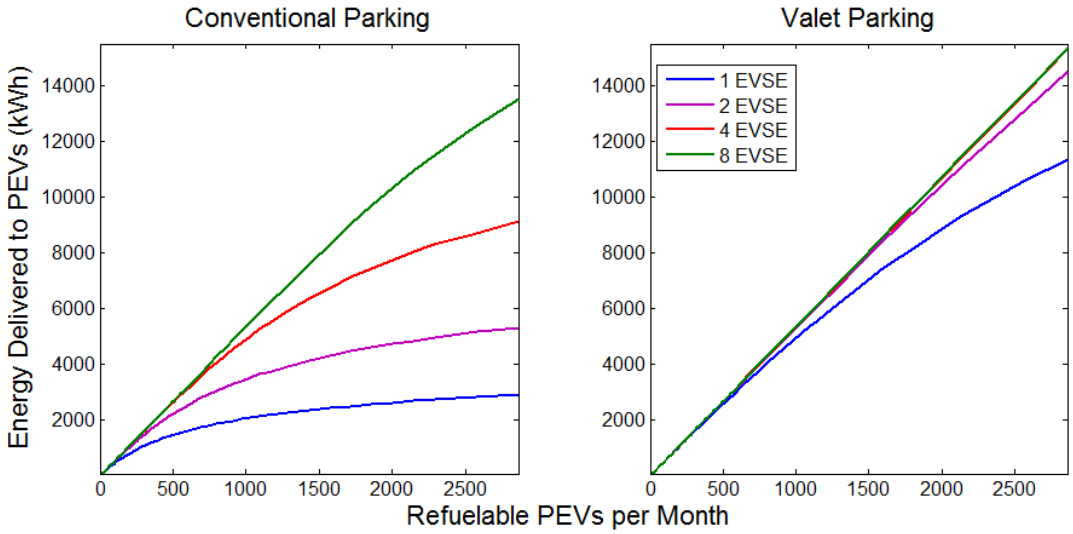

Figure 7-26: Energy delivered to the PEVs during refueling using one, two, four, and eight 44 kW EVSE operated using conventional and valet operations

When EVSE integration occurs, the demand charge cost associated with refueling PEVs according to the Shapley value is a combination of splitting already incurred demand charges between the building and PEVs as well as any increase to the overall demand serviced by the utility. The lowest cost achievable will occur when EVSE integration does not increase maximum utility demand, allowing for the demand charge already incurred by the building to be shared by multiple users. Deviation from this ideal situation is tied to any increases in maximum utility demand. Figure 7-27 shows the increase in maximum demand for all ten winter buildings when a single 44 kW EVSE is integrated. The ten buildings are characterized by the corresponding load factor. For both conventional and valet parking, buildings with the highest load factor consistently experience the largest increase to maximum demand. However, a decrease in load factor does not guarantee a small increase to maximum demand, as seen by the 0.66 load factor building having a smaller demand increase than the 0.29 load factor building.

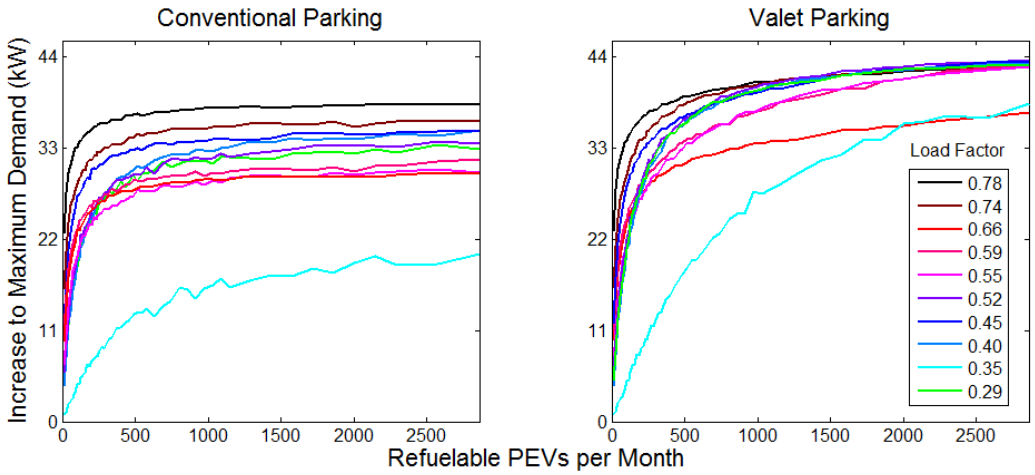

Figure 7-27: Increase to the 15 minute average maximum building demand for conventional and valet parking during the winter for a single 44 kW EVSE

Interestingly, the 0.35 load factor building experiences the smallest increase to maximum demand. Referring to Figure 4-14, the maximum demand for the 0.35 load factor building is

established during three instances late in the month. Each of these three instances result in the maximum or near maximum demand being achieved and maintained for a short duration of time. The other low load factor buildings (particularly the 0.40 and 0.29 load factor buildings) have a maximum demand established multiple times through the month and maintained for extended periods of time when shopping demand occurs most frequently. As a result, the 0.35 load factor building is less likely than the other low load factor buildings to have a PEV arrive and start refueling at the same time as when the building demand is highest. So while a high load factor typically translates to an increase in maximum utility demand on the order of the installed EVSE size, the best way to avoid an increase to maximum demand is to ensure that PEV refueling does not coincide with the maximum building demand.

Figure 7-28 and Figure 7-29 show the demand charge cost for all ten buildings normalized to a 100 kW average demand and the cost difference between EVSE integrated with a building and EVSE not integrated with a building (or standalone EVSE) for a single 44 kW EVSE. The demand charge costs used for the standalone EVSE were taken from [181]. For both Figure 7-28 and Figure 7-29, demand charges are high when PEV traffic is low, and decrease as PEV traffic increases. Comparing Figure 7-28 and Figure 7-29 to Figure 7-27 also shows that the buildings with the lowest PEV demand charge cost experience the smallest increase to maximum demand. For conventional parking, integrating a single 44 kW EVSE with a building almost always reduces overall cost to refuel a PEV. The building with the highest load factor provides almost no cost benefit for reducing demand charges unless there is little PEV traffic. The same is true under valet operations. For all scenarios, the greatest cost reductions occur when PEV

refueling does not coincide with the maximum building demand, reducing any increase to the maximum demand provided by the utility.

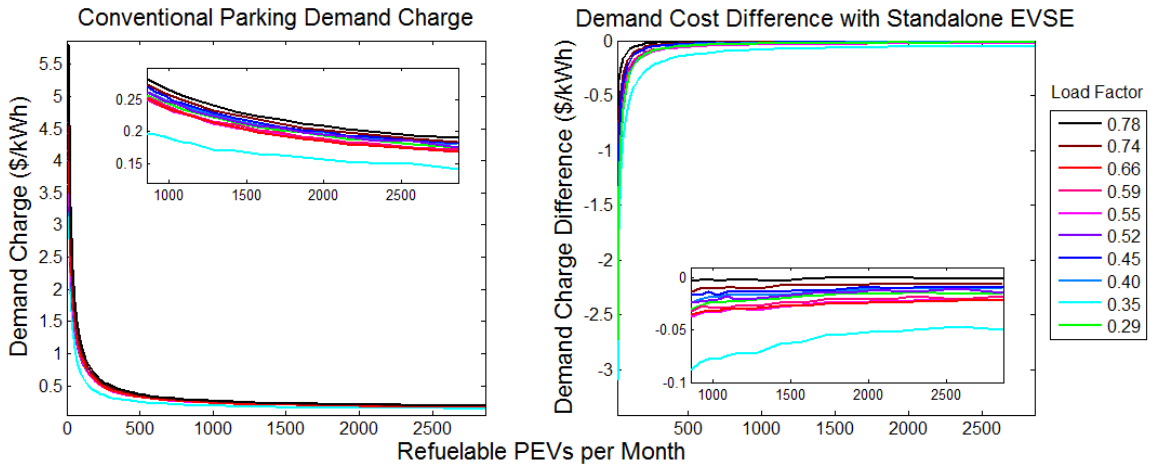

Figure 7-28: Winter demand charge cost and difference with a non-integrated EVSE system for a single 44 kW EVSE operated under conventional parking

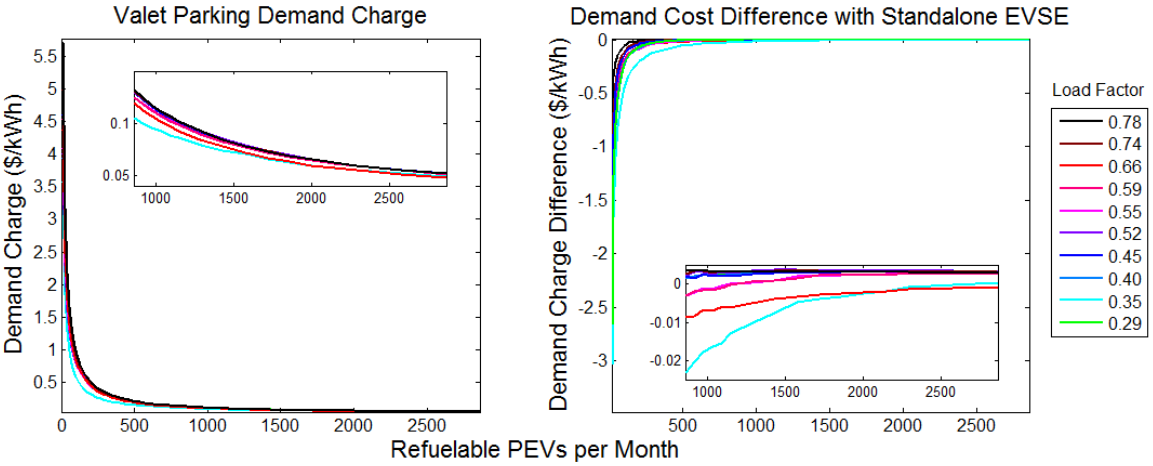

Figure 7-29: Winter demand charge cost and difference with a non-integrated EVSE system for a single 44 kW EVSE operated under valet parking when integrated with then ten building demand profiles normalized to 100 kW average demand

Since demand charges under TOU-8 are more expensive than TOU-EV-4, an increase in maximum utility demand as a result of EVSE integration can increase the building demand charge. Figure 7-30 shows any difference in demand charge cost that the ten buildings experience when a single 44 kW EVSE is integrated and the average demand of the buildings is 100 kW. Comparing Figure 7-30 to Figure 7-28 and Figure 7-29 shows both the refueled PEVs and the building simultaneously experience a cost increase or decrease. When the maximum utility demand is not increased by the full capacity of the installed EVSE, a benefit to both the building and EVSE is seen. However, when the maximum demand is increased by the full capacity, both the building and the PEVs experience higher cost. The PEVs experience a higher cost due to paying higher demand charge rates, and the building pays a higher demand charge cost due to being responsible for the increase in PEV demand charge rate. In other words, the additional demand charge savings cost incurred by EVSE integration is shared by all parties involved.

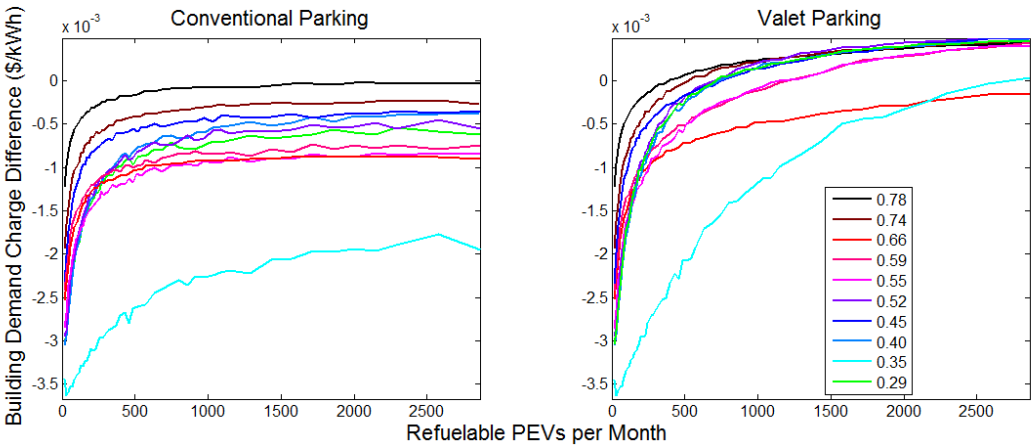

Figure 7-30: Building demand charge difference for a 100 kW average demand as a result of integrating a single 44 kW EVSE using conventional and valet parking operation during the winter

Figure 7-31 shows the demand charges for conventional and valet parking when one, two, four, and eight 44 kW EVSE are integrated with the 0.52 load factor building demand profile normalized to 100 kW average demand. For conventional operations, Figure 7-31 shows that increasing the number of EVSE increases demand charge cost slightly at low levels of PEV traffic, but decreases cost at high levels of PEV traffic. This occurs because the refueling of PEVs using multiple EVSE operated with conventional parking typically do not coincide with each other. As a result, while an increase in EVSE may result in increased demand, the increase does not increase linearly with the number of EVSE installed. Under valet parking, refueling of any queued PEVs begins as soon as a prior PEV is finished fueling, ensuring that multiple EVSE are refueled simultaneously and the full capacity of the EVSE station is achieved. This increased demand translates to an increase in maximum utility demand, resulting in increased demand charge cost when multiple EVSE are installed and operated using valet parking. The results presented in Figure 7-31 are for the 0.52 load factor building only. However, the results are similar for all other buildings with the difference being the absolute level of the demand charge cost. Buildings with higher or lower cost for a single EVSE respectively experience higher or lower cost with multiple EVSE than what is presented in Figure 7-31.

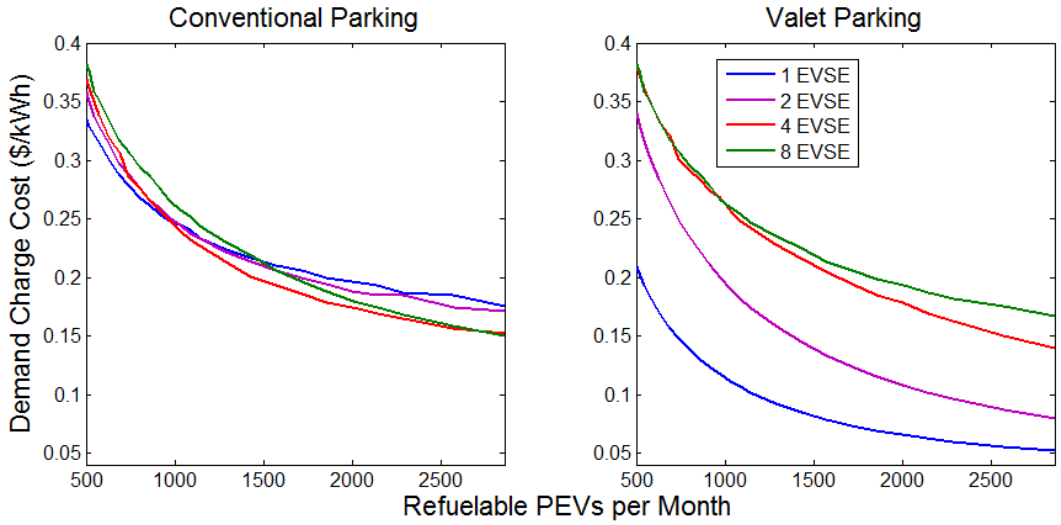

Figure 7-31: Winter demand charge cost for one, two, four, and eight 44 kW EVSE operated using conventional and valet parking while integrated with the 0.52 load factor building demand profile normalized to 100 kW average demand

An increase to maximum utility demand due to EVSE integration does not necessarily correlate to increased demand charges for the building. Figure 7-32 shows the difference in demand charge cost for the 0.29, 0.52, and 0.74 load factor buildings with 100 kW average demand when one, two, four, and eight 44 kW EVSE are installed. Under conventional operations, installing additional EVSE always reduced building demand charge costs. For the 0.29 and 0.52 load factor buildings, installing additional EVSE allows for demand charge savings when PEV traffic is low to be maintained or improved upon as PEV traffic increases. Referring back to Figure 7-27, the maximum utility demand is increased less under conventional parking. This result is also representative of the fact that the full capacity of the installed EVSE may not be fully utilized during the entire month if all arriving vehicles can be refueled in less than 15 minutes (or the time scale on which demand charges are applied). If PEV refueling produces a 15 minute average demand less than the full capacity of the installed EVSE, then the

only portion of the building demand charge that can be shared with the EVSE is reduced. Increasing the number of EVSE increases the load created by PEV refueling, increasing the amount of demand charge that can be shared between the building and EVSE load. As a result, increasing the number of EVSE also increases the savings that can be realized by the building by allowing for a larger portion of the demand charge to be shared with those refueling PEVs.

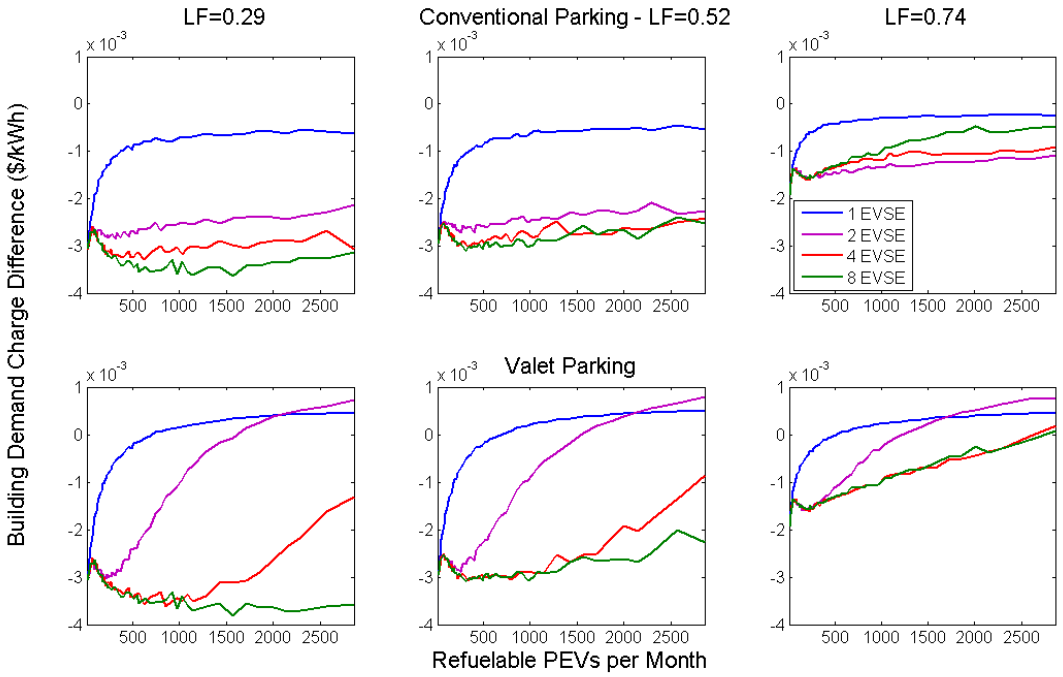

Figure 7-32: Building demand charge difference for the 0.29, 0.52, and 0.74 load factor building with 100 kW average demand one, two, four, and eight integrated 44 kW EVSE operated using conventional and valet parking during the winter

Increasing EVSE can also increase savings for valet parking. Figure 7-32 shows an increase in cost when two EVSE are installed, which is produced by increased maximum utility demand of the aggregated PEV and building load. However, cost is reduced at four and eight

EVSE. When multiple EVSE are installed for shopping travel, most PEVs begin refueling at time of arrival. While this increases demand charge cost for PEVs when multiple vehicles are simultaneously refueled, this may occur when building demand is relatively low. As a result, the peak refueling demand and building demand are not coincident, and the PEV refueling is primarily responsible for the increase to maximum demand. When this occurs, the building cost is reduced even though PEV demand charge cost increases.

Prior results have shown that costs for both the building and PEVs can be reduced by ensuring that refueling of PEVs is not coincident with maximum building demand. This may be accomplished by integrating EVSE with larger buildings. Figure 7-33 shows the demand charge for one and eight 44 kW EVSE integrated with the 0.52 load factor building normalized to 100 kW, 500 kW, 1000 kW, and 2000 kW average demand for both conventional and valet operations. By integrating the 44 kW EVSE with larger buildings, the relative size of the PEV refueling load is reduced compared to the building and the chances of the combined building and PEV load increasing the maximum utility is reduced. When this is accomplished, PEV demand charge cost is reduced. Keep in mind that once a building size has been increased sufficiently such that the additional PEV refueling load does not increase maximum utility demand, the largest demand charge cost reduction benefit has been realized and no further demand charge benefit can be realized as a result of increasing the building size. This is seen in Figure 7-33 as a decrease in improved savings as the size of the building increases beyond 500 kW.

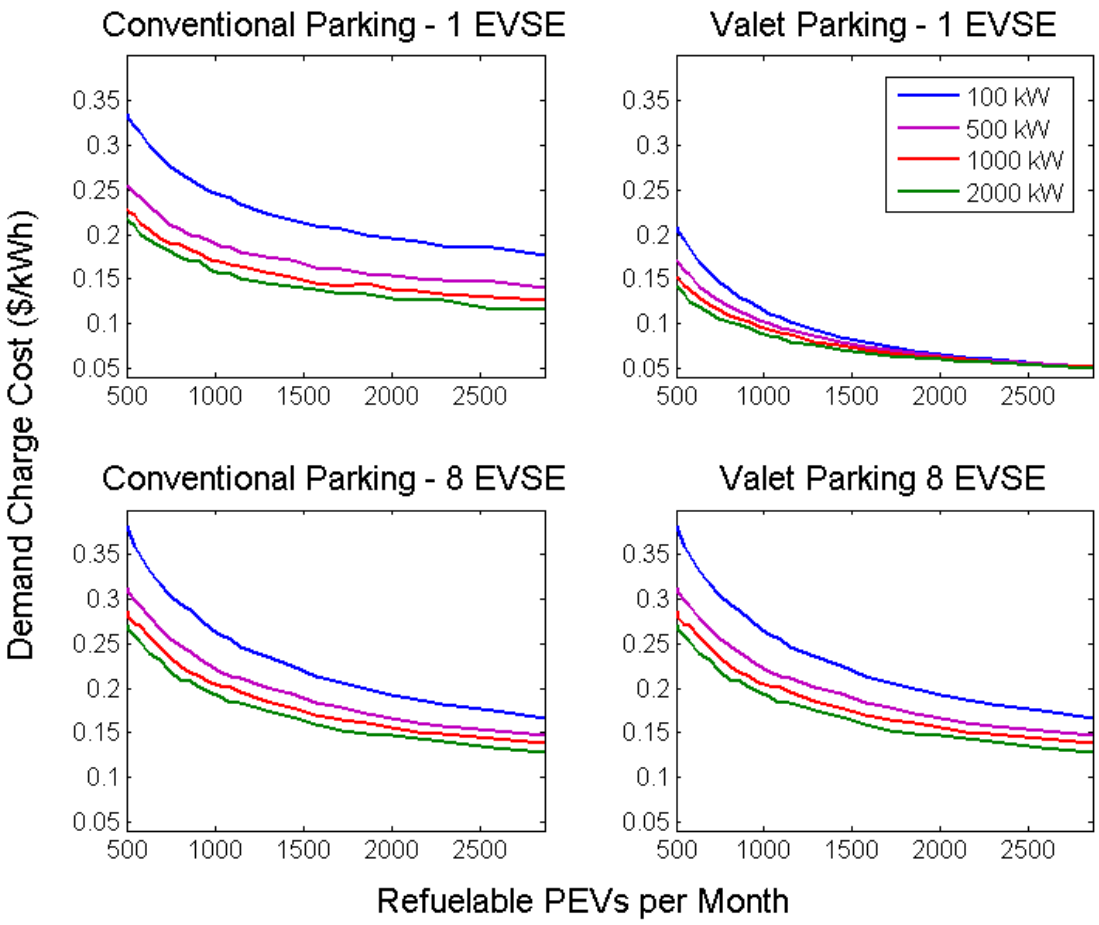

Figure 7-33: Winter demand charge cost for one and eight 44 kW EVSE operated while using conventional and valet operations while integrated with the 0.52 load factor building demand profile normalized to 100 kW, 500 kW, 1000, kW, and 2000 kW average demand

Contrary to some prior results, an increase in demand charge savings for PEVs is not coupled with an increase in demand charge savings for buildings. Figure 7-34 shows the building demand charge difference when a single 44 kW EVSE is integrated with the 0.52 load factor building with a 100, 500, 1000, and 2000 kW average demand. As discussed earlier, if the EVSE load can be integrated without increasing demand charges and the maximum amount of demand charge is shared between the building and EVSE, no further reduction in demand charge

cost can be realized. Clearly, an increase in building size naturally allows for EVSE integration to occur without an increase to maximum utility demand, possible realizing the maximum benefit. However, once the maximum benefit to the building has been realized, and any building demand increase yields no further savings, demand charge cost savings on a per unit energy basis decrease because the savings remain the same as the building size increases. From the perspective of the building, this is representative of sharing only a portion of the entire building demand charge with the EVSE load, indicating that the possible value created by EVSE integration is dwarfed by the sheer size of the building.

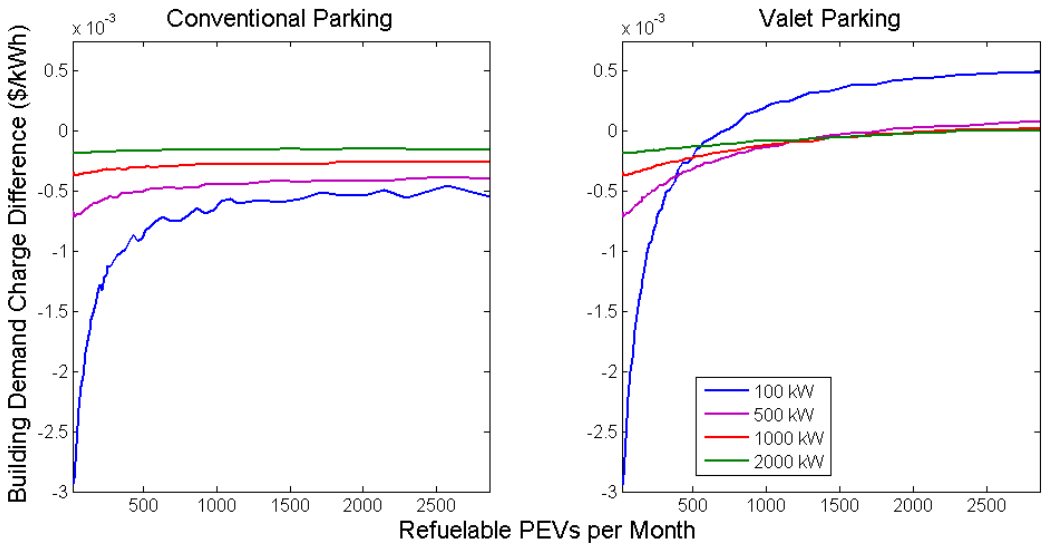

Figure 7-34: Building demand charge difference for a single EVSE integrated with the 0.52 load factor building with an average demand of 100, 500, 1000, and 2000 kW during the winter.

7.2.1.2 Summer Season and 44 kW EVSE

The two primary differences between summer and winter seasons are possible on-peak and mid-peak demand charges if the applicable rate under TOU-8 is rate B, and the possibility of EVSE integration resulting in a rate switch from the original rate to the other rate. The results for the number of simulations that did and did not result in a rate switch will be presented, followed

by the results for when a rate switch does and does not occur. Keep in mind that while the end user can select which rate (A or B) their building will operate under, this work assumes that the lower cost rate will always be adopted.

Of the ten buildings tested during the summer season, five originally took service under rate A and the other five took service under rate B. For a switch from A to B to occur, sufficient energy must be consumed without increasing the maximum utility demand in order to increase energy cost such that the more expensive demand charges used by rate B provide lower cost service. Since the purpose of Level 3 fast charging is to deliver a relatively small amount of energy quickly, the increase in energy consumption without an increase in maximum utility demand does not occur and no simulation of a building that previously preferred rate A resulted in a switch to B. However, the converse, where a building operating under rate B switches to rate A, does occur when the building profiles tested were sized to 100 and 500 kW average demand. A rate switch from B to A does not occur for the 1000 or 2000 kW buildings.

This type of rate switch is most common in the smallest building tested; that with 100 kW average demand. The percent of total simulations for which a rate switch occurred when EVSE is integrated with a 100 kW average demand is shown in Figure 7-35 for one and two EVSE. Information for four and eight EVSE is not shown because the results are the same as for two EVSE, with nearly every simulation for both operational strategies resulting in a rate change. The results show that the lower load factor buildings are more prone to a rate switch. Also, since valet parking results in more energy being sold to PEVs when only one or two EVSE are considered, a rate switch from B to A is not as common at moderate PEV traffic for the high load factor buildings and high PEV traffic for lower load factor buildings.

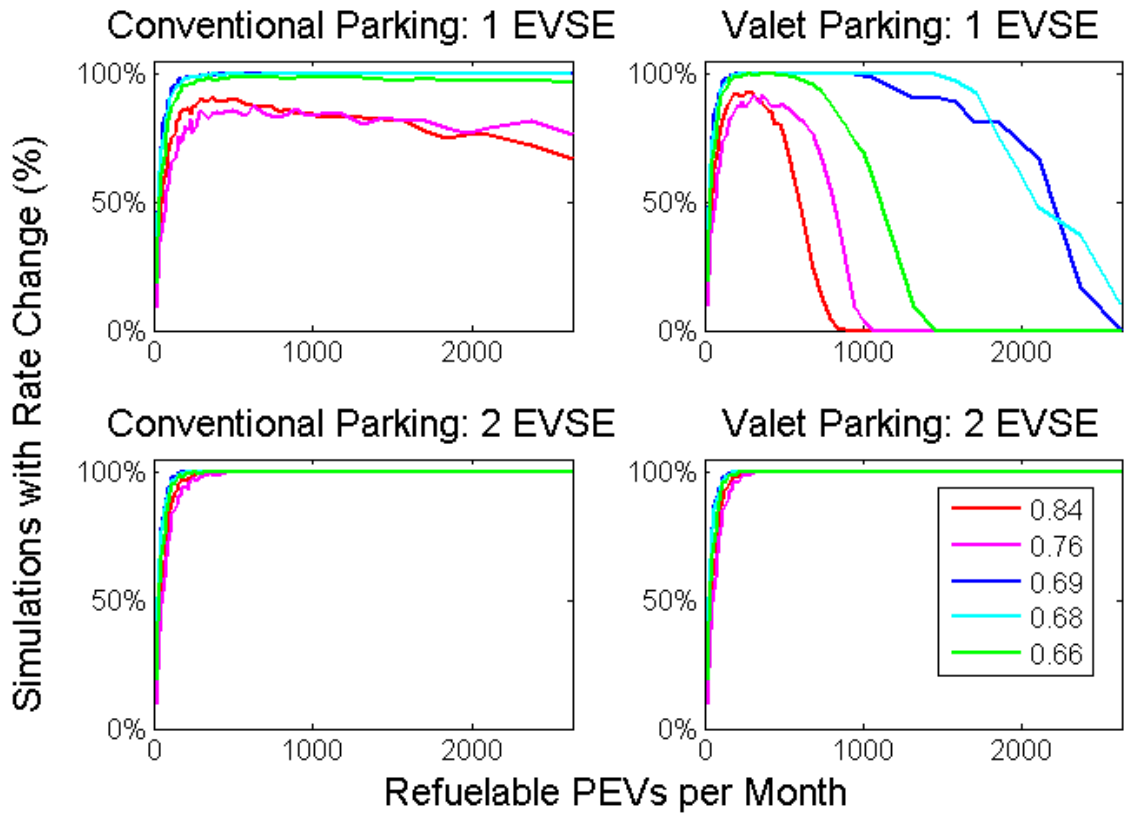

Figure 7-35: Percent of simulations in which a rate switch from B to A occurred for the five buildings with a 100 kW average demand that originally took service under rate B during the summer for one and two 44 kW EVSE

The rate switch from B to A occasionally occurs at 500 kW, but with less frequency than the 100 kW building. Also, rate switches only occur for the 0.68 and 0.66 load factor buildings. No rate switch occurs when only one 44 kW EVSE is integrated and when PEV traffic is low across all other scenarios. As PEV traffic increases, a rate switch is more common under valet operations for the 500kW average demand buildings. The maximum number of simulations for which a rate switch occurs is for 8 EVSE using valet operations, for which approximately a third of all simulations for both buildings resulted in rate switches. The cost results for both the buildings and PEVs are similar to what is presented for the 100 kW buildings. Keep in mind that

a rate switch only occurs when the maximum possible demand from the integrated EVSE is comparable to the building load. By simply integrating EVSE with large buildings, a rate switch will not occur. In fact, a rate switch is a relatively rare occurrence that was manifested in only a portion of the model runs when the tested average demand was relatively similar in size to the maximum capacity of the integrated EVSE. When a rate change does not occur, the aggregated PEV refueling and building demand remain on the same rate as the original building.

Since PEV travel does not significantly change between the winter and summer season, the energy cost associated with refueling PEVs during the summer is similar in shape to refueling PEVs in the winter. While having the same shape as winter energy charges, the summer energy charges are more expensive due to the increase in cost to purchase electricity during the middle of a summer day. For buildings that select A, PEV energy costs under conventional parking start at $0.194 per kWh at low traffic levels, and decrease linearly to $0.17 per kWh at the highest PEV traffic levels tested. Under valet parking, PEV energy costs are approximately $0.194 across all PEV traffic levels tested. EVSE integration with a building that operates under rate A results in an increase in electrical energy cost of approximately $0.03 per kWh versus if the EVSE received utility service under a single utility meter. For buildings that select B, PEV energy costs under conventional parking start at $0.125 per kWh at low traffic levels, and decrease linearly to $0.12 per kWh at the highest PEV traffic levels tested. Under valet parking, PEV energy costs are approximately $0.125 across all PEV traffic levels tested. EVSE integration with a building that operates under rate B results in a decrease in electrical energy cost of between $0.025 and $0.03 per kWh versus if the EVSE received utility service under a single utility meter

PEV demand charges during the summer have the same shape as during the winter. However, since half the buildings operate under rate A and the other half under rate B, the demand charge profile versus PEV traffic splits into an A and B group, as seen in Figure 7-36 for conventional parking and Figure 7-37 for valet parking. Both figures show results when a single EVSE is integrated with a 100 kW building. Since the rate A demand charge during the summer is the same as the winter, the results in terms of cost and difference versus a standalone EVSE system are virtually identical. The buildings that take service under rate B, however, have additional on-peak and mid-peak demand charges that increase costs to the point where demand charge cost increases are greater than the case of connecting the EVSE to a dedicated utility meter.

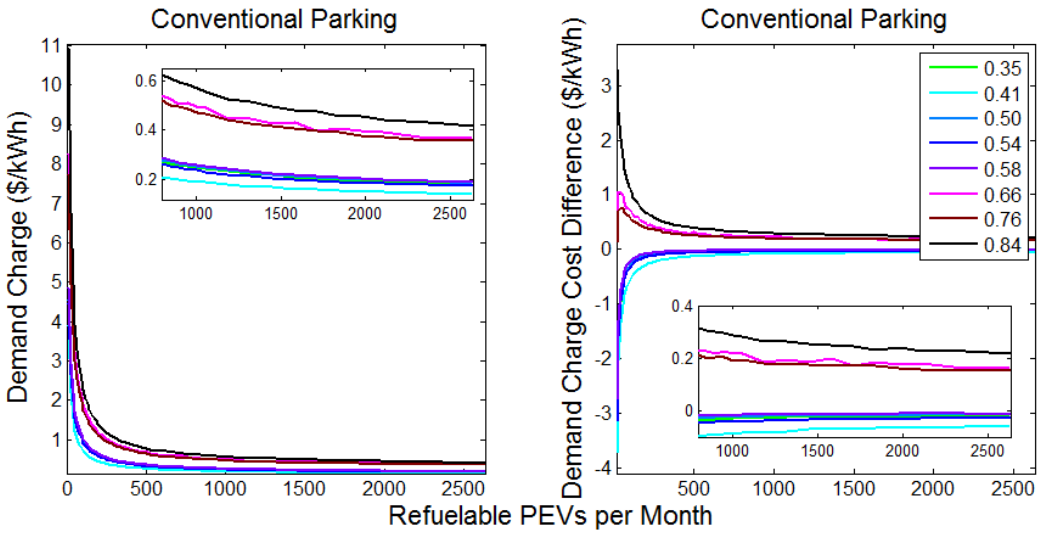

Figure 7-36: Demand charge cost and difference in cost with a standalone EVSE station operated using conventional parking when a single EVSE is integrated with 100 kW average building demand during the summer

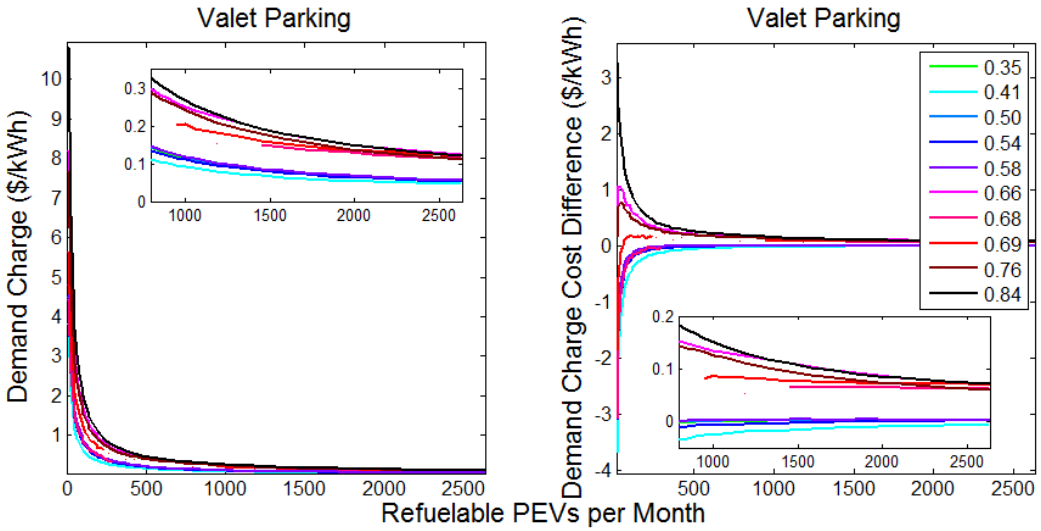

Figure 7-37: Demand charge cost and difference in cost with a standalone EVSE station operated using valet parking when a single EVSE is integrated with 100 kW average building demand during the summer

Buildings operating under rate A experience a similar demand charge cost difference, as seen in Figure 7-38. Buildings operating under rate B, however, can experience a larger increase to demand charge costs. The increased cost grows along with PEV traffic, and is consistently high or highest for the high load factor buildings. Keep in mind that some buildings always switched rates at an average demand of 100 kW, and do not have results for some levels of PEV traffic, resulting in only line segments appearing in Figure 7-38.

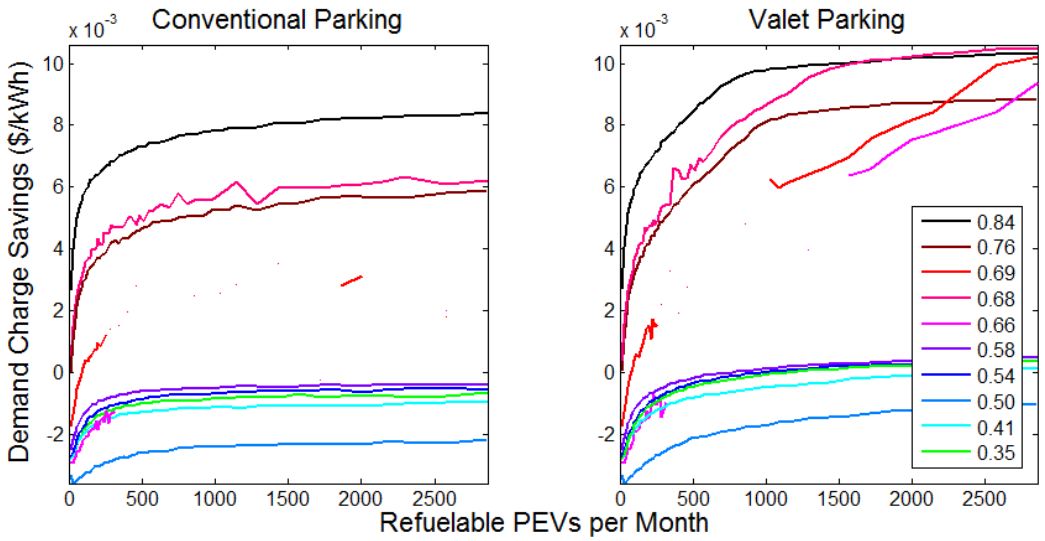

Figure 7-38: Building demand charge difference for a single EVSE integrated with 100 kW average demand during the summer

Increasing building size can help to reduce cost when rate B is applicable, as seen during the winter. However, for all buildings except the 0.76 load factor building, average demand must be increased to 2000 kW before savings can consistently be produced across most PEV traffic levels. Figure 7-39 shows only the difference in cost between multiple EVSE integrated with the 2000 kW 0.84 load factor building for both conventional and valet operations. The results show that the increase in cost due to EVSE integration can be significantly reduces and turned into a savings. Under conventional operations, these savings can be maintained unless eight EVSE are installed and under valet operations until PEV traffic reaches the highest levels tested in this work when four and eight EVSE are installed and moderate traffic levels when one or two EVSE are installed. Results for all other buildings are similar in shape. The values are also similar except for the prior mentioned 0.76 load factor building, which experiences a demand charge savings for all number of EVSE and operational strategies tested at 2000 kW and up until the highest PEV traffic levels tested for 1000 kW. Additionally, for all buildings, whenever a

demand charge savings can be realized for PEVs, a reduction in overall demand charge cost can be realized by the building as well, further indicating the importance of integrating EVSE in such a way that the maximum utility demand is not increased.

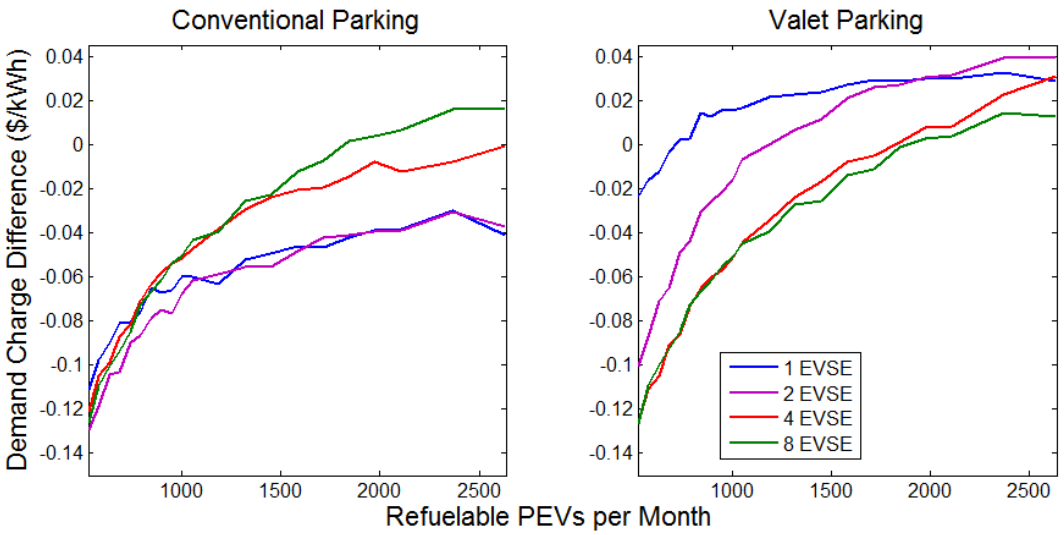

Figure 7-39: Difference in PEV demand charge cost when multiple EVSE are integrated with the 0.84 load factor building with an average demand of 2000 kW during the summer

A rate switch from B to A occurs when the maximum utility demand has been increased during peak periods such that the peak demand charges become overly expensive. As already discussed, this economic phenomena only occurs when the installed EVSE is similar in size to the building demand. In particular, the buildings with an average demand of 100 kW are prone to switching rates as a result of EVSE integration. Note that since the rate switch is driven by an increase in maximum utility demand, the exact PEVs that cause the increase can be determined and separated into a "switching" PEV group. The remaining PEVs belong to the "non switching" group. By separating between these two groups, the true cost of refueling the switching PEVs (or refueling vehicles during peak periods when building demand is highest) can be determined. Under conventional parking, the percent of vehicles creating the rate switch is between 5% and

15% of all refueled vehicles. Under valet parking, the percent of vehicles creating the rate switch is between 5% and 15 % for the 0.84, 0.76, and 0.66 load factor buildings and 5% and 30% for the 0.68 and 0.69 load factor buildings.

After the two groups of PEVs have been determined, the demand produced by refueling the two groups can be produced, and the cost to refuel the individual groups determined. Figure 7-40 shows the energy charges for both groups of PEVs when integrated with the five buildings that originally took service under rate B. For the group of PEVs that did not contribute to the rate switch, energy charges lie between the rate A and rate B charges, signifying that if only these PEVs had been refueled, the lower rate B energy rates would have applied, but the actual cost is greater due to the application of rate A energy rates. Energy rates for the group of PEVs that caused the rate switch are extremely high. Since the switching PEV group are responsible for all other participants (the building and the non-switching PEV group) paying higher energy charges, the switching group must bear some of the increased cost of every other kWh purchased by the building and other PEV group. Since the group of switching PEVs is a fraction of the total refueled PEVs, and the PEV load is a small portion of the total load, the resulting cost of energy ranges from the hundreds to the tens of dollars per kWh.

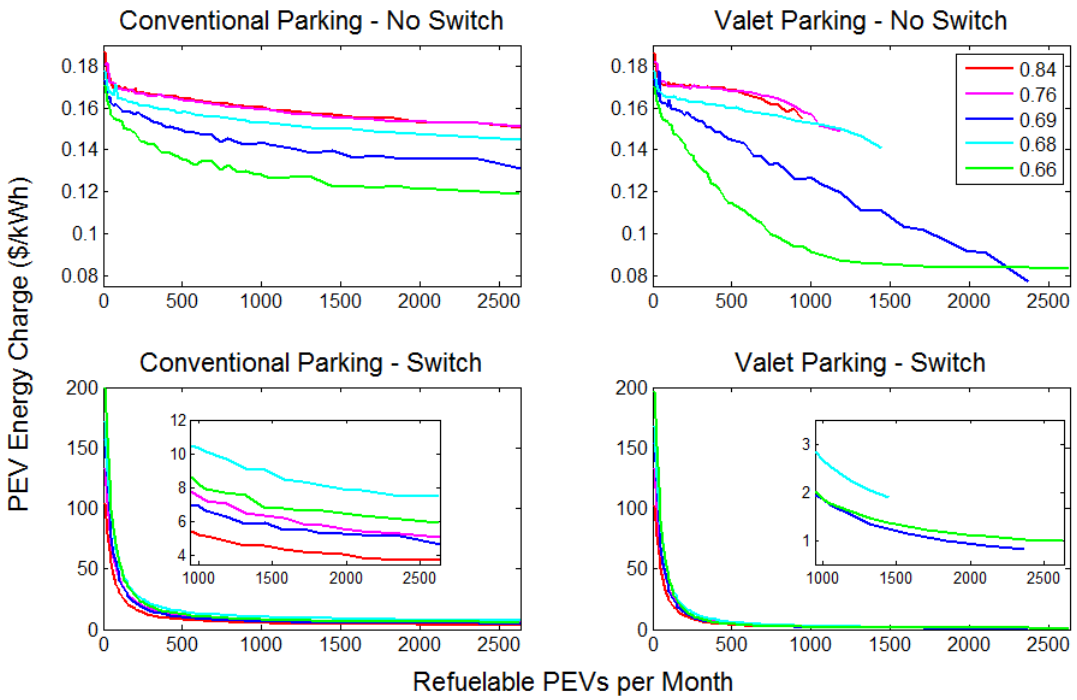

Figure 7-40: Energy cost for PEVs that did and did not cause a rate switch from B to A when 1 EVSE is integrated with a 100 kW average demand building during the summer

While the group of switching PEVs is responsible for an increase in energy cost for every kWh purchased, the same group is also responsible for the elimination of on-peak and mid-peak demand charges. Figure 7-41 shows the summer demand charge for both groups of PEVs under conventional and valet operations. While the non-switching PEV group experiences typical demand charges, the switching group experiences a significant demand charge savings as a result of eliminating peak demand charges. The combination of the energy charges and demand charges results in a more palatable cost to refuel this group of PEVs ranging between one to two dollars per kWh under conventional operations and between 0.35 and 0.65 dollars per kWh under valet operations.

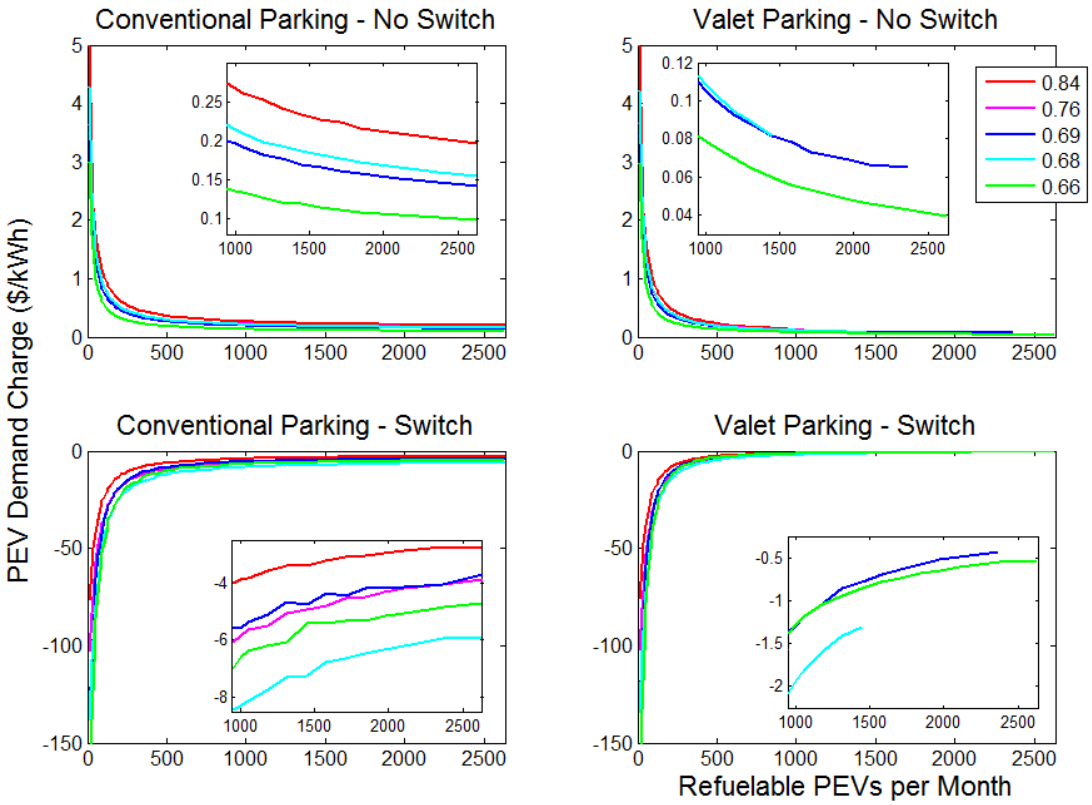

Figure 7-41: Demand cost for PEVs that did and did not cause a rate switch from B to A when 1 EVSE is integrated with a 100 kW average demand building during the summer

The total cost for the buildings with an average demand throughout the month of 100 kW and a single integrated 44 kW EVSE also changes, as shown in Figure 7-42. The results show that all buildings, except for the 0.68 load factor building under conventional operations or at low traffic levels under valet operations, experience an increase to cost. Similar to the situation where no rate switch occurs, reducing load factor may or may not create a cost reduction.

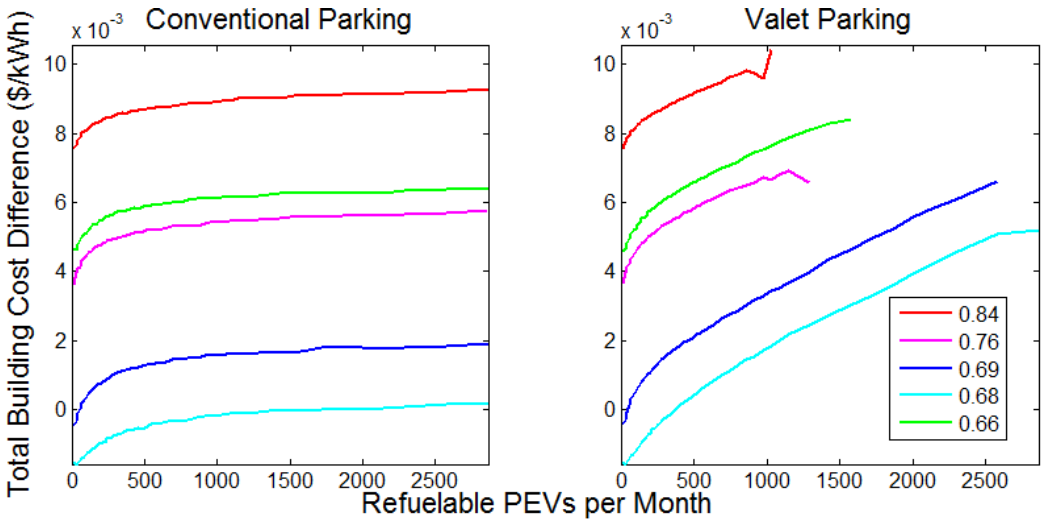

Figure 7-42: Difference in total building cost for the buildings with a 100 kW average demand that experience a rate switch from B to A during summer months

7.2.1.3 Difference between 44 kW and 120 kW EVSE

Prior work on non-building-integrated EVSE has shown that increasing the EVSE power output from 44 kW to 120 kW increases the number of PEVs that leave the EVSE station fully charged, increasing demand charges, but does not necessarily improve access to the station, especially if conventional parking is implemented [181]. When integrating EVSE with a building, the move to 120 kW also increases demand charges. Figure 7-43 shows the difference in demand charges between when a 120 kW and 44 kW EVSE are integrated with a 100 kW building during the winter. Increasing EVSE power output from 44 kW to 120 kW effectively doubles the demand charges for all buildings, operational scenarios, and PEV traffic levels.

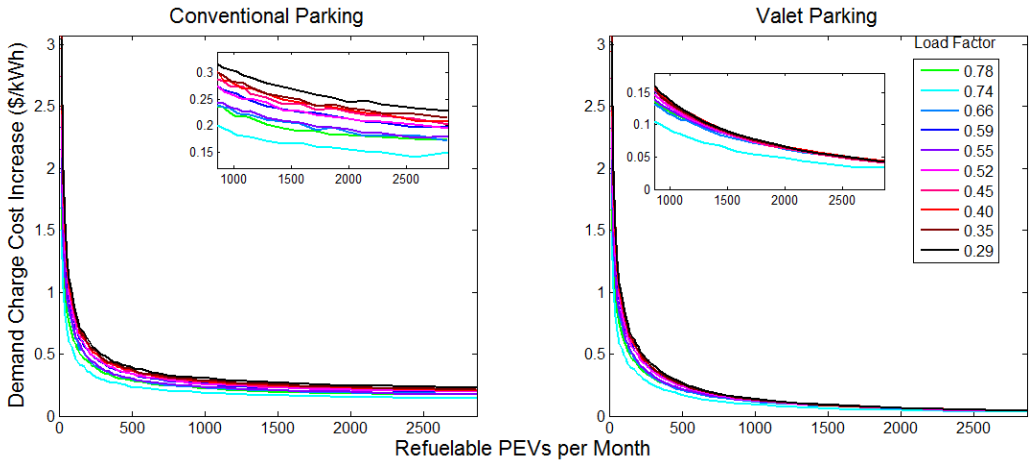

Figure 7-43: Difference in PEV demand charges between a single 44 kW and 120 kW EVSE integrated with 100 kW building during the winter

The increase in PEV demand charges is not always coupled with an increase in building demand charges, as seen in Figure 7-44. Figure 7-44 shows the difference in cost when a 100 kW building integrates a single 120 kW EVSE versus a 44 kW EVSE. Under conventional operations, the switch to a 120 kW EVSE always increases demand charge costs for the building as well. Under valet operations, cost increases except for the buildings that experienced either the largest cost increase or smallest savings when integrating 44 kW EVSE. These buildings, which also experienced the largest increase in maximum demand as a result of 44 kW EVSE integration, experience a reduction in cost because of faster refueling during off-peak times. Since the EVSE operates at 120 kW, demand charges would already be high prior to integration, and when the maximum utility demand is increased significantly when the building demand is relatively low, the increase in demand charge is due primarily to the EVSE only, resulting in a reduction in cost for the building. Keep in mind that any savings produced are on the order of $0.0001 per kWh. Also note that the buildings with the largest cost increases are the buildings that experience the greatest savings as a result of integrating 44 kW EVSE (versus 120 kW

EVSE). Switching to 120 kW EVSE eliminates any possible benefit of splitting the demand charge cost between multiple loads for these specific buildings.

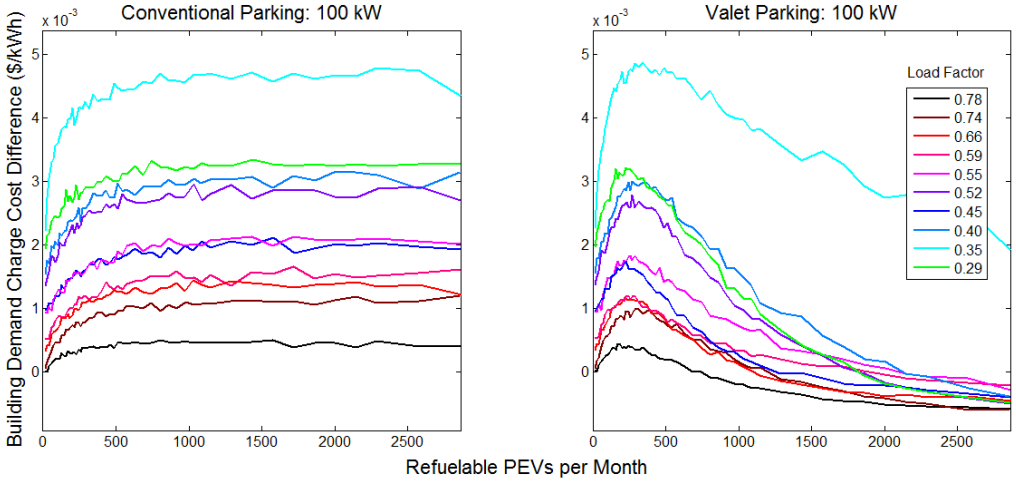

Figure 7-44: Difference in building demand charges produced by integrating either a single 120 kW or 44 kW EVSE with 100 kW building during the winter

Integrating multiple EVSE across any type of building demand will always increase PEV demand charges. Building demand charges will generally increase except when the switch from 44 kW to 120 kW creates a large increase in demand when the building demand is relatively low. During the summer, demand charges are increased for both PEVs and buildings except for the aforementioned scenario of an increase in utility demand during low building load periods. For the 100 kW building, rate switching from rate B to A occurs across all number of installed EVSE scenarios, all operation strategies, and all PEV traffic levels, and the resulting costs are similar to what is presented in Section 7.2.1.2.

7.2.2 Work Travel

The primary differences between work and shopping travel is the dwell time at work can be considerably longer than while shopping, the drivers arrive more frequently in the morning,

and the average vehicle miles travelled to work is higher. Due to the increase in vehicle miles traveled, approximately 38% of all vehicles arrive with a state of charge below 80% and can be refueled using Level 3 EVSE.

Just as with shopping travel, PEV energy charges are associated only with time of energy purchase, not with building shape or size. Figure 7-45 shows the PEV energy cost incurred when multiple EVSE are integrated and operated using conventional and valet operations. Since more vehicles arrive early in the morning during off-peak, electricity cost actually increases for all of conventional operations and valet operations when PEV traffic is low. If multiple EVSE are integrated, refueling of most arriving vehicles can be accomplished before mid-peak, increasing cost across all PEV traffic levels. If one or two EVSE are integrated and operated using valet operations, refueling of all queued vehicles extends into the mid-peak and on-peak, resulting in a reduction in energy cost only at high PEV traffic levels. PEV energy cost is increased by between $0.0015 and $0.002 per kWh for conventional operations and by $0.0005 per kWh for four and eight EVSE operated under valet operations. If one or two EVSE are installed and operated under valet operations, the cost increase at low PEV traffic is $0.005 per kWh, but turns into a savings of between $0.0006 and $0.001 per kWh at high PEV traffic.

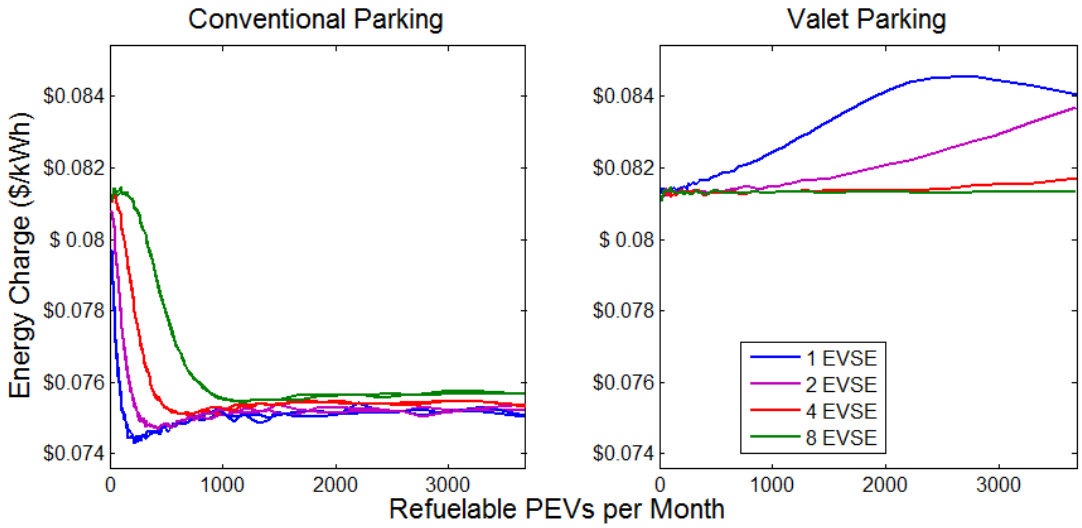

Figure 7-45: Energy charges for refueling PEVs performing shopping travel using one, two, four, and eight 44 kW EVSE for both conventional and valet parking during the winter

Predictably, any increase or decrease to PEV energy cost is coupled respectively with an increase or decrease to building energy cost. Figure 7-46 shows the difference in building energy cost when multiple 44 kW EVSE are integrated with a 100 kW building.

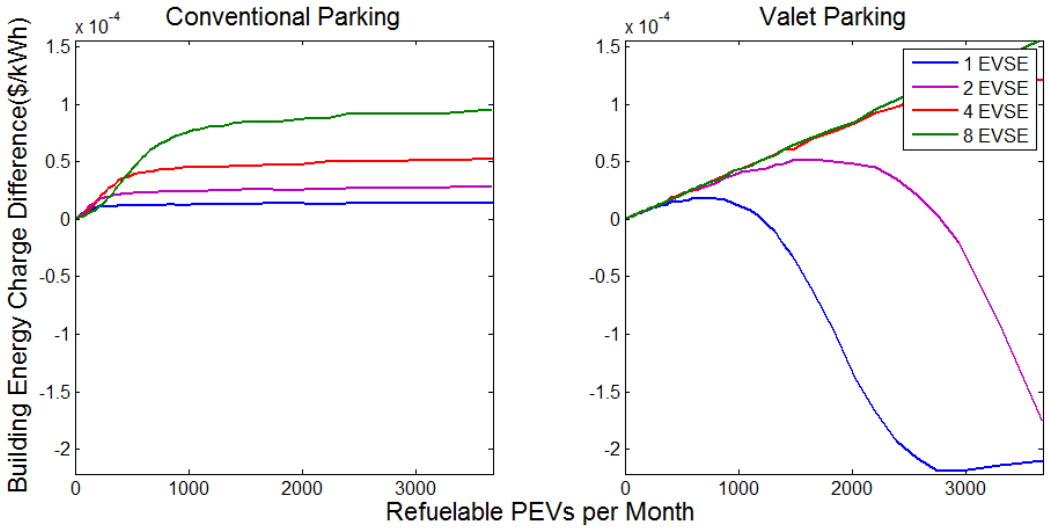

Figure 7-46: Building energy charge difference for a 100 kW average demand as a result of integration one, two, four, and eight 44 kW EVSE using conventional and valet parking operation during the winter and work travel

Figure 7-47 shows the difference in demand charge created by taking a standalone 44 kW EVSE and integrating the system with a 100 kW building. Clearly, cost can be significantly reduced under conventional parking. Note that the building that provided the greatest demand charge reduction for shopping travel continues to provide the greatest savings for work travel. Since work travel results in early arrivals, conventional operation results in PEV refueling occurring during off-peak times, which is commonly associated with low building demand. However, since work travel results in an increase in Level 3 eligible vehicles, valet operations result in an PEV refueling occurring consistently throughout the entire day, ensuring the maximum utility demand is increased and PEV demand charge cost is increased at nearly every building.

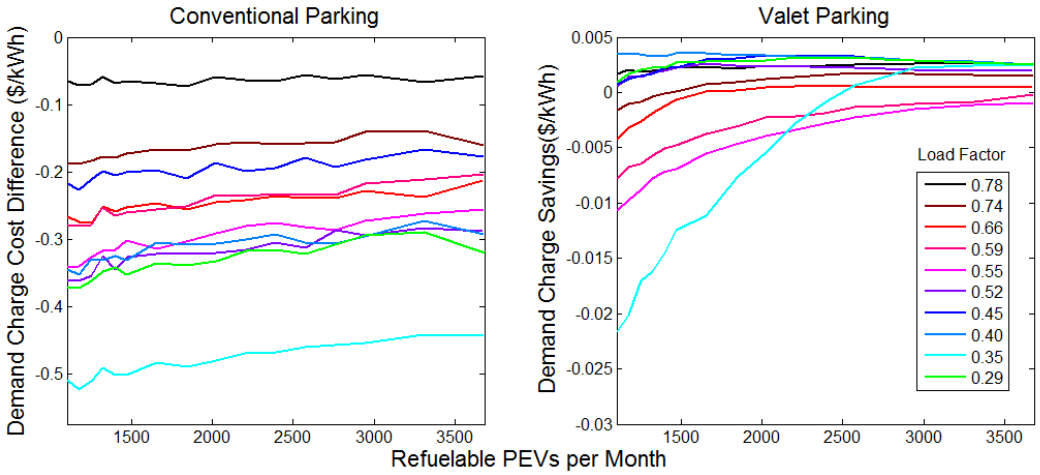

Figure 7-47: Difference in PEV demand charge cost for a single 44 kW EVSE servicing work travel integrated with a 100 kW building during the winter

The difference in PEV demand charge cost is correlated to the difference in building demand charge cost. Whenever EVSE integration produces savings for PEV customers, building demand charge cost is decreased. Whenever costs are increased for PEV customers, cost for the building is also increased.

The results presented for multiple EVSE, different building size, and season are all similar for work travel. In summary, increasing EVSE can reduce demand charge cost under conventional operations but increase cost under valet operations, increasing building size tends to reduce PEV demand charge cost and reduces any building impact, demand and energy charges increase significantly during the summer, and rate switches occur frequently for small buildings with a high load factor.

7.2.3 Discussion

The most obvious result of this work is that if EVSE integration provides lower cost energy for PEVs, then integration will reduce costs. However, for many of the scenarios presented in this work, the solution to the question of should we integrate EVSE with buildings is not clear cut. In the particular example of Southern California Edison rate structures, integration leads to increased demand charges that complicate the analysis. Clearly, when the maximum utility demand of the combined building and PEV load is increased by the capacity of all EVSE installed, cost is increased for both parties. Valet parking leads to the greatest increase for both shopping and work travel. Valet parking also leads to the overall lowest demand charge cost for PEVs, suggesting that any valet station in Southern California should not be integrated with a building. If conventional operations are to be used, then the opposite is true, where integration with a building can produce lower costs.

The most consistent cost reductions are achieved when integrating with larger buildings. While a building with a high load factor provides the least amount of opportunity to reduce cost, a building with a low load factor may not provide much more opportunity if the maximum building demand regularly coincides with PEV refueling. In addition, if building operations

change in the future, a previously attractive building for EVSE integration may cease to be attractive. From the perspective of reducing risk due to future uncertainty, integration with a larger building definitely reduces any variation in future performance.

The largest cost savings for PEVs and buildings is due to the sharing of demand charges. Even during the summer under rate B, savings can be produced for both parties. However, as the difference in demand charges from the EV to the building rate increases, the importance of PEV refueling not coinciding with maximum building demand becomes paramount to maintaining consistent savings. Whenever this is accomplished, EVSE integration with a building can continue to provide value. Controlled or smart charging could be used to assure PEV charging that does not coincide with building peak demand.

One important result of this work is the scale of savings or costs for both the PEV and building operators. While building integration can lead to savings of up to 50% for PEVs, the cost impact to a building is marginal. Even for the smallest building load evaluated with the highest load factors, total cost increases were within the range of hundreds of dollars. While this is not desirable from the perspective of a building operator, the other potential benefits associated with public EVSE may outweigh this potential cost. Keep in mind though that typically, a cost increase for the building is also coupled with a cost increase for PEVs as well. If the goal is the maximize the cost of refueling PEVs, and integration with a large building occurs, then the actual portion of the demand charge that is split is only a fraction of the total building demand charge, eliminating much of the benefit for the building. However, by integrating with a larger building, the impact of any cost increase is also reduced due to the sheer size of the building and corresponding total cost of electricity.

To add even more incentive to avoid integration with high load factor, low power demand buildings, the increase in cost for a building due to a possible rate switch can actually significantly increase the cost of electricity for a building, with a cost increase of nearly $0.01 per kWh being observed for the 0.84 load factor building with 100 kW average demand. This result is not necessarily specific to the Southern California Edison rates since other large utilities, such as Florida Power and Light, Georgia Power, and Xcel Energy all have multiple rates for commercial and industrial customers to select from. Such a rate switch is not automatic and would only occur under the direction of the utility customer. However, the rate switch always results in a reduced cost of electricity for the aggregated PEV refueling and building load, even if the PEVs or buildings may experience a higher allocated utility cost.

In addition, when a small number of PEVs are responsible for the rate switch, the cost associated with refueling those specific vehicles is very high. If the rate structure used to charge PEV drivers to refuel does not take into account the additional cost at refueling when building demand is high and a rate switch may occur, then the majority of drivers will be forced to subsidize the additional cost incurred by a few drivers. This can be avoided by electing to remain on the same rate, but at a higher total cost than the other available rates.

Much of the current research on PEV refueling treats the additional load as controllable in the sense that some operator can adjust the demand to meet some objective. This work further lends credence to the need for robust control of PEV refueling. When uncontrolled PEV refueling occurs (particularly for high load factor buildings), the cost benefits provided by building integration are reduced or eliminated, particularly when a rate switch occurs. By introducing some control of EVSE into the overall building system, the maximum benefits may

be retained regardless of the size and shape of the building load profile. However, for this level of control to be attractive for PEV drivers, rates charged for refueling PEVs would most likely need to be tied to energy delivered to the vehicle, not time spent at the EVSE (unless the PEV has been fully refueled) in order for future refueling rates to be acceptable to drivers.

8 Impact of PEV Refueling on Optimal DER System Design and Operation

The integration and operation of EVSE at a building to refuel electric vehicles will augment the electrical demand created by building operations. If the adoption of both DER and EVSE systems occurs simultaneously, the adoption and operation of one set of technology may influence the adoption and resulting operation of the other set of technology.

The problem of considering both DER and EVSE system adoption and operation has been formulated for three simple scenarios in this section of the current work. Section 3.4.3.1 presents a stochastic formulation of the DER system optimization model designed to also capture the decision to invest in and operate EVSE for the uncontrolled public refueling of PEVs or hybrid electric vehicles. Section 3.4.3.2.1 presents a deterministic formulation of the DER system optimization model designed to also capture the decision to invest in and operate vehicles (including electric vehicles) where the routes are already known. Finally, Section 3.4.3.2.2 further modified the DER system optimization to address the decision to invest in and operate vehicles when a set of destinations, or nodes, is known, but the routes to the different nodes is unknown and to also be optimized.

Countless scenarios and applications exist where the optimization models may be applied. The current work cannot consider all possible options of how electric vehicles impact building operations and the decision to invest in and operate a DER systems. These models can be used to begin to shed light into how the refueling of electric vehicles may affect DER system design and operation. In addition, as seen in Section 0, current PEV and EVSE prices are high enough to block the adoption if the goal is to minimize overall cost and conventional vehicle

options exist. With this in mind, the focus of this section will be on determining the capital cost at which electric vehicle technologies are adopted. For uncontrolled public refueling of PEVs, the focus will be on determining the capital cost at which a building operator may decide to invest in public EVSE, and will use the model described in Section 3.4.3.1. For fleet vehicles, the focus will be on determining the capital cost at which the adoption of PEVs occurs when a conventional vehicle option exists, and will use the model described in Section 3.4.3.2.2.

8.1 Adoption of Public EVSE

As discussed earlier, the decision to install and operate public EVSE depends upon the probability of certain scenarios occurring. This decision depends upon the expected number of vehicles that will show up to be refueled. The vehicle behavior can vary as the total number of electric vehicles on the road changes, or driving patterns change. Even if these parameters stay the same, random travel behavior may result in different operation from week to week or month to month. As a result, the stochastic formulation presented in Section 3.4.3.1 is designed to include any possible scenario that a building operator expects to occur, considering the probability that each event will occur.

Due to the uncertainty associated with travel patterns and future PEV adoption, as well as the different EVSE technology options available, a nearly infinite number of EVSE operation scenarios exist. Many of these scenarios can be eliminated from consideration prior to optimization. For example, the results presented in Section 0 suggest that the electricity demand profile created by Level 3 EVSE is undesirable. Coupled with the currently high capital cost associated with Level 3 EVSE, the decision to omit this technology from consideration can be made. Also, considering that Level 1 EVSE refuels electric vehicles slowly (perhaps too slowly

for public refueling), the technology scenarios evaluated in this section will be limited to those that consider Level 2 EVSE.

Within Level 2 EVSE, multiple power levels exist. The most commonly used power level associated with Level 2 EVSE is 6.6 kW. However, despite potential problems associated with demand charges, EVSE with higher power output may be desired in order to refuel electric vehicles more quickly. As a result, an additional set of Level 2 EVSE operating at 14.4 kW will be considered in the current analyses.

Considering the available technology, two different scenarios are considered. The first is 6.6 kW Level 2 EVSE operated using conventional parking installed at a building that experiences primarily shopping traffic. It is assumed that PEV traffic is low. The second scenario considers 14.4 kW Level 2 EVSE operated using valet parking installed at the same building considered during the first scenario. In this scenario, it is assumed that PEV traffic level is high. These two scenarios somewhat span the range of possibilities for consideration of adopting level 2 EVSE for integration with this particular building.

The building considered in this work is the UCI Natural Sciences 1 building. This building has an average electrical demand of 431 kW with an electrical load factor of 0.50. The heating demand is coincident with the electrical demand 93% of the time, and the ratio of the total heating load to the electrical load is 0.59. While other buildings exist with larger electrical demand, this building has a load small enough that EVSE may affect DER system optimization, while remaining large enough to adopt a DER system.

Note that the projected electrical demand as a result of EVSE adoption is determined using the EVSE operation model described in Section 3.3.2. This model assumes that any

electric vehicle arriving at this station that can be refueled, will be refueled, regardless of the cost to refuel. This is an overly optimistic model that most likely exaggerates the resulting EVSE operation for a given traffic level. However, the benefit of this model is that it establishes the most supportive scenario for EVSE adoption. In other words, if EVSE adoption does not occur under the conditions produced using the EVSE operation model at a given traffic level, it is unlikely that adoption would occur under more realistic conditions.

The current work does not attempt to resolve the probability that PEV adoption or traffic to a certain area will increase or decrease over time. Instead a specific probability associated with the set of PEVs and travel patterns considered or certain scenario is assumed for each case. Both the 6.6 and 14.4 kW scenarios have an assumed high, average, and low PEV traffic level from which a charging profile is generated. The assumed probability for these traffic levels are as follows: high traffic occurs 30% of the time, average traffic occurs 50% of the time, and low traffic occurs 20% of the time.

The stochastic model only considers the adoption of a CHP system consisting of a DG, HRU, and EES. The parameters used for the DG and CHP are the same as used in Section 5 and are described in Table 5-1. The parameters used for the EES are the same as used in Section 0 and are shown in Table 6-1. Three DER system scenarios are considered. They consist of 1) fuel cells, microturbines, and a heat recovery unity, 2) electrical energy storage only, and 3) fuel cells, microturbines, a heat recovery unit, and electrical energy storage. The optimization results for these three scenarios without an option to adopt public EVSE is shown in Table 8-1.

Table 8-1: Optimal DER system adoption for the three technology scenarios at the UCI Natural Sciences 1 building

Technology Scenario	Fuel Cell (100 kW)	Microturbine (65 kW)	HRU (kW)	EES (kWh)
FC/MTG/HRU	6	4	320	n/a
EES	n/a	n/a	n/a	115
FC/MTG/HRU/EES	6	3	320	66

The purpose of this part of the study is to determine the capital cost at which EVSE is adopted. The adoption of EVSE at a certain capital cost must balance the initial investment and cost of supplying electricity to the EVSE against the revenue generated by the equipment. Prior work performed by White has suggested that charging a customer $0.50 per kWh to refuel their PEV would cover operating costs and recoup the initial investment associated with Level 2 EVSE [182]. Assuming that a customer is charged $0.50 per kWh delivered, the EVSE capital cost will be reduced from an initial investment cost of $30,000 per EVSE by $1,000 until adoption occurs when no DER system is considered, and when all three of the DER system configurations are considered.

8.1.1 6.6 kW Level 2 EVSE

The assumed traffic levels for the 6.6 kW Level 2 EVSE analysis are 1000 PEVs per month (low traffic), 1500 PEVs per month (average traffic), and 2000 PEVs per month (high traffic). The travel and EVSE operation models were used to produce refueling profiles when one, two, three, and four 6.6 kW EVSE are operated under conventional parking. Three days of Level 2 EVSE operation are shown for all EVSE configurations in Figure 8-1.

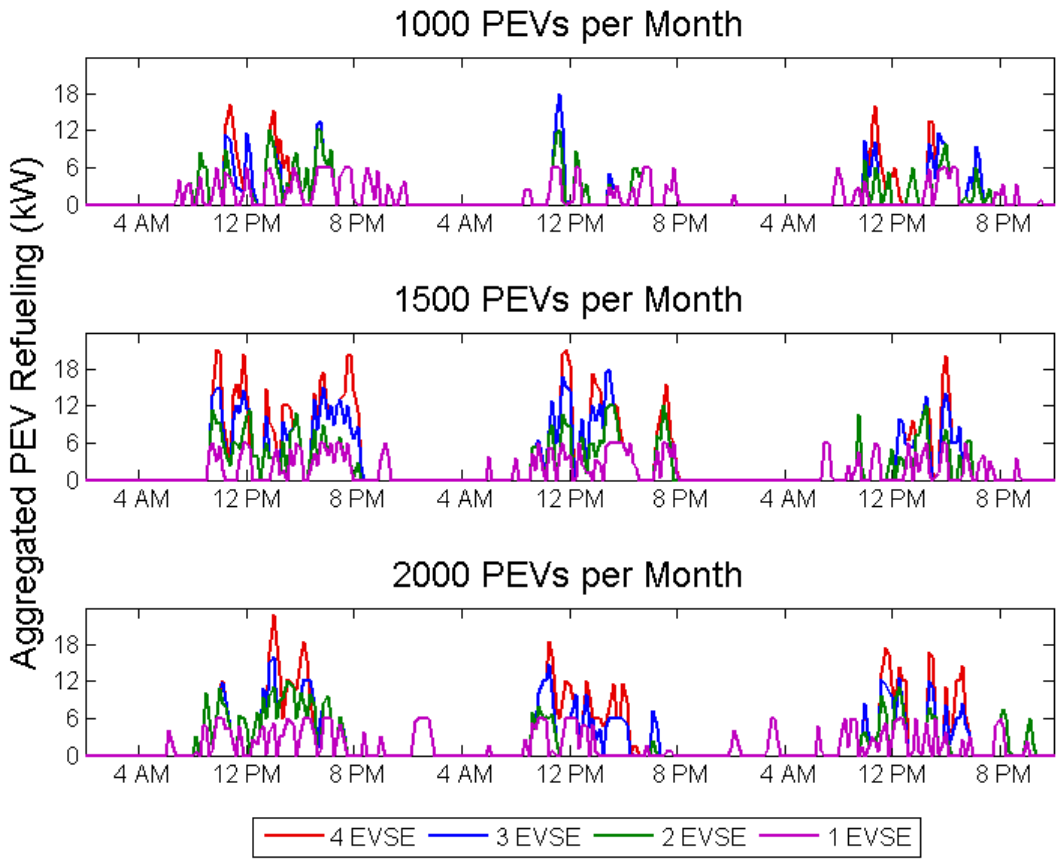

Figure 8-1: Refueling profiles generated by the three traffic scenarios when one, two, three, or four 6.6 kW EVSE are adopted and operated using conventional operations.

When no DER system was considered, adoption of 6.6 kW Level 2 EVSE did not occur until the capital cost of an individual 6.6 kW Level 2 EVSE was reduced to $4,000 per charger installed. Once capital cost had been reduced to this level, a single EVSE was adopted. This cost was then used in determining optimal DER and EVSE system adoption.

The resulting optimal DER and EVSE systems for the three technology scenarios is shown in Table 8-2. Note that the only difference in DER adoption occurs under the scenario where all technologies are considered. Under this scenario, the size of the EES is reduced from 66 kWh to 64 kWh. Also, under the EES scenario, Level 2 EVSE adoption did not occur.

Table 8-2: DER system adoption for the three technology scenarios at the UCI Natural Sciences 1 building when considering 6.6 kW Level 2 EVSE at $4,000 per charger

Technology Scenario	EVSE (6.6 kW)	Fuel Cell (100 kW)	Microturbine (65 kW)	HRU (kW)	EES (kWh)
FC/MTG/HRU	1	6	4	320	0
EES	0	0	0	0	115
FC/MTG/HRU/EES	1	6	3	320	64

In addition to adopting virtually the same systems, the operation of the DER systems remains nearly unchanged as a result of EVSE adoption. This results from the fact that the EVSE load is relatively small when compared to the load of the building. Figure 8-2 shows electrical demand for the UCI Natural Sciences 1 building for a single day with the three EVSE demand profiles shown in Figure 8-1 for a single 6.6 kW Level 2 EVSE. Since only a single 6.6 kW EVSE is adopted, the overall impact experienced by the building is very slight. These results suggest that low capital cost is required in order for 6.6 kW Level 2 EVSE adoption to occur when PEV traffic is low, and that the resulting impact on overall building operations is negligible.

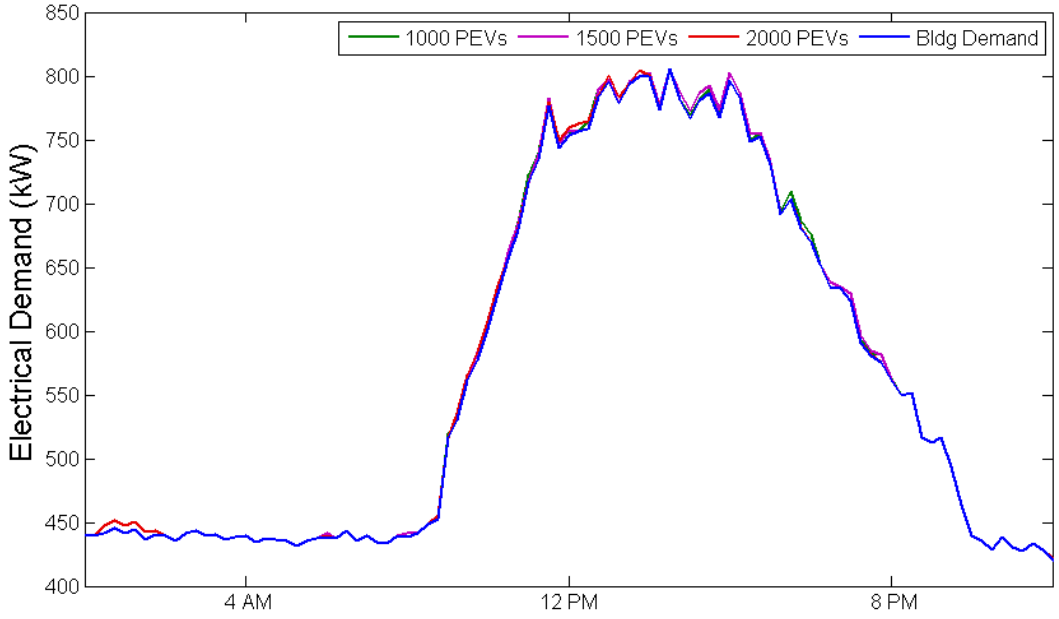

Figure 8-2: UCI Natural Sciences 1 electrical demand for a single day when a single 6.6 kW EVSE is adopted and experiences three separate PEV traffic level scenarios

8.1.2 14.4 kW Level 2 EVSE

The assumed traffic levels for the 14.4 kW Level 2 EVSE analyses are 6000 PEVs per month (low traffic), 8000 PEVs per month (average traffic), and 10000 PEVs per month (high traffic). The travel and EVSE operation models were used to produced refueling profiles when one, two, three, four, five, and six 14.4 kW Level 2 EVSE are operated under valet parking. Three days of Level 2 operation are shown for all EVSE configurations in Figure 8-3. Note that under valet operations, at high PEV traffic levels, the difference between the different scenarios begins to disappear.

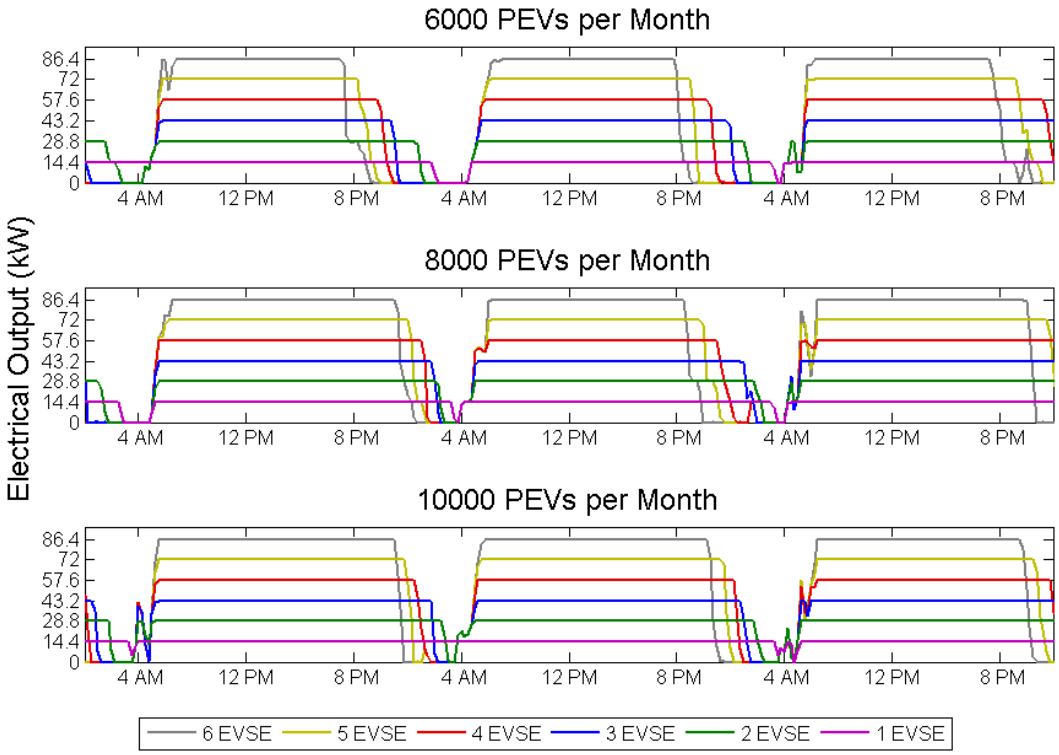

Figure 8-3: Refueling profiles generated by the three traffic scenarios when one, two, three, four, five, or six 14.4 kW EVSE are adopted and operated using valet operations.

When no DER system was considered, adoption of a single 14.4 kW Level 2 EVSE occurred at a capital cost of $24,000 per EVSE. At this cost level, a single charger was adopted. This cost was then used in determining optimal DER and EVSE system adoption.

The resulting optimal DER and EVSE systems for the three technology scenarios are shown in Table 8-3. The EES only scenario experiences no difference in adopted technology. However, at a cost of $24,000 per EVSE, not only are additional EVSE adopted under both CHP scenarios, but additional generators are also adopted. An additional fuel cell is adopted under the CHP only scenario, and an additional microturbine is adopted under the CHP and EES scenario.

Table 8-3: DER system adoption for the three technology scenarios at the UCI Natural Sciences 1 building when considering a 14.4 kW Level 2 EVSE at $24,000 per charger

Technology Scenario	EVSE (14.4 kW)	Fuel Cell (100 kW)	Microturbine (65 kW)	HRU (kW)	EES (kWh)
FC/MTG/HRU	4	7	3	324	0
EES	1	0	0	0	115
FC/MTG/HRU/EES	3	6	4	324	45

Figure 8-4 shows the combined building and EVSE electrical demand for one, three, and four EVSE. All three traffic scenarios are shown. For one EVSE, there is no difference between the three traffic scenarios. A slight difference is observed for three and four EVSE during the early morning and in the late evening. However, during the majority of the day, there no difference in operation between the different traffic levels.

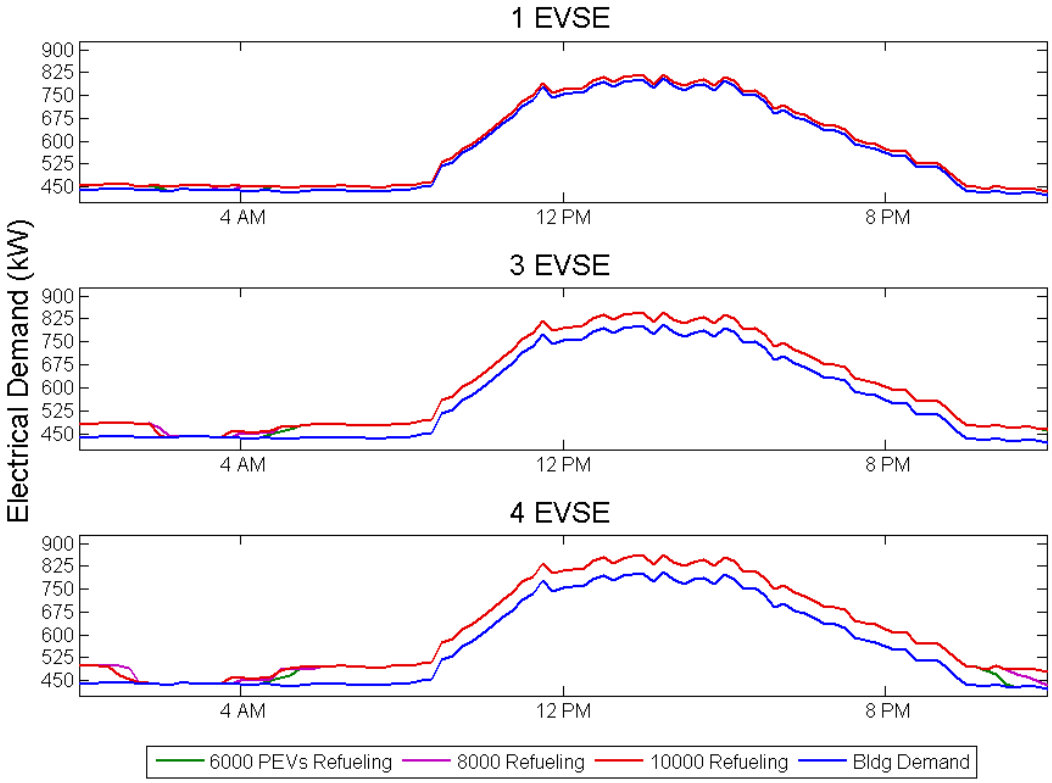

Figure 8-4: UCI Natural Sciences 1 electrical demand for a single day when one, three, and four EVSE are adopted

Under the EES only scenario, the dispatch of the EES does not experience any significant changes as a result of adopting a single EVSE. Operation for the CHP only and CHP with EES scenarios change as a result of adopting different technologies. Figure 8-5 and Figure 8-6 show DER system operation over the course of a week for the CHP and CHP with EES technology scenarios when EVSE is and is not included as an option respectively.

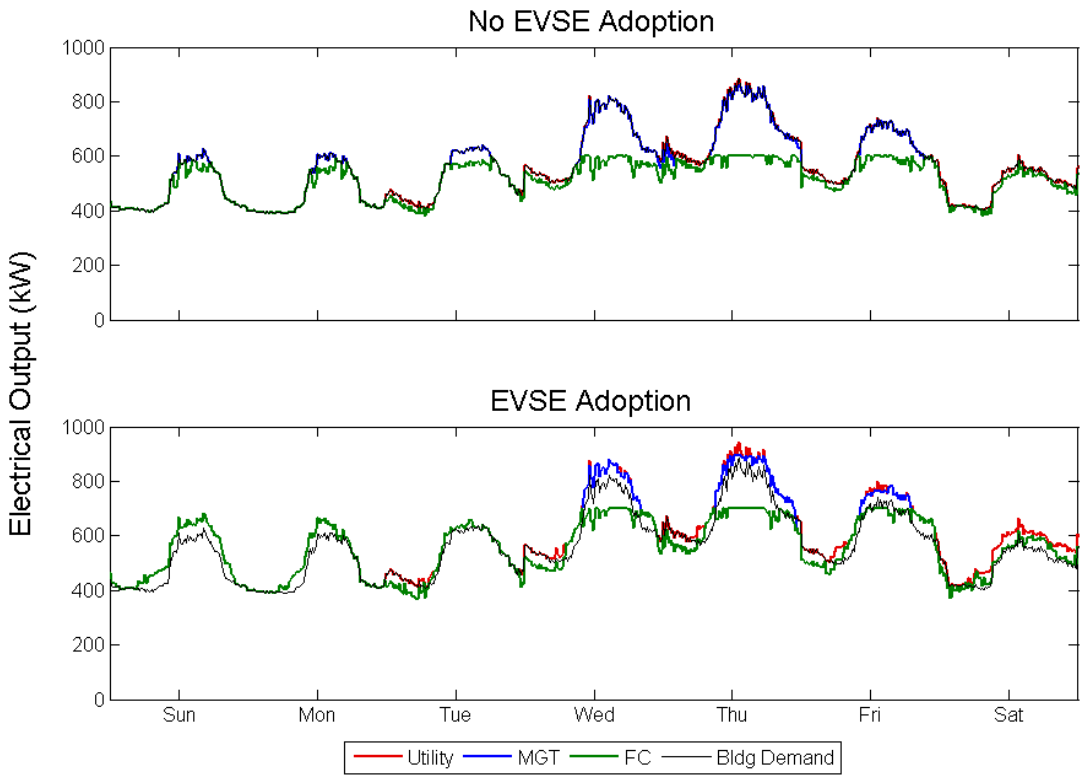

Figure 8-5: CHP system dispatch with and without EVSE adoption at the UCI Natural Sciences 1 building

Under the CHP only technology scenario, an additional fuel cell is adopted in lieu of a microturbine. As a result, microturbine operation decreases and the seven fuel cells are used to meet the majority of the building demand. Microturbine operation continues to only occur when the building and EVSE demand surpasses the maximum capacity of the fuel cell system. A side effect of the adoption of an additional fuel cell is increased dynamic operation of the entire set of fuel cells. Since the fuel cells are used to meet the majority of the building demand, the fuel cells are required to perform load following more frequently. Under this scenario, overall fuel utilization (electrical and thermal energy produced divided by fuel energy consumed) for the CHP system increases from 62.5% to 63.2% as a result of allowing for EVSE adoption.

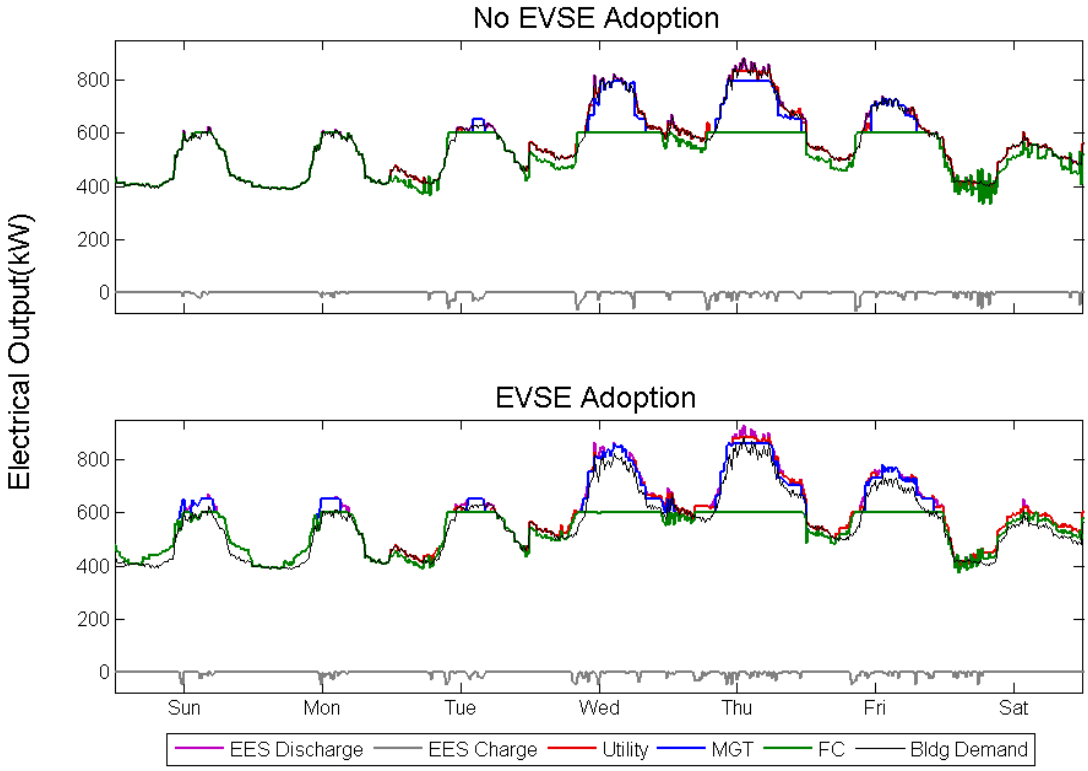

Figure 8-6: CHP and EES system dispatch with and without EVSE adoption at the UCI Natural Sciences 1 building

Under the CHP and EES technology scenario, an additional microturbine is adopted when EVSE is available for adoption. Fuel cell operation remains nearly the same regardless of EVSE adoption, with the largest change occurring to an increase in microturbine operation. Under this scenario, fuel utilization in the CHP system decreases from 63.6% to 61.8%.

8.1.3 Discussion

Currently, plug-in electric and hybrid vehicles make up a small portion of the overall vehicle fleet. Unless the EVSE installation is in a high electric vehicle traffic area, the resulting electrical demand created by refueling electric vehicles may resemble the intermittent profile shown in Figure 8-1. At these traffic levels, the electrical demand associated with EVSE is most

stochastic. However, the demand is also relatively small relative to the size of any building that would be a suitable candidate for DER system integration. As a result, the randomness associated with refueling electric vehicles may not matter simply because the additional electrical demand is so small relative to the DER system adopted. In this case, the decision to adopt a DER system can be uncoupled from the decision to adopt an EVSE system, with each being accepted based on the individual merit of the proposed system.

As PEV traffic increases and vehicle or parking technology improves such that valet parking becomes a realistic parking scenario, the resulting EVSE demand profiles become similar regardless of travel level. If a high level of PEV traffic to a certain area can be guaranteed, then the stochastic behavior associated with drivers begins to disappear from the perspective of the resulting refueling demand profile created by public EVSE. As a result, the problem appears to collapse from a problem governed by stochastic processes to a deterministic problem. Note that at this high level of PEV traffic, the resulting PEV refueling demand does affect the optimal design of a DER system and resulting operation. The actual problem of designing the optimal DER system, however, may be predictable enough to be accurately modeled using a deterministic model.

The travel model and probabilities associated with different travel levels were selected in part in order to demonstrate overall model performance. The optimization of DER and EVSE systems for two relatively fictitious scenarios does shed some light on the overall interplay (or lack of) the current need to take into account the public refueling of electric vehicles when designing a DER system for a building. The two scenarios, however, are only two points and do not define the entire space. At most, the model results show the importance of being able to

predict the resulting electrical demand associated with installing public EVSE. With some idea of how a potential EVSE system will behave, a building operator can determine if a stochastic or deterministic problem formulation is appropriate, or if the two systems will interact in a way that influences the design of each other.

8.2 Optimal DER System and Vehicle Fleet Design

Similar to the stochastic formulation for uncontrolled refueling of electric vehicles, the current state of the optimal DER and vehicle fleet design model is not well suited to analyze all options or scenarios for the integration of a DER system and electric fleet vehicles at a building. The primarily limitation is the solution method. The program used to solve the mixed integer linear program utilizes the branch and cut method. While well-suited for many optimization problems, the branch and cut method is limited to being useful only for small vehicle routing problems [115]. Increasing the problem size to beyond 20 nodes is impractical. For example, one simulation performed during this work included 25 nodes, allowed for only the adoption of electric vehicles, and did not include an option of adopting any DER technologies, could not converge to an optimal solution after five days of simulation.

Despite this shortcoming of the current solution method, the small set of nodes presented in Section 4.2.2 is small enough that an optimal solution can be found for the overall optimization problem presented in Section 3.4.3.2.2. Such an analysis provides the opportunity to showcase the potential benefit created by integrating the DER system and fleet design problems.

Using the UCI Natural Sciences 2 building and the node data set presented in Section 4.2.2, optimal DER system and fleet composition can be determined. This optimization took

place for a CHP system consisting of fuel cells, microturbines, and a heat recovery unit with cost and performance parameters defined in Table 5-1. All vehicle parameters, except for PEV capital cost, were assumed to be the same as the vehicle parameters used in Section 0 and shown in Table 6-3. No PEV adoption occurred with the PEV capital cost assumed in Table 6-3, so that the cost was step-wise reduced until PEV adoption occurred. The capital cost was reduced to $500,000 per PEV, or the same as a conventional vehicle, before adoption occurred. Note that this cost is the same as the electric bus included in the optimization occurring in Section 6. A single 30 kW EVSE was also adopted to refuel the PEV. The other adopted technologies included five 100 kW fuel cells, one 65 kW microturbine, a 320 kW heat recovery unit, and one conventional vehicle in addition to the adopted PEV.

Figure 8-7 shows the combined building demand and EVSE operation. The additional demand created by EVSE operation only occurs at night and does not increase building demand. The resulting DER system operation can be seen in Figure 8-8. DER system operation appears to be unaffected by EVSE operation, with the microturbine operation occurring only during the on-peak period, and the fuel cell performing thermal load following at night and base load production during the day.

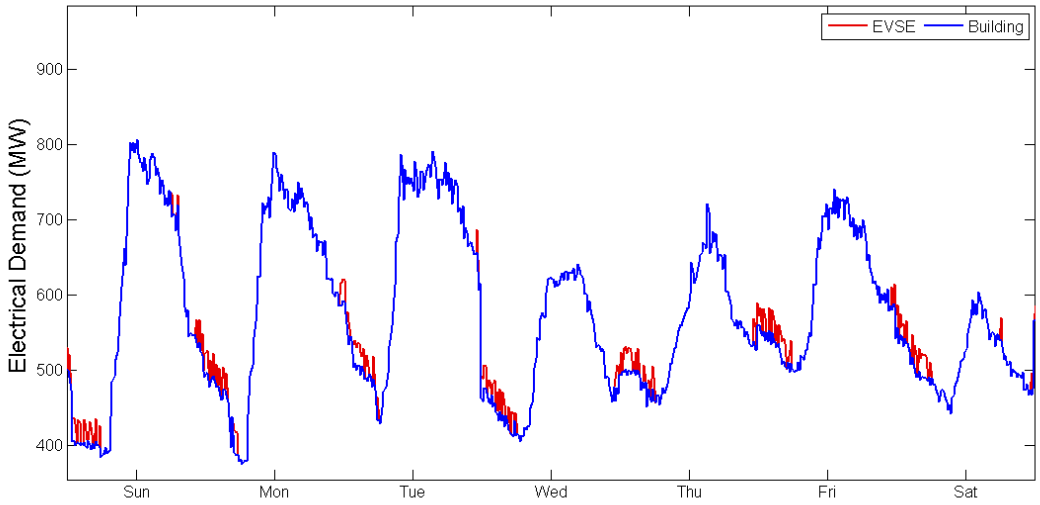

Figure 8-7: UCI Natural Sciences 2 building electrical demand with EVSE operation to refuel the adopted PEV

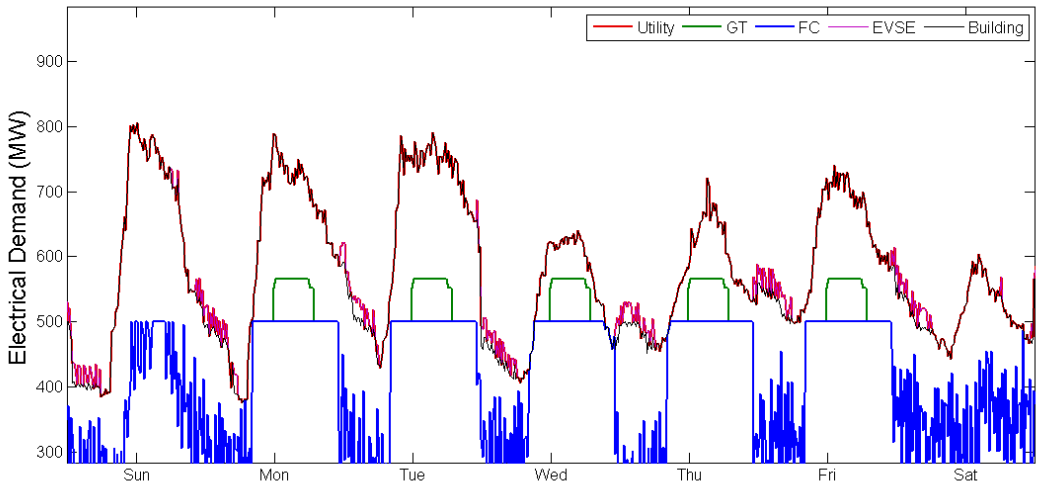

Figure 8-8: DER system operation and EVSE refueling at the UCI Natural Sciences 2 building

9 Summary, Conclusions, and Future Work

9.1 Summary

The goals of this dissertation were to 1) determine and evaluate the optimal mix and operation of distributed energy resources for a commercial or industrial building taking into account possible environmental constraints and the presence of plug-in electric vehicles, and 2) to determine the feasibility of public Level 3 refueling equipment. In order to accomplish these goals, numerous models were developed in order to perform qualitative analyses on the systems in question.

With regards to DER system design, a mixed integer linear program was developed based upon improving similar optimization models presented in the literature by including utility rate details and DER physical and operational characteristics that have been typically omitted. Additional constraints were added to take into account a desire to limit carbon emissions associated with building energy conversion. This model was further modified to resolve the stochastic nature created by considering the adoption of public EVSE, as well as the deterministic decision created by deciding to invest in a fleet of electric vehicles used to operate on pre-determined routes, or to travel to a series of nodes for which the overall trip is to be optimized in conjunction with routes travelled between the nodes.

The basic DER system formulation was used to design a CCHP system for numerous commercial and industrial buildings. The CCHP optimization results were then analyzed using cooperative game theory to evaluate the decision to use waste heat to meet either building heating or cooling demand. This analysis explored both the operational, economic, and environmental impacts created by deciding to install a CCHP system.

The DER system was then reformulated to explore the decision to use onsite power generation to help reduce carbon emissions at a university campus. This formulation included the option of adopting both electrical and thermal energy storage, photovoltaic panels, a renewable fuel source to power DG, and the ability to export excess electricity generated onsite.

The DER system model formulation that included electric vehicles was then executed for a small handful of cases in order to establish the viability of using such methods to fully evaluate the interaction between the decision to invest in a DER system and either EVSE or electric vehicles.

The primary contribution of this work is the DER optimization model developed for the first goal. The results produced by this model are the most valuable product of this work. The integration of typically neglected components, physical constraints, and rate structure parameters adds a level of detail that is needed for developing trust that any suggested system will perform as predicted and as expected from an economic and environmental perspective.

The analyses performed using this model have improved upon the state-of-the-art understanding of how DER systems make money when installed and operated in the built environment, or how these systems can be operated to assist with reducing carbon emissions associated with a building energy demand. The limited simulations that included electric vehicle interactions with the building dynamics have also shed light onto how future simulations can be used to more effectively capture the seemingly separate decisions to invest in a DER system and in electric vehicles or EVSE.

With regards to Level 3 EVSE evaluation, a PEV travel model was developed and combined with two different EVSE operation scenarios that span how EVSE are operated today.

These models were executed and used to assist with determining the cost of electricity to maintain EVSE operation when installed as a standalone system or integrated with a building. Cooperative game theory was used during this analysis, as well, in order to fairly allocate electrical utility costs between a building and integrated EVSE, and between individual drivers that use the EVSE.

9.2 Conclusions

The following conclusions are the primary findings of this dissertation:

- **Large buildings with consistent heating demand are the most attractive candidates for CCHP system integration.**

  This type of building provides numerous benefits when deciding to adopt a DR system. First, a large building is easily capable of consuming sufficient natural gas that the lowest cost natural gas is achieved when a declining block rate structure (the most common type of gas rate structure) is applied. Second, the size of the building energy loads allow for each of the individual components to behave in a flexible manner that maximizes the output of each system. Third, a large heating demand can be leveraged to create opportunities for increased absorption chiller operation during periods when the absorption chiller operation would otherwise be uneconomical. This allows for a large absorption chiller to be adopted and operated in such a way that the overall building electrical demand is reduced while not reducing potential savings during other times. Finally, the capture of waste heat in order to supply heating to the building provides an opportunity to reduce overall carbon emissions. On the other hand, meeting the

building cooling load through the use of an absorption chiller is likely to increase carbon emissions for a building in the state of California because the California grid has low carbon emissions and electric powered vapor compression chiller systems have a high coefficient of performance.

- **The export of electricity from a building to the electrical grid is key to finding the least expensive route to significant carbon emission reductions at a building.**

  Numerous technologies and options exist for reducing the carbon emissions associated with building operations. If the energy consumption of a building located in California has been minimized, and a DER system is to be adopted to further reduce carbon emissions, then the use of renewable fuel is necessary if the least expensive technologies are to be adopted. Further carbon reductions require the adoption of large photovoltaic systems. Without the ability to either store any excess energy produced by photovoltaics that cannot be used instantaneously, the cost to reduce carbon emissions are extremely high. While allowing for multiple storage options along with the ability to export excess solar energy to the utility grid network all reduce the cost of reducing carbon emissions. The ability to export excess solar power is particularly attractive due to the reduced overall DER system complexity and initial capital cost. While the system performance may become more difficult to manage from a utility grid network perspective, the ability to export excess solar power provides the lowest cost path to reducing carbon emissions.

- **Typical current demand charges are sufficiently high to singlehandedly block the adoption of Level 3 EVSE for any application other than possibly range extension or emergencies.**

  The demand charges associated with using Level 3 EVSE to refuel PEVs after performing common types of travel are on the order of $1 to $10 per kWh when PEV traffic is low. Increasing the EVSE power exacerbates demand charge costs while providing no additional improvements to customer access to EVSE. Integrating the equipment with a building can reduce cost substantially, particularly when PEV traffic is low. However, EVSE operation cannot occur when building electrical demand is high without risking increased overall costs for both the building and the PEVs refueling at the station. While demand charge costs decrease with increasing PEV traffic levels, the current number of PEVs on the road today that are Level 3 EVSE compatible result in the likelihood that demand charges will remain high.

- **A stochastic formulation may not be necessary for capturing the interactions between a building, DER system, and public EVSE.**

  PEV traffic patterns are stochastic from the perspective of a building. However, current PEV traffic levels are likely low enough at a typical building that the resulting EVSE demand profile is small enough to marginally impact the overall building operation. In this scenario, the decision to adopt and operate public EVSE does not impact the decision to adopt and operate a DER system. If PEV traffic increases and EVSE technology improves to increase access to a single EVSE, then the resulting demand profile becomes more predictable and may be

viewed as deterministic. In this scenario, EVSE operation does impact the decision to invest in and operate a DER system. In this case, the EVSE behavior is similar from week to week, month to month, and year to year. As a result, the stochastic problem can most likely be reduced to a deterministic problem. Note that a stochastic formulation may be required for PEV traffic between the high and low levels.

9.3 Future Work

As stated before, the primary contribution of this dissertation is the DER system optimization model developed for this work. Further work needs to be performed in order to validate the ability of the model to capture the physical characteristics of the different modeled components. In particular, the absorption chiller formulation in this current work should be compared to typical absorption chiller models presented in the literature by using the optimization model outputs to dictate how a physical absorption chiller model is operated.

The cooperative game theory analysis should be repeated. However, instead of determining the cost of each type pf energy produced by a CCHP system, the Shapley value for each cost component can be determined for each individual piece of technology in order to determine the associated savings. Such an analysis would allow for a DER system operator to determine the exact savings produced by each piece of technology. If energy storage were to be included in the analysis, then the value of including storage can be determined exactly.

Further work is required for the DER system and fleet vehicle optimization problem in order to extend the ability of the model to handle larger sets of nodes to be visited. In particular, decomposing the problem between the DER system and vehicle routing problem may provide a

promising route to allowing for the current branch and cut method to be used to solve the DER systems problem while using a more appropriate method for solving the vehicle routing problem. Such a decomposition would allow for large problems, such as DER system and electric vehicle adoption by a large courier service, to be solved.

With regards to the evaluation of different types of EVSE, a more realistic travel model is required. The largest missing piece is concerned with an individual driver's decision to refuel their PEV based upon competing options and the overall energy demand required by an individual's travel patterns. One potential model is the combination of a Markov chain to determine the discrete travel behavior of an individual driver coupled with an optimization that determines the location at which a vehicle driver will refuel their vehicle in order to minimize cost while maintaining their travel pattern. Resolving the driver's decision to refuel using public EVSE would create a more realistic demand at the public EVSE and also allow for a realistic evaluation of potential rates charged to customers who refuel their PEVs using public EVSE.

References

[1] U.S. Energy Information Administration. EIA - Annual Energy Outlook 2014 Early Release n.d.

[2] U.S. Energy Information Administration. U.S. Natural Gas Consumption by End Use 2015.

[3] U.S. Energy Information Administration. Heat Content of Natural Gas Delivered to Consumers n.d.

[4] Zhang L, Brown T, Samuelsen S. Evaluation of charging infrastructure requirements and operating costs for plug-in electric vehicles. J Power Sources 2013;240:515–24.

[5] El-Khattam W, Salama MMA. Distributed generation technologies, definitions and benefits. Electr Power Syst Res 2004;71:119–28.

[6] United States. Office of Coal Nuclear Electric and Alternate Fuels. Electric power annual 2010.

[7] Casten S. Are Standby Rates Ever Justified? The Case Against Electric Utility Standby Charges as a Response to On-Site Generation. Electr J 2003;16:58–65.

[8] Jackson J. Are US utility standby rates inhibiting diffusion of customer-owned generating systems? Energy Policy 2007;35:1896–908.

[9] Firestone R, Magnus Maribu K, Marnay C, Maribu M. The Value of Distributed Generation under Different Tariff Structures 2006.

[10] Mueller S. Missing the spark: An investigation into the low adoption paradox of

combined heat and power technologies. Energy Policy 2006;34:3153–64.

[11] United States. Energy Information Administration. State electricity profiles. Washington, D.C.: Energy Information Administration, Office of Coal, Nuclear, Electric and Alternate Fuels, U.S. Dept. of Energy; 2010.

[12] Goldstein HL, Institute GR, Laboratory NRE, Efficiency USD of EO of E, Energy R. Gas-fired Distributed Energy Resource Technology Characterizations. National Renewable Energy Laboratory; 2003.

[13] Brouwer J. On the role of fuel cells and hydrogen in a more sustainable and renewable energy future. Curr Appl Phys 2010;10:S9–17.

[14] Bruno JC, Ortega-López V, Coronas A. Integration of absorption cooling systems into micro gas turbine trigeneration systems using biogas: Case study of a sewage treatment plant. Appl Energy 2009;86:837–47.

[15] Alanne K, Saari A. Sustainable small-scale CHP technologies for buildings: the basis for multi-perspective decision-making. Renew Sustain Energy Rev 2004;8:401–31.

[16] Pilavachi P a. A. Mini- and micro-gas turbines for combined heat and power. Appl Therm Eng 2002;22:2003–14.

[17] Nanaeda K, Mueller F, Brouwer J, Samuelsen S. Dynamic modeling and evaluation of solid oxide fuel cell – combined heat and power system operating strategies. J Power Sources 2010;195:3176–85.

[18] Carles Bruno J, Valero A, Coronas A. Performance analysis of combined microgas

turbines and gas fired water/LiBr absorption chillers with post-combustion. Appl Therm Eng 2005;25:87–99.

[19] Ho JC, Chua KJ, Chou SK. Performance study of a microturbine system for cogeneration application. Renew Energy 2004;29:1121–33.

[20] Margalef P, Samuelsen S. Integration of a molten carbonate fuel cell with a direct exhaust absorption chiller. J Power Sources 2010;195:5674–85.

[21] Zhu Y, Tomsovic K. Development of models for analyzing the load-following performance of microturbines and fuel cells. Electr Power Syst Res 2002;62:1–11.

[22] Mueller F, Jabbari F, Gaynor R, Brouwer J. Novel solid oxide fuel cell system controller for rapid load following. J Power Sources 2007;172:308–23.

[23] Joos G, Ooi BT, McGillis D, Galiana FD, Marceau R. The potential of distributed generation to provide ancillary services. Power Eng. Soc. Summer Meet. 2000. IEEE, vol. 3, 2000, p. 1762–7 vol. 3.

[24] Chen H, Cong TN, Yang W, Tan C, Li Y, Ding Y. Progress in electrical energy storage system: A critical review. Prog Nat Sci 2009;19:291–312.

[25] Farid MM, Khudhair AM, Razack SAK, Al-Hallaj S. A review on phase change energy storage: Materials and applications. Energy Convers Manag 2004;45:1597–615.

[26] Siddiqui AS, Maribu K. Investment and upgrade in distributed generation under uncertainty. Energy Econ 2009;31:25–37.

[27] Al-Mansour F, Kožuh M. Risk analysis for CHP decision making within the conditions of

an open electricity market. Energy 2007;32:1905–16.

[28] Siler-Evans K, Morgan MG, Azevedo IL. Distributed cogeneration for commercial buildings: Can we make the economics work? Energy Policy 2012;42:580–90.

[29] Verbruggen A, Dufait N, Martens A. Economic evaluation of independent CHP projects. Energy Policy 1993;21:408–17.

[30] Gordijn J, Akkermans H. Business models for distributed generation in a liberalized market environment. Electr Power Syst Res 2007;77:1178–88.

[31] Ruan Y, Liu Q, Zhou W, Firestone R, Gao W, Watanabe T. Optimal option of distributed generation technologies for various commercial buildings. Appl Energy 2009;86:1641–53.

[32] Siddiqui A, Marnay C, Firestone R, Zhou N. Distributed Generation with Heat Recovery and Storage. J Energy Eng 2007;133:181–210.

[33] Becker WL, Braun RJ, Penev M, Melaina M. Design and technoeconomic performance analysis of a 1MW solid oxide fuel cell polygeneration system for combined production of heat, hydrogen, and power. J Power Sources 2012;200:34–44.

[34] Wang J-J, Jing Y-Y, Zhang C-F, Zhai ZJ. Performance comparison of combined cooling heating and power system in different operation modes. Appl Energy 2011;88:4621–31.

[35] Ziher D, Poredos A. Economics of a trigeneration system in a hospital. Appl Therm Eng 2006;26:680–7.

[36] Naimaster IV EJ, Sleiti AK. Potential of Fuel Cell Combined Heat and Power System for Energy-Efficient Commercial Buildings. Energy Build 2013;61:153–60.

[37] Medrano M, Brouwer J, McDonell V, Mauzey J, Samuelsen S. Integration of distributed generation systems into generic types of commercial buildings in California. Energy Build 2008;40:537–48.

[38] Maidment GG, Zhao X, Ri SB, Prosser G. Application of combined heat-and-power and absorption cooling in a supermarket 1999;63:169–90.

[39] Lai SM, Hui CW. Integration of trigeneration system and thermal storage under demand uncertainties. Appl Energy 2010;87:2868–80.

[40] Knizley AA, Mago PJ, Smith AD. Evaluation of the performance of combined cooling, heating, and power systems with dual power generation units. Energy Policy 2014;66:654–65.

[41] Flores RJ, Shaffer BP, Brouwer J. Dynamic distributed generation dispatch strategy for lowering the cost of building energy. Appl Energy 2014;123:196–208.

[42] Flores RJ, Shaffer BP, Brouwer J. Economic and sensitivity analyses of dynamic distributed generation dispatch to reduce building energy cost. Energy Build 2014;85:293–304.

[43] Pade L-L, Schröder ST. Fuel cell based micro-combined heat and power under different policy frameworks – An economic analysis. Energy Convers Manag 2013;66:295–303.

[44] Pruitt KA, Braun RJ, Newman AM. Establishing conditions for the economic viability of fuel cell-based, combined heat and power distributed generation systems. Appl Energy 2013;111:904–20.

[45] Cardona E, Piacentino A, Cardona F. Matching economical, energetic and environmental benefits: An analysis for hybrid CHCP-heat pump systems. Energy Convers Manag 2006;47:3530–42.

[46] Aki H, Oyama T, Tsuji K. Analysis of energy service systems in urban areas and their CO2 mitigations and economic impacts. Appl Energy 2006;83:1076–88.

[47] Fang F, Wang QH, Shi Y. A Novel Optimal Operational Strategy for the CCHP System Based on Two Operating Modes. IEEE Trans Power Syst 2012;27:1032–41.

[48] Lozano MA, Carvalho M, Serra LM. Operational strategy and marginal costs in simple trigeneration systems. Energy 2009;34:2001–8.

[49] Wang H, Yin W, Abdollahi E, Lahdelma R, Jiao W. Modelling and optimization of CHP based district heating system with renewable energy production and energy storage. Appl Energy 2015;159:401–21.

[50] Collazos A, Maréchal F, Gähler C. Predictive optimal management method for the control of polygeneration systems. Comput Chem Eng 2009;33:1584–92.

[51] Bozchalui MC, Sharma R. Optimal operation of commercial building microgrids using multi-objective optimization to achieve emissions and efficiency targets. 2012 IEEE Power Energy Soc. Gen. Meet., IEEE; 2012, p. 1–8.

[52] Keirstead J, Samsatli N, Shah N, Weber C. The impact of CHP (combined heat and power) planning restrictions on the efficiency of urban energy systems. Energy 2012;41:93–103.

[53] Liu P, Pistikopoulos EN, Li Z. An energy systems engineering approach to the optimal design of energy systems in commercial buildings. Energy Policy 2010;38:4224–31.

[54] Lozano MA, Ramos JC, Serra LM. Cost optimization of the design of CHCP (combined heat, cooling and power) systems under legal constraints. Energy 2010;35:794–805.

[55] Liu P, Gerogiorgis DI, Pistikopoulos EN. Modeling and optimization of polygeneration energy systems. Catal Today 2007;127:347–59.

[56] Wakui T, Yokoyama R. Optimal structural design of residential cogeneration systems with battery based on improved solution method for mixed-integer linear programming. Energy 2015;84:106–20.

[57] Bracco S, Dentici G, Siri S. DESOD : a mathematical programming tool to optimally design a distributed energy system. Energy 2016;100:298–309.

[58] Wang M, Wang J, Zhao P, Dai Y. Multi-objective optimization of a combined cooling, heating and power system driven by solar energy. Energy Convers Manag 2015;89:289–97.

[59] Li L, Mu H, Gao W, Li M. Optimization and analysis of CCHP system based on energy loads coupling of residential and office buildings. Appl Energy 2014;136:206–16.

[60] Zeng R, Li H, Liu L, Zhang X, Zhang G. A novel method based on multi-population genetic algorithm for CCHP-GSHP coupling system optimization. Energy Convers Manag 2015;105:1138–48.

[61] Pruitt KA, Braun RJ, Newman AM. Evaluating shortfalls in mixed-integer programming

approaches for the optimal design and dispatch of distributed generation systems. Appl Energy 2013;102:386–98.

[62] Siddiqui AS, Marnay C, Bailey O, Hamachi LaCommare K. Optimal selection of on-site generation with combined heat and power applications 2004.

[63] Marnay C, Venkataramanan G, Stadler M, Siddiqui AS, Firestone R, Chandran B. Optimal Technology Selection and Operation of Commercial-Building Microgrids. Power Syst IEEE Trans 2008;23:975–82.

[64] Stadler M, Groissböck M, Cardoso G, Marnay C. Optimizing Distributed Energy Resources and building retrofits with the strategic DER-CAModel. Appl Energy 2014;132:557–67.

[65] Marnay C, Venkataramanan G, Stadler M, Siddiqui AS, Firestone R, Chandran B. Optimal technology selection and operation of commercial-building microgrids. Power Syst IEEE Trans 2008;23:975–82.

[66] Stadler M, Kloess M, GroissbÃ¶ck M, Cardoso G, Sharma R, Bozchalui MC, et al. Electric storage in California's commercial buildings. Appl Energy 2013;104:711–22.

[67] Milan C, Stadler M, Cardoso G, Mashayekh S. Modeling of non-linear CHP efficiency curves in distributed energy systems. Appl Energy 2015;148:334–47.

[68] Carley S, Krause RM, Lane BW, Graham JD. Intent to purchase a plug-in electric vehicle: A survey of early impressions in large US cites. Transp Res Part D Transp Environ 2013;18:39–45.

[69] Egbue O, Long S. Barriers to widespread adoption of electric vehicles: An analysis of consumer attitudes and perceptions. Energy Policy 2012;48:717–29.

[70] Sierzchula W, Bakker S, Maat K, van Wee B. The influence of financial incentives and other socio-economic factors on electric vehicle adoption. Energy Policy 2014;68:183–94.

[71] Green EH, Skerlos SJ, Winebrake JJ. Increasing electric vehicle policy efficiency and effectiveness by reducing mainstream market bias. Energy Policy 2014;65:562–6.

[72] Joos G, de Freige M, Dubois M. Design and simulation of a fast charging station for PHEV/EV batteries. 2010 IEEE Electr Power Energy Conf 2010:1–5.

[73] Dharmakeerthi C, Mithulananthan N, Saha TK. Overview of the Impacts of Plug-in minor partein Electric Vehicles on the Power Grid. Innov Smart Grid Technol Asia (ISGT), 2011 IEEE PES 2011:1–8.

[74] Sadeghi-Barzani P, Rajabi-Ghahnavieh A, Kazemi-Karegar H. Optimal fast charging station placing and sizing. Appl Energy 2014;125:289–99.

[75] Eising JW, van Onna T, Alkemade F. Towards smart grids: Identifying the risks that arise from the integration of energy and transport supply chains. Appl Energy 2014;123:448–55.

[76] Salah F, Ilg JP, Flath CM, Basse H, Dinther C van. Impact of electric vehicles on distribution substations: A Swiss case study. Appl Energy 2015;137:88–96.

[77] Dharmakeerthi CH, Mithulananthan N, Saha TK. Impact of electric vehicle fast charging on power system voltage stability. Int J Electr Power Energy Syst 2014;57:241–9.

[78] Dubey a., Santoso S, Cloud MP. Understanding the effects of electric vehicle charging on the distribution voltages. IEEE Power Energy Soc Gen Meet 2013:1–8.

[79] Razeghi G, Zhang L, Brown T, Samuelsen S. Impacts of plug-in hybrid electric vehicles on a residential transformer using stochastic and empirical analysis. J Power Sources 2014;252:277–85.

[80] Harris CB, Webber ME. An empirically-validated methodology to simulate electricity demand for electric vehicle charging. Appl Energy 2014;126:172–81.

[81] Foley A, Tyther B, Calnan P, Ó Gallachóir B. Impacts of Electric Vehicle charging under electricity market operations. Appl Energy 2013;101:93–102.

[82] Zhang L, Jabbari F, Brown T, Samuelsen S. Coordinating plug-in electric vehicle charging with electric grid: Valley filling and target load following. J Power Sources 2014;267:584–97.

[83] Zakariazadeh A, Jadid S, Siano P. Integrated operation of electric vehicles and renewable generation in a smart distribution system. Energy Convers Manag 2015;89:99–110.

[84] Clement-Nyns K, Haesen E, Driesen J. The impact of Charging plug-in hybrid electric vehicles on a residential distribution grid. IEEE Trans Power Syst 2010;25:371–80.

[85] Soares FJ, Almeida PMR, Lopes JAP. Quasi-real-time management of Electric Vehicles charging. Electr Power Syst Res 2014;108:293–303.

[86] Iversen EB, Morales JM, Madsen H. Optimal charging of an electric vehicle using a Markov decision process. Appl Energy 2014;123:1–12.

[87] Su W, Wang J, Zhang K, Huang AQ. Model predictive control-based power dispatch for distribution system considering plug-in electric vehicle uncertainty. Electr Power Syst Res 2014;106:29–35.

[88] Xu Z, Hu Z, Song Y, Zhao W, Zhang Y. Coordination of PEVs charging across multiple aggregators. Appl Energy 2014;136:582–9.

[89] Tushar W, Saad W, Poor H V, Smith DB. Economics of electric vehicle charging: A game theoretic approach. Smart Grid, IEEE Trans 2012;3:1767–78.

[90] Zakariazadeh A, Jadid S, Siano P. Multi-objective scheduling of electric vehicles in smart distribution system. Energy Convers Manag 2014;79:43–53.

[91] Yang J, He L, Fu S. An improved PSO-based charging strategy of electric vehicles in electrical distribution grid. Appl Energy 2014;128:82–92.

[92] Momber I, Gómez T, Venkataramanan G, Stadler M, Beer S, Lai J, et al. Plug-in electric vehicle interactions with a small office building: An economic analysis using DER-CAM. IEEE PES Gen. Meet., IEEE; 2010, p. 1–8.

[93] Jia L, Hu Z, Song Y, Luo Z. Optimal siting and sizing of electric vehicle charging stations. Electr Veh Conf (IEVC), 2012 IEEE Int 2012:1–6.

[94] Su CL, Leou RC, Yang JC, Lu CN, Chun-Lien Su, Rong-Ceng Leou, et al. Optimal electric vehicle charging stations placement in distribution systems. IECON Proc (Industrial Electron Conf 2013:2121–6.

[95] Giménez-Gaydou D a., Ribeiro ASN, Gutiérrez J, Antunes AP. Optimal Location of

Battery Electric Vehicle Charging Stations in Urban Areas: A New Approach. Int J Sustain Transp 2014:141224080628007.

[96] Wagner S, Götzinger M, Neumann D. Optimal location of charging stations in smart cities: A points of interest based approach. 34th Int Conf Inf Syst (ICIS 2013) 2013:1–18.

[97] Xi X, Sioshansi R, Marano V. Simulation–optimization model for location of a public electric vehicle charging infrastructure. Transp Res Part D Transp Environ 2013;22:60–9.

[98] Xu H, Miao S, Zhang C, Shi D. Optimal placement of charging infrastructures for large-scale integration of pure electric vehicles into grid. Int J Electr Power Energy Syst 2013;53:159–65.

[99] Peterson SB, Michalek JJ. Cost-effectiveness of plug-in hybrid electric vehicle battery capacity and charging infrastructure investment for reducing US gasoline consumption. Energy Policy 2013;52:429–38.

[100] Ghavami A, Kar K. Nonlinear Pricing for Social Optimality of PEV Charging Under Uncertain User Preferences. 48th Annu Conf Inf Sci Syst 2014.

[101] Bayram IS, Michailidis G, Papapanagiotou I, Devetsikiotis M. Decentralized control of electric vehicles in a network of fast charging stations. GLOBECOM - IEEE Glob Telecommun Conf 2013:2785–90.

[102] Williams B, DeShazo JR. Pricing Workplace Charging. Transp Res Rec J Transp Res Board 2014;2454:68–75.

[103] U.S. Department of Energy. Alternative Fuels Data Center: Electric Vehicle Charging

Station Locations 2015.

[104] Schroeder A, Traber T. The economics of fast charging infrastructure for electric vehicles. Energy Policy 2012;43:136–44.

[105] Tarroja B, Zhang L, Wifvat V, Shaffer B, Samuelsen S. Assessing the stationary energy storage equivalency of vehicle-to-grid charging battery electric vehicles. Energy 2016;106:673–90.

[106] Skugor, Branimir, Deur J. Dynamic programming-based optimisation of charging an electric vehicle fleet system represented by an aggregate battery model. Energy 2014;92:456–65.

[107] Weiller C, Neely A. Using electric vehicles for energy services: Industry perspectives. Energy 2014;77:194–200.

[108] Kavousi-Fard A, Abunasri A, Zare A, Hoseinzadeh R. Impact of plug-in hybrid electric vehicles charging demand on the optimal energy management of renewable micro-grids. Energy 2014;78:904–15.

[109] Cardoso G, Stadler M, Bozchalui MC, Sharma R, Marnay C, Barbosa-P??voa A, et al. Optimal investment and scheduling of distributed energy resources with uncertainty in electric vehicle driving schedules. Energy 2014;64:17–30.

[110] Erdoğan S, Miller-Hooks E. A Green Vehicle Routing Problem. Transp Res Part E Logist Transp Rev 2012;48:100–14.

[111] Lin C, Choy KL, Ho GTS, Chung SH, Lam HY. Survey of Green Vehicle Routing

Problem: Past and future trends. Expert Syst Appl 2014;41:1118–38.

[112] Juan AA, Goentzel J, Bekta?? T. Routing fleets with multiple driving ranges: Is it possible to use greener fleet configurations? Appl Soft Comput J 2014;21:84–94.

[113] Hiermann G, Puchinger J, Hartl R. The Electric Vehicle Routing Problem with Time Windows and Recharging Stations. Transp Sci 2014;48:500–20.

[114] Desrosiers J, Sauvé M, Soumis F. Lagrangian Relaxation Methods for Solving the Minimum Fleet Size Multiple Traveling Salesman Problem With Time Windows. Manage Sci 1988;34:1005–22.

[115] Bektas T. The multiple traveling salesman problem: An overview of formulations and solution procedures. Omega 2006;34:209–19.

[116] Miller CE, Tucker a. W, Zemlin R a. Integer Programming Formulation of Traveling Salesman Problems. J ACM 1960;7:326–9.

[117] Laporte G, Norbert Y. A Cutting Planes Algorithm for the m-Salesman Problem. J Oper Res Soc 1980;31:1017–23.

[118] Christofides N, Mingozzi A, Toth P. Exact Algorithms for the Vehicle Routing Problem , Based on Spanning Tree and Shortest Path Relaxations. Math Program 1981;20:28.

[119] Golden B, Assad A, Levy L, Gheysens F. The fleet size and mix vehicle routing problem. Comput Oper Res 1984;11:49–66.

[120] Braysy O, Dullaert W, Hasle G, Mester D, Gendreau M. An Effective Multirestart Deterministic Annealing Metaheuristic for the Fleet Size and Mix Vehicle-Routing

Problem with Time Windows. Transp Sci 2008;42:371–86.

[121] Yuan Y, Mehrez A. Refueling strategies to maximize the operational range of a nonidentical vehicle fleet. Eur J Oper Res 1995;83:167–81.

[122] Chan Y, Baker SF. The multiple depot, multiple traveling salesmen facility-location problem: Vehicle range, service frequency, and heuristic implementations. Math Comput Model 2005;41:1035–53.

[123] Forsgren A, Gill P, Wright M. Interior Methods for Nonlinear Optimization. vol. 44. 2002.

[124] Song M-PSM-P, Gu G-CGG-C. Research on particle swarm optimization: a review. Proc 2004 Int Conf Mach Learn Cybern (IEEE Cat No04EX826) 2004;4:26–9.

[125] Webb GI. Posterior Probability. Encycl Mach Learn 2010:780.

[126] Inuiguchi M, Ramík J. Possibilistic linear programming: a brief review of fuzzy mathematical programming and a comparison with stochastic programming in portfolio selection problem. Fuzzy Sets Syst 2000;111:3–28.

[127] Tamaki H, Kita H, Kobayashi S. Multi-objective optimization by genetic algorithms: a review. Evol Comput 1996, Proc IEEE Int Conf 1996:517–22.

[128] Gopalakrishnan H, Kosanovic D. Operational planning of combined heat and power plants through genetic algorithms for mixed 0–1 nonlinear programming. Comput Oper Res 2015;56:51–67.

[129] Eksioglu B, Vural AV, Reisman A. The vehicle routing problem: A taxonomic review.

Comput Ind Eng 2009;57:1472–83.

[130] IBM. IBM CPLEX Optimizer - United States n.d.

[131] Gurobi. Gurobi Optimization - The Best Mathematical Programming Solver n.d.

[132] FICO. FICO Xpress Optimization Suite. n.d.

[133] OptiRisk. Products: FortMp n.d.

[134] MathWorks. Optimization Software - Optimization Toolbox - MATLAB n.d.

[135] Conforti M, Cornuejols G, Zambelli G. Integer Programming. 2014.

[136] Shapiro A, Philpott A. A tutorial on stochastic programming. Manuscript Available www2 Isye Gatech Edu … 2007:1–35.

[137] Cardoso G, Stadler M, Siddiqui A, C. Marnay, Deforest N, Barbosa-P??voa A, et al. Microgrid reliability modeling and battery scheduling using stochastic linear programming. Electr Power Syst Res 2013;103:61–9.

[138] Wickart M, Madlener R. Optimal technology choice and investment timing: A stochastic model of industrial cogeneration vs. heat-only production. Energy Econ 2007;29:934–52.

[139] Su W, Wang J, Member S, Roh J. Stochastic Energy Scheduling in Microgrids With Intermittent Renewable Energy Resources Stochastic Energy Scheduling in Microgrids With Intermittent Renewable Energy Resources 2013;5:1876–83.

[140] Najibi F, Niknam T. Stochastic scheduling of renewable micro-grids considering photovoltaic source uncertainties. Energy Convers Manag 2015;98:484–99.

[141] Gröwe-Kuska N, Römisch W. Stochastic unit commitment in hydrothermal power production planning. Appl Stoch Program 2005:633–53.

[142] Powell WB, Meisel S. Tutorial on Stochastic Optimization in Energy I : Modeling and Policies. IEEE Trans Power Syst 2015;PP:1–8.

[143] Powell WB, Meisel S. Tutorial on Stochastic Optimization in Energy II : An energy storage illustration. IEEE Trans Power Syst 2015;PP:1–8.

[144] Shmoys DB, Swamy C. Stochastic optimization is (almost) as easy as deterministic optimization. Found Comput Sci 2004 Proceedings 45th Annu IEEE Symp 2004:228–37.

[145] Higle JL. Stochastic Programming: Optimization When Uncertainty Matters. INFORMS, Tutorials Oper Res 2005:1–24.

[146] Curtin S, Gangi J. State of the States: Fuel Cells in America 2013. Fuel Cells 2000 - Breakthr Technol Inst 2013.

[147] Cardwell D. Utilities Push Into Fuel Stations for Electric Cars. New York Times 2015.

[148] The U.S Department of Transportation Federal Highway Administration. National Household Travel Survey 2009.

[149] Southern California Edison. Schedule TOU-8-S TIME-OF-USE - GENERAL SERVICE - LARGE STANDBY 2014.

[150] Southern California Edison. TOU-EV-3 GENERAL SERVICE TIME-OF-USE ELECTRIC VEHICLE CHARGING 2014.

[151] Southern California Edison. TOU-EV-4 GENERAL SERVICE TIME-OF-USE

ELECTRIC VEHICLE CHARGING - DEMAND METERED 2014.

[152] Gilbert, D. Fowler T. Natural Gas Glut Pushes Exports. Wall Str J 2012.

[153] United States. Office of Energy Markets and End Use., United States. Energy Information Administration. Office of Integrated Analysis and Forecasting. Annual energy outlook 2012:v.

[154] Smil V. Perils of Long-Range Energy Forecasting: Reflections on Looking Far Ahead. Technol Forecast Soc Change 2000;65:251–64.

[155] Hack, RL, McDonell, VG, Samuelsen GS. Realistic Application and Air Quality Implications of DG and CHP in California. California Energy Commission; 2011.

[156] Domínguez-Muñoz F, Cejudo-López JM, Carrillo-Andrés A, Gallardo-Salazar M. Selection of typical demand days for CHP optimization. Energy Build 2011;43:3036–43.

[157] U.S. Department of Energy. Alternative Fuels Data Center: Vehicle Search 2015.

[158] U.S. Department of Energy. Compare Electric Vehicles 2015.

[159] U.S. Department of Energy. U.S. PEV Sales by Model 2015.

[160] Pavley F, Nunez F. California Assembly Bill No. 32-Global Warming Solutions Act of 2006. Secretary 2006;5:38500–99.

[161] Winter E. The Shapley Value. Handb Game Theory 2002;3:2027–54.

[162] Littlechild SC, Owen G. A Simple Expression for the Shapley Value in a Special Case. Manage Sci 1973;20:370–2.

[163] California ISO n.d.

[164] Environmental Protection Agency. eGRID Subregion Representational Map n.d.;1/4/2012].

[165] Shaffer BP. UCI Microgrid Hardware Assets 2013:13.

[166] McLarty D. Thermodynamic Modeling and Dispatch of Distributed Energy Technologies including Fuel Cell - Gas Turbine Hybrids. University of California, Irvine, 2013.

[167] Irvine U of C at. System Map 2015-2016.pdf n.d.

[168] Hosford K. Design and Economic Potential of an Integrated High-Temparature Fuel Cell and Absorption Chiller Combined Cooling Heat and Power System 2013.

[169] DiMola A. Enabling the Distributed Generation Market of High Temperature Fuel Cell and Absorption Chiller Systems to Support Critical and Commercial Loads. University of California at Irvine, 2015.

[170] Flores RJ. Control of dispatch dynamics for lowering the cost of distributed generation in the built environment 2013.

[171] Fuel Cell Energy. DFC 300 Product Specifications 2013;2:2–3.

[172] Capstone. Product Specification Model C65 - Capstone MicroTurbine 2007:2007.

[173] Martz S. Modeling and Integration of a Combined Cooling , Heating and Power System with a High Temperature Fuel Cell and Absorption Chiller 2011.

[174] EPA. eGRID2012 Summary Tables. Clean Air Mark Div Off Atmos Programs US Environ Prot Agency 2015:3–8.

[175] California Air Resources Board. Subchapter 10 Climate Change, Article 5, Sections 95800 to 96023, Title 17, California Code of Regulations 2013:1–262.

[176] California Air Resource Board. Energy - Distributed Generation Program n.d.;1/3/2012].

[177] California U of. Carbon Neutrality Initiative | UCOP n.d.

[178] University of Californina at Irvine. UC Irvine Climate Action Plan 2013 Update 2013.

[179] BYD Company. BYD ebus, electric bus | Auto | BYD n.d.

[180] California Carbon Dashboard: Carbon Prices, the Latest News, and California Policy n.d.

[181] Flores RJ, Shaffer BP, Brouwer J. Electricity costs for an electric vehicle fueling station with Level 3 charging. Appl Energy 2016;169:813–30.

[182] White D. Important Factors for Early Market Microgrids: Demand Response and Plug-in Electric Vehicle Charging. University of California at Irvine, 2016.